Silver, Copper and Bronze in Early Dynastic Ur, Mesopotamia

A High-Resolution Analysis Approach

Eveline Salzmann

DBM Deutsches Bergbau-Museum Bochum

DER ANSCHNITT BEIHEFT 41

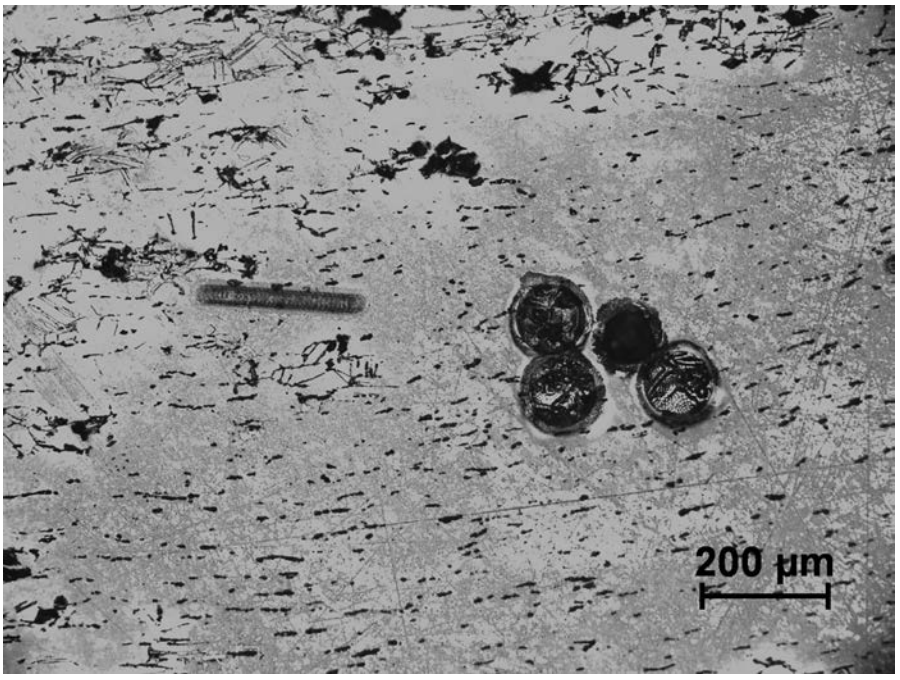
200 µm

Silver, Copper and Bronze in Early Dynastic Ur, Mesopotamia

A High-Resolution Analysis Approach

Eveline Salzmann

VML Verlag Marie Leidorf GmbH

Bochum 2019

Montanhistorische Zeitschrift Der ANSCHNITT. Beiheft 41
= Veröffentlichungen aus dem Deutschen Bergbau-Museum Bochum, Nr. 231

The dissertation with the title "The Royal Cemetery of Ur: Provenance studies on Early Bronze Age silver-, copper- and bronze artefacts in the collection of the University of Penn-sylvania Museum of Archaeology and Anthropology, Philadel-phia" was submitted in September 2017 to the Department of Geosciences/Geography of the Goethe-University Frankfurt am Main. This work represents mainly the state of research in 2017. Up to the printing time current literature and research results were taken into account.

Bibliografische Informationen der Deutschen Nationalbibliothek Die Deutsche Nationalbibliothek verzeichnet diese Publikation in der Deutschen Nationalbibliografie; detaillierte bibliografische Daten sind im Internet über http://dnb.d-nb.de abrufbar.
Zugl.: Univ. Frankfurt/Main, Diss. ; 2017

In Kommission bei
VML Verlag Marie Leidorf GmbH, Rahden/Westf.
Geschäftsführer: Dr. Bert Wiegel
Stellerloh 65 · D-32369 Rahden/Westf.
Tel: +49/(0)5771/ 9510-74
Fax: +49/(0)5771/ 9510-75
E-Mail: info@vml.de
Homepage: www.vml.de

Cover Image
Bronze Bull's Head as part of a harp. Image courtesy of the Penn Museum, Image #295652b, Object 30-12-696

Frontispiece
Microscope image of an arsenical copper needle of the Penn Museum (CBS16409). The round craters result from nanosecond the elongated crater from femtosecond laserablation measure-ments (Foto: E. Salzmann).

Reviewed by
Apl. Prof. Dr. Sabine Klein and Prof. Dr. Andreas Hauptmann, Goethe-Universität Frankfurt, Deutsches Bergbau-Museum Bochum

Editing
Bernd Lehnhoff, Bochum

Typesetting, Layout, Cover Design
Dr. Eveline Salzmann and Dr. Petra Eisenach, Bochum

Printing
druckhaus köthen GmbH & Co. KG, Köthen

ISBN 978-3-86757-033-6 (Print)
ISBN 978-3-96955-015-1 (Online)
ISSN 2749-6449 (Online)
ISSN 1616-9212 (Print)
DOI https://doi.org/10.46586/DBM.130

Except where otherwise noted, text and graphics ofthis work are licensed under a Creative Commons Attribution 4.0 International License.

Gefördert vom Land NRW

Content

Preface

Sir Charles Leonard Woolley of the British Museum, London, led the excavations at Tell al-Muqayyar in the 1920s and 1930s located in the southern area of the Euphrates and Tigris rivers, close to the Persian Gulf (Woolley, 1928a; -b; 1934). Ur had gained great importance amongst the many other Mesopotamian cities in Early Bronze Age. Woolley discovered approximately 2000 burials on the outskirts of Ur, among them 16 Royal Tombs dating mainly to Early Bronze Age (Early Dynastic III, about the middle of the 3rd millennium BCE). The Royal Tombs exhibit clearly distinguished burials of prominent females and males regularly accompanied to death by many dozens of individuals from the entourage. According to their social status the elite personalities were given rich burial gifts: an incredible amount of wonderful gold, silver, copper, and bronze artefacts could be salvaged.

The excavations of Ur and these outstanding grave finds quickly became world-renowned. The archaeological findings were divided among the participating institutions after the excavations ended, namely the British Museum, London, the National Museum of Iraq, Baghdad, and the University of Pennsylvania Museum of Archeology and Anthropology, Philadelphia.

The London-based Sumerian Metal Committee appointed by the Royal Anthropological Institute were inspired by the exceptional finds at the Royal Cemetery of Ur and decided to investigate the compositions, the origin and the evidence of the artefacts collected in this locality and from other excavations in the Mesopotamia. First wet-chemical analyses of copper artefacts by Desch (1928-1938) indicated, e.g. that their nickel content could be indicative of impurities to detect ore sources. He compared the data with a number of other ores from the Oman Mountain range in the south eastern Arabian Peninsula.

Harold J. Plenderleith (1934), on the other hand, focussed his first metallurgical investigations on the gold artefacts of Ur. He carried out his analytical investigations at the British Museum. He also worked on the aspects of corrosion and the associated desilvering of gold and depletion of copper, which was to be expected in the saline milieu of the alluvial soil of southern Mesopotamia.

In 1961 the director Froelich G. Rainey of the Penn Museum at Philadelphia established MASCA, the Museum Applied Science Center for Archeology. MASCA ran a radiocarbon laboratory and was involved in developing and testing remote sensing equipment as well as magnetometers, and engaged specialists in physics, chemistry, archaeobotany, and other sciences. This formed the basis for the research performed in Philadelphia, because the Penn Museum had a great interest in archaeology and especially in the development of the early metallurgy of Mesopotamia. The Museum's Mesopotamian Metals Project (MMP) was initiated in the 1980s to provide a reliable scientific framework for the social and economic interpretation of the metallurgical industry in the early urban complex that emerged in southern Iraq around 3000 BCE. Stuart Fleming, James D. Muhly, Vincent C. Pigott, Robert Maddin, Tamara Stech and later Sam Nash joined together to form a very active interdisciplinary research team. In the area of craft specialisation, Mesopotamia has yet received only a few words. Metallurgy was chosen as the vehicle of technological progress on the development of ancient cities. Many dozens of mounted samples of many silver and non-ferrous metal artefacts have been made to conduct chemical and metallographic analyses. Particle-induced X-ray emission (PIXE) analysis was performed in Delaware, and the major and minor constituents in the artefacts were determined to be copper, silver, arsenic, tin, and nickel.

In 2009 a collaboration was founded between the University of Pennsylvania Museum of Archaeology and Anthropology, Philadelphia, the Deutsches Bergbau-Museum Bochum and the Institute of Earth Sciences of J.W. Goethe University Frankfurt am Main in order to gain further analytical information from the metal artefacts of the Royal Tombs of Ur. In 2013, the first analytical investigations were intensified within a project funded by the German Research Foundation (DFG). Two topics were awarded in the framework of dissertations: The present study focussed on the copper and silver artefacts, the second, which is planned to follow in a later volume of this publication series deals with the gold artefacts of the Royal tombs.

The present publication thus is about the re-investigation of a collection of 88 mounts of metal specimens from Ur. Their preparation and metallographic analysis date back to the MASCA's Mesopotamian Metals Project MMP cooperator S. Nash. The metallographic results in form of S. Nash's hand-written notes were finally made available to the doctoral candidate and were helpful for the further investigations. Transliterated excerpts are incorporated in the present publication. The new investigations concentrated on a large series of trace elements and isotope analyses of lead and copper by means of laser ablation Inductively Coupled Plasma Mass Spectrometry. The analyses were carried out in the laboratories of the Institute of Geosciences at Frankfurt am Main.

Andreas Hauptmann and Sabine Klein

1 The “Ur-project” - main goals

This thesis is part of a joint project funded by the German Research Foundation (DFG) between the Goethe-Universität Frankfurt, Deutsches Bergbau-Museum Bochum, and the Pennsylvania Museum of Archaeology and Anthropology, Philadelphia (Penn Museum). The interdisciplinary project is divided into different specialities of Archaeometallurgy, Technology, Archaeology, and Assyriology. This thesis is dedicated to the provenance of the Ur copper-, bronze-, and silver metal and the involved technological know how of metal production in third millennium BCE Mesopotamia. Before the project could have started Andreas Hauptmann and Sabine Klein (Deutsches Bergbau-Museum Bochum, GER) established a cooperation with the Near Eastern section of the Penn Museum. They performed preliminary investigations on metal objects from Ur to prepare the project proposal at the German Research Foundation. Today they are consulting scholars at the Penn Museum‘s Near Eastern section. Richard L. Zettler and Brad Hafford (Penn University, Philadelphia, US) supported the scientific investigations with their profound knowledge of the Archaeology of Ur and Mesopotamia. Katherine Blanchard was of great support making this project possible regarding the sampling and study campaigns at the Penn Museum, Philadelphia, US.

Andreas Hauptmann and Sabine Klein investigated lead vessels from Pit X in Ur, analysed gold objects with non-destructive techniques, copper based artefacts from the collection of the British Museum, and cosmetic pigments. The analysis of lead isotopes and trace elements of the lead vessels dating to Early Dynastic I (Forest, 1983) indicates a potential origin of the material from Anatolia (Klein and Hauptmann, 2016). The non-destructive analysis of the gold artefacts provides indications on the application of depletion gilding on two gold artefacts (Hauptmann and Klein, 2016). Copper based, silver, and gold artefacts of the collection of the British Museum were analysed. The main element, trace element, and lead isotope compositions of the analysed copper based and silver artefacts will be compared and discussed in this dissertation, as well (Klein, La Niece, and Hauptmann, 2016). Furthermore they peformed scientific analyses of the cosmetic pigments of Ur, which were mostly on mineral base and likely produced from the intentional corrosion of copper based artefacts (Hauptmann, et al., 2016).

Moritz Jansen (Ruhr University Bochum, GER) is determining the provenance of the Ur gold artefacts with different analytical methods. Jansen, et al., (2016a; 2016b) investigated platinum group elements (PGE) and osmium isotopes in PGE inclusions within the gold and its possible assocation with Palaeozoic ophiolites close to potential placer deposits. Hendrik Wick (University Frankfurt, GER) analysed 6 samples of alabaster/calcite jars from five private and one Royal Tombs (PG 800)(Wick, 2015). Additionally, Wick investigated 14 samples of 7 different quarries located in Egypt. The results suggest that 4 of 6 samples of the calcite jars from Ur are potentially related to quarries in Egypt (Wick, 2015, 42).

Technological studies are performed by Barbara Armbruster (CNRS Toulouse, FR) aiming for a better understanding of the manufacture of the gold artefacts. Armbruster (2016) concluded, that the gold smiths of Ur were likely highly specialised craftsmen in very well organised workshop structures.

Paola Paoletti (University Munich, GER) supported the project with advice on technological aspects known from cuneiform texts resulting in a joint publication (Hauptmann, et al., 2018).

The ancient city of Ur, present day located in southern Iraq, was excavated in 1922-1934 by Sir Charles Leonard Woolley. Thousands of Early Bronze Age precious metal artefacts were discovered in the cemetery of Ur, including 16 Early Dynastic IIIa Royal Tombs. A large number of gold-, silver-, copper-, bronze-, lead-, lapis lazuli, and carnelian artefacts were recovered from the excavations, which were divided between the collections of the Penn Museum, Philadelphia, the British Museum, London, and the National Museum of Iraq in Baghdad. For the present thesis the Penn Museum in Philadelphia provided a number of 89 mounted samples as a loan, and additionally 20 drilled samples of silver artefacts for scientific investigations. The already mounted samples were investigated by Samuel K. Nash (volunteer at the Penn Museum) regarding their metallography. James D. Muhly, Vincent C. Pigott, Stuart Fleming, and Tamara Stech performed chemical analyses on the mounted samples regarding the main elements As, Ni, and Sn in the course of the Mesopotamian Metals Project (MMP).

In this thesis a more comprehensive set of chemical and isotope analysis is performed on the Ur artefacts. Electron microprobe analysis and single-collector mass spectrometry provides information on the main- and trace elements. Furthermore analysis of Pb and Cu iso-

tope composition is performed with multi-collector mass spectrometry.

During the Early Dynastic Period mining and smelting activities are evidenced in widely spread regions. All of these have to be taken into account as potential raw material‘s sources for the Ur metal. The material analysis is performed in order to narrow down the ore deposits, where the Ur metal has its origin. The results shall aid the reconstruction of ancient trade and cultural relationships.

2 The Fertile Crescent - cradle of civilisation

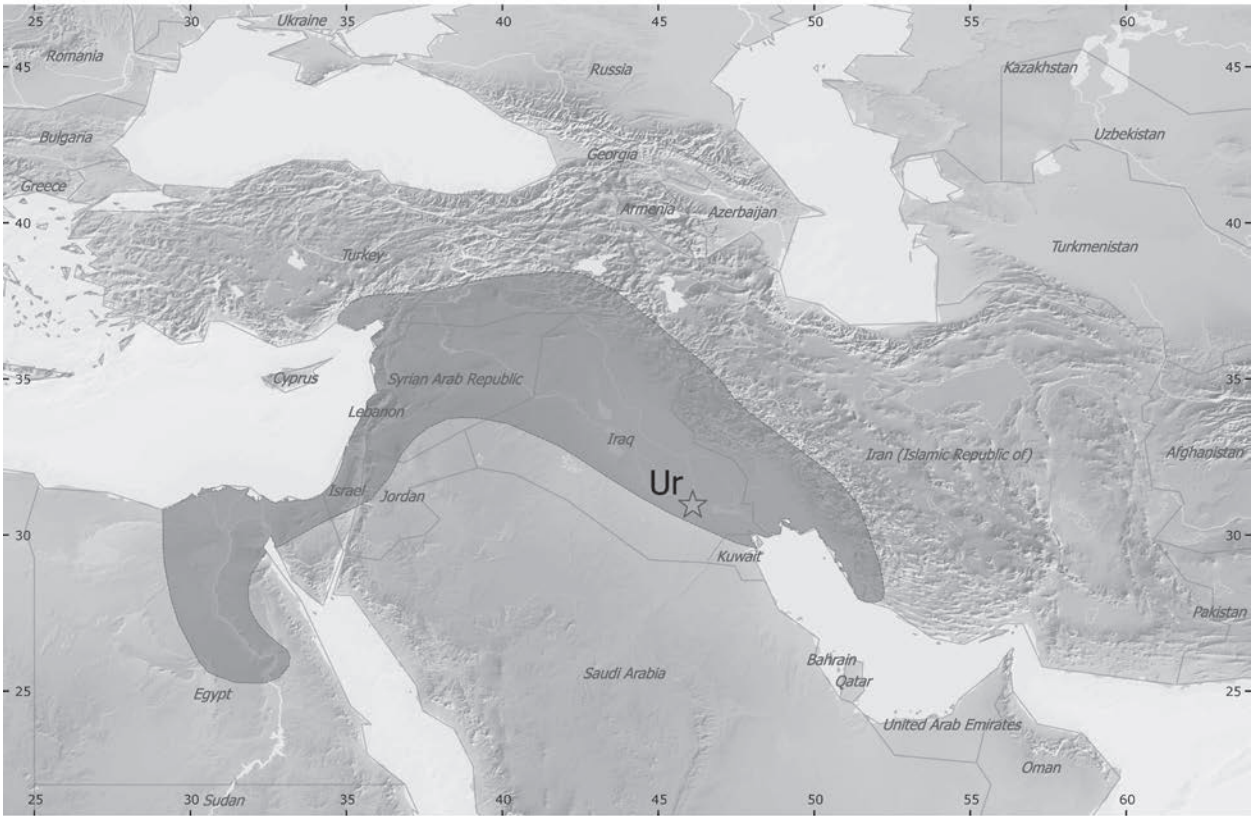

Fig. 2.1: Map of the Fertile Crescent highlighted in grey from Egypt to Mesopotamia (made with Natural Earth)

In the Neolithic period the Fertile Crescent was the cradle of civilisation. It was one of the the regions where early mankind put down its roots and abandoned their life as hunter-gatherers. The Fertile Crescent extends from modern Egypt, south-west Turkey and Syria to the Persian Gulf (cf. fig. 2.1). Northern Mesopotamia was settled at least since the 9th millennium BCE with evidence of pioneer animal husbandry and cereal cultivation (Moorey, 1994). The southern part of Mesopotamia has been settled since the Ubaid period (6th millennium BCE), as typical Ubaid pottery was recovered by excavations in this area (Woolley, 1946; Moorey, 1994; Zettler and Horne, 1998). Mesopotamia was the earliest civilisation and its name derived from its location “between the rivers” Euphrates and Tigris (Zettler and Horne, 1998). A higher sea level and different climate conditions at the time promoted the fertility of this region.

Though the usable land had to be extended by irrigation networks, which were essential for the development of permanent settlements (Bagg, 2012; Oates, 1983; Zettler and Horne, 1998). Due to arid climate conditions in southern Mesopotamia irrigation was necessary for agriculture. The created irrigation networks were surface channel systems and run along alluvial fans (Moorey, 1994; Oates, 1983). The earliest settlements of southern Mesopotamia concentrated on the delta area at the Persian Gulf, where the cities of Ur, Uruk, Larsa, and Umma are located (Bagg, 2012). After plants were domesticated, animals followed starting with sheep and goats in the 10th to 9th millennium BCE at the southern foothills of Zagros and Taurus (Arbuckle, 2012). As the management for sheep and goat became more sophisticated, pigs and cattle were domesticated in widely spread regions in the 8th millennium BCE (Arbuckle, 2012). By the 4th millennium BCE also donkeys

and horses were domesticated and animals were used for traction of ploughs and woollen textiles were produced (Moorey, 1994). The camel has not come into usage until the 1st millennium BCE (Moorey, 1994).

Due to the more extensive land use and the necessary management of the irrigation networks, Mesopotamia was extremely progressive in its development. The oldest writings are in Sumerian language, written in cuneiform and used for administration purposes. This major invention enabled other cultural and scientific developments as astronomy, literature, arts as well as the administration of the city states in Early Bronze Age. The cuneiform tablets found by archaeologists are of major importance in understanding the Mesopotamian culture.

The technological knowledge was very progressive as well at the time. Inventions as the wheel or shadoof (Bagg, 2012) promoted further technological development of agricultural innovation. A more complex architecture in the 5th millennium BCE northern and central Mesopotamia indicates the beginning of social stratification (Moorey, 1994). Resources as textiles, grains and livestock were produced to excess and could be traded to other regions in exchange for locally unavailable raw materials, as e.g. metals and timber. Urbanism progressed and resulted in the Uruk expansion (Moorey, 1994; Oates, 1983). Mesopotamia was dominated by independent city states in Early Dynastic times, when the city of Ur flourished (Zettler and Horne, 1998).

3 Ur – the site

“And ’Ûr, the son of Kesed, built the city of ’Ara of the Chaldees, and called its name after his own name and the name of his father.”

- Jubilees 11:3

3.1 Location, historic significance, and Trivia

The ancient city of Ur is located near the modern city of Nasiriyah 370 km from Baghdad in south-east Iraq. Its geological location lies within the south-western border of the flood area of the Euphrates river (Yacoub, 2011). Near the rivers of northern Mesopotamia the soil is more fertile, but the environment of Ur is still habitable. The big An Nafud desert is adjacent to the flood plains, extends to Saudi Arabia and is part of the Arabian desert connected to the Rub‘al Khali.

The soil of Ur itself consists mainly of sand and silt. During the excavations Woolley discovered a thin black layer in the soil. He correlated it to the biblic Flood (Woolley, 1946), although it is likely related to floods of the Euphrates river which occur periodically.

The big ziggurat temple has long been known and gave the place its modern name Tell al-Muqayyar (translated “mound of pitch”). This prominent landmark marked the considered home of Abraham, mentioned in the Old Testament (Genesis 11:28, 11:31, 15:7, Nehemiah 9:7, Jubilees 11:3). The excavations of Ur attracted attention in the media, and inspired Agatha Christie, who visited the excavation site of Ur and met her future husband Max Mallowan, to write the novel “Murder in Mesopotamia” in 1936 (Christie, 1936).

Indeed, the ancient city of Ur was of major importance in the past. Southern Mesopotamia is considered to be settled at least since the 7th to 6th millennium BCE (Zettler and Horne, 1998; Bagg, 2012**;** Oates, 2012). Further settlements dated to the Ubaid period have been discovered in Southern Mesopotamia (e.g. Tell Oueili, Uruk-Warka, Eridu, Tell Abada) (Oates, 2012). The following Uruk period (cf. fig. 3.1) is characterised by the invention of the cylinder seals and the mass-produced bevel rim bowl marking the Uruk expansion (Oates, 2012; Ur, 2012). During the Uruk expansion the ancient towns grew to cities in the 4th millennium BCE (Ur, 2012). In Early Dynastic I (ED I - beginning of 3rd millennium BCE) (cf. fig. 1.1) the urbanisation of the Sumerian cities reached its climax with a large number of emerging cities. Early texts written mostly in Sumerian but also not yet translated languages are found in ED I, although the record of cuneiform clay tablets of this period remains scarce (Ur, 2012). Ur is mentioned as one of Sumer’s major city-states in a pictograph of a group of clay sealings, dated to ED I (Matthews, 1993**;** Ur, 2012). Other emerged city-states included Nippur, Larsa, Uruk, Adab and Eridu, which competed for water, land use, and above all supremacy (Ur, 2012).

Within the Early Dynastic period the “kings and queens” were buried in the Royal Cemetery of the city-state Ur, leaving archaeological evidence of their wealth (cf. fig. 3.2) (Zettler and Horne, 1998). Each city has one principal deity as a guardian, Ur’s deity was the moon god Nanna (Woolley, 1934; Woolley and Steigerwald, 1956; Zettler and Horne, 1998). This deity ruled officially over its city and chose the city’s mundane ruler (lugal = “big man”, “king”; ensi / en = “governor”), whose duties involved maintenance of the deity’s temple and other matters, e.g. warfare against other city-states (Zettler and Horne, 1998). Conflicts between the competing city-states were inevitable and are well documented in the archaeological context. At the end of the Early Dynastic period king Sargon of Akkad unified Mesopotamia under his reign and formed the new empire, with the capital of Akkad, which gave the empire its name (Zettler and Horne, 1998). His daughter En-ḫedu-anna was assigned as high priestess of the Nanna temple in Ur (Korn, 2004). An inscription mentions, that he controlled the trade routes along the Persian Gulf to *Makan* and *Dilmun* as the access to timber from the Levant (Hirsch, 1963).

The Akkadian empire ended with the invasion of the Gutians from the Zagros mountains (Korn, 2004). Sumer and Akkad were then reunited under Ur-Nammu, governor of Ur, who established the IIIrd dynasty of Ur and hence the Ur III period began (Korn, 2004; Heinz, 2012). The empire and the ancient city of Ur flourished under a strict administration resulting in countless preserved cuneiform documents and with it the oversea trade (Korn, 2004).

At the beginning of the second millennium BCE the 3rd dynasty ended as the Akkadian empire had, with the invasion of Elamites, who destroyed Ur and founded a new dynasty in Larsa (Oates, 1990; Heinz, 2012). Due to a shift in the course of Euphrates, Ur became inhabitable, as irrigation became impossible (Korn, 2004).

3.2 Excavations

Before Sir Charles Leonard Woolley's excavations, Pietro della Valle was the first western visitor at Ur (Mid 17th Century) (Hall 1923, Zettler and Horne, 1998). After della Valle, J. B. Fraser and W. K. Loftus visited Ur separately later on. J. E. Taylor carried out the first excavations at the site in the mid of the 19th century (Taylor 1855, Zettler and Horne, 1998). Taylor focussed on the ziggurat temple of Ur and recovered cylinder seals with cuneiform inscriptions (Taylor 1855). Taylor cooperated with H. C. Rawlinson, who identified (cf. fig. 3.2) Tell al-Muqayyar as "Ur of the Chaldees" by the inscription on the cylinder seals (Zettler and Horne, 1998).

After World War I Mesopotamia fell into British hands although political instabilities delayed further excavations at the area of Ur. The British Museum of London sent Campbell-Thompson in 1918, who excavated Ur for a week, but was more interested in ancient Eridu (Zettler and Horne, 1998). H. R. Hall continued Campbell-Thompsons work and excavated trenches at Ur's city area (around the ziggurat and Ur-Nammu palace) in 1919 (Hall, 1923; Hall, 1925).

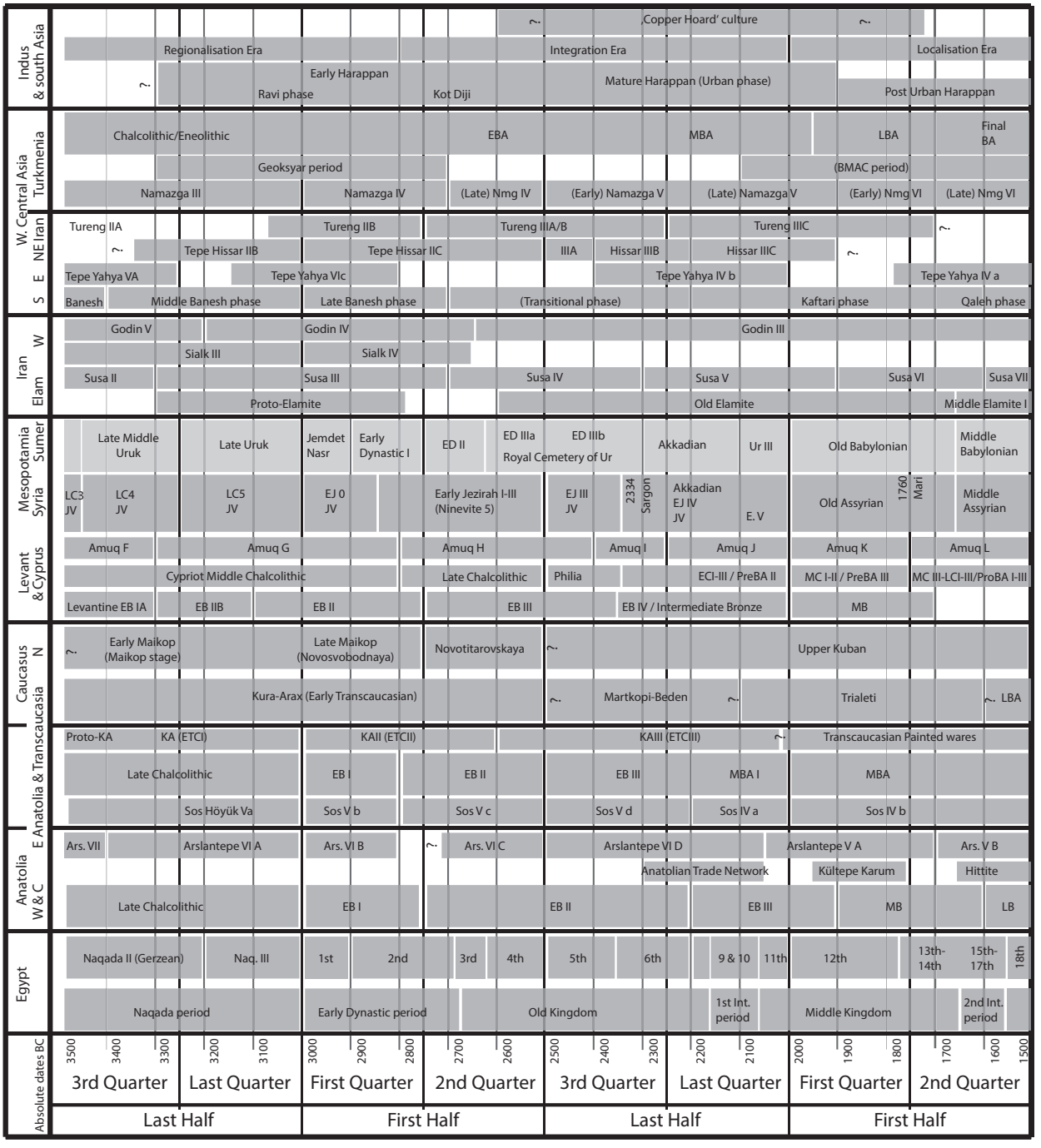

Fig. 3.1: Timeline of epochs and periods in regions mentioned in this thesis (after Wilkinson 2014)

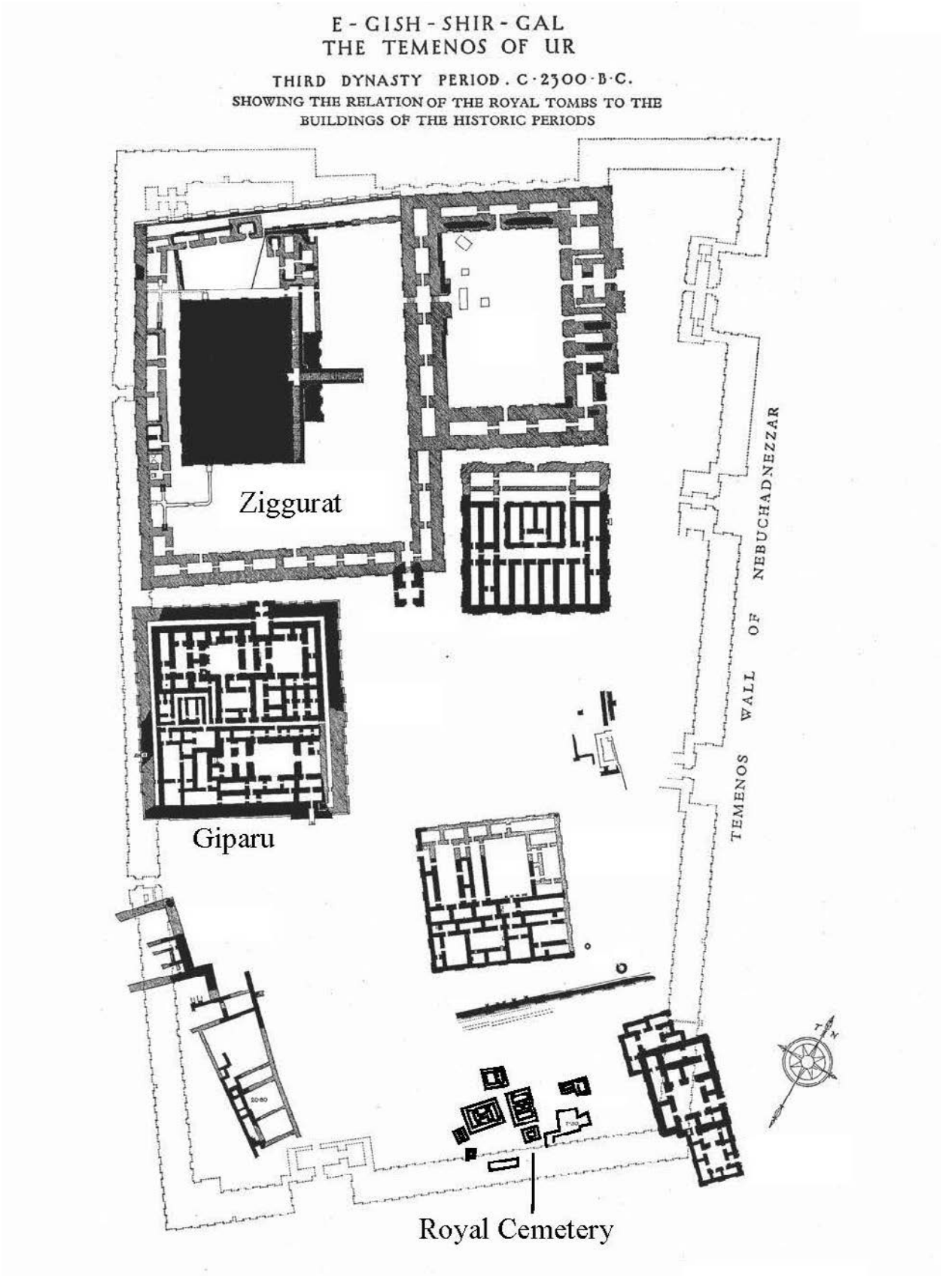

Fig. 3.2: Map of the ancient city of Ur, excavated by Sir Charles Leonard Woolley. The ziggurat is prominent in the NW section. The Royal Cemetery is displayed in the lower part of the plan (after Woolley, 1934).

Museumsnr.	Field Nr.	Material	Object	Dating	Tomb	EPMA	Traces	L. (Cul)	S. (Cul)	L. (LIA)	S. (LIA)
30-12-253.1	U.12355a	Ag	Lyre	Early Dynastic	PG 1237	x	x			x	
30-12-253.3	U.12355c	Ag	Lyre	Early Dynastic	PG 1237	x	x			x	
30-12-429	none	Ag	Toe rings, finger rings, earrings and beads	Not Dated	unknown	x					
30-12-446	U.12388g	Ag	Pin	Early Dynastic	PG 1237, body 30, renumbered body 49	x	x		x	x	x
30-12-487	U.10899	Ag	Fluted tumbler	Early Dynastic	PG 800B (068, 069)						
30-12-605	none	Ag	Hair coil	Not Dated	unknown	x	x	x	x	x	x
30-12-611	U.12425a	Ag	Rolled Ribbon	Early Dynastic	PG 1237/69 9 (renumbered body 56)	x					
30-12-754	U.12369c	Ag	Pins	Early Dynastic	PG 1237/11 (renumbered body 44)	x	x	x		x	
30-12-733	U.12423i	Ag	Pin	Early Dynastic	PG 1237/67 (renumbered body 9)	x	x	x		x	x
31-17-280a	U.14324	Ag	Ring	Not Dated	unknown	x		x		x	
B16926a	none	Ag	Pin	Akkadian/Late Akkadian	PG 673	x	x		x	x	x
B16931.1	U.9630a	Ag	Bracelets	Akkadian/Late Akkadian	PG 673	x	x		x	x	x
B16931.2	U.9630a	Ag	Bracelets	same as above	PG 673	x	x		x	x	x
B16958	U.8691	Lapis lazuli	Rings with beads	Early Dynastic	TTF PG 389						
B17000/ B17588	U.9786/ U.9787	Ag-Au Lapis lazuli	Fragments of a diadem	Early Dynastic	PG 777	x					
B17078a	U.10472	Ag	Spearhead	Early Dynastic	PG 789	x					x
B17082a	U.10860	Ag	Tumbler	Early Dynastic	PG 800						x
B17084	U.8013A	Ag	Bracelet	Early Dynastic	TTE PG 55	x	x	x			x
30-12-264.1	U.11486	As-Ni-Sn-Cu	Adze	Early Dynastic	PG 1038	x	x			x	
30-12-272.1	U.12740	Bz	Mirror	Not Dated	PG -5 m below surface, loose in soil	x	x	x		x	
30-12-272.2	U.12740	Bz	Mirror	Not Dated	same as above	x	x	x		x	
30-12-284.1	U.11866a	Bz	Dagger	Early Dynastic	PG 1162	x	x			x	
30-12-285.1	U.12005(?)	As-Cu	Chisel	Not Dated	PG 1321	x	x			x	
30-12-321.1	U.11494	Bz	Spatula	Early Dynastic	PG 1047	x	x	x		x	
30-12-373.1	U.11212c	As-Cu	Needle	Not Dated	PG 1249	x	x			x	
30-12-375.1	U.12606	As-Cu	Needle	Akkadian	PG 1339	x	x			x	
30-12-380.1	U.12054	As-Cu	Pin	Akkadian	PG 1230	x	x				x
30-12-382.1	U.12680F	Bz	Needle	Postakkadian-Ur III	PG 1387	x	x	x		x	
30-12-416.1	U.12350b	Bz	Needle	Ur III	PG 1336	x	x			x	
30-12-696	U.12435	Bz	Harp/Bull's Head	Early Dynastic	PG 1332	x	x	x	x	x	x
31-17-186.1	U.14238	Bz	Axe	Early Dynastic	PG 1687	x	x	x		x	
31-17-193.1	U.14301	As-Cu	Axe	Early Dynastic	PG 1738	x	x			x	
31-17-201.1	U.14304	As-Cu	Adze	Early Dynastic	PG 1739	x	x				
31-17-205.1	U.13528	Bz	Adze	Early Dynastic	PG 1520	x	x	x		x	
31-17-217.2	U.14252	Bz	Adze	Early Dynastic	PG 1694	x	x	x			
31-17-217.3	U.14252	Bz	Adze	Early Dynastic	PG 1694	x	x	x		x	
31-17-265.1	U.6642	Bz	Bow	Late 2nd Mill BCE or early 1st Mill BCE	K.P., L-M, 10-1 Giparu	x	x	x		x	
31-17-266.1	U.14061	As-Cu	Pin	Early Dynastic	PG 1625	x	x	x		x	
31-17-267.1	U.14924	As-Cu	Hook	Late Uruk	Pit F, T, square E7, level 8 - 8.5m	x	x			x	
31-17-352T	U.12778F	Cu	Needle/pin shaft	Jemdet Nasr/ ED I	Pit G, levels 7.5-8m below plano-convex brick pavement (dates 3100 BCE)	x	x			x	
33-35-79.1	U.18461	As-Cu	Pin	Jemdet Nasr	Pit W, JN 78b	x	x				
35-1-422.1	U.18935	Cu	Dagger	Akkadian	Pit X PJ/G series 100	x	x				
35-1-422.2	U.18935	As-Cu	Dagger	Akkadian	Pit X PJ/G series 100	x	x				
35-1-422.3	U.18935	As-Cu	Dagger	Akkadian	Pit X PJ/G series 100	x	x	x		x	
35-1-479.1	U.19102	As-Cu	Pin	Early Dynastic	Pit X PJ	x	x			x	
98-9-164	none	Cu	Copper ingot	Not Dated	unknown	x			x		x

Museumsnr.	Field Nr.	Material	Object	Dating	Tomb	EPMA	Traces	L. (CuI)	S. (CuI)	L. (LIA)	S. (LIA)
B16409.1	U.6510	As-Cu	Needle	Ur III - Isin Larsa	EH DT	x	x				
B16409.2	U.6510	As-Cu	Needle	Ur III - Isin Larsa	EH DT	x	x	x		x	
B16409.3	U.6510	As-Cu	Needle	Ur III - Isin Larsa	EH DT	x	x	x		x	
B16409.4	U.6510	As-Cu	Needle	Ur III - Isin Larsa	EH DT	x	x	x		x	
B16937.1	U.10744	Bz	Bracelet	Akkadian	PG 0906	x	x			x	
B16954.1	U.9599	Bz	Pin	Early Dynastic	PG 0662	x	x	x			
B16996.1	U.9964	Bz	Pin	Early Dynastic	PG 0777	x	x	x		x	
B17022.1	U.9720	Bz	Pin	Akkadian	PG 0681	x	x				
B17276.2	U.10794	As-Cu	Knife	Late Akkadi-an-Ur III	PG 0825	x	x	x		x	
B17317.1	U.9525	As-Cu	Pin	Early Dynastic	PG 0619	x	x			x	
B17327.1	U.8651	Bz	Dagger	Early Dynastic	PG 0049 TTE	x	x	x			
B17330.1	U.9138-39	Bz	Blade	Early Dynastic	PG 0537 (=PG 580)	x	x			x	
B17335.1	U.9963C	Cu	Spearhead	Early Dynastic	PG 0777	x	x				
B17347.1	U.9518	Bz	Spearhead	Early Dynastic	PG 0617	x					
B17351.1	U.10777	As-Cu	Dagger	Early Dynastic	PG 0849	x	x				
B17356.2	U.9904	As-Cu	Nail	Early Dynastic	PG 0580	x	x			x	
B17356.3	U.9904	As-Cu	Nail	Early Dynastic	PG 0580	x	x	x		x	
B17356.4	U.9904	As-Cu	Nail	Early Dynastic	PG 0580	x	x	x		x	
B17382.1	U.8992	Bz	Needle	Akkadian	PG 0521	x	x				
B17389.1	U.8649	As-Cu	Needle	Early Dynastic	PG 0049 TTE	x	x			x	
B17410.1	U.9017	Cu	Axe	Early Dynastic	PG 0466 TTF	x	x				
B17411.1	U.7931	Cu	Axe	Early Dynastic	PG 0068 TTE	x	x				
B17418.1	U.7856	Cu	Axe	Early Dynastic	PG 0016 TTE	x	x				
B17422.1	U.8986A	As-Cu	Anklet	Akkadian	PG 0503 TTF	x	x			x	
B17426.1	U.8546	As-Cu	Chisel	Early Dynastic (?)	PG not known	x	x	x		x	
B17426.2	U.8546	As-Cu	Chisel	Early Dynastic (?)	PG not known	x	x			x	
B17445.1	U.8366	As-Cu	Saw	Early Dynastic	PG 0121 TTE	x	x	x		x	
B17460.1	U.8474	As-Cu	Dagger	Ur III	PG 0304 TTE	x	x				
B17460.2	U.8474	As-Cu	Dagger	Ur III	PG 0304 TTE	x	x	x		x	
B17469.1	U.9013	Bz	Bracelet	Akkadian	PG 0478 TTF	x	x			x	
B17474.1	U.8318	As-Cu	Chisel	Early Dynastic	PG 0163 TTE	x	x				
B17478.1	U.8560	As-Cu	Chisel	Early Dynastic	PG 0317 TTE	x	x				
B17479.1	U.9353	Bz	Axe	Early Dynastic	PG 0580	x	x			x	
B17480.1	U.9141C-F	Bz	4 Spearheads	Early Dynastic	PG 0537 (= PG 580)	x	x	x		x	
B17488.1	U.10165	As-Cu	Pin	Early Dynastic	PG 0780	x					
B17494.1	U.10191	Bz	Pin	Akkadian	PG 0766	x	x			x	
B17495.1	U.10358	Bz	Pin	Akkadian	PG 0832	x	x			x	
B17496.1	U.10196	As-Cu	Pin	Late Akkadi-an-Ur III	PG 0762	x	x			x	
B17508.1	U.9933	Ni-Cu	Dagger	Early Dynastic	PG 0737	x	x				
B17508.2	U.9933	Ni-Cu	Dagger	Early Dynastic	PG 0737	x	x				
B17516.1 (?)	U.9213	As-Cu	Knife	Not Dated	PG 0556	x	x			x	
B17525.1	U.9342	Cu	Harpoon	Early Dynastic	PG 0580 TTE	x	x				
B17528a.1	U.9336	As-Cu	Spearhead	Early Dynastic	PG 0580	x	x			x	
B17528a.2	U.9336	As-Cu	Spearhead	Early Dynastic	PG 0580	x	x	x		x	
B17528b.1	U.9336	As-Cu	Spearhead	Early Dynastic	PG 0580	x	x			x	
B17551	U.9324	Cu	Rein Ring	Early Dynastic	PG 0580	x	x		x		x

Tab. 3.1: List of copper-based (As-Cu = Arsenical copper, Bz = Sn-bronze, Cu = pure copper) and silver artefacts (Ag) sampled for this dissertation. Informations include find contexts and dating. The dating of the artefacts is in correspondence to personal communication with Richard Zettler (July 2016). The table provides additional information, which artefacts were analysed by which method (EPMA = electron microprobe analysis, Traces = trace elements, CuI = Cu isotopes, LIA = Pb isotope analysis, S. = solution, L. = Laser, TT = Trial Trench)

In 1922 the local administrations gave permission for further fieldwork in Mesopotamia (Zettler and Horne, 1998). The excavations were carried out by Sir Charles Leonard Woolley (1880 - 1960) from 1922 to 1934 funded by the British Museum in London and the Penn Museum in Philadelphia (Woolley, 1946; Woolley and Steigerwald, 1956; Woolley, 1965a). After excavating parts of the ancient city and ziggurat area Woolley discovered in the season of 1926-27 approximately 600 graves within three months (Zettler and Horne, 1998). After four seasons he had uncovered around 1,700 graves (cf. fig. 3.2) and after the excavations were completed he discovered

a total number of approximately 1,850 graves (Woolley, 1946; Woolley and Steigerwald, 1956; Woolley, 1965a).

The three most famous untouched Royal Tombs are that of princess Puabi, Meskalamdug, and the Great Death Pit. The enormous number of finds in the graves revealed much of the Mesopotamian belief of the afterlife. The great excavations happened at the same time as the discovery of the grave of Tutankhamun in the Valley of the Kings. Both competed for the worldwide attention in the media.

The most famous metal finds are the Headdress of Queen Puabi, the helmet of Meskalamdug, the Ram Caught in a Thicket and the standard of Ur (Zettler and Horne, 1998).

One of the most surprising discoveries was the large number of metal objects found in the tombs. Plenty of gold, arsenical copper, tin bronze and silver objects were discovered. This fact is surprising as Ur is located in the flood plain of the Euphrates rivers and no metal resources occur in Mesopotamia, indicating the metals must have been imported from foreign regions (Zettler and Horne, 1998; Jassim and Goff 2006; Yacoub, 2011).

Further details about the excavations are to be found in the publication of Zettler and Horne (1998) as the Ur Excavation volumes published by Woolley and his co-workers (Woolley, 1923; Gadd, et al., 1928; Woolley, 1930; Woolley, 1934; Burrows, 1935; Woolley, 1939; Woolley, 1946; Woolley, 1955; Woolley and Steigerwald, 1956; Woolley, 1962; Woolley, 1965a; Woolley, 1965b; Woolley, 1974; Woolley and Mallowan, 1976).

3.3 The analysed artefacts

For the present project the so-called “Nash Collection” was provided as a loan by the Penn Museum, University of Pennsylvania. In total 89 silver, copper and bronze mounted samples taken from objects from the Philadelphia Ur collection were provided. Two of the 89 mounted samples were taken from gold objects and are currently investigated by Moritz Jansen.

In order to avoid confusion of artefact-numbers the Museum numbers of the artefacts are used in this dissertation. The numbers are given in the following notation. If an artefact was sampled multiple times, the sub numbers are given in the quotation: B16409.1, B16409.2, B16409.3, B16409.4. Some artefacts have the same museum number although they are different artefacts, in which case the artefacts are numbered, as follows: B17528a, B17528b (cf. tab. 3.1).

Most of the analysed samples of this dissertation were already sampled during the Mesopotamian Metals Project a few years ago. These objects include almost all of the copper-based metal artefacts, except for B17551 (a rein ring) and 98-9-164 (a copper ingot). The famous bronze bull’s head 30-12-696 is sampled both by the Mesopotamian Metals Project, and later by Sabine Klein. The older samples include also the unique silver lyre of Ur 30-12-253.

All samples of the Mesopotamian Metals Project were embedded into resin and mounted in order to perform metallography. Samuel K. Nash, a volunteer at the Penn Museum, studied the metallography of the Ur copper-based metal sections approximately ten years ago. Additionally chemical analyses of As, Ni and Sn were performed by Stuart Fleming and Tamara Stech. The notes taken by Samuel K. Nash on the metallography of the Ur copper-based metal sections were digitised and added to appendix C (catalogue) of this thesis.

Later in 2009 - 2010 Sabine Klein and Andreas Hauptmann visited the Penn Museum several times, in order to do preliminary pXRF-analysis and to take samples for the present project.

During later sampling campaigns the copper artefacts mentioned above were drilled with an additional set of 20 silver samples. Unfortunately some part of the silver artefacts were too corroded to gain sensible analytical data, therefore some had to be excluded.

3.3.1 The archaeological context of the sampled copper-based artefacts

In order to provide a better overview, the artefact’s context is displayed by date in first order and then by tomb in second order. As the single tombs exhibit a specific context, it is important to mention the specific find localities. The copper-based metal artefacts are mainly deriving from private tombs, but some were also discovered in Royal Tombs.

3.3.1.1 Uruk

The artefact of oldest dating is a hook (31-17-267) discovered by Woolley in pit F, square E7, at the levels of 8 to 8.5m below surface (Woolley, 1955).

3.3.1.2 Jemdet Nasr/Early Dynastic I

Only one artefact dates to Jemdet Nasr times. The pin 33-35-79 was found in Pit W (JN) in PG 78b. The needle or pin shaft 31-17-352 was found in Pit G NW of PG 777, at the levels 7.5-8m below planoconvex brick pavement (dates 3100 BCE). The planoconvex brick pavement determines the terminus ante quem at 3100 BCE, therefore 31-17-352 dates to either Jemdet Nasr or Early Dynastic I.

3.3.1.3 Early Dynastic III

PG 16

The axe B17418 was discovered in PG 16, in Trial Trench E, but not dated (Nissen 1966; Woolley’s Field Note Cards: http://www.ur-online.org/location/1019/; accessed in February 2019).

PG 49
One bronze dagger (B17327) and one arsenical copper needle (B17389) were located in the private tomb PG 49 in Trial Trench E, which Woolley dated to Early Dynastic III (R. Zettler, pers. comm., Jul. 2016; Woolley's Field Note Cards: http://www.ur-online.org/location/1232/; accessed in February 2019).

PG 68
This private tomb hosted one pure copper axe (B17411) (Woolley's Field Note Cards: http://www.ur-online.org/location/1106/; accessed in February 2019). The finding spot was approximately 1.8 m below surface in Trial Trench E.

PG 121
Among numerous copper artefacts found in this tomb in Trial Trench E, one arsenical copper saw (B17445) was sampled by the Mesopotamian Metals Project (Woolley's Field Note Cards: http://www.ur-online.org/location/1506/; accessed in February 2019).

PG 163
One arsenical copper chisel (B17474) was sampled from this tomb, discovered in Trial Trench E (Woolley's Field Note Cards: http://www.ur-online.org/location/1037/; accessed in February 2019).

PG 317
The arsenical copper chisel (B17478) was discovered in this relatively rich private tomb, where also silver and one gold artefact was recovered (Woolley's Field Note Cards: http://www.ur-online.org/location/935/; accessed in February 2019).

PG 466
This tomb contained one arsenical copper chisel (B17410) and another copper artefact, that was not sampled. This tomb was discovered in Trial Trench F (Woolley's Field Note Cards: http://www.ur-online.org/location/2201/; accessed in February 2019).

Royal Tomb PG 580
This tomb was originally numbered as PG 537 and then renumbered to PG 580. As this tomb is one of the Royal Tombs, plenty of precious metal artefacts were discovered in here (Woolley, 1934). Several copper-based weapons were sampled: four spearheads soldered together by oxidation (B17480), two additional spearheads (B17528a, and -b), one harpoon (B17525), one blade (B17330), and one axe (B17479) are to be named. One arsenical copper nail (B17356) was even sampled on four different locations. This tomb was dated by the find of a stone relief U.8557 (R. Zettler, pers. comm., Jul. 2016; Woolley's Field Note Cards: http://www.ur-online.org/location/1018/; accessed in February 2019).

PG 617
One bronze spearhead (B17347) was discovered in the Early Dynastic tomb of PG 617 (Woolley's Field Note Cards: http://www.ur-online.org/location/1496/; accessed in February 2019).

PG 619
In this tomb one arsenical copper pin (B17317) was uncovered and sampled (Woolley's Field Note Cards: http://www.ur-online.org/location/1240/; accessed in February 2019).

PG 662
A few copper artefacts were found in this tomb, of which one pin (B16954) was sampled (Woolley's Field Note Cards: http://www.ur-online.org/location/1211/; accessed in February 2019).

PG 737
One copper dagger with very high Ni-contents (>10 wt%) was sampled. Some other copper artefacts were also discovered in this tomb (Woolley's Field Note Cards: http://www.ur-online.org/location/4553/; accessed in February 2019).

Royal Tomb PG 777
This tomb hosted numerous precious metal artefacts, of which one spearhead B17335 (Woolley, 1934) and one pin (B16996) were sampled (Woolley's Field Note Cards: http://www.ur-online.org/location/1091/; accessed in February 2019).

PG 780
Among other artefacts on arsenical copper pin (B17488) was discovered in this tomb. It was dated by the associated find of a cylinder seal (U.10168) (Woolley's Field Note Cards: http://www.ur-online.org/location/1292/; accessed in February 2019).

PG 849
One arsenical copper dagger (B17351) was found in this tomb (Woolley's Field Note Cards: http://www.ur-online.org/location/4565/; accessed in February 2019).

PG 1038
This private tomb hosted one bronze adze (30-12-264) and some other decayed copper objects and lapis lazuli beads (Woolley's Field Note Cards: http://www.ur-online.org/location/1567/; accessed in February 2019).

PG 1047
One bronze spatula (30-12-321) was recovered from this private tomb (Woolley's Field Note Cards: http://www.ur-online.org/location/1851/; accessed in February 2019).

PG 1162
Some copper artefacts were found in this private grave, of which one bronze dagger (30-12-284) was sampled (Woolley's Field Note Cards: http://www.ur-online.org/location/1805/; accessed in February 2019).

PG 1321
An arsenical copper chisel (30-12-285) was discovered among other copper based, silver, and gold objects (Woolley's Field Note Cards: http://www.ur-online.org/location/945/; accessed in February 2019).

Royal tomb PG 1332
This tomb hosted a death pit of several bodies. Several silver-, gold-, lapis lazuli-, and copper artefacts were buried in this Royal Tomb (Woolley, 1934). One of the most intriguing artefacts of this study is the bronze bull's head (U.12435a, 30-12-696) sampled by both Mesopotamian Metals Project and Sabine Klein, thus both samples could be analysed (Woolley's Field Note Cards: http://www.ur-online.org/location/1586/; accessed in February 2019).

PG 1520
The bronze adze (31-17-205) was discovered in this tomb (Woolley's Field Note Cards: http://www.ur-online.org/location/1866/; accessed in February 2019).

PG 1625
Several gold- lapis lazuli-, silver-, and copper objects were uncovered in this private tomb (Woolley's Field Note Cards: http://www.ur-online.org/location/1126/; accessed in February 2019). One arsenical copper pin (31-17-266) was sampled.

PG 1687
One bronze axe (31-17-186) was buried and sampled in this tomb. Several additional copper artefacts were found (Woolley's Field Note Cards: http://www.ur-online.org/location/947/; accessed in February 2019).

PG 1698
One bronze adze (31-17-217) was sampled on three different spots, although one mounted sample was thoroughly corroded. The bronze adze was discovered among other copper objects (Woolley's Field Note Cards: http://www.ur-online.org/location/1477/; accessed in February 2019).

PG 1738
In this tomb one arsenical copper axe (31-17-193) was found (Woolley's Field Note Cards: http://www.ur-online.org/location/1578/; accessed in February 2019).

PG 1739
One arsenical copper adze (31-17-201) was buried in this private tomb (Woolley's Field Note Cards: http://www.ur-online.org/location/1604/; accessed in February 2019).

Pit X PJ
The arsenical copper pin (35-1-479) was discovered in pit X PJ and found with U 19101 (another copper pin) in the ruins of a grave of the B series (plundered) (Woolley, 1955.)

3.3.1.4 Akkadian

PG 478
Woolley discovered one bronze bracelet (B17469) in this tomb in Trial Trench F (Woolley's Field Note Cards: http://www.ur-online.org/location/2211/; accessed in February 2019).

PG 503
An arsenical copper anklet (B17422) was discovered together with a cylinder seal (cf. U.8988, BM 120572) with an inscription mentioning En-ḫedu-anna (daughter of Sargon) (R. Zettler, pers. comm., Jul. 2016; Woolley's Field Note Cards: http://www.ur-online.org/location/2235/; accessed in February 2019).

PG 521
This tomb hosted one single bronze needle (B17382) (Woolley's Field Note Cards: http://www.ur-online.org/location/2247/; accessed in February 2019).

PG 681
One bronze pin (B17022) was found in this tomb among other gold, lapis lazuli and carnelian artefacts (Woolley's Field Note Cards: http://www.ur-online.org/location/1223/; accessed in February 2019). It was dated by the associated find of a cylinder seal (cf. U.9721, B17024).

PG 766
Another bronze pin (B17494) was discovered in this tomb together with a cylinder seal (U.10192, B17594)(Woolley, 1934; Woolley's Field Note Cards: http://www.ur-online.org/location/1234/; accessed in February 2019).

PG 832
This bronze pin (B17495) was uncovered in a grave with another cylinder seal (U.10359, BM 121549) (Woolley's Field Note Cards: http://www.ur-online.org/location/1233/; accessed in February 2019).

PG 906
This bronze bracelet (B16937) was found in an Akkadian grave (Woolley's Field Note Cards: http://www.ur-online.org/location/2537/; accessed in February 2019).

PG 1230
This grave hosted two copper artefacts, of which one pin was sampled (30-12-380) (Woolley's Field Note Cards: http://www.ur-online.org/location/2834/; accessed in February 2019).

PG 1339
One arsenical copper needle (30-12-375) was discovered in this tomb (Woolley's Field Note Cards: http://www.ur-online.org/location/1218/; accessed in February 2019).

Pit X PJ
In pit X PJ one arsenical copper dagger (35-1-422) was found with a cylinder seal (U.18926) in a grave of the B series (Woolley, 1955).

3.3.1.5 Ur III

PG 304
One arsenical copper dagger (B17460) sampled two times was discovered in this tomb in Trial Trench E (Woolley's Field Note Cards: http://www.ur-online.org/location/1482/; accessed in February 2019). It was discovered with a cylinder seal (U.8476, B16887) depicting two heroes attacking a rampant lion (R. Zettler, pers. comm., Jul. 2016).

PG 762
The arsenical copper pin (B17496) was found in this tomb dating to Late Akkadian to Ur III (Woolley's Field Note Cards: http://www.ur-online.org/location/1219/; accessed in February 2019).

PG 825
This tomb hosted several finds, of which one arsenical copper knife (B17276) was sampled (Woolley's Field Note Cards: http://www.ur-online.org/location/1050/; accessed in February 2019).

PG 1336
The bronze needle (30-12-416) was discovered along with a cylinder seal (U.12350a, IM 14568) (Woolley, 1934), supposed to depict a spread eagle, Collon (1996) mentions it is Ur III in dating (Woolley's Field Note Cards: http://www.ur-online.org/location/1244/; accessed in February 2019).

PG 1387
The bronze needle (30-12-382) was found with a cylinder seal (U.12680, BM 122499, 122566, 123711) (Woolley's Field Note Cards: http://www.ur-online.org/location/2960/; accessed in February 2019).

3.3.1.6 Late Ur III to Isin-Larsa

The arsenical bronze pin (B16409) was discovered in the EH series of houses in the Dim-tabba area. It was sampled four times, although one sample might be misnamed and possibly belong to another artefact (cf. sec. 10.1.1.2).

3.3.1.7 Early Iron Age

One bronze bow (31-17-265) was found in the Giparu area (K.P., L-M, 10-1) with several Fe artefacts, thus dating to Early Iron Age (Late 2nd or early 1st millennium BCE) (Woolley's Field Note Cards: http://www.ur-online.org/location/15/; accessed in February 2019).

3.3.1.8 Without context

Six objects sampled by the Mesopotamian Metals Project are without known find context. These objects are an arsenical copper chisel (B17426), a bronze mirror (30-12-272), an arsenical copper chisel (PG 1212), an arsenical copper needle (30-12-373, PG 1249), a copper ingot (98-9-164), and an arsenical copper knife (B17516). Especially the copper ingot 98-9-164 is of unknown provenance, as it is only confirmed to be Mesopotamian, but not necessarily from Ur itself (M. Jansen, R. Zettler, pers. comm. Jul. 2017).

3.3.2 The archaeological context of the sampled silver artefacts

The silver artefacts were mostly buried in the Royal Tombs of Ur. In this summary of find contexts those artefacts were already excluded, which were too corroded for analysis.

PG55
One silver bracelet (B17084) was found in the Early Dynastic III private tomb.

PG333
In this private tomb dated to Early Dynastic III one silver bracelet was uncovered. The bracelet (B17553) was in very good shape and exhibits a spiral form (Woolley's Field Note Cards: http://www.ur-online.org/location/938/; accessed in February 2019).

PG386
This tomb is also a private grave (Early Dynastic III) exhibiting some silver rings and beads (B16958) which were agglutinated by corrosion. Of the beads, one was extracted and sampled in Frankfurt. By sampling the bead it revealed its true identity as a lapis lazuli bead, although the outside corrosion layer had the same greyish surface as corroded silver. The lapis lazuli bead was analysed by Electron microprobe and the results will be published separately (Woolley's Field Note Cards: http://www.ur-online.org/location/2120/; accessed in February 2019).

PG673
This private tomb is dated to Akkadian (Late Akkadian) and revealed three silver artefacts, including one pin (B16926a) and two bracelets (B16931a, -b).

PG777
The objects B17000/B17588 comprise a mixture of fragments belonging to a diadem, unfortunately the sample contains only gold, but is still included in the chemical analysis in the appendix, but will not be further discussed in this dissertation. These objects were found in the Early Dynastic IIIa Royal Tomb (Woolley's Field Note Cards: http://www.ur-online.org/location/1091/; accessed in February 2019).

PG789
Within the Early Dynastic IIIa Royal Tomb PG 789 a silver spearhead (B17078a) was discovered. This object was

unfortunately electrochemically restored and therefore chemical analysis proves to be difficult. Additionally, the rein ring (B17551) was discovered as part of a horse gear (Woolley's Field Note Cards: http://www.ur-online.org/location/1018/; accessed in February 2019).

PG800
Two of the silver samples were uncovered in Queen Puabis tomb PG800, also dated to Early Dynastic IIIa. These objects are two tumblers (30-12-487, B17082a) (Woolley's Field Note Cards: http://www.ur-online.org/location/942/; accessed in February 2019).

PG1237
Five silver artefacts were discovered in PG 1237 in the so-called Great Death Pit. These objects include the silver lyre (30-12-253), three silver pins (30-12-446, 30-12-733, 30-12-754), and rolled silver ribbon (30-12-611). The tomb PG1237 dates specifically to Meskalamdug, in Early Dynastic IIIa (Nissen 1966; Woolley's Field Note Cards: http://www.ur-online.org/location/931/; accessed in February 2019).

Without context:
Unfortunately three of the sampled objects are without verified archaeological context. Either the field notes did not tell anything about them or were lost in the meantime. Leonard Woolley did not describe every metal artefact in detail down in his notes. Anyhow these objects include several toe- and finger rings, earrings, and beads, one hair coil similar in shape to those of the contemporary silver hoard from Khafajeh (30-12-605), and a ring (30-12-280a).

4 Resource procurement and trade routes in 3rd millennium BCE Ur

The rise of the Sumerian city-states had an impact on social stratification and required a more complex level of organisation. Due to irrigation agriculture flourished and yielded more than the local population required for a living. The surplus could thus be traded for other goods to the people in the neighbouring highlands, where the environmental conditions were unfavourable for agriculture. The Mesopotamian palaces and temples required timber, stones, and different metals, which were procured by exchange, booty, tributes or gifts (Adams, et al., 1976**;** Moorey, 1994; Crawford, 2013). These resources had to be obtained from the nearby highlands or more distant sources. Mesopotamia is completely void of metal resources. However, textiles and grain were produced in excess of local consumption.

The ancient city of Ur is situated in an advantageous location with regard to water transport. On the one hand Ur was located at the coast of the Persian Gulf, as the sea level changed in the past 4500 years. On the other hand Ur is connected by the Euphrates river to Anatolia and Levant. Ubaid boat models provide evidence for the knowledge of watercraft at least since the 6th millennium BCE (Carter, 2012). At the Ur cemetery a small number of boat models was discovered in PG 1050 (e.g. U.11833) (Woolley, 1934). The route upriver to Anatolia was usually undertaken by a donkey caravan, as it was not possible to sail upriver (Moorey, 1994, p.6). Since the later 4th millennium BCE carts were pulled by donkeys or bovids (Arbuckle, 2012). There is textual evidence for the transport of textiles and tin from Mesopotamia to Kültepe (Kārum Kaneš) in the early 2nd millennium BCE (Moorey, 1994, Veenhof, 1972). From the texts Moorey (1994) calculates that one pack ass was able to take a load of 90 kg (180 lb.) with a range of up to 24 km (15 miles) per day. The donkeys were sold and the acquired metals, stones, and timber were transported by ships downriver to Mesopotamia (Veenhof, 1972). This route opened the potential to trade with Levant and therefore also with the Old Kingdom of Egypt as with the Transcaucasian cultures.

The Iranian Plateau was connected by land to Mesopotamia along the so-called “Great Khorasan Road” (Majidzadeh, 1982; Moorey, 1994). Further to the south lay the city of Susa in Khuzestan connecting to other trade routes in the north and turning west to Aššur providing a link between East and West (Moorey, 1994). The large amounts of lapis lazuli found at the cemetery of Ur are linking Mesopotamia to the East, as lapis lazuli occurs in a large scale deposit in Afghanistan (Tosi 1974 ; Crawford, 2013). Susa was the frontier to the East as the Proto-Harappa culture (Potts, 1993). Different forms of “Bactrian” or “Trans-Elamite” style metalwork, stonework, and glyptic occurred at various sites including Susa, Bactria and Baluchistan (Potts, 1993; Collon, 1996). The Diyala river branching of the Tigris was another important route taken to the northern parts of Iran.

The ships were probably able to sail along the coast of the Persian Gulf to the land of *Dilmun* and to *Makan* (Oman) (Moorey, 1994). Moorey (1994) doubts, whether the ships were able to reach the Indus Valley in the 3rd millennium BCE, although textual evidence for the trade of tin and copper in return for wool with *Dilmun* exists (Foster, 1997; Crawford, 2013). *Dilmun* was most likely an interstation of trade goods from further afar. The Indus Valley civilisation had cultural contacts to Mesopotamia as supposed by the findings of etched carnelian beads in Ur (e.g. U.12187 from grave PG 1284) (Crawford, 2013). *Meluḫḫa* had further outposts (e.g. Shortugai) upriver, in Afghanistan, and even to the eastern Iranian Plateau (Jansen et al. 2016). The Gulf route was used more frequently, when the political situation changed and independent city rulers wished to control the Euphrates route. Mesopotamian Jemdet Nasr pottery was discovered in graves along the Gulf route, suggesting early connections of *Makan* and Mesopotamia (Crawford, 2013).

5 A comprehensive GIS-based geological, archaeological and archaeometallurgical database

In the course of this dissertation it became apparent, that more than analytical data is needed for provenancing metals. Modern analytical methods, as Pb isotope, Cu isotope, trace element, and main element analysis, are getting more accurate and precise. More analytical data of archaeological artefacts, metallurgical by-products, and ancient mining areas are available, than ever. Studies arise, where researchers are gathering data from literature and condensing them in a new way, due to the progress of modern information technology. But provenancing metals remains an issue, as by analytical data alone, only an exclusion mechanism is provided. However, no positive confirmation is possible. As more comparative data of mineral deposits is published, the more complicated the situation of the vast mass of data becomes. Artefacts with only a small pool of comparative data available could be assigned clearly. But the larger this pool of data becomes, the more possibilities of assignment to mineral deposits arise. On that account an interaction of different analytical methods needs to be applied, to allow a better preliminary selection of mineral deposits. This takes also a good knowledge of archaeological reasonable locations of provenance and textual evidence into account. Hence both fields of Archaeology and Archaeometallurgy are mutually dependent. Both fields need to be connected, as understanding one cannot exclude the other.

A sound knowledge of mineral occurrences, their context, as well as archaeometallurgical finding spots allows the reconstruction of networks based on geospatial data. A map database does not only contain a large amount of valuable data, but gives information about distribution of metal finds, smelting, and mining locations in context of accessible raw materials. An innovative approach was already undertaken by Wilkinson (2014) in his dissertation, who connected archaeological data with mineral deposits, as well as network analysis in the Anatolian, Transcaucasian, and central Asian context.

This dissertation focusses on the provenance of copper-, bronze-, and silver artefacts from the Ur Cemetery and their relation to copper, tin, lead, and silver deposits in the large scale area of Egypt, Levant, Anatolia, Caucasus, Iran, Oman, Afghanistan, Pakistan, India, to the Central Asian steppe. This scale is reasonable, as textual evidence as well as archaeological investigations indicate intra- and intercultural relationships of these regions with Mesopotamia (Wilkinson, 2014). Therefore the database explained in the following is limited to these materials and regions.

The software used for this endeavour is the most current version of the Open Source program QuantumGIS (QGIS, version 2.18.8 - Las Palmas).

This project started with the aggregation of already online available data of mineral deposits (Mindat.org, 2018; USGS, 2018). Soon it became apparent, that these online resources only comprise data of larger scale mineral deposits with sufficient ore grade for modern mining companies. However, ancient miners were also exploiting ore occurrences, that are disregarded by modern miners. Therefore the next step included intensive literature research and the digitisation of a large number of published maps of smaller mineral occurrences. Mineral deposits form in specific geodynamic settings further explained in section 6. Informations about geological parameters, as geological unit, age, names, and deposit types were included, when available. In the case study of Ur, the map database illustrates the absence of mineral deposits in Mesopotamia for the large amount of metals found at the cemetery, although the surrounding highlands exhibit a variety of mineral deposits.

Further questions arise when studying the chaîne opératoire or supply chain of Ur with the question for the provenance of the ore being only the first of them. Where were the ores processed and smelted? Were the ores transported to a more central location, where they were smelted? In which state did the metals / raw materials arrive in Ur? Where was the metal worked and forged into artefacts?

Due to these questions the map database was then further extended. The expansion required more literature research and digitisation of smelting and metal working locations. In order to understand the spreading and distribution of metals, locations with metal findings were digitised and included in the database. Informations about context and dating of archaeological locations were incorporated. The example of Ur demonstrates that smelting locations are found near the raw material sources in the highlands. However, Woolley focussed his excavations on the ziggurat and cemetery area and further excavations are currently carried out at the settlement area of Ur. So far no metal workshops were discovered at Ur, yet. One shall await further archaeological research in the southern Mesopotamian floodplain. Although some golden and

copper chisels with traces of usage were buried in the Ur Cemetery. This is indicating that some artefacts might have been worked in Ur. But still the question remains, if all the artefacts were processed in Ur itself. Certainly some artefacts were worked at other locations, as indicated by the form of the golden leaves of queen Puabis headdress resembling the Sissoo tree (*Dalbergia sissoo Roxb.*) species, which is occurring nowadays in the Indo-Iranian borderlands and is not indigenous in Mesopotamia (Tengberg, Potts and Francfort, 2008).

Further results of the presented geospatial database are referred to in the discussion (cf. sec. 10.3 and 13.3) of this dissertation and shall help to visualise the interpretation of analytical data and their coherence with archaeological data. This interdisciplinary approach helps to illustrate the variety of different trade networks, partially known from textual and typological evidence and further emphasises the importance of geospatial analysis to reconstruct networks.

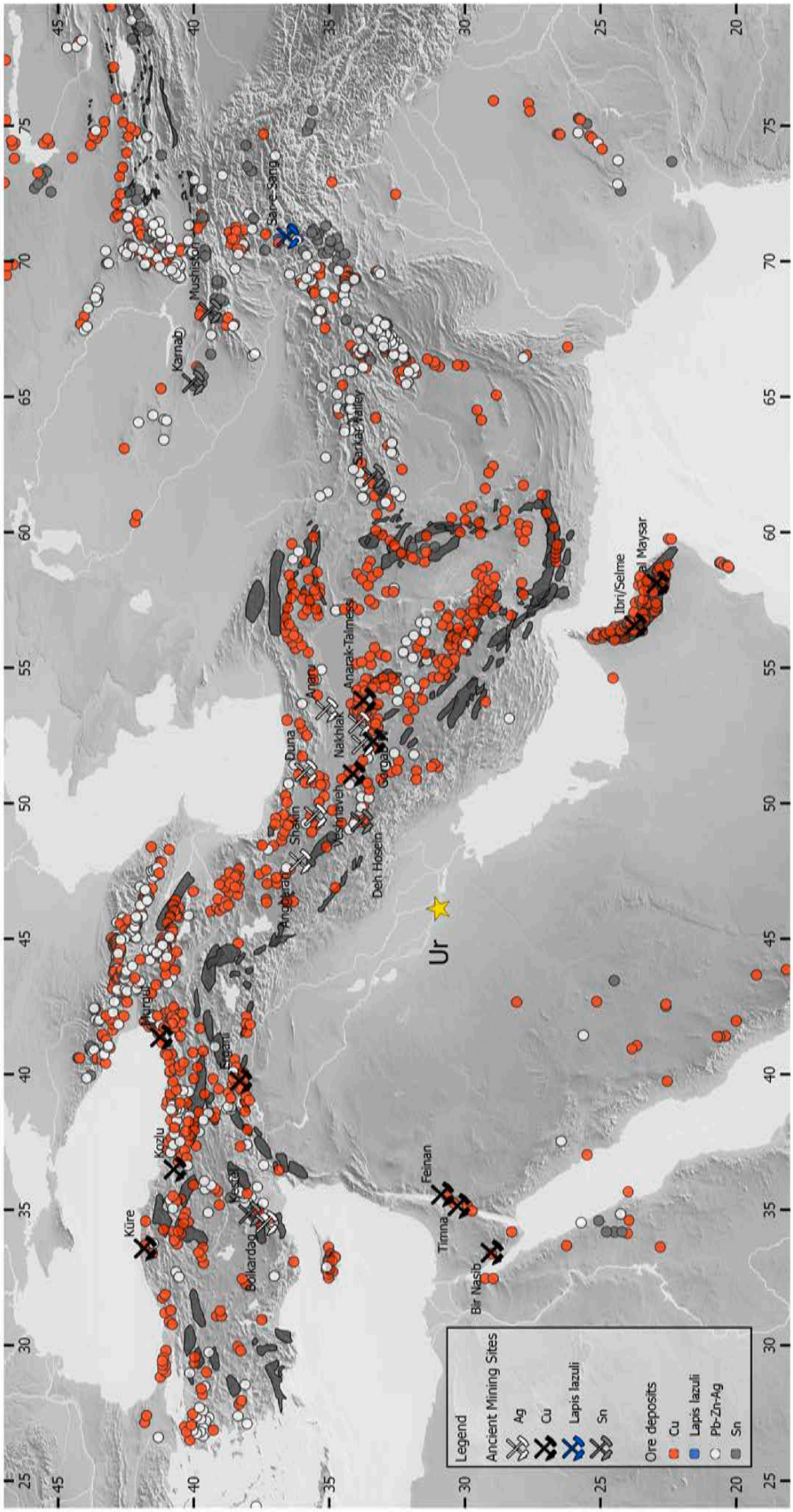

Fig. 5.1: Map of metal deposits in the Near and Middle East. Major mining and smelting sites dated to the third millennium BCE are marked. The grey polygons represent ophiolite occurrences.

(Data sources: Hauptmann, 1985; Yener, et al., 1991; Pigott 1999; Hauptmann, 2000; Prange, 2001; Orris and Bliss, 2002; Twaltschrelidze 2002; Hauptmann, Rehren und Schmitt-Strecker, 2003; Weeks, 2003; Momenzadeh, 2004; Pigott 2004; Weisgerber 2004; Nezafati, 2006; Murao, Deb and Furuno, 2008; Nezafati, et al., 2009; Seltmann 2009; Begemann, et al., 2010; Lehner and Yener 2010; Lyckberg, 2011; Mirnejad, Simonetti and Molasalehi, 2011; Chakrabarti, 2012; Dhavalikar, 2012; Garner, 2012; Nezafati and Pernicka, 2012; Seltmann, 2013; Merkel, et al., 2016; Mindat.org, 2018; USGS, 2018; Made with Natural Earth)

6 Geodynamic settings of copper, silver and tin occurrences in the Near and Middle East

For provenance studies of metal objects a comprehensive knowledge of geodynamic settings and mineralogical assemblages of metal deposits is essential. The geologic framework has influence on the individual mineral occurrences, and the tectonic evolution and regional geology give information about the expected mineralogical assemblages and geologic ages, which both have to be well understood, when it comes to the chemical and Pb isotope analysis of archaeological objects on the quest for provenance. For a general overview of the palaeolocations of the ancient terranes and super terranes and the development within the plate tectonic model see the papers of Ruban, Al-Husseini and Iwasaki (2007) and Burtman (2010) and the cited references within. The most important marks in Earth's history are displayed in fig. 6.1 and mentioned in the following chapter repeatedly, as they are essential for understanding the formation of relevant ore deposits. The figure exhibits the disjuncture of the supercontinent Rodinia resulting in a number of smaller terranes and the opening of the Prototethys ocean at the Neoproterozoic-Palaeozoic boundary. The continents are evolving in more than one full Wilson Cycle, as the Palaeotethys ocean closes again while the Hun super terrane breaks apart from Gondwana and the Palaeotethys opens. Meanwhile the continents of Laurentia, Baltica, Avalonia and a number of smaller terranes collide to the supercontinent Laurussia during the Caledonian orogeny. The formation of the supercontinent Pangaea marks the Hercynian / Variscan orogeny and the beginning of the closure of Palaeotethys in Carboniferous times. The Mesozoic is characterised by the complete closure of Palaeotethys, the subsequent opening of Neotethys and the disjunction of Pangaea. The African-Arabian plate collides with the Eurasian plate in the Cenozoic, the Neotethys closes again during the Alpide orogeny, the Indian plate breaks apart from the Australian plate, collides with the Eurasian plate and forms the Himalayas.

The rifting process of the ocean floors of Proto-, Palaeo-, and Neotethys gave passage to hydrothermal fluids percolating the oceanic crust, resulting in large number of volcanic-hosted massive sulphide deposits and related sedimentary-exhalative, vein-type and stockwork deposits. The intrusion of magmatic bodies caused the development of skarn and greisen deposits. Remnants of oceanic crust of the different Tethys oceans were obducted onto continental crust, as the origin of the Tethyan Eurasian Metallogenic Belt (TEMB) along the old Tethyan suture zones (Anatolia, Southern Caucasus, Zagros mountains, Iranian plateau, Oman, Baluchistan, Hindu Kush, Pamir, and Himalayas) (Janković, 1977). In several subduction zone settings parallel to the Tethyan oceans magmatic arcs and consequently associated porphyry copper deposits formed. Mississippi-Valley-type or carbonate-hosted lead-Zn deposits, which often host silver, are occurring along the carbonate platforms of the passive continental margins.

This chapter provides an overview about the geological settings and background information on regional geology and tectonic evolution in potential regions of provenance for the Ur copper-based and silver metal artefacts. For more detailed information see the cited literature in the text and the references within.

6.1 Anatolia

The geology of Anatolia or Asia Minor is mainly dominated by the opening and closure of the Tethys ocean and is part of the Tethyan Eurasian Metallogenic Belt (TEMB) extending from the Alps to the Himalayas (Janković, 1977). It can be divided into 3 major different tectonic units, according to Kettin (1966):

Pontides: The northern unit of Anatolia (cf. fig. 6.1) was folded during the Alpide orogeny (Okay, 2008). A great number of thrusts were faulted, but no metamorphosed rocks occur (Okay, 2008). The Pontides themselves are subdivided in three terranes: Strandja, Istanbul and Sakarya (Okay, 2008). The Strandja massif belongs to a terrane which also includes the Rhodopes and the Serbo-Macedonian massifs to the NW (Okay 2001, 2008). The orogenes formed in the Mesozoic and a magmatic belt occurred during the subduction of the Tethys oceanic plate in the Upper Cretaceous (Robinson, et al., 1995; Okay, 2008). The Istanbul terrane is approximately 400 km long and 55 km wide and extends along the southern coast of the Black Sea (Okay, 2008). The basement consists of Precambrian rocks, is followed by Ordovician to Carboniferous sediments (Akıncı, 1984; Bozkurt, et al., 2008), and both are part of Laurasia's passive continental margin (Yiğitbaş, et al., 2004; Okay, 2008). The evidence

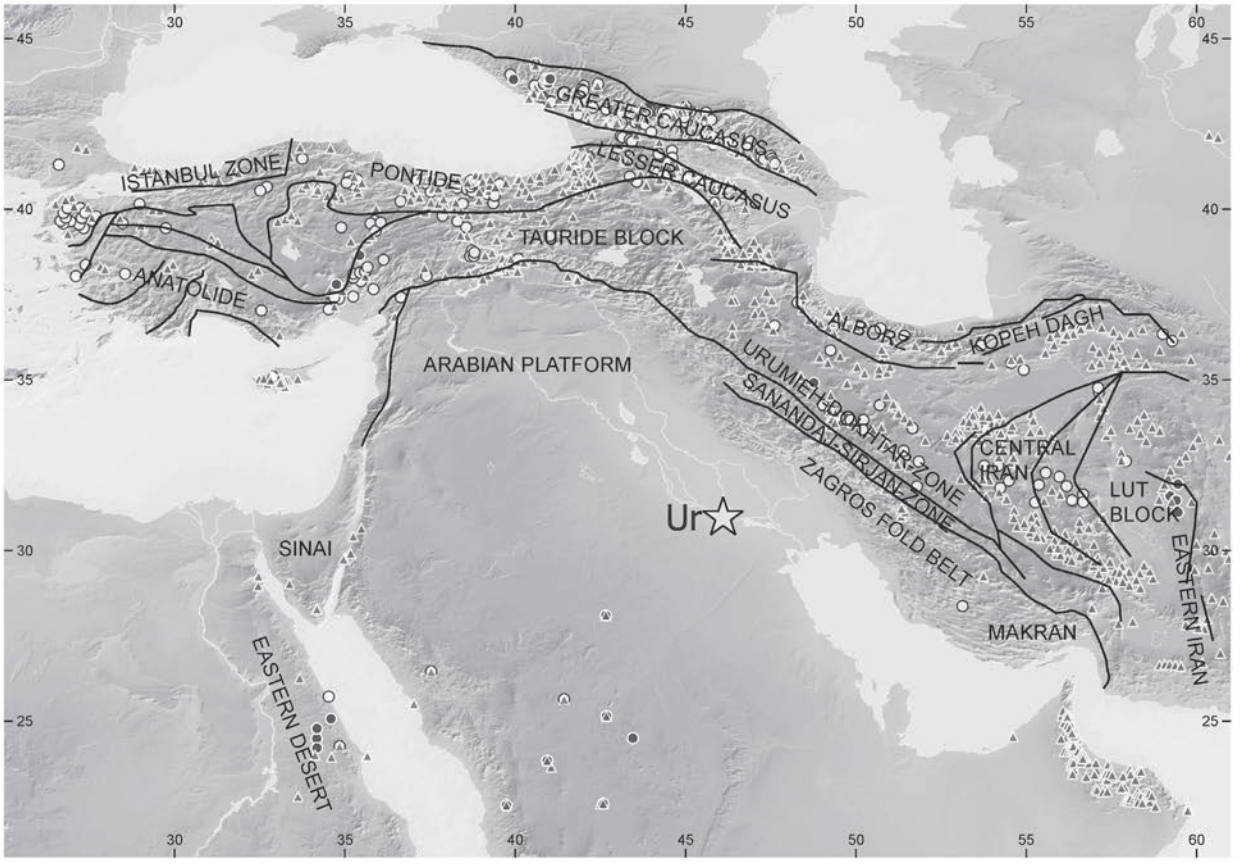

Fig. 6.1: Simplified map of tectonic units in Anatolia, Levant, Egypt, Caucasus, and Iran. The triangles represent copper occurrences, the white circles silver occurrences, the dark grey circles tin occurrences (after Okay, 2008, fig. 3; after Mirnejad, Simonetti and Molasalehi, 2011, fig. 1; Data sources: Hauptmann, 1985; Yener, et al., 1991; Pigott 1999; Hauptmann, 2000; Prange, 2001; Orris and Bliss, 2002; Twaltschrelidze 2002; Hauptmann, Rehren und Schmitt-Strecker, 2003; Weeks, 2003; Momenzadeh, 2004; Pigott 2004; Weisgerber 2004; Nezafati, 2006; Murao, Deb and Furuno, 2008; Nezafati, et al., 2009; Seltmann 2009; Begemann, et al., 2010; Lehner and Yener 2010; Lyckberg, 2011; Mirnejad, Simonetti and Molasalehi, 2011; Chakrabarti, 2012; Dhavalikar, 2012; Garner, 2012; Nezafati and Pernicka, 2012; Seltmann, 2013; Merkel, et al., 2016; Mindat.org, 2018; USGS, 2018; made with Natural Earth).

for Variscan influence is missing in the terrane (Bozkurt, et al., 2008). A suture separates the Istanbul from the Sakarya terrane which exhibits a heterogeneous crystalline basement influenced by Variscan orogeny, Palaeozoic intrusives and Permo-Triassic complex subduction and accretion of the Palaeo-Tethys (Ruban, Al-Husseini and Iwasaki, 2007; Okay, 2008). As the other two terranes the Sakarya zone is characterised of a succession of marine sediments and an ophiolitic melange is observed in the East (Akin, 1979; Okay, 2008). The deformation and metamorphism of Late Triassic to Early Jurassic age are caused by the Cimmeride orogeny (Okay, 2008). The Pontides as a single terrane formed during the closure of the intrapontidic ocean and the opening of the Black Sea (Okay, 2008). In Late Cretaceous a magmatic arc came into existence due to subduction caused by the collision of the Anatolides-Taurides with the Pontides, which generated a large number of Pb-Zn and Cu deposits mainly in the eastern part of the Pontides (Akıncı, 1984; Okay, 2008; Lehner and Yener, 2014; Revan, et al., 2014). Extension related volcanism started again in the Eocene by the opening of the Eastern basin of the Black Sea (Okay, 2008). The Cu and Pb-Zn deposits which bear Ag in a sometimes considerably high amount are mostly volcanic massive hosted sulphide deposits (VHMS), but also occur as stockwork or veins (Akıncı, 1984; Santoro, et al., 2013; Revan, et al., 2014). Numerous mineral occurrences are outcropping in the eastern Pontides (Akıncı, 1984). Murgul is the largest VHMS deposit in the Pontides containing mainly chalcopyrite and haematite (Yigit, 2009; Santoro, et al., 2013).

In north-western Anatolia complex Cu, Pb, Ag and Au deposits are occurring (Pernicka, et al., 1984; Wagner, et al., 1986; Pernicka, et al., 2003). There are many known porphyry Cu-Mo-Au deposits in the Pontides, as e.g. Dereköy (NW) or Gümüşhane (NE) (Yigit, 2009).

Anatolides/Taurides: The southern Anatolian peninsula comprises mainly the Anatolides and Taurides (Okay, 2008). The basement of the Anatolides/Taurides is of Precambrian crystalline rocks followed by glacial deposits of Late Ordovician age and clastic carbonates (Okay, 2008). During the Mesozoic from Upper Triassic to Upper Cretaceous a large carbonate sequence followed, while features of the Variscan orogeny are

missing (Okay, 2008). The terrane underwent regional metamorphism and Alpide deformation during the Late Cretaceous episodes of continental collision (Okay, 2008; Yigit, 2009). During the Late Cretaceous episodes of obduction large ophiolite bodies were emplaced on the Anatolide/Tauride terrane which are part of the Tethyan Eurasian Metallogenic Belt (TEMB) (Okay, 2008). VHMS copper deposits of the Cyprus-type are associated with the ophiolite bodies (Yigit, 2009). Further features of continental collision during the Palaeocene are observed (Okay, 2008; Yigit, 2009).

In the eastern Taurus mountains Ergani Maden is one of the largest copper sulphide deposits, where also Cu-As-Ni sulphide mineralisations occur (Bamba, 1976; Çagatay, 1977; Lehner and Yener, 2014). Ergani and Küre are the largest VHMS copper deposits of the Cyprus-type in the central Taurus (Akin, 1979; Lehner and Yener, 2014; Yigit, 2009). In the modern Bolkardağ mining district are argentiferous lead ores (sulphides and oxides) as well as stannites and cassiterite to be found (Lehner and Yener, 2014). In this area there is evidence for large scale tin ore smelting (Kestel) and metal working (Göltepe) (Earl and Yener, 1995; Yener, et al., 1989; Yener, et al., 1991; Yener, 2000; Yener and Vandiver, 1993). Pb-Zn-Ag skarn deposits occur in central Anatolia e.g. in the Akdağmadeni district or southern central Anatolia in Yahyalı (Yigit, 2009).

Arabian platform: The Arabian platform is present in the south-eastern part of Anatolia and collided with the Anatolides/Taurides in the Miocene (Okay, 2008). The basement of the terrane consists of Precambrian crystalline rocks which are overlain by a sedimentary sequence of Palaeozoic to Tertiary age (Okay, 2008).

6.2 Caucasus

The geology of the Caucasus was highly influenced by the opening and closure of the Proto-, Palaeo-, and Neotethys and evolved in a series of complex plate tectonic settings (Twaltschrelidze, 2001; Manafi, et al., 2013; Ruban, Al-Husseini and Iwasaki, 2007). According to Gamkrelidze (1997) the geological units of the Caucasus can be classified by three terranes (cf. fig. 6.1):

Greater Caucasus: The formation of the Greater Caucasus terrane is a result of the subduction of the Prototethys under the Baltic terrane (Manafi, et al., 2013). The terrane is assigned to the Hun super terrane by Ruban, Al-Husseini and Iwasaki (2007). Volcanoclastic and volcanic rocks were deposited in the Middle to Late Devonian possibly associated with the opening of the Rheic ocean (Ruban, Al-Husseini and Iwasaki, 2007). Meta ophiolite slices dated to Devonian / Early Carboniferous were emplaced on the crystalline core of Greater Caucasus, as the Prototethys ocean closed and the Palaeotethys reached its complete extension (Gamkrelidze, 1986; Manafi, et al., 2013). Remnants of a Jurassic ensialic volcanic arc are reported in the Greater Caucasus (Lipman, et al., 1993). VHMS copper deposits formed in a deep sea setting during the Cimmerian event (disjuncture of the Cimmeride terrane from Pangaea and formation of Neotethys ocean in Permian times) (Twaltschrelidze, 2001; Ruban, Al-Husseini and Iwasaki, 2007). The Greater Caucasus mountain range formed during the continental collision of the Arabian and Eurasian plate and the complete closure of the Neotethys ocean in the Miocene (Lipman, et al., 1993).

Trans Caucasus: This terrane evolved in a complex geologic and tectonic history. The basement consists of Precambrian to Palaeozoic rocks that were part of an island arc and fragmented Prototethys slices (Adamia, et al., 2011; Manafi, et al., 2013; Twaltschrelidze, 2001). The island arc developed during the subduction of the Prototethys ocean under the Baltic terrane in Late Proterozoic to Early Palaeozoic times parallel to the opening of the Palaeotethys between the Baltic and the Arabian-African terrane in middle Silurian along the Hun super terrane (Ruban, Al-Husseini and Iwasaki, 2007; Manafi, et al., 2013). Outcrops of the basement are composed of granitoid bodies that intruded in the island arc in the Late Palaeozoic (Variscan) (Adamia, et al., 2011). In the Palaeozoic Palaeotethys was then subducted under the Trans Caucasus terrane (Manafi, et al., 2013). In the southern and northern periphery of Trans Caucasus two island arcs formed in the Cretaceous resulting in vein-type and stratabound Pb-Zn as well as polymetallic VHMS deposits (Au-Ag-Cu-Pb-Zn-Ba) (Twaltschrelidze, 2001). Cenozoic magmatic activity occurred within the Transcaucasian terrane presumably caused by plate convergence, extension of the Red Sea rift system or a transtensional system related to the collision of the African-Arabian and Iranian-Anatolian terranes (Lipman, et al., 1993). In Miocene times during the main uplift of the Alpide orogeny several deposits formed that are characteristic of orogeny related mineralisations, as Mo-W-deposits (bound to granites), As-Sb-Hg-ore bodies, and porphyry Cu deposits (Twaltschrelidze, 2001).

Lesser Caucasus: The terrane was separated with the rifting of Cimmeria away from Pangaea resulting in the closure of Palaeotethys and opening of Neotethys ocean (Ruban, Al-Husseini and Iwasaki, 2007). The position of Lesser Caucasus in Palaeozoic times remains uncertain to this date (Ruban, Al-Husseini and Iwasaki, 2007). An ophiolitic melange is evident in this terrane along the suture formed by the disruption and erosion of emplaced Palaeozoic ophiolites at the rim of the Palaeotethys throughout the Mesozoic (Adamia, et al., 2011; Gamkrelidze, 1986). Metal deposits formed in this terrane during magmatic activity from Jurassic to Miocene (Janković, 1977; Philip, et al., 1989). Porphyry Cu-Mo deposits related to the collisional and postcollisional setting at the closure of Neotethys occur along dikes in the Lesser Caucasus (Janković, 1977; Moritz, et al., 2016).

6.3 Levant and Sinai

The Levant (cf. fig. 6.1) is geologically located at the north-western rim of the Arabian-Nubian Shield in between the African and Eurasian plate (Hauptmann, 2000). The Precambrian basement of the Arabian Shield is outcropping at the southern Sinai, in the Wadi Arabah, and to the SE of the Arabian coast with a succession of carbonatic shelf rocks (Segev, 1987; Hauptmann, 2000; Rybakov and Segev, 2004). In Proterozoic times a graben began to extend roughly N-S and it divided the Arabian-Nubian-Shield in the Miocene (Zak and Freund, 1981; Hauptmann, 2000). From south to north the thickness of sediments (Cambrian to Quaternary) increases up to 1900m (Bender, 1974; Hauptmann, 2007). Due to the thick coverage of sediments on the region north of the Dead Sea no metal deposits are occurring to the north until the Taurus mountains begin (Hauptmann, 2007). During Triassic to lower Cretaceous as well as Cenozoic times volcanic activities were occurring, related to the graben formation (Hauptmann, 2007). In Wadi Arabah and Sinai copper and copper/Mn mineralisations are to be found in the Precambrian basement, in Cambrian rhyolites and Cambrian to Cretaceous sediments (Hauptmann, 2007). The ore deposits in the southern Levant and Sinai differ from other deposits discussed in this section. The levantine and Sinai deposits are mainly characterised as stratiform sedimentary with mostly oxidic ores while sulphide ores occur very rarely (Hauptmann, 2007).

Bronze Age mining and archaeometallurgical activities on a grand scale have been reported in Timna, Faynan and Bir Nasib (Bartura, Hauptmann and Schöne-Warnefeld, 1980; Conrad and Rothenberg, 1980; Hauptmann, 2000; Hauptmann, 2007; Pfeiffer, 2013a).

6.4 Eastern Desert of Egypt

Egypt and Nubia (cf. fig. 6.1) are characterised by a Precambrian basement representing the earliest crustal remains in Africa and Arabia (Stern, Gottfried and Hedge, 1984). The craton grew during Neoproterozoic times, as the ocean between the eastern and western Gondwana closed, through accretion of island arcs along the continental margins (Abd El-Rahman, et al., 2009). The collision of the supercontinents caused the Pan-African orogeny followed by the eruption of the Dokhan Volcanics in the Eastern Desert, the deposition of the Hammamat sediments and emplacement of younger granites (Eliwa, Kimura and Itaya, 2006; Abd El-Rahman, et al., 2009). The Precambrian rocks are mostly outcropping between the Red Sea and the Nile due to rift shoulder uplift during the opening of the Red Sea (Stern, 1981; Ali, et al., 2016). The basement of the north-eastern desert comprises different components. The melasse-type Hammamat Formation (1) consists mostly of sediments probably deriving from older crusts, that were disrupted (Stern, Gottfried and Hedge, 1984; Eliwa, Kimura and Itaya, 2006). The Dokhan Volcanics (2) are composed of intermediate to felsic volcanic rocks, erupted at subaerial and subaqueous levels, that underwent lowgrade metamorphic events (Stern, Gottfried and Hedge, 1984). Dikes (3) comprising basaltic, rhyolitic, calcalkaline to alkaline compositions are intruding the north-eastern desert in swarms trending E-NE (Stern, Gottfried and Hedge, 1984). Furthermore plutonic rocks (4) as granodiorites and granites are emplaced in various kinds in the Hammamat and Dokhan formation (Stern, Gottfried and Hedge, 1984; Eliwa, Kimura and Itaya, 2006).

The Neoproterozoic ophiolites formed as a result of the closure of the Mozambique Ocean and the continental collision of the eastern and western Gondwana supercontinents and were emplaced in different parts of the Eastern Desert (Abd El-Rahman, et al., 2009; Furnes, Dilek and de Wit, 2015). Across the Egyptian ophiolites podiform chromitites are reported (Ahmed, Arai and Attia, 2011). Further magmatic intrusions occurred during Mesozoic times (mainly Jurassic and Cretaceous) and Neogene times (Mio- to Pliocene) as the opening of the Red Sea begun (Klitzsch, 1986).

Wide regions of Egypt are covered by younger continental and marine sediments (Klitzsch, 1986). Therefore most of the metal deposits are to be found in the Eastern Desert and Sinai (for Sinai see subsection 6.3). The Eastern Desert comprises mostly vein type, hydrothermal and metamorphic copper deposits (Pfeiffer, 2013; Salem, et al., 2013). The Pb-Ag deposits of Egypt are predominantly hydrothermal replacement deposits (Stos-Gale and Gale, 1981). In addition gold was mined in Egypt as early as the 5th millennium BCE which occurs near juvenile Proterozoic granodiorite intrusions (Klemm and Klemm, 2014).

6.5 Iranian Plateau and Zagros Mountains

Generally Iran can be divided into 10 major geological units, which are dominated by the subduction structures along the NE margin of the Tethys ocean in the Late Jurassic to Early Cretaceous and belong to the Tethyan Eurasian Metallogenic Belt and super ordinate to the Alpine-Himalayan Metallogenic belt (Janković, 1977; Nezafati, 2006; Nezafati, Pernicka and Momenzadeh, 2008; Moghadam and Stern, 2014; Moghadam and Stern, 2015) (cf. fig. 6.1):

Khuzestan plain: The plain is predominantly covered by alluvial sediments of Quaternary age and hosts no metal deposits (Nezafati, 2006).

Zagros fold belt: The general Zagros orogenic belt trends NE-SW and stretches for ca. 2000 km from eastern Turkey to the Oman line in southern Iran (Alavi, 1994; Nezafati, Pernicka and Momenzadeh, 2008). The basement was believed to comprise Precambrian rocks (Stocklin, 1968; Stocklin and Nabavi, 1973), however, is of Mesozoic or Paleozoic age (Alavi, 1994). The basement is covered

by successions of a evaporite-dolomite unit, a sequence of prevalent shallow continental shelf rocks, followed by a progression of Carboniferous to Upper Cretaceous continental shelf carbonate (Alavi, 1994). The uppermost sedimentary layer includes marine to non marine carbonates and siliciclastics of Cretaceous to Recent age (Alavi, 1994). In this zone only one significant Pb-Zn deposit of Mississippi-Valley-type occurs: Kuh-e Sormeh (Mirnejad, Simonetti and Molasalehi, 2011).

Sanandaj-Sirjan zone: This structural zone trends NE-SW and lies between the Zagros fold belt and the Urumieh-Dokhtar zone (Nezafati, 2006). The width is between 150 to 250 km and the ranges extend to 1500 km (Alavi, 1994**;** Nezafati, 2006; Ehya, Lotfi and Rasa, 2010). The Sanandaj-Sirjan zone joins the Taurus orogenic belt in Turkey and is characterised by rocks of mainly Mesozoic age, although in the south-east also Palaeozoic rocks occur (Nezafati, 2006). Associated with this zone are complex metamorphic and deformed rocks, intrusive bodies as well as volcanic rocks of Mesozoic age (Nezafati, 2006; Mirnejad, Simonetti and Molasalehi, 2011).

The Sanandaj-Sirjan zone is one of the three most important metallogenic provinces in Iran and hosts many Pb-Zn deposits, especially in the central part, the Malayer-Esfahan belt (Ehya, Lotfi and Rasa, 2010). There the Pb-Zn-deposits are mainly stratabound and hosted by Cretaceous limestones, dolomites, shale and sometimes sandstones (Ehya, Lotfi and Rasa, 2010; Momenzadeh, 2004). At the NE margin also Mississippi-Valley type deposits occur hosted by Permian-Triassic rocks (Rajabi, Rastad and Canet, 2013).

In this unit also Au-Sn-W-Cu mineralisations occur in Deh Hosein (Nezafati, 2006).

Main Pb-Zn deposits are Angouran (Daliran, et al., 2013) and Emarat (Ehya, Lotfi and Rasa, 2010).

Urumieh-Dokhtar zone: The magmatic assemblage extends along the entire length of the Zagros orogenic belt (Alavi, 1994). This geological unit formed due to subduction of the Neo-Tethys beneath the Central Iranian plate (Mirnejad, Simonetti and Molasalehi, 2011). The main magmatic activity is dated to Eocene (Alavi, 1994). The Urumieh-Dokhtar zone hosts the main part of porphyry copper deposits in the SE (Mirnejad, Simonetti and Molasalehi, 2011; Daliran, et al., 2013). The copper deposits are mostly Cu-Mo porphyry, VHMS, stratiform, vein- and skarn-type deposits (Nezafati, Momenzadeh and Pernicka, 2005). The latter is primarily associated with Tertiary magmatic activity (Nezafati, Momenzadeh and Pernicka, 2005). The mostly vein-type Pb-Zn deposits occur predominantly in the NW part of this unit (Mirnejad, Simonetti and Molasalehi, 2011).

Main metal production areas are: Arisman, Tappeh Sialk, Veshnaveh (Nezafati, Pernicka and Momenzadeh, 2008**;** Nezafati and Pernicka, 2012**;** Weeks, 2013).

Alborz mountains: The Alborz unit trends E-W and ranges over 500 km (Rajabi, Rastad and Canet, 2013). The range is a result of the opening and subduction of the Palaeo-Tethys under the Turan plate and remnants of Palaeozoic ophiolites are outcropping between the Alborz and Kopeh Dagh unit (Ruban, Al-Husseini and Iwasaki, 2007; Mirnejad, Simonetti and Molasalehi, 2011; Moghadam and Stern, 2014). This zone comprises sedimentary and magmatic rocks of Precambrian to Recent age (Moghadam and Stern, 2014). The Pb-Zn deposits are predominantly of the Mississippi-Valley-type and hosted by Permian-Triassic sand- and siltstones, dolomites and limestones (Rajabi, Rastad and Canet, 2013; Mirnejad, Simonetti and Molasalehi, 2015). Vein and skarn type Pb-Zn deposits due to Tertiary magmatic activity are also to be found in this unit (Mirnejad, Simonetti and Molasalehi, 2015). Furthermore stratabound Pb-Zn-deposits occur in the Alborz zone related to Cenozoic volcanic rocks (Mirnejad, Simonetti and Molasalehi, 2015).

This unit hosts next to the Urumieh-Dokhtar zone and Central Iran unit the main quantity of copper deposits related to Tertiary volcanism (Nezafati, Pernicka and Momenzadeh, 2008).

Kopeh Dagh: This geological unit comprises sediments of Mesozoic to Tertiary age and hosts only few metal deposits and is part of the Turan block (Moghadam and Stern, 2014; Nezafati, 2006).

Eastern Iran: This suture zone is mainly characterised by emplacement of Cretaceous ophiolites and flysch sedimentation (Moghadam and Stern, 2014). The ancient copper production site of Shahr-i Sokhta is located in this unit (Hauptmann, Rehren und Schmitt-Strecker, 2003).

Central Iran/Lut Block: This block is divided by three major faults and hosts rocks of Precambrian to Cambrian age (Alavi, 1994, Moghadam and Stern, 2014). The unit is the largest and also the most complicated geological unit of Iran due to at least three episodes of orogenic activity (Mirnejad, Simonetti and Molasalehi, 2015). More detailed information on this unit are found in the publication of Mirnejad, et al., (2015) and the references within. Many Pb-Zn-deposits are hosted in Cretaceous carbonates in this zone (Mirnejad, Simonetti and Molasalehi, 2015). In the Central Iranian unit ancient silver production is reported in Nakhlak in the Anarak region by Nezafati and Pernicka (2012).

Copper deposits related to Tertiary volcanism occur as well (Nezafati, Pernicka and Momenzadeh, 2008). Furthermore have Michigan type native copper occurrences been reported in this area, namely Darhand, and Talmessi (Nezafati, Pernicka and Momenzadeh, 2008**;** Pernicka, et al., 2011).

Makran: As the eastern Iranian suture zone the Makran zone consists of Cretaceous ophiolites and flysch sediments (Moghadam and Stern, 2014).

6.6 *Makan* - Oman and *Dilmun* - East coast of Arabian peninsula

Oman's geology (cf. fig. 6.1) is highly dominated by a sequence of Mesozoic ophiolites, its associated hydrothermal copper deposits, and the archaeological evidence for a large scale copper smelting and metal production

(Hauptmann and Weisgerber, 1980; Hauptmann, 1985; Hauptmann, 1987; Prange, et al., 1999; Prange, 2001). It has been well established in literature that Oman is indeed the ancient *Makan* (Moorey, 1994; Glassner, 1996; Begemann et al., 2010). The peninsula of Bahrain hosts no metal deposits but previous research identified Bahrain and its surrounding continental areas (the eastern coast of the Arabian peninsula) as ancient *Dilmun* (Muhly, 1973; Larsen, 1983, 118; Moorey, 1994; Glassner, 1996, 130; Foster, 1997; Weeks, 2003; Crawford, 2013). In many cuneiform texts the metal trade between ancient Mesopotamia and *Dilmun* is mentioned (Moorey, 1994; Foster, 1997; Weeks, 2003; Crawford, 2013;). This matter is addressed further in section 4.

The basement is comparable with other parts of the Arabian Shield and consists of Palaeozoic rocks covered with Permian shelf carbonates (Coleman, 1981; Hauptmann, 1985).

The oceanic crust of the emplaced ophiolites formed during sea floor spreading of the Tethys ocean. The sea floor underwent hydrothermal activity in the Upper Cretaceous (Hauptmann, 1985; Haymon, Koski and Abrams, 1989). The ophiolites were then obducted in a supra subduction setting in the Palaeocene (Searle, Robb and Gardiner, 2016). A change in the axial trend of the mountains from NW to N-S occurred due to the rotation of the Arabian plate in the Miocene caused by the opening of the Red Sea (Mahfoud and Beck, 1997). The resulting compressional stress and rotational effects gave passage to the rise of diapiric, peridotitic mantle material (Mahfoud and Beck, 1997). Across the Oman mountains a number of mantle diapirs are observed and there is a correlation between stockwork copper mineralisation and the upward movement of peridotitic mantle material along discontinuities (Mahfoud and Beck, 1997; Prange, 2001).

Hydrothermal fluids were circulating through the sea floor resulting in mineralisations of hydrothermal polymetallic ore deposits (Haymon, Koski and Abrams, 1989). The main ore is pyrite carrying the copper ore chalcopyrite and other commodities (Hauptmann, 1985). The ophiolites host large VHMS deposits of the Cyprus-type in the lava sequence (Searle, Robb and Gardiner, 2016). The Aarja ore body is one of the biggest VHMS deposits of this type and contains apart from pyrite, bornite, and chalcopyrite also tennantite and galena (Mahfoud and Beck, 1997). But also dissemination type mineralisations occur in serpentinised gabbro and peridotite (Mahfoud and Beck, 1997). In the deeper parts of the ophiolite series stockwork and vein type copper mineralisations occur bearing higher levels of Ni, Co, As, and Sb (Prange, 2001).

6.7 Central Asia and Himalayas

The geology of Central Asia evolved in a complex tectonic history and comprises several crustal terranes as a result of the disjuncture of the supercontinent Rodinia in the Neoproterozoic era and Gondwana in the Palaeozoic (Burtman, 2010; Steinmüller, et al., 2010). The ranges formed in relatively younger time of Earth's history during the Alpide orogeny and the formation of the Himalayas. Due to the different stages of continental evolution which affected the different conditions of ore forming processes the different units are displayed by age and continental origin.

6.7.1 Precambrian to Palaeozoic geodynamics

The Hindu Kush is situated in Afghanistan and Pakistan and forms the western part of the Himalayan region (cf. fig. 6.2). The Pamir mountain range joins the Hindu Kush in north-western Afghanistan. North of Pamir lies the Tien Shan mountain range, which extends over 2500 km, trending NW (Garner, 2013). The Tien Shan range is transitioning in the Altai mountain range to the NE.

As mentioned above the geological history of this region is very complex and characterised by the collision and break down of different terranes and ancient continents (Şengör, Natal'in and Burtman, 1993; Steinmüller, et al., 2010; Benham, et al., 2013; Seltmann, 2013). The northern terrane of Afghanistan is part of the Eurasian plate (Tajik block), while the southern terranes were disjoined from Gondwana in the Palaeozoic (Farad, Helmand, and Nuristan blocks) (Steinmüller, et al., 2010). The fragments of Gondwana were merged with the Eurasian plate during the closure of the Palaeotethys ocean in Mesozoic times (Ruban, Al-Husseini and Iwasaki, 2007, Steinmüller, et al., 2010). In the Cenozoic the Indo-Pakistan plate collided with the Eurasian continent resulting in the orogeny of the Himalayas and the complete closure of the Neotethys ocean (Steinmüller, et al., 2010).

Precambrian rocks composed of Archaean metamorphic gneisses, amphibolites, marbles, quartzites, and calc-silicates as well as Proterozoic amphibolite and greenschist facies rocks are outcropping in the Kabul, Nuristan, Helmand blocks, in Badakhshan, and the Altai-Tarim craton (Krumsiek 1967; Steinmüller, et al., 2010; Seltmann, 2013; Seltmann, Porter and Pirajno, 2014). In the Kabul block a number of stratabound copper deposits are hosted in Late Proterozoic metamorphic carbonate rocks, e.g. Mes Aynak (Steinmüller, et al., 2010; Thomalsky, et al., 2013).

During the extention of the Palaeotethys marine carbonates and clastic rocks were deposited at a passive continental margin and volcanic rocks of intermediate composition occur (Steinmüller, et al., 2010; Tapponier, et al., 1981). The marine carbonate rocks of Ordovician to Carboniferous age host stratabound Pb-Zn-deposits (Ghor, Parwan and Khost province), e.g. Farenjal and Spira (Steinmüller, et al., 2010). Along the Tien Shan range outcrop Palaeozoic (Devonian to Carboniferous) magmatic rocks, which developed in a back-arc subduc-

tion zone setting, overlying a Neoproterozoic basement (Garner, 2013). In the Altai mountains Cambrian-Ordovician and Devonian porphyry copper (island arc related) and polymetallic Cu-Pb-Zn (VHMS) deposits occur (Seltmann, 2013). Further mineral occurrences in the Altaides are reported for Variscan times (Devonian-Carboniferous) by Seltmann (2013): stratabound, sedimentary exhalative (SEDEX), VHMS copper deposits associated with mafic volcanism; carbonate-hosted Pb-Zn deposits associated with Fe and baryte; sedimentary and supergene enriched copper deposits (also containing Mo, Pb, Zn, Ag, Re, Os, Cd); porphyry Cu-Mo-Au deposits.

In Early Permian the Cimmerian terranes were separated from Gondwana through the strong slab-pull of the subduction zone along the southern rim of Eurasia (Ruban, Al-Husseini and Iwasaki, 2007, Steinmüller, et al., 2010). As a result two back-arc basins formed along the Palaeotethys and Palaeo-Pacific margins which led to the intrusion of mafic volcanic and plutonic rocks (Dronov and Chmyriov, 2008; Schwab, et al., 2004, 204; Steinmüller, et al., 2010).

In Late Permian ophiolite complexes were emplaced on the Precambrian Karakum and Altai-Tarim terranes along the Palaeotethys suture (Kabul block, Pamir, Karakoram) (Burtman, 2010; Seltmann, Porter and Pirajno, 2014).

6.7.2 Mesozoic ophiolites and volcanic activity

The separated Gondwana terranes were accreted to the Eurasian plate in Triassic times (Srimal 1986; Natal'in 1993). In the area of the Tien Shan mountain range several postcollisional porphyry Cu-Mo deposits occur (Mao, et al., 2014). The main Mesozoic feature in Central Asia can be characterised as intraplate magmatic activity (cf. fig. 6.2), uplift and emergence of large fault zones (Schwab, et al., 2004, Seltmann, Porter and Pirajno, 2014). Along the Tethyan suture zone Mesozoic ophiolites were obducted in Cretaceous times (Tapponier, et al., 1981; Burtman, 2010; Benham, et al., 2013). A large number of copper deposits are hosted in the Tethyan Eurasian Metallogenic Belt (TEMB), mainly of volcanic-sedimentary, VHMS, and porphyry Cu-Mo type (Janković, 1977). Furthermore are vein and skarn-type copper deposits as well as Pb-Zn and Au deposits reported (Janković, 1977).

6.7.3 Cenozoic Himalayan orogeny associated units

Along the Karakoram and Pamir ranges crustal thickening occurs during the Oligocene and Miocene, as the Indian-Asian collision resulted in the Himalayan orogeny, and only a few mineral occurrences are reported in this area (Schwab, et al., 2004, Searle, Robb and Gardiner, 2016). In Afghanistan several mineral occurrences are reported related to felsic and intermediate rocks of magmatic origin which developed along fault zones (Ganss 1965, 105, Steinmüller, et al., 2010). In the Kabul block a large number of deposits is mentioned in connection with Eocene ultramafic and Quaternary carbonatite rocks (Orris and Bliss, 2002; Steinmüller, et al., 2010). Cu deposits, Pb-Zn skarns, polymetallic Cu-Pb-Zn (associated with Au, W, and Sn) veins, as well as Sn-W veins, greisen and skarns are hosted by a magmatic arc outcropping in Kandahar, Ghazni and Zabul province (dated to Late Cretaceous - Oligocene) (Steinmüller, et al., 2010).

6.8 The Indus Valley and Aravalli-Delhi range in NW India

The craton of the Indian subcontinent preserved one of the oldest continental rock formations of Earth's history (Deb and Sarkar, 1990). The basement of NW India in the present day Rajasthan / Gujarat region consists of an Archaean banded gneiss complex (with the oldest Sm-Nd isotope date being 3.5 Ga) and granites (Naha and Roy, 1983; Choudhary, et al., 1984; Macdougall, 1984; Deb and Sarkar, 1990). Around 2.6 Ga intraplate rifting occurred in the banded gneiss complex marked by the intrusion of the Berach granite and resulted in the formation of the Bhilwara belt (Deb, et al., 1989). Hydrothermal seawater percolated the rift basin resulting in stratiform polymetallic mineralisations within the Aravalli-Delhi complex (Deb and Sarkar, 1990). Sedimentary rocks were deposited on the banded gneiss complex along the subsequent passive continental margin (2-1.7 Ga) and are outcropping in the Aravalli range (Deb, et al., 1989; Deb and Sarkar, 1990). In this process (cf. fig. 6.2) an island arc (present day Delhi supergroup) formed and collided with the Aravalli continental margin at 1.5 Ga (Deb, et al., 1989). Although there are different theories about the exact number of subduction zones involved and in which direction the island arc collided, the ultimate result was lower crust of the banded gneiss complex being thrust over the Bhilwara formation (Deb, et al., 1989; Deb and Sarkar, 1990; Deb, et al., 2001).

This complex geodynamic setting supported the formation of several polymetallic ore deposits, which are according to Deb, et al., (1989):

The Rampura-Agucha orebody is hosted by synorogenic highly metamorphosed granulite facies rocks of the Bhilwara belt and contains mostly sphalerite and galena. The Bhilwara belt hosts the stratiform Rajpura-Dariba orebody, which comprises Pb-Zn minerals in the central part and copper in the footzone.

The formation of the deposits is associated with volcano-sedimentary activity in a shallow marine intracontinental rift setting (Deb, et al., 1989; Deb, et al., 2001). The Pb-Zn mineralisation also includes rare Ag-As

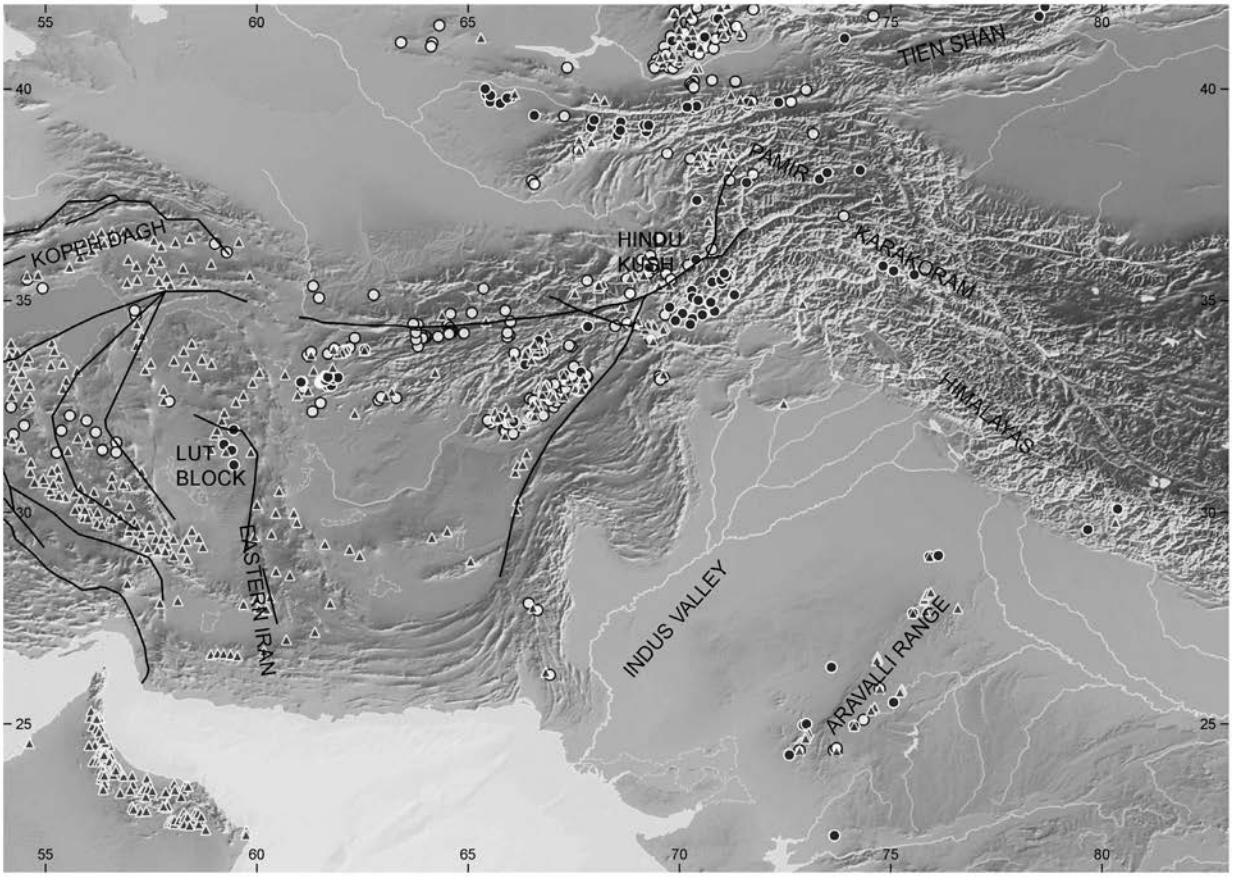

Fig. 6.2: Simplified map of tectonic units in Central Asia and Indus Region. The triangles represent copper occurrences, the white circles silver occurrences, the dark grey circles tin occurrences (Data sources: Hauptmann, 1985; Yener, et al., 1991; Pigott 1999; Deb and Sarkar, 2000; Hauptmann, 2000; Prange, 2001; Orris and Bliss, 2002; Twaltschrelidze 2002; Hauptmann, Rehren und Schmitt-Strecker, 2003; Weeks, 2003; Momenzadeh, 2004; Pigott 2004; Weisgerber 2004; Nezafati, 2006; Murao, Deb and Furuno, 2008; Nezafati, et al., 2009; Seltmann 2009; Begemann, et al., 2010; Lehner and Yener 2010; Lyckberg, 2011; Mirnejad, Simonetti and Molasalehi, 2011; Chakrabarti, 2012; Dhavalikar, 2012; Garner, 2012; Nezafati and Pernicka, 2012; Seltmann, 2013; Merkel, et al., 2016; Mindat.org, 2018; USGS, 2018; made with Natural Earth).

sulphosalts and native metals (Deb, et al., 1989). The largest Pb-Zn-mineralisation is the Zawar orebody, which is found in the lower part of the Aravalli belt (Deb, et al., 1989; Deb and Sarkar, 1990).

Further stratiform Zn-Pb-Cu deposits are hosted in the Delhi belt (Deb, et al., 1989). The stratabound Khetri copper belt, the Kho-Dariba Cu-, and the Tosham Sn-W deposits represent other important mineralisation of the Delhi belt (Sarkar and Dasgupta, 1980; Deb and Sarkar, 1990; Law, 2008). The tin deposit in Tosham is a polymetallic vein-type deposit containing (In-bearing) cassiterite and Cu-Sn-sulphides (stannites) of Neoproterozoic age hosted by greisenised metasediments, granite-, and rhyolite intrusions (Murao, Deb and Furuno, 2008).

This region includes the Indus Valley to the West, which hosts geologically recent sediments. In the fertile region of the Indus river the Harappa culture emerged in Early Bronze Age and trade connections are reported between Early Dynastic Ur and Harappa (Hirsch, 1963; Heimpel, 1987; Moorey, 1994, 8; Prange et al. 1999, 187).

The western margin of the Indian subcontinent is marked by the Tethyan suture and the associated Late Cretaceous Tethyan Eurasian Metallogenic belt, where the Waziristan-, Muslim Bagh-, and Bela ophiolites of Baluchistan (Pakistan) are to be found (Jan, Windley and Khan, 1985; Zaigham and Mallick, 2000; Siddiqui, et al., 2011; Siddiqui, Qasim Jan and Asif Khan, 2012). The ophiolites host VHMS polymetallic (Mn-Cu-Pb-Zn) deposits, due to hydrothermal seawater percolation through the oceanic crust in Mesozoic times (Zaigham and Mallick, 2000).

The Chagai porphyry copper belt, situated in Baluchistan, formed during multiple ore forming stages in several superimposed magmatic arcs of Miocene to Pliocene age and hosts one of the biggest copper deposits in the world, namely Reko Diq (Perelló, et al., 2008).

7 Methods: Electron microprobe analysis

7.1 Requirements and procedure

The analytical question requires spatial resolving techniques. Electron microprobe analysis was applied to gain information about the structure, the corrosion status and the main and trace element composition of the metal objects. The sample surface is analysed by an electron beam. The electrons penetrate into the samples to a certain depth dependent on the high voltage as well as molecular weight and density of the sample. The electron beam causes an electron transition in energy levels in the sample atoms. This transition emits excess energy as characteristic x-radiation which is measured by detectors behind different spectrometer crystals. Due to the high sample density of copper, bronze, and silver metal the penetration depth is low. Therefore the surface of a sample can be analysed to a depth of approximately 1-2 µm. For the applied measurements wavelength dispersive analysis (WDS) is applied, having the advantage of lower detection limits compared to energy dispersive methods (EDS).

As a requirement for a good analysis the surface has to be completely even, clean, and fresh. Superficial corrosion has to be removed from the metal before it can be analysed. The samples were sawn and a small fragment from each specimen was extracted for metallography and PIXE analysis at the Penn Museum. To ensure representative bulk chemical compositions by point analysis a statistically relevant number of measurement points is set randomly across the metal surface of the specimens. The chemical composition of the metal and specific phases can be determined. Measurements on corroded surfaces can be ruled out in contrast to e.g. portable x-ray fluorescence analysis (XRF). Lacking the possibility to drill the samples, it is the only way to gain information about the composition of these objects. For comparison there are older particle-induced x-ray emission (PIXE) and energy-dispersive x-ray microanalysis data about the mounted objects available, which were carried out by Tamara Stech and Vincent Pigott in the Penn Museum in the 1980's. The method itself is non-destructive on the samples surface but fragments of the samples have to be extracted for preparation.

7.2 Limitations

Limitations of *in situ* analysis are chemical inhomogeneities within the metals due to alloying. Metal artefacts are not as homogeneous as e.g. glass. Tin bronze in particular exhibits strong inhomogeneities due to complex metastable phases occurring at different temperatures and Sn concentrations. Point analysis of heterogeneous phases leads to problems with the analysis of chemical composition. To provide an accurate mean a higher number of points have to be spread across the sample's surface. To exclude accidental preference of certain sample areas by the operator the points had to be set randomly by grid analysis if possible.

7.3 Sample preparation

The Nash Collection samples were already mounted in resin and just needed to be reduced to diameter of 1 inch in order to fit the sample holders.
19 silver samples and 3 copper-based samples were prepared for electron microprobe measurements differently. The material sampled by drilling was fixed on an adhesive foil. From the others small pieces were chopped off and mounted. The samples were embedded in epoxy resin and then sanded and polished with cloth to provide a clean surface and avoid lead contamination.

All samples were cleaned in an ultrasonic bath and coated with carbon before measuring.

7.4 Electron Microprobe Analysis

All measurements were carried out with the Jeol JXA 8900R at the Institute for Geosciences of Goethe University Frankfurt. In 74 copper- and bronze sections the following 12 elements were analysed: Cu, Sn, S, Mn, Fe, Co, Ni, Zn, As, Ag, Sb and Pb. All measurements were carried out with a current of 30 nA, beam diameter of 6µm and a high voltage of 20kV. The results were ZAF corrected. Some were measured with a probe diameter

Element	X-ray	Crystal	Channel	Detection Limit	Peak		Background (BG)			
				[ppm]	Time	Position	Time [sec]		Position [mm]	
					[sec]	[mm]	BG+	BG-	BG+	BG-
Sb	Lα	PETJ	2	290	60	110.1	60	0	3.6	0
Ag	Lα	PETJ	2	230	60	133.1	60	0	2.3	0
Cu	Kα	LIF	2	370	20	107.2	10	10	2	1.5
As	Lα	TAP	3	310	60	105.5	60	0	4	0
Sn	Lα	PETJ	4	350	30	115.2	15	15	1.52	1.5
Pb	Mα	PETJ	4	520	90	169.2	0	90	0	2.5
S	Kα	PETJ	4	73	60	172.1	60	0	1.6	0
Zn	Kα	LIFH	5	470	20	100.1	10	10	3	1.5
Fe	Kα	LIFH	5	100	60	135	30	30	3	3.8
Ni	Kα	LIFH	5	150	40	115.7	20	20	1.5	1.5
Co	Kα	LIFH	5	170	40	124.8	20	20	3	4.5
Mn	Kα	LIFH	5	150	40	146.4	40	0	1.5	0

Table 7.1 Measurement conditions of the electron microprobe analysis for the copper-based artefacts as well as detection limits.

Element	X-ray	Crystal	Channel	Detection Limit	Peak		Background (BG)			
				[ppm]	Time	Position	Time [sec]		Postition [mm]	
					[sec]	[mm]	BG+	BG-	BG+	BG-
Sb	Lα	PETJ	2	330	60	110.1	60	0	3.6	0
Ag	Lα	PETJ	2	450	30	133.1	30	0	2.3	0
Pd	Lα	PETJ	2	260	60	139.9	60	0	4	0
Bi	Mβ	PETJ	2	500	60	157.2	30	30	4.1	5.5
Au	Lα	LIF	2	1580	60	88.8	0	60	0	1.7
Cu	Kα	LIF	2	220	60	107.2	30	30	2	1.5
As	Lα	TAP	3	360	60	105.6	60	0	4	0
Cr	Kα	PETJ	4	130	60	73.1	30	30	2.5	2
Sn	Lα	PETJ	4	210	60	115.3	30	30	1.52	1.5
Pb	Mα	PETJ	4	470	90	169.3	0	90	0	2.5
Ti	Kα	PETJ	4	1690	60	91.9	30	30	1.9	4.4
Zn	Kα	LIFH	5	240	60	100.4	30	30	3	1.5
Ni	Kα	LIFH	5	230	40	115.8	20	20	1.5	1.5
Co	Kα	LIFH	5	170	40	124.8	20	20	3	4.5
Mn	Kα	LIFH	5	180	50	146.4	50	0	1.5	0

Table 7.2 Measurement conditions and detection limits of the electron microprobe analysis for the silver artefacts.

of 3 µm due to smaller sample sizes caused by heavy corrosion.

The measurement condition avoids most of the interferences, though these could not be ruled out completely. Cobalt Kα interferes with Ni. When measured on pure Co, there is a signal of 1.5 wt% Ni. Due to the low Co contents in the samples the effect is below the detection limit and shows no effect on the results. Other interferences could be corrected (see below): Sn interferes with As and Sb (tin bronzes), Cu interferes with Ag, As and Mn (copper-based metals).

The exact measurement procedures used in the beginning and the progress are shown in the appendix A.1. The final measurement conditions are given in the table 7.1.

The silver samples were analysed with a different program. The measurement times had to be adjusted to a different element content. Therefore measurement time for silver was reduced and for copper extended. Further elements were included and some omitted. A total of 16 elements was analysed in the silver samples: Ag, Cu, Sb, Pd, Bi, Au, As, Cr, Sn, Pb, Ti, Pt, Zn, Ni, Co, and Mn. Inter-

Channel	1	2	3	4	5
Spectrometer crystal		PETJ/ LIF	TAP	PETJ	LIFH
Position		Sb (PETJ)	As	Sn	Zn
		Ag (PETJ)		Pb	Fe
		Cu (LIF)		S	Ni
					Co
					Mn

Table 7.3 Spectrometer configuration for copper samples.

Channel	1	2	3	4	5
Spectrometer crystal		PETJ/ LIF	TAP	PETJ	LIFH
Position		Sb (PETJ)	As	Cr	Pt
		Ag (PETJ)		Sn	Zn
		Pd (PETJ)		Pb	Ni
		Bi (PETJ)		Ti	Co
		Au (LIF)			Mn
		Cu (LIF)			

Table 7.4 Spectrometer configuration for silver samples.

ferences could be avoided but not completely. An interference of Pd and silver could not be eliminated. There is no detectable Pd in our samples so this interference has no consequences for this work. The exact parameters and measurement orders are given in the table 7.2 and 7.4

The interferences of Cu with Ag, As and Mn as well as Sn with Sb and As were corrected by the following formula:

$$EL_{COR} = EL_{RAW} - \left(\frac{EL_{RAW}(std)}{EL_{INT}(std)}\right) \times EL_{INT}$$

EL_{COR} Corrected Netto signal intensity of the interfered element in the sample

EL_{RAW} Measured netto signal intensity of the element that was interfered in the sample

$EL_{RAW}(std)[cts]$ Netto signal intensity of the interfered element in the standard

$EL_{INT}(std)[cts]$ Netto signal intensity of the interfering element in the standard

$EL_{INT}[cts]$ Netto signal intensity of the interfering element in the sample

After these corrections, the following method determined the detection limits (LOD):

(1) When measured on both slopes of the peak the mean of both measurements was determined. If the background was measured on one side of the peak, this value was used.

(2) For the detection limits 3σ of the background measurements (BG) were calculated to ensure a 99% probability of the detection limits. Therefore the follwing method was used:

$$LOD[cts] = 3 \times \sqrt{2} \times \sqrt{BG[cts]}$$

(3) As the detection limits were calculated as Netto signal intensity they have to be converted to wt%:

$$LOD\ [wt\%] = LOD[cts] \times \frac{conc_{sample}[wt\%]}{conc_{sample}[cts]}$$

The detection limits are given in table 7.1 and table 7.2.

8 Methods: Mass spectrometry

8.1 Requirements and procedure

With Mass spectrometry multiple measurements can be performed. First of all trace element contents as well as isotope ratios can be measured. Two different types are distinguished regarding the detection: Single collector (SC) and multi-collector (MC). The single collector mass spectrometer measures one isotope at a time whereas the multi collector mass spectrometer measures multiple isotopes parallel. The latter is very useful for isotope measurements because errors induced by fluctuating plasma beam are cancelled out. When measured one by one this fluctuation leads to big errors in the isotope ratios due to changes in the ionisation rate. When the isotopes are measured parallel, the errors caused by beam fluctuations are eliminated and the ratios are much more constant.

Modern mass spectrometers can determine very small element contents and do need comparably little sample material in order to measure isotopes. This method was not as precise in the 80's when the Nash Collection samples were examined the first time.

The Nash Collection samples are analysed with laser ablation. This method is applied to ablate material directly from the solid surface and to transport into the mass spectrometer for ionisation. The other samples taken with drilling or sawing were dissolved, diluted and then ionised after passing through a spray chamber into the plasma. For quality control the drilled samples are mounted as well to compare the results by solution and laserablation measurements.

Heavily corroded samples are excluded from this method. There can not be gained any information from oxides about trace elements or isotopes due to their chemical purity.

8.2 Sample Preparation

For Laserablation the already mounted samples were re-polished to remove recent superficial oxidation and carbon coating. Before the measurements the samples were cleaned with ethanol.

11 silver, 3 copper-based samples and 3 silver standards were selected for trace element measurement by solution-SC-ICP-MS: silver: 30-12-446, 30-12-605, 30-12-773, B16926a, B16931a-b, B17078a, B17082a, B17084, B17553a-b; copper-based: 30-12-696, 98-9-164, B17551; standards: AgA1, AgA2, AgA3.

For sample solutions Beakers were bleached with HNO_3 for 4 days. Samples and standards were weighed and solved in a solution of 0.5 ml 6M HCl and 0.5 ml 6M HNO_3. After dissolution the samples and standards were evaporated and taken up by 2% HNO_3. Different dilution factors due to different element contents. The dilution factor for silver is 40, for copper 20 and for the standards 50. In addition two multi element standard solutions were mixed and weighed for the silver and copper-based samples.

8.3 Laserablation

8.3.1 Trace Elements

To provide a clean surface the samples were polished and cleaned with ethanol. The measurements were carried out with a ThermoFinnigan Element2 single-collector inductively coupled plasma mass spectrometer at the Institute for Geosciences at Goethe Universty Frankfurt. A Resonetics RESOlution M-50 laser system with a wavelength of 193 nm was coupled with the mass spectrometer. The ICP-MS settings used for the measurements are described in table 8.1 and 8.2.

All elements were measured in low resolution mode. The gas flows and forward power were adjusted at each day of measurement for optimal signal intensity. For laserablation the measurable elements are limited to the available certified standards.

The used multiple certified copper and silver standards as well as the acquired isotopes are given in table 8.3.

Due to detector overload ^{60}Ni and ^{75}As were only measured in tin bronzes and ^{114}Cd, ^{115}In and ^{119}Sn in arsenical copper. The standards were measured before and after each set of 30 sample analyses. Per sample 10 points were randomly spread across the metal surface. The corroded areas of the samples were excluded from the measurements.

Since the analytical results gained by analysis are given in counts per second (cps) for each isotope measured

Parameter	Setting
Spotsize	67 µm
Laser energy	70 mJ
Repetition rate	4 Hz
Attenuator	25%
Pulse duration	20 nsec
Energy density on sample	< 2 J/m²

Tab. 8.1: Laser parameters during SC-ICP-MS measurements

Parameter	Setting
Carrier gas He/N	550/1.5 ml/min
Sample gas (Ar)	0.846 L/min
Auxiliary gas (Ar)	0.78 L/min
Oxidation rate	< 1 %
Forward Power	1250 W
Scanning Mode	Peak hopping
Samples per peak	30
Data acquisition	Electric Scan (EScan)
Dwell time	10 ms
Preablation	3 pulses
Analysis duration	60 sec
sample / skimmer cones	Al

Tab. 8.2: Tune settings of the SC-ICP-MS.

Silver	
Standards:	AgA1, AgA2, AgA3, AgRM1, AgRM2
Acquired Isotopes:	^{24}Mg, ^{27}Al, ^{28}Si, ^{48}Ti, ^{53}Cr, ^{55}Mn, ^{57}Fe, ^{59}Co, ^{60}Ni, ^{63}Cu (int. std), ^{65}Cu, ^{66}Zn, ^{72}Ge, ^{75}As, ^{77}Se, ^{103}Rh, ^{105}Pd, ^{106}Pd, ^{111}Cd, ^{114}Cd, ^{113}In, ^{115}In, ^{118}Sn, ^{121}Sb, ^{209}Bi
As-Ni-Copper	
Standards:	AgA1, AgA2, AgA3, AgRM1, AgRM2, BAM 376, Bronze A, C1251, C1252, 319 CKD, UE15
Acquired Isotopes:	^{24}Mg, ^{27}Al, ^{31}P, ^{48}Ti, ^{53}Cr, ^{55}Mn, ^{57}Fe, ^{59}Co, ^{66}Zn, ^{72}Ge, ^{77}Se, ^{103}Rh, ^{105}Pd, ^{106}Pd, ^{111}Cd, ^{114}Cd, In, ^{115}In, ^{119}Sn, ^{121}Sb (int. std.), ^{128}Te, ^{130}Te, ^{194}Pt, ^{195}Pt, ^{197}Au, ^{206}Pb, ^{209}Bi
Tin bronze	
Standards:	AgA1, AgA2, AgA3, AgRM1, AgRM2, BAM 376, Bronze A, C1251, C1252, 319 CKD, UE15
Acquired Isotopes:	^{24}Mg, ^{27}Al, ^{31}P, ^{48}Ti, ^{53}Cr, ^{55}Mn, ^{57}Fe, ^{59}Co, ^{60}Ni, ^{66}Zn, ^{72}Ge, ^{75}As, ^{77}Se, ^{103}Rh,^{105}Pd, ^{106}Pd, ^{11}Cd, ^{113}In, ^{121}Sb(int. std), ^{128}Te, ^{130}Te, ^{194}Pt, ^{195}Pt, ^{197}Au, ^{206}Pb, ^{209}Bi

Tab. 8.3: List of standards and acquired isotopes used for trace element analysis. Different standards were used for different metals.

the data had to be processed. To acquire corrected data in ppm the Glitter™ Software was used for processing. The software provides a tool for selection of preablation blank and sample to execute blank correction for each analysis. For element concentrations the internal standard

Measured isotope	Interfering isotope / molecule
^{24}Mg	$^{12}C_2^+$
^{27}Al	$^{12}C^{15}N^+$, $^{13}C^{14}N^+$, $^{1}H^{12}C^{14}N$
^{31}P	$^{15}N^{16}O^+$, $^{14}N^{17}O^+$, $^{13}C^{18}O^+$, $^{12}C^{18}O^{1}H^+$ etc.
^{48}Ti	$^{36}Ar^{12}C^+$, $^{14}N^{17}N_2^+$, $^{32}S1^{6O+}$ etc.
^{57}Fe	$^{40}Ar^{17}O$
^{60}Ni	$^{120}Sn^{2+}$
^{75}As	$^{40}Ar^{35}Cl$, $^{38}Ar^{37}Cl$, $^{59}Co^{16}O$, $^{36}Ar^{38}Ar^{1}H$
^{103}Rh	$^{63}Cu^{40}Ar$, $^{206}Pb^{2+}$
^{105}Pd	$^{65}Cu^{40}Ar$
^{106}Pd	^{106}Cd
^{113}In	^{113}Cd
^{114}Cd	^{114}Sn
^{115}In	^{115}Sn
^{130}Te	^{130}Ba

Tab. 8.4: List of isobaric and polyatomic interferences with the acquired isotopes.

as well as the standards with certified values for each element are selected for data processing to calculate the concentration with regard to the particular standard used. The results are corrected as well for fractionation effects induced by laserablation.

Multiple isobaric interferences were identified during the measurements (cf. tab. 8.4).

Cd and Ba show no impact on the results as for In, Pd and Te two isotopes were measured. Cd is below 6 ppm in the copper-based samples and therefore ^{106}Pd and ^{113}In could be used for results. The main elements Sn, Cu and Pb significantly influence the analytical results of the interfered isotopes ^{103}Rh, ^{105}Pd, ^{114}Cd and ^{115}In, which hence had to be excluded from the results. The isotope ^{57}Fe showed highly erroneous results in all measurements as a result of the interference with ArO and was therefore excluded. The light isotopes ^{24}Mg, ^{27}Al, ^{31}P and ^{48}Ti have multiple polyatomic interferences with the gases in the atmosphere as well as carrier gases for the laser. Therefore these elements were excluded from the results.

Matrix effects occurred during laserablation measurements due to the presence of different main elements. The following different matrices were involved: Sn bronze, copper, leaded bronze and silver. The different matrices affect in varying degrees each element measured. Especially Pb and Bi were heavily affected by silver and copper matrix and matrix matched standards have to be used. The presence of Sn affects the matrix of Cu and other elements strongly. For the tin bronzes partly silver standards could be used, whereas for As-Ni-Copper more matrix effects were observed using silver standards. Furthermore the pure copper standard C1251 as well as the leaded bronze were excluded as these are no matrix matched standards for these specific standards. All of the silver samples were calculated on the basis of the three silver standards: AgA1, AgA2, AgA3.

Isotope	Standards
^{31}P	BAM 376, Bronze A, C1251, C50, CKD319, UE 15
^{48}Ti	AgA1, AgA2, AgA3, AgRM2, BAM 376
^{53}Cr	AgA1, AgA2, AgA3, AgRM1, AgRM2, BAM 376, C1251, C1252
^{55}Mn	BAM 376, C50, CKD 319, UE 15
^{59}Co	AgA1, AgA2, AgA3, BAM 376, C1251, C1252
^{60}Ni	BAM 376, C1251, C1252, C50, CKD 319, UE 15
^{66}Zn	BAM 376, C1251, C1252, C50, CKD 319, UE 15
^{72}Ge	AgA1, AgA2, AgA3
^{75}As	AgA1, AgA2, AgA3, AgRM1, AgRM2, BAM 376, C1251, C1252, C50, CKD 319, UE 15
^{77}Se	AgA1, AgA2, AgA3, AgRM1, AgRM2, BAM 376, C1251, C1252
^{106}Pd	AgA1, AgA2, AgA3, AgRM1, AgRM2
^{11}Cd	AgA1, AgA2, AgA3, AgRM1, AgRM2, BAM 376, C1251, C1252
^{113}In	AgA1, AgA2, AgA3, AgRM1, AgRM2
^{128}Te	AgA1, AgA2, AgA3, AgRM1, AgRM2, BAM 376, C1251, C1252
^{130}Te	AgA1, AgA2, AgA3, AgRM1, AgRM2, BAM 376, C1251, C1252
^{194}Pt	AgA1, AgA2, AgA3, AgRM1, AgRM2
^{195}Pt	AgA1, AgA2, AgA3, AgRM1, AgRM2
^{197}Au	AgA1, AgA2, AgA3, AgRM1, AgRM2, C1251,C1252
^{206}Pb	BAM 376, Bronze A, C1251, C1252, C50, CKD 319
^{209}Bi	BAM 376, C1251, C1252, C50, CKD 319

Table 8.5: Tin Bronzes: List of elements referred to individual standards.

Isotope	Standards
53Cr	AgA1, AgA2, AgA3, AgRM1, AgRM2,
	BAM 376, C1252
55Mn	BAM 376, C50, CKD 319, UE 15
59Co	AgA1, AgA2, AgA3, BAM 376, C1252
66Zn	BAM 376, C1252, CKD 319
72Ge	AgA1, AgA2, AgA3
77Se	BAM 376, C1252
106Pd	AgA1, AgA2, AgA3, AgRM1, AgRM2
111Cd	AgA1, AgA2, AgA3, AgRM1, AgRM2,
	BAM 376, C1252
113In	AgA1, AgA2, AgA3, AgRM1, AgRM2
119Sn	BAM 376, Bronze A, C1252, CKD 319, UE 15
128Te	BAM 376, C1252
130Te	BAM 376, C1252
194Pt	AgA1, AgA2, AgA3, AgRM1, AgRM2
195Pt	AgA1, AgA2, AgA3, AgRM1, AgRM2
197Au	AgA1, AgA2, AgA3, AgRM1, AgRM2, C1252
206Pb	BAM 376, Bronze A, C1252, CKD 319
209Bi	BAM 376, C1252, CKD 319

Tab. 8.6: As-Ni-Copper: List of elements referred to individual standards.

Lists for each isotope related to the specific standards used for calculation of the copper-based metals according to different sample matrices is given in tab. 8.5 and 8.6.

This approach highlights the importance of multiple matrix matched standards used for laserablation, rather than using a single standard for calculation. Although the standards used in this study are not ideal, the usage of multiple standards repeal the matrix effect induced errors. The maximum relative deviation for each isotope at 10% on each standards is in good agreement with other studies of laserablation-based trace element analysis.

8.3.2 Lead Isotopes

To perform Pb isotope measurements a Resonetics RESOlution M-50 laser system with a wavelength of 193 nm was coupled with the mass spectrometer. The mass spectrometer ThermoScientific Neptune was used. All measurements were performed at the Institute for Geosciences at Goethe University Frankfurt. On two days the Aridus and Aridus II were connected to the mass spectrometer to introduce Tl to the system for mass bias correction. Some samples were measured with and without Tl and compared to solution-based Pb isotope data from Begemann and Schmitt-Strecker (2009).

The laser- and mass spectrometer settings were used according to tab. 8.7 and 8.8.

The NIST SRM 610 was measured every 5-6 samples to provide an overview over the drift in the plasma during the measurements. NIST 610 was measured with 4.4 J/cm² fluence and a spotsize of 213µm. For comparison a bronze standard (Bronze A by MBH)(dissolved in 0.5 ml 6M HCl and 0.5 ml 6M HNO_3), two silver standards RAgGP6 and AgA2 (dissolved in 1 ml HNO_3) were diluted to 1 ppm and measured by solution MC-ICP-MS as well as laserablation for matrix corrections.

Due to differences in the samples microstructure, corrosion status, Pb concentration as well as material types (silver, bronze, As-Ni-copper) the fluence as well as the spotsize had to be adjusted for each sample individually. Especially for the copper-based metals it was difficult to reach a ^{204}Pb signal above 100 mV. It was observed that absolute errors increase above 10^{-2} when the ^{204}Pb signal drops below 100 mV. It is desired to reduce absolute errors below 10^{-3} therefore the laser parameters were adjusted individually whereas the tune parameters of the mass spectrometer stayed the same for each measurement day. Each sample was measured at least three times on different spots, to evaluate inhomogeneities and minimise errors.

For evaluation purposes a R-script was written to perform all the corrections explained in the following, except for standard-sample-bracketing. The script is given in the appendix (cf. A.2). For background correction the blank was measured in between the measurements and observed over the day.

Parameter	Setting
Spotsize	120-380 µm
Laser energy	60-100 mJ
Repetition rate	12-20 Hz
Attenuator	25%
Fluence	1.7 - 3.5 Jcm²
Pulse duration	20 ns

Table 8.7 Laser parameters during MC-ICP-MS measurements of Pb isotopes

Parameter	Setting
Coolant (torch)	15.25 - 15.5 L/min
Carrier gas He / N_2	150 - 450 / 0.5 - 2 ml/min
Sample gas (Ar)	0.9 - 1.2 L/min
Auxiliary gas (Ar)	0.7 - 1 L/min
Additional Gas (Ar)	0.3 - 0.6 L/min
Extraction Voltage	~2000 V
Forward Power	1200 - 1270 W
Scanning Mode	static
Integration Time	0.524 s
Cycles	80
Collector configuration	L4(201Hg), L3(202Hg), L2(203Tl), L1(204Pb), C(205Tl), H1(206Pb), H2 (207Pb), H3(208Pb)
Sample / Skimmer cones	Ni-H

Tab. 8.8 Tune settings of the MC-ICP-MS Neptune (Pb isotopes).

The mean of the blanks of the same measurement day was used to correct the background:

$$I_{BG} - corr = I_{sample} - I_{BG}$$

$I_{BG} - corr$ Background corrected intensity of the acquired isotope
I_{sample} Raw intensity of the acquired isotope
I_{BG} Background intensity of the measured isotope without ablation

After subtracting the background ^{204}Pb was corrected for the interference of ^{204}Hg. First the ratio is mass bias corrected and then corrected for mercury. For the mass bias correction see the described calculations below. As in some of the samples an elevated Hg-Signal was observed, this interference correction is very important:

The Hg-corrected ^{204}Pb intensity is then used to calculate the raw Pb isotope ratios $^{208}Pb/^{204}Pb$, $^{207}Pb/^{204}Pb$ and $^{206}Pb/^{204}Pb$.

8.3.2.1 Mass bias correction with Tl (Solution)

This correction was applied only to the samples measured of the chromatographically separated Pb solution. The laser measurements were corrected in a different way. This step involves the calculation of the mass bias with Tl. The natural Tl ratio is assumed as: $^{205}Tl/^{203}Tl = 2.3872$. The measured Tl-ratio is different to the natural ratio as mass fractionation occurs.

The Tl-correction is performed with the Exponential Law by (Russel, Papanastassiou, Tombrello, 1980):

$$\left[\frac{(^{y}Pb)}{(^{x}Pb)}\right]_{Tl} = \left[\frac{(^{y}Pb)}{(^{x}Pb)}\right]\left[\frac{M(^{205}Tl) = 204.974}{M(^{203}Tl) = 203.973}\right]^{\beta}$$

β is the exponential which is used in the next step:

$$\beta = \frac{ln\frac{2.3872}{(^{205}Tl/^{203}Tl)_{meas}}}{ln\frac{M(^{205}Tl) = 204.974}{M(^{203}Tl) = 202.972}}$$

The standard errors of the first day of silver measurements are averaged 0.12 % for $^{206}Pb/^{204}Pb$, 0.086 % for $^{207}Pb/^{204}Pb$, 0.11 % for $^{208}Pb/^{204}Pb$, 0.059 % for $^{207}Pb/^{206}Pb$ and 0.080 % for $^{208}Pb/^{206}Pb$. On the second day of silver measurements the standard errors are on average 0.025 % for $^{206}Pb/^{204}Pb$, 0.029 % for $^{207}Pb/^{204}Pb$, 0.034 % for $^{208}Pb/^{204}Pb$, 0.010 % for $^{207}Pb/^{206}Pb$ and 0.012 % for $^{208}Pb/^{206}Pb$.

8.3.2.2 Standard-sample bracketing (Laserablation)

The mounted copper-based samples were mass bias and drift corrected by standard-sample bracketing (SSB) on the mean of the NIST 610 measured before and after each sample block. The measured NIST 610 values were normalised to the published values of Woodhead and Hergt (2001).

Although this method was applied successfully the measured ratios of this study differed from the MC-ICP-MS data of the same artefacts of Begemann and Schmitt-Strecker (2009). The offset is most likely caused by a laser induced difference in mass bias between the NIST 610 glass and the metal matrix. Another possible reason is the difference in mass discrimination within the plasma due to the presence of copper or silicium ions. Therefore a matrix correction was performed on the laserablation data explained in the following.

8.3.2.3 Matrix correction with the exponential law

It is assumed, that the thermal effects of the laser cause a difference in mass bias when it comes to laserablation of different sample matrices. Glass behaves in a different way when thermally heated than metal. The mass bias is corrected via the exponential law of Russel, Papanastas-

siou, Tombrello (1980). The β value is calculated from the differences in measured Pb isotope ratios (cf. sec. 8.3.2.1). As some artefacts of this study were also analysed with MC-ICP-MS out of a separated Pb solution and published by Begemann and Schmitt-Strecker (2009), both laser- and solution data were combined to calculate the β of the laser induced matrix effects. This calculation was performed for the ^{204}Pb normalised Pb isotope ratios of each artefact. The molar mass M of the different isotopes has to be included as the mass bias is dependent on the relative mass differences. The β was calculated as follows with the ^{206}Pb/^{204}Pb ratio as an example:

$$\beta = \frac{ln\frac{(^{206}Pb/^{204}Pb)_{Beg-S-Str2009}}{(^{206}Pb/^{204}Pb)_{laser}}}{ln\frac{M(^{206}Pb) = 205.9745}{M(^{204}Pb) = 203.973}}$$

The calculated β-values of the three ratios ^{206}Pb/^{204}Pb, ^{207}Pb/^{204}Pb, and ^{208}Pb/^{204}Pb were averaged with a result of β = 0.0723545. The measured ratios were then corrected with the same formula, as the Tl-correction, with the calculated β as exponential:

$$\left[\frac{(^{y}Pb)}{(^{x}Pb)}\right]_{corr} = \left[\frac{(^{y}Pb)}{(^{x}Pb)}\right]_{meas}\left[\frac{M(^{y}Pb)}{M(^{x}Pb)}\right]^{\beta=0.0723545}$$

8.3.3 Copper Isotopes

The samples were polished and cleaned with ethanol before the measurements to provide a clean surface.

Cu isotope measurements were carried out with deep ultraviolet femtosecond laser ablation multi-collector inductively coupled plasma mass spectrometry (UV-fsLA-MC-ICP-MS) at the Institute of Mineralogy, Leibniz University Hannover in cooperation with Marina Lazarov. The femtosecond laser system was chosen for Cu isotope measurements due to less fractionation effects as well as less material consumption. The latter is particularly interesting for archaeological artefacts as considerably less material is consumed compared to nanosecond laser systems. The MC-ICP-MS used is a Thermo Scientific Neptune Plus and the coupled laser system is a Spectra Physics Solstice, USA. The output beam of the laser has a wavelength 194 nm in deep ultraviolet region (Lazarov and Horn, 2015). Due to different sample matrices the repetition rate varied between 5 and 7 Hz and the fluence between 0.3 and 0.4 J/cm² to provide similar Cu signal intensities. A spray chamber was coupled before the plasma torch to add the spike of 1-2 ppm NIST SRM 986 Nickel standard solution. A concentration of 2 ppm Ni was added to the high-Ni-copper-based samples (Ni > 1 wt%). The isotopes ^{60}Ni, ^{61}Ni, ^{62}Ni, ^{64}Ni, as well as ^{63}Cu and ^{65}Cu were measured simultaneously. The ratio ^{62}Ni/^{60}Ni was used for internal mass bias correction, because it is better reproducible than ^{61}Ni/^{60}Ni (Lazarov and Horn, 2015). The following settings were used for the measurement:

Parameter	Setting
Spotsize	20 - 25 µm
Laser energy	0.03 mJ
Repetition rate	5 - 7 Hz
Pulse duration	200 fs
Energy density on sample	0.3-0.4 J/m²

Table 8.9 Laser parameters during SC-ICP-MS measurements

Parameter	Setting
Coolant (torch)	15.6 L/min
Carrier gas He	0.4 L/min
Sample gas (Ar)	0.9 - 1 L/min
Auxiliary gas (Ar)	0.9 Lmin
Extraction Voltage	~2000 V
Forward Power	1300 W
Scanning Mode	static
Collector configuration	L3(60Ni), L2(61Ni), L1(62Ni), C(63Cu), H1(64Ni (64Zn)), H3(65Cu)
Nebuliser	PFA micro-flow
Sample uptake	~100 µl/min
Sample / Skimmer cones	Al-H

Tab. 8.10 Tune settings of the MC-ICP-MS Neptune

The gas flows and spotsize were adjusted after each sample change for optimal signal intensity. Line analyses were performed on samples and standards to avoid fractionation effects. The copper metal NIST SRM 976 was used as a standard for mass bias correction with sample-standard bracketing method. The NIST SRM 976 was measured before and after each block of 3 samples. For matrix matched correction one brass and copper metal sample were analysed for comparison.

Offline background corrections and mass discrimination corrections were carried out with a modified Excel-Macro (LamTool written by Jan Košler, University Bergen, Norway) (Lazarov and Horn, 2015). These corrections were applied individually on each cycle of the analyses.

The results are displayed as δ^{65}Cu ratios [‰] with the following equation:

$$\delta^{65}Cu = \left[\left(\frac{\left(\frac{^{65}Cu}{^{63}Cu}\right)_{sample}}{\left(\left(\frac{^{65}Cu}{^{63}Cu}\right)_{NIST\ SRM\ 976}\right)} - 1\right) \times 1000\right]$$

The errors are between 0.004 and 0.2 SE ‰.

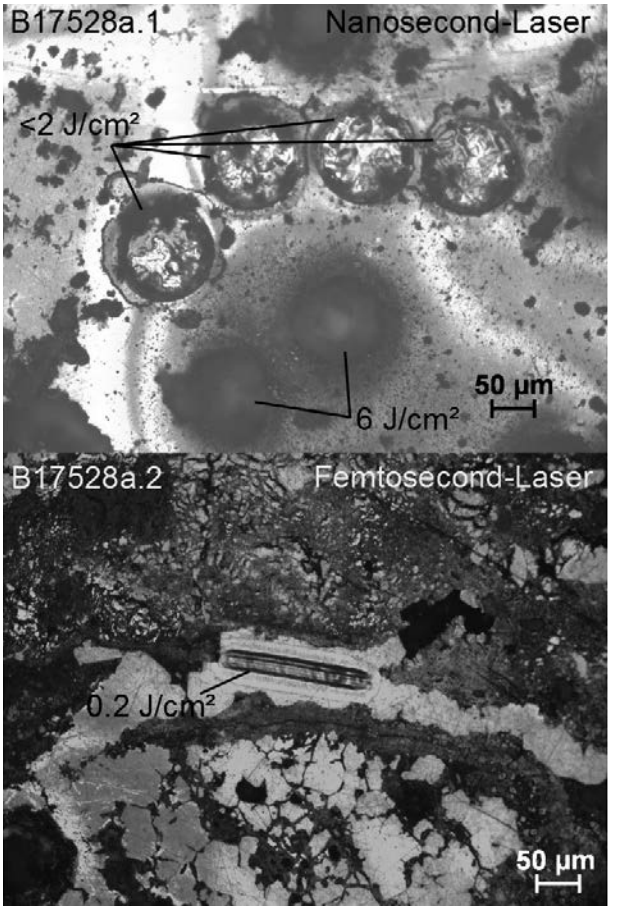

Fig. 8.1: Comparison of nanosecond- and femtosecond-laser-ablation craters. Above: point analysis with the nanosecond-laser where craters created by a laser beam with <2 J/cm² and 6 J/cm² are displayed. Below: line scan of the femtosecond-laser with 0.2 J/cm².

8.3.4 Destructive Laserablation

Nanosecond-laserablation consumes a lot of the sample material, although it is generally considered a non-destructive analysis. The metal ablated by the laser is gone after analysis and the ablated areas are visible with the naked eye. Therefore laserablation is *not* a non-destructive type of analysis. A femtosecond-laser consumes much less sample material compared to the nanosecond-laser and is therefore recommended for archaeological objects, although the femtosecond laser irretrievably consumes material as well. A few samples had to be excluded from further analysis as there was no sample material left after laserablation.

The picture reveals the destructive impact of the laser beam on the sample's surface (see fig. 8.1). In the figure above the difference between 6 J/cm² and less than 2 J/cm² becomes clear. A higher energy density on the sample surface induces a deeper crater surrounded by a bigger radius of sputtered material. Whereas a lower energy density causes a crater less deep with less sample material sputtered on the surface. A lower energy density shows less melting effects on the samples as well. As melted metal especially when containing Pb causes fractionation effects between the elements or isotopes with lower or higher melting points. The femtosecond laser shows even less thermal effects as melting compared to the nanosecond laser (LaHaye, et al., 2015). It removes less material and is therefore recommendable for archaeological objects, where limited material is available. It is considerably useful for measurement of isotope ratios as the femtosecond laser induces less fractionation effects (Lazarov and Horn, 2015).

8.4 Wet chemical measurements of Pb and Cu isotopes

The sample preparation method was performed in the clean laboratory of the Goethe-University of Frankfurt. In the process were ultra-pure chemicals used only. Three copper-based metal samples were dissolved in HNO_3 and HCl (30-12-696, B17551, 98-9-164). Eleven silver metal samples were dissolved in 1ml 6M HNO_3 (30-12-446, 30-12-605, 30-12-773, B16926a, B16931a-b, B17078a, B17082a, B17084, B17553a-b). Both were evaporated and converted in 0.6 M HBr for column chemistry procedure. The columns were filled with Dowex 1x8 100-200 mesh resin. The cleaning of the columns and resin before separation involved different steps of MilliQ-water, HNO_3 and HCl, the Cu and Pb solution were separated in ion exchange columns by 0.6 M HBr and 6 M HCl (Horwitz, et al., 1994). Both solutions were evaporated and taken up by 2 % HNO_3. The resulting 1 ppm lead solution was spiked with a 100 ppb Tl-solution (NIST SRM 997), whereas the Cu solution was spiked with 1 ppm Ni-solution (NIST SRM 986) for mass bias correction. A blank was prepared for each Cu and Pb as well as each day of ion exchange separation following the same procedures as the samples.

8.4.1 Wet chemical Pb isotope measurements

The Pb isotope measurements were performed with the MC-ICP-MS Thermo Scientific Neptune of the Institute for Geosciences at Goethe University Frankfurt. The Standard NIST SRM 981 with a dilution of 500ppb was measured before and after a set of three samples. The samples were diluted individually to achieve the same signal intensity as the standard (500 ppb). The exact parameters used for measurements are displayed in tab. 8.11. The measurement errors are on average 0.027 % for $^{206}Pb/^{204}Pb$, 0.031 % for $^{207}Pb/^{204}Pb$, 0.035 % for $^{208}Pb/^{204}Pb$, 0.0086 % for $^{207}Pb/^{206}Pb$ and 0.012 % for $^{208}Pb/^{206}Pb$ in two times standard deviation.

Parameter	Setting
Coolant (torch)	15.5 L/min
Sample gas (Ar)	1.155 L/min
Auxiliary gas (Ar)	0.95 L/min
Extraction Voltage	~2000 V
Forward Power	1190 W
Scanning Mode	static
Integration Time	2.054 s
Cycles	40
Collector configuration	L4(201Hg), L3(202Hg), L2(203Tl), L1(204Pb), C(205Tl), H1(206Pb), H2 (207Pb), H3(208Pb)
Sample uptake	~50 µl/min
Sample / Skimmer cones	Al-H
Resolution	Low

Tab. 8.11: Tune settings of the MC-ICP-MS Neptune (Pb isotopes)

Parameter	Setting
Coolant (torch)	15.25 L/min
Sample gas (Ar)	1.057 L/min
Auxiliary gas (Ar)	0.9 L/min
Extraction Voltage	~2000 V
Forward Power	1221 W
Scanning Mode	static
Integration Time	2.054 s
Cycles	40
Collector configuration	L3(60Ni), L2(61Ni), L1(62Ni,) C(63Cu), H1(64Ni), H2(64.5), H3(65Cu), H4(65.5)
Sample uptake	~50 µl/min
Sample / Skimmer cones	Al-H
Resolution	Low

Tab. 8.12: Tune settings of the MC-ICP-MS Neptune (Cu isotopes)

8.4.2 Wet chemical Cu isotope measurements

The Pb isotope measurements were performed with the MC-ICP-MS Thermo Scientific Neptune. The Standard NIST SRM 976 with a dilution of 300ppb was measured before and after a set of five to six samples. The samples were diluted individually to achieve the same signal intensity as the standard (300 ppb). The exact parameters used for measurements are displayed in tab. 8.12. The measurement errors are between 0.03 and 0.13 ‰ in two times standard deviation.

8.5 Accuracy and precision - Laserablation in comparison with wet chemical measurements

The standard NIST 610 was measured over 6 days and could be reproduced on each day (cf. fig. 8.4). Even though the errors are higher than from wet chemical measurements, the measured values are in good agreement with literature data (Woodhead and Hergt, 2001).

Only a few samples could be measured by both laserablation and wet chemical procedure. As the silver metal was drilled, as well as the bulls head (30-12-696), a proportion of the drilling was embedded in epoxy resin and another proportion dissolved. The comparison of both analysis methods is displayed in the diagrams in fig. 8.3. In the ^{204}Pb-normed diagrams the laserablation analyses show an offset to lower Pb isotope ratios, whereas the ^{206}Pb-normed data shows a smaller offset to higher ratios regarding the laserablation analysis. During the laserablation analysis of the silver metal the washout time was considerably higher (> 15 min.) than that of the measurement days with copper-based metals due to the dirty membrane in the Aridus used at this day. This had an impact on the blank as well, as it was still higher than on copper-based metal measurements. This could be one factor leading to higher errors when measuring Pb isotopes in a silver matrix with laserablation. On the other hand the Pb isotope measurement by laserablation was repeated another day with the same result that the results are not fitting to the wet chemical data.

Furthermore the mass bias of the Pb isotopes is possibly influenced by the different matrices. Silver ions have a higher mass (107 and 109 amu) than copper (63 and 65 amu). This could have an effect on the mass discrimination occurring in the plasma. It is expected that lower masses are not influencing the higher Pb isotope masses (204, 206, 207 and 208 amu) within the plasma. The more ions of a higher mass are present in the plasma the more likely is an influence on the mass discrimination.

In addition laser induced thermal effects occur during the laser pulses on the samples surface. The thermal effects are highly influenced by the laser energy density, repetition rate, pulse length, the spotsize and the depth of the laser crater (I. Horn, pers. comm., Oct. 2016). So one factor is the ablated volume. The other is the pulse duration, the longer the pulse, the higher the thermal effect. A nanosecond-laser has a relatively high pulse duration. When the laser pulse hits the sample's surface heat conduction occurs and for a nanosecond laser pulse a zone of approximately a few µm is heat affected and shows melting effects on the surface (Chichkov, et al., 1996; Horn, Guillong and Günther, 2001). The melting effects are affecting the ablation behaviour of the target material. The ablation behaviour is dependent on several factors as thermal conductivity, melting point, critical temperature etc. (Miotello and Kelly, 1999; Lorazo, Lewis

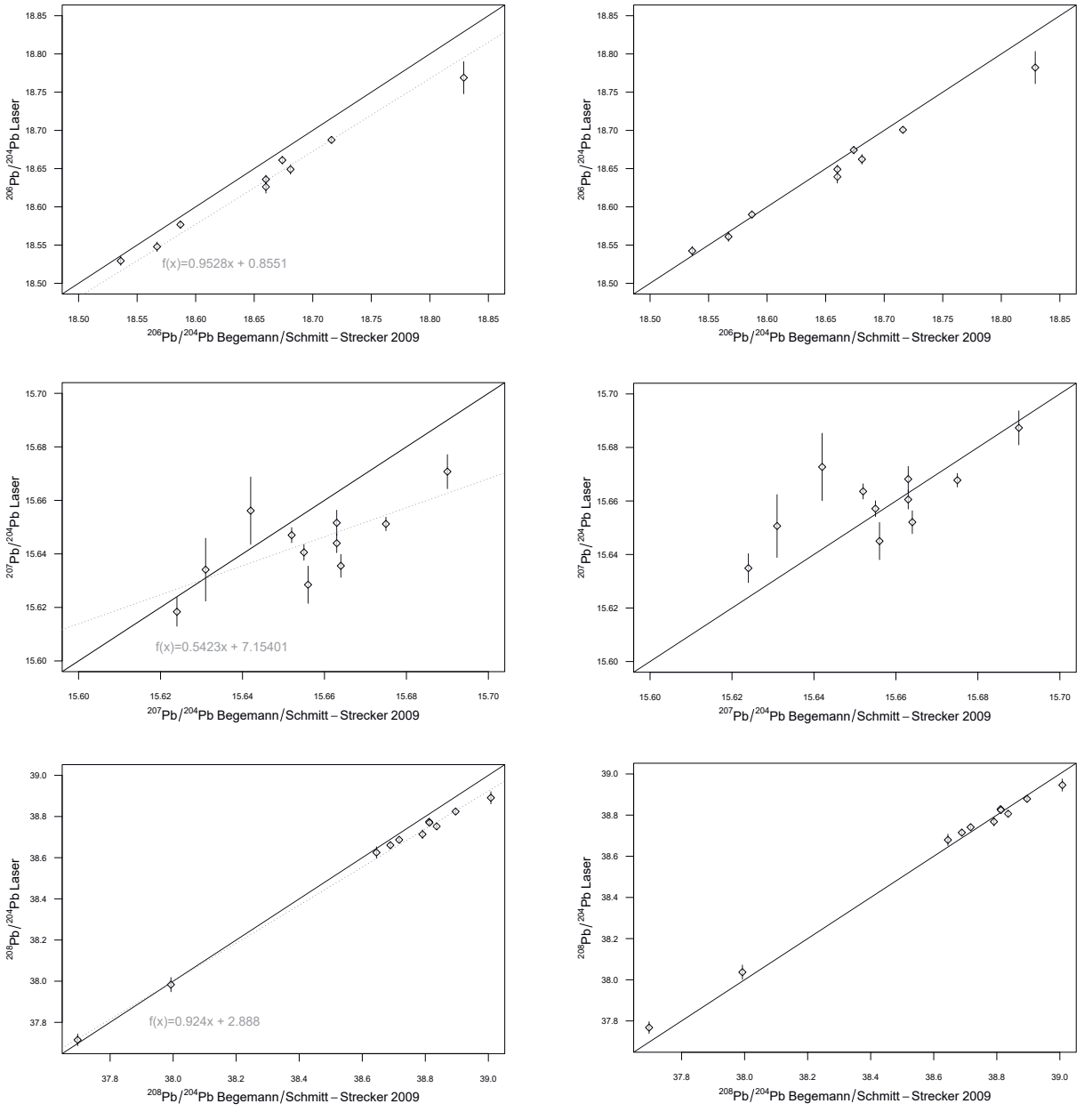

Fig. 8.2: Comparison of different Pb isotope ratios of laserablation measurements of those samples that were measured also by Begemann and Schmitt-Strecker (2009). The laser induced mass bias corrected data are displayed on the the right side, whereas the not corrected data are on the left.

and Meunier, 2006); for a good laser ablation analysis melting effects should be kept to a minimum, due to its influence on the particle size distribution. Melting effects are supporting the formation of bubbles which are leading to irregular distributed particles and particle sizes (Miotello and Kelly, 1999). This is affecting the ionisation behaviour in the plasma, as smaller particles are easier ionised than bigger particles which additionally bear the danger of damaging the slits of the mass spectrometer (Guillong, Horn and Günther, 2003; Horn and Blanckenburg, 2007). Changes in the particle size distribution due to deep drilling or melting effects are effecting the ionisation in the plasma and therefore the mass bias massively (Horn, Guillong and Günther, 2001; Guillong, Horn and Günther, 2003). Ag has a lower melting point, a higher thermal conductivity, a lower ionisation potential and a lower bond dissociation energy than Cu. Because of its thermodynamic proportions it is easier affected by heating effects than Cu and therefore more sensitive to the laser ablation process. Although for the measurements in this study a low energy density of 1.8 J/cm² was chosen, the pulse length of the nanosecond-laser was probably too high and caused melting effects in the silver metal. For this reason only the wet chemical measurements were used for further evaluation and interpretation of the Pb isotope analysis of the silver metal.

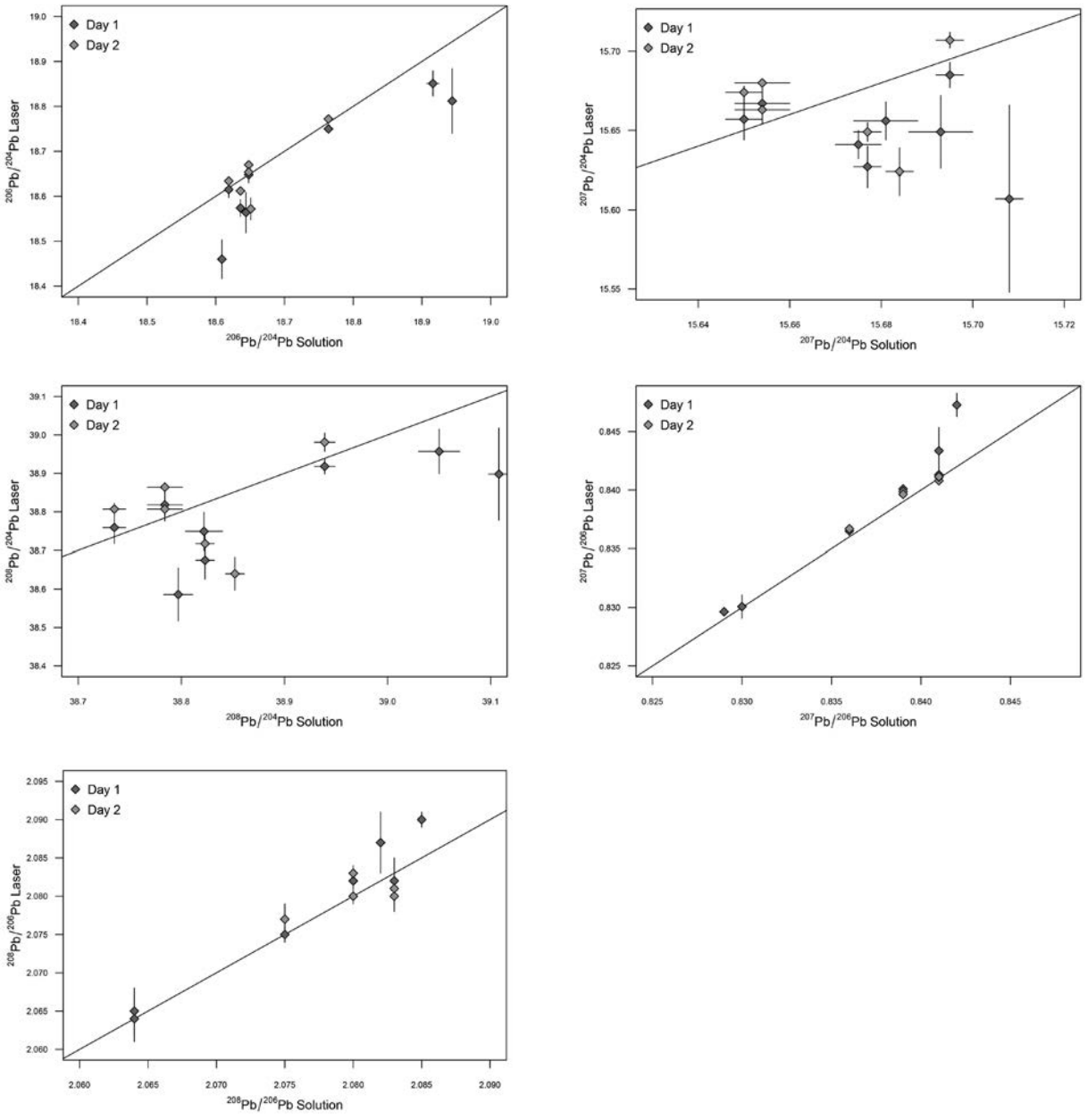

Fig. 8.3: Comparison of different Pb isotope ratios of wet chemical (solution) and laserablation (laser) measurements of those samples that were measured with both methods.

The Pb isotope ratios of the copper-based metal samples display a difference compared to the values measured by Begemann and Schmitt-Strecker (2009) of those artefacts measured by both working groups. This difference is most likely caused by laser induced matrix effects and a therefore different mass bias (cf. fig. 8.2). The matrix effect corrected data are in better agreement with those of Begemann and Schmitt-Strecker (2009), although not perfectly. The 207Pb/204Pb-ratio shows a bigger offset, although the natural variability of the 207Pb is smaller than the other Pb isotopes. As the intensity of the 204Pb was very low during the measurement, ratios based on 204Pb are likely to have a higher error than the 206Pb based ratios. As the errors of the Pb isotope data of Begemann and Schmitt-Strecker (2009) are not published, an evaluation, whether some outliers are still within error range, cannot be determined. Further deviation could be caused by small heterogeneities within the artefacts.

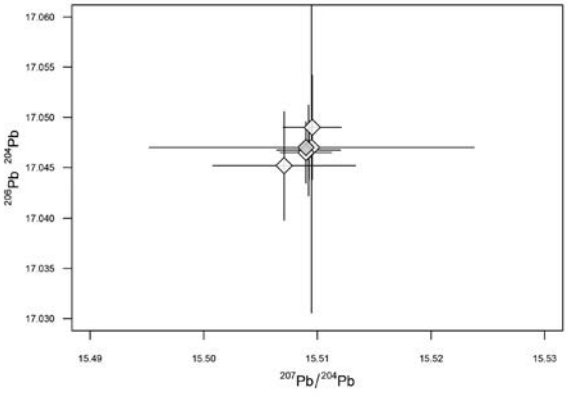

Fig. 8.4: $^{207}Pb/^{204}Pb$ versus $^{206}Pb/^{204}Pb$ ratios of the NIST 610 of laser-ablation measurements in comparison with double-spike corrected measurements of Woodhead and Hergt, 2001 (grey diamond).

8.6 Graphics

All diagrams of chemical and isotope data in the results and discussion section of this thesis were conducted with the program RStudio. For the plots the following R packages were used: ggplot2 (Wickham, 2009), ggtern (Hamilton, 2017), viridis (created by Stéfan van der Walt and Nathaniel Smith).

9 Beginnings of copper metallurgy

9.1 The emergence of copper base metal and its alloys

9.1.1 11th to 9th millennium BCE

Before early mankind discovered metal as a useful material for many applications, the use of copper ores (e.g. malachite) for the manufacture of beads and other kinds of adornment could be considered as predecessor of metal working. The outcrops of gossans and the colourful minerals occurring there as well as the metallic lustre of sulphide minerals beneath the secondary mineralisation (e.g. galena, pyrite, etc.) might have drawn the attention of humans already in the Neolithic period.

The earliest intentional use of copper ores was established at the Neolithic sites (11th to 9th millennium BCE) of Shanidar, Zawi Chemi (NE Iraq), Hallan Çemi (E Turkey), and Rosh Horesha (Israel) (cf. fig. 9.1) (Roberts, Thornton and Pigott, 2009) .

9.1.2 8th to 7th millennium BCE

Çayönu Tepesi (cf. fig. 9.1) is one of the oldest sites (7250 - 6750 BCE) where copper artefacts were uncovered (approximately 100 artefacts made of native copper) (Stech, 1999; Roberts, Thornton and Pigott, 2009), although publications differ in date for the copper beads: Pernicka (1990) states a calibrated ^{14}C-date of 8400 - 7500 BCE, whereas Stech's (1999) dating is based on Braidwood, Çambel and Schirmer, 1981 (7250 - 6750 BCE). Anyhow the youngest date of Çayönu Tepesi's copper beads can be roughly set in the first half of the 7th millennium BCE. Furthermore hundreds of malachite disc beads as well as debris from malachite processing were discovered in Çayönu Tepesi (Stech, 1999). These findings are roughly contemporary with copper beads from Aşıklı Höyük (Stech, 1999). Other presumably early copper artefacts were excavated at Nevalı Çori, although the chemical composition suggests the artefacts to be made of smelted copper rather than native copper and thus indicating a potentially later dating for these findings. Though the theory of the first use of native copper prior to development of smelting technology is debatable (see sec. 9.2.1). In the Levant at Tell Ramad, where one further copper bead was discovered, that is related to the 8th millennium BCE (Roberts, Thornton and Pigott, 2009). Malachite has been discovered in archaeological excavations at the preceramic Neolithic sites of Basta, Barga, Beidha, Nahal Issaron, Uvda valley, Ain Ghazal, and Feinan in the Levant (Hauptmann, 2000).
Çatalhöyük revealed a few copper metal artefacts likely produced of native copper, dating to the 7th millennium BCE (Birch, Rehren and Pernicka, 2013). Several ore minerals as galena were discovered in Çatalhöyük, probably in order to manufacture beads, rather than smelting (Stech, 1999; Hauptmann, 2000; Roberts, Thornton and Pigott, 2009). In neolithic Mesopotamia the first evidence for metallurgy is found at Tell Maghzaliyah (copper awl), Tell es-Sawwan (copper knife), and Yarim Tepe I-II (two copper rings, copper seal / pendant, and a lead bracelet) dating to the 7th and 6th millennium BCE (Merpert and Munchaev, 1987; Stech, 1999). Especially the lead bracelet is one of the earliest records for lead metallurgy.

The earliest evidence for copper metal in Iran is a rolled copper bead found at Ali Kosh and dated to the transition of the 8th to 7th millennium BCE (Thornton, 2014). Isolated copper metal artefacts were discovered at the site of Mehrgarh, further to the east in present day Pakistan, dated to the end of the 7th until the beginning of the 6th millennium BCE (Thornton, 2014).

9.1.3 6th millennium BCE

In the Transcaucasus region the earliest evidence for copper metal is identified at Aratashen (Neolithic, level IId) with the finding of 57 arsenical copper beads dated to early 6th millennium BCE (Courcier, 2014).

A few copper artefacts have been recovered from Gargalar-Tepesi, Khramis Didi-Gora, Arukhlo, and Göy Tepe associated with the Shomu-Shulaveri Culture (cf. fig. 9.2) (Courcier, 2014). In Göy Tepe a vitreous slag with copper prills was discovered suggesting extractive metallurgy in the middle of the 6th millennium BCE in this area (Courcier, 2014). Two copper awls were discovered at Chalagan Tepe in a funerary context dated to the end of the 6th millennium BCE (Kawtaradze, 2001).

Within the 6th millennium BCE falls the site of Tal-i Iblis, where a firepit filled with fragments of a crucible,

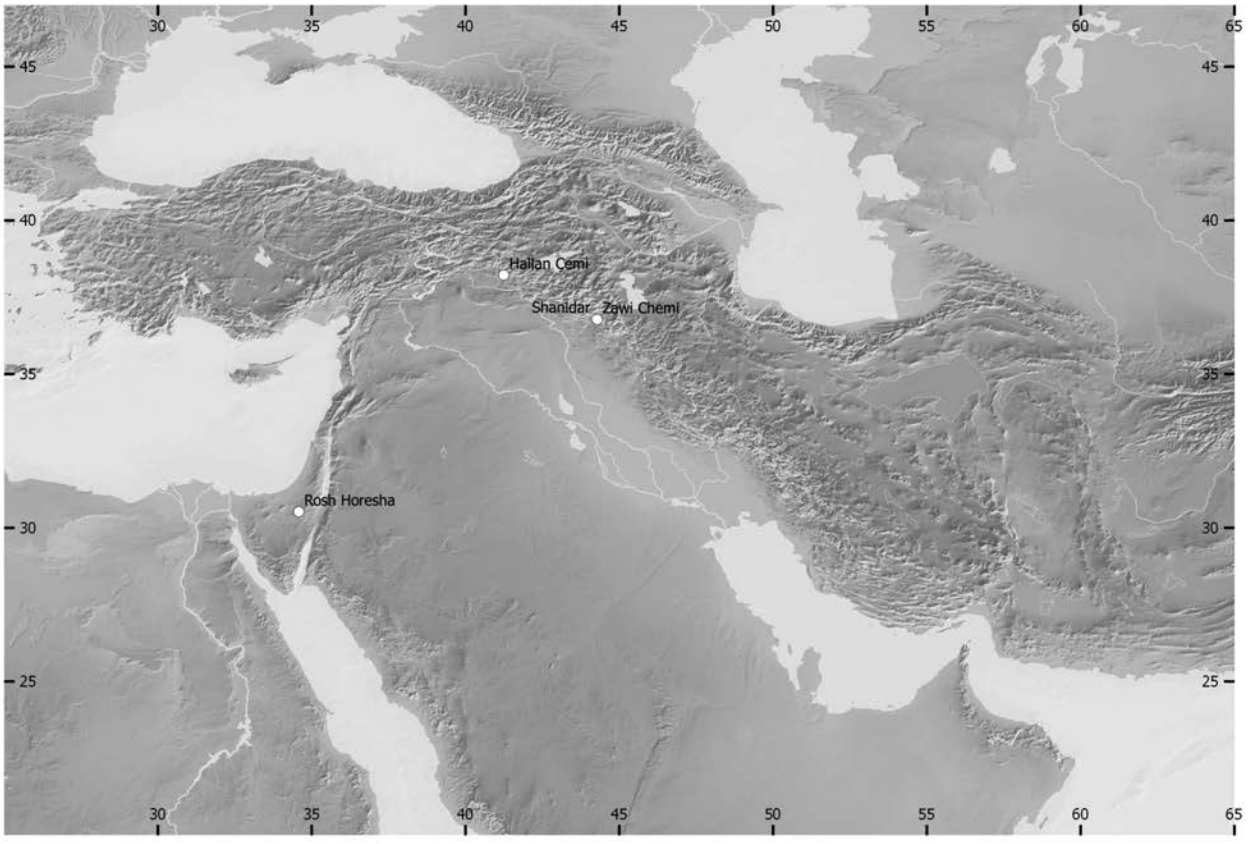

Fig. 9.1: Distribution map of early copper ore findings in an archaeological context of the 11th to 9th millennium BCE (data source: Roberts, Thornton and Pigott, 2009; made with Natural Earth).

malachite, and charcoal was discovered between the layers of Period I and II, as well as more than 100 "slagged crucible fragments", dated to Period II (Thornton, 2014). These could be seen as one of the earliest evidence for copper smelting activity at the end of the 6th to the beginning of the 5th millennium BCE, although copper smelting activities were also uncovered at Belovode in Serbia (Roberts, Thornton and Pigott, 2009; Radivojević, 2013).

The oldest archaeological site in the Levant, where copper artefacts have been discovered, is Tell Tsaf, dated to the late 6th millennium BCE (Garfinkel, et al., 2014). These findings suggest the beginning of levantine copper metallurgy already in Chalcolithic times.

The oldest tin bronze artefacts were discovered at Ghar-i-Mar in Afghanistan in the so-called snake cave (Thomalsky, et al., 2013). In the cave were several bronze sheets and fragments of a rectangular rod discovered dated to 5500-5300 BCE (Thomalsky, et al., 2013), although the date for these findings is debatable and further investigations have to be performed for verification purposes.

9.1.4 5th to 4th millennium BCE

One of the oldest tin bronze artefacts was discovered at the site of Pločnik in Serbia dated to the mid 5th millennium BCE, which is associated with the Vinča culture (cf. fig. 9.3) (Radivojević, et al., 2013; Radivojević and Rehren, 2016). Indeed, it predates the discovered tin bronze sheet at other sites where early tin bronzes occur (Mesopotamia and Anatolia) by 1500 years (Radivojević, et al., 2013).

At the same time the evidence for the 5th and 4th millennium BCE copper artefacts in Anatolia and Mesopotamia remains scarce and more research has to be done for these time periods. At the end of the 4th millennium BCE, in the Jemdet Nasr period, pure copper artefacts occur at Tello/Girsu, Tepe Gawra, and Niniveh (Stech, 1999).

The Uruk expansion caused large migration waves to the Levant, eastern Anatolia, and up to the northern Caucasus region, where the first pure and arsenical copper artefacts appear at the sites of Svobodnoe, Skala, Meshoko, and Veselogo (Courcier, 2014). In the southern Transcaucasian region three beads and an awl from Alikemek Tepesi and seven copper artefacts from Kültəpə (Nakhchivan) were discovered dated to the beginning of the 5th millennium BCE associated with the Alikemek-Kültəpə culture (Courcier, 2014; Kawtaradze, 2001). The site of Mentesh Tepe revealed the evidence for a local metallurgical chain from slag to copper objects in the second half of the 5th millennium BCE (Courcier, 2014). Further metal objects associated with the Sioni culture were discovered at Alazani III, Tsiteli Gorebi, and Chalagan Tepe. The north-western Caucasus and Black Sea is characterised by the Darkveti culture (second half of 5th millennium BCE) with important early metal finds at the sites of

Fig. 9.2: Distribution map of early archaeological copper metal and ore findings dated to the 8th to 6th millennium BCE (data source: Stech, 1999; Hauptmann, 2000; Kawtaradze, 2001; Roberts, Thornton and Pigott, 2009; Courcier, 2014; Garfinkel, et al., 2014; Thornton, 2014; Lyonett et al. 2016; made with Natural Earth).

Samele-Klde, Chikhori, Natsar Gora, Sagvardzhile, Guad ikhu, Kistrik, and Tetri Mgvime (Neolithic to Chalcolithic times, no ^{14}C-dates available)(Courcier, 2014).

Later the Maikop culture dominated the north-western Caucasus with more complex metal artefact types, as also socketed weapons appear at this stage. Copper pickaxes resembling stone tools were discovered at Ust'Labinskaja and El'brus, socketed axes at Maikop, Kostromskaja, Ust'Dzhegusta, Pjatigorsk, Apsheronskaja, and Balaklava (Courcier, 2014). Furthermore copper vessels, daggers with flat blades and tripartite spearheads occurred in the Maikop phase (Courcier, 2014).

Early evidence for levantine copper metallurgy has been uncovered at the cave of Nahal Mishmar, where a treasure was buried exhibiting the application of lost-wax casting technique (Garfinkel, et al., 2014). Ben-Yosef, et al., (2016) reported also the appearance of the first leaded copper in the Levant in the 5th millennium BCE at Bet Shemesh in Israel. Further important Chalcolithic sites regarding early metallurgy in the Levant are at Abu Matar, Bir Safadi, Neve Noy, Gilat, Shiqmim, Jericho, Teleilat Ghassul, Abu Hamid, and Nahal Qana (Hauptmann, 2000). The ancient mining and smelting site of Timna (Israel) was active in the 4th millennium BCE (Conrad and Rothenberg, 1980). 4th millennium copper smelting activities were also reported in Feinan and Abu Matar (Hauptmann, 2000).

The beginning of the levantine Bronze Age falls in the second half of the 4th millennium BCE (Early Bronze Age I), to which several sites with copper finds are dated (Nahal Besor, Ashkelon Afridar, Tell Halif, Tell esh-Shuna, Tell Maqass, and Hujayrat al-Ghuzlan) (Hauptmann, 2000).

In Iran late 5th millennium BCE copper artefacts were discovered at the sites of Susa, Tappeh Hissar, Tappeh Yahya, and Tappeh Sialk suggesting the beginning of more widespread use of metal in this region (Thornton, 2014; Vatandoust, Parzinger and Helwing, 2011). An important 4th millennium site is certainly Tappeh Ghabristan, where two hearths, smelting crucibles, casting moulds, and copper oxide ores were discovered, identifying Tappeh Ghabristan as both smelting site and workshop (Thornton, 2014). Further sites with similar types of crucibles compared to Ghabristan are Tappeh Sialk and Arisman. 4th millennium BCE Tappeh Hissar revealed smelting activity of copper sulphide Fe ores, as chalcopyrite (Thornton, 2014). Further to the East in the plane of Baluchistan lie the sites of Shahr-i Sokhta and Gardan Rig, where copper production emerged in the 4th millennium BCE and continued later in the 3rd millennium BCE (Hauptmann, Rehren und Schmitt-Strecker, 2003; Thomalsky, et al., 2013).

At the Eurasian steppe copper and silver were common by late 4th millennium BCE (Roberts, Thornton and Pigott, 2009). In Namazga Tepe a significant increase of copper objects was noticed in the 4th millennium BCE and intentional alloys with tin joined the copper artefacts in the early third millennium BCE in Namazga IV (Garner, 2013).

9.1.5 3rd millennium BCE

In Jemdet Nasr times the first arsenical copper artefacts appear at Tepe Gawra, Tell Fara, Jemdet Nasr, Arslantepe, and in the early graves of Ur (cf. fig. 9.4) (Stech, 1999). Already in Early Dynastic I arsenical copper became quite common and was excavated at Kheit Qassem, Kiš, Ur, and several sites in Anatolia (Stech, 1999). The first verified tin bronzes in Mesopotamia emerge at the cemetery of Kiš in Early Dynastic I (Stech, 1999). In Early Dynastic III tin bronzes only played an important role at the Royal Cemetery of Ur and Stech (1999, 64) suggests this is due

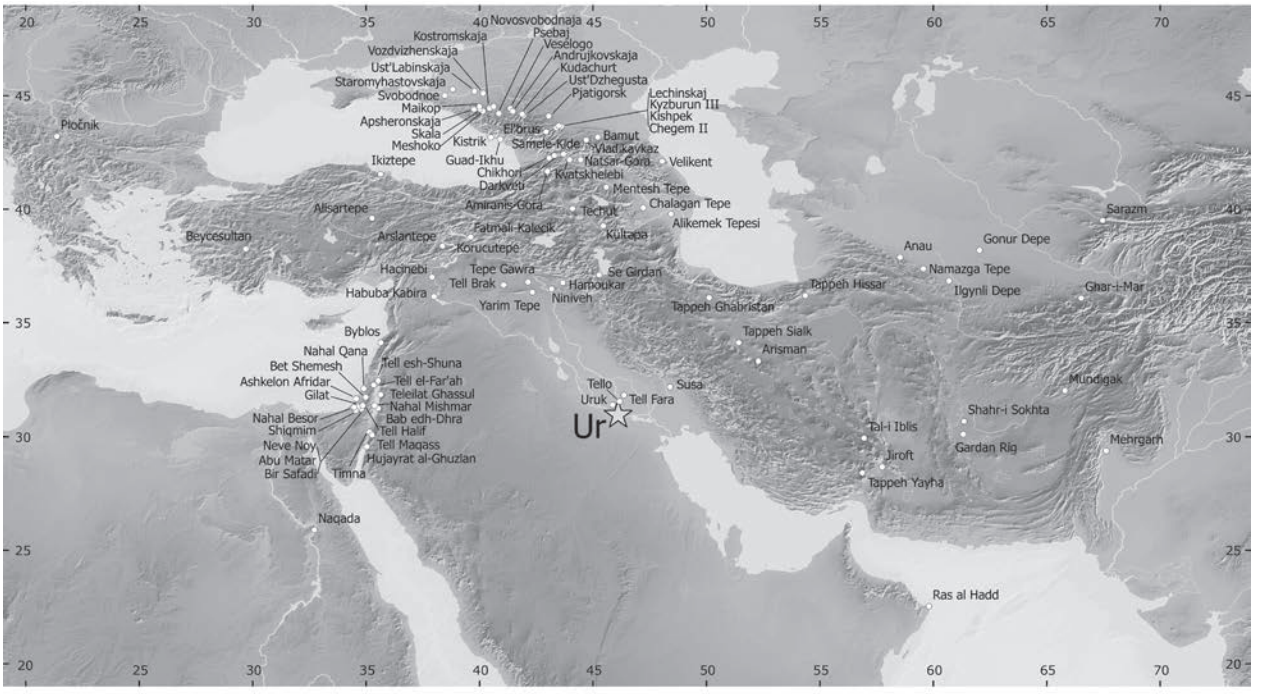

Fig. 9.3: Distribution maps of early archaeological copper-based metal findings dated to the 5th to 4th millennium BCE (data source: Conrad and Rothenberg, 1980; Philip and Rehren, 1996; Stech, 1999; Hauptmann, 2000; Kawtaradze, 2001; Meyers, 2003; Radivojevic, 2007; Roberts, Thornton and Pigott, 2009; Begemann, et al., 2010; Nezafati and Pernicka, 2012; Garner, 2013; Thomalsky, et al., 2013; Courcier, 2014; Garfinkel, et al., 2014; Helwing, 2014; Thornton, 2014; Ben-Yosef, et al., 2016; Lyonnet, et al., 2016; made with Natural Earth).

to passing the political control from Kiš to Ur reflecting the restriction of the access to the precious tin / bronze trade. Arsenical (-Ni rich) copper occurred contemporarily with tin bronzes in Early Bronze Age Mesopotamia. The occurrences of tin bronze remained scarce in Akkadian to Ur III times and were identified at the cemetery of Ur, Tepe Gawra, Kiš, Fara, and Nippur (Stech, 1999). In Anatolia tin bronzes were discovered at the sites of Troy (level II), Alaca Höyük, Ahlatıbel, Alişar, Polatlı, Kültepe, Horuztepe, Tarsus and Mersin (Stech, 1999). In general the level of complex metal artefacts of Early Bronze Age Mesopotamia is very evolved compared to other cultures.

The Levant exhibits an abrupt rise of copper production in Feinan, and copper artefacts were discovered in settlements of Bab edh-Dhra, Numeira, Kfar Monash, and Arad (Hauptmann, 2000). Tin bronze artefacts began to spread at the end of the 3rd millennium BCE and there are no local tin ores available in the Levant indicating an import of tin as ore or ingot (Hauptmann, 2000).

Northern Mesopotamia had close relations to north- and eastern Anatolia, and Transcaucasia already in the Late Chalcolithic and continued to have these in the 3rd millennium BCE (Courcier, 2014). The north-western Caucasus was dominated by the Novosvobodnaja phase (late Maikop phase: 3300 - 2600 BCE) with copper axe-hammers along with pickaxes at the sites of Klady, Vozdvizhenskaja, Lechinskaj, and Vladikavkaz. Socketed axes with differing type of blades were discovered at Novosvobodnaja, Andrjukovskaja, Klady, Chegem II, Kishpek, Miziev, Bamut, Dolinka, Kyzburun III, Lakshukaj, and Psebaj (Courcier, 2014). Also daggers with flat and ribbed blades are typical for this period and appear later at 2600 BCE in Tell Melebiya, Tell Brak, Uruk, and Mari (Courcier, 2014). The type of tripartite spearhead spreads even to southern Caucasus, eastern Anatolia, northern Syria, and Turkmenistan by the first half of the 3rd millennium BCE (Courcier, 2014). A new type of spearhead (a pike with a square section) emerges in the Novosvobodnaja phase and similar forms are found in the Kura-Araxes culture, and at Early Bronze Age (II/III) Tell Kara Hassan, Jerablus-Tahtani, and Carchemish (Courcier, 2014). The Kura-Araxes culture in Transcaucasia dominated the region for over a thousand years of continuity and spread even to eastern and Central Anatolia, as well as the Levant (Courcier, 2014). There is evidence for local metal production activity in this region at Amiranis Gora, Baba Dervish II, Shortepe, Shengavit, Igdir, and Pichori, as well as metalworking at Velikent (Dagistan), Mokhra-Blur, Kabaz-Kutan (3000 BCE)(Courcier, 2014). Most of the copper artefacts of the Kura-Araxes culture are arsenical copper artefacts with As contents of as high as 20 wt% (Courcier, 2014; Kawtaradze, 2001). Tin bronzes occur in the Caucasus for the first time at the tombs of Velikent associated with the Kura-Araxes culture (Courcier, 2014).

Smelting and alloying techniques evolve in Iran at the end of the 4th to the beginning of the 3rd millennium BCE. The first tin bronze artefacts were discovered at the cemetery of Kalleh Nisar in Luristan (Thornton, 2014). Furthermore there is a shift from arsenical copper to a more pure copper composition similar to the Kura-Araxes culture in the Transcaucasus and in general metal production boomed in the 3rd millennium BCE Iranian region (Thornton, 2014).

Oman started copper production in the 4th millennium and had a peak in the 3rd millennium BCE. Copper artefacts dating to the 3rd millennium BCE were discovered at several sites (cf. fig. 9.6). The copper artefacts of Oman are in general characterised by high As and Ni levels indicating smelting activities with local ores as a source. The ancient land of *Makan* was connected by sea trade with Southern Mesopotamia via the Persian Gulf (Moorey, 1994; Glassner, 1996; Prange, et al., 1999).

Western Central Asia is characterised by the Oxus civilisation and the Bactro-Margiana Archaeological Complex (BMAC) comprising NE Iran, Northern Afghanistan, S Uzbekistan and Tajikistan with important metal finds at Gonur Depe, Altyn Depe, and Tepe Fullol (Kosh Tepe) (Thomalsky, et al., 2013).

The Harappa culture further to the east in the fertile region of the Indus river has been acknowledged to be the land of *Meluḫḫa* mentioned in Akkadian texts (Hirsch, 1963). Mesopotamia and *Meluḫḫa* were connected by sea via *Makan* and *Dilmun* and presumably by land via the Iranian plateau (Kenoyer and Miller, 1999; Kenoyer, Price and Burton, 2013). The evidence for copper smelting in the Early Bronze Age Indus valley is very scarce and archaeological investigations suggest the presence of local melting technologies, rather than smelting, although the use of copper was widely spread and copper appears to have been available to all walks of life (Hoffman and Miller, 2014). Hoffman and Miller (2014) suggest that the Harappa culture engaged more in the trade of copper ingots than in producing copper themselves. The Indus civilisation influenced also sites to the west in southern and even northern Afghanistan. In southern Afghanistan the site of Mundigak was an important centre of metal production and trade in close contact with Harappan merchants and culture (Thomalsky, et al., 2013). The influence stretched even as far as the Iranian borderlands with important sites of copper metal production in Shahr-i Sokhta, Jiroft, or Gardan Rig (Thomalsky, et al., 2013). To the north there were an Harappan outpost named Shortugai and the Dashli oasis where some bronze and copper objects were obtained (Thomalsky, et al., 2013). Further metal objects were uncovered at Said Qala, Deh Morasi Ghundai, Aq Kupruk, and Darra-i-Kur (Thomalsky, et al., 2013).

In Western Central Asia tin bronzes occur first in the beginning of the 3rd millennium BCE at the site of Namazga and later at the sites of Dzharkutan, Sapalli Tepe, Altyn Tepe, and Dashli (Garner, 2013). At the end of the 4th millennium BCE copper artefacts were discovered in Sarazm (Garner, 2013). It is interesting to note that the copper artefacts of Sarazm are similarly worked as artefacts in Mesopotamia, Indus valley, and Iran (Garner, 2013).

9.2 Copper ores

A wide range of copper ores occurs in nature and these shall be discussed in this subsection. The different ore minerals are described in short as a lengthy description is beyond the scope of this dissertation. The element copper has a global abundance of 75 µg/g or ppm in the Earth's crust, which is ca. 1000 times higher than silver and 25,000 times higher than gold (Taylor and McLennan, 1985; Pernicka, 1990).

Native copper: First of all copper exists as native copper in nature. Although native copper requires specific redox-environments for formation and therefore occurs concentrated at specific locations. Not every ore body exhibits native copper. Part of the native copper does not outcrop at the surface but is found at deeper levels of the ore bodies. Examples for native copper are the Darhand copper deposit (Nezafati, Momenzadeh and Pernicka, 2005) or the Anarak-Talmessi occurrence (Tarkian, Bock and Neumann, 1983).

Copper oxides: Copper oxides are usually found at oxidation zones of sulphide deposits intergrown with other copper carbonates, as the sulphides are exposed to weathering in the surface near environment, although pure copper oxides are rarely occurring in nature in significant quantities for smelting. Natural copper oxides are cuprite and tenorite.

Copper carbonates: Malachite and azurite are usually the main constituents of oxidation zones, as they form under oxidising and aqueous conditions. The colour is also a striking feature of these ores, which is a good indicator for exploration of copper deposits.

Copper chloride: Atacamite is a common weathering product of copper minerals in aride climate conditions. It is also occurring frequently in corrosion products of copper artefacts.

Copper sulphides are usually the primary copper ore of a deposit. Different copper sulphides form under different conditions but mostly in hydrothermal environments and in supergene enrichment zones. Important copper sulphide minerals are: chalcopyrite, bornite, chalcocite, covellite, digenite, enargite, cubanite, and many more.

Fahlores are the solid solution of tennantite-tetrahedrite usually occurring intergrown with other sulphide minerals and form in hydrothermal or contact metamorphic settings. They are important for smelting of arsenical copper and silver exploitation.

Copper silicates, mainly chrysocolla occur in oxidation zones of copper ore deposits. The mineral is often intergrown with other common minerals in oxidising environments, e.g. malachite.

Copper sulfates form at aride climate or very oxidising conditions copper sulfates with brochantite and its corrosion product antlerite being the most common among them.

9.2.1 Early unalloyed copper: Native copper versus smelted copper ores from oxidation zones

The question remains, how early copper smelting technology started, as most researchers assume the use of native

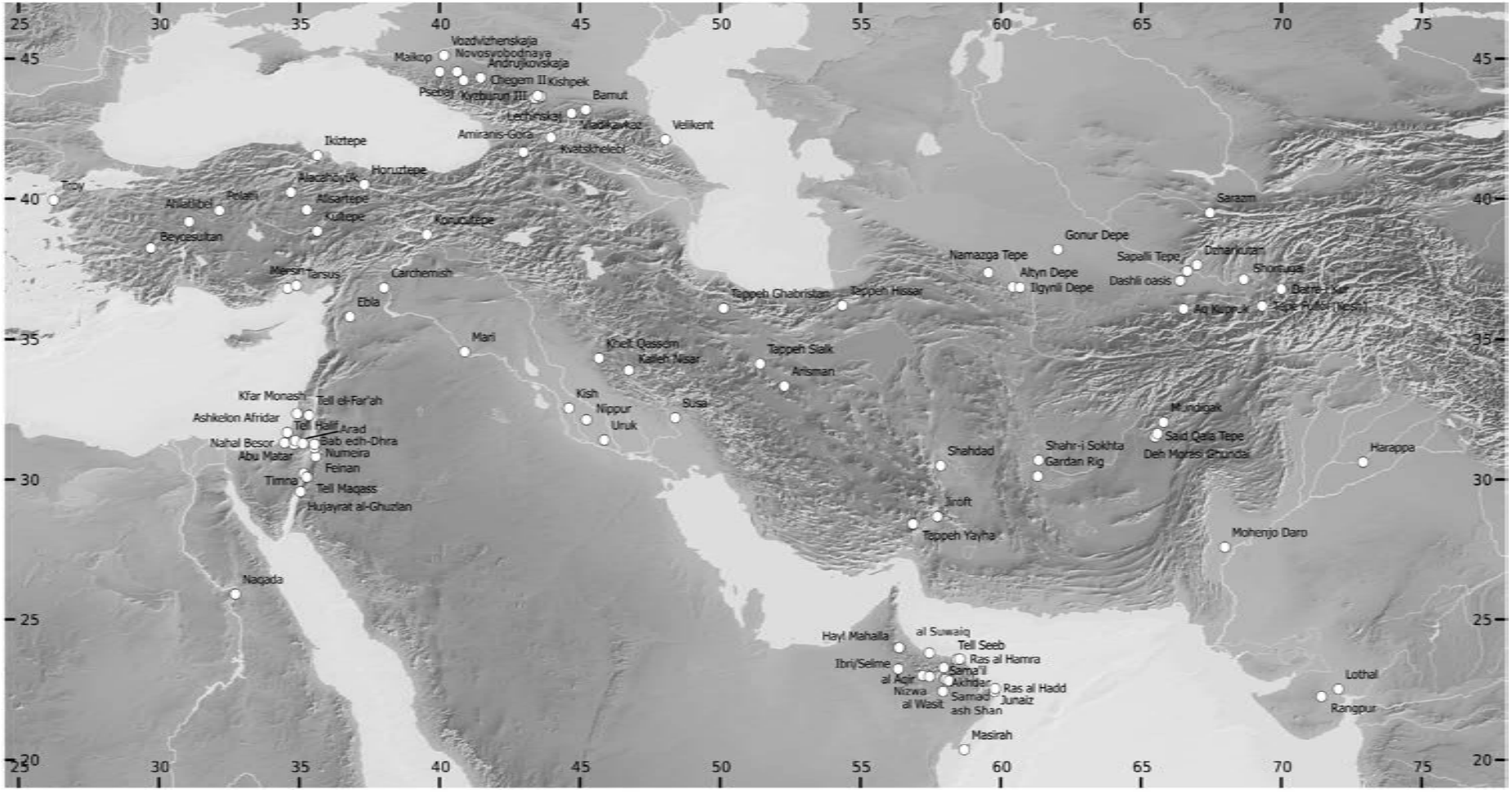

Fig. 9.4: Distribution map of early archaeological copper-based metal findings dated to the 3rd millennium BCE (data source: Conrad and Rothenberg, 1980; Philip and Rehren, 1996; Stech, 1999; Hauptmann, 2000; Kawtaradze, 2001; Prange, 2001; Meyers, 2003; Radivojevic, 2007; Paoletti, 2008; Roberts, Thornton and Pigott, 2009; Begemann, et al., 2010; Nezafati and Pernicka, 2012; Garner, 2013; Thomalsky, et al., 2013; Courcier, 2014; Garfinkel, et al., 2014; Helwing, 2014; Hoffman and Miller, 2014; Thornton, 2014; Ben-Yosef, et al., 2016; Lyonnet, et al., 2016; made with Natural Earth).

copper before smelting oxide or sulphide ores. This theory is based on the absence of sulphide inclusions and the high purity of early copper metal (Thornton, et al., 2002; Birch, Rehren and Pernicka, 2013), although this could also be obtained by smelting pure oxide ores. Besides, no slags or almost none would have been left as evidence by smelting copper oxides. Maddin, Wheeler and Muhly (1980) state that "scholars have sometimes been influenced by the date of the object in determining the type of copper from which it was made". Some "native copper artefacts" were determined as those only by metallography or by date. The earliest copper metal artefacts of Çayönü were determined to be made of native copper (Stech, 1999; Roberts, Thornton and Pigott, 2009). But the question of the source of these very early copper metal finds remains. It is supposed that the native copper was extracted from the nearby Ergani district (Griffitts, et al., 1972, Wertime 1964), but there has been no evidence for native copper occurrences in Ergani (Maddin, Wheeler and Muhly, 1980). The relation of a potential native copper artefact found at Tappeh Sialk to the Anarak-Talmessi native copper occurrence seems more likely, but this artefact is dated to the 5th millennium BCE, around 3000 years later than the findings of Çayönü (Maddin, Wheeler and Muhly, 1980). Pernicka (1990) estimates that around 1000 native copper occurrences existed in the Old World. But it is uncertain, if all of these were available for ancient metallurgists. Put together the quantity of early copper findings is not very high and could be explained by the exploitation of the very limited sources of native copper, though the earliest findings do not overlap with potential nearby native copper sources. Smelting of secondary copper ores seems more likely, as copper ores from oxidation zones (e.g. malachite) (1) were locally available in large quantities, (2) were known as raw material for jewellery since the 11th millennium BCE, (3) would result in very pure copper artefacts with no sulphide inclusions, provided that early metallurgists were using pure malachites (or other ores), (4) are more easily smelted (one step process) as compared to sulphide ores (two step process). On the other hand even for non-sulphide ores specific conditions have to be fulfilled. Pernicka (1990) states that a delicate equilibrium of sufficient air supply for burning charcoal in order to reach higher temperatures and simultaneous absence of air is required for complete reduction to copper metal, which is not easily reached by very ancient technology. On the other hand the question arises if modern researchers do not exhibit enough confidence in early metallurgists. Neolithic humans most certainly had other criteria to observe temperature or other specific conditions (e.g. by colour of the embers) to evaluate manufactured pyromaterials, abilities which modern humans lack. Annealing was already known to early metallurgists, as otherwise they could not have forged copper metal into artefacts (Pernicka, 1990). Besides, native copper and smelted copper artefacts cannot be distinguished by microstructure, if the artefacts have been worked, which is the case at Çayönü (Maddin, Wheeler and Muhly, 1980; Stech, 1999). Further evidence for early smelting activities accumulates, as the discovery of a lead bracelet at Yarim Tepe suggests, dated to the 7th to 6th millennium BCE (Merpert and Munchaev, 1987; Stech, 1999). Lead metal has to be obtained by smelting of lead ores, as lead does not or very rarely occur in native form in nature (Maddin, Wheeler and Muhly, 1980; Stech, 1999). Summarising one should evaluate general statements on early copper metal being made of native copper with a critical eye. It cannot be completely excluded, that native copper had been in use in ancient times, but one should not disregard the possibility of early copper smelting activities. This matter would be an excellent starting point for further chemical and metallographical analysis of the earliest copper artefacts for future research.

9.3 Smelting of copper ores

9.3.1 Smelting of oxidic copper ores

The smelting of oxidic ores (e.g. malachite) is a more simple process than compared to smelting of sulphide ores. The copper ore was crushed first to ensure a bigger surface and therefore increased reaction rates (Tylecote, Ghaznavi and Boydell, 1977). It requires only an one step process and can be easily acquired by putting oxidic copper ore in a crucible and covering it with charcoal to obtain reducing conditions. The crucible was then heated in a fire and tuyères were used to enhance the necessary air supply (Tylecote, Ghaznavi and Boydell, 1977). The critical temperature for the reduction to copper metal is at 1083°C (Tylecote, Ghaznavi and Boydell, 1977). But a more sophisticated method with a higher copper output is achieved by adding gangue as a flux to create a liquid fayalite slag, which is described in the following.

In the initial phase the added air leads to burning of the charcoal, in order to reach the higher temperatures, as the reaction (1) is exothermic. The redox conditions within the crucible or furnace are highly influenced by the oxygen and carbon dioxide partial pressure. Carbon excess is required to achieve a Boudouard equilibrium.

(1a) $C + O_2 \rightarrow CO_2$

(1b) $CO_2 + C \leftrightarrow 2\,CO$ Boudouard equilibrium

According to Tylecote, Ghaznavi and Boydell (1977) several tuyères were used for heating the fire up to 1100 - 1200°C. Additionally gangue has to be added as a flux (the required components of Fe and silicate rich gangue) (Tylecote, Ghaznavi and Boydell, 1977). Bachmann (1982) describes the following reactions occurring in the crucible / furnace:

(2a) Decomposition of the ore:

$CuCO_3.Cu(OH)_2 \rightarrow 2\,CuO + CO_2\uparrow + H_2O\uparrow$

(2b) Reduction 1: $2\,CuO + CO \rightarrow Cu_2O + CO_2\uparrow$

(2c) Reduction 2: $Cu_2O + CO \rightarrow 2\,Cu + CO_2\uparrow$

(2d) Slag formation: $SiO_2 + 2\,FeO \rightarrow Fe_2SiO_4$

The (II)-copper ions are reduced to copper in a two-step reduction. The unwanted components are collected in the slag, which remains due to lower density in the upper part of the crucible, whereas copper metal is to be found in the lower part of the crucible (Tylecote, Ghaznavi and Boydell, 1977). At the lining of the crucible remains of fritted sand adhere (Tylecote, Ghaznavi and Boydell, 1977).

Elemental partitionining	Byproduct	Density
Siliceous melt	Slag	3-4
CU-sulfides Fe-sulfides	Matte	5
(Ferous speiss) (Fe-Arsenides) (+base metal speiss)	(Speiss)	(7-8)
Copper	Metal	>8

Fig. 9.5: The metallurgical (by-)products of polymetallic smelting (after Keesmann (1993), fig. 6). The distribution between different phases takes place in different layers, separated by density.

9.3.2 Smelting of sulphide ores

Smelting of copper sulphides is more complex than of copper oxides, as it requires a step of roasting before the actual smelting. The sulphides (e.g. chalcopyrite) have to be decomposed to copper sulphide, Fe oxide, and S dioxide which escapes into the atmosphere. For this step a simple hearth is used with charcoal, which is heated up to 300 - 400°C (Ryndina, Indenbaum and Kolosova, 1999). The reaction takes place as follows depending on the level of reaction (Bachmann, 1982):

(3a) Dead roasting:

$$CuFeS_2 + 3\,O_2 \rightarrow FeO + CuO + 2\,SO_2\uparrow$$

(3b) Partial roasting:

$$4\,CuFeS_2 + 7\,O_2 \rightarrow 2\,Fe_2O_3 + 4\,CuS + 4\,SO_2\uparrow$$

Dead roasting (3a) of the ore was not desired, as it prevents the separation of Fe from the copper. For the following smelting operation of copper a partially roasted ore was produced (3b). The next step involves the addition of charcoal and high temperatures (1000 - 1200°C) (Ryndina, Indenbaum and Kolosova, 1999), where multiple reactions occur simultaneously. The formation of matte is necessary, in order to bind components affecting the resulting metal in a negative way, as for example high As, Pb, or Sb levels, which would not separate into the siliceous slag. Therefore the sulphide ores were not dead roasted, as some sulphides have to remain in the ore in order to produce matte. The reactions are according to Bachmann (1982):

(4a) Matting:

$$CuFeS_2 + 5\,O_2 + 2FeS_2 \rightarrow FeS + CuS + 2FeO + 4SO_2$$

(4b) Matte roasting:

$$CuS + FeS + 3\,O_2 \rightarrow CuO + FeO + 2\,SO_2$$

(4c) Reduction: $CuO + CO \rightarrow Cu + CO_2$

(4d) Slagging: $2\,FeO + SiO_2 \rightarrow Fe_2SiO_4$

The final reaction from sulphide / oxide requires the presence of sulphides next to the oxides. In order to achieve this at first the so-called matte forms (4a). The matte comprises copper and Fe sulphides. In the next step the matte is oxidised to copper and Fe oxides, which further react to copper metal and fayalite slag. Due to differences in density, the by-products separate in different layers (see fig. 9.7). The slag has the lowest density and remains in the uppermost layer of the crucible. The matte is of intermediate density and therefore separates in the central layer. Depending on the ores used for smelting and the process conditions, the matte can contain ferrous speiss or even base metal speiss comprising different arsenides or antimonides, if polymetallic ores are smelted (which is often the case). The lowest layer with the highest density consists of the reduced copper metal. The copper metal can now be cold worked or cast into an artefact and usually contains some remnant Fe sulphide inclusions.

9.3.3 Smelting of arsenical copper

There are different theories about smelting of arsenical copper and whether As is added intentionally to the copper, although from a mineralogical point of view the most reasonable way is the selection of polymetallic copper ores, which are associated with arsenides. As this is a quite common mineral association and a large number of polymetallic copper deposits occur in the Near and Middle East, these type of ores were widely accessible. Natural As-bearing minerals in association with copper deposits are for example: enargite, domeykite, arsenopyrite, orpiment, Niine, rammelsbergite, and löllingite.

Lechtman and Klein (1999) conducted experiments on smelting of As bearing copper ores. In general the main processes are the same as for smelting sulphide ores. The ores have to be roasted before smelting. The chemical reaction is different, when As is present, according to Lechtman and Klein (1999):

(5a) roasting of copper sulfide:

$$CuS + 1.5\,O_2 \rightarrow CuO + SO_2\uparrow$$

(5b) roasting of arsenides:

$$8\,CuAsS + 22.5\,O_2 \rightarrow 6\,CuAsO_4 + 2\,CuO + As_2O_3\uparrow + 8\,SO_2\uparrow$$

The arsenides are oxidised during roasting and some As is emitted as fume. When the roasted ores are directly smelted, the chemical reactions would take place, as follows (Lechtman and Klein, 1999):

(6a) direct smelting:

$$CuAsO_4 + 4\,CO \rightarrow Cu.As + 4\,CO_2\uparrow$$

Although Lechtman and Klein (1999) exhibited, that cosmelting is also possible:

(6b) Cosmelting of Cu_3AsS_4:

$$8\ CuCO3 + Cu_3AsS_4 \rightarrow Cu.As + 4\ SO_2\uparrow + 8\ CO_2\uparrow$$

(6c) Cosmelting of FeAsS:

$$3\ CuCO_3 + FeAsS \rightarrow Cu.As + FeO + SO_2\uparrow + 3\ CO_2\uparrow$$

The S is oxidised and emitted as a gas from the crucible. This process involves as during smelting of copper sulphides the formation of matte and slag, in order to provide a separation by density. The As bearing fumes are big hazards for human health and the environment. This might be one of the reasons, why smelting of arsenical copper was abandoned in later times and arsenical copper replaced by tin bronzes (Lechtman and Klein, 1999).

Opposed to the presented process of arsenical copper production, Thornton, et al., (2008; 2009) suggest another mechanism by means of “speiss slags” found at Tepe Hissar. They argue that ferrous speiss was intentionally produced at Tepe Hissar which was used further for arsenical copper production, although there are certain problems with this hypothesis. First of all ferrous speiss is usually an undesired by-product, which was discarded. Speiss minerals are commonly minor contents of matte and occur as skeletal crystals or small inclusions. Even if one intentionally produced enough ferrous speiss, the ancient smelter would have had difficulties to alloy it with copper to arsenical copper due to the high melting point of speiss minerals. The high levels of Fe in the copper would produce a very brittle metal not suitable for forging into an artefact. Indeed, the main problem of this theory is the high Fe amount within the resulting copper metal and how to extract it afterwards. Thornton, et al., (2008) noticed the absence of different base metals in the speiss phase and concluded, that the smelted ore was therefore no copper ore. However, the absence of base metals does not necessarily mean that no copper ore was smelted, since it depends on the selection of copper ores for the process, as they can be very variable in their particular base metal contents.

9.3.4 Smelting of copper and tin

According to Coghlan (1975), there are four different ways of copper and tin smelting to tin bronze (Oudbashi, Emami and Davami, 2012):

(1) Mixing copper and tin metal: This is the most obvious method. The tin metal is simply added to the copper metal at high temperatures in order to reduce the melting point and viscosity, so the tin bronze is better castable. The controlled amount of tin in the tin bronze is better manageable, as in the other smelting processes.

(2) Addition of cassiterite to copper metal under reducing conditions: Cassiterite is added to the copper metal mixed with charcoal. In order to reduce the cassiterite to tin metal, a temperature of about 1200°C has to be reached. This might be one of the reasons, why tin bronzes occur in a later stage of copper metallurgy, as higher temperatures have to be controlled. The charcoal is needed to maintain reducing conditions in the crucible. This type of smelting would lead to variable concentrations of Sn in copper.

(3) Co-smelting of copper ore and cassiterite: Copper ores and cassiterite are directly smelted together, in order to produce the alloy of tin bronze. The process temperature is at around 1200°C. The ores are crushed before smelting then put into a crucible with charcoal and are heated in an open fire (Rovira, Montero-Ruiz and Renzi, 2009).

Rovira, Montero-Ruiz and Renzi (2009) did some experiments on this method with malachite and cassiterite and obtained metal prills with very variable Sn concentrations in the copper. Gowland already achieved a tin bronze with 22 % Sn in an experiment, where he smelted malachite and cassiterite (Gowland, 1906).

(4) Smelting of natural copper-tin ore (e.g. stannites, mushistonite): Gowland claimed already in his article in 1906, that “bronze had its origin in the simple smelting of an ore in which copper ore and tin ore were naturally associated”. This theory is continued in recent times. Experiments were conducted by Lutz and Pernicka, but the results still remain to be published (Garner, 2013). Potential copper-tin-ores would be stannite, e.g. occurring in Iran (Nezafati, 2006), or mushistonite, e.g. occurring in Mushiston, Kazakhstan (Garner, 2013). In theory the smelting of these ores would lead to a tin bronze, with very variable amounts of Sn.

Although some work has been undertaken regarding experiments of copper tin smelting, there are still certain problems, which need to be discussed. One of the problems is the difference in redox conditions needed for reducing copper versus Sn. Sn as the less noble element and in a 4+ redox state needs more reducing conditions than copper. In order to achieve these conditions in the presence of copper, a Boudouard equilibrium and therefore a carbon excess has to be existent or at least approximating it. Depending on the exact process large amounts of Fe could be easily introduced into the tin bronze metal, which would lead to an undesirable brittle alloy.

Co-smelting of copper sulphides and cassiterite is difficult, as the reaction of copper sulphide / oxide to metallic copper could easily block the reaction from cassiterite to tin metal, as several intermediate Sn oxides would probably remain in the copper metal. Cassiterite would be easier reduced to tin without the presence of copper, and leading to more homogeneous results regarding the metal, when copper and tin metal are melted together. Although a thermodynamic modelling for these reactions would be desirable, this is beyond the scope of this dissertation. Also further experimental investigations could bring the feasibility of these processes to light.

9.4 The “tin problem”

The question for the provenance of early tin in the Near East goes back to the 1970’s (Muhly, 1973). The so-called “tin problem” has caused many discussions and different attempts to solve the old question. The first tin bronzes in the Near East appear in late 4th millennium BCE Tappeh Sialk, Susa, and Mundigak relatively near to potential tin sources (Cleuziou and Bethoud 1982). Whereas the occurrences of tin bronzes in the 3rd millennium BCE at the prominent cemeteries of Kiš and Ur were far away from tin deposits (s. sec. 9.1) (Stech, 1999). Back in the 1970’s to 80’s Cleuziou and Berthoud (1982) did surveys in Afghanistan and discovered some tin deposits in this region. In the Akkadian texts tin is supposed to come from the lands of *Makan* and *Dilmun* (Muhly, 1973), which were most likely an interstation of the metals trade from further East. The land of *Meluḫḫa*, mentioned in Akkadian texts, was connected to Mesopotamia (Hirsch, 1963; Muhly, 1973; Kenoyer and Miller, 1999; Kenoyer, Price and Burton, 2013). Up the rivers from the Arabian Sea *Meluḫḫa* had different trade outposts, for example at Shortugai, reaching as far as Central Asia and Eastern Iran. In Central Asia tin mining areas have been identified at the Zeravshan valley (Karnab, Lapas, Changali, and Mushiston), which are presumed to have started in the second half of the 3rd millennium BCE (Alimov, et al., 1998; Cuenod, Bray and Pollard, 2015; Garner, 2013). A potential tin source in Iran was discovered by Nezafati at the Deh Hosein copper-tin deposit, although there has been no evidence for exploitation in the 3rd millennium BCE, yet (Nezafati, 2006; Nezafati, Pernicka and Momenzadeh, 2006; Nezafati, Pernicka and Momenzadeh, 2008).

Whether tin was traded from or to Anatolia is not clear, as Yener claims the ancient site of Kestel near Göltepe was exploited for cassiterite in the 3rd millennium BCE and even identified cassiterite remains in crucibles (Yener and Vandiver, 1993; Earl and Yener, 1995; Yener, et al., 1989). Yener discovered further evidence for tin processing near Kültepe, starting in the 3rd millennium BCE (Karum Kaneš) (Yener, et al., 2015).

Thus the most reasonable provenance estimation comes from Akkadian texts. But scientific investigations until today failed to solve the old question. There were different approaches to solve the analytical question. Lead isotope analysis displays the geological age of lead minerals (e.g. galena), which are intergrown with copper minerals. But the tin deposits occur primarily near granites or pegmatites and secondarily in placer deposits nearby. Therefore this method is to be excluded. Trace elemental analysis is very difficult to separate between the trace elements deriving from the copper or tin ore. For example Mn incrustations can occur at tin nuggets in placer deposits, but can also be associated with copper mineralisations. One newer approach in research is the investigation of Sn isotopes, although first results are not very promising and cannot separate between different deposits (e.g. Erzgebirge and Cornwall) (Haustein, Gillis and Pernicka, 2010; Brügmann, Berger and Pernicka, 2017). But further investigations whether Sn isotopes fractionate during smelting, smithing, phase separation within the final alloy, and corrosion effects (e.g. tin pest) have to be awaited, until the feasibility of this method can truly be evaluated.

A more promising approach is the attempt of Cuenod, Bray and Pollard (2015), who were assembling a large amount of published chemical data of early bronze artefacts to observe a general trend over vast regions, as many publications only refer to a smaller scale. They investigated the Sn content of the analysed artefacts and enabled them to answer some question. Cuenod, Bray and Pollard (2015) theorise that tin from eastern sources was added at a late stage of trade, possibly even by the Mesopotamians themselves, whereas tin from the west might have travelled already as finished alloys to Mesopotamia. These constrains will be further addressed in section 10.3.

10 The copper-based artefacts: Results and discussion

10.1 Quantitative analysis

10.1.1 Results: electron microprobe analysis

For the copper-based metal objects a number of 74 samples were analysed by electron microprobe analysis. The difficulty of point analysis of alloys lies within the occurring inhomogeneities. In order to avoid accidentally preferential selection of point locations by the operator, a set of more than twenty points was spread randomly as a grid across the fresh metal surface, when possible. Therefore some points were set randomly on the corrosion resulting in sums of sometimes less than 95 %. As some of the standards used for standardisation of the electron microprobe were less dense and/or higher porous than the metal samples, sometimes sums with more than 100 % were obtained on the samples. The single point analysis results with less than 95 % as well as sums with more than 102 % were excluded from the calculation of the bulk chemical composition of the individual sample. The samples of a copper ingot (98-9-164), a spearhead (B17335), an axe (B17411), and a harpoon (B17525) were excluded. 98-9-164 is of unknown context, and it is not verified, if the sampled ingot was even buried in Ur. It is surely Mesopotamian, but no more information is available (M. Jansen, R. Zettler, pers. comm., Jul. 2017). B17411 and B17525 are very small sections sampled from objects, that were electrochemically restored. The microstructure is thoroughly corroded with only small remnants of the original metal. Thus these samples were excluded from further discussion.

During the electron microprobe measurements spot analysis was performed on corrosion layers, sulphides, and other inclusions. Most analyses exhibit no clear distinguishable phases, as most inclusions were smaller than the 6 µm spotsize of the electron beam. Most inclusions in the metal's matrix displayed elevated levels of Fe and S. In the tin bronzes tin sweat or tin pest is observed around the grain boundaries of the original metal where Sn was dissolved preferentially and then precipitated as a Sn rich Cu containing oxide or metallic salt phase in between the tin bronze grains. Specifically in the electrochemically restored samples Pb and As-rich inclusions are observed indicating redox conditions, where arsenides could form during the restoration process. The results of the metal's matrix are given for the total of the 74 copper-based metal samples in table 10.1.

The main element Cu constitutes between 86.5 and 99.0 wt% of the samples and it averages 93.2 wt%, whilst the median is 92.1 wt%. Sn is also one of the major elements measured with very heterogeneous results. The Sn content varies between 0.031 and 12.8 wt% and averages 3.9 wt%, the median exhibits 0.39 wt%. The difference in the mean and the median displays already the heterogeneity of the element Sn in the samples. The other two major components are As and Ni. The As content varies between 0.011 and 4.66 wt% and averages 1.45 wt%. Ni varies between 0.021 and 11.1 wt% and averages 1.2 wt% with a median of 0.68 wt%. These four elements are the main constituents of the copper-based metal matrix.

10.1.1.1 Differing alloys and metals by their main elements

Based on the four main elements Cu, Sn, As, and Ni the artefacts were subdivided in different groups of alloys, displayed in fig. 10.1.

1. Unalloyed copper rich in As (As > 0.9 wt%): The artefacts with more than 0.9 wt% As are showing a clear

	S	Mn	Fe	Co	Ni	Cu	Zn	As	Ag	Sn	Sb	Pb
Mean	0,25	b.d.l.	0,25	0,073	1,15	92	b.d.l.	1,44	0,096	3,9	0,13	0,21
Median	0,07	b.d.l.	0,18	0,03	0,66	93,1	b.d.l.	1,35	0,064	0,39	0,088	0,14
Sdev	0,39	b.d.l.	0,21	0,1	1,78	11,2	b.d.l.	1,1	0,094	4,5	0,12	0,17
Min	0,014	b.d.l.	0,012	0,01	0,021	2,4	b.d.l.	0,011	0,024	0,031	0,01	0,052
Max	2,03	b.d.l.	0,96	0,49	11,07	99	b.d.l.	4,66	0,49	12,8	0,66	0,74

Tab. 10.1: Mean, median, standard deviation (Sdev), minimum (Min) and maximum (Max) values in wt% of the bulk copper-based metal samples analysed by electron microprobe (n=74). Mn and Zn are below detection limit (b.d.l.) in all samples.

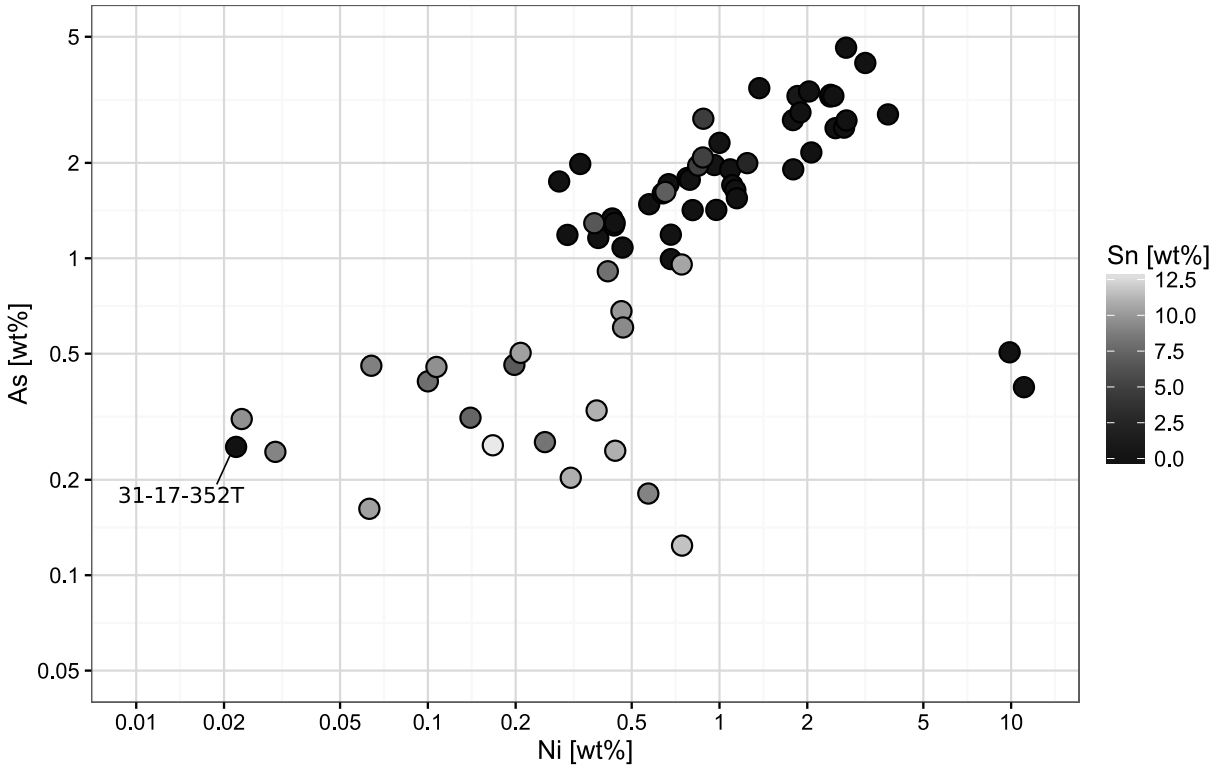

Fig. 10.1: Arsenic vs. Ni in the copper-based samples. The colours are scaled after the Sn content with 12.5 wt% as the highest (light grey) and 0 wt% as the lowest (black).

correlation in the diagram As versus Ni. These artefacts exhibit very low levels of Sn.

2. Sn-Bronze (Sn > 2 wt%): The majority of the artefacts having more than 2 wt% Sn are lower in As and Ni compared to the copper rich in As. A few artefacts of this composition fall into the correlation of the As-rich copper. The others are showing no distinctive correlation. The mark of 2 wt% Sn content was chosen as Stech (1999) states that the material characteristics of the metal changes with 2 wt% Sn but also another value could be set as threshold. Another plausible value is also when the colour of the material changes from the typical copper red to a more golden tone at 5 wt%. This is displayed in fig. 10.2. This changes only a few artefacts from tin bronze to copper rich in As.

3. Pure Copper (As < 0.9 wt%, Sn<2 / 5 wt%): Only one artefact (31-17-352T) has a Cu content of 99 wt% and is therefore considered as pure copper. This artefact exhibits low As and Ni levels, as well as no Sn contents.

4. Copper rich in Ni (Ni > 5 wt%): Only one artefact (B17508) with two samples taken exhibits very high Ni contents compared to the other copper-based metal samples with a range of 9.9 to 11.1 wt%. These two samples are different from the other copper-based artefacts as they exhibit low As concentrations (0.37 to 0.48 wt%), while yielding very high Ni.

The Sb level in the artefacts is correlated to the As content (cf. fig. 10.4). The copper rich in As and Ni exhibits also higher Sb concentrations compared to the artefacts with lower As and higher Sn levels. Most of the copper rich in As and Ni displays Sb concentrations five to ten times higher than in the tin bronze artefacts. The Sn-rich copper yields lower Sb, but there is a transition zone, where a few artefacts of each kind are similar in their Sb content. The pure copper and the copper high in Ni yield the lowest Sb levels.

The Co/Ni ratios of the overall copper-based metal artefacts are between 0.01 and 0.1. A few artefacts exhibit smaller or higher ratios in Co/Ni (cf. fig. 10.2). The tin bronze artefacts display lower Co concentrations than the copper rich in Ni and As. Cobalt is in some tin bronze artefacts below the detection limit and therefore not diagrammed in fig. 10.2. The artefact B17508 yields the highest Co and Ni levels, compared to the other copper-based metal artefacts. This artefact can also be described with the modern term cupro-nickel: an alloy of Cu and Ni. No pure copper artefact is displayed in fig. 10.2, as the Co levels are below detection limit (0.011 to 0.015 wt%). The overall copper-based metal artefacts reveal a correlation of Co and Ni.

10.1.1.2 Homogeneity of copper-based metal artefacts

Of some artefacts multiple samples were extracted from different locations. Hence the homogeneity of the artefacts can be evaluated. The As and Ni contents are displayed in multiple samples of one artefact in fig. 10.3. It is important to investigate, if all results of the different measurement

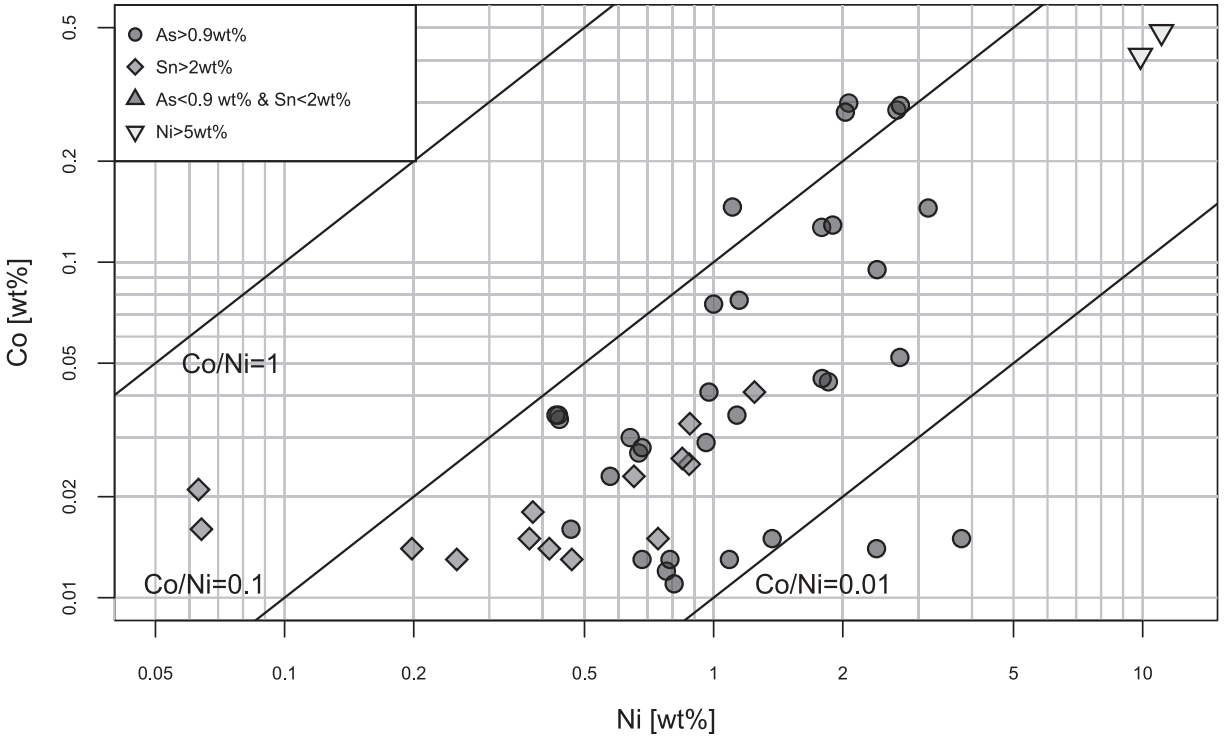

Fig. 10.2: Cobalt versus Ni in the copper-based metal samples. The symbols are distinguished by their As, Sn and Ni content.

techniques agree with each other to verify the internal reproducibility.

The artefacts 30-12-272, 31-17-217, B17356 and B17508 agree well in their electron microprobe results from different sample locations of the objects. For the artefacts B17426.1 and -2 as well as B17460.1 and -2 the analyses exhibit a transition in the As content of one part of the artefact to the other where as the Ni concentrations are consistent. The sample 35-1-422.1 differs in its As content from the other two samples of the object 35-1-422.2 and -3. Possibly As is enriched due to corrosion in the tip of the blade, where 35-1-422.1 was sampled, as it exhibits a higher corrosion status than the other samples from side and grip. Also B17528a.1 differs in its Ni levels from the other part of the same spearhead B17528a.2 due to corrosion. B17528a.2 is less corroded than -1 and therefore its electron microprobe analyses are more likely to be trusted. The other spearhead B17528b.1 resembles in its As and Ni contents B17528a.2. The two spearheads B17528a and b were analysed repeatedly on different days, while the results of the samples as well as the standards were reproduced and therefore verified. Heterogeneities in As and Ni contents in between corrosion and metal are likely, as the copper oxides do not take up all elements, the metal contained originally.

Furthermore the needle B16409 was sampled four times and the electron microprobe results of their As and Ni content are displayed in fig. 10.3. In the upper diagram the sample B16409.1 exhibits considerably higher As and Ni levels than the other three parts B16409.2 to -4. In the lower diagram only the more homogeneous As and Ni contents are displayed in focussed on the parts B16409.2 to -4. These three different analyses agree well with each other and as they were analysed on different measurement days the internal reproducibility is good.
In order to exclude that some artefacts were labelled wrong, all results of all different measurement techniques should agree with each other. Especially the Pb isotope ratios are expected to be homogeneous even if the chemistry is not.

10.1.2 Discussion: The main elements

The analysis of the main elements gives already valuable information on the general characteristics of the copper-based metal samples. As discussed in subsec. 10.1.1.1 the copper-based artefacts can be distinguished between high and low Sn levels, as well as the correlated high As and Ni content. Those artefacts with higher Sn levels exhibit no correlation in As and Ni, except for the pure copper artefact 31-17-352T. The artefacts with elevated As and Ni concentrations are in general low in Sn and the other way around with a few exceptions. As displayed in fig. 10.1 some artefacts are high in Sn additional to As and Ni. With the Sn content as colour scale in the diagram As versus Ni the indication of a transition becomes clear. The Sn content decreases gradually with increasing As and Ni levels. This trend portends a possible intentional mixing of As- and Ni-rich copper with tin bronze.

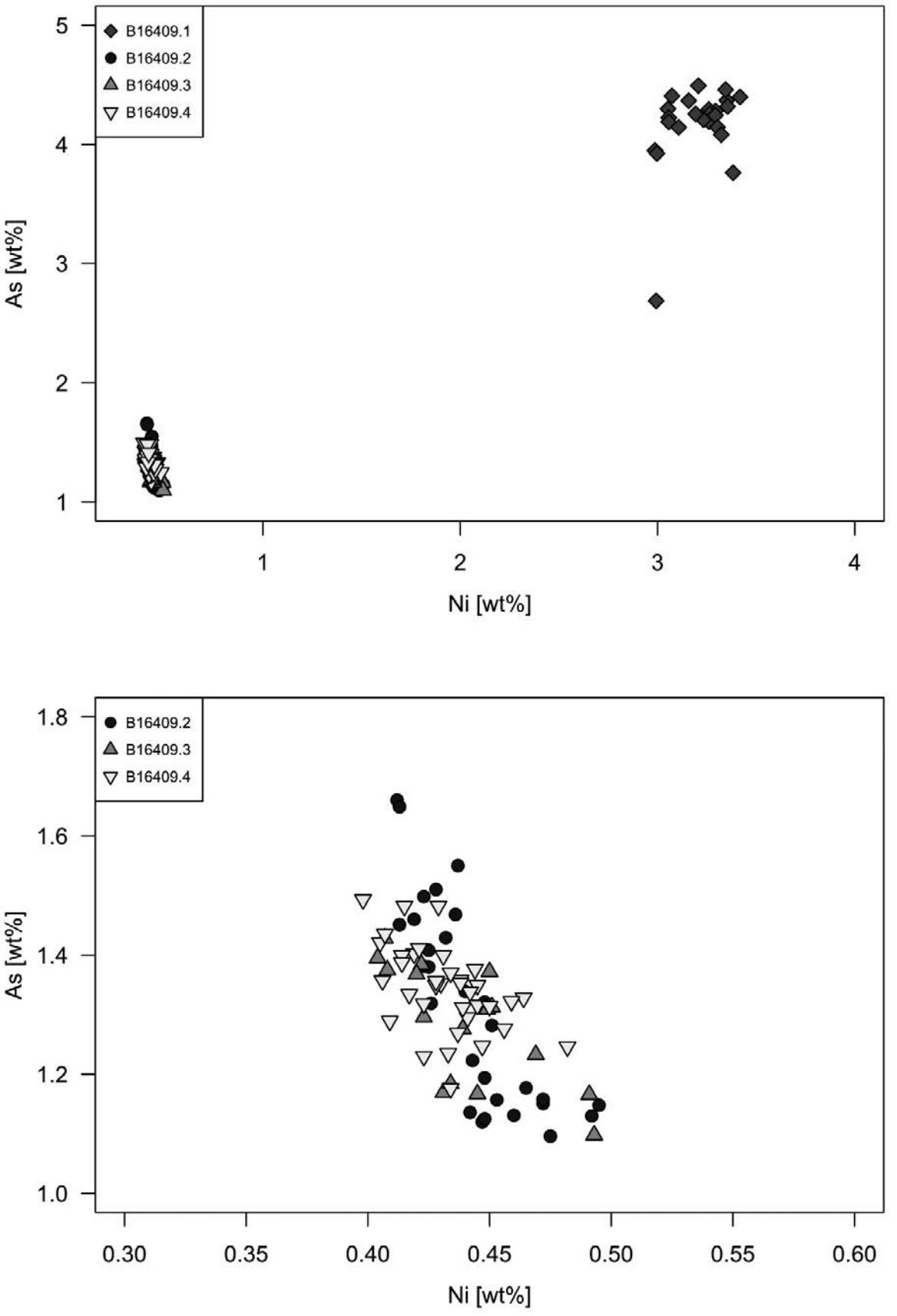

Fig. 10.3: Arsenic versus Ni of single point analyses in four independently analysed samples of the artefact B16409.1-4. The upper diagram displays all four parts of the needle. The lower diagram displays parts two to four of the artefact.

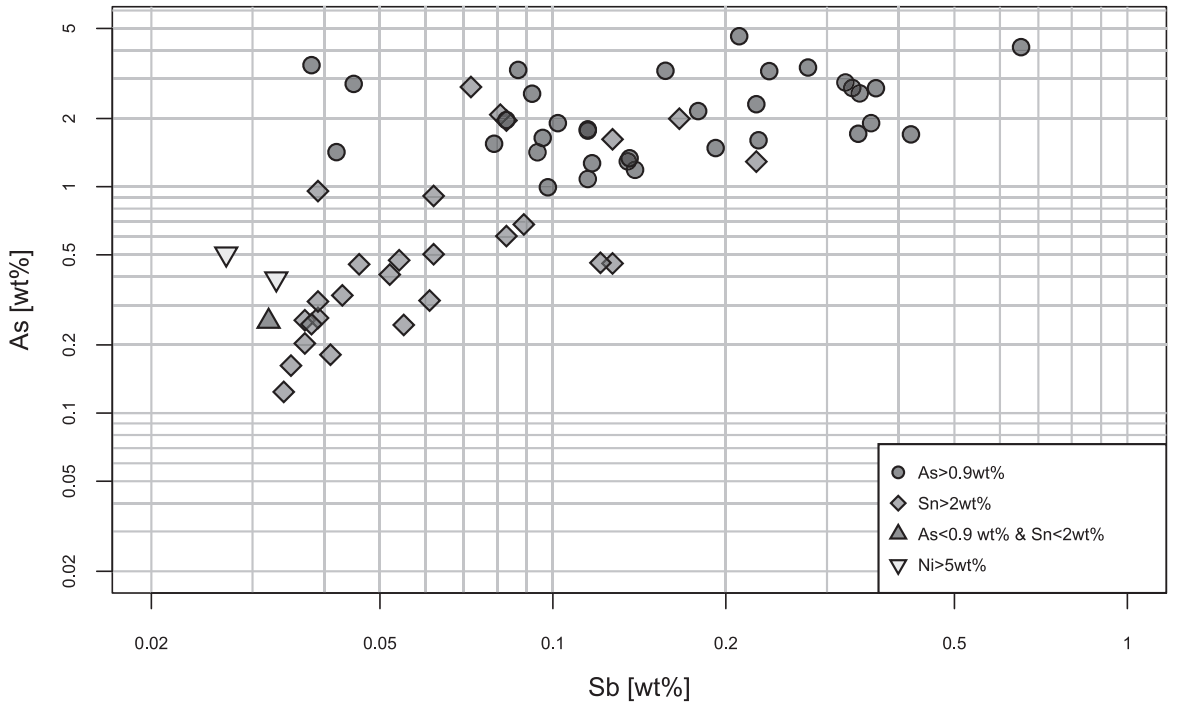

Fig. 10.4: Arsenic versus Sb in the copper-based metal samples. The symbols are distinguished by their As, Sn and Ni content.

This observation is confirmed by the ternary diagram of copper, Sn, and total of As and Ni (cf. fig. 10.5). The same artefacts forming a transition with increasing As and Ni and decreasing Sn content exhibit a transition between artefacts characterised as tin bronze and As-Ni rich copper. Interestingly, most of these transitional metals are dating to Early Dynastic III. This is further confirmed when comparing the electron microprobe data of this study to the particle-induced x-ray emission (PIXE) measurements conducted by the Museum Applied Science Center for Archaeology (MASCA).

The Mesopotamian Metals Project analysed further artefacts of Ur dating from Jemdet Nasr to Akkadian times. These data are displayed in fig. 10.7 and exhibit similar trends as the measurements of this study. Additionally the pXRF data of Müller-Karpe (2004) are diagrammed in the same ternary diagram emphasising the same trend in low to high Sn contents, where the Sn content is in general very variable with further artefacts in the transition of As-Ni-copper to tin bronze. The potential for intentional mixing will be further discussed in sec. 10.1.5 and 10.2.4.

The diagram in fig. 10.5 exhibits other essential information. The artefacts oldest in date display no high Sn contents. The Late Uruk hook 31-17-267 consists of arsenical copper with 1.18 wt% As, as does the Jemdet Nasr pin 33-35-79 with 2.57 wt% As. However, the Jemdet Nasr to ED I needle or pin shaft 31-17-352T exhibits low As contents with 0.25 wt%. In the chronological sequence the Early Dynastic III artefacts account for the bulk of the copper-based samples. These objects have a wide range of main element compositions, as discussed before. The Akkadian and Ur III to Isin Larsa dating artefacts display roughly the same range of compositions as the Early Dynastic III dating ones. The same applies for the one Early Iron Age tin bronze handle 31-17-265 and the artefacts of unknown date.

The earliest artefacts exhibit no significant amounts of Sn. In Early Dynastic III tin bronze started to be accessible on a grand scale. The pure copper artefact 31-17-352T is not only different in chemical composition, but also in its microstructure, as it has irregular clusters of slag inclusions showing, unlike the other Ur artefacts (cf. fig. 10.6). This might indicate a different origin than the other artefacts, what seems reasonable, due to the date of Jemdet Nasr/ Early Dynastic I. The access to a copper rich in As and Ni is already noted for Jemdet Nasr times indicated by the pin 33-35-79 of Jemdet Nasr grave 18, which has Ni contents of 2.5 wt%. The early phases of Ur are generally characterised by only few metal finds but the number increases massively in Early Dynastic III.

Regarding the type of artefact, jewellery exhibits no or only little mixing composition of Sn with As- and Ni-rich copper. The transitional artefacts between both compositions are mostly tools and weapons. One pin (B17022), three adzes (30-12-264, 31-17-205, 31-17-217), two chisels (B17426, B17478), one axe (B17479), and one dagger (B17351) show this composition. Except for B17022 (Akkadian) the other transitional copper metal artefacts all are Early Dynastic in date. The chisels have exclusively higher As and Ni contents and only slightly higher Sn levels. The mirror 30-12-272 was most likely, intentionally made of tin bronze, due to its high reflectivity. The daggers have either high Sn or As and Ni levels. The majority of the pins and needles is made of As-Ni-copper.

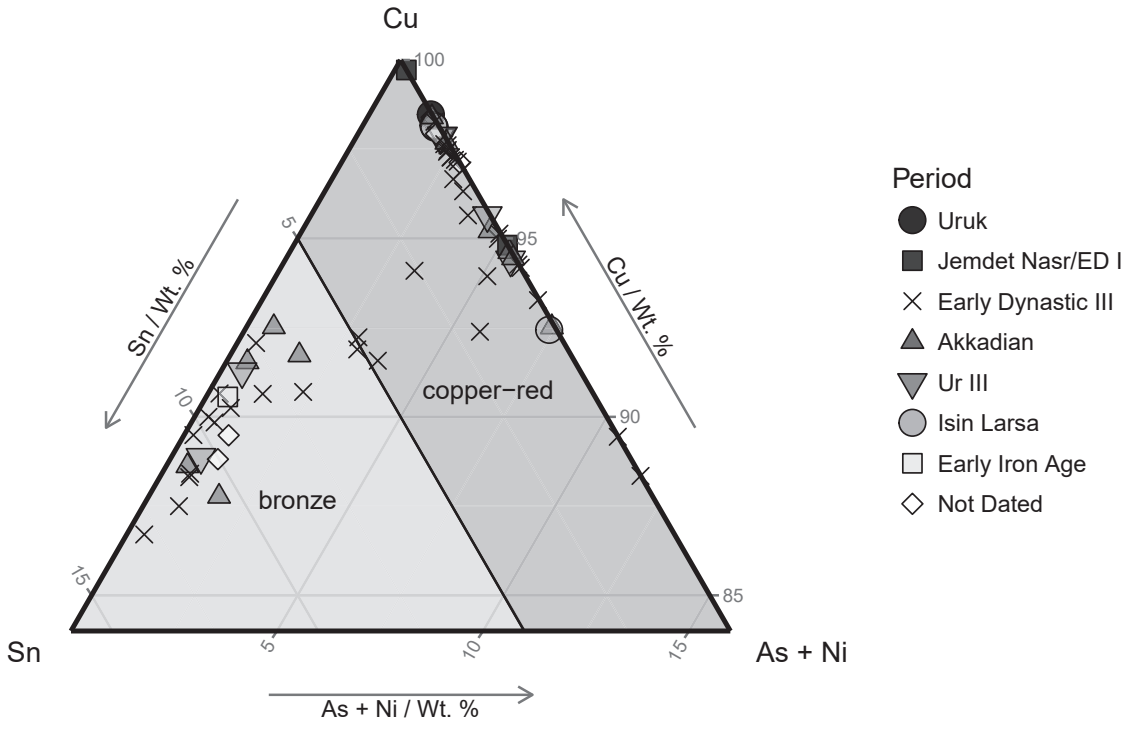

Fig. 10.5: Ternary diagram of copper, Sn, As + Ni content of the copper-based samples. The symbols represent the dating of the displayed artefacts. The optical colour shift from copper red to bronze of the metal by changing Sn content is displayed by the background colours of the diagram.

Of the bracelets sampled two are made of tin bronze and one of silver. Otherwise there is no clear trend observed, whether certain types of artefacts were made of a specific alloy. The same applies to the tombs the objects were found in. Tin bronzes are not limited to the Royal Tombs.

10.1.2.1 The chemistry of the inclusions

The majority of the copper-based metal exhibits inclusions mostly of sulphide phases. The analysis of the pure inclusions was impossible, due to their size being mostly smaller as the electron beam of the electron microprobe. Although only mixed analysis of inclusion and surrounding metal was performed, elevated S and Fe contents were observed in part of the inclusions. A few artefacts exhibited inclusions rich in As and Pb. These inclusions are likely to be characterised as speiss and are remnants of the smelting process. These inclusions are not limited to the As-Ni-copper and occur in tin bronzes. The electron microprobe results of inclusion analysis is given in the appendix. Some silver rich inclusions were also analysed by electron microprobe. The majority of these inclusions is a mixture of copper and silver possibly in consequence of mixed analysis. These inclusions form usually within intergranular voids and corrosion. This can easily happen during the corrosion process. The conditions during the 4500 years the artefacts rested in the soil were not ideal for metals. Ur is located in a floodplain in an arid climate and near the Persian gulf, therefore the soil contains salt and groundwater levels are high. The combination of humidity and salt increase the corrosion rate of the artefacts. Likely some silver was dissolved and then precipitated, when the pH or other conditions changed over time (McNeil and Little, 1992). Whether the silver inclusions came from dissolved Ag contents within the copper metal itself or derive from silver artefacts stored next to the copper-based artefacts is not clear.

10.1.3 Results: trace elements - nanosecond-laserablation-SC-ICP-MS

As discussed in section 10.1.1.1 the results are displayed by their type of material. As a total number of eleven standards were measured to calculate the correct means of each isotope. The standard measurements are displayed as medians of all four measurement days compared to the certified values in table 10.2.

The results are mostly within an 10 % error range and comparable with other laserablation results of trace elements measured by LA-ICP-MS. All of the results in the wt% range exhibit higher deviation from the certified values as the detector of the ELEMENT2 in analogue mode reaches saturation. Each isotope of each standard exhibiting higher than 10% deviation of the certified value was excluded for the calculation of the results based on

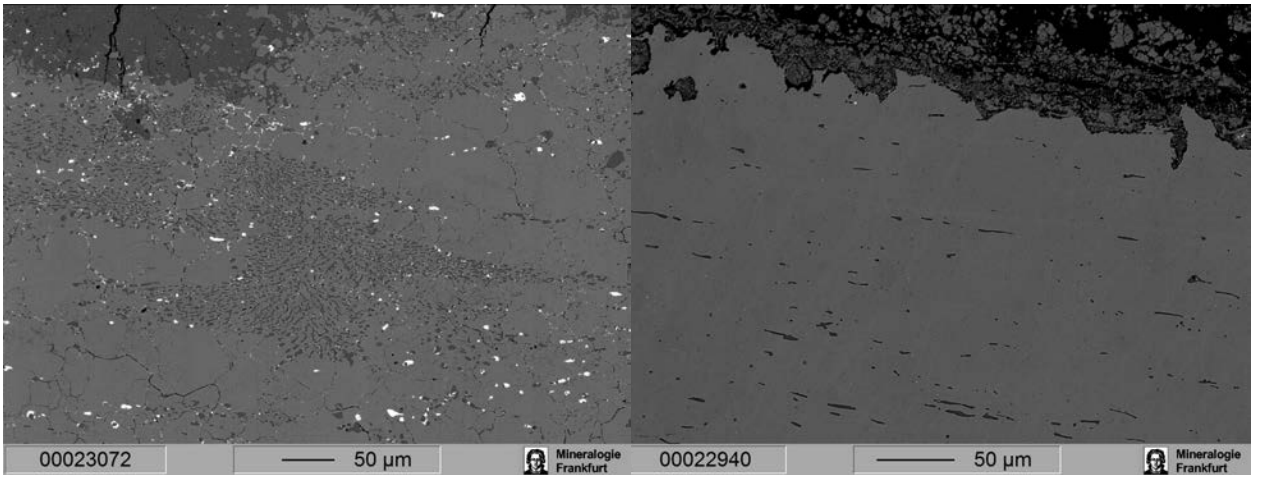

Fig. 10.6: Microstructures of 31-17-352 (left) and B17528b (right) in comparison with each other in the backscatter-electron image. B17528b exhibits typical sulphide type slag inclusions (darker grey) elongated by hammering, whereas the slag inclusions appear in 31-17-352 in clusters. Lead inclusions are observed as white in the BSE image.

the measured standards. Antimony proved to be a reliable internal standard for the copper-based samples, as it is distributed within the matrix very homogeneously. Also the levels are in an ideal range for the mass spectrometers detectors. In general the median agrees better with the certified values than the mean. Therefore the median value is given for both standards and samples in the results.

The results of the LA-ICP-MS trace element analysis are displayed in table 10.4 with mean, median, standard deviation, as well as maximum and minimum values.

Mn was already below detection limit in the electron microprobe results and as well in many samples measured by LA-ICP-MS. In general Mn is very low in most of the samples above detection limit. The Mn content varies between 0.5 and 739 ppm and averages 30 ppm. ^{59}Co is distributed more heterogeneously between the samples.

In sample B17508 Co had to be excluded from the results, as the high Ni content of more than 10 wt% causes an overlap with the rims of the peaks ^{58}Ni and ^{60}Ni on the mass of ^{59}Co. ^{60}Ni was completely excluded from the results, due to the high concentrations in a large number of samples and because of the interference with $^{120}Sn^{2+}$ in the Sn-rich samples. The same is applied for ^{75}As as it has an interference with $^{40}Ar^{35}Cl$. Sn is one of the main constituents of some samples and is enriched in corroded areas and in between grain boundaries of the samples. As the spotsize of the laser is much larger than of the electron microprobe, it was almost impossible to avoid measuring at least small corroded parts of the artefact sections. The object 30-12-696 (Bull's head) e.g. exhibits a Sn content of 7.4 wt % (EPMA), whereas the Sn content measured by LA-ICP-MS shows 11.5 wt %. As the electron microprobe results are more reliable for main elements, Ni, As and Sn were excluded from the LA-ICP-MS results.

Pd is mostly below 1 ppm. The Pd content varies between 0.1 and 65.5 ppm and averages 1.4 ppm. Also the elements In and Cd are mainly below 1 ppm. The element Te exhibits larger variations consistent in both measured isotopes ^{128}Te and ^{130}Te. The Te content varies between 3.3 and 3390 ppm. Platinum is mostly below 10 ppm levels. Except for the samples 31-17-352, 31-17-193, 35-1-479, B17276, B17418, B17422, B17525 and B17551 the Pt level exceeds 10 ppm.

The Pb content varies between 9.1 and 28043 ppm and averages 2557 ppm. As lead and copper are not forming homogeneous alloys, Pb is incorporated as tiny inclusions, therefore the total Pb content is difficult to determine by small spotsizes. Thus the Pb contents measured by electron microprobe differ from the LA-ICP-MS results. Due to the larger spotsizes the Pb content is likely to be better determined by LA-ICP-MS, as a better mean is provided by analysing a larger area. B17382 and B17410 had to be excluded from the results due to their corrosion status.

The sample 98-9-164 of a copper ingot displays trace element concentrations differing from all other copper-based samples. It exhibits high Cr (3345 ppm), Mn (856 ppm), Zn (2092 ppm), Ge (75 ppm), Se (11496 ppm), Cd (88 ppm), In (100 ppm), Te (3541 ppm), Pt (165 ppm), and Au levels (149 ppm). The ingot itself is unfortunately of unknown origin, as it has no u- or field-number. No tomb is noted for it, therefore the ingot's dating is unclear. The results for this artefact are given in the appendix, but are not further discussed regarding provenance, as its context is unknown.

10.1.3.1 The bulk chemical composition of the copper-based artefacts

As discussed in section 10.1.1.1 the material is displayed by type of material. In fig. 10.8 and 10.9 the LA-ICP-MS results are complemented by electron microprobe results for the elements S, Fe, Ni, As, Ag, Sn, and Sb. So all chemical results are summarised in the following spider diagrams.

Standard		53Cr	55Mn	59Co	60Ni	66Zn	72Ge	75As	77Se	106Pd	111Cd	113In	128Te	130Te	194Pt	195Pt	197Au	206Pb	209Bi
BAM376	median	310	121	208	216	231	0,3	205	218	6,5	200	45	207	215	0,1	0,1	0,1	226	182
BAM376	SE%	77,3	8,6	-	3,5	6,5	29,1	1,2	5,7	142,3	2,8	22	6,6	6,7	8,9	6,3	24041	3,6	4,3
BAM376	certified	400	205,9	208	209	217	-	199	210	-	186	-	215	215	-	-	-	236	200
Bronze A	median	1,5	3	5,2	295	14212	0,4	591	61,6	0,5	10	5	1,3	1,2	0	0	0,3	18300	337
Bronze A	SE%	24,7	280,3	46,1	0,4	17,3	8,4	4,2	27,5	22,1	32,3	24	28	37,7	21,6	59,7	3,8	4,5	12,7
Bronze A	certified	-	-	-	300	18400	-	600	-	-	-	-	-	-	-	-	-	18300	-
C1252	median	6,8	9,7	89	133	49	0,2	114	76,1	0,5	14	1,9	51	53	0,01	0,1	31,5	60	23
C1252	SE%	49,9	35,5	10	2,4	7,5	723,5	1,4	2,6	219,6	3,9	61	3	3,4	-	2961,9	19,2	13,1	2,2
C1252	certified	7,4	17	90	128	60	-	115	53,6	-	14	-	51	51	-	-	34,9	60	21
CKD319	median	2,9	146	39,5	3936	22128	1,1	861	19	0,5	8,3	4,2	1,9	2,4	0,01	0,2	0,5	22579	438
CKD319	SE%	18,6	11,2	8,9	1,2	5,3	12,3	2,1	153,7	4,1	40,6	20	68,3	92,1	5,5	5,5	4,6	7,6	5,5
CKD319	certified	NA	150	-	4000	23000	NA	800	-	-	-	-	-	-	-	-	-	24000	450
UE15	median	1,4	50	26,5	2477	1191	0,2	852	12,8	0,1	0,6	0,4	2,1	1,7	0	0,1	0,2	5317	20
UE15	SE%	18,8	13,6	83,4	2,4	3,9	40,2	5,8	108,2	8,1	77,2	21	147	108,1	28,1	7,1	1,9	1,6	58,2
UE15	certified	NA	50	-	2300	1700	-	900	-	-	-	-	-	-	-	-	-	5000	NA
AgA2	median	46	115	109,2	187	4351	53	126	87,1	68	87	28	101	99	82	83	4884	9333	1028
AgA2	SE%	29,3	9,1	74,9	18,4	5,1	3	3,5	8,4	0,8	22,2	39	17,6	18,1	1,4	1,5	2,9	2	7,6
AgA2	certified	76	115	163	264	5020	47	144	78	76	113	65	98	98	114	114	5070	10200	1130

Tab. 10.2: Measured medians, relative standard errors (SE%) and certified values for each measured isotope on the standards used for the arsenical copper samples. Not detected values (-) are marked.

Standard		53Cr	55Mn	59Co	60Ni	66Zn	72Ge	75As	77Se	106Pd	111Cd	113In	128Te	130Te	194Pt	195Pt	197Au	206Pb	209Bi
BAM376	median	310	121	208	216	231	0,3	205	218	6,5	200	45	207	215	0,1	0,1	0,1	226	182
BAM376	SE%	77,3	8,6	-	3,5	6,5	29,1	1,2	5,7	142,3	2,8	22	6,6	6,7	8,9	6,3	24041	3,6	4,3
BAM376	certified	400	205,9	208	209	217	-	199	210	-	186	-	215	215	-	-	-	236	200
Bronze A	median	1,5	3	5,2	295	14212	0,4	591	61,6	0,5	10	5	1,3	1,2	0	0	0,3	18300	337
Bronze A	SE%	24,7	280,3	46,1	0,4	17,3	8,4	4,2	27,5	22,1	32,3	24	28	37,7	21,6	59,7	3,8	4,5	12,7
Bronze A	certified	-	-	-	300	18400	-	600	-	-	-	-	-	-	-	-	-	18300	-
C1252	median	6,8	9,7	89	133	49	0,2	114	76,1	0,5	14	1,9	51	53	0,01	0,1	31,5	60	23
C1252	SE%	49,9	35,5	10	2,4	7,5	723,5	1,4	2,6	219,6	3,9	61	3	3,4	-	2961,9	19,2	13,1	2,2
C1252	certified	7,4	17	90	128	60	-	115	53,6	-	14	-	51	51	-	-	34,9	60	21
CKD319	median	2,9	146	39,5	3936	22128	1,1	861	19	0,5	8,3	4,2	1,9	2,4	0,01	0,2	0,5	22579	438
CKD319	SE%	18,6	11,2	8,9	1,2	5,3	12,3	2,1	153,7	4,1	40,6	20	68,3	92,1	5,5	5,5	4,6	7,6	5,5
CKD319	certified	NA	150	-	4000	23000	NA	800	-	-	-	-	-	-	-	-	-	24000	450
UE15	median	1,4	50	26,5	2477	1191	0,2	852	12,8	0,1	0,6	0,4	2,1	1,7	0	0,1	0,2	5317	20
UE15	SE%	18,8	13,6	83,4	2,4	3,9	40,2	5,8	108,2	8,1	77,2	21	147	108,1	28,1	7,1	1,9	1,6	58,2
UE15	certified	NA	50	-	2300	1700	-	900	-	-	-	-	-	-	-	-	-	5000	NA
AgA2	median	46	115	109,2	187	4351	53	126	87,1	68	87	28	101	99	82	83	4884	9333	1028
AgA2	SE%	29,3	9,1	74,9	18,4	5,1	3	3,5	8,4	0,8	22,2	39	17,6	18,1	1,4	1,5	2,9	2	7,6
AgA2	certified	76	115	163	264	5020	47	144	78	76	113	65	98	98	114	114	5070	10200	1130

Tab. 10.3: Measured medians, relative standard errors (SE%) and certified values for each measured isotope on the standards used for the tin bronze samples. Not detected values (-) are marked.

	53Cr	55Mn	59Co	66Zn	72Ge	77Se	106Pd	111Cd	113In	119Sn	128Te	130Te	194Pt	195Pt	197Au	206Pb	209Bi
Mean	143	29,6	674	102	8,3	478	1,4	2,3	4,1	73153	114	117	13,6	11,1	46	2557	122
Median	4,5	3,5	373	19,8	0,9	167	0,2	0,3	0,7	1664	38,7	39,6	0,5	0,6	19,6	1181	29,2
σ	829	111	890	377	43,6	1466	8,4	12,4	19,6	347643	426	436	63	52,3	87	4212	272
Min	0,3	0,5	0,8	2,3	0,1	19,4	0,03	0,03	0,1	4	3,4	3,3	0,03	0,06	2,2	9,1	2,3
Max	6269	739	3892	2621	366	11522	65,5	93	162	2201630	3285	3390	410	413	550	28043	2015

Tab. 10.4: Results of the trace element analysis with LA-ICP-MS (n=73 samples). Displayed are mean, median, standard deviation (σ), minimum and maximum values for the bulk copper-based metal analysis.

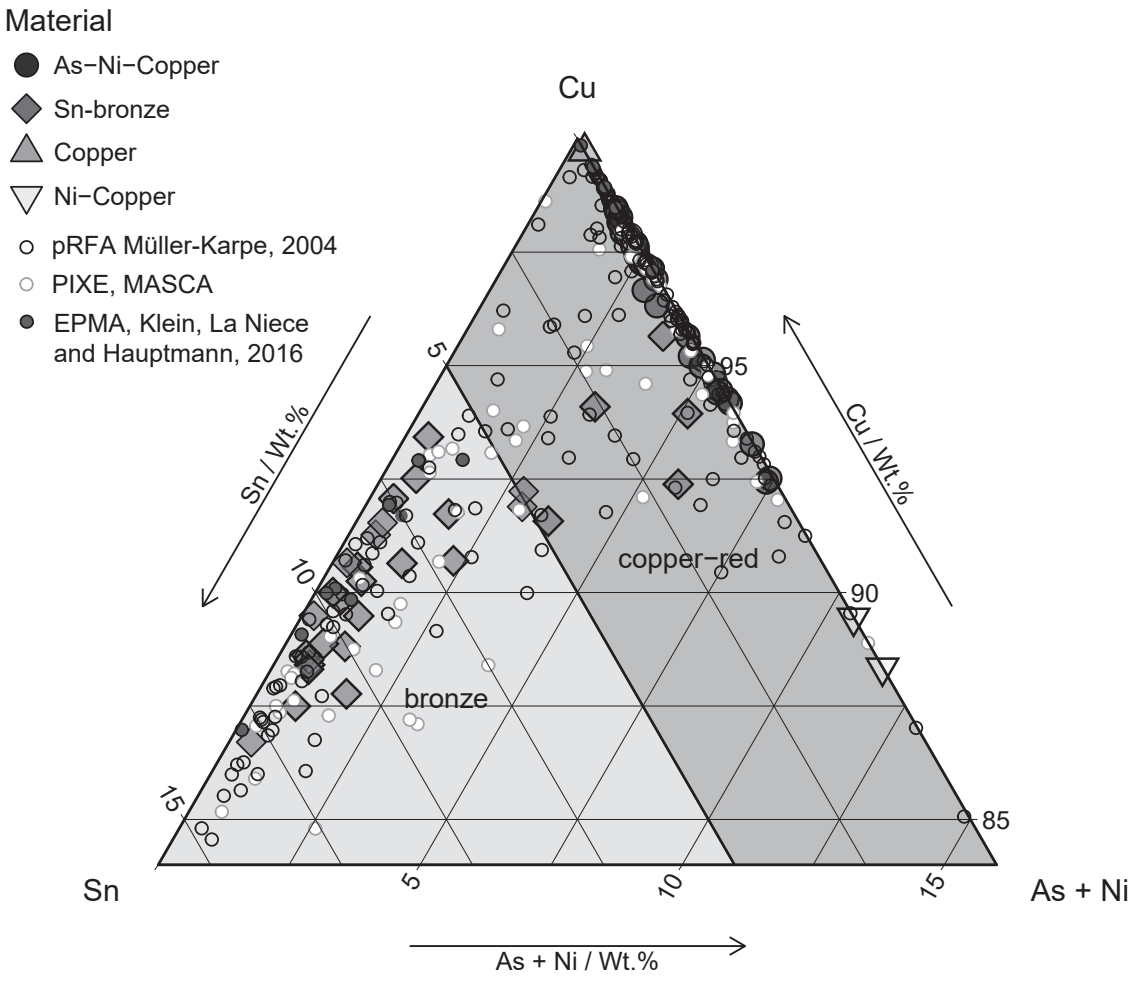

Fig. 10.7: Ternary diagram of copper, Sn, As + Ni. The symbols are distinguished by material type of the Ur electron microprobe results. Additionally, the PIXE analysis of the Mesopotamian Metals Project from the Museum Applied Science Center for Archaeology (MASCA) are displayed as white circles with reddish contours, the pXRF data of Müller-Karpe (2004) are diagrammed as black open circles, and the EPMA analyses of Klein, La Niece and Hauptmann (2016) are displayed as small blue circles with black contours.

A total number of 38 copper rich in As and Ni samples was analysed for trace elements. The highest means of concentrations are As and Ni in the weight percent range. They are followed by the range of 0.1 to 1 wt% of the elements S, Fe, Co, Ag, Sn, Sb, and Pb. In the range of 100 to 1000 ppm only Se is to be ranked. Cr, Zn, Te, Au, and Bi are on average within the range of 10 to 100 ppm. In the very low ppm range below 10 ppm are Mn, Ge, Pd, Cd, In, and Pt to be found. The range between maximum and minimum differs as well. As for example Fe, Co, Ge, Sn, and Pt exhibit a larger range of differing concentrations compared to e.g. As.

The chemical composition of the tin bronze samples which exhibit more than 2 wt% Sn are summarised in the spider diagram in fig. 10.9. Apart from Sn the most abundant elements in the tin bronze samples are S, Fe, Ni, As and Pb within 0.1 and 1 wt% as mean values. These elements are followed by Co, Zn, Se, Ag, Sb, Te, and Bi in the range of 100 ppm to 1000 ppm. Between 10 and 100 ppm are Cr, Mn, and Au. In the low ppm range below 10 ppm are Ge, Pd, Cd, In and Pt to be ranked.

The two samples of B17508 having more than 10 wt% Ni are not included in the spider diagrams, but they are displayed in the scatter plots below. The only true pure copper artefact 31-17-352T is not diagrammed in the spider plots, either.

Comparing the tin bronze to the As-Ni-copper artefacts exhibits elevated levels of Mn, Zn, Se and Pd in the tin bronze artefacts. Cd and In contents are also slightly enriched in the tin bronzes, as are the heavy elements Te, Pt, Au, Pb, and Bi.

These elements reveal a higher range between maximum and minimum values in the tin bronzes. The As-Ni-copper artefacts display higher levels of Sb and Co besides As and Ni. However the general trend of the tin bronzes compared to the As-Ni-copper exhibits only small differences in the trace element composition.

10.1.4 Discussion: Trace element analysis

The trace element composition of the copper-based artefacts exhibits only small differences in between the

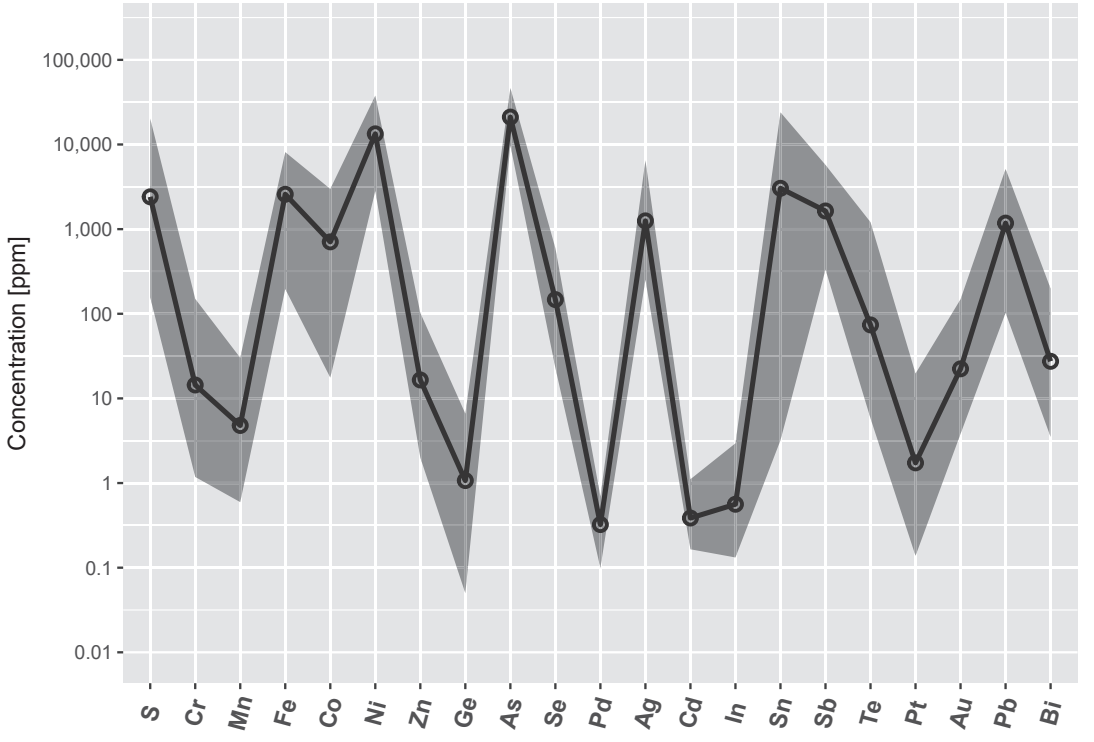

Fig. 10.8: Spider diagram of the LA-ICP-MS results of the As-Ni-Cu artefacts. S, Fe, Ni, As, Ag, Sn and Sb are complemented electron microprobe results. The blue line and points represent the mean, the filled contour exhibits the minimum and maximum values.

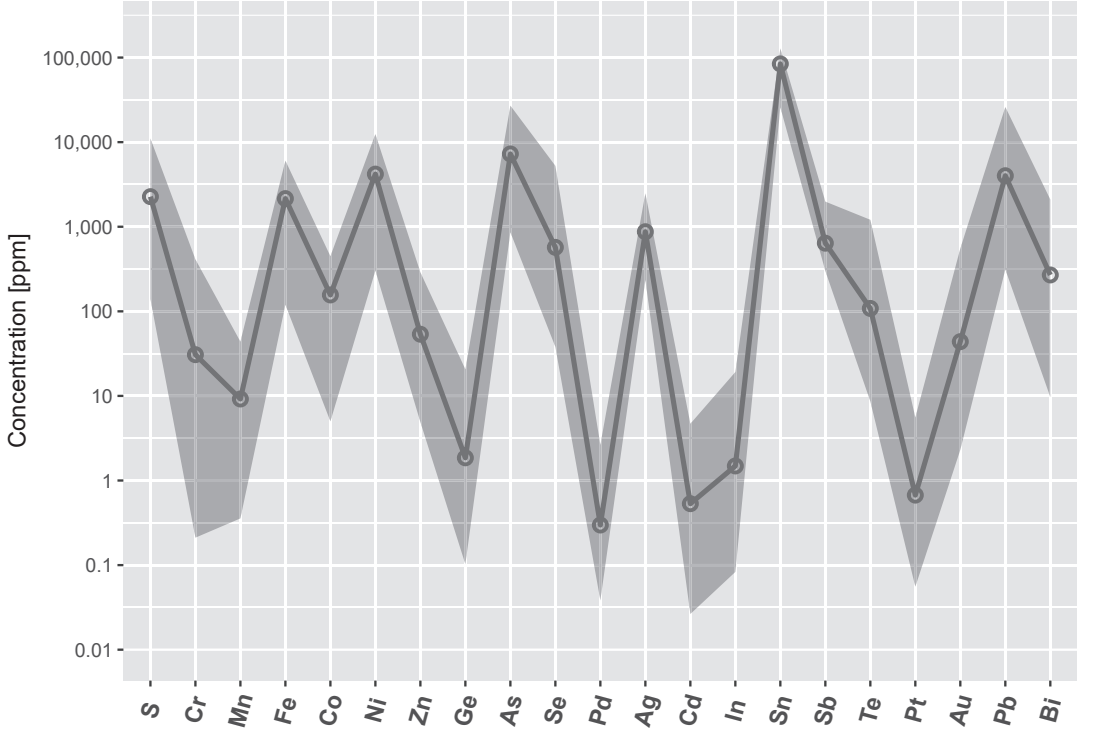

Fig. 10.9: Spider diagram of the LA-ICP-MS results of the Sn bronze artefacts. S, Fe, Ni, As, Ag, Sn and Sb are complemented electron microprobe results. The orange line and points represent the mean, the filled contour exhibits the minimum and maximum values.

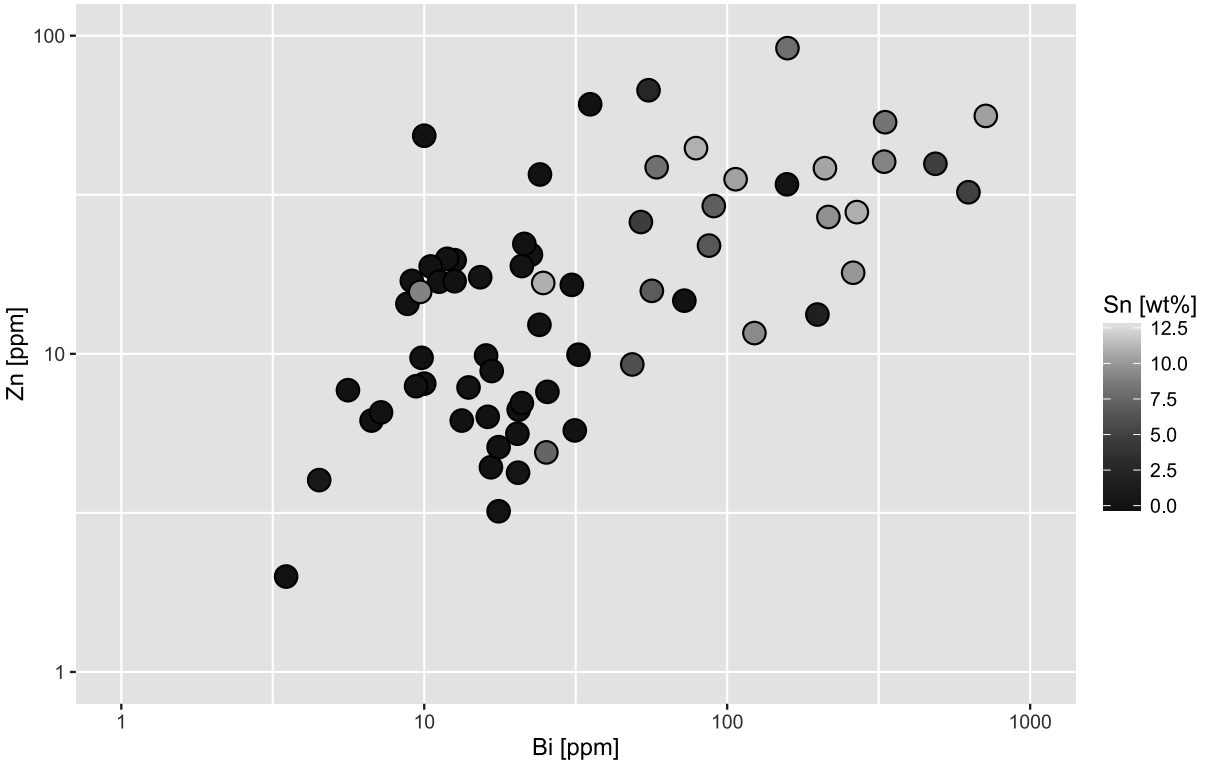

Fig. 10.10: Bi versus Zn in the copper-based artefacts. The colour scale of the symbols represents the Sn content.

tin bronze- and As-Ni-copper artefacts. The copper rich in As and Ni has a tendency to slightly higher Co, Sb, Cr, Pd, and Pt levels, as well as slightly lower concentrations of Zn, Pb, and Bi compared to the tin bronze artefacts (cf. fig. 10.8 and 10.9), although the differences are not outstanding.

The Pt group elements (PGE) exhibit no trend, though only the Pd-group elements (PPGEs: Rh, Pt, Pd) were measured. The measurement of the Ir-group elements (IPGEs: Os, Ir, Ru) was not possible, due to the lack of a suitable laserablation standard. The elements characteristic of placer tin (e.g. Mn, Pt, Au, Pb, Bi) are not significantly higher although the presumed input of 1 part of placer tin to 6 or 8 parts of copper is expected to be only small. Other elements typical of primary cassiterite deposits, as Ta, Nb, or W, could not be measured, as there are no matrix-matched standards available, but could be worth investigating for the future.

As in the ternary diagram of Sn, Cu, As + Ni, there is no clear threshold of high to low Zn and Bi levels between tin bronze and As-Ni-copper. This transition can be explained by the general presence of certain base metals in copper ores, the only difference being the quantity of associated minerals. But even the accessory minerals can vary within one deposit in between individual veins or ore stages. Therefore expectations should not be risen to be able to differ between even individual veins or specific areas of one single deposit, when comparing trace elements. Nevertheless, trace element levels give valuable information on accessory minerals and thus additional implications on the ore resources, even if they hold only general informations. The larger part of the associated base metals were also extracted during the smelting process and the primary ore composition was most certainly different, which should be taken into account, when evaluating trace elements. The exact depletion of trace elements can only be reconstructed by knowing the original process parameters. As the trace elements behave differently during roasting, smelting, and refining, the ratios change usually compared to the original ore and not all elements, which were correlated in the ore, remain correlated in the resulting metal. Therefore the observed trends should be handled with care.

10.1.5 Implications of the chemistry on the ore source

The main elements of the copper-based metal give information on the ore sources. As discussed in sec. 10.1.1.1 the artefacts can be subdivided by Sn, As, and Ni levels. On the one hand there are artefacts with high Sn concentrations and low As and Ni levels, on the other hand artefacts with low Sn content and high As and Ni levels as well as compositions in between.

The S contents and inclusions emphasise the usage of sulphide ores. Due to the wide range and the smooth transition from low to higher As and Ni levels a natural alloy in consequence of associated Ni arsenide mineralisation

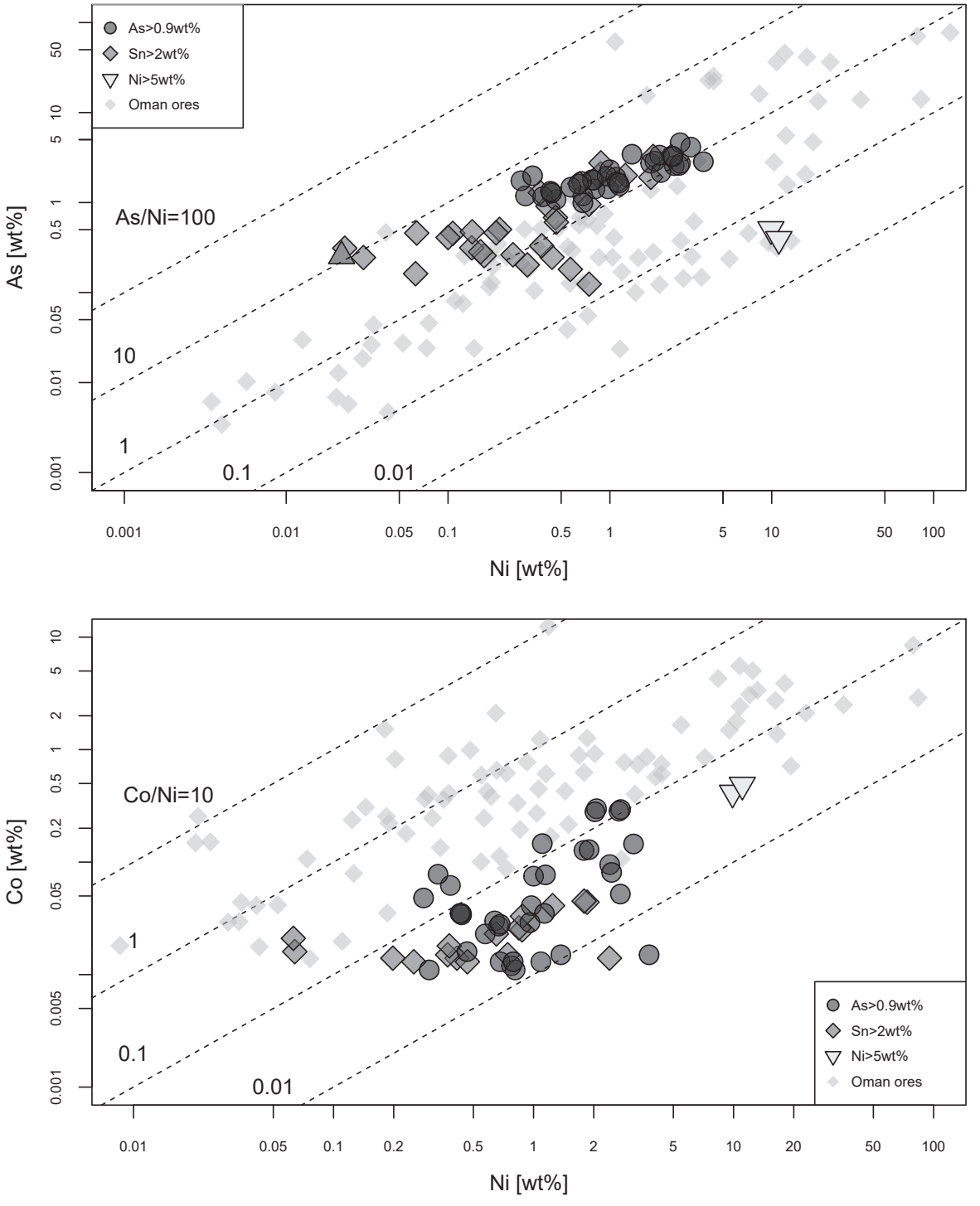

Fig. 10.11: Arsenic versus Ni (upper) and Co versus Ni (lower) of the Ur copper-based artefacts. The Omani copper ores are displayed as grey diamonds and normalised to their Cu content (Prange, 2001).

is indicated. If arsenic had been alloyed intentionally, a treshold at a certain As content and a narrow range of As and Ni concentrations would have been present.

Typical Ni arsenides / sulphides are for example nickeline, gersdorffite, rammelsbergite, and pentlandite. Especially the high Ni levels indicate an ore associated with ultramafic rocks, which occur in ophiolites. As discussed in sec. 6 the Tethyan Eurasian Metallogenic Belt (TEMB) is an ophiolite belt extending over Anatolia, Iran, Oman and further East to the Himalayas. The copper deposits in the Iranian highlands are not associated with the ophiolites, whereas the Ergani Maden and Siirt-Madenköy deposits in Anatolia and the rich deposits in Oman are related to ophiolites (Lorand, 1988; Bartura, Hauptmann and

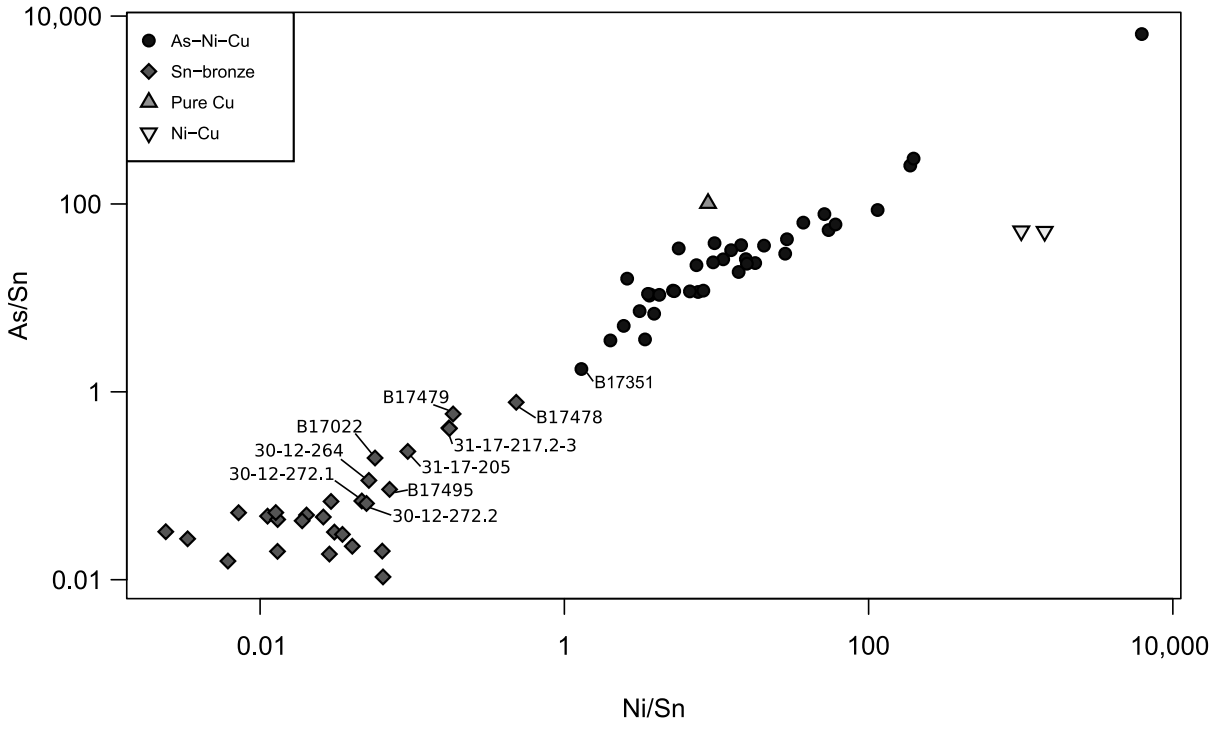

Fig. 10.12: The ratios of Ni/Sn vs. As/Sn of the Ur copper-based artefacts. The artefacts in the transition zone between As-Ni-copper and Sn-bronze are labelled.

Schöne-Warnefeld, 2008; Akıncı, 2009). The copper deposit in Oman formed in the lower mantle-near sequence of the ophiolite body and underwent a partial melting event, where the residual sulphides were enriched in Cu and Ni (Lorand, 1988). In Ergani and Siirt-Madenköy are volcanic massive sulphide deposits of the Cyprus-type to be found, where the pyrites are locally enriched in Co and Ni (Akıncı, 2009). The deposits of both regions have also an arsenic component, as commonly associated with hydrothermal deposits (Griffitts, et al., 1972; Prange, 2001).

The Ur copper-based artefacts are partially in agreement with the chemical data of Oman ores (Prange, 2001). The chemical data of Prange (2001) were normalised to Cu before plotting. The ratio of As/Ni of the Ur artefacts is slightly higher than the ore data, whereas the ratio of Co/Ni is lower than the Oman ores (cf. fig. 10.11). Begemann, et al., (2010) made the same observations when comparing Mesopotamian artefacts with Oman ores. Regarding the Co content it is likely, that Co is more easily oxidised during smelting than Ni and thus removed from the metal phase (Hauptmann, 2007; Begemann, et al., 2010). However, As is expected to be removed partially by smelting due to its volatile character. Therefore the As/Ni ratio should decrease to some extent in the copper artefacts compared to the original ore ratios. Although the copper artefacts still being partially in range of the As/Ni ratios of the Oman ores could be the result of intentional selection of As-rich Oman copper ores, as the ancient smelters did likely notice the technological advantages of an arsenical copper with higher hardness (Northover, 1989).

The majority of the tin bronze artefacts has to the order of ten lower As and Ni levels than compared to the As-Ni-copper with a few exceptions. These are still not very low and indicate arsenides associated with the copper ore source. This is not unusual for copper sulphide ores, as a large number deposits bear some quantities of arsenopyrite, for example. The same applies to other base metals, as Co. The high base metal levels in the artefacts are most likely indicating a copper, that has not been intentionally purified. The general trend of the tin bronzes being lower in As, Sb, and Co indicate lower fahlore contents as in the source of the As-Ni-copper. However, the tin bronzes appear to be from a source rather associated with Zn-Pb-Bi-ores. This type of polymetallic mineralisation is not very rare. Levy et al., (2002) mention that no evidence for intentional refinement of impurities, such as As, Ni, Pb, and Fe, has yet been discovered at any Early Bronze Age workshop site. The high impurity levels in the Sn-bronze artefacts of Ur analysed in this study support this argument.Further implications on the ore source can be gained by isotope analysis and shall be discussed in sec. 10.2.4.

10.1.5.1 Intentional alloying of tin bronze

The majority of the tin bronze artefacts exhibits lower contents of As, Ni, Co, and Sb (cf. fig. 10.8 and 10.9). The transition in fig. 10.5 and 10.7 between high and low Sn contents is very smooth and no clear boundary

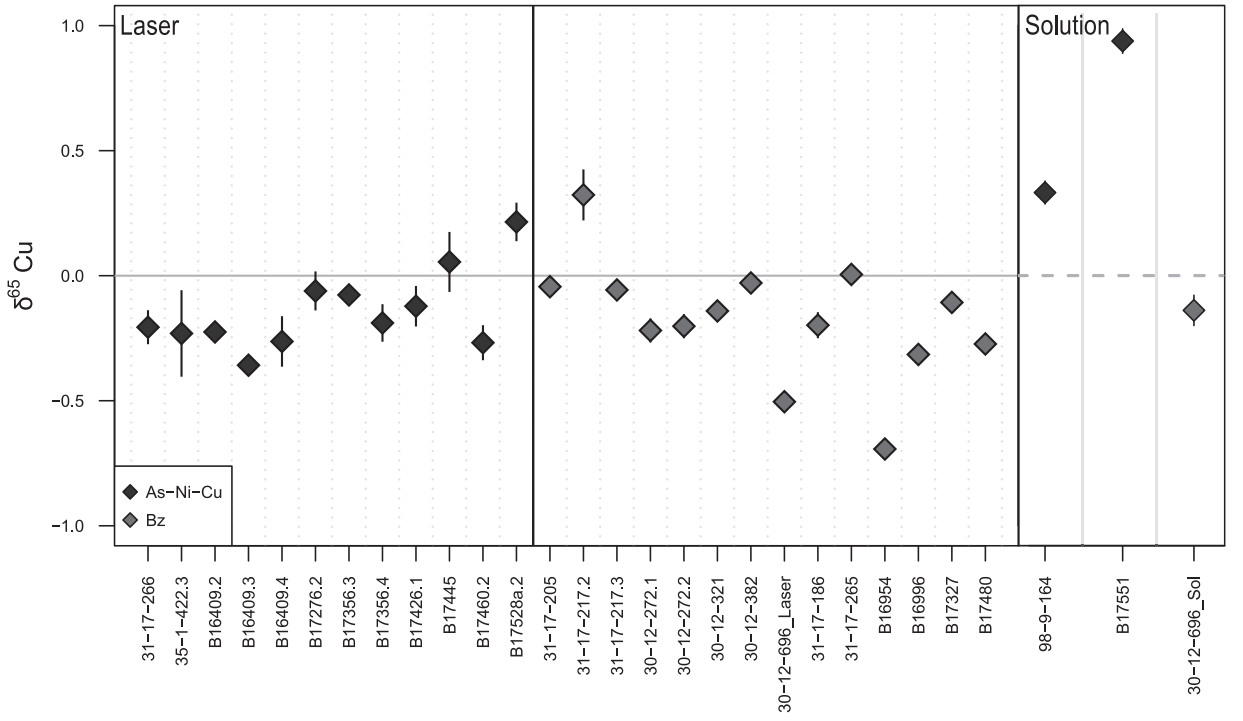

Fig. 10.13: Copper isotope signatures of the copper-based metal samples analysed by fs-Laserablation MC-ICP-MS (left) and solution-based MC-ICP-MS (right).

is observed, where tin can be visualised to be added intentionally. Although the higher the Sn content, the purer is the copper regarding other base metals. Tin bronze recipes were known in Akkadian times and passed down as cuneiform tablets in the archaeological record (Reiter, 1997). The earliest reference of tin in administration texts was discovered in an Early Dynastic text from Lagaš, where Baranamtara, wife of Lugalanda, sent copper and tin for bronze to the wife of the city ruler of Adab (Reiter, 1997, pp. 261-262). This text indicates, that tin was known as individual component. Unfortunately no archaeological evidence for the mid 3rd millennium BCE exists so far for tin ingots or other pure tin metal that could have been traded. The translation of AN.NA (annākum) with tin is still debated (Salonen, 1970; Adams, et al., 1974; Waetzoldt and Bachmann, 1984; Reiter, 1997). Salonen (1970, p. 146) references a text, where “four columns of bronze in which (copper) was mixed with tin in the ratio of (one part of tin to) six parts (of copper)” were produced. Waetzoldt and Bachmann (1984, pp. 9-10) mention a ratio of 56 shekel (471,33 g) copper to 8 shekel (67,33 g) tin, equalling 7 parts of copper to 1 part of tin.

It is also noted, that “washed” copper was used for alloying with tin (Waetzoldt and Bachmann, 1984). Whether this term refers to a refined copper or if the term “washed” is indicating a ritual of ceremonial cleaning, is not clear. Indeed, the analysed artefacts with Sn levels of 6 to 13 wt% are relatively pure regarding their As, Ni, and other base metal contents when compared to the copper rich in As and Ni. The Fe and S contents are in the same range as the unalloyed copper indicating no recycling or specific refining. It is possible, that ancient smelters knew already about the disadvantages of a high Sn-As-copper alloy and therefore chose a purer copper for alloying originating from a source with less base metal contents. As the Akkadian word AN.NA is not completely confirmed to mean tin metal in that sense, it is also possible it to mean tin ore (cassiterite) or even bronze, although cassiterite is unlikely as it is more useful to trade metal in semi processed form, as ingots for example. Possibly a bronze was produced in the region, where tin was mined and maybe even copper nearby, making it easier to trade or transport over long distances. The diagram in fig. 10.12 gives information on the changing ratio of Sn to As and Ni. The threshold value of 2 wt% Sn is marking the difference in As-Ni-copper and tin bronze. Those tin bronzes exhibiting no correlation between As and Ni are clusters in the lower left corner of the diagram, where some are transitioning in a linear fashion to the As-Ni-copper. Interestingly those artefacts have quite high Sn contents (6-10 wt%) hinting towards a admixture of small quantities of unalloyed As-Ni-copper to the tin bronzes and not the other way around. The linear trend in the upper right corner of the As-Ni-copper is a result of the correlation of both elements. Sn is present in the range of 0.01 to ca. 0.1 wt% in the unalloyed copper and could be a natural contamination, as small quantities of Sn are commonly present as stannites in association with hydrothermal veins. This amount is not necessarily indicating recycling, as it is unlikely at this early stage of bronze metallurgy in Mesopotamia. But the valuable trade

good of tin bronze was possibly diluted to some extent in order to increase the amount of the precious alloy. This matter shall be further discussed in sec. 10.2.4.

Due to the textual evidence it is likely that tin was intentionally added. Although no clear compositional threshold is observed in fig. 10.5 and 10.7, it seems reasonable, that tin was added in order to change the colour of the metal, bringing out more brightness and shininess to the metal. Apart from its technological advantages, tin bronze was most likely rather a metal of prestige. However, tin bronzes were not limited to the Royal Tombs, as a number of private tombs contained tin bronze artefacts. When it comes to the colour, the threshold Sn content is between 4 and 6 wt%, where the colour changes to bronze (Mödlinger, et al., 2017; Radivojević, et al., 2018). But as natural copper-Sn sulphides, as stannites, occur on a regular basis in hydrothermal deposits, there exists some input of Sn in unalloyed copper. Mixing and recycling further complicates the picture, although potentially occurring only on a smaller scale in earlier times. In summary potential mixing of As-Ni-copper with tin bronze is observed in 8 to 10 artefacts, analysed in this study, depending on the eye of the beholder. Those tin bronze artefacts exhibiting no correlation in fig. 10.12 are in the ideal range of 6 to 13 wt% Sn and therefore highly likely to be deliberately alloyed.

10.2 Isotope analysis

10.2.1 Results: Copper isotopes - fs-Laserablation-MC-ICP-MS and solution MC-ICP-MS

The copper-based metal samples display a low variation in their Cu isotope signature (cf. fig. 10.13). The As-Ni-copper varies in its δ^{65}Cu between -0.36 and +0.33 ‰ with a mean of -0.11 ‰. These samples exhibit higher errors compared to the tin bronze samples, as they have higher levels of Ni. Therefore the mass bias had to be calculated by using the Ni spike in the blank of the two measurements before and after each measurement. The tin bronze samples display a variation between -0.69 and +0.32 ‰ with a mean of -0.17 ‰. Only the sample B17551 exhibits a Cu isotope signature of +0.94 ‰, which is slightly higher than the other copper artefacts. The bronze bull's head (30-12-696) was measured by fs-Laserablation as well as out of a separated copper solution. The solution-based δ^{65}Cu value is -0.14 ‰ and the laserablation value is -0.50 ‰. The Cu isotope signature is not homogeneous within the artefacts. A small quantity of corroded material is able to alter the Cu isotope signature. Therefore the solution-based δ^{65}Cu values have to be handled with care, as small amounts of corroded material can easily be included in drilled metal samples. In addition the possibility occurs that a Cu isotope fractionation takes place in the columns due to the chemical separation method (M. Jansen, pers. comm., Feb. 2017). As a small part of copper remains in the resin within the columns a slight Cu isotope fractionation cannot be excluded. Therefore the laserablation-δ^{65}Cu data are considered as more reliable.

The metal analysed by fs-laserablation MC-ICP-MS exhibits a relatively homogeneous trend in all artefacts, with only slight variations. However, the secondary phases surrounding the metal formed by corrosion show differences in their δ^{65}Cu isotope signature. The inner corrosion layer of cuprite and other copper oxides displays a trend to more positive values compared to the metal. In sample B16996 the metal exhibits δ^{65}Cu values of between -0.34 to -0.27 ‰. The copper oxide layer's δ^{65}Cu signature is around -0.02 to +0.08 ‰. The malachite is very heterogeneous in its δ^{65}Cu values, as it differs between +0.19 near the copper oxide up to -1.60 ‰, depending on the location and vicinity to the rim.

The sample 30-12-382 displays δ^{65}Cu values at 0 ‰ in the metal, but more heterogeneous values in the copper oxide layer between -0.21 and +1.09 ‰. However, the outer malachite layer shows a δ^{65}Cu signature more variable than the metal but less than the copper oxide layer. The values differ between -0.35 to +0.16 ‰.

The δ^{65}Cu signature of sample 30-12-321 varies between -0.15 to -0.13 ‰ in the metal, whereas the δ^{65}Cu values in the copper oxide layer display at +0.62 and +0.78 ‰. The malachite's δ^{65}Cu values exhibit -0.19 and -0.98 ‰. The corrosion layers of the copper-based metal samples show large differences compared to the metal in the core. Due to limited time no more sample could be measured in the corrosion layers. But a general idea of the differences between metal, copper oxide and malachite layers could be acquired.

10.2.2 Discussion: Cu isotopes

Copper isotope ratios fractionate in nature during redox processes and are therefore proxies for the ore being of primary, secondary or supergene type (Markl, Lahaye and Schwinn, 2006; Braxton and Mathur, 2011; Mathur, et al., 2011). There are different zones typically occurring in ore deposits. As an example serves the common primary sulphide mineral chalcopyrite $CuFeS_2$. Chalcopyrite and pyrite occur commonly in volcanic massive sulphide or porphyry deposits. During weathering chalcopyrite reacts with water and oxygen to goethite, which remains in the leached zone or gossan. The forming sulfates and copper ions are transported to deeper levels. At the deeper levels above groundwater table form usually green copper oxides (e.g. malachite), whereas below the groundwater table copper precipitates to secondary sulphides (e.g. chalcocite). With time the Cu content increases in the supergene enrichment zone of secondary sulphides and can even be higher than in the original chalcopyrite (Reich and Vasconcelos, 2015). Below lies usually the remaining primary ore. The

layers thicknesses depend on time, general weathering conditions and initial structure.

This process has an impact on the δ^{65}Cu signature of the different zones. The leached cap is usually heavily depleted in δ^{65}Cu, whereas it is δ^{65}Cu enriched in the enrichment zone (Mathur and Fantle, 2015). Primary sulphide ores commonly exhibit a δ^{65}Cu-signature of -0.5 to +0.5 ‰ (Markl, Lahaye and Schwinn, 2006). Although this range also depends on the primary Cu isotope signature the deposit forms from and can differ in a wider range. The amount of depletion and enrichment in δ^{65}Cu is usually determined by weathering conditions and time and can result in several per mill difference (Mathur and Fantle, 2015).

As Cu isotopes are more sensitive to low temperature redox processes, the amount of fractionation during smelting of copper ores is expected to be low, although the exact mechanisms are not well understood, yet. In theory the δ^{65}Cu signature of the artefacts can give information on whether ancient smelters used the primary sulphide, oxide, or supergene ore for copper production, although these conclusions need to be handled with care and additional informations have to be taken into account, e.g. the chemistry. Also the potential fractionation during roasting and smelting processes needs to be investigated. The Ur copper-based artefacts measured regarding Cu isotopes exhibit the typical primary sulphide range of -0.5 to +0.5 ‰. The only two exceptions being B16954 with -0.69 ‰ and B17551 with +0-94 ‰, although both are still in the range of between -1 and 1 ‰, which can still be considered as primary. This result is in accordance with the elemental analysis, as the omnipresent S contents and inclusions in the artefacts indicated already an sulphide ore as a source. No significant difference between tin bronzes and As-Ni-copper is observed and emphasises the widely spread knowledge of the two-step process of smelting sulphides in the Early Bronze Age.

10.2.3 Results: Lead isotopes - Laserablation-MC-ICP-MS and solution MC-ICP-MS

The Pb isotope results for the copper-based metal samples are diagrammed in fig. fig. 10.14. The Pb isotope ratios of the copper rich in As and Ni range from 18.35 to 18.90 for ^{206}Pb/^{204}Pb, 15.567 to 15.690 for ^{207}Pb/^{204}Pb, 38.431 to 38.997 for ^{208}Pb/^{204}Pb, 0.82951 to 0.85219 for ^{207}Pb/^{206}Pb and 2.06325 to 2.09652 for ^{208}Pb/^{206}Pb. These artefacts form an almost interrelated field with a few exceptions in the outer range. The three pure copper artefacts show an overlap with the As-Ni-copper artefacts and are therefore included in the range mentioned above.

However, most of the tin bronze artefacts have ratios differing from the As-Ni-copper artefacts. The ratios display a huge range between 17.36 to 18.93 for ^{206}Pb/^{204}Pb, 15.600 to 15.719 for ^{207}Pb/^{204}Pb, 37.304 to 39.271 for ^{208}Pb/^{204}Pb, 0.82931 to 0.89859 for ^{207}Pb/^{206}Pb and 2.06754 to 2.14836 for ^{208}Pb/^{206}Pb. It appears that the tin bronze artefacts form no specific connected cluster, except at both margins, supposedly.

In order to evaluate, if comparable copper deposit data are within error range of the measured artefacts, the data are plotted as open symbols and error ellipses with the height and width of the standard errors. The copper ingot 98-9-164 exhibits high errors in the ^{204}Pb based isotope ratios, therefore only the ^{206}Pb based ratios are used for this artefact. Regarding the homogeneity of the artefacts the samples 35-1-422.1-3, B16409.2-4, B17426.1-2, and B17356.2-4 exhibit an overlap within error range. As mentioned in sec. 10.1.1.2 the sample B16409.1 exhibits not only a different main element composition (cf. fig. 10.3), but also a different Pb isotope signature. The needle or pin B16409 was sampled only at the lower end resulting in similar cross sections of the different samples, as several slices of the same end were extracted and embedded in epoxy. The cross section of B16409.1 is distinct from B16409.2-4, therefore it is highly likely that B16409.1 was sampled from another artefact and misnamed. Nevertheless, it exhibits a similar signature as other artefacts rich in As and Ni and remains included regarding the question of provenance.

The Pb isotope measurements of this study agree well with the results of Begemann and Schmitt-Strecker (2009) and of Klein, La Niece and Hauptmann (2016), who analysed parts of the analysed artefacts of this study as well as other copper-based metal artefacts of the Ur cemetery (cf. fig. 10.17 and 10.18). This study complements these data with 56 additional samples that were measured successfully. The Pb isotope ratios of the present study exhibit a similar trend as the data of Begemann and Schmitt-Strecker (2009). The general course of the Sn-Bronze artefacts showing a tendency to more extreme differences in their Pb isotope ratios compared to the As-Ni- and pure copper is verified by the connection of these two independent studies.

10.2.4 Discussion: Lead isotopes

The Pb isotope data of the copper artefacts reveal different trends in between the tin bronze and As-Ni-copper artefacts.

The copper rich in As and Ni exhibits a more narrow range of Pb isotope ratios. In fig. 10.15 are the model ages of the copper-based artefacts displayed. In the Stacey and Kramers (1975) two-stage model the As-Ni-copper artefacts have geological ages from 300 Ma to recent ages. The peak is at 118 Ma corresponding to Cretaceous age. The age fits almost perfectly to the emplacement of the mesozoic ophiolites in Oman and Turkey, which are part of the Tethyan Eurasian Metallogenic Belt (TEMB) (Janković, 1977).

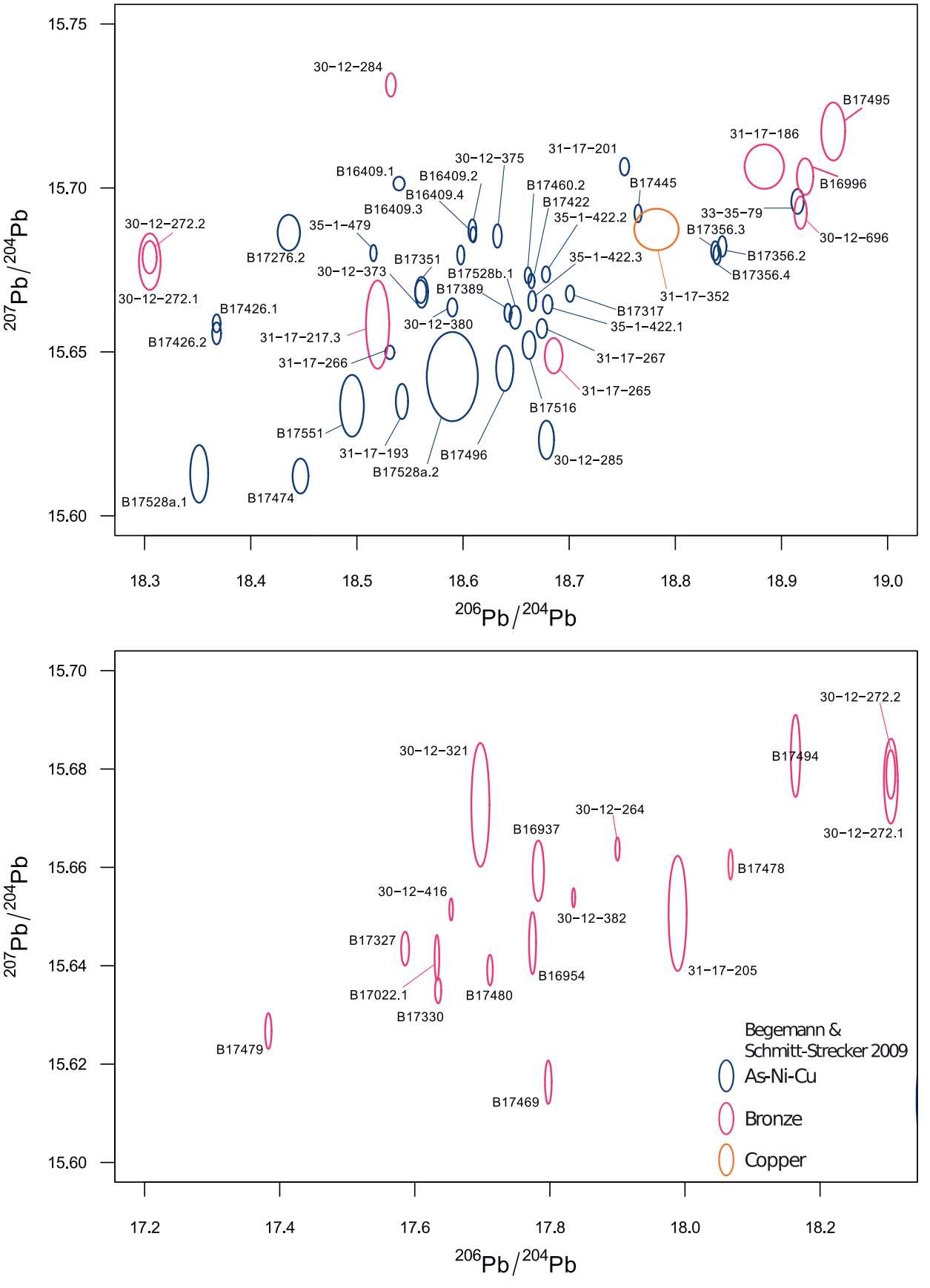

Fig. 10.14: $^{206}Pb/^{204}Pb$ vs. $^{207}Pb/^{204}Pb$ ratios of the copper-based metal samples measured by laserablation MC-ICP-MS. The data are displayed as error ellipses: The ellipses have the width and height of the absolute standard errors 2 SE of each analysis with the measured Pb isotope ratio as the centre.

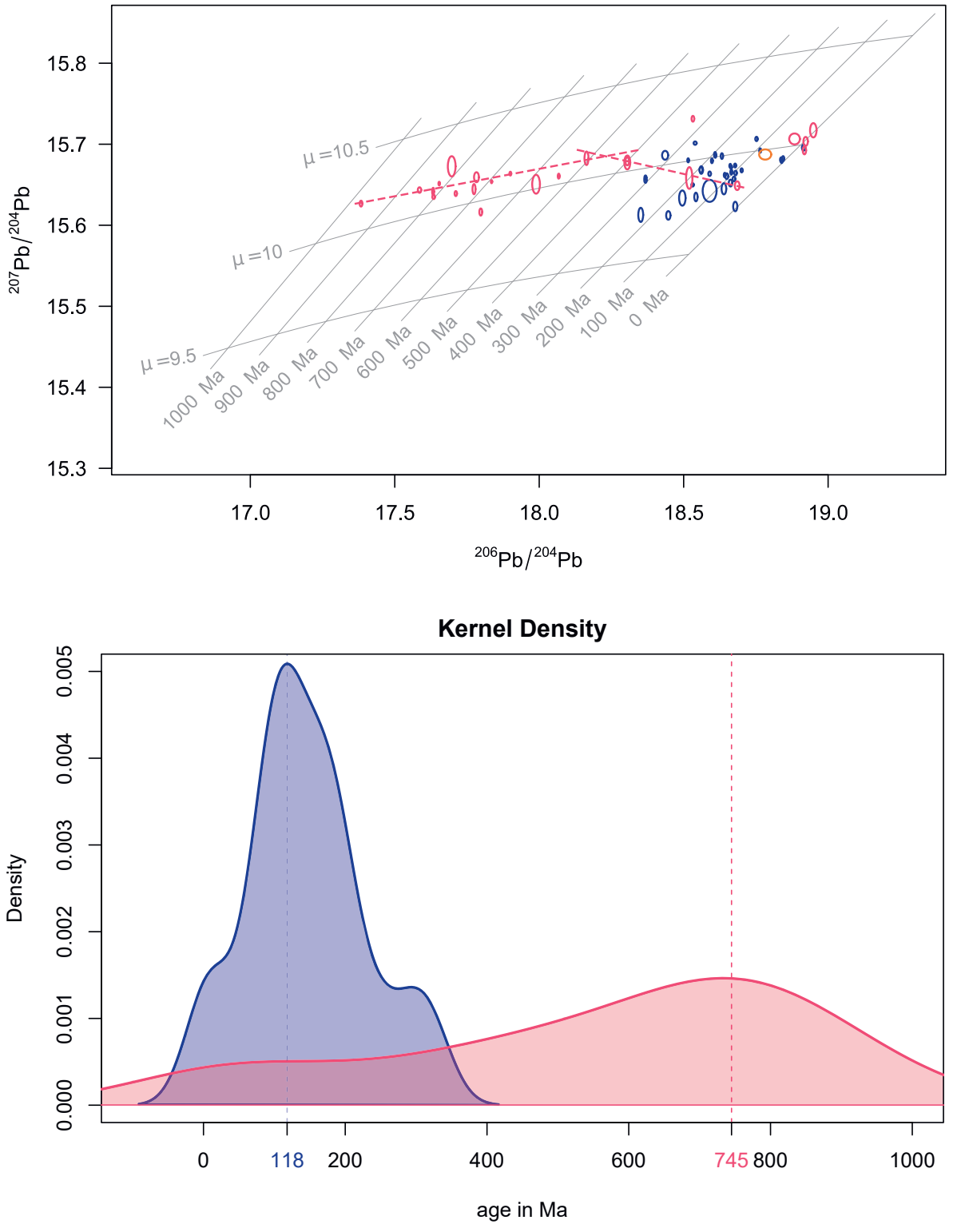

Fig. 10.15: (Upper) The $^{206}Pb/^{204}Pb$ vs. $^{207}Pb/^{204}Pb$ ratios of the Ur copper-based artefacts in the two stage model of Stacey and Kramers (1975) plotted with an R-Script written by T. Rose (2017). The dark grey colour represents the As-Ni-copper and the lighter grey colour the tin bronze artefacts. The lines exhibit potential mixing lines. (Lower) The Kernel density of the calculated model ages of the copper-based artefacts as histogram.

In contrast to the As-Ni-copper the tin bronze artefacts exhibit a wide range of Pb isotope ratios. The peak in the Kernel density plot is not as clear as the As-Ni-copper artefacts and has its maximum at 745 Ma corresponding to Neoproterozoic age. The model ages ranging from recent to approximately 1000 Ma and following a linear trend indicate a mixture of different ores or metal of different geological ages.

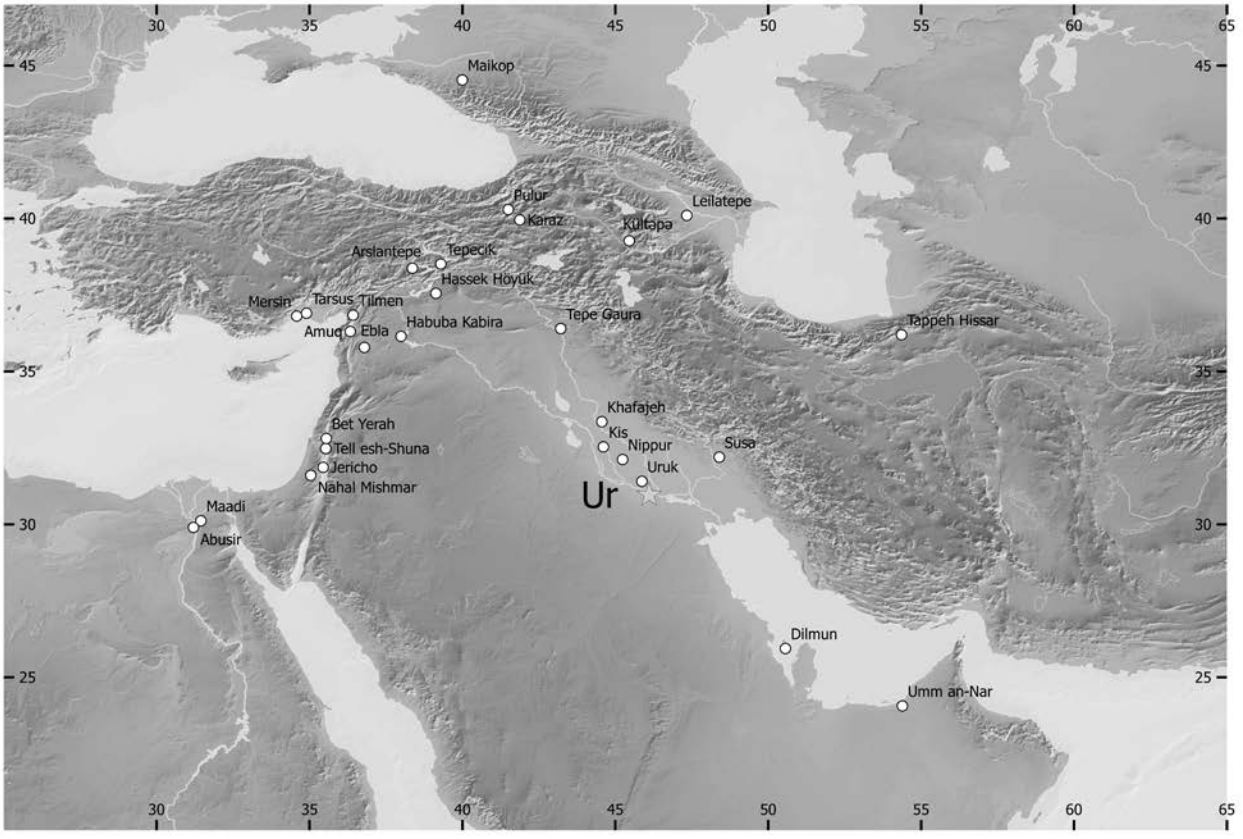

Fig. 10.16: Distribution of As-Ni-copper artefact findings across the Near East in the third millennium BCE (after Hauptmann, 2000 with additional data from Tallon, 1987; made with natural earth).

The linear trend appears consistently in all diagrams and all ratios. This trend was already observed in previous diagrams regarding the chemistry and is therefore further confirmed (cf. sec. 10.1.2 and 10.1.5). The trend from old to younger model ages appears to be a mixture of a geologically very old ore source with a Cretaceous ore source, as the tin bronzes having an Mesozoic age trend to the centre of the As-Ni-copper artefacts. The majority of the tin bronze artefacts falls in between the model ages of 500 to 900 Ma indicating a mixture of two different ore stages and both geologically old sources. In addition the linear trend in the older Pb isotope data of the tin bronze artefacts appears to change directions in a small angle at the mark of 500-400 Ma, thus hinting towards a mixing between Precambrian/Cambrian and Mesozoic sources as well as in between different Neoproterozoic sources (cf. lines in fig. 10.15).

The very old Pb isotope signature is potentially related to ore sources in an old craton. Remnants of old cratons exist in India and the Eastern Desert of Egypt (Stern, Gottfried and Hedge, 1984; Deb and Sarkar, 1990). The artefact with the highest model age B17479 (axe, ED IIIa, PG 580) is characterised by 4.7 wt% Sn, 2.7 wt% As, and 0.88 wt% Ni. When mixing is considered, B17479 falls into the transitional group with both elevated As, Ni, and Sn levels and is thus not the end member regarding the calculated geological ages.

The recent tin bronze artefacts are only a minority as are the As-Ni-copper artefacts falling into the same area of the diagram possibly indicating an origin from a source of similar age. Copper sources of younger age correspond to deposits formed after the collision of the Arabian plate with Eurasia and the subsequent opening of the Red Sea causing extension tectonics and magmatism in the Miocene along the Taurus, Caucasus, and Zagros mountains (Okay, 2008). Due to the long half-life of U and Th decaying to Pb, younger model ages are less precise and more likely erroneous. Therefore the model ages have to be considered to be approximating the true geological age, however, giving only general information. The pure copper artefact 31-17-352T has a model age corresponding to Late Cretaceous / Early Cenozoic.

10.3 Comparison of potential raw material sources with the Ur copper-based metal

10.3.1 Provenance of the As-Ni-copper

The high Ni content in the As-Ni-copper already indicates a copper source in an ophiolitic context (cf. sec. 10.1.5).

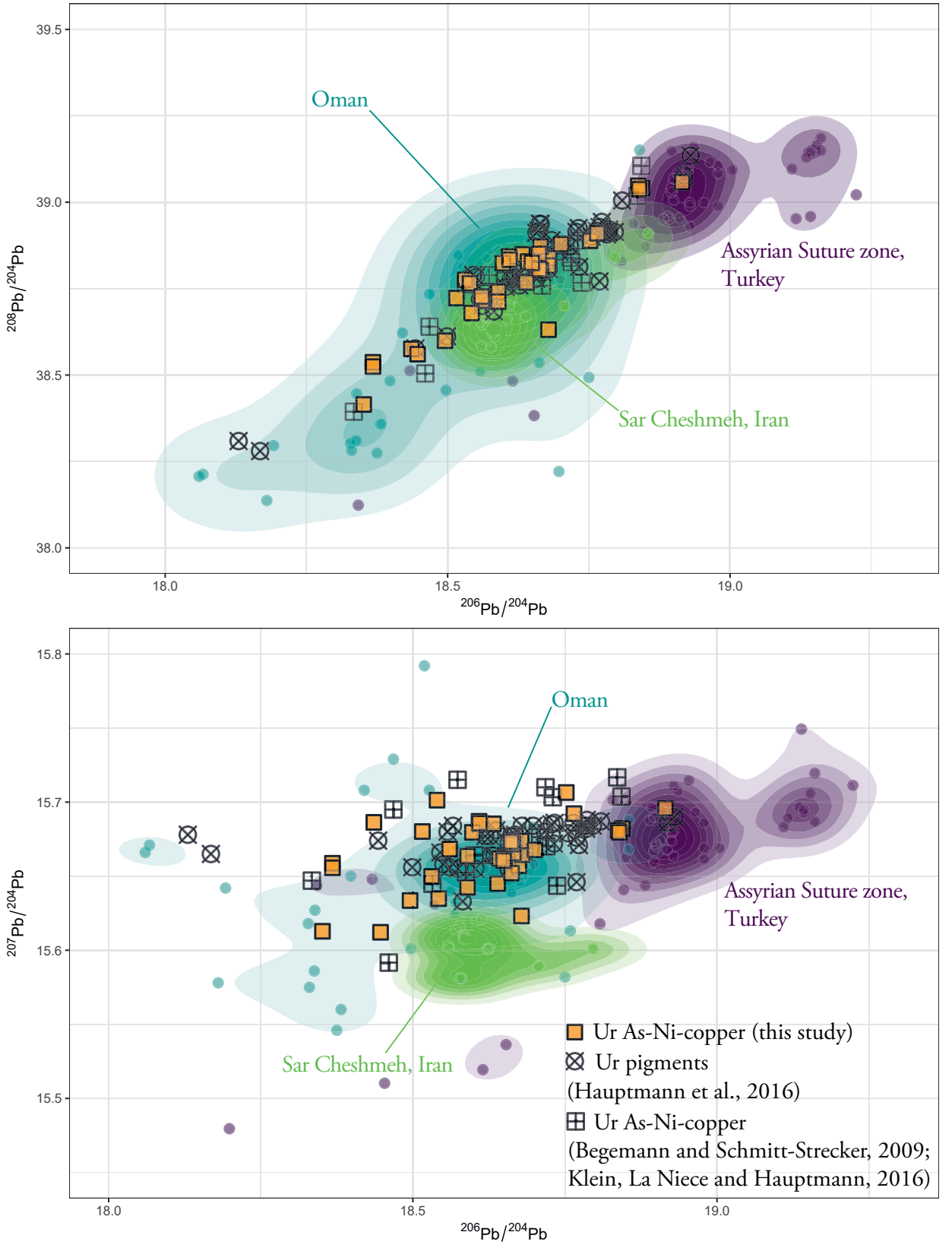

Fig. 10.17: $^{208}Pb/^{204}Pb$ vs. $^{206}Pb/^{204}Pb$ (upper) and $^{207}Pb/^{204}Pb$ vs. $^{206}Pb/^{204}Pb$ (lower) ratios of the As-Ni-copper samples measured by laserablation MC-ICP-MS in comparison with Pb isotope data of As-Ni-copper artefacts from Ur analysed by Begemann and Schmitt-Strecker, 2009, and Klein, La Niece and Hauptmann, 2016, and mineral pigments analysed by Hauptmann et al., 2016, as well as ores and metallurgical by-products from the Assyrian Suture zone in Turkey, Oman, and Sar Cheshmeh in Iran. (Seeliger, et al., 1985; Wagner, et al., 1986; Shahabpour and Kramers, 1987; Wagner, et al., 1989; Hirao, Enomoto and Tachikawa, 1995; Hauptmann, et al., 2002; Begemann and Schmitt-Strecker, 2009; Begemann, et al., 2010; Shafiei, 2010; Hauptmann et al., 2016; Klein, La Niece and Hauptmann, 2016). The coloured areas represent the Kernel density estimation of the ore data.

Copper deposits associated with Ni arsenides occur in Oman and Ergani, which are both known mining areas in the 3rd millennium BCE and therefore are considerable sources for the copper of Ur (Wagner and Öztunali, 2000; Begemann and Schmitt-Strecker, 2009). The mesozoic Pb isotope signature of Oman fits well to the As-Ni-copper artefacts, whereas the very few younger Pb isotope signatures are in agreement with the source of Ergani in the Assyrian Suture zone in Turkey, as well as metallurgical by-products from Arslantepe (Seeliger, et al., 1985; Wagner, et al., 1986; Wagner, et al., 1989; Hirao, Enomoto and Tachikawa, 1995; Hauptmann, et al., 2002; Begemann, et al., 2010).

Although close to each other, copper deposits north of the Makran coast in Iran and Oman on the opposite side of the Persian Gulf are different. The Volcanic Massive Sulphide deposits of Oman formed at an active continental margin, whereas the Porphyry copper deposits in Iran are associated with an magmatic arc. Iran can be excluded as a potential source due to the copper deposits not being associated with ophiolites (c.f. fig. 10.17; e.g. the Sar Cheshmeh porphyry copper deposit is not in accordance with Pb isotope data of the As-Ni-copper artefacts from Ur).

Interestingly the Jemdet Nasr pin 33-35-79 fits well to the Assyrian Suture zone Pb isotope data. The Early Dynastic pin B17356 is in the transition of the Assyrian Suture zone and Oman and cannot be clearly assigned. Both sources are reasonable. The remaining Pb isotope data of the As-Ni-copper artefacts are in good agreement with the Oman Pb isotope signature (Begemann, et al., 2010). This also coincides with the results of Begemann and Schmitt-Strecker (2009) and Klein, La Niece and Hauptmann (2016), who analysed a number of other Ur copper-based artefacts. The data are in general agreement with each other and further confirm the hypothesis, that the land of copper *Makan* is indeed Oman (Prange, 2001; Weisgerber, 2007; Begemann, et al., 2010). The majority of the As-Ni-copper agrees well in both chemistry and Pb isotope signatures with Oman. This also corresponds well to the archaeological and textual evidence (Hirsch, 1963; Hauptmann and Weisgerber, 1980; Heimpel, 1987; Weisgerber, 1991; Moorey, 1994; Glassner, 1996). Large scale copper production in Oman has been evidenced for the third millennium BCE. The distribution of copper artefacts with significantly elevated As and Ni contents is hinting towards the connection of Oman, Mesopotamia, SE Turkey, Levant, and Egypt (cf. fig. 10.16) (Hauptmann and Weisgerber, 1980; Hauptmann, 1985; Prange, 2001; Weisgerber, 2007; Begemann, et al., 2010). Tepe Hissar exhibits also findings of As-Ni-copper artefacts and is therefore likely connected with Mesopotamia. The copper travelled in all likelihood by ship along the coast via *Dilmun* to Mesopotamia. The As-Ni-copper coming from SE Turkey could be simply transported down the Euphrates river by ship (Moorey, 1994). The distribution westwards to other sites in Turkey, southwards to the Levant and Egypt, as well as northwards to Maikop went most likely overland.

In the map of Hauptmann (2000) Troy was included, as often a connection of Troy and Ur is made in literature (Bass, 1966; Pernicka, et al., 1984; Stos-Gale, Gale and Gilmore, 1984; Pernicka, et al., 2003). While parallels in technology and typology especially regarding the gold jewellery cannot be denied, high Ni contents in the unalloyed copper are only found in one dagger (HDM 258, Stuttgart Nr. 9877) with 1.24 wt% Ni and 2.4 wt% As (Pernicka, et al., 1984) and in no sample analysed by Stos-Gale, Gale and Gilmore, 1984. The dagger is likely related to the Ergani ore deposit in the Assyrian Suture zone according to chemistry and Pb isotope signature. Although a connection of Ur and Troy is in all probability, this does not necessarily include the same copper sources. The majority of the unalloyed copper in Troy dated to the third millennium BCE agrees with local sources in western Anatolia (Begemann, Schmitt-Strecker and Pernicka, 2003). In a land with rich copper resources it seems unnecessary to exploit foreign copper sources from further afar. Whereas in Mesopotamia itself no metal resources occur and therefore the sources of metal and other commodities had to be accessed from further distant regions. The extensive demand for copper in Mesopotamia was most likely satisfied by the large scale copper production in Oman, as the resources are not exhausted until today. The transport by ship allows large quantities of copper to be transported to Mesopotamia in an efficient and convenient way and is therefore the most likely transportation route of choice corresponding to the distribution of As-Ni-copper artefacts along the Persian Gulf coast.

10.3.2 Provenance of the tin bronzes

The very old geological model ages of the tin bronze artefacts narrow down the potential provenance of the copper used for tin bronze production considerably. As discussed before (cf. sec. 10.2.4) the linear trend in the Pb isotope signatures of the tin bronze artefacts is likely the result of mixing of ores or metal. The very old geological age of the higher Pb isotope signatures in the ^{206}Pb-based ratios leaves only India and Egypt as possible sources, as no other deposits in the Near and Middle East are of Precambrian age. Two tin bronze artefacts (BM-nr.: EA35571; EA35572) from Egypt have been identified so far in the tomb of Khasekhemwy in Abydos dating to the early 27th century BCE (Kmošek, et al., 2018; http://www.britishmuseum.org/). Yet, it is unknown whether the material had been imported to Egypt. When looking at the distribution of tin bronze findings as well as tin deposits it becomes clear that the majority of tin deposits lie to the east of Ur (cf. fig. 10.19). Indeed, the Pb isotope signatures of deposits in the Aravalli-range in Rajasthan as well as other deposits in Gujarat and possibly Jammu and Kashmir province in NW India fit isotopically to the old Pb isotope signatures of the Ur tin bronze artefacts. As different Precambrian ore stages occur in this region and the majority of the

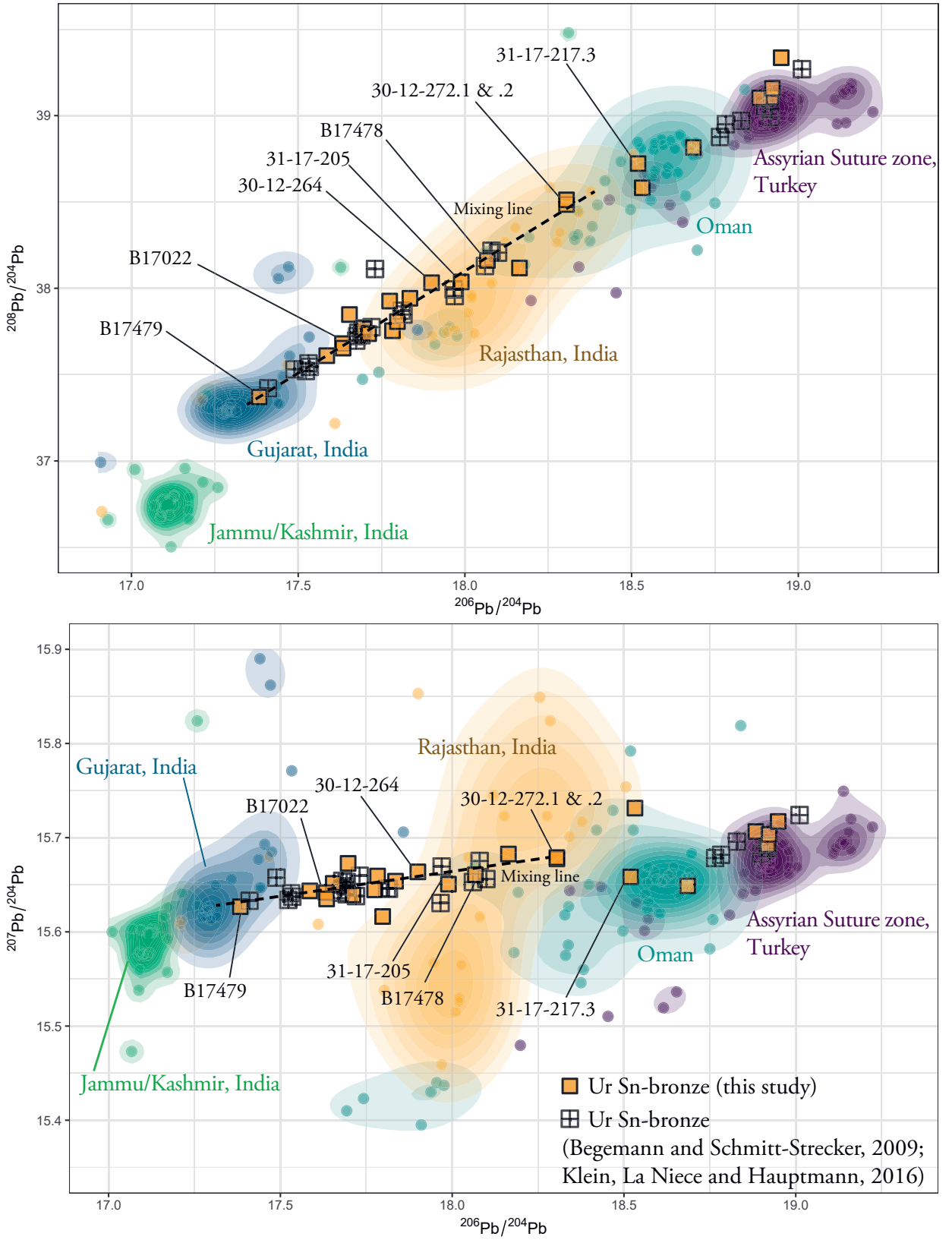

Figure 10.18 $^{208}Pb/^{204}Pb$ vs. $^{206}Pb/^{204}Pb$ (upper) and $^{207}Pb/^{204}Pb$ vs. $^{206}Pb/^{204}Pb$ (lower) ratios of the Sn-bronze metal samples measured by laserablation MC-ICP-MS in comparison with Pb isotope data of As-Ni-copper artefacts from Ur analysed by Begemann and Schmitt-Strecker, 2009, and Klein, La Niece and Hauptmann, 2016, as well as ores and metallurgical by-products from the Assyrian Suture zone in Turkey, Oman, Gujarat, Jammu/Kashmir, and Rajasthan in India (Seeliger, et al., 1985; Wagner, et al., 1986; Deb, et al., 1989; Wagner, et al., 1989; Hirao, Enomoto and Tachikawa, 1995; Deb, et al., 2001; Hauptmann, et al., 2002; Law, 2008; Begemann and Schmitt-Strecker, 2009; Begemann, et al., 2010; Klein, La Niece and Hauptmann, 2016). The named artefacts exhibit a mixing trend in the As/Sn and Ni/Sn ratios in fig. 10.12. The dashed line is a potential extrapolation of a possible mixing with ores from older rock formations, indicated by the As/Sn and Ni/Sn ratios.

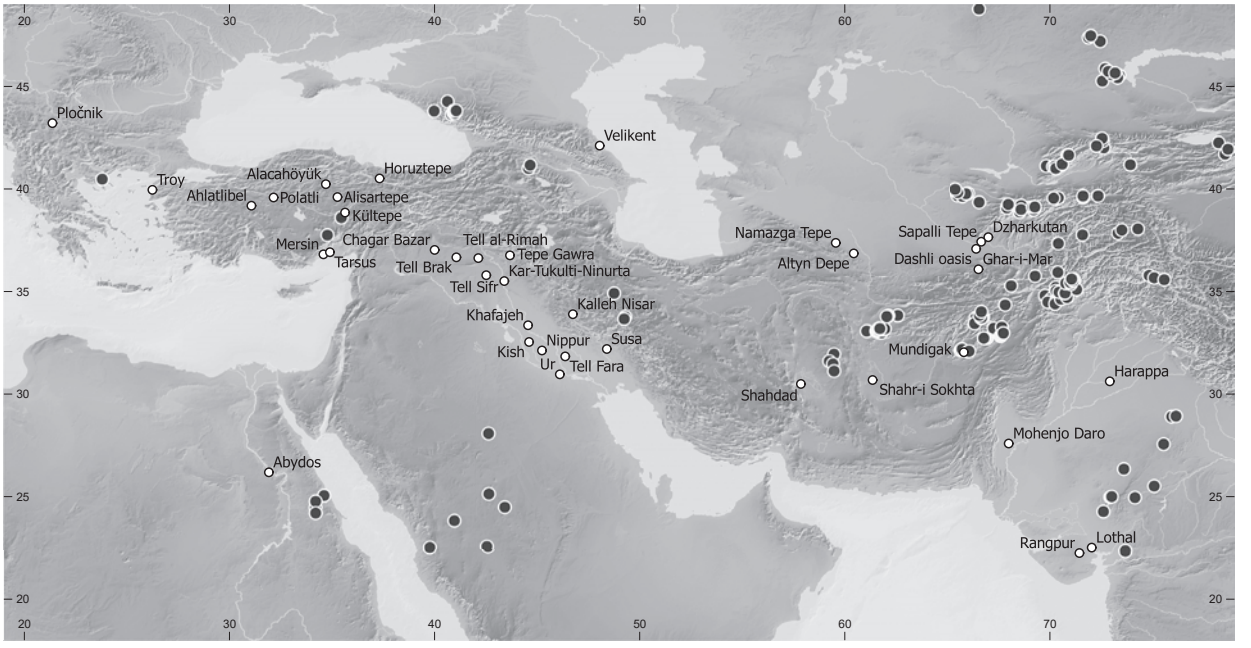

Fig. 10.19: Distribution of tin bronze artefact findings across the Near East until the third millennium BCE (white points) in relation to the locations of tin deposits (black points) (data source: Tallon, 1976; Deb and Sarkar, 1990; Kenoyer, 1999; Stech, 1999; Orris and Bliss, 2002; Twaltschrelidze, 2002; Weeks, 2003; Pigott, 2004; Nezafati, 2006; Murao, Deb and Furuno, 2008; Seltmann, 2009; Lehner and Yener, 2010; Lyckberg, 2011; Chakrabarti, 2012; Garner, 2013; Radivojevic, et al., 2013; Seltmann, 2013; Thomalsky, et al., 2013; Courcier, 2014; Thornton, 2014; http://mrdata.usgs.gov/; http://www.mindat.org/; made with natural earth).

tin bronze artefacts lie in between different ore stages in Rajasthan and Gujarat province a mixture of these ores is highly likely. In figure 10.18 are those artefacts labelled showing a mixing trend in the chemistry (cf. fig. 10.12). Interestingly, the artefact B17479 exhibits an intermediate As-Ni-Sn-composition and therefore is unlikely the end member of a potential mixture.

Therefore the Pb isotope signature is potentially a mixture of the Mesozoic As-Ni-copper and an older source. Those artefacts in between Rajasthan and Oman are possibly a mixture in between these ore sources. The younger Pb isotope signatures of the tin bronze artefacts are not quite matching copper deposits in the Taurus mountains. Indeed, so far no published Pb isotope of potential copper ore sources match these geologically younger Sn-bronze artefacts. A linear trend from the Oman Pb isotope ore field to an unknown source could also indicate mixing of copper from at least two sources. (cf. fig. 10.18). The problem of provenancing mixed Pb isotope signatures is, that the end members have to be known. One end member is the geologically older Pb isotope signature hinting towards Oman. However, the geologically younger end member is unclear, as it could be an ore source in e.g. Afghanistan or in the Taurus mountains.

If one considers the possibility of mixing Oman and Indian copper, the question remains, where this was performed. If the tin bronze travelled as semi- or fully processed artefact or ingot from the Indus Valley to Mesopotamia via Oman and *Dilmun*, tin bronze or copper artefacts/ingots with a similar Pb isotope signature would be discovered. This is not the case (Begemann, et al., 2010).

Copper and tin travelled separated from each other to their destinations, as it is mentioned in cuneiform texts (Reiter, 1997). Even if only copper from India travelled via *Makan* and *Dilmun*, as it is mentioned in the texts, this would be evident in the Pb isotope signatures of copper findings in *Makan* and *Dilmun*. Begemann, et al., (2010) theorised, that the copper used for tin bronze production was under the same restrictions as tin, and therefore only shipped directly to Mesopotamia and not used as exchange good for local authorities at the interstations. This seems likely, yet remains a matter for debate. The artefact 31-17-217 exhibits also an intermediate composition of 5 wt% Sn, 0.86 wt% Ni, and 2 wt% As. Yet it is unknown, whether tin bronze metal and As-Ni-copper was mixed or tin was alloyed to As-Ni-copper. The fact, that mostly tools and weapons have an intermediate As-Ni-Sn-composition, could indicate a potential use of the artefacts during the lifetime of the individuals and mending with an admixture of other As-Ni-copper before the burial. Although this is purely speculative, it is a possibility. Undoubtedly the metal artefacts buried in the Royal and Private Tombs of Ur were used and worn by their owners during lifetime, as was evident by traces of use on the gold artefacts (B. Armbruster, pers. comm., Feb. 2017). More conclusions on the end members of the mixing will be able to draw, if more combined chemical and Pb isotope analysis Early Bronze Age Mesopotamian tin bronze artefacts are available.

Unfortunately it is not yet possible to provenance tin, therefore conclusions on provenance can only be drawn for the copper metal used for tin bronze production. Nevertheless, it is possible, that tin and copper resources

are occurring in the vicinity of each other, which were combined to tin bronze and travelled in semi-processed form to their destination. Although no archaeological evidence exists, it seems a reasonable possibility. So far, no tin ingots have been discovered dating to the third millennium BCE, therefore it is unknown, how tin bronzes were were produced or the raw materials travelled.

From an archaeological point of view the connection between NW-India and Mesopotamia is highly likely, since numerous textual evidence exist for ships coming from *Meluḫḫa* to Ur and Mesopotamia bringing tin and copper (Moorey, 1994; Foster, 1997, 86; Crawford, 2013). The source of tin lies probably not in the Indus Valley itself, but more to the North in NE Afghanistan, where cassiterite occurs in plenty (Orris and Bliss, 2002). The Harappa culture had several outposts in the north, and Shortugai, in particular, is located nearby to the cassiterite occurrences (Kenoyer and Miller, 1999). This connection is further confirmed by the findings of etched carnelian beads from *Meluḫḫa* in Ur as well as plentiful lapis lazuli artefacts deriving from Sar-e Sang in Afghanistan. The trade goods travelled most likely by ship to Mesopotamia, as indicated by cuneiform texts (Hirsch, 1963). Due to the missing link in Oman it is likely the copper for tin bronze travelled along the Makran coast of southern Iran to Mesopotamia and not via *Makan* and *Dilmun* (Begemann, et al., 2010). This would indicate that potential mixing and even alloying had been performed in Mesopotamia itself. Until recently no archaeological evidence for metal workshops exists in Ur, yet Woolley put most of his efforts to the cemetery area and not to the settlement. The ongoing excavations of the Penn Museum, Philadelphia, will hopefully contribute to a better understanding, where the metal working and alloying had taken place.

10.3.3 Provenance of the pure copper artefact 31-17-352T

The only pure copper artefact 31-17-352T analysed in this study exhibits a Late Mesozoic to Cenozoic Pb isotope signature. As only one data point exists for this kind of material the euclidean distances are a more reliable tool for provenancing (for the formula cf. sec. 13.3.2), as in the Mesozoic Pb isotope signatures many overlaps occur with numerous copper deposits.

The nearest neighbours in the 3-dimensional space fit best to Serçeören Köy, NW Turkey. Interestingly this is also the most likely source for the early Troy copper (Begemann, Schmitt-Strecker and Pernicka, 2003). This artefact dated to Jemdet Nasr/Early Dynastic I could be a link between the Troad and Southern Mesopotamia. As mentioned above (cf. sec. 10.3.1) there are parallels in typology and technology in metal finds from Ur and Troy (Bass, 1966). Therefore an exchange of knowledge had most likely taken place. An exchange of material goods seems thus all the more likely. As this object exhibits also differences in its microstructure than compared to the other copper-based artefacts, it is possible, that it was forged at another location (cf. fig. 10.6). This could hint towards the artefact being traded as artefact from the Troad to Ur and not as semi-processed form possibly as a gift or in exchange for other goods as textiles or grain. Although this is speculative, an exchange of gifts in between Ur and foreign regions had most certainly taken place.

11 The copper-based artefacts: Conclusion

The analysis of the copper-based artefacts with *in situ* methods could be accomplished successfully. The artefacts could be chemically distinguished due to their different As, Ni, and Sn content. The Sn content varies between 0 and 13 wt% and ca. one third of the analysed artefacts can be characterised as tin bronzes. The majority of the copper-based artefacts, however, exhibits elevated and correlated As (0.1 to 4.66 wt%) and Ni (0.02 to11.07 wt%) levels and are therefore characterised as As-Ni-copper. Due to the very variable contents As and Ni were most likely not intentionally alloyed, but entered the metal due to the presence of Ni arsenides in the copper ore used for smelting. One Jemdet Nasr/Early Dynastic I pure copper artefact 31-17-352T stands out also in its microstructure. Differences in trace elements are only small and the tin bronze artefacts have slightly elevated Bi and Zn levels compared to the As-Ni-copper. The S contents as well as the Cu isotope signature mostly between -0.5 and +0.5 ‰ indicate smelting of primary sulphide ores for the copper production.

The majority of Pb isotope signatures of the As-Ni-copper artefacts are in accordance with ore data from Oman and two artefacts are more likely related to the copper deposit of Ergani in Turkey (33-35-79 and B17356). The copper ores in Oman are associated with Ni arsenides occurring in the deeper parts of the related Mesozoic ophiolite, which could likely enter the copper metal during smelting. This mineralogical feature is only observed in Oman and partially in the Ergani area, while other common copper deposits in the Near and Middle East do not appear to have Ni arsenides in larger quantities. Therefore other regions could be excluded due to the chemical data. Oman was in all likelihood identified as *Makan* the 'land of copper'. It was most likely the main supplier of copper for Mesopotamia (Hauptmann and Weisgerber, 1980**;** Hauptmann, 1985**;** Prange, 2001**;** Weisgerber, 2007; Begemann, et al., 2010), a fact, which is further confirmed due to the results of this thesis. Only small quantities of copper were accessed from SE Turkey, where evidence for large scale copper production is scarce. In contrast a large scale copper production was evidenced in Oman for the third millennium BCE and seems to have supplied Mesopotamia and possibly other locations in all cardinal directions from Mesopotamia (cf. fig. 10.18). The copper travelled most likely by sea via *Dilmun* to southern Mesopotamia, as indicated by cuneiform texts (Hirsch, 1963; Heimpel, 1987).

The majority of the copper used for the tin bronzes came most likely from India according to Pb isotopes. The Pb isotope signatures of most of the Ur tin bronze artefacts exhibits geologically very old signatures of Neo- to Mesoproterozoic age and appear to follow a linear trend in between different ore stages of NW Indian copper sources in Rajasthan and possibly Gujarat province (Aravalli range). The only other potential candidate is the Eastern Desert of Egypt, though Egypt could be excluded, as tin bronze does not appear in Egypt contemporarily with the Ur artefacts. The very young Pb isotope signatures of four Sn-Bronze artefacts (30-12-696, 31-17-186, B16996, B17495) hints towards a provenance in an unknown source region, as no published Pb isotope data matches these artefacts. Additionally, a linear trend in Pb isotope data of the geologically younger tin bronze artefacts could indicate mixing of copper from Oman with the other unknown source.

In between the Precambrian and Cenozoic Pb isotope signatures mixing seems to have taken place also with As-Ni-copper from Oman. Whether this had been performed in Mesopotamia itself or at another location is not clear. This mixing trend was also observed in the chemistry and could be related to mending used tin bronze tools or weapons, which were in use before burial. Due to the fact, that no Oman copper or tin bronze artefacts with a similar old Pb isotope signature has been discovered and analysed, it is possible, that the copper for the tin bronze travelled not via *Makan* and *Dilmun*, but along the Makran coast of southern Iran (Begemann, et al., 2010).

With the currently available analytical methods it was impossible to provenance the tin used for production of the Ur tin bronze artefacts. However, most of the copper used for the tin bronze originating in NW India indicates a possible relation to the Indus Valley civilisation. The Harappa culture had several outposts to the north (Kenoyer and Miller, 1999). Particularly Shortugai is of interest, as it is located in NE Afghanistan and in close distance to several rich cassiterite occurrences (Orris and Bliss, 2002). Furthermore Shortugai lies in the vicinity of the major lapis lazuli deposit of Sar-e Sang, where the large amounts of lapis beads discovered in Ur most likely originate. The tin could have travelled down from Afghanistan to the Indus Valley, where most likely the copper used for tin bronze was produced, and then shipped together to Mesopotamia.

The pure copper artefact 31-17-352T is most likely related to the copper deposits of Serçeören Köy in NW Turkey, which is interestingly also the likely main supplier of the early copper artefacts of Troy. A connection is in all likelihood, and possibly this artefact was also forged in the Troad due to the differing microstructure from all other copper-based artefacts (cf. fig. 10.11).

As mentioned above it is desirable to provenance the tin sources. The tin question could not be answered with the available analytical techniques applied in this study and therefore remains unanswered. Several approaches exist already, as the study of tin isotopes (Haustein, Gillis and Pernicka, 2010), although this method still has to be further investigated regarding feasibility. Another approach could be the analysis of cassiterite-related trace elements, as Ta, Nb, W, or Zr and further elements. Though these elements are expected to fractionate into the slag during smelting, elevated contents should be measurable in the tin bronze metal, if they were present in larger quantities in the original ore in the first place. Cassiterite can contain several weight percent of these elements, which could therefore give information, whether the cassiterite was associated with e.g. greisen or skarn deposits.

Another approach could be the analysis of all Pt group elements, as they are expected to be present in the ophiolite related copper deposits. The PGE signature could give further information of the specific deposits, as they behave differently in their geochemistry. This could lead to further implications on the potential mixture of Indian and Oman copper, and which of the latter two deposits was a source for mixing with the Indian copper.

Additionally further copper-based artefacts from other Mesopotamian sites as well as of other dating should be analysed. This enables the observation, whether there is a continuation or a break in cultural and trade contacts and how far the supply chain from the East went further up the Euphrates river or possibly even further to Iran or northwards.

This study highlights the importance of scientific and analytical investigations regarding provenance studies. Although numerous textual evidence from cuneiform tablets exists, the names of the metal suppliers could not have been identified without the scientific analysis of metal artefacts and comparison with potential raw material sources. This study contributes to a better understanding of intercultural relationships of Ur with other regions and gives more information of the main and minor contacts. As mentioned above Turkey appears to have been only a minor supplier for copper. However, when it comes to As-Ni-copper, tin, copper for tin bronze as well as carnelian and lapis lazuli, the main suppliers are more likely to be found to the east in Oman and India. This further emphasises the connection of Mesopotamia and the Indus Valley civilisation, as well as *Makan* and *Meluḫḫa* being Oman and the land of the Harappa culture, respectively.

12 Beginnings of Silver metallurgy

The metallurgy of silver emerged later than copper and gold. The use of native silver has been proposed as well, yet native silver occurrences are very scarce and appear only on a smaller scale, unlike copper and gold (Pernicka, 1990). Another theory is the early reduction of silver from silver chlorides, as chlorargyrite (Mishara and Meyers 1974). These minerals occur in nature only sporadic. Therefore silver had most likely to be extracted from lead ores in the first place. In the first step lead metal has to be smelted from galena, which required more sophisticated knowledge of smelting techniques. A condition that was fulfilled, when copper smelting became more common. In the next step silver can be extracted by the cupellation process from lead metal.

The oldest evidence for silver working in the form of two silver beads was discovered at the site of Domuztepe in south-eastern Anatolia, dated to the 6th millennium BCE (Carter, Campbell and Gauld, 2003; Roberts, Thornton and Pigott, 2009). In the 4th millennium BCE silver objects occur more widespread at the sites of Tappeh Sialk, Susa, Beycesultan, Korucutepe, Alişar Höyük, Arslantepe, Uruk, and Naqada (Meyers, 2003**;** Nezafati and Pernicka, 2012). 4th millennium BCE silver production has been accounted for Ilgynli Depe, Fatmalı-Kalecik, Tappeh Sialk, Tappeh Hissar, and Arisman, due to the finds of litharge (Nezafati and Pernicka, 2012; Helwing, 2014).

In Mesopotamia silver was a limited source and was kept under the higher authority's control, but their policy involved luckily for archaeologists a "state treasury policy", where silver treasures were hoarded for safekeeping (Helwing, 2014). Otherwise silver was used for decorative and higher status jewellery, as for example at the Royal Tombs of Ur and Kiš (Helwing, 2014). In the Ur III dynasty silver became a weight currency (Paoletti, 2008; Helwing, 2014). It was exchanged for barley and copper in order to maintain the flow of these staple goods (Paoletti, 2008; Helwing, 2014).

Silver appeared in northern Caucasus first in the first half of the 4th millennium BCE in Maikop, Staryj Urukh, and Staromyshastovskaja in the Maikop phase (Courcier, 2014). Later on in the Novosvobodnaja phase silver artefacts were discovered at the sites of Novosvobodnaja, Klady, Kubina Aul, Kishpek, Chegem I, Nal'chik, and Bamut (Courcier, 2014). Silver was also known to the Kura-Araxes culture in the Transcaucasian region at the sites of Amiranis-Gora, Kvatskhelebi, and Velikent and its ornaments appear to have parallels with the so-called 'Royal Tomb' of Arslantepe (Courcier, 2014, Kawtaradze, 2001), although silver remained limited in use and was usually associated with burials of individuals of higher social status (Helwing, 2014).

In the Levant silver appeared in a large amount of 230 objects at Byblos in the 4th millennium BCE (Philip and Rehren, 1996). Contemporary with Byblos is the find of a silver vessel in Tell esh-Shuna, comprising 4.6-4.8 wt% Au and 1.1-1.8 wt% Cu next to the Ag content (Philip and Rehren, 1996). Furthermore a silver pin has been uncovered at Bab edh-Dhra in Jordan (Philip and Rehren, 1996). An early 4th millennium BCE lead object has been recently discovered in the Ashalim cave and is supposed to be a spinning whorl (Langgut, et al., 2016). In the northern Levant at the transition to Anatolia has silver production been evidenced at Habuba Kabira in the late Uruk period (Pernicka, Rehren and Schmitt-Strecker, 1998).

At the beginning of the 4th millennium BCE the process of cupellation was known and applied to lead ores across South-west Asia and spread even to Central Asia by mid of the 4th millennium BCE (Roberts, Thornton and Pigott, 2009), although this process might have his origins in South-east Europe, as a silver hoard in the cave of Alepotrypa was discovered, which is dated to the mid 5th / early 4th millennium BCE (Roberts, Thornton and Pigott, 2009). In Namazga III central Asian silver artefacts were uncovered dating to the early 3rd millennium BCE (Garner, 2013). In Western Central Asia the most important find of a gold and silver treasure was at Tepe Fullol (Kosh Tepe), dated to the 3rd and 2nd millennium BCE, which exhibits a very sophisticated level of metal working and decoration (Thomalsky, et al., 2013).

The Harappa culture includes silver objects at the major sites. Kenoyer and Miller (1999) mention, that silver might have been even more common than gold in contrast to Mesopotamia. Silver occurrences are widely spread near the Indus Valley in the Aravalli range, Baluchistan, and Afghanistan (Kenoyer and Miller, 1999).

12.1 Lead- and silver ores

The most common silver ore is galena, which incorporates or is associated with certain silver minerals. Galena is usually associated with Zn sulphides and together

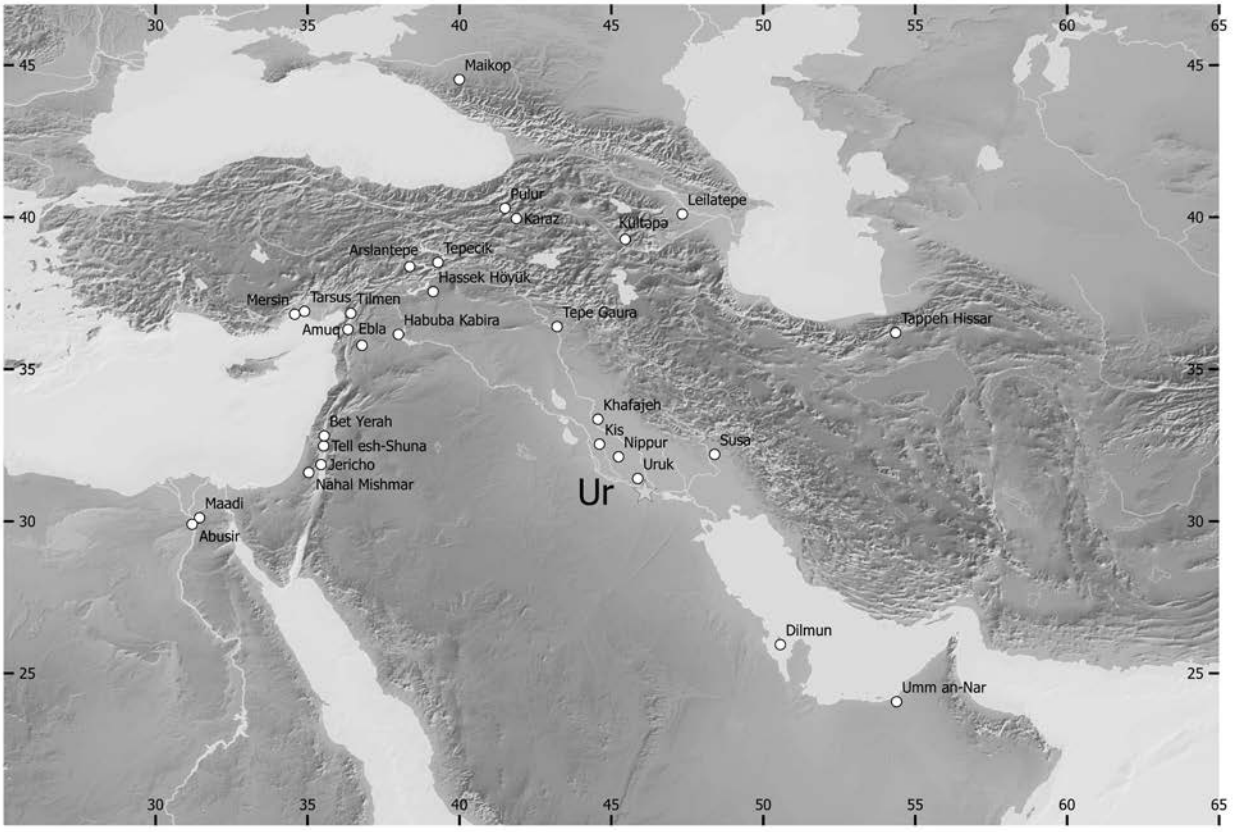

Fig. 12.1: Distribution map of early silver artefact findings across the Near and Middle East in the 6th to 3rd millennium BCE [data source: Philip and Rehren, 1996; Pernicka, Rehren and Schmitt-Strecker, 1998; Kenoyer and Miller, 1999; Stech, 1999; Hauptmann, 2000; Kawtaradze, 2001; Carter, Campbell and Gauld, 2003; Meyers, 2003; Paoletti, 2008; Roberts, Thornton and Pigott, 2009; Romer and Born 2009; Nezafati and Pernicka, 2012; Courcier, 2014; Helwing, 2014; Hoffman and Miller, 2014; Thornton, 2014, made with natural earth)

they form large scale Zn-Pb-(Ag)-deposits. The silver solubility in galena via the substitution of $2Ag + \leftrightarrow Pb^{2+}$ is low (0.4 mol% at 615°C) (van Hook 1960). Silver minerals commonly hosted by galena as solid solution or micro scale inclusions are: pyrargyrite, proustite, and stephanite (Westner, 2016). The mineral acanthite is found within galena minerals as well. The incorporation of silver ions is enhanced by the presence of both Bi and Sb (Chutas, et al., 2008 , Westner, 2016).

Further important silver bearing minerals are fahlores of the argentotennantite-freibergite solid solution system and argentojarosite.

In contact with salty water chlorargyrite is formed, which is easier to smelt then sulphides. The same is applied for cerussite, which is commonly enriched in the oxidation zones of Zn-Pb-deposits. Cerussite can contain more silver than galena.

Silver can be enriched in supergene environments by Bacteria (Sillitoe, Folk and Saric, 1996). Sillitoe, Folk and Saric (1996) reported, that carrier solutions of metal ions resulting from sulphide dissolution can be precipitated under reducing conditions near the groundwater table. This process is enhanced by activity of bacteria leading to silver enrichment of upto several thousand ppm (Sillitoe, Folk and Saric, 1996).

Certain copper ores have also the ability of carrying high levels of silver, as in bornites for example silver can be as high as several thousands ppm (Cook, et al., 2011). Chalcocite and digenite can exhibit even higher Ag concentrations than bornite (0.3 - 0.8 wt%) in contrast to chalcopyrite (up to 0.3 wt%) (Cook, et al., 2011).

12.2 Smelting of polymetallic ores

To produce silver from lead ores, one has to reduce lead metal from the ore first. The reactions of the main lead ore galena are displayed as an example in the following. According to Nezafati and Pernicka (2012) galena can be smelted directly. However, there are different approaches for smelting lead minerals:

12.2.1 Roast reduction process:

Crushed lead sulphides are heated resulting in the reduction of Pb and the oxidation of the S, which is escaping as SO_2

(Gowland, 1914). The reactions are as follows (Nezafati and Pernicka, 2012, Westner, 2016):

(1a): $2\ PbS + 3\ O_2 \rightarrow 2\ PbO + 2\ SO_2$
(1b): $PbO + 2\ SO_2 + O_2 \rightarrow 2\ PbSO_4$

This process is highly temperature dependent, as at lower temperatures the unwanted $PbSO_4$ preferentially forms, partially reacting back to PbS (3f).

12.2.2 Roast reaction process:

The crushed ore is oxidised in the upper part of the furnace. Under these conditions the previously formed (1a, 1b) $PbSO_4$ and PbO react with galena. In the process forms lead metal, which is accumulating in the lower part of the furnace, due to higher density, whereas S is emitted as SO_2 (Nezafati and Pernicka, 2012; Westner, 2016):

(2a): $PbS + 2\ PbO \rightarrow 3\ Pb + SO_2$
(2b): $PbS + PbSO_4 \rightarrow 2\ Pb + 2\ SO_2$

The limiting factor of this process is the high purity of galena required (Gowland, 1914). However, the advantage of the relatively pure lead metal, as opposed to the roast reduction process, is compensating the disadvantage (Westner, 2016).

12.2.3 Smelting process:

Charcoal is added to the roasted ores resulting from the roast reduction process. The charcoal reacts with the O_2 put in through the tuyère to CO_2 (3a), which then further reacts with the remaining charcoal to CO (3b), provided that O_2 input is kept at lower levels, resulting in reducing conditions. Under reducing conditions PbO is reacting to lead metal, although the presence of $PbSO_4$ can diminish the lead output (3f). The reactions are as follows (Nezafati and Pernicka, 2012, Westner, 2016):

(3a) $C + O_2 \rightarrow CO_2$
(3b) $CO_2 + C \leftrightarrow 2\ CO$ Boudouard equilibrium
(3c): $PbO + CO \rightarrow Pb + CO_2$
(3d): $PbO + C \rightarrow Pb + CO$
(3e): $PbSO_4 + Pb \rightarrow 2\ PbO + SO_2$
(3f): $PbSO_4 + 4\ CO \rightarrow PbS + 4\ CO_2$

As the precious metals are more noble than Pb, they are reduced and collected within the lead metal.

Elemental partitionining	Byproduct	Density
Siliceous melt	Slag	3-4
Copper-iron-sulfides	Matte	5
(Ferous speiss) (Fe-Arsenides) (+base metal speiss)	(Speiss)	(7-8)
Lead + silver (Bi, Au) + Cu-Sb	Metal	>8

Fig. 12.2: The metallurgical (by-)products of polymetallic smelting (after Keesmann, 1993, fig. 6). The distribution between different phases takes place in different layers, separated by density.

12.3 Cupellation of silver

The lead metal achieved by the prior roasting and smelting process is further processed during cupellation. This task is performed in a small crucible or cupelle. The lead metal is given into the crucible or cupelle and heated under oxidising conditions to approximately 900°C (melting point of PbO: 996°C) (Nezafati and Pernicka, 2012). Lead is less noble than silver, therefore it is oxidised first.

(4a): $2\ Pb + O_2 \rightarrow PbO + Pb(Ag)$

Lead melts due to its low melting point, oxidises to litharge and collects other unwanted metals and components. The litharge has to be removed, as the forming lead-silver droplet will prevent further oxidation of lead metal. This is ensured by the low surface tension of the litharge, which is absorbed by the porous cupelle or hearth lining (Nezafati and Pernicka, 2012). The hearth is further heated to 1000°C, so the silver droplet remains in the liquid form, when further Pb is oxidised (Nezafati and Pernicka, 2012). Due to the higher surface tension of liquid silver metal, it floats on the surface of the cupelle or crucible (Nezafati and Pernicka, 2012). Volatile elements are evaporating at high temperatures, as As or Sb (Nezafati and Pernicka, 2012). Copper is more noble than Pb and less noble than silver, therefore some losses occur in the litharge, while some copper is trapped in the silver droplet depending on the reaction time. Bi is difficult to remove, as it will oxidise after all Pb is oxidised, thus it is remaining in the silver, although possibly not completely (Merkel, et al., 2013). If Au, Pt, and Pd is present in the ore, it will also remain in the silver metal.

This process might also be repeated, in order to obtain a silver of higher purity (Moorey, 1994).

13 The silver artefacts: Results and discussion

13.1 Quantitative analysis

13.1.1 Results: Electron Microprobe Analysis

The silver samples were measured with a different microprobe program than the copper-based metal samples. New elements were included: Ti, Cr, Pd, Pt and Bi. Some samples were already deeply corroded resulting in a total number of 14 artefacts analysed by Electron Microprobe. Again the results with sums more than 102 % and below 95% were excluded. The mean, median, standard deviation as well as minimum and maximum of the bulk analysed silver samples are displayed in tab. 13.1.

The major constituents of the silver metal are Ag, Cu and Pb, which were detected in each sample. The Ag content varies between 89.6 and 99.7 wt%, averaging 96.6 wt%. The Ag levels are followed by differing concentrations of copper with a minimum of 0.12 wt% and a maximum of 6.95 wt%, averaging 2.68 wt%. Lead varies between 0.11 and 1.48 wt% with an average of 0.48 wt%. Ti, Mn, Co, Zn, Pd, Sn and Bi were below detection limit in all 14 samples. Cr was detected in the silver lyre (30-12-253-1 and -3), only. The samples 30-12-253.1 and -3 as well as B17078a and B17082a exhibit a different composition than the other 10 analysed silver samples, as they have lower copper and higher Fe levels. The other 10 silver samples have Fe contents below detection limit. The element Ni was only detected in the silver lyre as well. Small quantities of As could be found in the samples B17082a and B17553b. 510 ppm of Sb were detected in sample 30-12-446. The element Pt is mostly below detection limit, except for 30-12-253.1, 30-12-605, B16931a and B17084. Au was detected with more than 4000 ppm in the two bracelets B16931a and -b.

As most of the measured elements are below detection limit, only a correlation of Pb and Cu was observed in the silver samples. The artefacts 30-12-253, B17078a and B17082a with lower Cu content display no correlation as the other artefacts with more than 2 wt% copper. The pin 30-12-446 found at PG 1237 exhibits the highest Cu content of 6.95 wt% combined with the highest Pb levels at 1.48 wt%.

13.1.2 Discussion: The main elements

The four samples 30-12-253.1, -2, B17078a and B17082a exhibit a different microstructure than the other silver metal samples. The remaining silver metal in these four samples forms a skeletal structure of dendrites with no indication of structures caused by forging. Another difference is the surface of the artefacts, as the three low Cu artefacts exhibit a silvery surface, whereas the other artefacts have corrosion layers of silver halogenides on the surface.

It turns out that these objects were restored electrochemically (R. Zettler, pers. comm., Jul. 2016). The objects were bathed in a Cr containing fluid and an electrical potential was put to it resulting in reducing conditions on the surface of the objects, so the silver halogenides were reduced to silver metal again. The restoration method has an impact on the microstructure and the trace element composition as well, further discussed in the following subsection 13.1.3. Due to the chemical alteration caused by this process, these artefacts were excluded from further interpretation regarding provenance.

The plot of the remaining silver artefacts sorted by date visualises, that the Early Dynastic silver artefacts exhibit higher Pb and Cu levels than the Akkadian artefacts as well as the artefact of unknown date. Although the statistics of nine artefacts are not ideal.

The picture changes when compared to the pXRF analyses of Müller-Karpe (2004) (cf. fig. 13.2). The published pXRF analyses by Müller-Karpe (2004) were sorted by corrosion status, before further evaluation, as a large number of analyses had to be excluded, due to bad quality of analysis on corroded surfaces. Of the Ur objects 20 analyses of silver artefacts remained that exhibited low alteration by corrosion. These are diagrammed in fig. 13.2 and sorted by dating. When combined with the microprobe analyses of this study, it becomes apparent, that all samples do not form a clear correlation and do not differ in Cu and Pb contents across the time periods, as before. PXRF analyses are more susceptible to errors. It is not mentioned in the publication of Müller-Karpe, in which mode the samples were measured, neither how the pXRF was calibrated. Furthermore it is desirable to know, if the artefacts were measured several times and if a mean was calculated from different analyses. Therefore these data have to be a handled with care and the large scatter could also be explained by high measurement errors of pXRF.

The general trend of elevated Cu and Pb contents is observed in all silver artefacts, regardless. Both elements are an indicator of cupelled silver from argentiferous lead ores. Other elements were not or rarely detected by

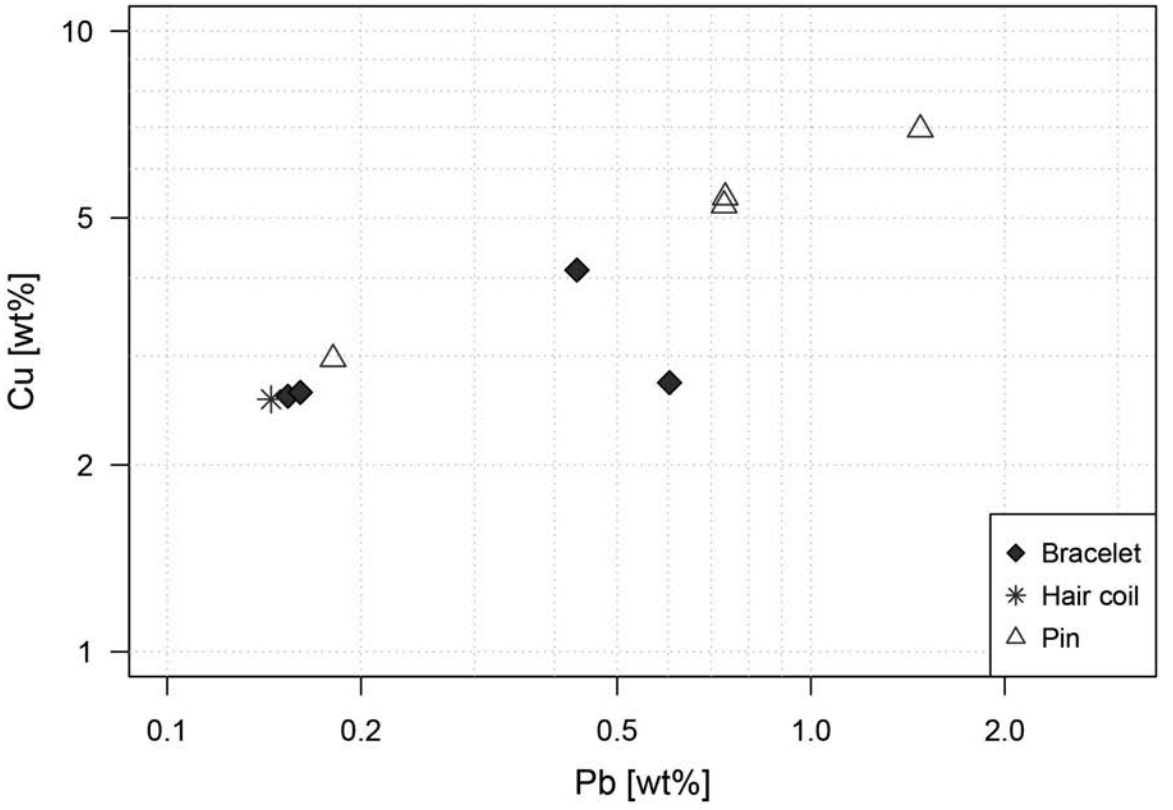

Fig. 13.1: Lead vs. copper in the silver metal samples of Ur. The electrochemically restored samples were excluded from this diagram.

electron microprobe and are therefore very low. Some local enrichment of Pt was observed during microprobe measurements, but the contents could not be quantified reliably with this method.

Au was detected only in the two bracelets B16931a and -b with ca. 4500 ppm. Interestingly, these two artefacts differ also by dating (Akkadian) and exhibit Cu and Pb levels at the lower edge. The lower levels of Cu and Pb could also be related to different process parameters during smelting. Possibly for some silver artefacts cupellation was carried out more than one time, in order to refine the silver. This would lead to reduced Cu and Pb concentrations.

One further possibility for the elevated Cu is the intentional addition of copper metal to save some of the precious silver. This has the advantage of increased hardness of the silver metal (Mishara and Meyers, 1974). The silvery colour is not affected by the copper, as higher Cu concentrations are needed for the change of colour until a more reddish tone is noticeable (cf. fig. 13.3). For latter consideration the evaluation of trace element data is needed, to investigate if other elements are correlated with copper.

Whether the difference of B16931a and -b in Au content reflects a silver from a different source will be discussed further in sec. 13.1.4, 13.2.4, and 13.3.

	Cr	Fe	Ni	Cu	As	Ag	Sb	Pt	Au	Pb
	(3 0 - 1 2 - 253.1-3)	(n=4)	(3 0 - 1 2 - 253.1-3)	(n=14)	(n=2)	(n=14)	(3 0 - 1 2 - 446)	(n=4)	(B16931a-b)	n=14)
Mean	0,032	0,07	0,029	2,68	0,033	96,6	0,051	0,081	0,46	0,48
Median	0,032	0,07	0,03	2,6	0,033	96,7	0,051	0,081	0,46	0,43
Sdev	0,006	0,046	0,008	2,15	0,002	2,8	1 sample	0,004	0,006	0,41
Min	0,027	0,022	0,021	0,12	0,031	89,6	0,051	0,077	0,46	0,11
Max	0,036	0,119	0,038	6,95	0,034	99,7	0,051	0,086	0,47	1,48

Tab. 13.1: Mean, median, standard deviation (Sdev), minimum (Min) and maximum (Max) values of the silver metal samples analysed by Electron Microprobe. Ti, Mn, Co, Zn, Pd and Bi are below detection limit (b.d.l.) in all samples and there fore not displayed. Sb was detected only in one sample.

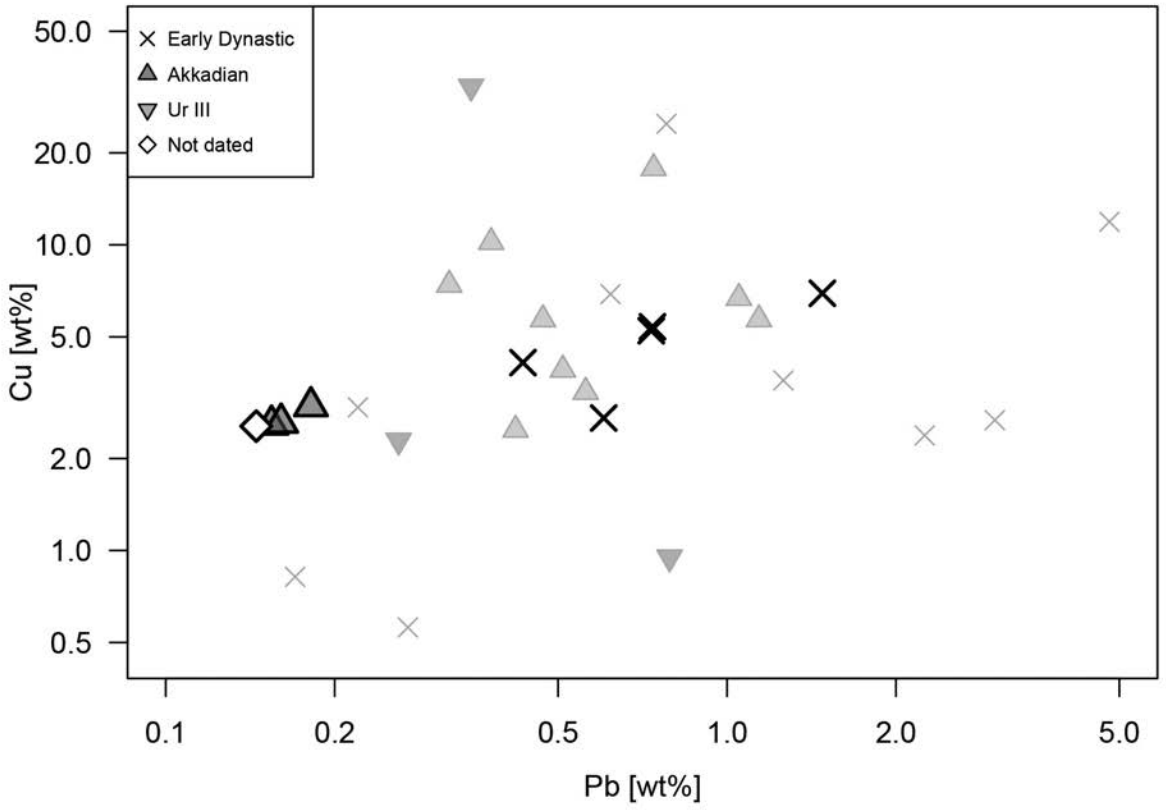

Fig. 13.2: Lead vs. copper in the silver artefacts of Ur. The samples are displayed by dating. The bigger symbols with a thicker black outline represent the analysed samples of this study. The silver artefacts measured with pXRF by Müller-Karpe (2004) are plotted as smaller symbols with grey outline and lighter colour.

13.1.3 Results: trace elements - nanosecond-laserablation-SC-ICP-MS

As mentioned in subsection 13.1.1 a few artefacts had to be excluded due to electrochemical restoration. As the artefacts 30-12-253, B17078a and B17082a behave differently compared to the other "normally" restored artefacts, when it comes to trace element concentrations, the data were evaluated carefully before further discussion. The three objects exhibit higher levels of Cr, Mn, Ni, Zn, and Sn and lower levels of Cu, Pb and Bi, which are most likely altered by the chemicals used for electrochemical restoration. Therefore these objects had to be excluded from further evaluation of the chemical data, unfortunately.

The results of the remaining 9 samples analysed by laserablation SC-ICP-MS are further discussed in the following. The mean, median, standard deviation, minimum and maximum values are displayed in tab. 13.3. The mean as well as the minimum and maximum values are also diagrammed in fig. 13.4. As mentioned in section 10.1.3 the median is in better agreement with the certified values of the standards. Therefore the median of the 10 points measured is given for the trace element results of the silver artefacts (cf. tab. 13.2 for the results of the standards).

In general most of the trace element levels in the measured artefacts are very low. As discussed in subsection 13.1.1 Cu and Pb are the two major constituents besides Ag. However, they are followed by Au and Bi. In the range of 100 to 1000 ppm only falls the mean of Mg, which is, like Al and Ti, problematic due to polyatomic interferences.

Between 10 and 100 ppm are the means of Ni, Zn, As, Sb and Te to be found. Cr, Se, Rh, Pd, Cd, Sn and Pt are in the lower ppm range of 1 to 10 ppm. Below 1 ppm and thus near the detection limit are Mn, Co, Ge and In. Rh is displayed in this diagram, but has to be excluded from further discussion as it displays an interference with $^{63}Cu^{40}Ar$ which is still noticeable at Cu contents of 2 to 7 wt%.

13.1.4 Discussion: Trace elements

The measured trace elements of the silver artefacts exhibit some differences in between the artefacts. The elevated Cu levels display no clear correlation with As and Sb, although the Early Dynastic artefacts 30-12-754 and 30-12-733 have higher levels of As and Sb paired with higher Cu concentration (cf. fig. 13.5). This indicates, that fahlore of the tennantite-tetrahedrite series was possibly associated with the argentiferous lead ore smelted for both artefacts. Both As and Sb are expected to be partially lost during roasting and smelting. Although potentially forming speiss has a similar density as the crude lead and could thus be introduced as inclusions in the silver

Standard		^{53}Cr	^{55}Mn	^{59}Co	^{60}Ni	^{66}Zn	^{72}Ge	^{75}As	^{77}Se	^{103}Rh	^{105}Pd	^{106}Pd	^{111}Cd	^{115}In	^{118}Sn	^{121}Sb	^{128}Te	^{195}Pt	^{197}Au	^{208}Pb	^{209}Bi
AgA1	median	23,6	57,8	529	125	2137	101	274	139	18,5	58,8	54,7	166	39,9	2911	501	272	71,9	14706	2074	1975
AgA1	SE%	1,4	0,08	1,5	0,75	0,13	0,24	0,53	1,3	0,55	0,33	0,097	0,14	0,27	0,15	0,15	0,02	3,8	0,016	0,13	0,016
AgA1	certified	20	61	406	118	2110	107	255	169	16	54	54	165	37	2910	500	271	67	14800	2070	1940
AgA2	median	59,5	116	116	267	4977	51,8	144	111	11,7	76,4	76,5	112	61,4	5197	1984	101	117	5076	10602	1117
AgA2	SE%	1,1	1,5	1,5	0,53	0,35	0,87	1,4	3,4	1,4	0,1	0,13	0,34	0,67	0,65	1	1,1	1,3	0,072	0,26	0,65
AgA2	certified	76	115	163	264	5020	47	144	78	13	76	76	113	65	5200	1920	98	114	5070	10200	1130
AgA3	median	101	94,6	48,9	395	8081	34,4	65,2	39,3	17,1	141	146	43	134	9375	4316	48,6	336	2653	18208	409
AgA3	SE%	2,2	0,21	3,3	0,49	0,056	1,2	0,98	1,7	0,79	0,15	0,068	0,061	0,044	0,012	0,099	0,37	0,5	0,028	0,069	0,011
AgA3	certified	86	98	50	450	8160	45	80	44	17	156	156	42	134	9210	4590	54	256	2580	18900	480
AgRM1	median	48,4	3,3	0,27	42,3	18	0,23	9,5	8,3	9,1	2,6	4,2	3,9	0,074	18,8	1,8	1,5	3,8	2,8	14,2	8,6
AgRM1	SE%	22,4	82,6	32,3	22,4	5,3	11,4	39,1	42,7	45,4	65,7	50,2	64,5	238	62,2	55,4	56,8	30,6	56,3	46,9	51,4
AgRM1	certified	62,9	8,9	0,1	66,1	26,9	0,1	19	23	13,4	5,2	5,2	8	0,1	49,2	4,5	4,7	5,5	6,1	37,5	7,3
AgRM2	median	8,9	7,5	0,24	10,3	9,2	0,19	3,5	4,8	2,2	12,2	14,6	11,4	0,011	2,5	12,8	19,5	18,9	13,3	3,1	41,2
AgRM2	SE%	30,2	48,9	5,4	44,1	9,1	4,5	42,1	84	1593	39,7	28,8	40,7	345	38,3	45	50,3	24,8	43,9	30,8	17,7
AgRM2	certified	8,8	16,1	0,1	10,6	5,2	0,1	5,5	8,6	4,6	23,1	23,1	23,5	0,1	4,5	23,6	38,1	20,9	26,2	5,6	40,8

Tab. 13.2: Measured medians, relative standard errors (SE%) and certified values for each measured isotope on the standards used for the silver samples. Not detected values (n.d.) are marked.

	^{53}Cr	^{55}Mn	^{57}Fe	^{59}Co	^{60}Ni	^{65}Cu	^{68}Zn	^{72}Ge	^{75}As	^{77}Se	^{103}Rh	^{106}Pd	^{111}Cd	^{113}In	^{119}Sn	^{121}Sb	^{128}Te	^{195}Pt	^{197}Au	^{206}Pb	^{209}Bi
Mean	2,2	0,7	862	0,6	12,1	35837	50,8	0,2	55,8	3,4	2,5	4,9	2,5	0,2	7,2	11,7	11,7	5,2	1691	6294	812
Median	1,4	0,4	263	0,5	4,9	27591	3,9	0,3	5	3,8	1,8	4,6	2,3	0,2	4,4	5	1,6	2,7	719	4811	747
Sdev	2	0,6	1522	0,4	14,5	14914	112	0,1	111	1,9	1	1,1	0,6	0	7,8	13,5	17,4	5,9	2039	4957	377
Min	0,3	0,1	95,5	0,2	1,2	23000	1,8	0,1	2,7	1,1	1,4	3,8	1,9	0,2	1	1,1	0,7	1,2	316	1468	260
Max	5,5	1,8	4267	1,2	42	63623	342	0,3	333	5,9	4,4	7,6	3,9	0,3	26,6	36,7	43	17,5	5698	16583	1231

Tab. 13.3: Silver: Mean, median, standard deviation (Sdev), minimum (Min) and maximum (Max) values of trace elements analysed by laserablation SC-ICP-MS (n=9 samples).

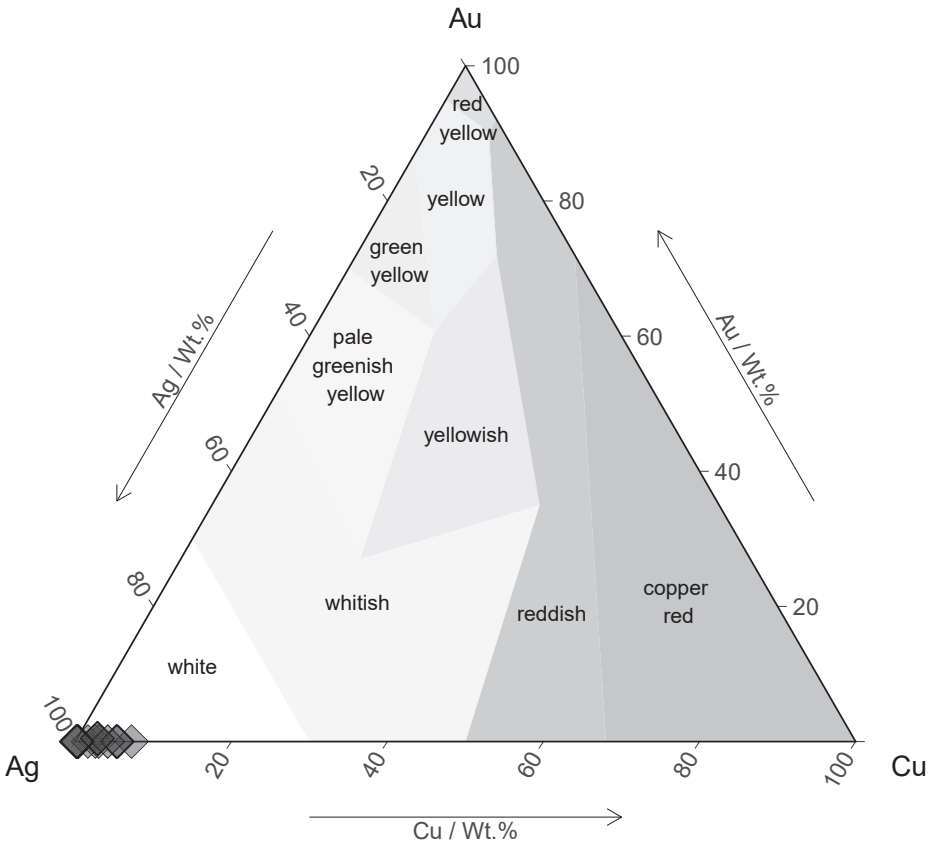

Fig. 13.3: Ternary diagram of Cu, Ag, and Au with the analysed silver artefacts of this study as violet diamonds. The diagram exhibits also the colour of the metal resulting from different compositions. Diagram after German, Guzowski and Wright, 1980.

metal. Depending on the composition of the original ore and the process parameters some As and Sb can remain in the metal as inclusions or even within the metal's matrix in small quantities.

The Zn levels are low. Sphalerite is one of the most common minerals associated with galena. Nevertheless, Zn is expected to go into the slag during the process of silver production. Therefore Zn is not necessarily correlated with Pb, even though it might be in the original ore.

Due to the alterations of trace element composition from ore to silver metal during smelting and refining it is essential to investigate those elements, that stay the same regarding the ratio to silver. Though Bi is partially oxidised during silver production, a proportion enters the silver metal. Hence the ratio of Bi and Au might provide a clue. Bi and Au are geochemically associated with each other, although not in the same minerals.

Since Bi and Au stay in the silver metal due to Au being more noble than Ag and Bi being oxidised after eventual oxidation of Pb, their ratio could give some indications on different ore sources. The ratio is supposed to stay the same in the silver metal, as in the original ore mixture. It is considered, that ancient smelters did not take pure ores of modern standards but ores with impurities, which were desired to some extent, as they aid the matte formation in the smelting process (cf. sec. 12.2). Most of the silver artefacts exhibit a Bi-Au ratio of around one, except for 30-12-446, B16931a-, and -b (cf. fig. 13.6). 30-12-446 has a higher Bi-Au ratio combined with the highest Cu and Pb contents of all analysed silver artefacts. The high Cu content of 6.95 wt% is more likely to be explained by low refinement or purification of the silver metal. The combination of high Cu and Pb is reflecting a silver that was probably directly used after the first or second cupellation step. Pernicka and Bachmann observed significant amounts of copper to remain in the silver metal produced by cupellation (Pernicka and Bachmann 1983).

The general composition of the silver artefacts might reflect a silver bearing lead ore with high impurities of tennantite-tetrahedrite and aikinite-Biinite series used for the production. Biinite is a very common impurity in galena and enhances the solubility of argentite in galena (van Hook 1960).

The two bracelets B16931a and -b dated to Akkadian times from PG 673 exhibit significantly higher Au levels, than the other silver artefacts (cf. fig. 13.7). This trend is further reinforced by the higher Pt and Te concentrations in both bracelets reflecting a similar ore used for both artefacts. The Early Dynastic bracelet B17084 from PG 55 displays elevated Au and Te, although not as high

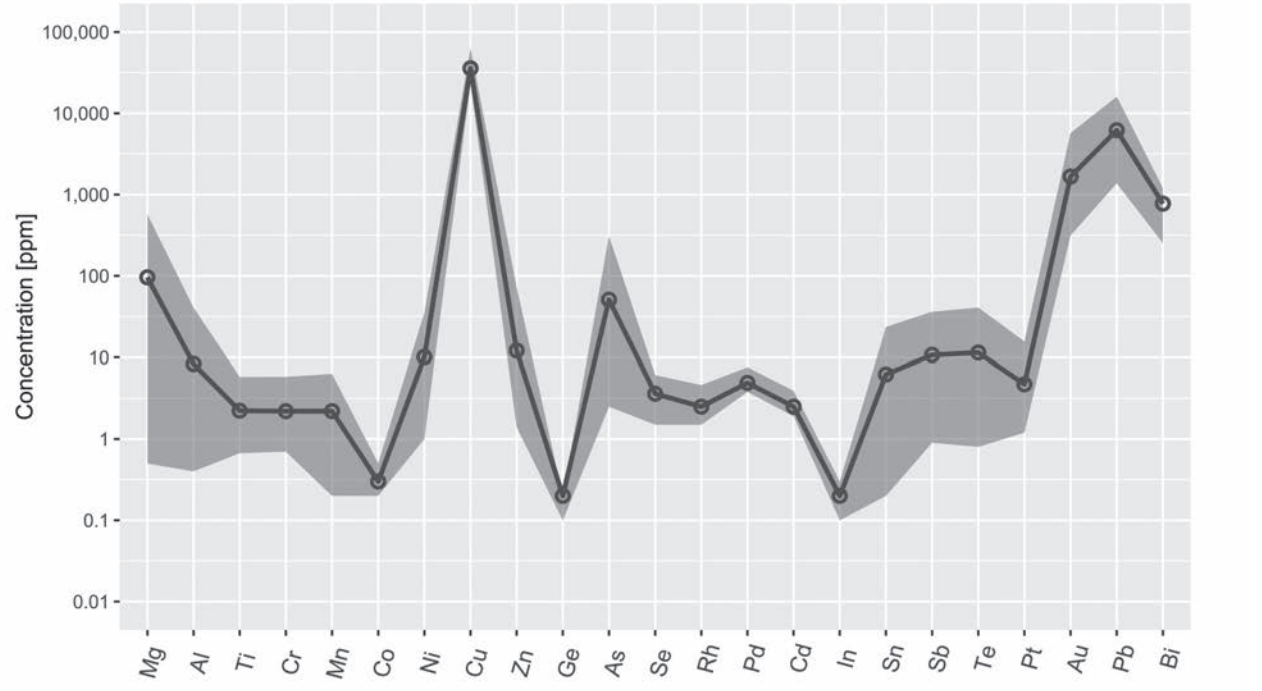

Fig. 13.4: Spider diagram of trace elements measured by laserablation SC-ICP-MS. The line represents the mean and the shaded contour exhibits the range between minimum and maximum.

as the Akkadian bracelets. The Au concentrations of B16931a and -b measured by LA-ICP-MS are within error range of the electron microprobe data. Pt in B17084 is low in contrast to B16931a and -b. Natural telluride minerals are rarely found and occurring in hydrothermal deposits forming at temperatures below 354°C or even 250 °C (Afifi, Kelly and Essene, 1988). Typical telluride minerals occurring also with galena and sphalerite in epithermal deposits are: sylvanite, calaverite, empressite, altaite, tetradymite, coloradoite, kostovite, and melonite (Afifi, Kelly and Essene, 1988). Rarely also Pt containing tellurides occur, as e.g. maslovite. Although Pt exhibits some local enrichment within the samples matrices, that cannot exactly be quantified, the elevated Pt, Au, and Te concentrations appear to be significant. As Te containing ores are rare it shall help to narrow down the potential raw material source locations. Kekelia, et al., (2008) mention gold tellurides in the Greater Caucasus region, although other regions have to be considered. The trace element results are investigated further in combination with the Pb isotope data in sec. 13.2.4 and 13.3.

13.2 Isotope analysis

13.2.1 Results: Copper isotopes - fs-laserablation- and solution-MC-ICP-MS

Six samples of the silver metal could be analysed by fs-Laserablation-MC-ICP-MS: 30-12-429, 30-12-605, 30-12-754, 30-12-733, 31-17-280a and B17084. 30-12-605 and five other not corroded samples were dissolved, the copper was separated by column chemistry, and the Cu isotopes measured by MC-ICP-MS. Both results are displayed in fig. 13.8. The Cu isotopes of the silver metal exhibit a mean of 0.38 ‰ and the variation is between -0.17 to 1.52 ‰. 10 of the analysed samples are in the range between -0.5 and +0.5 ‰, two exceptions are the samples 30-12-733 and B16931a with both exceeding δ^{65}Cu isotope signature of more than 1 ‰. The sample B16931a differs from sample B16931b with more than 1 ‰ deviation, as the samples -a and -b are two different bracelets, therefore they do not have to agree necessarily in their Cu isotope signature. 30-12-605 was analysed by both fs-Laserablation and from a separated copper solution by MC-ICP-MS. Both results differ by 0.2 ‰, which can be explained by inhomogeneities in the metal or small quantities of corroded material, that was dissolved with the silver metal for the separated copper solution (see fig. 10.13). Another factor is the potential Cu isotope fractionation due to the chemical separation method, as an amount of copper remains in the resin (cf. sec. 10.2.1, M. Jansen, pers. comm., Feb. 2017).

13.2.2 Discussion: Copper isotopes

Copper isotopes do fractionate in geological setting within different parts of metal deposits. Primary copper deposits usually exhibit a δ^{65}Cu signature of 0 ± 0.5 ‰ relative to the NIST standard SRM 976 (Markl, Lahaye and Schwinn,

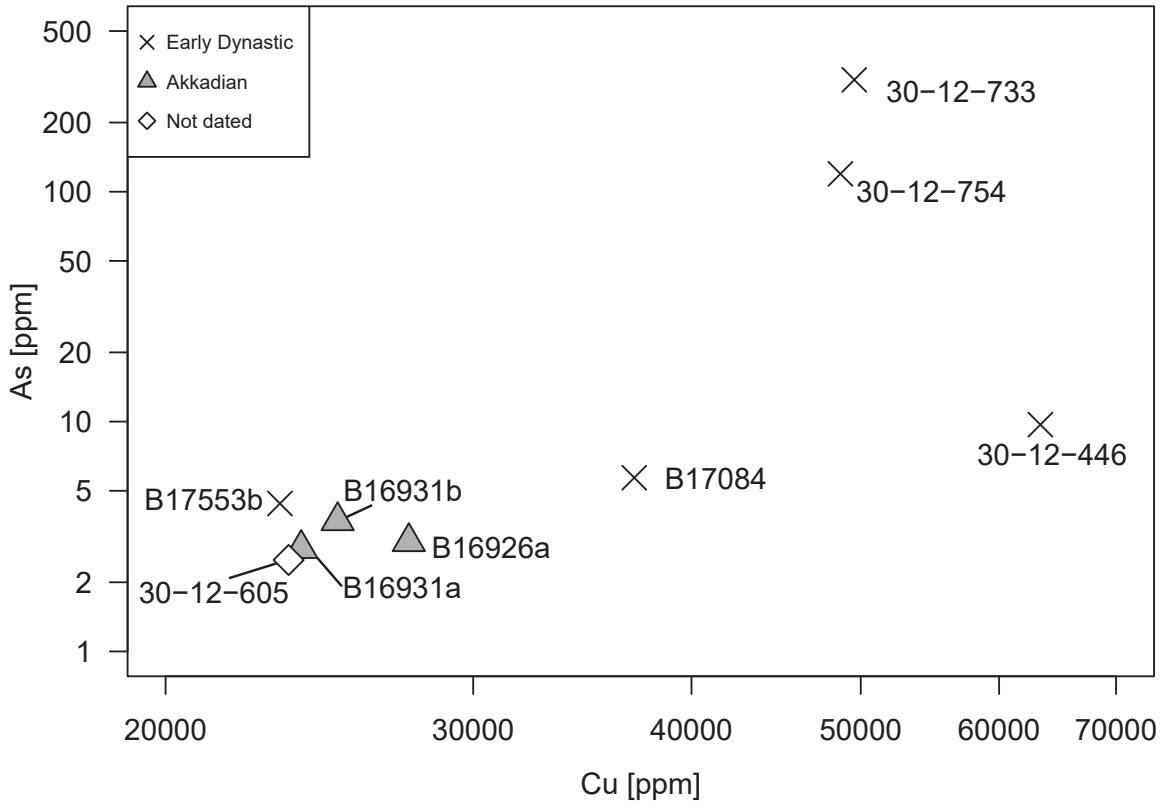

Fig. 13.5: Cu vs. As of the Ur silver artefacts measured by LA-ICP-MS.

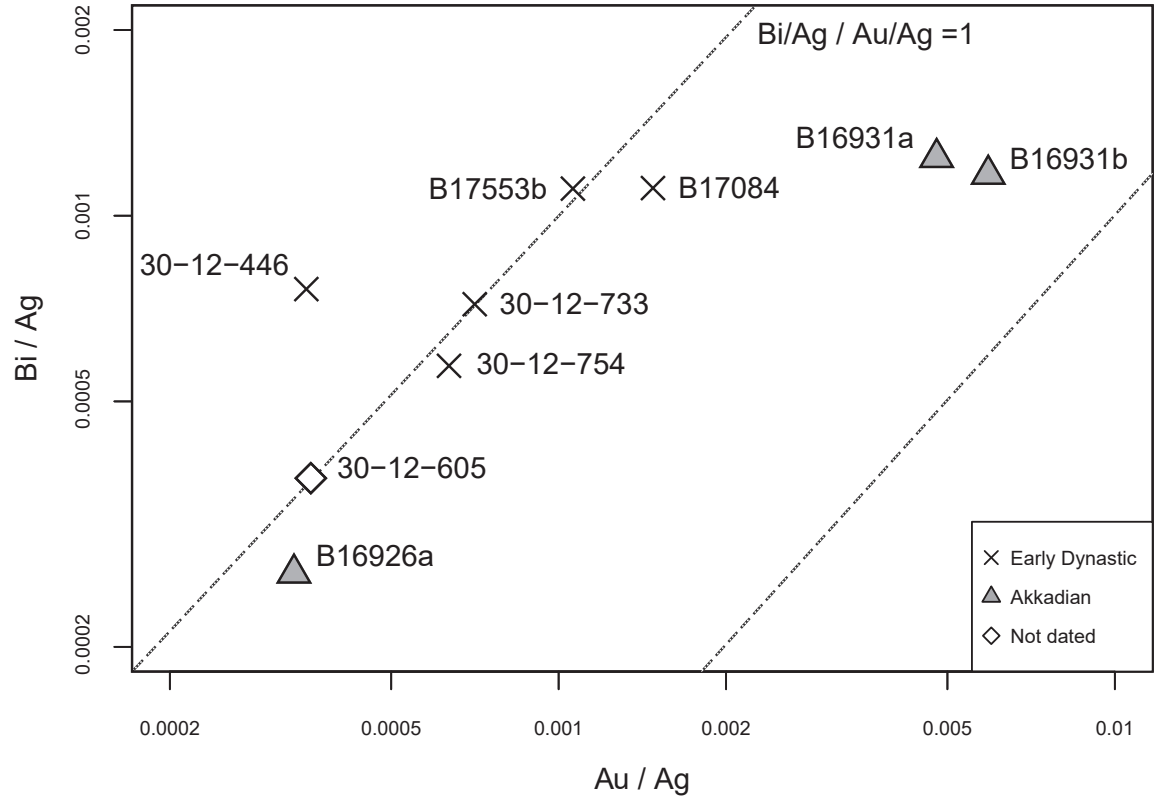

Fig. 13.6: Bi vs. Au in the silver artefacts measured by LA-ICP-MS.

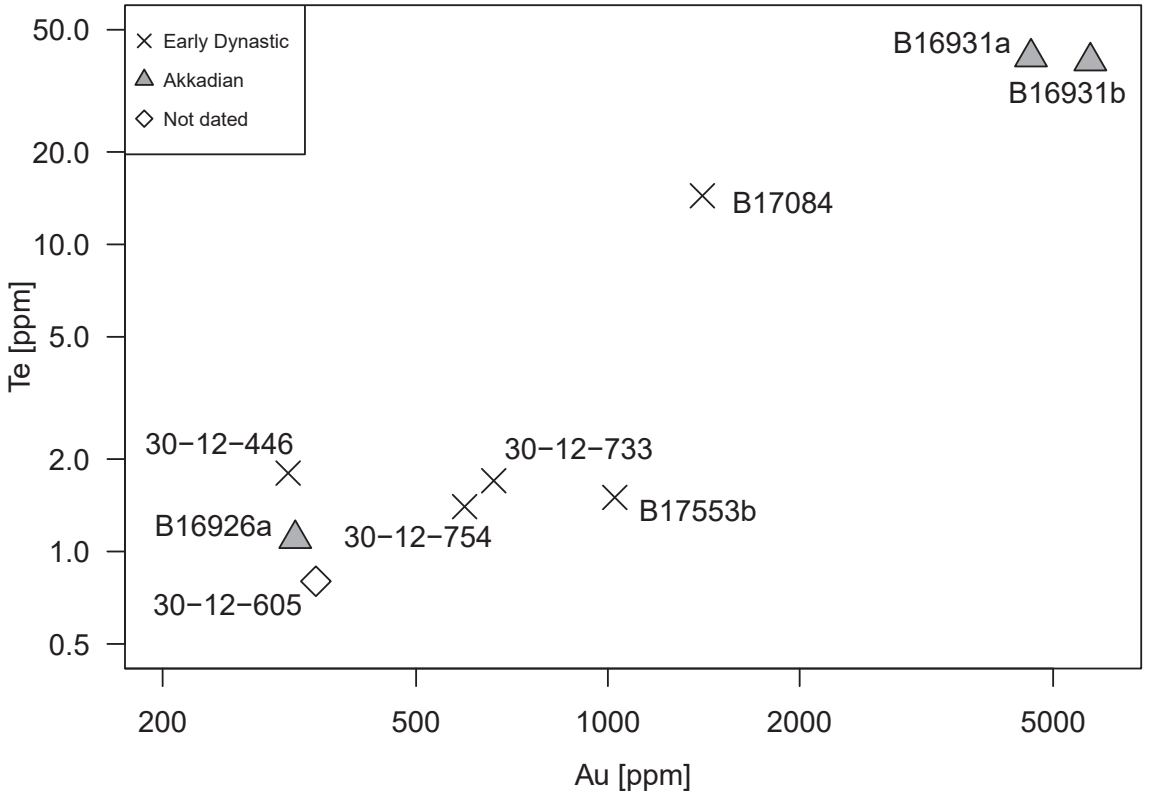

Fig. 13.7: Au vs. Te in the silver artefacts measured by LA-ICP-MS.

2006). The basic thermodynamic mechanisms have yet to be better researched. Nevertheless, studies have been indicating, that ^{65}Cu is dissolved preferentially under oxidising conditions resulting in a solution enriched in ^{65}Cu and thus with a more positive δ^{65}Cu signature (Braxton and Mathur, 2011; Markl, Lahaye and Schwinn, 2006; Mathur, et al., 2011).

As mentioned in sec. 10.2.2 Cu isotope fractionation is observed due to corrosion of the artefacts. Therefore it is crucial, when measuring artefacts for Cu isotope measurements out of a copper solution, to ensure no corroded material is included in the dissolution and separation process. Depending on the corrosion state of the artefact it cannot be prevented for small proportions of corroded material to enter the analysed solution. The difference of 0.2 ‰ in δ^{65}Cu signature of 30-12-605 measured by laserablation and solution is most likely to be explained by corroded material being dissolved with the metal. Another possibility are small inhomogeneities within an artefact, although the artefacts exhibit fairly homogeneous δ^{65}Cu signatures. Copper isotope fractionation during chromatographic separation is likely, as the protocol of Bendall was not investigated for Cu isotope fractionation, before. Bendall (2003, 47) wrote: “This method does not recover all the copper and may produce incorrect δ^{65}Cu values due to chemical fractionation induced by the chromatographic method.” The separation protocol used for copper separation was originally developed for lead separation and adapted by Bendall for copper to be able to separate both Cu and Pb in one cycle. Due to the high quality of the Cu isotope measurements of samples and standards by fsLA-ICP-MS, these results are considered to be more accurate than the measurements from a copper solution, although an offset of + 0.2 ‰ of the separated solution in comparison with the laserablation data was observed by Jansen (M. Jansen, pers. comm, Feb. 2017). Nonetheless, the solution-based Cu isotope data give a general information on oxidation state of the ore used for metal production.

Nine out of eleven silver artefacts have a δ^{65}Cu signature in between ± 0.5 and thus resemble a primary ore signature from a hydrothermal deposit (Markl, Lahaye and Schwinn, 2006; Klein, et al., 2010). Nevertheless, one should take into account potential fractionation processes during cupellation. The Cu content in the silver metal is low and most likely survived the smelting and cupellation process with its highly oxidising conditions from the original ore. The different process steps conducted for silver metallurgy is likely to have an impact on the Cu isotope signature. Both artefacts B16931a and 30-12-733 exhibit a δ^{65}Cu signature of more than +1 ‰. The difference to the other bulk silver artefacts is out of error range and could potentially indicate a secondary ore used for silver production. Secondary ores form after the oxidising dissolution of the primary ore (galena) and secondary precipitation of the ^{65}Cu enriched fluid (e.g. malachite), although Cu isotopes give information on the setting of the ore within a metal deposit, varying δ^{65}Cu signatures

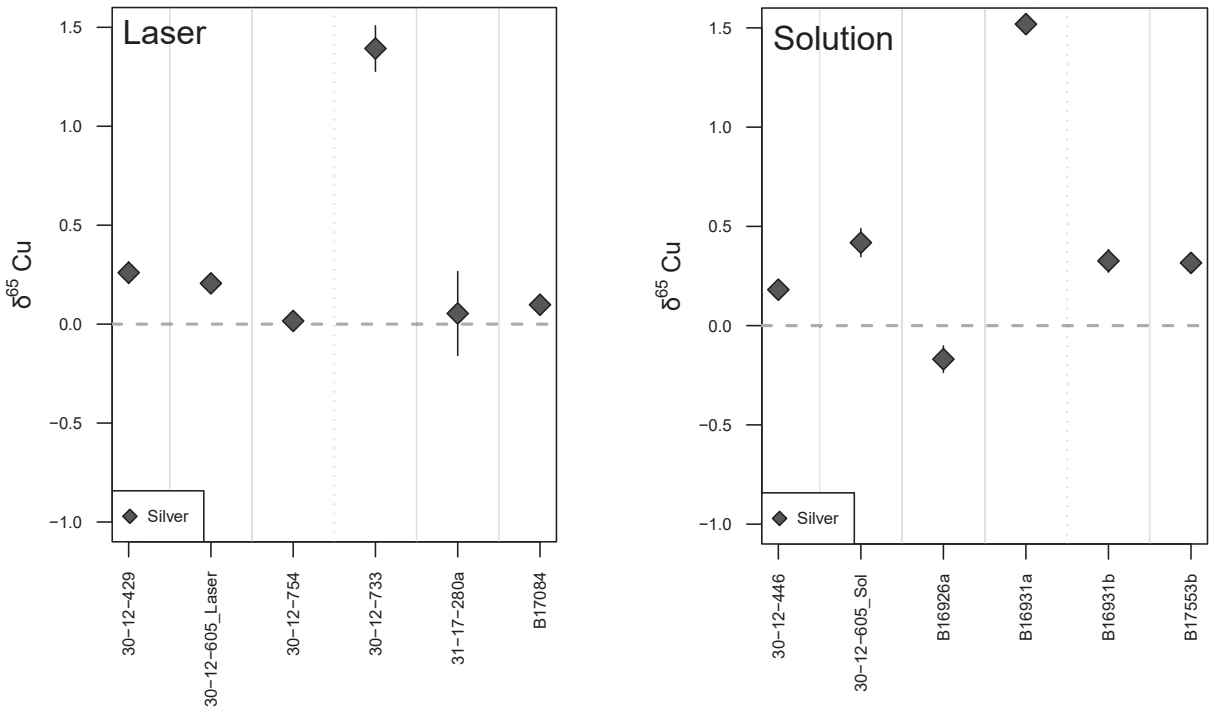

Fig. 13.8: Copper isotopes of the silver metal samples of Ur. The left diagram displays the fs-laserablation data, whereas the right diagram exhibits the solution-based data.

of different artefacts do not necessarily indicate disparate ore sources. It is entirely possible, that ores from the same deposit but differing proportions of secondary/primary ores have been used for metal production. However, the Cu isotopes can aid in understanding the ore's redox-environment within an ore deposit used for metal production and possibly the process and weathering conditions the silver was exposed to.

13.2.3 Results: Lead isotopes - MC-ICP-MS

Eleven of the 20 silver samples could be analysed by MC-ICP-MS out of a pure Pb solution separated by column chemistry methods. The ratios exhibit a more narrow range than the copper-based metal samples. The ratios of $^{206}Pb/^{204}Pb$, $^{207}Pb/^{204}Pb$, $^{208}Pb/^{204}Pb$ vary between 18.564 and 18.944, 15.629 and 15.708 as well as 38.650 and 39.108, respectively. The results are displayed in fig. 13.9. The ^{206}Pb-normalised ratios range from 0.82916 to 0.84276 for $^{207}Pb/^{206}Pb$ and from 2.06437 to 2.08481 for $^{208}Pb/^{206}Pb$. The bulk of the analysed silver samples forms a relatively close cluster, with the exceptions of the samples B17084, B16931a and -b. The two bracelets B16931a and -b appear to form a small array out of error range compared to the other silver artefacts. The bracelet B17084 displays an intermediate Pb isotope composition in between the bulk silver artefacts and the other two bracelets (B16931a and-b). The Pb isotope data of the silver artefacts anaylsyed in this study agree well with Pb isotope data of further silver artefacts from Ur of the collection of the British Museum published by Klein, La Niece and Hauptmann (2016)(cf. fig. 13.11).

13.2.4 Discussion: Lead isotopes

The measured Pb isotope ratios were plotted in a Stacey and Kramers (1975) two stage model to evaluate general geological ages and therefore the age of the ore used for metal production. The plot and the age calculation were performed with an R script written by Thomas Rose (2017). The Stacey-Kramers model ages of the silver artefacts give a general idea of the geological age. The calculated model ages have to be handled with care, as they do not take into account the measurement errors (cf. tab. 13.4).

The silver artefacts forming a closer cluster at Jurassic age are 30-12-446, 30-12-605, B16926a, and B17078a. While B17082a exhibits a different μ value and has an age at the Jurassic-Cretaceous boundary. 30-12-733, B17553a, -b, and B17084 display Cretaceous ages. The two Akkadian bracelets B16931a and -b have distinct very young ages. Due to the long half-life of ^{235}U and ^{238}U decaying to ^{207}Pb and ^{206}Pb, respectively, young stable Pb isotope signatures are highly erroneous.

The kernel density plot (cf. lower fig. 13.10) exhibits two peaks: one at the second half of Mesozoic, the other at possibly Tertiary or Quaternary age. It can be concluded that the ores used for the Mesozoic artefacts originate in an area along the Neotethys suture zone, as the age fits the breakup of Pangaea and the closure of the Neotethys ocean (cf. sec. 6) (Ruban, Al-Husseini and Iwasaki, 2007). The so-called Tethyan Eurasian Metallogenic Belt (TEMB) fits the geological age of these artefacts (Okay, 2008). The TEMB extends from the Taurides to the Zagros and further to the East even to the Himalayas. Tertiary metal deposits occur in the Caucasus and in Iran (Kovalenker, et al., 1990; Moritz, et al., 2006).

13.3 Comparison of potential raw material sources with the Ur silver metal

13.3.1 The ore type

The results presented before emphasise the importance of synergetic application of different analytical methods. Main and trace element results indicate at least two different mineralogical compositions of ores having been used for silver production. One had higher fahlore content, while the other was associated with gold, possibly tellurides, and lower fahlore contents. The measured Cu isotopes suggest, that both primary sulphide ore (galena and associated Cu sulphides) and secondary oxide ores were used. Lead isotope analysis hints to different deposits of Mesozoic and Tertiary to Quaternary age.

In summary, the silver artefacts can be subdivided in at least two different source ore types and associated minerals:

1. Lead-silver deposit of Tertiary to Quaternary age containing galena and secondary lead minerals associated with gold, tellurides, and lower fahlore contents.
2. Lead-silver deposit of Mesozoic (Jurassic-Cretaceous) age containing galena and secondary lead minerals associated with fahlores.

13.3.2 Comparing Pb isotope signatures of ores with the silver artefacts

The corresponding Pb-Ag ore searched for has now been characterised and narrows down potential ore sources. Ore sources in Egypt, Levant, Indus Valley, and Central Asia are to be excluded from further considerations, as they do not fit the geological age and the chemical composition of the silver artefacts (cf. sec. 6). Oman has mainly copper mineralisations and is not considered further as a source for the Ur silver metal. As potential ore sources remain mineral deposits in Anatolia (Taurus, Pontides), Caucasus, and Iran. As mentioned in sec. 13.2.4 the TEMB extends across the highlands of Turkey, the Caucasus, and the Zagros mountains. A multitude of Pb-Ag deposits occurs along the metallogenic belt. While ores from Iran and Turkey are characterised very well regarding Pb isotope analysis, the Greater Caucasus is an analytical void in terms of Pb isotope data. Ores from Transcaucasian region have been analysed by Begemann and Schmitt-Strecker (2009) and Meliksetian and Pernicka (2010), but none are published from the Greater Caucasus.

From an archaeological point of view the connection of Mesopotamia with ore sources in Iran, Turkey, and Caucasus is reasonable, as textual evidence and archaeological studies suggest, that intensive exchange of different trade goods (e.g. textiles and grain from Mesopotamia for metal from the surrounding highlands) had taken place (Postgate, 1992; Moorey, 1994; Meyers, 2003; Paoletti, 2008; Crawford, 2013).

When comparing Pb isotope data from Turkey with the Ur silver artefacts, it occurs, that the objects B16931a and -b exhibit the highest resemblance with ore sources in the Taurus mountains, along the Assyrian Suture / Zagros Suture zone in all Pb isotope ratios, while B17084 has the most conformity with the Taurus mountains and the Pontide Sakarya zone, the northern border between Taurus and Pontides (cf. fig. 13.11). The remaining silver objects are in better agreement with the Urumieh-Dokhtar zone in Iran in all Pb isotope ratios (cf. fig. 13.11). The Transcaucasian ore data do not match the silver artefacts of Ur.

The diagrams of the ratios of $^{207}Pb/^{206}Pb$ and $^{208}Pb/^{206}Pb$ are highlighting that conformity in these ratios does not necessarily prove a provenance, as Pb isotope ratios based on ^{204}Pb exhibit higher variations and thus are better suitable for investigating the provenance of artefacts in comparison with ore sources. For example, in fig. 13.11 the silver artefacts agree well with the Taurus in the ratios of $^{207}Pb/^{206}Pb$ and $^{208}Pb/^{206}Pb$, while they fall into a gap between different Anatolian geological units in the ^{204}Pb based ratios. The use of only ^{206}Pb based ratios in Archaeometry has its roots in former measurement techniques, when ^{204}Pb could be measured only with high measurement errors, as the interference with ^{204}Hg could not be properly resolved, and was thus not suitable for provenancing. However, the modern analytical techniques with MC-ICP-MS facilitate the measurements of all stable Pb isotopes with low measurement errors and therefore all its ratios should be used for provenancing.

Another approach involved the calculation of the Euclidean distance d in the 3-dimensional space for each silver artefact to all Pb isotope data of ores available in the Near and Middle East.

Each ^{204}Pb based Pb isotope ratio of each artefact is subtracted by the corresponding ratio of each individual ore sample, then squared, summed up, and the square root extracted. The lower the value for the Euclidean distance, the closer is the corresponding ore to the artefact in 3-dimensional space (cf. fig. 13.12). The cited data in the diagrams were used for comparison (cf. fig. 13.11).

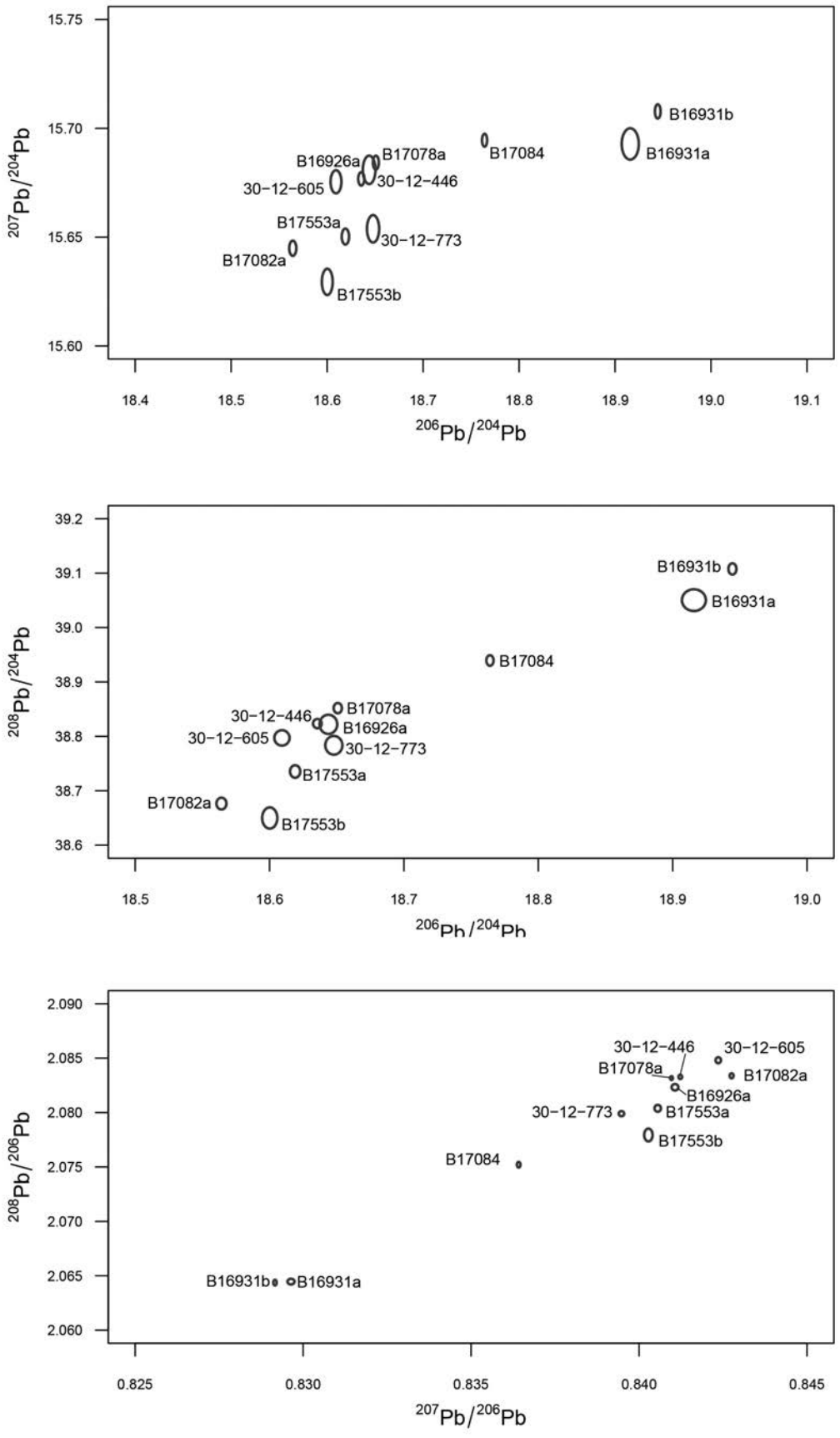

Fig. 13.9: $^{208}Pb/^{206}Pb$ vs. $^{207}Pb/^{206}Pb$ (upper), $^{208}Pb/^{204}Pb$ vs. $^{206}Pb/^{204}Pb$ (middle), $^{206}Pb/^{204}Pb$ vs. $^{207}Pb/^{204}Pb$ (lower) ratios of the silver metal samples measured by solution-based MC-ICP-MS. The data are displayed as error ellipses: The ellipses have the width and height of the absolute errors 2σ of each analysis with the measured Pb isotope ratio as the centre.

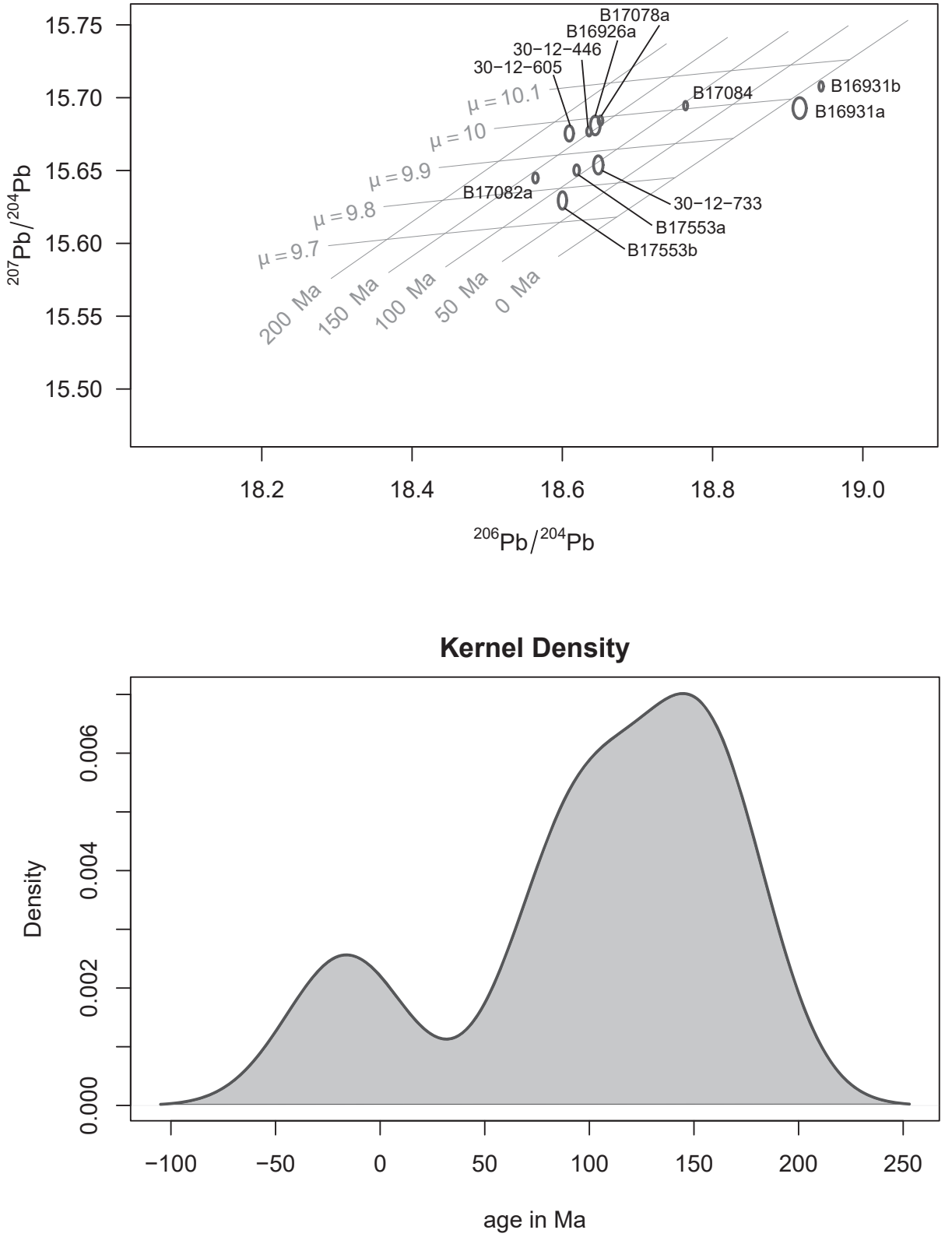

Fig. 13.10: $^{206}Pb/^{204}Pb$ vs. $^{207}Pb/^{204}Pb$ of the Ur silver artefacts in the two-stage model of Stacey and Kramers (1975), plotted with a R-script written by T. Rose (upper). A kernel density histogram of the calculated model ages of the Ur silver artefacts (lower).

The calculated nearest neighbours for 30-12-446, 30-12-605, B17082a, B17553a, and -b are the Karkas mountains, Isfahan province of Iran in the Urumieh-Dokhtar zone. This is further emphasised by the pXRF analysis performed in February 2017 (M. Jansen, B. Hafford, A. Hauptmann, E. Salzmann, pers. comm., Feb. 2017) of a contemporary hack silver hoard in Khafajeh exhibiting similar copper and Pb contents. The location is directly at

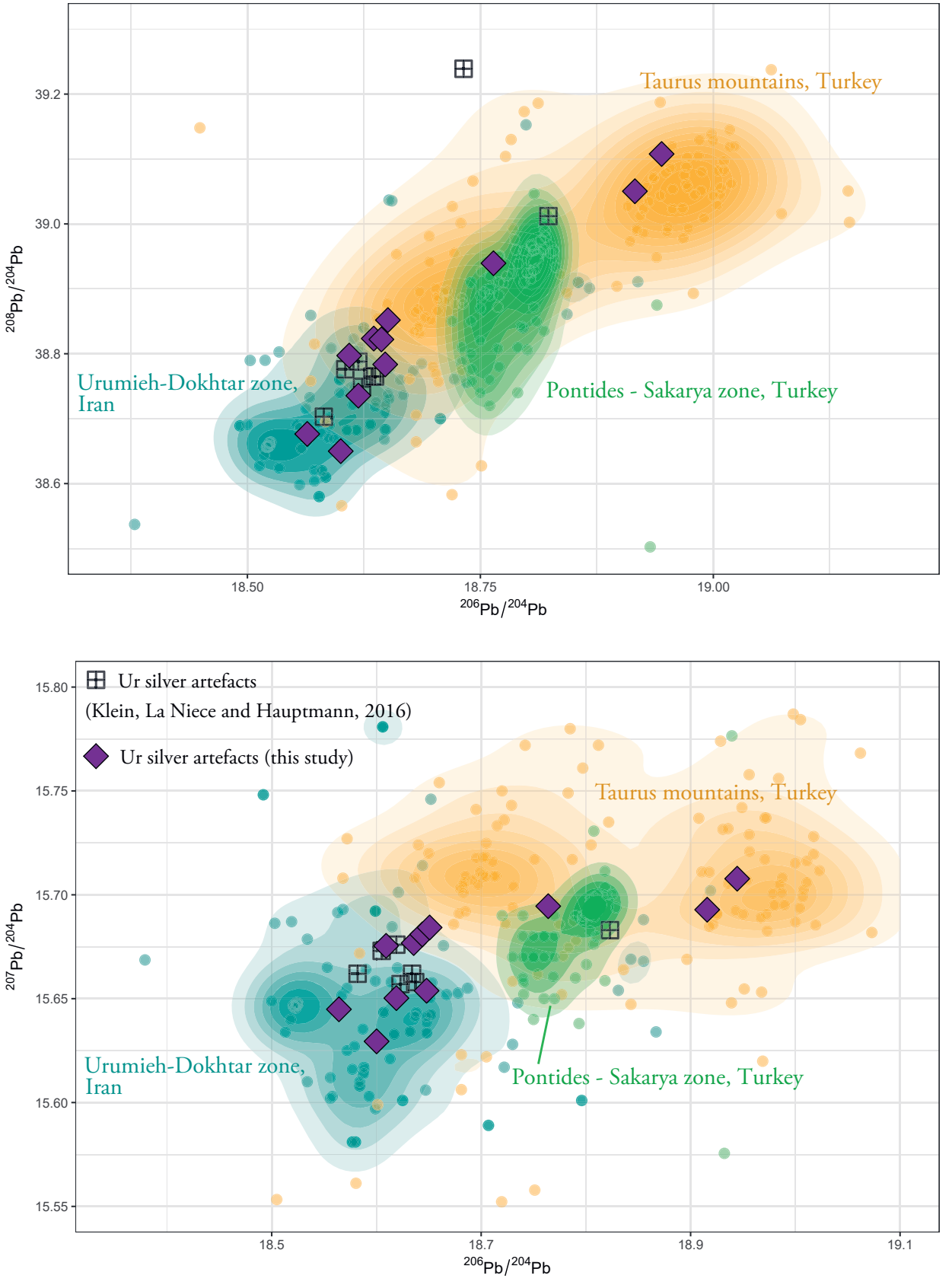

Fig. 13.11: $^{208}Pb/^{204}Pb$ vs. $^{206}Pb/^{204}Pb$ (upper) and $^{207}Pb/^{204}Pb$ vs. $^{206}Pb/^{204}Pb$ (lower) ratios of the Ur silver artefacts in comparison with selected lead isotope data of further Ur silver artefacts from the collection of the British Museum (Klein, La Niece and Hauptmann, 2016), and ores from Iran and Turkey (Chevrim, 1984; Wagner et al., 1984; Vavelidis et al., 1985; Wagner et al. 1986; Wagner et al., 1989; Yener et al., 1991; Hirao, Enomoto and Tachikawa, 1995; Sayre et al., 2001; Begemann, Schmitt-Strecker and Pernicka, 2003; Koptagel et al., 2007; Nezafati, Pernicka and Momenzadeh, 2008; Mirnejad, Simonetti and Molasalehi, 2011; Pernicka et al., 2011).

$$d = \sqrt{\left(\frac{^{206}Pb}{^{204}Pb}_{Ag} - \frac{^{206}Pb}{^{204}Pb}_{ore}\right)^2 + \left(\frac{^{207}Pb}{^{204}Pb}_{Ag} - \frac{^{207}Pb}{^{204}Pb}_{ore}\right)^2 + \left(\frac{^{208}Pb}{^{204}Pb}_{Ag} - \frac{^{208}Pb}{^{204}Pb}_{ore}\right)^2}$$

Fig. 13.12: Formula for calculation of the Euclidean Distances in three dimensional space of the artefact's lead isotope ratios from the compared ore's lead isotope ratios.

the route along the Diyala river from the Zagros mountains to the plains of Mesopotamia, which could link both regions. As for 30-12-733 and B16926a the Euclidean distances (Fig. 13.11) display equal values for the Taurus mountains and Zagros mountains. The Bolkardağ mining district in the Taurus is in shortest distance of B17078a, while B17084 best fits to Pb isotope data from Taurus and Sakarya zone in the Pontides. The two bracelets B16931a and -b are matching the Ergani area in Turkey.

As only small proportions of silver could be produced in a single cupellation step, it is not unlikely that silver might have been mixed from different sources. This could be the case for the objects 30-12-733 and B16926a, although, when examining patterns in the Pb isotope diagrams (cf. fig. 13.11), Iranian ores appear to be a better match. Additionally, the As and Sb contents of 30-12-733 are expected to be lower, when mixed with silver from another source, as As would evaporate during the melting process. Mixing seems unlikely regarding 30-12-733, since it exhibits the highest As and Sb levels of all silver artefacts. However, the As and Sb levels in B16926a are very low (cf. fig. 13.5). Moreover, B16926a was discovered in the same Akkadian tomb PG 673 as B16931a and -b. As for the two bracelets the provenance in the foothills of Taurus (near Ergani) seems more likely, it is possible, that B16926a was produced of a silver from sources in the foothills of Taurus and Zagros mixed together. From mineralogical and geodynamic point of view ores in the Greater Caucasus could fit to the two objects B16931a and -b, as the age fits the closure of the Neotethys and numerous Pb-Ag deposits combined with some gold mineralisation occur there. Unfortunately no comparative Pb isotope data of the Greater Caucasus exists, but it should be noted for future studies. The Meghradzor ore field in Armenia exhibits galena-fahlore mineralisation of Tertiary age and tellurides occurring within the deposit (Kovalenker, et al., 1990), yet Pb isotope data from Armenia provide no match for the Ur silver artefacts.

In summary, the Pb isotope data of 30-12-446, 30-12-605, B17082a, B17553a, and -b, and possibly 30-12-733 fit best to data from the Karkas mountains, Isfahan province, Iran, while Anatolian ore sources suit better B17078a (Bolkardağ mining district), B17084 (Taurus and Sakarya zone in the Pontides), B16931a, and -b (Ergani area at the foothills of the Taurus). B16926a could be from either Anatolian and Iranian ore sources or mixed from both sources.

sample	model age in Ma	geological era
30-12-446	153	Jurassic
30-12-605	170	Jurassic
30-12-733	96	Cretaceous
B16926a	155	Jurassic
B16931a	-22	Tertiary-Quaternary
B16931b	-11	Tertiary-Quaternary
B17078a	157	Jurassic
B17082a	140	Jurassic - Cretaceous
B17084	95	Cretaceous
B17553a	110	Cretaceous
B17553b	80	Cretaceous

Tab. 13.4: Model ages of the silver artefacts calculated with an R-script written by T. Rose.

14 The silver artefacts: Conclusion

The 11 non-corroded silver artefacts from Royal and private tombs of Ur were analysed regarding main and trace elements, Cu isotopes, and Pb isotopes. They are characterised by high correlating Pb and Cu contents indicating lead ores containing copper ores being cupelled for silver production. As, Sb, and Bi suggest that fahlores were associated with the lead ores smelted for the production of 30-12-446, 30-12-605, 30-12-733, B17078a, B17082a, B17553a, and -b, while low fahlore contents are noted for B17084, B16926a, B16931a, and -b. The two Akkadian bracelets are high in Au and exhibit elevated Pt and Te contents indicating an ore associated with gold mineralisation and possibly tellurides. The Cu isotopes are hinting towards both primary sulphide and secondary oxide ores having been mined. The Pb isotope ratios match with different ore sources in the Zagros and Taurus mountains. The Early Dynastic artefacts 30-12-446, 30-12-733, B17082a, B17553a, and -b, and 30-12-605 of unknown date fit to Pb isotope data of ores from the Karkas mountains, Isfahan province, Iran. Furthermore the Ur silver artefacts exhibit chemical similarities with a contemporary hack silver hoard in Khafajeh located at the trade route along the Diyala river connecting Iran and Mesopotamia hinting towards a connection with Ur. The remaining two Early Dynastic artefacts B17078a and B17084 are resembling lead ores from the Taurus (Bolkardağ mining district) and Sakarya zone in the Pontides. The three silver artefacts from the Akkadian tomb PG 673 exhibit a different provenance. B16931a and -b match Pb isotope data from the Ergani area at the foothills of the Taurus, while B16926a could be a mixture of silver from Anatolian and Iranian source or derive from either one of both sources.

This study emphasises the possibilities of modern analytical techniques for silver metal. Only little research has been undertaken concerning the analytics of ancient silver, and none for Early Bronze Age silver in Mesopotamia. The silver artefacts analysed and evaluated in this study permit new insights in the provenance of silver in early Mesopotamia. An answer, that has been demanded in literature, repeatedly (Paoletti, 2008). Provenance studies offer scientific solutions for questions, that cannot be answered by Archaeology or Philology alone. The possible origin of the Ur silver metal in Zagros and Taurus mountains highlights the long-term connection with these regions, although further research should be carried out regarding Pb isotope analysis and geochemical characterisation of ores from the Greater Caucasus. The picture could change, if ores from the Greater Caucasus matched the Ur silver artefacts. The analysis of more silver artefacts would improve the statistics and give insights into the proportion of silver metal coming from different sources. Especially future Pb isotope analysis of the hack silver hoard discovered at Khafajeh could proof further connections of Ur with Iran as main silver supplier. Which region was the main supplier and was there even one? This question remains unanswered for now. The scientific indications support future research regarding intercultural contacts and exchange in the early societies of mankind. This enables further insights into development and history of humanity. The results of this study shall help to better understand the relationship between Ur specifically with other regions, the intercultural exchange, and economic relations.

15 Conclusions

The ancient city of Ur is located in the floodplain of the Euphrates and Tigris river: an area completely void of metal resources. Thousands of precious metal artefacts had been uncovered by Sir Charles Leonard Woolley, indicating a massive import of metals. A set of 89 mounted copper-, bronze-, and silver samples as well as 20 drilled samples of silver artefacts were provided as a loan by the Penn Museum in Philadelphia for analytical work. The main goal of this dissertation is the analytical investigation on the quest for provenance of the copper- , bronze-, and silver artefacts from the cemetery of Ur. This has been accomplished by the analysis of main elements with electron microprobe, trace elements with LA-SC-ICP-MS, stable Cu isotopes with both fs-LA-MC-ICP-MS and MC-ICP-MS, and Pb isotopes with both LA-MC-ICP-MS and MC-ICP-MS.

Analytical limitations

Before the results could be evaluated regarding the research question, the analytical methods had to be refined and evaluated. New procedures had to be established for *in situ* analysis with electron microprobe and LA-ICP-MS. The microprobe analysis for main element characterisation involved a set of sufficient point analyses to provide a reliable mean. This was a fundamental problem for tin bronze samples, in particular, as the binary alloy of Cu and Sn exhibits decomposition into several phases, especially after corrosion. Therefore more than 20 point analyses were set as a grid randomly across the fresh metal's surface in order to prevent accidentally preferential point location by the operator. Analysing corroded parts of the artefacts was avoided for the calculation of the mean or intentionally performed to chemically characterise the corrosion. The same was performed for the silver samples, which were mounted for electron microprobe.

Lead is also distributed inhomogeneously as small inclusions below the µm-scale. Therefore the mean Pb concentrations differ between electron microprobe and laserablation results. Due to the bigger spotsizes of the laser, the mean Pb contents determined with laserablation are considered to be more accurate, as it is estimated that the number and size of small lead inclusions is approximately the same for the area of each laser spot.

The analysis with laserablation coupled with ICP-MS had to be evaluated first regarding the fluence settings for the laser. Laser induced thermal heating occurred at high fluence settings and led to fractionation effects, which could not be corrected. However, at lower fluence (< 1.8 J/cm^2) the thermal effects were reduced. One further problem was the oxidation of the metals surface. This affected the first µm in depth because the ablation behaviour of oxidised metal is different to the original metal. Due to this effect a preablation of 3 laser pulses was performed before the actual measurement in order to remove the oxidised metal layer.

Furthermore an offset of approximately +0.2 ‰ within the δ^{65}Cu values between MC-ICP-MS and fs-LA-ICP-MS is observed for the separated copper solution. This could be a result of fractionation during the chemical chromatographical separation method or small quantities of corroded metal entering the solution. Due to the precise and accurate measurements with fs-LA-ICP-MS performed at the Institute of Mineralogy, Leibniz-University Hannover, these data are considered to be more reliable.

For Pb isotope analysis with LA-MC-ICP-MS several setups were tried and measured with ARIDUS and Tl as well as without. Eventually the best results were accomplished by measuring without Tl-addition. The drift and mass bias correction was achieved by standard-sample-bracketing. Due the unavailability of matrix matched Pb isotope standards only the NIST SRM 610 was used. Therefore an additional matrix correction was performed by determining the mass bias offset in β by the comparison of those artefacts measured by both LA-MC-ICP-MS and MC-ICP-MS. Begemann and Schmitt-Strecker (2009) measured 10 artefacts, that were also analysed in this dissertation. With the known offset the matrix induced mass bias could be corrected and the results are in good agreement with each other.

For the silver metal, however, the matrix effects could not be corrected. Due to the lack of comparable results and matrix matched standards, this issue could not be solved. Therefore only the MC-ICP-MS data are used for interpretation.

The provenance of the silver artefacts from Ur

Due to the correlated Pb and Cu contents in the wt%-range the origin in cupelled lead-silver ores could be determined. Due to the presence of As, Sb, and Bi as trace elements

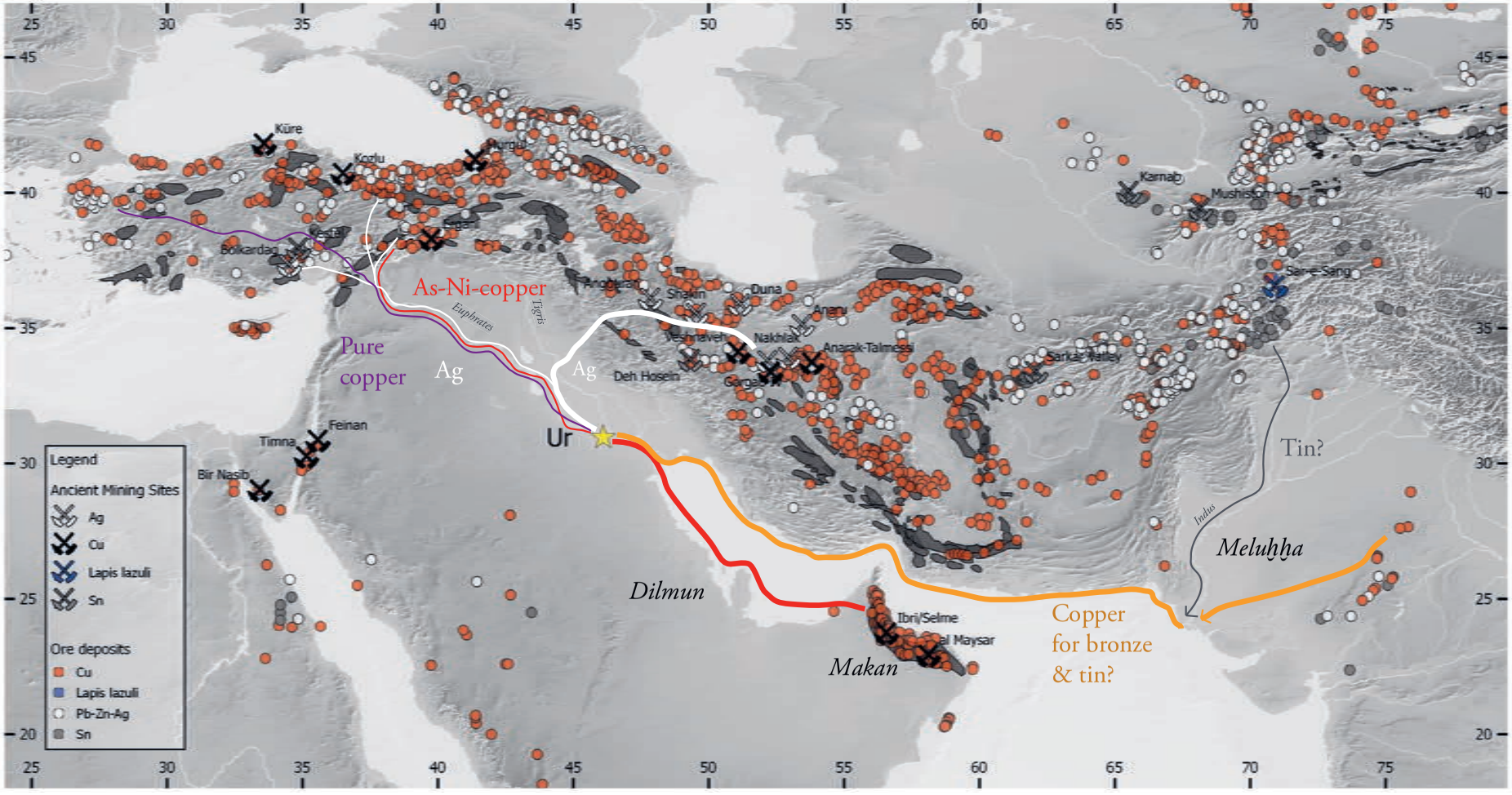

Fig. 15.1: Map of metal deposits in the Near and Middle East. Major mining and smelting sites dated to the third millennium BCE are marked. The grey polygons represent ophiolite occurrences. The thick lines represent the most probabale main supplier. The thinner lines represent the most likely minor suppliers of Ur. In general the lines follow the potential path the different metals travelled to Ur.

(Data sources: Begemann, et al., 2010; Chakrabarti, 2012; Dhavalikar, 2012; Garner, 2012; Hauptmann, 1985; Hauptmann, 2000; Hauptmann, Rehren und Schmitt-Strecker, 2003; Lehner and Yener 2010; Lyckberg, 2011; Merkel, et al., 2016; Mirnejad, Simonetti and Molasalehi, 2011; Momenzadeh, 2004; Murao, Deb and Furuno, 2008; Nezafati, 2006; Nezafati, et al., 2009; Nezafati and Pernicka, 2012; Orris and Bliss, 2002; Pigott 1999; Pigott 2004; Prange, 2001; Seltmann 2009; Seltmann 2013; Twaltschrelidze 2002; Weeks, 2003; Weisgerber 2004; Yener, et al., 1991; http://mindat.org; http://mrdata.usgs.gov.)

the association with fahlores is indicated. The Cu isotope ratios hint towards a primary sulphide ore being smelted. Lead sulphide ores are common in the highlands of the Near East. More specific information is given by the Pb isotope ratios and the Au levels of the silver artefacts. B16931a, and -b (both bracelets) exhibit higher Au contents of approximately 4500 ppm, while the other silver artefacts have Au levels below 1000 ppm. The Pb isotope ratios of the two bracelets appear to have Cenozoic model ages, whereas the other silver artefacts are of Mesozoic geological age. The euclidean distances were used as an additional tool, in order to calculate the distance in 3-dimensional space to comparable Pb isotope data of potential sources.

In conclusion the artefacts 30-12-446, 30-12-733, B17082a, B17553a, and -b, and 30-12-605 have their origin most likely in the Karkas mountains, Isfahan province, Iran. Further indication for a provenance from the Iranian highlands is indicated by the comparable main element contents of a hack silver hoard discovered at Khafajeh at the Diyala river, an important trade route between Mesopotamia and Zagros mountains (cf. fig. 15.1).

B17078a and B17084 have the most accordance with data from the Bolkardağ area in the Taurus or the Sakarya-zone of the Pontides. B16931a and -b fit best to data from the Assyrian Suture zone, where besides copper, also lead ores occur. B16926a cannot be assigned clearly, although a provenance in Iranian or Turkish highlands is likely as is a mixture of both sources.

The provenance of the copper-based artefacts from Ur

The copper-based artefacts differ chemically by their As, Ni, and Sn content. While approximately two third exhibit low Sn, but high correlated As and Ni levels, the other third has high Sn contents and low As and Ni levels. The first is characterised as As-Ni-copper, the latter as tin bronze. One artefact (31-17-352T, Jemdet Nasr/Early Dynastic I) differs in microstructure and pure copper composition from the other copper-based artefacts. A few artefacts have an intermediate As-Ni-Sn-composition in between both alloys indicating a potential mixture of both metals. The copper rich in As and Ni has elevated Co and Sb levels, other elemental differences in between tin bronze and As-Ni-copper are small. The tin bronze artefacts have slightly elevated Zn and Bi levels compared to the As-Ni-copper artefacts.

All artefacts exhibit inclusions rich in S and Fe. A number of artefacts has additionally speiss inclusions, indicating polymetallic sulphide ores as source.

The Cu isotope signature is mostly in the range of -0.5 to +0.5 ‰ further hinting towards smelting of primary sulphide ores for copper production. The Pb isotope signatures differ between the As-Ni-copper, pure copper, and tin bronze artefacts.

The As-Ni-copper artefacts could be assigned with two exceptions to the rich copper deposits in Oman (cf. fig. 15.1). This is in accordance with Pb isotope data from further As-Ni-copper artefacts analysed by Begemann and Schmitt-Strecker (2009) and Begemann et al. (2010). For the two As-Ni-copper artefacts 33-35-79 and B17356 the Pb isotope data are a better fit to Pb isotope data from the Ergani area in Turkey as well as metallurgical by-products from Arslantepe. Both are reasonable sources, as Ni arsenides are associated with the copper mineralisation in an ophiolite context, which likely entered the metal resulting in a natural As-Ni-copper alloy with differing concentrations.

The tin bronze artefact's Pb isotopes have a wide range of linear trending ratios. The larger number is most likely a mixture between different ore stages in the Aravalli range in NW India. The tin possibly travelled as separate trade or exchange good and has its potential origin north to the Indus Valley in the highlands of NE Afghanistan (cf. fig. 15.1). Four tin bronze artefacts (30-12-696, 31-17-186, B16996, B17495) are in better agreement with copper ores from an unknown source area and could also be a potential mixture of copper from Oman and an unknown source. Those artefacts showing a trend of mixing in their chemistry, exhibit a similar trend in between Oman and the NW Indian ores. The pure copper artefact 31-17-352T has the most accordance with Pb isotope data from Serçeören Köy in NW Turkey near Troy. The same copper deposit likely served as a source for early copper in Troy (Begemann, Schmitt-Strecker and Pernicka, 2003). As the artefact exhibits also a different microstructure than all other copper-based artefacts investigated in this study, it was even potentially forged in the same region and could indicate further cultural relationships between Ur and Troy.

The scientific results in context of Archaeology and Textual evidence

The provenance of the copper-based and silver metal of Ur emphasises the intense exchange in between widely spread regions. Most interesting is the fact, that the major sources for silver and copper lay to the East. Textual evidence has long been hinting towards the provenance for the copper from the 'land of copper' *Makan* and the Harappa culture in the Indus Valley (Waetzoldt and Bachmann, 1984; Kenoyer and Miller, 1999**;** Begemann and Schmitt-Strecker, 2009**;** Begemann, et al., 2010). Oman has been established to be the land of *Makan*, mentioned in cuneiform texts (Waetzoldt and Bachmann, 1984**;** Heimpel, 1987; Weisgerber, 1991; Reiter, 1997; Begemann, et al., 2010). This study offers scientific reinforcement for this theory, as both sources appear to be the major suppliers for the copper found in Ur. The copper from Oman has a very distinct chemical signature of high Ni contents in correlation with high As concentrations (Hauptmann and Weisgerber, 1980; Hauptmann, 1985; Hauptmann, 1987; Weisgerber, 1991; Prange, et al., 1999; Prange, 2001; Begemann, et al., 2010). The find distribution of copper rich in As and Ni matches the pattern of the Tethyan Eurasian Metallogenic

Belt from Oman to Turkey even goes down to the Levant and northern Egypt. Although no copper metal analysed in this thesis matches with copper ores from the Levant, an exchange between Mesopotamia and Levant is likely. Whereas the tin bronze artefacts exhibit a very distinct mixed Pb isotope signature of both very old and young geological age, leaving only little space for speculation. For alloying copper and tin a more pure copper composition is desired, as high contents of both As and Sn lead to a brittle metal unsuited for cold working. Therefore another source of copper is necessary and evidenced by differences in Pb isotope signatures, though on a smaller scale mixing is observed in between As-Ni-copper and tin bronze. The mixing was most likely performed in Mesopotamia, as artefacts with the Indian Pb isotope signature would have been evidenced in Oman, if it had travelled via Oman. The Indian copper and possibly tin travelled therefore most likely not via *Makan* and *Dilmun*, but possibly along the Makran coast of southern Iran (Begemann, et al., 2010). The provenance of the silver has only been assumed to originate in the highlands of Iran and Turkey, yet. The analysis of the Ur silver metal confirms this hypothesis, as sources in both Karkas mountains, Isfahan province, Iran, as well as Taurus and Pontides in Turkey are identified as the most likely silver sources. The silver reached Mesopotamia in all likelihood along the known trade route along the Diyala river from Iran as well as the Euphrates river from Anatolia.

Outlook

This study emphasises the importance and possibilities of modern scientific investigations regarding provenancing of metals. Due to the interplay of different analytical techniques and methods the potential sources for the Ur metal could be narrowed down significantly.

The provenance of the tin used for the production of the tin bronze was beyond the scope of this dissertation, although possibilities arise with the analysis of Sn isotopes (Haustein, Gillis and Pernicka, 2010). Potential lies also in analysing trace elements as W, Ta, Nb, and Zr, to be able to distinguish between different types of tin deposits.

For better statistics it is desired to analyse more silver artefacts in order to investigate, which region was the main supplier or if there even existed one.

Further information on trade route patterns could be gained by the analysis of metal objects from other Mesopotamian cities and of metal objects dating to earlier or later periods. This could provide further implications on a change in time ore location of potential source regions and thus lead to a better understanding of exchange patterns in the Early Bronze Age Near East.

16 Abstract / Zusammenfassung

In the course of the DFG project „The Royal Cemetery of Ur: Analytical, Archaeological and Technological Investigations of Early Bronze Age artefacts from the collection of the Penn Museum, University of Pennsylvania, Philadelphia“, the copper-, bronze-, and silver artefacts were successfully analysed and evaluated. A total number of 89 sections of metal artefacts from the MASCA collection of the Penn Museum were made available. Another 20 silver artefacts were sampled by Sabine Klein and Andreas Hauptmann. Some artefacts had to be excluded due to the complete corrosion of the metal. A total of 13 sections and 6 silver samples were excluded from the analytical work. 3 of the 20 drilled samples were mistakenly identified as silver artefacts, although they are in fact copper artefacts with an unusual dark grey corrosion layer. Two of the sections are gold artefacts made available to Moritz Jansen and his dissertation project. This left 74 mounts (2 of which were silver artefacts, 72 copper artefacts), 11 silver metal drilled samples, 1 lapis lazuli sample, and 3 copper metal drilled samples. The drilled samples were split. A part of the drillings were embedded in epoxy resin and mounted. Another part was dissolved in nitric acid (silver) or with a hydrochloric acid - nitric acid mixture (copper) and evaporated. The samples were then taken up in HBr, centrifuged and chromatographically separated for Pb and Cu isotope analysis using MC-ICP-MS. Both Pb and Cu isotope analysis were successfully carried out with MC-ICP-MS (Thermo Scientific Neptune) at the Goethe University Frankfurt. The sections were first analysed with electron microprobe (Jeol JXA 8900R) at Goethe University Frankfurt regarding main and minor elements. If possible, at least 20 point analyses were randomly distributed across the uncorroded sample surface. Subsequently, trace element analysis was performed by means of laser ablation (Resonetics RESOlution M-50) coupled SC-ICP-MS (Thermo Scientific Element 2) at Goethe University Frankfurt. In situ Cu isotope analysis was carried out in cooperation with Dr. Marina Lazarov (Institute for Mineralogy of the Leibniz University of Hanover) with femtosecond laserablation (Spectra Physics Solstice) and MC-ICP-MS (Thermo Scientific Neptune Plus). For this purpose, a different laser system was chosen since Cu isotopes are susceptible to thermally induced matrix effects which occur by the application of nanosecond laser ablation (Lazarov and Horn, 2015). Finally, the microstructures of the MC-ICP-MS (Thermo Scientific Neptune) coupled with laser ablation (Resonetics RESOlution M-50) at Goethe University in Frankfurt were tested for the analysis of stable Pb isotope ratios. The results were verified by comparative analyses on 10 artefacts published by Begemann and Schmitt-Strecker (2009), which were analysed in both studies. The sections of the MASCA collection have also been studied in the past with PIXE at Penn Museum, University of Pennsylvania. The samples present as drilling chips were measured from a chromatographically separated Cu and Pb solution with the addition of a Ni and Tl spike, respectively, using MC-ICP-MS. A deviation between the Cu isotope data measured by solution and laserablation was determined. This could be either due to fractionation during the separation method according to Bendall (2003) or to the presence of small amounts of corroded metal.

In addition to the analytical work, a GIS-based database of copper, tin, and lead-silver deposits of the Near and Middle East was established, which was carried out by intensive literature research and i.a. digitisation of offline maps. In addition, important archaeological sites, such as mining regions and smelting sites, were added to the database in order to enable a better reconstruction of the archaeometallurgical landscape of the third millennium BCE. Also, finding locations of Bronze Age metal artefacts were mapped. This allows the reconstruction of ancient distribution patterns and which regions were connected with each other. Further conclusions can be drawn regarding provenance of the metals and which way they travelled to or from Mesopotamia. The map additionally helps to visualise the results of this study for a better understanding of the ancient networks.

The main element analyses with electron microprobe are highly consistent with the PIXE analyses performed at the Penn Museum, Philadelphia. The unalloyed copper artefacts are mainly characterised by high Ni and As contents, which correlate with one another (As to 4 wt%, Ni to 10 wt%). Only a single artefact (31-17-352T) consists of more than 99 wt% Cu and has been identified as „pure copper“. The tin bronzes have Sn contents of 2 to 12 wt%. The main elements in all copper and tin bronze artefacts are accompanied by low concentrations of Co (0.011-0.49 wt%), Sb (0.01-0.66 wt%), Fe (0.012-0.96 wt%) , S (0.014 - 2.03wt%) and Pb (0.052 - 0.74 wt%). The trace elements of the unalloyed and tin bronze artefacts are relatively similar to each other. In addition to the main

elements the following trace elements were measured: Mn (0.5-739 ppm), Zn (2.3-2261 ppm), Ge (0.1-366 ppm), Se (19.4-11522 ppm), Pd (0.03 to 65.5 ppm), Cd (0.03 to 93 ppm) ,In (0.1 to 162 ppm), Te (3.3 to 3390 ppm), Pt (0.06 to 413 ppm), Au (2.2 - 550 ppm) and Bi (2.3 - 2015 ppm).

Cu isotope analysis was carried out on a large part of the artefacts. The As- and Ni-rich, as well as the tin bronze artefacts have δ^{65}Cu values of -0.7 to +0.5 ‰. The As-Ni-rich copper artefact B17551 with a δ^{65}Cu value of +1 ‰ is the only outlier. The unalloyed copper artefacts show a range from Mesozoic to Tertiary age in their Pb isotope ratios, while the tin bronzes show a range from Proterozoic to Tertiary geological age. The unalloyed copper artefacts with high Ni- and As-contents can be assigned to the deposits of Oman (Begemann, et al., 2010) and the Assyrian Suture zone (Seeliger, et al., 1985), since these copper deposits have formed in ophiolites. The high Ni contents are likely to result from the association of Ni arsenides with the copper mineralisation used for smelting activities, which migrate into the copper during smelting. The older Pb isotope signals spread over a wide range and follow a linear trend in all Pb isotope ratios. It is possible that this trend is indicating a mixture since some of the tin bronze artefacts with intermediate Pb isotope signatures also contain increased contents of As and Ni. The oldest signature agrees with data from the Aravalli-Delhi range in NW-India (Deb, et al., 1989). Such old signatures are found only in the Indian Cratone or in the Eastern Desert of Egypt. In Egypt, however, there are no or hardly any tin deposits in noteworthy quantities, additionally tin bronzes occur later in Egypt than in Mesopotamia. The connection with India appears to be reasonable, since Mesopotamia had contact with the Indus civilisation, and trade goods from the Indus Valley reached Ur by coastal shipping along the Makran coast of southern Iran (Begemann, et al., 2010). The origin of the tin could not be determined in this dissertation, yet the highly probable origin of the copper used for tin bronze production from India might indicate a similar origin. Copper and tin from Meluḫḫa are mentioned in cuneiform texts. The Harappa culture had several outposts in the Afghan highlands. In particular, the Shortugai outpost, located in north-eastern Afghanistan, is close to numerous tin deposits. It is possible that the tin extracted there went to the south to the Indus Valley and from there to Mesopotamia. The Indian copper does not appear to have been transported via Makan and Dilmun, since no copper with an Indian signature has been discovered there (Begemann, et al., 2010). It is possible that additional copper from Oman was added to the tin bronzes in Mesopotamia, which results in a mixture becoming apparent both in the main element contents and in the Pb isotope ratios. The geologically young Pb isotope signatures of the tin bronze artefacts correspond to no comparative data of copper ores, although a linear trend is indicating a potential mixing of copper from Oman and another unknown source. Due to the fact that mostly weapons and tools exhibit a mixed signature, a repair of the objects after intensive use during the lifetime of the individual person would be conceivable. Possibly, the original tin bronze was „diluted“ with copper from more favourable sources, as Oman, to save precious tin. However, this is purely speculative.

The silver artefacts have elevated Cu (2-7 wt%) and Pb contents (0.15-1.5 wt%), which correlate with one another. Furthermore, the two bracelets B16931a and -b contain 0.44-0.46 wt% Au and lower Cu and Pb concentrations, and thus differ from the other silver artefacts. The trace element contents of the silver artefacts are low in general except for Au (318 - 5698 ppm) and Bi (260 - 1231 ppm). As (2,7 - 333 ppm) and Sb (1,1 - 36,7 ppm) are in weak correlation in the Early Dynastic artefacts. In addition to the increased Au concentrations, the bracelets B16931a and -b show slightly increased Te (43 ppm) and Pt (10-20 ppm). In the Cu isotope ratios the silver artefacts differ only slightly. The δ^{65}Cu values are between -0.5 and +0.5 ‰, suggesting a primary sulphide ore (Markl, Lahaye and Schwinn, 2006; Klein, et al., 2010), which has been cupelled. Only the two artefacts 30-12-733 and B16931b exhibit δ^{65}Cu values of approx. +1.5 ‰ and thus the signature of an ore of secondary, oxidic origin. Differences between B16931a, -b and the other silver artefacts are also found in the Pb isotope ratios. The majority of the silver artefacts have Pb isotope signatures of Mesozoic age (Jurassic to Cretaceous), whereas the artefacts B16931a and -b have a distinctly younger geological age. Both B17084 and B16931a- and -b are in good agreement with Pb isotope ratios of ores in the Taurus Mountains (Hauptmann, et al., 2002). More precisely, B17084 agrees well with data in the transition area of the Pontides and Taurus (Sakarya zone). B16931a and -b fit well to Pb isotope data in southeastern Anatolia. Except for B16926a, the remaining silver artefact's Pb isotope ratios fit well into the area of the Karkas Mountains, Isfahan Province, Iran, which belongs to the geological unit of the Urumieh Dokhtar Zone (Pernicka, et al., 2011). Artefact B16926a could be a mixed isotope signature consisting of ores in the Taurus and Zagros mountains, since the calculation of the Euclidean distances to the nearest neighbours did not yield any clear results. An origin from one of the two regions is also possible, but this can not be clearly assigned. A further reference to a possible origin of the Early Dynastic silver from Iran comes from the pXRF analyses, which the project carried out in February 2017 at the silver hort of Khafajeh. The hack silver showed similar Pb and Cu contents as the original silver artefacts. Khafajeh is located in the area of the Diyala river and dates to Early Dynastic. Thus Khafajeh occupies an important position along the trade route of the Diyala River into the Iranian highlands. A link could be scientifically proven by further analyses, especially Pb isotope and trace element analyses, of the Khafajeh silver hort. There is also further potential for a possible provenance of the Au-rich silver artefacts in the Caucasus. However, the lead-silver deposits in the Caucasus (Kovalenker, et al., 1990), particularly in the Great Caucasus, have so far hardly been characterised by scientific investigations. Lead-silver mineralisations exist

in the Great Caucasus, that can yield higher Au contents which could not be used for the comparison since no published comparative data exist so far.

In summary, the copper-, bronze-, and silver artefacts of the cemetery of Ur were successfully analysed. The results of the provenance studies are promising and can prove a possible provenance of the As-Ni-containing copper artefacts from Oman and two artefacts likely from the Assyrian Suture zone, Turkey. In addition, a possible connection between the tin bronzes of Ur and deposits in the Aravalli-Delhi mountains, NW-India could be established for the first time, as well as one further unknown source. The pure copper artefact 31-17-352 has its most likely origin in Serçeören Köy, Turkey. The results of the silver artefacts of Ur show evidence of a possible origin of the silver from the Taurus Mountains, Turkey, and Karkas Mountains, Iran. For the future, scientific studies of other artefacts from other Mesopotamian cities and at best further locations on important trade routes (e.g. Khafajeh, Tepe Hissar) are indicated. This makes it possible to reconstruct the routes the metals came to Ur, whether by land or sea. Furthermore, due to the small number of investigated artefacts, the chronological development has only been insufficiently investigated. Interesting findings would be the investigation of earlier and later-dated artefacts, which would allow the reconstruction of the chronological change in the areas of provenance. Also, the PIXE analyses of the Penn Museum are of high quality since they are in good agreement with the electron microprobe data of the present dissertation. On the basis of the main elements, some conclusions have already been drawn regarding the origin of the artefacts. In order to allow better statistics, future access to the complete PIXE analyses of the Penn Museum within the „Mesopotamian Metals Project“ would be desirable in order to evaluate these statistically.

Zusammenfassung

Im Zuge des DFG-Projekts “Der Königsfriedhof von Ur: Analytische, archäologische und technologische Untersuchungen der frühbronzezeitlichen Artefakte aus der Sammlung des Penn-Museums, University of Pennsylvania, Philadelphia“ wurden die für die vorliegende Dissertation zur Verfügung gestellten Kupfer-, Bronze- und Silberartefakte erfolgreich analysiert und ausgewertet. Insgesamt wurden 89 Anschliffe von Metallartefakten aus der MASCA-Sammlung des Penn Museums zur Verfügung gestellt. Weitere 20 Silberartefakte wurden von Sabine Klein und Andreas Hauptmann beprobt. Einige Artefakte mussten aufgrund von vollständiger Korrosion des Metalls ausgeschlossen werden. Insgesamt wurden 13 Anschliffe und 6 Silberproben für die Analytik exkludiert. 3 der 20 Bohrspan-Proben wurden irrtümlich als Silberartefakte identifiziert, in Wahrheit handelt es sich um Kupferartefakte, die eine ungewöhnliche, dunkelgraue Korrosionsschicht aufweisen. Eine Perle, die als Ganzes beprobt wurde, stellte sich als Lapis Lazuli-Perle heraus. Bei zweien der Anschliffe handelt es sich um Goldartefakte, die Moritz Jansen und seinem Dissertationsprojekt zur Verfügung gestellt wurden. Somit verblieben 74 Anschliffe (davon 2 Silberartefakte, 72 Kupferartefakte), 11 Silbermetall-Bohrspan-Proben, 1 Lapis Lazuli-Probe und 3 Kupfermetall-Bohrspan-Proben. Die Bohrspan-Proben wurden aufgeteilt. Ein Teil der Bohrspäne wurde eingebettet und zu Anschliffen präpariert. Ein anderer Teil wurde mit Salpetersäure (Silber) oder mit einem Salzsäure-Salpetersäure-Gemisch (Kupfer) aufgeschlossen und eingedampft. Die Proben wurden im Anschluss in Lösung gebracht, zentrifugiert und chromatographisch abgetrennt für Blei- und Kupferisotopen-Analytik mittels MC-ICP-MS. Sowohl Blei- als auch Kupferisotopenanalytik wurden mit MC-ICP-MS (Thermo Scientific Neptune) an der Goethe-Universität Frankfurt erfolgreich durchgeführt. Die Anschliffe wurden zunächst mit der Elektronenstrahl-Mikrosonde (Jeol JXA 8900R) der Goethe-Universität Frankfurt auf Haupt- und Nebenelemente analysiert. Dabei wurden nach Möglichkeit mind. 20 Punktanalysen zufällig über die unkorrodierte Probenoberfläche verteilt. Im Anschluss wurde Spurenelement-Analytik mittels Laserablation (Resonetics RESOlution M-50) gekoppeltem SC-ICP-MS (Thermo Scientific Element 2) an der Goethe-Universität Frankfurt durchgeführt. In situ Kupferisotopen-Analytik wurde in Kooperation mit Dr. Marina Lazarov (Institut für Mineralogie der Leibniz-Universität Hannover) mit Femtosekunden-Laserablation (Spectra Physics Solstice) und MC-ICP-MS (Thermo Scientific Neptune Plus) vorgenommen. Hierfür wurde ein anderes Laser-System gewählt, da Kupferisotope anfällig für thermisch bedingte Matrix-Effekte sind, welche durch Anwendung von Nanosekunden-Laserablation auftreten (Lazarov und Horn, 2015). Abschließend konnten die Anschliffe mittels Laserablation (Resonetics RESOlution M-50) gekoppeltem MC-ICP-MS (Thermo Scientific Neptune) an der Goethe-Universität Frankfurt auf stabile Bleiisotopen-Verhältnisse untersucht werden. Die Ergebnisse wurden durch Vergleichsanalysen an ca. 10 Artefakten publiziert von Begemann und Schmitt-Strecker (2009) verifiziert, welche in beiden Studien analysiert wurden. Die Anschliffe der MASCA-Sammlung wurden zudem bereits in der Vergangenheit mit PIXE am Penn Museum, University of Pennsylvania, untersucht. Die als Bohrspäne vorliegenden Proben wurden aus einer chromatographisch abgetrennten Kupfer- bzw. Blei-Lösung unter Zugabe eines Ni- bzw. Tl-spikes am MC-ICP-MS

gemessen. Dabei wurde eine Abweichung zwischen den mittels Lösung- und Laserablation-gemessenen Kupferisotopendaten festgestellt. Dies könnte entweder in einer Fraktionierung während der angewendeten Abtrennungsmethode nach Bendall (2003) oder aber durch die Präsenz von geringen Mengen von korrodiertem Metall begründet sein.

Zusätzlich zu der Analytik wurde eine GIS-basierte Datenbank von Kupfer-, Zinn- und Blei-Silber-Vorkommen des Nahen und Mittleren Ostens aufgebaut, die durch intensive Literaturrecherche erarbeitet wurde. Ferner wurden wichtige archäologische Fundorte, wie Bergbauregionen und Verhüttungsplätze in die Datenbank aufgenommen, um eine bessere Rekonstruktion der archäometallurgischen Landschaft des dritten Jahrtausends v. u. Z. zu ermöglichen.

Die Hauptelement-Analysen mit Elektronenstrahl-Mikrosonde stimmen sehr gut mit den PIXE-Analysen überein. Die unlegierten Kupfer-Artefakte zeichnen sich größtenteils durch hohe Ni- und As-Gehalte aus, die miteinander korrelieren (As bis 4 Gew%, Ni bis 10 Gew%). Nur ein einzelnes Artefakt (31-17-352T) besteht zu über 99 Gew% aus Kupfer und wurde aufgrund dessen als „Reinkupfer“ identifiziert. Die Zinn-Bronze-Artefakte weisen Sn-Gehalte von 2 bis 12 Gew% auf. Begleitet werden die Hauptelemente in allen Kupfer- und Zinn-Bronze-Artefakten von geringen Konzentrationen von Co (0,011 – 0,49 Gew%), Sb (0,01 – 0,66 Gew%), Fe (0,012 – 0,96 Gew%), S (0,014 – 2,03 Gew%) und Pb (0,052 – 0,74 Gew%). Die Spurenelemente der Arsenkupfer- und Zinnbronze-Artefakte sind einander relativ ähnlich. Es konnten zusätzlich zu den Hauptelementen Mn (0,5 – 739 ppm), Zn (2,3 – 2621 ppm), Ge (0,1 – 366 ppm), Se (19,4 – 11522 ppm), Pd (0,03 – 65,5 ppm), Cd (0,03 – 93 ppm), In (0,1 – 162 ppm), Te (3,3 – 3390 ppm), Pt (0,06 – 413 ppm), Au (2,2 – 550 ppm) und Bi (2,3 – 2015 ppm) nachgewiesen werden. Kupferisotopen-Analytik konnte an einem Großteil der Artefakte ausgeführt werden. Die As- und Ni-reichen, sowie die Zinnbronze-Artefakte weise δ^{65}Cu-Werte von -0,7 bis +0,5 ‰ auf. Als einziger Ausreißer zeigt sich das As-Ni-reiche Kupfer-Artefakt B17551 mit einem δ^{65}Cu-Wert von +1 ‰.

Die unlegierten Kupfer-Artefakte weisen eine Spanne von Mesozoischem bis Tertiärem Alter in ihren Bleiisotopen-Verhältnissen auf, wohingegen die Zinnbronzen eine Spanne von präkambrischem bis tertiärem geologischen Alters zeigen. Die unlegierten Kupferartefakte mit hohen Ni- und As-Gehalten können mit den Lagerstätten von Oman (Begemann, et al., 2010) und der Assyrischen Sutur-Zone (Seeliger, et al., 1985) in Verbindung gebracht werden, da sich hier Kupferlagerstätten in Ophioliten gebildet haben. Die hohen Nickel-Gehalte resultieren wahrscheinlich aus der Assoziation von Nickelarseniden mit der Kupfermineralisation, aus welcher Erze zur Verhüttung gewonnen wurden, und können in das hergestellte Kupfermetall übergehen. Die älteren Bleiisotopensignaturen streuen über einen weiten Bereich und folgen einem linearen Trend in allen Bleiisotopen-Verhältnissen. Es ist möglich, dass es sich hier um eine Mischung handelt, da auch einige der Zinnbronze-Artefakte mit mittleren Bleiisotopensignaturen erhöhte Gehalte an As und Ni enthalten. Die älteste Signatur stimmt mit den Daten aus dem Aravalli-Delhi-Gebirge in NW-Indien überein (Deb, et al., 1989). Derart alte Signaturen finden sich nur im Indischen Kraton, oder aber in der Ostwüste von Ägypten. In Ägypten jedoch gibt es keine, bzw. kaum Zinnlagerstätten in nennenswerten Mengen, zumal Zinnbronzen hier erst deutlich später als in Mesopotamien auftreten. Die Verbindung mit Indien erscheint sinnvoll, da Mesopotamien Kontakt zur Indus-Zivilisation hatte und Waren aus der Indus Region durch Küstenschifffahrt entlang der Makran-Küste des südlichen Irans nach Ur gelangten (Begemann, et al., 2010). Die Provenienz des Zinns konnte in dieser Dissertation nicht ermittelt werden, jedoch könnte die höchstwahrscheinliche Herkunft des Kupfers der Zinnbronzen aus Indien auf eine ähnliche Herkunft hindeuten. In Keilschrift-Texten wird Kupfer und Zinn aus Meluḫḫa erwähnt. Die Harappa-Kultur hatte mehrere Außenposten im afghanischen Hochland. Insbesondere der Außenposten Shortugai, der im nordöstlichen Afghanistans gelegen ist, befindet sich nahe zahlreicher Zinnvorkommen. Möglicherweise reiste das dort gewonnene Zinn gen Süden ins Indus-Tal und von dort weiter nach Mesopotamien. Das indische Kupfer scheint nicht via Magan und Dilmun transportiert worden zu sein, da bislang kein Kupfer mit indischer Signatur von dort analysiert wurde (Begemann, et al., 2010). Möglicherweise wurde weiteres Kupfer aus Oman in Mesopotamien den Zinnbronzen hinzulegiert, welches in einer Mischung resultiert, die sowohl in den Hauptelement-Gehalten als auch in den Bleiisotopenverhältnissen sichtbar wird. Die jungen Bleiisotopensignaturen der geologisch jüngeren Zinnbronze-Artefakte zeigen keine Überlappung mit Vergleichsdaten von Kupfererzen, jedoch eine potentielle Mischung von omanischem Kupfer mit Kupfer aus einer möglicherweise unbekannten Quelle. Aufgrund der Tatsache, dass größtenteils Waffen und Werkzeuge eine Mischsignatur aufweisen, wäre eine Reparatur der Gegenstände nach intensivem Gebrauch zu Lebzeiten der individuellen Person denkbar. Möglicherweise wurde die ursprüngliche Zinnbronze mit Kupfer aus günstigeren Bezugsquellen, wie dem Oman, “verdünnt”, um kostbares Zinn zu sparen. Jedoch ist dies rein spekulativ.

Die Silber-Artefakte weisen erhöhte Kupfer- (2 – 7 Gew%) und Blei-Gehalte (0,15 – 1,5 Gew%) auf, die miteinander korrelieren. Weiterhin enthalten die beiden Armreife B16931a und -b 0,44 – 0,46 Gew% Au bei gleichzeitig niedrigeren Kupfer- und Blei-Konzentrationen und unterscheiden sich somit von den anderen Silber-Artefakten. Die Spurenelement-Gehalte der Silber-Artefakte sind insgesamt niedrig, außer Au (318 – 5698 ppm) und Bi (260 – 1231 ppm). As (2,7 – 333 ppm) und Sb (1,1 – 36,7 ppm) befinden sich in den frühdynastischen Artefakten in schwacher Korrelation. Die Armreife B16931a und -b zeigen neben erhöhten Au-Konzentrationen auch leicht erhöhte Te- (43 ppm) und Pt-Gehalte (10-20 ppm). In den Kupferisotopen-Verhältnissen unterscheiden sich die Silber-Artefakte nur wenig. Die δ^{65}Cu-Werte liegen i.

d. R. zwischen -0,5 und +0,5 ‰ und deuten somit auf ein primäres sulfidisches Erz hin (Markl, Lahaye and Schwinn, 2006; Klein, et al., 2010), welches verhüttet wurde. Lediglich die beiden Artefakte 30-12-733 und B16931b zeigen δ^{65}Cu-Werte von ca. +1,5 ‰ und somit die Signatur eines Erzes von sekundärer, oxidischer Herkunft. Auch in den Blei-Isotopen-Verhältnissen zeigen sich Unterschiede zwischen B16931a, -b und den übrigen Silber-Artefakten. Der Großteil der Silber-Artefakte weist Bleiisotopen-Signaturen Mesozoischen Alters auf (Jura-Kreide), wohingegen die der Artefakte B16931a und -b ein deutlich jüngeres geologisches Alter besitzen. Sowohl B17084, als auch B16931a- und -b befinden sich in guter Übereinstimmung mit Bleiisotopen-Verhältnissen von Erzen im Taurus-Gebirge (Hauptmann, et al., 2002). Genauer stimmt B17084 gut mit Daten im Übergangsbereich Pontiden und Taurus (Sakarya zone) überein. B16931a und -b passen hingegen gut zu Bleiisotopen-Daten in Südost-Anatolien. Ausgenommen von B16926a passen die übrigen Bleiisotopen-Verhältnisse gut in den Bereich des Karkas-Gebirges, Isfahan-Provinz, Iran, welches der geologischen Einheit der Urumieh-Dokhtar-Zone zuzuordnen ist (Pernicka, et al., 2011). Bei Artefakt B16926a könnte es sich um eine gemischte Isotopen-Signatur handeln, bestehend aus Erzen des Taurus und Zagros-Gebirges, da die Berechnung der euklidischen Distanzen zu den nächsten Nachbarn keine eindeutigen Ergebnisse lieferte. Möglich ist auch eine Herkunft aus einer der beiden Regionen. Jedoch lässt sich diese nicht eindeutig zuordnen. Ein weiterer Hinweis auf eine mögliche Herkunft des frühdynastischen Silbers aus dem Iran entstammt zudem den pRFA-Analysen, die das Projekt im Februar 2017 am Silberhort von Khafajeh ausführte. Das Hacksilber zeigte ähnliche Blei- und Kupfer-Gehalte, wie die Ur-Silber-Artefakte. Khafajeh ist im Bereich des Diyala-Flusses lokalisiert und datiert frühdynastisch. Somit befindet sich Khafajeh an einer wichtigen Position entlang der Handelsroute des Diyala-Flusses ins iranische Hochland. Ein Zusammenhang könnte durch weitere Analysen, ins Besondere Bleiisotopen- und Spurenelement-Analysen, des Silberhortes Khafajeh naturwissenschaftlich belegt werden. Auch besteht weiteres Potential für eine mögliche Provenienz der goldreicheren Silber-Artefakte im Kaukasus. Jedoch wurden die Blei-Silber-Lagerstätten im Kaukasus (Kovalenker, et al., 1990), ins Besondere im Großen Kaukasus, bislang kaum bis nicht durch naturwissenschaftliche Analytik charakterisiert. Jedoch existieren auch Blei-Silber-Mineralisationen im Großen Kaukasus, die z. T. höhere Au-Gehalte aufweisen können, die nicht zum Vergleich herangezogen werden konnten, da hier bisher keine publizierten Vergleichsdaten existieren.

Insgesamt konnten die Kupfer-, Bronze- und Silber-Artefakte des Friedhofs von Ur erfolgreich analysiert werden. Die Ergebnisse der Provenienzstudien sind vielversprechend und können eine mögliche Provenienz der As-Ni-haltigen Kupfer-Artefakte im Oman und der Assyrischen Sutur-Zone, Türkei, nachweisen. Zudem konnte erstmalig ein möglicher Zusammenhang der Zinnbronzen von Ur mit Lagerstätten des Aravalli-Delhi-Gebirges, NW-Indien, sowie vermutlich einer weiteren unbekannten Quelle hergestellt werden. Das Ausgangsmaterial des Reinkupfer-Artefakts 31-17-352T stammt vermutlich aus der Region um Serçeören Köy, Türkei. Die Ergebnisse der Silber-Artefakte von Ur zeigen Hinweise auf eine mögliche Herkunft des Silbers aus dem Taurus-Gebirge, Türkei, und Karkas-Gebirge, Iran. Für die Zukunft sind naturwissenschaftliche Untersuchungen an weiteren Artefakten anderer mesopotamischer Stadtstaaten und bestenfalls Fundorte an wichtigen Handelsrouten (z. B. Khafajeh, Tepe Hissar) angezeigt. Dies ermöglicht die Rekonstruktion, auf welchem Wege die Metalle nach Ur gelangten, ob über Land oder See. Des Weiteren konnte die zeitliche Entwicklung bislang aufgrund der geringen Anzahl an untersuchten Artefakten nur unzureichend untersucht werden. Interessante Aufschlüsse würde die Untersuchung von früher und später datierenden Artefakten geben, welches die Rekonstruktion der zeitlichen Veränderung in den Herkunftsgebieten ermöglichen würde. Auch sind die PIXE-Analysen des Penn Museum von hoher Qualität, da sie gut mit den Elektronenstrahl-Mikrosonden-Daten der vorliegenden Dissertation übereinstimmen. Aufgrund der Hauptelement-Gehalte konnten bereits einige Schlussfolgerungen, was die Herkunft der Artefakte betrifft, gezogen werden. Um eine bessere Statistik zu ermöglichen, wäre daher zukünftiger Zugriff auf die vollständigen PIXE-Analysen des Penn Museums im Rahmen des „Mesopotamian Metals Project“ wünschenswert, um diese statistisch auszuwerten.

17 Bibliography

Abd El-Rahman, Y., Polat, A., Dilek, Y., Fryer, B. J., El-Sharkawy, M. and Sakran, S., 2009. Geochemistry and tectonic evolution of the Neoproterozoic incipient arc–forearc crust in the Fawakhir area, Central Eastern Desert of Egypt. *Precambrian Research*, [e-journal] 175(1-4), pp.116-134. http://dx.doi.org/10.1016/j.precamres.2009.09.008.

Abdullah, S. H. and Chmyriov, V. M., eds., 2008. *Geology and Mineral Resources of Afghanistan. Book 1 - Geology*.

Adamia, S., Zakariadze, G., Chkhotua, T., Sadradze, N., Tsereteli, N., Chabukiani, A. and Gventsadze, A., 2011. Geology of the Caucasus. A Review. *Turkish Journal of Earth Sciences*, (20), pp.489-544.

Adams, R. M., Adovasio, J. M., Brentjes, B. and Chittick, H. N., 1974. Anthropological Perspectives on Ancient Trade [and Comments and Replies]. *Current Anthropology*, (15, No. 3), pp.239-258.

Afifi, A. M., Kelly, W. C. and Essene, E. J., 1988. Phase Relations among Tellurides, Sulfides, and Oxides: II. Applications to Telluride-Bearing Ore Deposits. *Economic Geology*, (83), pp.395-404.

Ahmed, A. H., Arai, S. and Attia, A. K., 2001. Petrological characteristics of podiform chromitites and associated peridotites of the Pan African Proterozoic ophiolite complexes of Egypt. *Mineralium Deposita*, [e-journal] 36(1), pp.72-84. http://dx.doi.org/10.1007/s001260050287.

Akin, H., 1979. Geologie, Magmatismus und Lagerstättenbildung im ostpontischen Gebirge/Türkei aus der Sicht der Plattentektonik. *Geologische Rundschau*, [e-journal] 68(1), pp.253-283. http://dx.doi.org/10.1007/BF01821131.

Akıncı, Ö. T., 1984. The Eastern Pontide volcano-sedimentary belt and associated massive sulphide deposits. Geological Society, London, Special Publications, (17), pp.415-428.

Akıncı, Ö. T., 2009. Ophiolite-hosted Copper and Gold Deposits of Southeastern Turkey: Formation and Relationship with Seafloor Hydrothermal Processes. *Turkish Journal of Earth Sciences*, (18), pp.475509.

Alavi, M., 1994. Tectonics of the Zagros orogenic belt of Iran. New data and interpretation. *Tectonophysics*, (229), pp.211-238.

Ali, K. A., Zoheir, B. A., Stern, R. J., Andresen, A., Whitehouse, M. J. and Bishara, W. W., 2016. Lu–Hf and O isotopic compositions on single zircons from the North Eastern Desert of Egypt, Arabian–Nubian Shield. Implications for crustal evolution. *Gondwana Research*, [e-journal] 32, pp.181-192. http://dx.doi.org/10.1016/j.gr.2015.02.008.

Alimov, K., Boroffka, N., Bubnova, M., Burjakov, J., Cierny, J., Jakubov, J., Lutz, J., Parzinger, H., Pernicka, E., Radilikovskij, V., Ruzanov, V., Shirinov, T., Starshinin, D. and Weisgerber, G., 1998. Prähistorischer Zinnbergbau in Mittelasien. Vorbericht der Kamapagne 1997. *Eurasia Antiqua*, (4), pp.137-199.

Arbuckle, B. S., 2012. Animals in the Ancient World. In: D. T. Potts, ed. 2012. *A companion to the archaeology of the ancient Near East*. Chichester: Wiley-Blackwell, pp.201-219.

Armbruster, B., 2016. Technological Aspects of Selected Gold Objects from Ur - Preliminary Results and Perspectives. *Metalla*, (22.1), pp.113-135.

Bachmann, H.-G., 1982. *The Identification of slags from Archaeological sites*. London.

Bagg, A. M., 2012. Irrigation. In: D. T. Potts, ed. 2012. *A companion to the archaeology of the ancient Near East*. Chichester: Wiley-Blackwell, pp.261-278.

Bamba, T., 1976. Ophiolite and related copper deposits of the Ergani mining district, southeastern Turkey. *Bulletin of the Mineral Research and Exploration*, (86), pp.36-57.

Bartura, Y., Hauptmann, A. and Schöne-Warnefeld, G., 1980. Zur Mineralogie und Geologie der antik genutzten Kupferlagerstätte im Timna-Tal. In: H. G. Conrad, and B. Rothenberg, eds. 1980. *Antikes Kupfer im Timna-Tal. 4000 Jahre Bergbau und Verhüttung in der Arabah.* Bochum, pp.41-56.

Bass, G. F., 1966. *Troy and Ur. Gold links Between Two Ancient Capitals.* Expedition, pp.26-39.

Begemann, F., Hauptmann, A., Schmitt-Strecker, S. and Weisgerber, G., 2010. Lead isotope and chemical signature of copper from Oman and its occurrence in Mesopotamia and sites on the Arabian Gulf coast. *Arabian Archaeology and Epigraphy*, (21), pp.145-179.

Begemann, F. and Schmitt-Strecker, S., 2009. Über das Frühe Kupfer Mesopotamiens. *Iranica Antiqua*, (44), pp.1-45.

Begemann, F., Schmitt-Strecker, S. and Pernicka, E., 2003. On the composition and provenance of metal finds from Beşiktepe(Troia). In: G. A. Wagner, E. Pernicka, and Uerpmann H.-P., eds. 2003. *Troia and the Troad. Scientific Approaches*. Berlin, Heidelberg, pp.173-201.

Bendall, C., 2003. *The Application of Trace Element and Isotopic Analyses to the Study of Celtic Gold Coins and their Metal Sources.* Dissertation. Frankfurt am Main.

Bender, F., 1974. Explanatory Notes on the Geological Map of the Wadi Araba, Jordan. *Geologisches Jahrbuch Reihe B*, (B10), pp.1-62.

Benham, A. J., Kováč, P., Petterson, M. G., Rojkovic, I., Styles, M. T., Gunn, A. G., McKervey, J. A. and Wasy, A., 2013. Chromite and PGE in the Logar Ophiolite Complex, Afghanistan. *Applied Earth Science*, [e-journal] 118(2), pp.45-58. http://dx.doi.org/10.1179/174327509X434957.

Ben-Yosef, E., Vassal, Y., van den Brink, Edwin C.M. and Beeri, R., 2016. A new Ghassulian metallurgical assemblage from Bet Shemesh (Israel) and the earliest leaded copper in the Levant. *Journal of Archaeological Science*: Reports, [e-journal] 9, pp.493-504. http://dx.doi.org/10.1016/j.jasrep.2016.08.010.

Birch, T., Rehren, T. and Pernicka, E., 2013. The Metallic Finds from Çatalhöyük. A Review and Preliminary New Work. In: I. Hodder, ed. 2013. *Substantive technologies at Çatalhöyük. Reports from the 2000 - 2008 seasons*. London, Los Angeles, Ca.: British Institute of Archaeology at Ankara; Cotsen Inst. of Archaeology, pp.307-318.

Bozkurt, E., Winchester, J. A., Yiğitbaş, E. and Ottley, C. J., 2008. Proterozoic ophiolites and mafic–ultramafic complexes marginal to the İstanbul Block. An exotic terrane of Avalonian affinity in NW Turkey. *Tectonophysics*, [e-journal] 461(1-4), pp.240-251. http://dx.doi.org/10.1016/j.tecto.2008.04.027.

Braidwood, R. J., Çambel, H. and Schirmer, W., 2013. Beginnings of Village-Farming Communities in Southeastern Turkey. Çayönü Tepesi, 1978 and 1979. *Journal of Field Archaeology*, [e-journal] 8(3), pp.249-258. http://dx.doi.org/10.1179/009346981791504950.

Braxton, D. and Mathur, R., 2011. Exploration Applications of Copper Isotopes in the Supergene Environment: A Case Study of the Bayugo Porphyry Copper-Gold Deposit, Southern Philippines. *Economic Geology*, (106), pp.1447-1463.

Brügmann, G., Berger, D. and Pernicka, E., 2017. Determination of the Tin Stable Isotopic Composition in Tin-bearing Metals and Minerals by MC-ICP-MS. *Geostandards and Geoanalytical Research*, [e-journal] 405, p. 2973-2973. http://dx.doi.org/10.1111/ggr.12166.

Burrows, E., 1935. *Ur Excavations. Texts II. Archaic Texts.* Philadelphia.

Burtman, V. S., 2010. Tien Shan, Pamir, and Tibet. History and geodynamics of phanerozoic oceanic basins. Geotectonics, [e-journal] 44(5), pp.388-404. http://dx.doi.org/10.1134/S001685211005002X.

Çagatay, A., 1977. Genetische Ergebnisse einer geologisch-mineralogischen Untersuchung der Kupfererzlagerstätten und -vorkommen in Südostanatolien. *Bulletin of the Mineral Research and Exploration in Turkey*, (89), pp.48-74.

Carter, E. F., Campbell, S. and Gauld, S., 2003. Elusive Complexity. New Data from late Halaf Domuztepe in South Central Turkey. *Paléorient*, (29-2), pp.117-133.

Carter, R. A., 2012. Watercraft. In: D. T. Potts, ed. 2012. *A companion to the archaeology of the ancient Near East*. Chichester: Wiley-Blackwell, pp.347-372.

Chegini, N. N., Momenzadeh, M., Parzinger, H., Pernicka, E., Stöllner, T., Vatandoust, A. and Weisgerber, G., 2000. Preliminary Report on archaeometallurgical investigations around the prehistoric site of Arisman near Kashan, western Central Asia. *Archäologische Mitteilungen aus Iran und Turan*, (32), pp.281-318.

Chichkov, B. N., Momma, C., Nolte, S., Alvensleben, F. von and Tünnermann, A., 1996. Femtosecond, picosecond and nanosecond laser ablation of solids. *Applied Physics A*, pp.109-115.

Choudhary, A.K., Gopalan, K., Anjaneya-Sastry, C., 1984. Present status of the Geochronology of the Precambrian rocks of Rajasthan. *Tectonophysics* (105), pp.131-140.

Christie, A., 1936. *Murder in Mesopotamia*: Collins Crime Club.

Chutas, N. I., Kress, V. C., Ghiorso, M. S. and Sack, R. O., 2008. A solution model for high-temperature PbS-$AgSbS_2$-$AgBiS_2$ galena. American Mineralogist, [e-journal] 93(10), pp.1630-1640. http://dx.doi.org/10.2138/am.2008.2695.

Cleuziou, S. and Berthoud, T., 1982. Early Tin In The Near East. A reassessment in the Light of New Evidence from Western Afghanistan. *Expedition*, (25), pp.14-19.

Collon, D., 1996. Mesopotamia and the Indus. The evidence of the seals. In: J. E. Reade, ed. 1996. *The Indian Ocean in Antiquity*. London, pp.209-225.

Conrad, H. G. and Rothenberg, B., eds., 1980. *Antikes Kupfer im Timna-Tal. 4000 Jahre Bergbau und Verhüttung in der Arabah*. Bochum.

Cook, N. J., Ciobanu, C. L., Danyushevsky, L. V. and Gilbert, S., 2011. Minor and trace elements in bornite and associated Cu–(Fe)-sulfides. A LA-ICP-MS studyBornite mineral chemistry. *Geochimica et Cosmochimica Acta*, [e-journal] 75(21), pp.6473-6496. http://dx.doi.org/10.1016/j.gca.2011.08.021.

Courcier, A., 2014. Ancient Metallurgy in the Caucasus from the Sixth to the Third Millennium BCE. In: B. W. Roberts, and C. P. Thornton, eds. 2014. *Archaeometallurgy in global perspective. Methods and syntheses*. New York: Springer, pp.579-664.

Crawford, H., 2013. Trade in the Sumerian World. In: H. Crawford, ed. 2013. *The Sumerian World*. London, pp.447-461.

Cuenod, A., Bray, P. and Pollard, A. M., 2015. The „tin problem“ in the prehistoric Near East. Further insights from a study of chemical datasets on copper alloys from Iran and Mesopotamia. *Iran*, (53), pp.29-48.

Daliran, F., Pride, K., Walther, J., Berner, Z. A. and Bakker, R. J., 2013. The Angouran Zn (Pb) deposit, NW Iran. Evidence for a two stage, hypogene zinc sulfide–zinc carbonate mineralization. *Ore Geology Reviews*, [e-journal] 53, pp.373-402. http://dx.doi.org/10.1016/j.oregeorev.2013.02.002.

Deb, M., Thorpe, R. I., Cumming, G. L. and Wagner, P. A., 1989. Age, source and stratigraphic implications of Pb isotope data for conformable, sediment-hosted, base metal deposits in the Proterozoic Aravalli-Delhi orogenic belt, northwestern India. *Precambrian Research*, [e-journal] 43(1-2), pp.1-22. http://dx.doi.org/10.1016/0301-9268(89)90002-8.

Deb, M. and Sarkar, S.C., 1990. Proterozoic tectonic evolution and metallogenesis in the Aravalli-Delhi orogenic complex, northwestern India. *Precambrian Research*, [e-journal] 46(1-2), pp.115-137. http://dx.doi.org/10.1016/0301-9268(90)90069-3.

Deb, M., Thorpe, R. I., Krstic, D., Corfu, F. and Davis, D. W., 2001. Zircon U–Pb and galena Pb isotope evidence for an approximate 1.0 Ga terrane constituting the western margin of the Aravalli–Delhi orogenic belt, northwestern India. *Precambrian Research*, [e-journal] 108(3-4), pp.195-213. http://dx.doi.org/10.1016/S0301-9268(01)00134-6.

Doonan, R., Hanks, B., Zdanovich, D. G., Kupriyanova, E., Pitman, D., Batanina, N.'y. and Johnson, J., 2014. Metals, Society, and Economy in the Late Prehistoric Eurasian Steppe. In: B. W. Roberts, and C. P. Thornton, eds. 2014. *Archaeometallurgy in global perspective. Methods and syntheses*. New York: Springer, pp.755-784.

Dronov, V. I. and Chmyriov, V. M. The main features of Afghanistan's geological structure. In: S. H. Abdullah, and V. M. Chmyriov, eds. *Geology and Mineral Resources of Afghanistan. Book 1 - Geology,* pp.19-30.

Dschaparidze, O., 2001. Zur frühen Metallurgie Georgiens vom 3. bis zum 1. Jahrtausend v. Chr. In: I. Gambaschidze, A. Hauptmann, R. Slotta, and Ü. Yalçın, eds. 2001. Georgien. Schätze aus dem Land des goldenen Vlies. Bochum, pp.92-119.

Earl, B. and Yener, K. A., 1995. Tin smelting at the Oriental Institute. *The Oriental Institute*, (149), pp.2-5.

Ehya, F., Lotfi, M. and Rasa, I., 2010. Emarat carbonate-hosted Zn–Pb deposit, Markazi Province, Iran. A geological, mineralogical and isotopic (S, Pb) study. *Journal of Asian Earth Sciences*, [e-journal] 37(2), pp.186-194. http://dx.doi.org/10.1016/j.jseaes.2009.08.007.

Eliwa, H.A., Kimura, J.-I. and Itaya, T., 2006. Late Neoproterozoic Dokhan Volcanics, North Eastern Desert, Egypt. Geochemistry and petrogenesis. *Precambrian Research*, [e-journal] 151(1-2), pp.31-52. http://dx.doi.org/10.1016/j.precamres.2006.08.005.

Farr, T. G., Rosen, P. A., Caro, E., Crippen, R., Duren, R., Hensley, S., Kobrick, M., Paller, M., Rodriguez, E., Roth, L., Seal, D., Shaffer, S., Shimada, J., Umland, J., Werner, M., Oskin, M., Burbank, D. and Alsdorf, D., 2007. The Shuttle Radar Topography Mission. *Reviews of Geophysics*, [e-journal] 45(2), p.1485-1485. http://dx.doi.org/10.1029/2005RG000183.

Faure, M. and Natal'in, B.A., 1992. The geodynamic evolution of the eastern Eurasian margin in Mesozoic times. *Tectonophysics*, (208.4), pp.397-411.

Forest, J.-D., 1983. *Les pratiques funéraires en Mésopotamie du 5e millénaire au début du 3e: étude de cas*. Paris.

Foster, B. R., 1997. A Sumerian Merchant's Account of the Dilmun Trade. *Acta Sumerologica*, (19), pp.53-62.

Furnes, H., Dilek, Y. and de Wit, M., 2015. Precambrian greenstone sequences represent different ophiolite types. Gondwana Research, [e-journal] 27(2), pp.649-685. http://dx.doi.org/10.1016/j.gr.2013.06.004.

Gadd, C. J., Legrain, L., Smith, S. and Burrows, E., 1928. *Texts I. Royal Inscriptions*. Philadelphia.

Gamkrelidze, I. P., 1986. Geodynamic evolution of the Caucasus and adjacent areas in Alpine time. *Tectonophysics*, [e-journal] 127(3-4), pp.261-277. http://dx.doi.org/10.1016/0040-1951(86)90064-8.

Gamkrelidze, I. P., 1997. Terranes of the Caucasus and Adjacent Areas. *Bulletin of Georgian Academy of Science*, (155, No. 3), pp.391-394.

Ganss, O., 1965. Geosynklinalbecken, Tektonik, Granite und junger Vulkanismus in Afghanistan. *Geologische Rundschau*, [e-journal] 54(2), pp.668-698. http://dx.doi.org/10.1007/BF01820751.

Garfinkel, Y., Klimscha, F., Shalev, S. and Rosenberg, D., 2014. The beginning of metallurgy in the southern Levant: a late 6th millennium CalBC copper awl from Tel Tsaf, Israel. *PloS one*, (9 (3)), 1-6. http://dx.doi.org/10.1371/journal.pone.0092591.

Garner, J., 2013. *Das Zinn der Bronzezeit in Mittelasien II. Die montanarchäologischen Forschungen an den Zinnlagerstätten*. Darmstadt.

German, R. M., Guzowski, M. M. and Wright, D. C., 1980. Color and Color Stability as Alloy Design Criteria. *JOM*, [e-journal] 32(3), pp.20-27. http://dx.doi.org/10.1007/BF03354551.

Glassner, J.-J., 1996. Dilmun, Magan and Meluhha. Some observations on Language, Toponymy, Anthroponymy and Theonymy. In: J. E. Reade, ed. 1996. *The Indian Ocean in Antiquity*. London, pp.235-250.

Gowland, W., 1906. Presidential Address: Copper and Its Alloys in Prehistoric Times. *The Journal of the Anthropological Institute of Great Britain and Ireland*, (36), pp.11-38.

Gowland, W., 1914. *The metallurgy of the non-ferrous metals*. London.

Griffitts, W. R., Albers, J. P. and Oener, O., 1972. Massive Sulfide Copper Deposits of the Ergani-Maden Area, Southeastern Turkey. *Economic Geology*, [e-journal] 67(6), pp.701-716. http://dx.doi.org/10.2113/gsecongeo.67.6.701.

Guillong, M., Horn, I. and Günther, D., 2003. A comparison of 266 nm, 213 nm and 193 nm produced from a single solid state Nd:YAG laser for laser ablation ICP-MS. J. Anal. At. *Spectrom*., [e-journal] 18(10), pp.1224-1230. http://dx.doi.org/10.1039/B305434A.

Hall, H. R., 1923. Ur and Eridu: The British Museum Excavations of 1919. *The Journal of Egyptian Archaeology*, (9), pp.177-195.

Hall, H. R., 1925. The Excavations of 1919 at Ur, el-'Obeid, and Eridu, and the History of Early Babylonia. A Monthly Record of Anthropological Science, (25), pp.1-7.

Hamilton, N., 2017. *ggtern: An extension to ‚ggplot2', for the Creation of Ternary Diagrams. R package version 2.2.2.* https://CRAN.R-project.org/package=ggtern

Hassan, A. A. and Hassan, F. A., 1981. Source of galena in Predynastic Egypt at Nagada. *Archaeometry*, (23), pp.77-82.

Hauptmann, A., Klein, S., Paoletti, P., Zettler, R. L. and Jansen, M., 2018. Types of Gold, Types of Silver: The Composition of Precious Metal Artifacts Found in the Royal Tombs of Ur, Mesopotamia. *Zeitschrift für Assyriologie und Vorderasiatische Archäologie*, [e-journal] 108(1), pp.100-131. http://dx.doi.org/10.1515/za-2018-0007.

Hauptmann, A. and Klein, S., 2016. Golden Artifacts from the Royal Tombs of Ur, Mesopotamia. *Metalla*, (22.1), pp.84-88.

Hauptmann, A., Schmitt-Strecker, S., Begemann, F. and Palmieri, A., 2002. Chemical Composition and Lead Isotopy of Metal Objects from the „Royal" Tomb and Other Related Finds at Arslantepe, Eastern Anatolia. *Paléorient*, [e-journal] 28(2), pp.43-69. http://dx.doi.org/10.3406/paleo.2002.4745.

Hauptmann, A., 1985. *5000 Jahre Kupfer in Oman. Band 1: Die Entwicklung der Kupfermetallurgie vom 3. Jahrtausend bis zur Neuzeit.* Bochum.

Hauptmann, A., 1987. Kupfer und Bronzen der Südostarabischen Halbinsel. *Der Anschnitt*, (39), pp.209-218.

Hauptmann, A., 2000. *Zur frühen Metallurgie des Kupfers in Fenan/Jordanien*. Bochum.

Hauptmann, A., 2007. *The archaeometallurgy of copper. Evidence from Faynan, Jordan*. Berlin, New York: Springer.

Hauptmann, A. and Klein, S., 2016. An Introduction. *Metalla*, (22.1), pp.77-83.

Hauptmann, A., Klein, S., Zettler, R. L., Baumer, U. and Dietemann, P., 2016. On the Making and Provenancing of Pigments from the Early Dynastic Royal Tombs of Ur, Mesopotamia. *Metalla*, (22.1), pp.41-74.

Hauptmann, A., Rehren, T. and Schmitt-Strecker, S., 2003. Early Bronze Age copper metallurgy at Shahr-i Sokhta (Iran), reconsidered. In: T. Stöllner, G. Körlin, G. Steffens, and J. Cierny, eds. 2003. *Man and Mining - Mensch und Bergbau. Bochum*, pp.197-213.

Hauptmann, A. and Weisgerber, G., 1980. Third millenium BC copper production in Oman. Revue d'Archéometrie, (3), pp.131-138.

Hauptmann, H. and Pernicka, E., eds., 2004. Die Metallindustrie Mesopotamiens von den Anfängen bis zum 2. Jahrtausend v. Chr. Rahden /Westf.

Haustein, M., Gillis, C. and Pernicka, E., 2010. Tin isotopy. A new method for solving old questions. *Archaeometry*, [e-journal] 52(5), pp.816-832. http://dx.doi.org/10.1111/j.1475-4754.2010.00515.x.

Haymon, R. M., Koski, R. A. and Abrams, M. J., 1989. Hydrothermal discharge zones beneath massive sulfide deposits mapped in the Oman ophiolite. *Geology*, (17), pp.531-535.

Heinz, M., 2012. The Ur III , Old Babylonian, and Kassite Empires. In: D. T. Potts, ed. 2012. *A companion to the archaeology of the ancient Near East*. Chichester: Wiley-Blackwell, pp.706-721.

Helwing, B., 2009. Rethinking the tin mountains. Patterns of usage and circulation of tin in Greater Iran from the 4th to the 1st millennium BC. *Türkiye Bilimler Akademisi Arkeoloji Dergisi*, (12), pp.209-221.

Helwing, B., 2014. Silver in the early state societies of Greater Mesopotamia. In: H. Meller, R. Risch, and E. Pernicka, eds. 2014. *Metalle der Macht - Frühes Gold und Silber. Halle (Saale)*, pp.411-421.

Hirao, Y., Enomoto, J. and Tachikawa, H. Lead Isotope ratios of Copper, Zinc and Lead minerals in Turkey - In relation to the provenance study of artefacts. In: . Mikasa (Hg.) 1985 – *Essays on ancient Anatolia*, pp.89-114.

Hirsch, H., 1963. Die Inschriften der Könige von Agade. *Archiv für Orientforschung (AfO),* (20), pp.1-82.

Hoffman, B. C. and Miller, H. M.-L., 2014. Production and Consumption of Copper-Base Metals in the Indus Civilization. In: B. W. Roberts, and C. P. Thornton, eds. 2014. *Archaeometallurgy in global perspective. Methods and syntheses.* New York: Springer, pp.697-728.

Horn, I. and von Blanckenburg, F., 2007. Investigation on elemental and isotopic fractionation during 196 nm femtosecond laser ablation multiple collector inductively coupled plasma mass spectrometry. *Spectrochimica Acta Part* B: *Atomic Spectroscopy*, pp.410-422.

Horn, I., Guillong, M. and Günther, D., 2001. Wavelength dependant ablation rates for metals and silicate glasses using homogenized laser beam profiles — implications for LA-ICP-MS. *Applied Surface Science*, [e-journal] 182(1-2), pp.91-102. http://dx.doi.org/10.1016/S0169-4332(01)00465-2.

Horwitz, E. P., Dietz, M. L., Rhoads, S., Felinto, C., Gale, N. H. and Houghton, J., 1994. A lead-selective extraction chromatographic resin and its application to the isolation of lead from geological samples. *Analytica Chimica Acta*, (292), pp.263-273.

Jan, M. Q., Windley, B. F. and Khan, A., 1985. The Waziristan Ophiolite, Pakistan: General Geology and Chemistry of Chromite and Associated Phases. *Economic Geology,* (80), pp.294-306.

Janković, S., 1977. The copper deposits and geotectonic setting of the Thethyan Eurasian Metallogenic Belt. *Mineralium Deposita*, [e-journal] 12(1), pp.37-47. http://dx.doi.org/10.1007/BF00204503.

Jansen, M., Aulbach, S., Hauptmann, A., Höfer, H. E., Klein, S., Krüger, M. and Zettler, R. L., 2016a. Platinum group placer minerals in ancient gold artifacts – Geochemistry and osmium isotopes of inclusions in Early Bronze Age gold from Ur/Mesopotamia. *Journal of Archaeological Science*, [e-journal] 68, pp.12-23. http://dx.doi.org/10.1016/j.jas.2016.02.004.

Jansen, M., Hauptmann, A. and Klein, S., 2016b. Where Does the Gold from the Cemetery of Ur Come From? – Provenancing Gold Sources Using Analytical Methods. *Metalla*, (22.1), pp.98-106.

Jassim, S. Z. and Goff, J. C., 2006. *Geology of Iraq.* Prague, Brno: Dolin; Moravian Museum.

Kawtaradze, G. I., 2001. Die frühesten Metallobjekte in Zentral-Transkaukasien. In: I. Gambaschidze, A. Hauptmann, R. Slotta, and Ü. Yalçın, eds. 2001. *Georgien. Schätze aus dem Land des goldenen Vlies.* Bochum, pp.136-141.

Keesmann, I., 1993. Naturwissenschaftliche Untersuchungen zur antiken Kupfer- und Silberverhüttung in Südwestspanien. In: H. Steuer, and U. Zimmermann, eds. 1993. Montanarchäologie in Europe. Sigmaringen, pp.105-122.

Kekelia, S., Kekelia, M., Otkhmezuri, Z., Özgür, N. and Moon, C., 2004. Ore-forming systems in volcanogenic-sedimentary sequences by the example of base metal deposits of the Caucasus and East Pontic metallotect. *Bulletin of the Mineral Research and Exploration in Turkey*, (129), pp.1-16.

Kenoyer, J. M. and Miller, H. M.-L., 1999. Metal technologies of the Indus Valley Tradition in Pakistan and Western India. In: V. C. Pigott, ed. 1999. *The emergence and development of metallurgy.* Philadelphia: University Museum, pp.107-151.

Kenoyer, J. M., Price, T. D. and Burton, J. H., 2013. A new approach to tracking connections between the Indus Valley and Mesopotamia: initial results of strontium isotope analyses from Harappa and Ur. *Journal of Archaeological Science*, [e-journal] 40(5), pp.2286-2297. http://dx.doi.org/10.1016/j.jas.2012.12.040.

Ketin, I., 1966. Tectonic units of Anatolia (Asia Minor). *Bulletin of the Mineral Research and Exploration*, (66), pp.23-37.

Klein, S., Brey, G. P., Durali-Müller, S. and Lahaye, Y., 2010. Characterisation of the raw metal sources used for the production of copper and copper-based objects with copper isotopes. *Archaeological and Anthropological Sciences*, [e-journal] 2(1), pp.45-56. http://dx.doi.org/10.1007/s12520-010-0027-y.

Klein, S., La Niece, S. and Hauptmann, A., 2016. Objects from the Ur collection of the British Museum Sampling and Analytical Investigations. *Metalla*, (22.1), pp.89-97.

Klein, S. and Hauptmann, A., 2016. Ur, Mesopotamia: The Lead Metal from Pit X. *Metalla*, (22.1), pp.136-140.

Klemm, R. and Klemm, D., 2014. Früher Goldbergbau in Ägypten und Nubien. In: H. Meller, R. Risch, and E. Pernicka, eds. 2014. *Metalle der Macht - Frühes Gold und Silber. Halle (Saale)*, pp.141-149.

Klitzsch, E., 1986. Plate tectonics and cratonal geology in Northeast Africa (Egypt, Sudan). *Geologische Rundschau*, [e-journal] 75(3), pp.755-768. http://dx.doi.org/10.1007/BF01820645.

Kmošek, J., Odler, M., Fikrle, M. and Kochergina, Y. V., 2018. Invisible connections. Early Dynastic and Old Kingdom Egyptian metalwork in the Egyptian Museum of Leipzig University. *Journal of Archaeological Science*, [e-journal] 96, pp.191-207. http://dx.doi.org/10.1016/j.jas.2018.04.004.

Kohl, P. L., 2009. T*he Making of Bronze Age Eurasia*. Cambridge: Cambridge University Press.

Korn, W., 2004. *Mesopotamien. Wiege der Zivilisation*. Stuttgart.

Kovalenker, V. A., Zalibekyan, M. A., Laputina, I. P., Malov, V. S., Sandomirskaya, S. M., Garas'ko, M. I. and Mkhitaryan, D. I., 1990. Sulfide-Telluride Mineralization of the Megradzor ore field, Armenia. *International Geology Review*, [e-journal] 32(7), pp.705-720. http://dx.doi.org/10.1080/00206819009465812.

Kronz, A., 1997. *Phasenbeziehungen und Kristallisationsmechanismen in fayalitischen Schmelzsystemen - Untersuchungen an Eisen- und Buntmetallschlacken.* Dissertation. Mainz.

Krumsiek, K. Zur Bewegung der Iranisch-Afghanischen Platte. *Geologische Rundschau*, 1967(65.1), pp.909-929.

LaHaye, N. L., Kurian, J., Diwakar, P. K., Alff, L. and Harilal, S. S., 2015. Femtosecond laser ablation-based mass spectrometry. An ideal tool for stoichiometric analysis of thin films. *Scientific Reports,* [e-journal] 5, p.13121-13121. http://dx.doi.org/10.1038/srep13121.

Lamberg-Karlovsky, C. C. and Tosi, M., 1973. Shahr-i Sokhta and Tepe Yahya: Tracks on the Earliest History of the Iranian Plateau. East and West, (23), pp.21-57.

Langgut, D., Yahalom-Mack, N., Lev-Yadun, S., Kremer, E., Ullman, M. and Davidovich, U., 2016. The earliest Near Eastern wooden spinning implements. *Antiquity*, [e-journal] 90(352), pp.973-990. http://dx.doi.org/10.15184/aqy.2016.99.

Larsen, C. E., 1983. *Life and land use on the Bahrain Islands. The geoarcheology of an ancient society.* [e-book]. Chicago: University of Chicago Press. Available at: Larsen, Curtis E. (VerfasserIn). <http://www.loc.gov/catdir/enhancements/fy0609/83005085-b.html>.

Law, R. W., 2008. *Inter-Regional Interaction and Urbanism in the Ancient Indus Valley: A Geologic Provenience Study of Harappa's Rock and Mineral Assemblage*. Dissertation. Madison.

Lazarov, M. and Horn, I., 2015. Matrix and energy effects during in-situ determination of Cu isotope ratios by ultraviolet-femtosecond laser ablation multicollector inductively coupled plasma mass spectrometry. *Spectrochimica Acta Part B: Atomic Spectroscopy,* [e-journal] 111, pp.64-73. http://dx.doi.org/10.1016/j.sab.2015.06.013.

Lechtman, H. and Klein, S., 1999. The Production of Copper–Arsenic Alloys (Arsenic Bronze) by Cosmelting: Modern Experiment, Ancient Practice. Journal of Archaeological Science, (26), pp. 497–526.

Lehner, J. W. and Yener, K. A., 2014. Organization and Specialization of Early Mining and Metal Technologies in Anatolia. In: B. W. Roberts, and C. P. Thornton, eds. 2014. *Archaeometallurgy in global perspective. Methods and syntheses*. New York: Springer, pp.529-558.

Lipman, P. W., Bogatikov, O. A., Tsvetkov, A. A., Gazis, C., Gurbanov, A. G., Hon, K., Koronovsky, N. V., Kovalenko, V. I. and Marchev, P., 1993. 2.8-Ma ash-flow caldera at Chegem River in the northern Caucasus Mountains (Russia), contem-

poraneous granites, and associated ore deposits. J*ournal of Volcanology and Geothermal Research*, [e-journal] 57(1-2), pp.85-124. http://dx.doi.org/10.1016/0377-0273(93)90033-N.

Lorand, J. P., 1988. Fe-Ni-Cu sulfides in tectonite peridotites from the Maqsad district, Sumail ophiolite, southern Oman: implications for the origin of the sulfide component in the oceanic upper mantle. *Tectonophysics*, (151), pp.57-73.

Lorazo, P., Lewis, L. J. and Meunier, M., 2006. Thermodynamic pathways to melting, ablation, and solidification in absorbing solids under pulsed laser irradiation. *Physical Review B*, [e-journal] 73(13). http://dx.doi.org/10.1103/PhysRevB.73.134108.

Macdougall, J.D., Willis, R., Lugmair, G.W., Roy, A.B., Gopalan, K., 1984. *The Aravalli sequence of Rajasthan, India: a Precambrian continental margin. Workshop on the early Earth: the interval from accretion to the older Archaean.* Lunar Planet. Inst., Houston, Texas, pp. 55- 56.

Maddin, R., Wheeler, T. S. and Muhly, J. D., 1980. Distinguishing artifacts made of native copper. *Journal of Archaeological Science,* [e-journal] 7(3), pp.211-225. http://dx.doi.org/10.1016/S0305-4403(80)80025-2.

Mahfoud, R. F. and Beck, J. N., 1997. Copper Mineralizations in the Ophiolite of Oman. The Genesis and Emplacement Relationship with the Orogenic Movements of Serpentinized Peridotite. *International Geology Review*, (39), pp.252-286.

Majidzadeh, Y., 1982. Lapis Lazuli and the Great Khorasan Road. *Paléorient*, (8/1), pp.59-69.

Manafi, M., Arian, M., Raeesi, S. H. T. and Solgi, A., 2013. Tethys Subduction History in Caucasus Region. *Open Journal of Geology,* (03), pp.222-232. http://dx.doi.org/10.4236/ojg.2013.33026.

Mao, J., Pirajno, F., Lehmann, B., Luo, M. and Berzina, A., 2014. Distribution of porphyry deposits in the Eurasian continent and their corresponding tectonic settings. *Journal of Asian Earth Sciences,* [e-journal] 79, pp.576-584. http://dx.doi.org/10.1016/j.jseaes.2013.09.002.

Markl, G., Lahaye, Y. and Schwinn, G., 2006. Copper isotopes as monitors of redox processes in hydrothermal mineralization. *Geochimica et Cosmochimica Acta*, [e-journal] 70(16), pp.4215-4228. http://dx.doi.org/10.1016/j.gca.2006.06.1369.

Mathur, R. and Fantle, M. S., 2015. Copper Isotopic Perspective on Supergene Processes. Implications for the Global Cu cycle. *Elements*, (11), pp.323-329.

Matthews, R. J., 1993. *Cities, Seals and Writing. Archaic Seal Impressions from Jemdet Nasr and Ur*. Berlin.

McNeil, M. B. and Little, B. J., 1992. Corrosion mechanisms for copper and silver objects in near-surface environments. *Journal of American Institute for Conservation*, (31, 3), pp.355-366.

Meliksetian, K. and Pernicka, E., 2010. Geochemical characterisation of Armenian Early Bronze Age metal artefacts and their relation to copper ores. In: S. Hansen, ed. 2010. *Von Majkop bis Trialeti. Gewinnung und Verbreitung von Metallen und Obsidian in Kaukasien im 4.-2. Jt. v. Chr. ; Beiträge des Internationalen Symposiums in Berlin vom 1. - 3. Juni 2006.* Bonn: Habelt, pp.41-58.

Merkel, S., Bräutigam, B., Klein, S. and Hauptmann, A., 2013. The Analysis of Slag from the Panjhir Mining Region, Afghanistan: An Investigation of (Medieval) Silver Production Technology. *Archäologische Mitteilungen*, (45), pp.231-249.

Merkel, S. W., 2016. *Silver and the Silver Economy at Hedeby.* Raw Materials, Innovation, Technology of Ancient Cultures RITaK 2./ Der Anschnitt. Beiheft 33. Rahden, Westf.: Marie Leidorf.

Merpert, N. Y. and Munchaev, R. M., 1987. The Earliest Levels at Yarim Tepe I and Yarim Tepe II in Northern Iraq. *Iraq*, (49), pp.1-36.

Méry, S., Phillips, C. and Calvet, Y., 1998. Dilmun. Potteries in Mesopotamia and Magan from the end of the 3rd and of the 2nd Millennium B.C. In: C. S. Phillips, D. T. Potts, and S. Searight, eds. 1998. *Arabia and her Neighbours. Essays on Prehistorical and Historical Developments*. Essays Presented in Honour of Beatrice de Cardi. Brepols, pp. 165–180.

Meyers, P., 2003. Production of Silver in Antiquity: Ore Types Identified Based Upon Elemental Compositions of Ancient Silver Artifacts. In: L. van Zelst, ed. 2003. *Patterns and Process*. A Festschrift in honor of Dr. Edward Sayre. Suitland, Maryland, pp.271-288.

Miotello, A. and Kelly, R., 1999. Laser-induced phase explosion: new physical problems when a condensed phase approaches the thermodynamic critical temperature. *Applied Physics A Materials Science and Processing*, [e-journal] 69(S1), S67-S73. http://dx.doi.org/10.1007/s003399900296.

Mirnejad, H., Simonetti, A. and Molasalehi, F., 2011. Pb isotopic compositions of some Zn–Pb deposits and occurrences from Urumieh–Dokhtar and Sanandaj–Sirjan zones in Iran. *Ore Geology Review*s, [e-journal] 39(4), pp.181-187. http://dx.doi.org/10.1016/j.oregeorev.2011.02.002.

Mirnejad, H., Simonetti, A. and Molasalehi, F., 2015. Origin and formational history of some Pb-Zn deposits from Alborz and Central Iran. Pb isotope constraints. *International Geology Review*, [e-journal] 57(4), pp.463-471. http://dx.doi.org/10.1080/00206814.2015.1013510.

Mishara, J. and Meyers, P., 1974. Ancient Egyptian Silver - A Review. In: A. Bishay, ed. 1974. *Recent Advances in Science and Technology of Materials*, pp.29-45.

Moghadam, H. S. and Stern, R. J., 2014. Ophiolites of Iran. Keys to understanding the tectonic evolution of SW Asia: (I) Paleozoic ophiolites. *Journal of Asian Earth Sciences*, [e-journal] 91, pp.19-38. http://dx.doi.org/10.1016/j.jseaes.2014.04.008.

Mödlinger, M., Kuijpers, M. H.G., Braekmans, D. and Berger, D., 2017. Quantitative comparisons of the color of CuAs, CuSn, CuNi, and CuSb alloys. *Journal of Archaeological Science*, [e-journal] 88, pp.14-23. http://dx.doi.org/10.1016/j.jas.2017.09.001.

Moghadam, H. S. and Stern, R. J., 2015. Ophiolites of Iran. Keys to understanding the tectonic evolution of SW Asia: (II) Mesozoic ophiolites. *Journal of Asian Earth Sciences*, [e-journal] 100, pp.31-59. http://dx.doi.org/10.1016/j.jseaes.2014.12.016.

Momenzadeh, M., 2004. Metallische Bodenschätze in Iran in antiker Zeit. Ein kurzer Überblick. In: T. Stöllner, R. Slotta, and A. Vatandoust, eds. 2004. *Persiens Antike Pracht. Bergbau - Handwerk - Archäologie.* Bochum, pp.8-21.

Moorey, P. R. S., 1994. *Ancient Mesopotamian Metals and Industries. The Archaeological Evidence*. Oxford.

Moritz, R., Melkonyan, R., Selby, D., Popkhadze, N., Gugushvili, V., Tayan, R. and Ramazanov, V., 2016. Metallogeny of the Lesser Caucasus: From Arc Construction to Postcollision Evolution. In: J. P. Richards, ed. 2016. *Tectonics and Metallogeny of the Tethyan Orogenic Belt.* Cheyenne, Wyoming, pp.157-192.

Muhly, J. D., 1973. *Copper and tin. The distribution of mineral resources and the nature of the metals trade in the Bronze Age.* New Haven.

Muhly, J. D., 1985. Sources of Tin and the Beginnings of Bronze Metallurgy. *American Journal of Archaeology*, (89), pp.275-291.

Muhly, J. D., 1989. Çayönü Tepesi and the Beginnings of Metallurgy in the Ancient World. In: A. Hauptmann, E. Pernicka, and G. A. Wagner, eds. 1989. *Archäometallurgie der Alten Welt. Beiträge zum Internationalen Symposium „Old World Archaeometallurgy" Heidelberg 1987*. pp.1-11.

Müller-Karpe, M., 2004. Katalog I. Untersuchte Metallobjekte aus Mesopotamien. In: H. Hauptmann, and E. Pernicka, eds. 2004. *Die Metallindustrie Mesopotamiens von den Anfängen bis zum 2. Jahrtausend v. Chr*. Rahden /Westf., pp.1-92.

Murao, S., Deb, M. and Furuno, M., 2008. Mineralogical evolution of indium in high grade tin-polymetallic hydrothermal veins — A comparative study from Tosham, Haryana state, India and Goka, Naegi district, Japan. *Ore Geology Reviews*, [e-journal] 33(3-4), pp.490-504. http://dx.doi.org/10.1016/j.oregeorev.2007.02.004.

Naha, K. and Roy, A. B., 1983. The problem of the Precambrian basement in Rajasthan, western India. *Precambrian Research*, (19), pp.217-223.

Natal'in, B. A., 1993. History and modes of Mesozoic accretion in Southeastern Russia. *The Island Arc,* (2), pp.15-34.

Nezafati, N., 2006. *Au-Sn-W-Cu-Mineralization in the Astaneh-Sarband Area, West Central Iran*. Dissertation. Tübingen.

Nezafati, N., Momenzadeh, M. and Pernicka, E., 2005. Darhand copper occurrence: An example of Michigantype native copper deposits in central Iran. In: J. Mao, and F. P. Bierlein, eds. 2005. *Mineral Deposit Research: Meeting the Global Challenge*. Berlin, Heidelberg: Springer Berlin Heidelberg, pp.165-166.

Nezafati, N. and Pernicka, E., 2012. Early Silver Production in Iran. *Iranian Archaeology,* (2), pp.38-45.

Nezafati, N., Pernicka, E. and Momenzadeh, M., 2006. Ancient tin: Old question and a new answer. *Antiquity*, (80 (308)).

Nezafati, N., Pernicka, E. and Momenzadeh, M., 2008. Iranian Ore Deposits and Their Role in the Development of the Ancient Cultures. In: Ü. Yalçın, ed. 2008. *Anatolian Metal IV.* Bochum: Dt. Bergbau-Museum, pp.77-90.

Nissen, H. J., 1966. *Zur Datierung des Königsfriedhofes von Ur. Unter besonderer Berücksichtigung der Stratigraphie der Privatgräber.* Bonn.

Northover, J. P., 1989. Properties and Use of Arsenic-Copper Alloys. In: A. Hauptmann, E. Pernicka, and G. A. Wagner, eds. 1989. *Archäometallurgie der Alten Welt. Beiträge zum Internationalen Symposium „Old World Archaeometallurgy" Heidelberg 1987*. Heidelberg, pp.111-118.

Oates, J., 1983. Urban trends in prehistoric Mesopotamia. In: F. Brüschweiler, Y. Christie, R. Martin-Achard, B. Urio, and J. Vicari, eds. 1983. *La ville dans le Proche-Orient ancien. Actes du Colloque de Cartigny 1979*. Leuven, pp.81-92.

Oates, J., 1990. *Babylon. Stadt und Reich im Brennpunkt des Alten Orien*t. Bindlach.

Oates, J., 2012. Southern Mesopotamia. In: D. T. Potts, ed. 2012. *A companion to the archaeology of the ancient Near East*. Chichester: Wiley-Blackwell, pp.466-484.

Okay, A., Satır, M., Tüysüz, O., Akyüz, S. and Chen, F., 2001. The tectonics of the Strandja Massif: late-Variscan and mid-Mesozoic deformation and metamorphism in the northern Aegean. *International Journal of Earth Sciences*, [e-journal] 90(2), pp.217-233. http://dx.doi.org/10.1007/s005310000104.

Okay, A. I., 2008. Geology of Turkey: A Synopsis. In: Ü. Yalçın, ed. 2008. *Anatolian Metal IV*. Bochum: Dt. Bergbau-Museum, pp.19-42.

Orris, G. J. and Bliss, J. D., 2002. *Mines and Mineral Occurrences of Afghanistan*.

Oudbashi, O., Emami, M. and Davami, P., 2012. Bronze in Archaeology. A Review of the Archaeometallurgy of Bronze in Ancient Iran. In: L. Collini, ed. 2012. *Copper alloys. Early applications and current performance: enhancing processes.* Rijeka: InTech, pp.153-178.

Paoletti, P., 2008. Elusive Silver? Evidence for the circulation of silver in the Ur III state. *Rivista di storia, ambienti e culture del Vicino Oriente Antico*, (5), pp.127-158. http://dx.doi.org/10.1002/9783527617272.

Perello, J., Razique, A., Schloderer, J. and Asad-ur-Rehman, 2008. The Chagai Porphyry Copper Belt, Baluchistan Province, Pakistan. *Economic Geology*, [e-journal] 103(8), pp.1583-1612. http://dx.doi.org/10.2113/gsecongeo.103.8.1583.

Pernicka, E., 1990. Gewinnung und Verbreitung der Metalle in prähistorischer Zeit. *Jahrbuch des Römisch-Germanischen Zentralmuseums Mainz*, (37), pp.21-136.

Pernicka, E., Adam, K., Böhme, M., Hezarkhani, Z., Nezafati, N., Schreiner, M., Winterholler, B., Momenzadeh, M. and Vatandoust, A., 2011. Archaeometallurgical research on the western Central Iranian Plateau. In: A. Vatandoust, H. Parzinger, and B. Helwing, eds. 2011. *Early mining and Metallurgy on the Western Central Iranian Plateau. The first five years of work.* Mainz, pp.633-687.

Pernicka, E. and Bachmann, H.-G., 1983. Archäometallurgische Untersuchungen zur antiken Silbergewinnung in Laurion. Das Verhalten einiger Spurenelemente beim Abtreiben des Bleis. *Erzmetall*, (36), pp.592-597.

Pernicka, E., Eibner, C., Öztunali, Ö. and Wagner, G. A., 2003. Early Bronze Age metallurgy in the North-East Aegean. In: G. A. Wagner, E. Pernicka, and Uerpmann H.-P., eds. 2003. *Troia and the Troad. Scientific Approaches*. Berlin, Heidelberg, pp.143-172.

Pernicka, E., Rehren, T. and Schmitt-Strecker, S., 1998. Late Uruk silver production by cupellation at Habuba Kabira, Syria. *Metallurgica Antiqua,* Der Anschnitt, Beiheft 8, pp.123-134.

Pernicka, E., Seelinger, T., Wagner, G. A., Begemann, F., Schmitt-Strecker, S., Eibner, C., Öztunali, Ö. and Baranyi, I., 1984. Archäometallurgische Untersuchungen in Nordwestanatolien. *Jahrbuch des Römisch-Germanischen Zentralmuseums Mainz*, (31), pp.533-599.

Pfeiffer, K., 2013. Archaeometallurgy in Sinai. The Innovation of Copper Metallurgy. In: S. Burmeister, S. Hansen, M. Kunst, and N. Müller-Scheeßel, eds. 2013. *Metal Matters. Innovative Technologies and Social Change in Prehistory and Antiquity*. Rahden/Westf.: Marie Leidorf, pp.91-103.

Pfeiffer, K., 2013. *Forschungscluster 2 / Neue Untersuchungen zur Archäometallurgie des Sinai. Die Entwicklungsgeschichte der Innovation „Kupfermetallurgie".* Rahden/Westf.: Marie Leidorf.

Philip, G. and Rehren, T., 1996. Fourth millennium BC silver from Tell esh-Shuna, Jordan. Archaeometallurgical investigation and some thought on ceramic skeuomorphs. *Oxford Journal of Archaeology*, (15-2), pp.129-150.

Philip, H., Cisternas, A., Gvishiani, A. and Gorshkov, A., 1989. The Caucasus. An actual example of the initial stages of continental collision. *Tectonophysics*, [e-journal] 161(1-2), pp.1-21. http://dx.doi.org/10.1016/0040-1951(89)90297-7.

Pigott, V. C., 1999. The Development of Metal Production on the Iranian Plateau. In: V. C. Pigott, ed. 1999. The Archaeometallurgy of the Asian Old World. Philadelphia, pp.73-106.

Pollock, S., 1985. Chronology of the Royal Cemetery of Ur. *Iraq*, (47), pp.129-158.

Potts, T. F., 1993. Patterns of Trade in Third-Millennium BC Mesopotamia and Iran. *World Archaeology*, (24, No. 3), pp.379-402.

Prange, M. K., Götze, H.-J., Hauptmann, A. and Weisgerber, G., 1999. Is Oman the Ancient Magan? Analytical Studies of Copper from Oman. In: S. M. M. Young, A. M. Pollard, P. Budd, and R. A. Ixer, eds. 1999. *Metals in Antiquity.* Oxford, pp.187-192.

Prange, M., 2001. *5000 Jahre Kupfer in Oman. Band 2: Vergleichende Untersuchungen zur Charakterisierung des omanischen Kupfers mittels chemischer und isotopischer Analysemethoden.* Bochum.

Rademakers, F. W., Rehren, T. and Pernicka, E., 2017. Copper for the Pharaoh. Identifying multiple metal sources for Ramesses' workshops from bronze and crucible remains. *Journal of Archaeological Science*, [e-journal] 80, pp.50-73. http://dx.doi.org/10.1016/j.jas.2017.01.017.

Radivojević, M., 2013. Archaeometallurgy of the Vinča culture: a case study of the site of Belovode in eastern Serbia. *Historical Metallurgy*, (47 (1)), pp.13-32.

Radivojević, M., Pendić, J., Srejić, A., Korać, M., Davey, C., Benzonelli, A., Martinón-Torres, M., Jovanović, N. and Kamberović, Ž., 2018. Experimental design of the Cu-As-Sn ternary colour diagram. *Journal of Archaeological Science*, [e-journal] 90, pp. 106-119. http://dx.doi.org/10.1016/j.jas.2017.12.001.

Radivojević, M. and Rehren, T., 2016. Paint It Black. The Rise of Metallurgy in the Balkans. *Journal of Archaeological Method and Theory*, [e-journal] 23(1), pp.200-237. http://dx.doi.org/10.1007/s10816-014-9238-3.

Radivojević, M., Rehren, T., Kuzmanovi´c-Cvetkovi´c, J., Jovanovi´c, M. and Northover, J. P., 2013. Tainted ores and the rise of the tin bronzes in Eurasia, c. 6500 years ago. *Antiquity*, (87), pp.1030-1045.

Rajabi, A., Rastad, E. and Canet, C., 2013. Metallogeny of Permian–Triassic carbonate-hosted Zn–Pb and F deposits of Iran. A review for future mineral exploration. *Australian Journal of Earth Sciences*, [e-journal] 60(2), pp. 197–216. http://dx.doi.org/10.1080/08120099.2012.754792.

Reich, M. and Vasconcelos, P. M., 2015. Geologic and Economic Significance of Supergene Metal Deposits. Elements, (11), pp.305-310.

Reiter, K., 1997. *Die Metalle im alten Orient. Unter besonderer Berücksichtigung altbabylonischer Quellen.* Münster.

Revan, M. K., Genç, Y., Maslennikov, V. V., Maslennikova, S. P., Large, R. R. and Danyushevsky, L. V., 2014. Mineralogy and trace-element geochemistry of sulfide minerals in hydrothermal chimneys from the Upper-Cretaceous VMS deposits of the eastern Pontide orogenic belt (NE Turkey). *Ore Geology Reviews*, [e-journal] 63, pp.129-149. http://dx.doi.org/10.1016/j.oregeorev.2014.05.006.

Roberts, B.W. and Thornton, C. P., eds., 2014. *Archaeometallurgy in global perspective. Methods and syntheses*. New York: Springer.

Roberts, B. W., Thornton, C. P. and Pigott, V. C., 2009. Development of metallurgy in Eurasia. *Antiquity*, [e-journal] 83(322), pp.1012-1022. http://dx.doi.org/10.1017/S0003598X00099312.

Robinson, A. G., Banks, C. J., Rutherford, M. M. and Hirst, J. P. P., 1995. Stratigraphic and structural development of the Eastern Pontides, Turkey. *Journal of the Geological Society,* [e-journal] 152(5), pp.861-872. http://dx.doi.org/10.1144/gsjgs.152.5.0861.

Rovira, S., Montero-Ruiz, I. and Renzi, M., 2009. Experimental Co-smelting to Copper-tin Alloys. In: T. L. Kienlin, and B. W. Roberts, eds. 2009. Metals and Societies. Studies in honour of Barbara S. Ottaway. Bonn.

Ruban, D.A., Al-Husseini, M.I. and Iwasaki, Y., 2007. Review of Middle East Paleozoic plate tectonics. *GeoArabia,* (12.3), 35-56.

Russel, W.A., Papanastassiou, D.A. and Tombrello, T.A., 1980. Ca isotope fractionation on the Earth and other solar system materials. *Geochimica et Cosmochimica Acta,* (42), pp.1075-1090.

Rybakov, M. and Segev, A., 2004. Top of the crystalline basement in the Levant. G*eochemistry, Geophysics, Geosystems*, [e-journal] 5(9). http://dx.doi.org/10.1029/2004GC000690.

Ryndina, N., Indenbaum, G. and Kolosova, V., 1999. Copper Production from Polymetallic Sulphide Ores in the Northeastern Balkan Eneolithic Culture. *Journal of Archaeological Science*, [e-journal] 26(8), pp.1059-1068. http://dx.doi.org/10.1006/jasc.1999.0410.

Salem, S. M., Arafa, S. A., Ramadan, T. M. and El Gammal, E. S.A., 2013. Exploration of copper deposits in Wadi El Regeita area, Southern Sinai, Egypt, with contribution of remote sensing and geophysical data. Arabian *Journal of Geosciences*, [e-journal] 6(2), pp.321-335. http://dx.doi.org/10.1007/s12517-011-0346-z.

Salonen, E., 1970. *Über das Erwerbsleben im alten Mesopotamien. Untersuchungen zu den akkadischen Berufsnamen.* Helsinki.

Santoro, L., Boni, M., Herrington, R. and Clegg, A., 2013. The Hakkari nonsulfide Zn–Pb deposit in the context of other nonsulfide Zn–Pb deposits in the Tethyan Metallogenic Belt of Turkey. *Ore Geology Reviews*, [e-journal] 53, pp.244-260. http://dx.doi.org/10.1016/j.oregeorev.2013.01.011.

Sarkar, S. C. and Dasgupta, S., 1980. Geologic setting, genesis and transformation of sulfide deposits in the northern part of Khetri copper belt, Rajasthan, India? An outline. *Mineralium Deposita,* [e-journal] 15(2). http://dx.doi.org/10.1007/BF00206508.

Schwab, M., Ratschbacher, L., Siebel, W., McWilliams, M., Minaev, V., Lutkov, V., Chen, F., Stanek, K., Nelson, B., Frisch, W. and Wooden, J. L., 2004. Assembly of the Pamirs. Age and origin of magmatic belts from the southern Tien Shan to the southern Pamirs and their relation to Tibet. *Tectonics*, [e-journal] 23(4), 1-31. http://dx.doi.org/10.1029/2003TC001583.

Searle, M. P., Robb, L. J. and Gardiner, N. J., 2016. Tectonic Processes and Metallogeny along the Tethyan Mountain Ranges of the Middle East and South Asia (Oman, Himalaya, Karakoram, Tibet, Myanmar, Thailand, Malaysia). In: J. P. Richards, ed. 2016. *Tectonics and Metallogeny of the Tethyan Orogenic Belt.* Cheyenne, Wyoming, pp.301-327.

Seeliger, T. C., Pernicka, E., Wagner, G. A., Begemann, F., Schmitt-Strecker, S., Eibner, C., Öztunalı, Ö. and Baranyi, I., 1985. Archäometallurgische Untersuchungen in Nord- und Ostanatolien. *Jahrbuch des Römisch-Germanischen Zentralmuseums Mainz*, (32), pp.597-659.

Segev, A., 1987. The age of the latest precambrian volcanism in southern israel, northeastern sinai and southwestern jordan - a re-evaluation. *Precambrian Research*, [e-journal] 36(3-4), pp.277-285. http://dx.doi.org/10.1016/0301-9268(87)90025-8.

Seltmann, R., 2013. Erzreichtum Kasachstans. In: T. Stöllner, and Z. Samašev, eds. 2013. *Unbekanntes Kasachstan. Archäologie im Herzen Asiens*. Bochum, pp.67-76.

Seltmann, R., Porter, T. M. and Pirajno, F., 2014. Geodynamics and metallogeny of the central Eurasian porphyry and related epithermal mineral systems. *A review. Journal of Asian Earth Sciences*, [e-journal] 79, pp.810-841. http://dx.doi.org/10.1016/j.jseaes.2013.03.030.

Şengör, A. M. C., Natal'in, B. A. and Burtman, V. S., 1993. Evolution of the Altaid tectonic collage and Paleozoic crustal growth in Eurasia. *Nature*, (364), pp.299-307.

Siddiqui, R. H., Mengal, J. M., Hoshino, K., Sawada, Y. and Brohi, I. A., 2011. Back-Arc Signatures represented by the Sheeted Dykes from the Muslim Bagh Ophiolite Complex, Balochistan, Pakistan. Sindh University Research Journal, (43.1), pp.51-62.

Siddiqui, R. H., Qasim Jan, M. and Asif Khan, M., 2012. Petrogenesis of Late Cretaceous lava flows from a Ceno-Tethyan island arc. The Raskoh arc, Balochistan, Pakistan. *Journal of Asian Earth Sciences*, [e-journal] 59, pp.24-38. http://dx.doi.org/10.1016/j.jseaes.2012.05.004.

Siehl, A., 1967. Zur Stratigraphie und Paläogeographie des Perm in Afghanistan. *Geologische Rundschau*, (56.1), pp.795-812.

Sillitoe, R. H., Folk, R. L. and Saric, N., 1996. *Bacteria as Mediators of Copper Sulfide Enrichment During Weathering. Science*, (272), pp.1153-1155.

Sosson, M., Rolland, Y., Müller, C., Danelian, T., Melkonyan, R., Kekelia, S., Adamia, S., Babazadeh, V., Kangarli, T., Avagyan, A., Galoyan, G. and Mosar, J., 2010. *Subductions, obduction and collision in the Lesser Caucasus (Armenia, Azerbaijan, Georgia), new insights*. Geological Society, London, Special Publications, [e-journal] 340(1), pp.329-352. http://dx.doi.org/10.1144/SP340.14.

Srimal, N., 1986. India-Asia collision: Implications from the geology of the eastern Karakoram. *Geology*, (14), pp.523-527.

Stech, T., 1999. Aspects of Early Metallurgy in Mesopotamia and Anatolia. In: V. C. Pigott, ed. 1999. T*he Archaeometallurgy of the Asian Old World*. Philadelphia, pp.59-71.

Steinmüller, K., Coats, S., Bräutigam, B. and Garry, J., 2010. *The Metalliferous Mineral Potential of Afghanistan. Synthesis of geology and metallogeny with suggestions for mineral resource development* [Accessed 5 April 2017].

Stern, R. J., Gottfried, D. and Hedge, C. E., 1984. Late Precambrian rifting and crustal evolution in the Northeastern Desert of Egypt. *Geology*, [e-journal] 12(3), pp.168-172. http://dx.doi.org/10.1130/0091-7613(1984)12<168:LPRACE>2.0.CO;2.

Stern, R. J. and Hedge, C. E., 1985. Geochronologic and isotopic constraints on Late Precambrian crustal evolution in the Eastern Desert of Egypt. *American Journal of Science*, (285), pp.97-127.

Stern, R. J., 1981. Petrogenesis and tectonic setting of late Precambrian ensimatic volcanic rocks, central eastern desert of Egypt. *Precambrian Research*, [e-journal] 16(3), pp.195-230. http://dx.doi.org/10.1016/0301-9268(81)90013-9.

Stocklin, J., 1968. Structural History and Tectonics of Iran: A Review. *AAPG Bulletin,* (52.7), pp.1229-1258.

Stocklin, J. and Nabavi, M. H., 1973. *Tectonic map of Iran. Geological Survey of Iran.*

Stos-Gale, Z. A., Gale, N. H. and Gilmore, G. R., 1984. Early Bronze Age Trojan metal sources and Anatolians in the Cyclades. *Oxford Journal of Archaeology*, [e-journal] 3(3), pp.23-44. http://dx.doi.org/10.1111/j.1468-0092.1984.tb00120.x.

Stos-Gale, Z. A. and Gale, N. H., 1981. Sources of Galena, lead and silver in Predynastic Egypt. *Revue d'Archéometrie*, pp.285-295.

Tallon, F., 1987. *Métallurgie susienne I.* Paris: Ed. de la Réunion des Musées Nationaux.

Tapponnier, P., Mattauer, M., Proust, F. and Cassaigneau, C., 1981. Mesozoic ophiolites, sutures, and arge-scale tectonic movements in Afghanistan. *Earth and Planetary Science Letters*, [e-journal] 52(2), pp.355-371. http://dx.doi.org/10.1016/0012-821X(81)90189-8.

Tarkian, M., Bock, W.-D. and Neumann, M., 1983. Geology and mineralogy of the Cu-Ni-Co-U ore deposits at Talmessi and Meeskani, central Iran. *TMPM Tschermaks Mineralogische und Petrologische Mitteilungen*, (32), pp.111-133.

Taylor, J.E., 1855. Notes on the Ruins of Muqeyer. *Journal of the Royal Asiatic Society of Great Britain and Ireland*, (15), pp.260-276.

Taylor, S. R. and McLennan, S. M., 1995. The geochemical evolution of the continental crust. *Reviews of Geophysics*, [e-journal] 33(2), p.241-241. http://dx.doi.org/10.1029/95RG00262.

Tengberg, M., Potts, D. T. and Francfort, H.-P., 2008. The golden leaves of Ur. *Antiquity*, (82), pp.925-936.

Thomalsky, J., Bräutigam, B., Karaucak, M. and Kraus, S., 2013. Early mining and metal production in Afghanistan: The first year of investigations. *Archäologische Mitteilungen*, (45), pp.199-230.

Thornton, C. P., Rehren, T. and Pigott, V. C., 2009. The production of speiss (iron arsenide) during the Early Bronze Age in Iran. *Journal of Archaeological Science*, [e-journal] 36(2), pp.308-316. http://dx.doi.org/10.1016/j.jas.2008.09.017.

Thornton, C. P., 2014. The Emergence of Complex Metallurgy on the Iranian Plateau. In: B. W. Roberts, and C. P. Thornton, eds. 2014. *Archaeometallurgy in global perspective. Methods and syntheses*. New York: Springer, pp.665-696.

Thornton, C. P., Lamberg-Karlovsky, C. C., Liezers, M. and Young, S. M.M., 2002. On Pins and Needles. Tracing the Evolution of Copper-base Alloying at Tepe Yahya, Iran, via ICP-MS Analysis of Common-place Items. *Journal of Archaeological Science*, [e-journal] 29(12), pp.1451-1460. http://dx.doi.org/10.1006/jasc.2002.0809.

Thornton, C. P. and Rehren, T., 2009. A truly refractory crucible from fourth millennium Tepe Hissar, Northeast Iran. *Journal of Archaeological Science*, [e-journal] 36(12), pp.2700-2712. http://dx.doi.org/10.1016/j.jas.2009.08.008.

Tosi, M., 1974. The Lapis Lazuli Trade across the Iranian Plateau in the 3rd Millennium B.C. In: Naples, ed. 1974. *Gururajamanjarika. studi in onore di Giuseppe Tucci*. Naples, pp.3-28.

Twaltschrelidze, A. G., 2001. Erzlagerstätten in Georgien. In: I. Gambaschidze, A. Hauptmann, R. Slotta, and Ü. Yalçın, eds. 2001. *Georgien. Schätze aus dem Land des goldenen Vlies.* Bochum, pp.78-89.

Tylecote, R. F., Ghaznavi, H. A. and Boydell, P. J., 1977. Partitioning of trace elements between the ores, fluxes, slags and metal during the smelting of copper. *Journal of Archaeological Science,* [e-journal] 4(4), pp.305-333. http://dx.doi.org/10.1016/0305-4403(77)90027-9.

Ur, J., 2012. Southern Mesopotamia. In: D. T. Potts, ed. 2012. *A companion to the archaeology of the ancient Near East*. Chichester: Wiley-Blackwell, pp.533-555.

van Hook, H. J. The ternary system Ag 2 S-Bi 2 S 3 -PbS. Economic *Geology*, (55 (4)), pp.759-788.

Vatandoust, A., Parzinger, H. and Helwing, B., eds., 2011. *Early mining and Metallurgy on the Western Central Iranian Plateau. The first five years of work*. Mainz.

Veenhof and K. R., 1972. *Aspects of old Assyrian Trade and its terminology.* Leiden.

Waetzoldt, H. and Bachmann, H.-G., 1984. Zinn- und Arsenbronzen in den Texten aus Ebla und aus dem Mesopotamien des 3. Jahrtausends. *Oriens Antiquus*, (23), pp.1-18.

Wagner, G. A., Pernicka, E., Seeliger, T. C., Öztunali, Ö., Baranyi, I., Begemann, F. and Schmitt-Strecker, S., 1984. Geologische Untersuchungen zur frühen Metallurgie in NW-Anatolien. Bulletin of the Mineral Research and Exploration in Turkey, (101/102), pp.45-81.

Wagner, G. A., Begemann, F., Eibner, C., Lutz, J., Öztunalı, Ö., Pernicka, E. and Schmitt-Strecker, S., 1989. Archäometallurgische Untersuchungen an Rohstoffquellen des Frühen Kupfers Ostanatoliens. *Jahrbuch des Römisch-Germanischen Zentralmuseums Mainz*, (36), pp.637-686.

Walley, C. D., 1998. Some outstanding issues in the geology of Lebanon and their importance in the tectonic evolution of the Levantine region. *Tectonophysics*, [e-journal] 298(1-3), pp.37-62. http://dx.doi.org/10.1016/S0040-1951(98)00177-2.

Warren, C. J., Parrish, R. R., Searle, M. P. and Waters, D. J., 2003. Dating the subduction of the Arabian continental margin beneath the Semail ophiolite, Oman. *Geology*, [e-journal] 31(10), p.889-889. http://dx.doi.org/10.1130/G19666.1.

Weeks, L., 2003. *Early Metallurgy of the Persian Gulf. Technology, Trade, and the Bronze Age World*. Boston, Leiden.

Weeks, L., 2013. Iranian metallurgy of the fourth millennium BC in its wider technological and cultural contexts. In: C. A. Petrie, and J. R. Alden, eds. 2013. *Ancient Iran and its neighbours. Local developments and long-range interactions in the fourth millennium BC*. Oxford, Oakville: Oxbow Books, pp.277-292.

Weisgerber, G., 1991. Die Suche nach dem altsumerischen Kupferland Makan. *Das Altertum*, (37), pp.76-90.

Weisgerber, G., 2007. Copper from Magan for Mesopotamian Cities. In: S. Cleuziou, and M. Tosi, eds. 2007. *In the Shadow of the Ancestors: The Prehistoric Foundations of the Early Arabian Civilization in Oman*: Ministry of Heritage and Culture, Sultanat of Oman, pp.195-196.

Wertime, T. A., 1964. *Man's first Encounters With Metallurgy. Science*, (146 (3649)), pp.1257-1267.

Westner, K.J., 2016. *Roman mining and metal production near the antique city of ULPIANA (Kosovo).* Dissertation. Frankfurt a. Main.

Wick, H., 22.09.2015. *Geochemische und isotopische Charakterisierung von karbonatischen Gefäßen aus den Gräbern von Ur, Mesopotamien und der Vergleich mit Kalkstein aus ägyptischen Steinbrüchen.* Masterarbeit. Frankfurt am Main.

Wickham, H., 2009. *Elegant Graphics for Data Analysis*. Springer Verlag New York.

Wilkinson, T. C., 2014. *Tying the Threads of Eurasia. Trans-regional routes and material flows in eastern Anatolia and western central Asia, c. 3000-1500 BC*. Leiden: Sidestone Press.

Woodhead, J. D. and Hergt, J., M., 2001. Strontium, Neodymium and Lead Isotope Analyses of NIST Glass Certified Reference Materials: SRM 610, 612, 614. *Geostandards Newsletter*, (25 - 2-3), pp.261-266.

Woolley, C. L., 1923. Excavations at Ur of the Chaldees. *The Antiquaries Journal,* [e-journal] 3(04), pp.311-333. http://dx.doi.org/10.1017/S0003581500014980.

Woolley, C. L., 1939. *Ur Excavations V. The Ziggurat and its surroundings*. Philadelphia.

Woolley, C. L., 1962. *Ur Excavations IX. The Neo-Babylonian and Persian Periods.* Philadelphia.

Woolley, C. L., 1965. *Ur Excavations VIII. The Kassite Period and the period of Assyrian Kings.* Philadelphia.

Woolley, C. L., 1974. *Ur Excavations VI. The buildings of the Third Dynasty.* Philadelphia.

Woolley, L., 1930. *Vor 5000 Jahren. Die Ausgrabungen von Ur und die Geschichte der Sumerer*. Stuttgart.

Woolley, L., 1934. *Ur Excavations II. The Royal Cemetery. A report on the predynastic and Sargonid graves excavated between 1926 and 1931*. London.

Woolley, L., 1946. Ur. The first phases. London, New York.

Woolley, L., 1955. Ur Excavations IV. The early periods. a report on the sites and objects prior in date to the third dynasty of Ur discovered in the course of the excavations. London.

Woolley, L., 1965. *Excavations at Ur: A Record of Twelve Years' Work.*

Woolley, C. L. and Mallowan, M., 1976. *Ur Excavations VII. The Old Babylonian Period.* Philadelphia.

Woolley, L. and Steigerwald, G., 1956. *Ur in Chaldäa. 12 Jahre Ausgrabungen in Abrahams Heimat.* Wiesbaden.

Yacoub, S. Y., 2011. Stratigraphy of the Mesopotamia plain. Iraqi *Bulletin of Geology and Mining*, (4), pp.1-36.

Yener, K. A., 2000. *The domestication of metals. the rise of complex metal industries in Anatolia*. Leiden, Boston, Köln.

Yener, K. A., Sayre, E. V., Joel, E. C., Özbal, H., Barnes, I. L. and Brill, R. H., 1991. Stable lead isotope studies of central taurus ore sources and related artifacts from eastern mediterranean chalcolithic and bronze age sites. *Journal of Archaeological Science*, [e-journal] 18(5), pp.541-577. http://dx.doi.org/10.1016/0305-4403(91)90053-R.

Yener, K. A., Kulakoğlu, F., Yazgan, E., Kontani, R., Hayakawa, Y. S., Lehner, J. W., Dardeniz, G., Öztürk, G., Johnson, M., Kaptan, E. and Hacar, A., 2015. New tin mines and production sites near Kültepe in Turkey. A third-millennium BC highland production model. *Antiquity*, [e-journal] 89(345), pp.596-612. http://dx.doi.org/10.15184/aqy.2015.30.

Yener, K. A., Özbal, H., Kaptan, E., Pehlivan, A. N. and Goodway, M., 1989. Kestel: An Early Bronze Age Source of Tin Ore in the Taurus Mountains, Turkey. *Science*, (244), pp.200-203.

Yener, K. A. and Vandiver, P. B., 1993. Tin processing at Göltepe, an Early Bronze Age Site in Anatolia. *American Journal of Archaeology*, (97), pp.207-238.

Yigit, O., 2009. Mineral Deposits of Turkey in Relation to Tethyan Metallogeny: Implications for Future Mineral Exploration. *Economic Geology,* (104), pp.19-51.

Yiğitbaş, E., Kerrich, R., Yılmaz, Y., Elmas, A. and Xie, Q., 2004. Characteristics and geochemistry of Precambrian ophiolites and related volcanics from the Istanbul–Zonguldak Unit, Northwestern Anatolia, Turkey. Following the missing chain of the Precambrian South European suture zone to the east. *Precambrian Research*, [e-journal] 132(1-2), pp.179-206. http://dx.doi.org/10.1016/j.precamres.2004.03.003.

Zaigham, N. A. and Mallick, K. A., 2000. Bela ophiolite zone of southern Pakistan. Tectonic setting and associated mineral deposits. *Geological Society of America Bulletin*, (112.3), 478-189.

Zak, I. and Freund, R., 1981. Asymmetry and basin migration in the dead sea rift. *Tectonophysics*, [e-journal] 80(1-4), pp.27-38. http://dx.doi.org/10.1016/0040-1951(81)90140-2.

Zettler, R. L. and Horne, L., eds., 1998. *Treasures from the Royal Tombs of Ur.* Philadelphia.

A Methods

A.1 Documentation of changes in Electron-Microprobe measurement conditions

Element	X-Ray	Crystal	Channel	Time [sec]	Position [mm]	Time [sec]		Position [mm]	
						BG+	BG-	BG+	BG-
Sb	Lα	PETJ	2	40	110.1	0	40	0	1.5
Ag	Lα	PETJ	2	40	133.1	20	20	1.5	1.5
Cu	Kα	LIF	2	40	107.2	20	20	2	2
Au	Lα	LIF	2	40	88.8	20	20	1.7	1.3
As	Lα	TAP	3	40	105.5	0	40	0	4
Sn	Lα	PETJ	4	40	115.2	20	20	1.5	1.9
Pb	Mα	PETJ	4	40	169.2	20	20	2.5	0
S	Kα	PETJ	4	40	172.1	20	20	1.7	1.7
Bi	Mα	PETJ	4	40	163.9	20	20	4.4	1.6
Zn	Kα	LIFH	5	40	100.1	20	20	1.5	1.5
Fe	Kα	LIFH	5	40	135	20	20	2.6	3
Ni	Kα	LIFH	5	40	115.7	20	20	1.5	1.5
Co	Kα	LIFH	5	40	124.8	20	20	4.5	3

Tab. A.1: Program: Ur1

Element	X-Ray	Crystal	Channel	Time [sec]	Position [mm]	Time [sec]		Position [mm]	
						BG+	BG-	BG+	BG-
Sb	Lα	PETJ	2	60	110.1	0	60	0	1.5
Ag	Lα	PETJ	2	60	133.1	30	30	1.5	1.5
Cu	Kα	LIF	2	20	107.2	10	10	2	2
As	Lα	TAP	3	60	105.5	0	60	0	4
Sn	Lα	PETJ	4	30	115.2	15	15	1.5	1.9
Pb	Mα	PETJ	4	90	169.2	90	0	2.5	0
S	Kα	PETJ	4	60	172.1	30	30	1.7	1.7
Zn	Kα	LIFH	5	20	100.1	10	10	1.5	1.5
Fe	Kα	LIFH	5	40	135	20	20	2.6	3
Ni	Kα	LIFH	5	40	115.7	20	20	1.5	1.5
Co	Kα	LIFH	5	40	124.8	20	20	4.5	3
Mn	Kα	LIFH	5	40	146.4	0	40	0	1.5

Tab. A.2: Program: Ur2-Ur6.

Element	X-Ray	Crystal	Channel	Time [sec]	Position [mm]	Time [sec]		Position [mm]	
						BG+	BG-	BG+	BG-
Sb	Lα	PETJ	2	60	110.1	0	60	0	1.5
Ag	Lα	PETJ	2	60	133.1	30	30	1.5	2.3
Cu	Kα	LIF	2	20	107.2	10	10	1.5	2
As	Lα	TAP	3	60	105.5	0	60	0	4
Sn	Lα	PETJ	4	30	115.2	15	15	1.5	1.52
Pb	Mα	PETJ	4	90	169.2	90	0	3.8	0
S	Kα	PETJ	4	60	172.1	30	30	1.7	1.7
Zn	Kα	LIFH	5	20	100.1	10	10	1.5	1.5
Fe	Kα	LIFH	5	40	135	20	20	2.6	3
Ni	Kα	LIFH	5	40	115.7	20	20	1.5	1.5
Co	Kα	LIFH	5	40	124.8	20	20	4.5	3
Mn	Kα	LIFH	5	40	146.4	0	40	0	1.5

Tab. A.3: Program: Ur7-16 and Ur18-Ur20.

Element	X-Ray	Crystal	Channel	Time [sec]	Position [mm]	Time [sec]		Position [mm]	
						BG+	BG-	BG+	BG-
As	Lα	TAP	3	60	105.5	0	60	0	4
Sb	Lα	PETJ	4	60	110.1	0	60	1.5	0
Ag	Lα	PETJ	4	60	133.1	30	30	2	3.7
Cu	Kα	LIF	4	20	107.2	10	10	1.5	1.5
Sn	Lα	PETJ	4	30	115.2	15	15	1.5	1.52
Pb	Mα	PETJ	4	90	169.2	90	0	3.8	0
S	Kα	PETJ	4	60	172.1	30	30	1.7	1.7
Zn	Kα	LIFH	5	20	100.1	10	10	1.5	1.5
Fe	Kα	LIFH	5	40	135	20	20	2.6	3
Ni	Kα	LIFH	5	40	115.7	20	20	1.5	1.5
Co	Kα	LIFH	5	40	124.8	20	20	4.5	3
Mn	Kα	LIFH	5	40	146.4	0	40	0	1.5

Tab. A.4: Program: Ur17-Without spectrometer 2.

A.2 R-Script for Pb isotope evaluation

```
############################################################
                Script for Lead Isotope Evaluation
############################################################

#### Setting directory: setwd("C:\\Users\\yourpath
mass<- read.table("mass_bias.csv", sep=";",header=TRUE)
# example mass<- read.table("Laser_25-11-16_Intensities.csv",
sep=";",header=TRUE)
#real data

#### First select all blanks:
blank<-mass[which(mass$sample2=="blank"),]
#selects all blanks

#### Calculate mean of the blanks raw intensities:
# ignore warnings
blank <- colMeans(blank[sapply(blank, is.numeric)])
# must do colMeans functions for mean of the columns
blank <- as.data.frame(blank) # back as dataframe, note, that mean Inten-
sities are written in rows not columns

#### Substract blank from samples raw intensities:
# First predefine a dataframe, with the dimensions of the finished dataset
blank_corr<-data.frame(matrix(0,nrow=length(mass$-
sample),ncol=length(mass)))
# Substract the mean of the blank from the raw intensities:
# ignore warnings
for (i in 1:length(mass$sample)) {
blank_corr[i,5:12]<- mass[i,5:12]-blank[3:10,]
}
# Add the row- and column names again:
blank_corr[,1:4]=mass[,1:4]
colnames(blank_corr) <- colnames(mass)

#### MERCURY CORRECTION ################################
Hg204_mass<-203.9730
Hg202_mass<-201.971
Hg202_204blk_corr<-blank_corr$X202Hg/blank_corr$X204Pb
Hgfactor <- 1/4.34788937409025
X204Hg<-Hg202_204blk_corr*blank_corr$X204Pb*Hgfactor
Pb204_Hgcorr <- blank_corr$X204Pb-X204Hg

# Add Hg-corrected 204Pb: blank_corr$X204Pb <- Pb204_Hgcorr
#### Calculate raw ratios: ####
Pb206_204 <- (blank_corr$X206Pb/blank_corr$X204Pb)
Pb207_204 <- (blank_corr$X207Pb/blank_corr$X204Pb)
Pb208_204 <- (blank_corr$X208Pb/blank_corr$X204Pb)
Pb207_206 <- (blank_corr$X207Pb/blank_corr$X206Pb)
```

```
Pb208_206 <- (blank_corr$X208Pb/blank_corr$X206Pb)
Pb208_207 <- (blank_corr$X208Pb/blank_corr$X207Pb)
Pb204_206 <- 1/Pb206_204

#### bind ratios together: ####
# as.character -> sample and sample2 are the names of the samples
ratios_raw <- as.data.frame(cbind(as.character(blank_corr$sample), as.character(blank_corr$sample2), blank_corr$number, blank_corr$Cycle, Pb206_204, Pb207_204, Pb208_204, Pb207_206, Pb208_206, Pb208_207, Pb204_206))
# replace headers of first 4 columns with the original names
colnames(ratios_raw)[1:4]<-colnames(blank_corr)[1:4]

# the ratios were bound together as factors and listed.
# They first have to be unlisted, then written as characters
# Otherwise R would not recognize the numbers and just write NAs
# Then convert to numeric for further calculation
ratios_raw[,3:11] <- as.numeric(as.character(unlist(ratios_raw[3:11])))

#### Outlier correction beyond the quantiles: #####
# The basic principle: The cycles count from 1-80, thus when
# jumping from cycle 80 to 1 at a new sample, it tells the loop
# to stop there, and calculate the outliers in the 3 sigma interval
# and replace the outliers with NAs.
# # As from 1-80 the next i is always bigger then the previous, it
# will stop, when 1<80
# # The quantile range is introduced at quantile(probs=c())
# -> and can be adapted to other values as well
# here 3 sigma is used (0.27 %, 99,73 %) i=1 k=1
# resets variable k if used several times in a row

while (i<length(ratios_raw[,1]))
        {
# i counts all rows until the very last row
                if (ratios_raw[i,4]<ratios_raw[i+1,4])
                {i=i+1}
# does loop until condition is not true -> e.g. 80 < 1
# the 4th column is the cycle column
                        else { for(a in 5:11)
                                {
# for the numerical data columns -> Pb isotope ratios
                                qnt <- quantile(ratios_raw[k:i,a], probs=c(0.0027,0.9973), na.rm=TRUE);
# calculates quantiles for 3 sigma
                                        for (b in k:i)
# loop for excluding the outliers within a sample
# break
# Check if the difference of k and i is the number of cycles of the last sample
                                                {
                                if (ratios_raw[b,a]<qnt[1] || ratios_raw[b,a]>qnt[2] ) {ratios_raw[b,a]<-NA}
# excludes outliers beyond 3 sigma
                                }} i=i+1; k=i}
# i=i+1 -> jumps to next row, k=i -> next sample
        }
i=1   # if used several times in a row -> resets row counts

############################################################
#### same same:
#### Does basically the same, as the outlier correction above.
#### The only difference is, that it compares the text strings of the sample names
#### It is useful, if samples are not ordered by time of measurement
# if (ratios_raw[i,1]==ratios_raw[i+1,1]) {i=i+1}
# alternative if data are not ordered by
# time, then see if the row's names are the same
# this takes longer, because it compares strings not integers:
#k=1
#while (i<length(ratios_raw[,1])) {
# i counts all rows until the very last row
# if (ratios_raw[i,1]==ratios_raw[i+1,1]) {i=i+1}
# does loop until condition is not true -> e.g. 80 < 1
#else { # for(a in 5:11) { # for the numerical data columns -> Pb isotope ratios
# qnt <- quantile(ratios_raw[k:i,a], probs=c(0.0027,0.9973), na.rm=TRUE);
# calculates quantiles for 3 sigma
# for (b in k:i)
# break
# Schauen ob i bis 80 zählt, bzw. Ende der cycles
# {
# if (ratios_raw[b,a]<qnt[1] || ratios_raw[b,a]>qnt[2] ) {ratios_raw[b,a]<-NA}
# excludes outliers beyond 3 sigma
# }} # i=i+1; k=i}
# i=i+1 -> jumps to next row, k=i -> next sample
#}
#i=1


############################################################
        If you want to do Tl-Correction -> jump to 2nd possibility
############################################################

#### 1. possibility: extract Raw ratios: ####
# aggregate puts all means together
# Calculate the mean
# Take note to 'pass' NA's, not OMIT (will ignore entire row/case)
# ignore warnings
#colnames(ratios_raw)[,2:3] <- c("number","cycle")
mass_mean<-aggregate(ratios_raw[,3:11], list(ratios_raw$sample), na.rm=TRUE, na.action = "na.pass", mean)

# ignore warnings
# Calculate standard error:
# First introduce function stderr:
# sqrt = square root
# NA are excluded

stderr <- function(x) sqrt(var(x,na.rm=TRUE)/length(na.omit(x)))

# Put all standard errors together in one file:
mass_se<-aggregate(ratios_raw[,3:11], list(ratios_raw$sample), na.rm=TRUE, stderr)

# Adding number column back on:
mass_se$number <- mass_mean$number

# Change column names so you know its the SE:
colnames(mass_se)[4:10] <- c("Pb206_204se","Pb207_204se","Pb208_204se", "Pb207_206se","Pb208_206se","Pb208_207se", "Pb204_206se")

#colnames(mass_mean)[2:3] <- c("number","cycle")
# bind standard errors to means:
mass_mean_se <- as.data.frame(cbind(mass_mean, mass_se[4:10]))

# Add the sample2 column back on:
sample2 <- aggregate(blank_corr, list(blank_corr$sample),
#na.rm=TRUE,
FUN = head)

mass_mean_se$sample2 = sample2$sample2

# order dataset by measurement order for standard-sample-bracketing:
mass_mean_se <- mass_mean_se[order(mass_mean_se$number),]

#### save file: #####
write.csv(mass_mean_se, file="yourname.csv")
# enter file names


############################################################
        If you want to do only standard-sample-bracketing, stop here
############################################################

############################################################
############################################################


############################################################
                2. possibility: Tl-Correction:
############################################################

# Natural abundance of lead Isotopes: ####
Pb204_mass<-203.9730
Pb206_mass<-205.974468
Pb207_mass<-206.9759
Pb208_mass<-207.9767

#### Beta Calculation ########################################
Tl205_Tl203_rat<-(blank_corr$X205Tl/blank_corr$X203Tl)
Tl203_mass<-202.97200
Tl205_mass<-204.97400
nat_Tl<-2.3895
beta<-log(nat_Tl/Tl205_Tl203_rat)/log(Tl205_mass/Tl203_mass)

# Calculate mass bias with Tl: ####
```

```
Pb206_204mbc <- (blank_corr$X206Pb/Pb204_Hgcorr)*(Pb206_mass/Pb204_mass)^beta
Pb207_204mbc <- (blank_corr$X207Pb/Pb204_Hgcorr)*(Pb207_mass/Pb204_mass)^beta
Pb208_204mbc <- (blank_corr$X208Pb/Pb204_Hgcorr)*(Pb208_mass/Pb204_mass)^beta
Pb207_206mbc <- (blank_corr$X207Pb/blank_corr$X206Pb)*(Pb207_mass/Pb206_mass)^beta
Pb208_207mbc <- (blank_corr$X208Pb/blank_corr$X207Pb)*(Pb208_mass/Pb207_mass)^beta
Pb208_206mbc <- (blank_corr$X208Pb/blank_corr$X206Pb)*(Pb208_mass/Pb206_mass)^beta
Pb204_206mbc <- Pb206_204mbc

#### bind ratios together: ####
# as.character -> sample and sample2 are the names of the samples
ratios_raw <- as.data.frame(cbind(as.character(blank_corr$sample), as.character(blank_corr$sample2), blank_corr$number, blank_corr$Cycle, Pb206_204mbc, Pb207_204mbc, Pb208_204mbc, Pb207_206mbc, Pb208_206mbc, Pb208_207mbc, Pb204_206mbc))

# replace headers of first 4 columns with the original names
colnames(ratios_raw)[1:4]<-colnames(blank_corr)[1:4]

# the ratios were bound together as factors and listed.
# They first have to be unlisted, then written as characters
# Otherwise it would not recognise the numbers and just write NAs
# Then convert to numeric in order to further calculate with them
ratios_raw[,3:11] <- as.numeric(as.character(unlist(ratios_raw[3:11])))
#### Outlier correction beyond the quantiles: #####
# The basic principle: The cycles count from 1-80, thus when
# jumping from cycle 80 to 1 at a new sample, it tells the loop
# to stop there, and calculate the outliers in the 3 sigma interval
# and replace the outliers with NAs. #
# As from 1-80 the next i is always bigger then the previous, it
# will stop, when 1<80 #
# The quantile range is introduced at quantile(probs=c())
# -> and can be adapted to other values as well
# here 3 sigma is used (0.27 %, 99,73 %)

k=1

# resets variable k if used several times in a row

while (i<length(ratios_raw[,1]))
        {
# i counts all rows until the very last row
        if (ratios_raw[i,4]<ratios_raw[i+1,4]) {i=i+1}
# does loop until condition is not true -> e.g. 80 < 1
                else { for(a in 5:11) {
# for the numerical data columns -> Pb isotope ratios
                        qnt <- quantile(ratios_raw[k:i,a], probs=c(0.0027,0.9973), na.rm=TRUE);
# calculates quantiles for 3 sigma for (b in k:i)
# loop for excluding the outliers within a sample
# break
# Check if the difference of k and i is the number of cycles of the last sample
                        { if (ratios_raw[b,a]<qnt[1] || ratios_raw[b,a]>qnt[2] ) {ratios_raw[b,a]<-NA}
# excludes outliers beyond 3 sigma
                        }} i=i+1; k=i}
# i=i+1 -> jumps to next row, k=i -> next sample
        }

i=1
# if used several times in a row -> resets row counts

#############################################################
#
#### same same:
#### Does basically the same, as the outlier correction above.
#### The only difference is, that it compares the text strings of the sample names
#### It is usefull, if samples are not ordered by time of measurement
# if (ratios_raw[i,1]==ratios_raw[i+1,1]) {i=i+1}
# alternative if data are not ordered by
# time, then see if the row's names are the same # this takes longer, because it compares strings not integers:
# k=1 while (i<length(ratios_raw[,1])) {
# i counts all rows until the very last row if (ratios_raw[i,1]==ratios_raw[i+1,1]) {i=i+1}
# does loop until condition is not true -> e.g. 80 < 1
# else { for(a in 5:11) {
# for the numerical data columns -> Pb isotope ratios
# qnt <- quantile(ratios_raw[k:i,a], probs=c(0.0027,0.9973), na.rm=TRUE);
# calculates quantiles for 3 sigma for (b in k:i)
# break
# Schauen ob i bis 80 zählt, bzw. Ende der cycles
# { if (ratios_raw[b,a]<qnt[1] || ratios_raw[b,a]>qnt[2] ) {ratios_raw[b,a]<-NA}
# excludes outliers beyond 3 sigma
# }} i=i+1; k=i}
# i=i+1 -> jumps to next row, k=i -> next sample
# } i=1



#############################################################
                aggregate the means and standard errors
#############################################################

###############         Calculate the mean          ###############

# Take note to 'pass' NA's, not OMIT (will ignore entire row/case)
mass_mean<-aggregate(ratios_raw[,2:11], list(ratios_raw$sample), na.rm=TRUE, na.action = "na.pass", mean) mass_sd<-aggregate(ratios_raw[,2:11], list(ratios_raw$sample), na.rm=TRUE, sd)

###############       Calculate standard error      ###############
# First introduce function stderr:
# sqrt = square root
# NA are excluded

stderr <- function(x) sqrt(var(x,na.rm=TRUE)/length(na.omit(x)))

#### Put all standard errors together in one file: ####
mass_se<-aggregate(ratios_raw[,3:11], list(ratios_raw$sample),
#na.rm=TRUE,
stderr)

# Adding number column back on: mass_se$number <- mass_mean$number
#### save file: #####

write.csv(mass_mean, file="yourname.csv")
write.csv(mass_se, file="yourname.csv")

#############################################################
#####################  ##############################
#################################################
#### If you did standard-sample-bracketing with Excel: #####
#### Calculate means of finished data ####
std_spl_bracket<- read.table("yourname.csv", sep=";",header=TRUE) # read in data
lead_means<-aggregate(std_spl_bracket[,6:12], list(std_spl_bracket$sample),
#na.rm=TRUE,
mean)

#### Error Propagation #####
errorprop <- function(x,y) sqrt(na.pass(x)^2+na.pass(y)^2)
lead_SE<-aggregate(std_spl_bracket[,6:12], list(std_spl_bracket$sample),
#na.rm=TRUE,
stderr)

lead_SE2 <- aggregate(std_spl_bracket[,13:19], list(std_spl_bracket$sample),
#na.rm=TRUE,
mean)


lead_errors <- errorprop(lead_SE[,2:8],lead_SE2[,2:8])
lead_means <- as.data.frame(cbind(lead_means, lead_errors))

#############################################################
##################
##### If you measured copper artefacts with laserablation: ####
#### After standard sample bracketing, and calculations of each mean per sample
#### Laser mass bias correction for copper:
# Natural abundance of lead Isotopes: ####

Pb204_mass<-203.9730
Pb206_mass<-205.974468
Pb207_mass<-206.9759
Pb208_mass<-207.9767

# the beta was calculated, as follows:
# after Russel (1980): beta = ln(Solution Pb206/204//Laser Pb206/204)/
# ln(atomic mass Pb206 / atomic mass Pb204) #
```

```
beta206_204 <- (log(begemann$Pb206_204/begelaser$Pb206_204))/(log(Pb206_mass/Pb204_mass))

# The beta was calculated for each 204 based ratio:
# beta206_204 <- (log(begemann$Pb206_204/begelaser$Pb206_204))/(log(Pb206_mass/Pb204_mass))
# beta207_204 <- (log(begemann[,6]/begelaser[,5]))/(log(Pb207_mass/Pb204_mass))
# beta208_204 <- (log(begemann[,7]/begelaser[,6]))/(log(Pb208_mass/Pb204_mass))
# This lead to different betas of which the mean was calculated:
# betamean <- mean(c(betamean206_204, betamean207_204, betamean208_204))
# This is the result calculated from the Laser and solution data of this thesis
# and the artefacts measured by Begemann and Schmitt-Strecker, 2009 for copper:

betamean <- 0.0723545138687956

# Here are the ratios corrected with the normal mass bias correction and the # calculated beta:

lead_means$Pb206_204 <- lead_means$Pb206_204*(Pb206_mass/Pb204_mass)^betamean
lead_means$Pb207_204 <- lead_means$Pb207_204*(Pb207_mass/Pb204_mass)^betamean
lead_means$Pb208_204 <- lead_means$Pb208_204*(Pb208_mass/Pb204_mass)^betamean
lead_means$Pb207_206 <- lead_means$Pb207_206*(Pb207_mass/Pb206_mass)^betamean
lead_means$Pb208_206 <- lead_means$Pb208_206*(Pb208_mass/Pb206_mass)^betamean
lead_means$Pb208_207 <- lead_means$Pb208_207*(Pb208_mass/Pb207_mass)^betamean
lead_means$Pb204_206 <- 1/lead_means$Pb206_204

# save as csv-file write.csv(lead_means, file = "yourname.csv")
```

B Analytical Results

B.1 Electron microprobe results

sample nr.	n	S	± 2SE	Fe	± 2SE	Co	± 2SE	Ni	± 2SE	Cu	± 2SE	As
30-12-264.1	19	0,127	0,037	0,170	0,011	0,014	0,001	0,41	0,01	90,2	1,0	0,87
30-12-272.1	20	1,106	0,182	0,185	0,011	<0.011	b.d.	0,46	0,02	87,6	0,6	0,65
30-12-272.2	22	0,592	0,734	0,279	0,140	0,013	0,001	0,47	0,02	88,5	0,9	0,58
30-12-284.1	18	0,052	0,057	0,171	0,017	<0.012	b.d.	0,17	0,01	86,5	0,9	0,22
30-12-285.1	18	0,568	0,198	0,074	0,016	0,062	0,004	0,38	0,07	97,6	0,6	1,13
30-12-321.1	23	0,057	0,013	0,120	0,005	<0.014	b.d.	0,107	0,004	89,6	0,4	0,42
30-12-373.1	15	0,150	0,166	0,240	0,034	0,013	0,001	0,68	0,03	96,7	0,5	1,17
30-12-375.1	13	0,080	0,084	0,168	0,011	0,016	0,003	0,47	0,02	97,7	0,4	1,06
30-12-380.1	12	0,039	0,030	0,118	0,013	0,127	0,003	1,79	0,02	94,5	0,1	2,73
30-12-382.1	16	0,017	0,005	0,139	0,010	<0.011	b.d.	0,21	0,01	88,1	0,9	0,47
30-12-416.1	26	0,014	0,002	0,127	0,004	0,013	0,001	0,253	0,004	91,0	0,7	0,23
30-12-696.1	17	0,675	0,122	0,012	0,001	<0.012	b.d.	0,140	0,004	91,4	0,7	0,28
30-12-696.2	8	n.m.	n.m.	<0.02	b.d.	<0.017	b.d.	0,16	0,01	93,1	2,4	0,25
31-17-186.1	25	0,029	0,003	0,132	0,007	<0.014	b.d.	0,57	0,01	90,1	1,2	0,14
31-17-193.1	14	0,058	0,061	0,070	0,005	0,041	0,003	0,98	0,04	97,2	0,3	1,40
31-17-201.1	26	0,192	0,259	0,027	0,015	0,095	0,003	2,41	0,07	93,7	0,5	3,26
31-17-205.1	33	0,066	0,013	0,035	0,002	0,023	0,004	0,65	0,06	90,2	1,0	1,59
31-17-217.2	9	0,719	0,777	0,343	0,026	0,025	0,004	0,88	0,08	90,6	1,9	2,06
31-17-217.3	39	1,001	0,083	0,338	0,009	0,027	0,002	0,85	0,01	90,5	0,3	1,94
31-17-265.1	39	0,037	0,039	0,079	0,007	0,016	0,001	0,064	0,002	90,1	0,5	0,42
31-17-266.1	15	0,065	0,021	0,171	0,111	0,129	0,005	1,90	0,05	94,3	0,3	2,88
31-17-267.1	25	0,054	0,075	0,162	0,009	0,011	0,001	0,30	0,01	98,0	0,2	1,16
31-17-352.1	15	0,025	0,004	<0.01	b.d.	<0.012	b.d.	0,022	0,003	99,1	0,7	0,22
33-35-79.1	20	1,661	0,114	0,020	0,006	<0.01	b.d.	2,50	0,03	92,8	0,2	2,56
35-1-422.1	6	0,234	0,265	0,223	0,019	0,052	0,004	2,72	0,10	91,6	0,4	4,66
35-1-422.2	17	0,109	0,079	0,216	0,005	0,284	0,006	2,68	0,03	93,5	0,3	2,58
35-1-422.3	13	0,055	0,080	0,219	0,009	0,293	0,006	2,73	0,04	93,5	0,3	2,74
35-1-479.1	21	0,330	0,187	0,175	0,005	0,075	0,002	1,00	0,02	95,2	0,3	2,31
98-9-164	7	n.m.	n.m.	0,05	0,01	0,026	0,003	0,39	0,03	99,4	0,8	0,017
B16409.1	23	0,016	0,003	0,196	0,008	0,145	0,006	3,17	0,06	91,5	0,5	4,15
B16409.2	29	0,021	0,004	0,162	0,007	0,034	0,002	0,44	0,01	97,8	0,2	1,27
B16409.3	16	0,114	0,106	0,170	0,011	0,035	0,003	0,44	0,01	97,7	0,3	1,24
B16409.4	36	0,018	0,003	0,168	0,005	0,035	0,002	0,43	0,01	97,7	0,2	1,31
B16937.1	19	0,017	0,008	0,184	0,006	<0.012	b.d.	0,31	0,01	88,4	0,8	0,17
B16954.1	29	0,018	0,004	0,025	0,002	0,021	0,002	0,063	0,003	89,4	0,8	0,12
B16996.1	28	0,033	0,024	0,152	0,005	<0.011	b.d.	0,44	0,01	88,3	0,6	0,21
B17022.1	24	0,015	0,002	0,459	0,008	0,015	0,001	0,372	0,004	91,0	0,4	1,26
B17276.2	31	0,021	0,009	0,267	0,008	0,048	0,002	0,282	0,005	97,2	0,1	1,73
B17317.1	22	0,139	0,055	0,544	0,016	0,013	0,001	1,09	0,02	95,5	0,3	1,86
B17327.1	14	0,126	0,025	0,249	0,147	<0.012	b.d.	0,74	0,02	87,2	0,6	b.d.
B17330.1	25	0,395	0,169	0,402	0,025	<0.012	0,000	0,030	0,005	89,9	0,4	0,21
B17335.1	12	0,042	0,016	0,094	0,050	<0.01	b.d.	0,021	0,004	99,4	0,7	0,31
B17347.1	15	0,023	0,004	0,195	0,009	<0.011	b.d.	0,023	0,003	89,4	0,9	0,27

± 2SE	Ag	± 2SE	Sn	± 2SE	Sb	± 2SE	Pb	± 2SE	Total norm	Total
0,09	0,054	0,008	7,99	0,92	0,056	0,006	0,06	0,01	100,0	100,1
0,03	<0.023	b.d.	9,89	0,69	0,08	0,009	<0.054	b.d.	100,0	100,7
0,04	<0.023	b.d.	9,33	0,63	0,08	0,008	0,13	0,05	100,0	101,8
0,01	<0.023	b.d.	12,84	0,42	0,03	0,003	<0.048	b.d.	100,0	101,0
0,27	<0.023	b.d.	0,05	0,01	0,13	0,019	<0.046	b.d.	100,0	100,5
0,01	0,058	0,008	9,57	0,21	0,04	0,004	<0.046	b.d.	100,0	100,7
0,04	0,038	0,007	0,17	0,01	0,14	0,003	0,69	0,57	100,0	101,7
0,06	<0.023	b.d.	0,042	0,005	0,12	0,009	0,37	0,13	100,0	101,2
0,02	<0.023	b.d.	0,24	0,01	0,34	0,007	0,17	0,09	100,0	101,4
0,03	<0.023	b.d.	10,32	0,72	0,06	0,005	0,74	0,51	100,0	101,2
0,01	<0.023	b.d.	8,19	0,46	0,03	0,003	0,09	0,02	100,0	100,5
0,02	<0.023	b.d.	7,42	0,73	0,06	0,007	0,06	0,00	100,0	100,3
0,11	0,05	0,03	6,1	2,3	0,055	0,018	<0.047	b.d.	100,0	102,5
0,03	<0.023	b.d.	8,98	1,02	0,03	0,005	<0.048	b.d.	100,0	100,9
0,08	0,032	0,006	0,12	0,01	0,043	0,003	0,06	0,01	100,0	101,2
0,14	<0.023	b.d.	<0.035	b.d.	0,088	0,005	0,21	0,07	100,0	100,3
0,17	0,085	0,015	6,98	0,73	0,12	0,03	0,21	0,09	100,0	100,3
0,37	0,189	0,054	5,04	0,49	0,077	0,008	0,09	0,02	100,0	100,8
0,04	0,249	0,041	4,82	0,12	0,080	0,004	0,20	0,11	100,0	100,6
0,01	<0.023	b.d.	8,87	0,32	0,121	0,005	0,27	0,11	100,0	101,1
0,14	0,072	0,007	0,037	0,004	0,33	0,02	0,20	0,12	100,0	100,9
0,10	0,091	0,012	0,031	0,001	0,081	0,007	0,17	0,09	100,0	101,5
0,06	0,044	0,020	<0.028	b.d.	0,032	0,003	0,57	0,16	100,0	100,6
0,04	0,052	0,004	<0.028	b.d.	0,093	0,005	0,28	0,16	100,0	100,7
0,47	0,055	0,013	0,07	0,01	0,214	0,009	0,20	0,20	100,0	101,5
0,11	<0.023	b.d.	0,05	0,01	0,347	0,014	0,31	0,16	100,0	101,4
0,10	<0.023	b.d.	0,05	0,01	0,372	0,013	0,08	0,01	100,0	101,8
0,11	<0.023	b.d.	0,32	0,02	0,229	0,011	0,39	0,26	100,0	101,2
0,011	<0.041	b.d.	<0.013	b.d.	0,036	0,003	<0.047	b.d.	100,0	100,9
0,15	0,049	0,007	0,18	0,01	0,661	0,029	<0.054	b.d.	100,0	101,0
0,06	<0.023	b.d.	0,12	0,01	0,137	0,010	0,069	0,004	100,0	101,3
0,05	<0.023	b.d.	0,12	0,01	0,118	0,007	0,07	0,01	100,0	101,1
0,02	<0.023	b.d.	0,12	0,01	0,137	0,006	0,070	0,005	100,0	100,6
0,01	<0.023	b.d.	10,84	0,44	0,029	0,003	0,063	0,005	100,0	101,2
0,01	0,078	0,006	10,27	0,49	0,027	0,001	<0.052	b.d.	100,0	100,5
0,01	<0.023	b.d.	10,89	0,29	0,029	0,002	<0.055	b.d.	100,0	101,1
0,02	<0.023	b.d.	6,54	0,08	0,222	0,005	0,16	0,07	100,0	100,3
0,10	0,256	0,013	0,11	0,01	0,096	0,004	0,06	0,01	100,0	100,9
0,07	<0.023	b.d.	0,05	0,01	0,356	0,015	0,46	0,26	100,0	99,4
b.d.	<0.023	b.d.	11,59	0,34	0,025	0,001	<0.052	b.d.	100,0	99,4
0,01	<0.023	b.d.	8,99	0,45	0,048	0,005	<0.048	b.d.	100,0	100,7
0,54	0,057	0,024	<0.028	b.d.	0,040	0,004	<0.048	b.d.	100,0	101,2
0,02	0,092	0,016	9,60	0,42	0,032	0,004	0,37	0,28	100,0	100,3

Tab. B1: Results of electron microprobe analysis of the copper-based artefacts in wt%. The errors are given as two standard errors. Zn and Mn were below detection limit in all artefacts and are not given. The results are normalised to 100 wt% and the original sum is given behind. (abbr.: n=number of point analysis, n.m.=not measured, b.d.=below detection limit).

sample nr.	n	S	± 2SE	Fe	± 2SE	Co	± 2SE	Ni	± 2SE	Cu	± 2SE	As
B17351.1	24	0,310	0,166	0,626	0,038	0,014	0,001	2,40	0,06	90,9	0,3	3,21
B17356.2	20	0,066	0,011	0,154	0,075	0,012	0,001	0,78	0,04	96,7	0,3	1,77
B17356.3	15	0,039	0,014	0,105	0,009	0,011	0,001	0,81	0,03	97,3	0,1	1,39
B17356.4	29	0,043	0,015	0,134	0,038	0,013	0,001	0,79	0,02	96,8	0,2	1,76
B17389.1	14	0,024	0,005	0,521	0,011	0,027	0,003	0,67	0,02	96,4	0,5	1,69
B17410.1	6	0,040	0,014	0,147	0,022	<0.014	b.d.	0,14	0,04	88,3	3,1	0,43
B17411.1	8	0,903	0,835	0,019	0,005	<0.011	b.d.	<0.014	b.d.	99,0	1,1	0,01
B17418.1	4	0,412	0,525	0,119	0,009	0,077	0,009	1,15	0,07	96,6	3,3	1,50
B17422.1	15	0,159	0,092	0,437	0,015	0,030	0,003	0,64	0,01	96,7	0,2	1,59
B17426.1	15	0,027	0,005	0,178	0,008	0,044	0,003	1,85	0,08	93,5	0,3	3,26
B17426.2	21	2,028	0,504	0,194	0,012	0,045	0,002	1,79	0,04	92,9	0,7	1,89
B17445.1	16	0,049	0,010	0,148	0,004	0,029	0,003	0,96	0,03	96,2	0,2	1,95
B17460.1	14	0,317	0,177	0,488	0,015	0,299	0,011	2,07	0,04	94,4	0,4	2,15
B17460.2	18	0,128	0,111	0,472	0,027	0,281	0,012	2,03	0,05	93,1	0,4	3,33
B17469.1	34	0,020	0,003	0,314	0,011	<0.013	b.d.	0,101	0,004	91,1	0,3	0,37
B17474.1	15	0,138	0,098	0,707	0,039	0,015	0,002	1,37	0,03	94,0	0,4	3,43
B17478.1	22	0,188	0,037	0,605	0,010	0,041	0,002	1,25	0,02	92,8	0,3	1,97
B17479.1	28	0,133	0,037	0,197	0,009	0,033	0,003	0,88	0,03	91,1	0,7	2,70
B17480.1	25	0,105	0,117	0,363	0,031	0,018	0,002	0,38	0,01	87,8	0,5	0,30
B17488.1	25	0,839	0,483	0,666	0,026	0,081	0,004	2,46	0,07	92,4	0,5	3,25
B17494.1	32	0,058	0,016	0,427	0,012	0,014	0,001	0,198	0,003	91,9	0,5	0,42
B17495.1	21	0,072	0,017	0,065	0,002	0,015	0,002	0,74	0,02	87,3	0,6	0,93
B17496.1	18	0,036	0,019	0,285	0,005	0,023	0,002	0,57	0,01	96,8	0,4	1,47
B17508.1	15	0,260	0,117	0,797	0,156	0,413	0,072	9,89	1,23	88,1	1,6	0,48
B17508.2	23	0,137	0,017	0,963	0,112	0,486	0,051	11,07	0,86	87,0	0,9	0,37
B17516.1	16	1,102	0,303	0,235	0,013	0,147	0,005	1,11	0,03	95,2	0,4	1,67
B17525.1	15	0,697	0,254	0,018	0,004	<0.015	b.d.	<0.015	b.d.	99,2	0,4	b.d.
B17528a.1	16	0,173	0,169	0,309	0,041	0,078	0,004	0,33	0,04	97,1	0,5	1,96
B17528a.2	19	0,044	0,045	0,324	0,152	0,028	0,004	0,68	0,24	97,6	1,0	0,97
B17528b.1	17	0,052	0,036	0,813	0,013	0,035	0,002	1,13	0,02	96,1	0,3	1,61
B17551	6	n.m.	n.m.	<0.014	0,03	0,015	0,001	3,78	0,52	92,3	2,4	<0.024

sample nr.	n	Ag	± 2SE	Cu	± 2SE	Pb	± 2SE	Cr	± 2SE	Ni	± 2SE	Fe
30-12-253.1	18	98,8	0,47	0,34	0,39	0,530	0,014	0,027	0,005	0,034	0,006	0,119
30-12-253.3	25	99,6	0,32	0,12	0,03	<0.047	b.d.	0,036	0,010	0,038	0,007	0,099
30-12-446	10	89,6	3,84	6,95	2,73	1,479	3,037	<0.013	b.d.	<0.019	b.d.	<0.013
30-12-605	8	97,2	0,60	2,55	0,08	0,145	0,021	<0.013	b.d.	<0.019	b.d.	<0.013
30-12-754	17	93,9	0,44	5,24	0,20	0,734	0,015	<0.012	b.d.	<0.016	b.d.	<0.013
30-12-773	13	93,8	0,53	5,40	0,35	0,737	0,022	<0.012	b.d.	0,021	0,003	<0.013
31-17-280a	14	98,2	0,42	1,60	0,18	0,113	0,016	<0.012	b.d.	<0.019	b.d.	<0.013
B16926a	15	96,7	0,41	2,97	0,14	0,182	0,012	<0.01	b.d.	0,025	0,004	<0.013
B16931a	13	96,6	0,45	2,58	0,36	0,155	0,047	<0.012	b.d.	<0.017	b.d.	<0.013
B16931b	8	96,7	0,64	2,62	0,62	0,161	0,066	<0.013	b.d.	<0.019	b.d.	<0.013
B17078a	12	99,7	0,55	0,14	0,07	<0.047	b.d.	<0.012	b.d.	<0.017	b.d.	0,022
B17082a	9	99,6	0,95	0,21	0,09	<0.047	b.d.	<0.013	b.d.	<0.019	b.d.	0,041
B17084	10	95,3	0,41	4,12	0,38	0,433	0,031	<0.013	b.d.	<0.018	b.d.	<0.011
B17553b	9	96,7	1,38	2,71	0,41	0,603	0,096	<0.013	b.d.	<0.023	b.d.	<0.014

± 2SE	Ag	± 2SE	Sn	± 2SE	Sb	± 2SE	Pb	± 2SE	Total Norm	Total
0,11	0,070	0,006	1,85	0,07	0,237	0,010	0,36	0,13	100,0	100,0
0,21	0,157	0,024	0,15	0,02	0,116	0,013	0,10	0,01	100,0	100,7
0,07	0,134	0,014	0,12	0,01	0,094	0,005	<0.056	b.d.	100,0	100,6
0,10	0,155	0,015	0,15	0,01	0,116	0,007	0,061	0,002	100,0	101,3
0,12	<0.023	b.d.	0,16	0,07	0,344	0,046	0,19	0,10	100,0	101,1
0,07	0,027	0,011	10,82	1,03	0,045	0,009	0,08	0,03	100,0	97,8
0,03	0,032	0,028	<0.028	b.d.	b.d.	b.d.	<0.048	b.d.	100,0	100,5
0,23	<0.023	b.d.	0,08	0,02	0,079	0,026	<0.052	b.d.	100,0	99,0
0,07	0,025	0,005	0,04	0,01	0,232	0,012	0,14	0,04	100,0	101,6
0,20	<0.023	b.d.	0,92	0,06	0,159	0,017	0,14	0,09	100,0	101,3
0,29	<0.023	b.d.	0,53	0,09	0,103	0,011	0,52	0,44	100,0	100,9
0,11	0,073	0,009	0,39	0,03	0,084	0,007	0,129	0,004	100,0	100,6
0,28	<0.023	b.d.	0,07	0,01	0,182	0,020	0,08	0,01	100,0	101,6
0,13	<0.023	b.d.	0,13	0,01	0,278	0,013	0,22	0,11	100,0	100,1
0,01	<0.023	b.d.	7,91	0,29	0,046	0,004	0,11	0,04	100,0	100,2
0,24	<0.023	b.d.	0,14	0,02	0,038	0,003	0,14	0,04	100,0	100,7
0,05	0,040	0,005	2,58	0,07	0,165	0,006	0,36	0,14	100,0	100,4
0,31	0,042	0,010	4,74	0,40	0,068	0,008	0,09	0,01	100,0	99,4
0,01	0,024	0,005	10,91	0,26	0,034	0,003	0,09	0,01	100,0	100,9
0,20	<0.023	b.d.	<0.034	b.d.	0,264	0,008	0,09	0,02	100,0	101,1
0,02	<0.023	b.d.	6,77	0,32	0,116	0,006	0,05	0,01	100,0	100,4
0,03	<0.023	b.d.	10,46	0,28	0,031	0,002	0,43	0,26	100,0	100,8
0,05	<0.023	b.d.	0,046	0,005	0,195	0,014	0,56	0,39	100,0	101,6
0,07	<0.023	b.d.	<0.029	b.d.	0,027	0,001	<0.065	b.d.	100,0	101,6
0,05	<0.023	b.d.	<0.029	b.d.	0,033	0,002	<0.053	b.d.	100,0	102,2
0,07	<0.023	b.d.	<0.028	b.d.	0,422	0,020	0,09	0,02	100,0	100,4
b.d.	<0.023	b.d.	0,08	0,04	0,031	0,001	<0.059	b.d.	100,0	100,5
0,30	<0.023	b.d.	0,06	0,01	0,039	0,004	<0.059	b.d.	100,0	100,4
0,49	0,113	0,095	0,04	0,01	0,100	0,022	0,06	b.d.	100,0	101,9
0,05	0,094	0,006	0,039	0,005	0,096	0,004	0,08	0,02	100,0	100,5
2,1	<0.026	0,49	<0.02	b.d.	0,045	0,010	<0.069	b.d.	100,0	102,3

Tab. B2: Continuation of results of electron microprobe analysis of the copper-based artefacts in wt%. The errors are given as two standard errors. Zn and Mn were below detection limit in all artefacts and are not given. The results are normalised to 100 wt% and the original sum is given behind. (abbr.: n=number of point analysis, n.m.=not measured, b.d.=below detection limit).

± 2SE	As	± 2SE	Sb	± 2SE	Sn	± 2SE	Au	± 2SE	Total norm	Total
0,054	<0.036	b.d.	<0.033	b.d.	<0.021	b.d.	<0.158	b.d.	100,00	101,07
0,025	<0.036	b.d.	<0.03	b.d.	<0.02	b.d.	<0.144	b.d.	100,00	100,79
b.d.	<0.036	b.d.	<0.03	b.d.	<0.021	b.d.	<0.158	b.d.	100,00	101,35
b.d.	<0.036	b.d.	<0.033	b.d.	<0.021	b.d.	<0.158	b.d.	100,00	99,931
b.d.	<0.036	b.d.	<0.03	b.d.	<0.02	b.d.	<0.144	b.d.	100,00	100,41
b.d.	<0.036	b.d.	<0.03	b.d.	<0.02	b.d.	<0.144	b.d.	100,00	100,24
b.d.	<0.036	b.d.	<0.03	b.d.	<0.02	b.d.	<0.144	b.d.	100,00	99,745
b.d.	<0.036	b.d.	<0.03	b.d.	<0.02	b.d.	<0.144	b.d.	100,00	100,32
b.d.	<0.036	b.d.	<0.03	b.d.	<0.02	b.d.	0,468	0,044	100,00	100,23
b.d.	<0.036	b.d.	<0.033	b.d.	<0.021	b.d.	0,458	0,047	100,00	100,11
0,007	<0.036	b.d.	<0.03	b.d.	<0.02	b.d.	<0.144	b.d.	100,00	100,35
0,008	0,034	0,003	<0.033	b.d.	<0.021	b.d.	<0.158	b.d.	100,00	94,86
b.d.	<0.036	b.d.	<0.033	b.d.	<0.021	b.d.	<0.158	b.d.	100,00	100,0
b.d.	0,031	0,004	<0.033	b.d.	<0.021	b.d.	<0.158	b.d.	100,00	95,53

Tab. B3: Results of electron microprobe analysis of the silver artefacts in wt%. The errors are given as two standard errors. Ti, Mn, Zn, Pt, and Bi were below detection limit in all artefacts and are not given. The results are normalised to 100 wt% and the original sum is given behind. (abbr.: n=number of point analysis, n.m.=not measured, b.d.=below detection limit).

B.2 Mass spectrometry results

sample nr.	Cr	± 2SE	Mn	± 2SE	Co	± 2SE	Zn	± 2SE	Ge	± 2SE	Se	± 2SE	Pd	± 2SE	Cd
30-12-285	8,8	2,0	4,3	0,9	751	200	19,7	0,5	0,8	0,07	220	57	0,6	0,08	b.d.
30-12-380	2,3	0,7	1,4	0,3	1541	377	102,4	18,5	b.d.	b.d.	155	18	0,2	0,02	0,3
30-12-696	38,7	8,3	25,8	4,7	5	1	4,9	1,4	0,5	0,08	127	28	0,5	0,08	0,9
31-17-193	16,3	4,6	1,3	0,3	231	59	12,3	3,1	0,8	0,04	86	7	b.d.	b.d.	0,2
31-17-201	1,2	b.d.	b.d.	b.d.	987	347	4,4	1,3	0,4	0,09	70	27	b.d.	b.d.	0,3
31-17-266	4,8	0,9	2,6	0,5	1361	354	7,6	0,1	1,3	0,10	79	20	b.d.	b.d.	0,2
31-17-267	8,9	2,5	4,0	0,9	87	24	9,9	2,8	0,8	b.d.	76	5	b.d.	b.d.	b.d.
31-17-352	31,3	15,8	b.d.	b.d.	0	0	9,9	2,8	2,9	0,56	392	110	b.d.	b.d.	5,1
30-12-373	b.d.	b.d.	b.d.	b.d.	105	26	20,5	5,1	b.d.	b.d.	275	24	0,4	0,06	b.d.
30-12-375	16,0	4,5	b.d.	b.d.	164	44	8,1	2,2	b.d.	b.d.	140	11	0,3	0,04	0,3
33-35-079	b.d.	b.d.	b.d.	b.d.	18	5	2,0	0,1	0,5	0,04	43	11	0,1	0,01	0,3
35-1-344.1	2,9	0,9	b.d.	b.d.	686	168	9,7	1,6	b.d.	b.d.	23	3	0,2	0,03	0,3
35-1-344.3	b.d.	b.d.	b.d.	b.d.	3405	836	7,7	1,2	b.d.	b.d.	59	7	b.d.	b.d.	b.d.
35-1-422.2	2,0	0,5	b.d.	b.d.	2729	664	6,2	0,7	0,2	0,01	60	14	0,1	0,01	0,2
35-1-479	7,3	2,2	6,7	1,2	1156	288	17,4	2,2	b.d.	b.d.	64	9	0,7	0,09	b.d.
B16409.1	1,7	0,5	b.d.	b.d.	1764	423	3,2	0,4	0,2	0,01	45	11	0,1	0,01	b.d.
B16409.2	3,7	1,0	4,0	0,9	464	110	19,9	3,2	0,4	0,03	387	90	0,4	0,06	0,5
B16409.3	b.d.	b.d.	2,4	0,6	491	112	17,0	3,6	0,5	0,03	224	50	0,4	0,06	b.d.
B16409.4	b.d.	b.d.	b.d.	b.d.	521	117	18,8	4,4	1,6	0,09	135	30	0,5	0,06	b.d.
B17276.2	8,3	2,4	b.d.	b.d.	812	178	60,9	15,7	4,0	0,25	368	79	0,5	0,06	0,2
B17317	3,0	0,9	b.d.	b.d.	110	27	6,2	1,3	b.d.	b.d.	90	9	0,2	0,02	0,3
B17335	4,8	1,4	b.d.	b.d.	32	8	2,7	0,3	b.d.	b.d.	17	2	0,3	0,05	1,2
B17351	1,7	0,5	1,4	0,3	106	23	13,3	4,1	0,3	0,01	92	19	0,1	0,02	0,2
B17356.2	b.d.	b.d.	b.d.	b.d.	76	19	5,1	1,3	2,2	0,12	182	26	0,2	0,03	0,3
B17356.3	3,1	1,0	1,4	0,3	85	20	5,6	1,5	1,5	0,09	100	13	0,1	0,02	0,2
B17356.4	2,2	0,7	b.d.	b.d.	82	18	6,7	1,7	0,1	0,01	249	25	0,2	0,02	b.d.
B17382	19,4	5,6	30,2	6,4	287	71	34,1	8,1	0,7	0,06	170	15	0,5	0,06	0,9
B17389	2,8	0,8	b.d.	b.d.	328	89	18,9	5,2	0,2	0,02	222	41	0,2	0,03	0,5
B17411	18,8	5,5	24,4	4,9	151	37	889	185	1,3	0,11	118	12	0,5	0,06	6,0
B17418	12,0	3,5	1,2	0,2	289	71	5,7	1,3	1,5	0,12	51	5	0,3	0,04	0,3
B17422	3,3	1,0	b.d.	b.d.	420	89	22,2	7,3	0,3	0,01	261	52	0,7	0,09	0,4
B17426.1	b.d.	b.d.	b.d.	b.d.	406	131	4,0	1,2	0,9	0,17	48	15	b.d.	b.d.	0,4
B17426.2	2,2	0,7	b.d.	b.d.	612	128	4,2	1,5	0,5	0,02	56	11	b.d.	b.d.	b.d.
B17445	3,6	1,1	b.d.	b.d.	335	69	7,8	3,2	0,5	0,01	75	14	0,4	0,06	b.d.
B17460.1	b.d.	b.d.	b.d.	b.d.	2145	430	6,5	1,6	0,5	0,02	40	3	0,2	0,03	b.d.
B17460.2	b.d.	b.d.	b.d.	b.d.	3362	626	8,8	2,1	b.d.	b.d.	59	2	b.d.	b.d.	b.d.
B17474	b.d.	b.d.	3,6	0,9	346	70	6,3	2,7	b.d.	b.d.	61	11	0,6	0,08	b.d.
B17508.1	166,1	58,9	15,4	3,4	22456	7664	14,4	4,2	71,9	3,83	91	33	2,7	0,39	b.d.
B17508.2	187,3	b.d.	b.d.	b.d.	39597	13270	16,9	4,9	43,7	2,16	99	34	b.d.	b.d.	b.d.
B17516	b.d.	b.d.	b.d.	b.d.	1782	360	16,9	7,7	3,1	0,01	52	9	b.d.	b.d.	0,9
B17525	46,9	13,2	103,8	23,8	169	28	47,5	16,1	2,5	3,95	433	30	66,9	8,49	3,0
B17528a.1	10,9	3,8	b.d.	b.d.	2704	469	14,7	3,5	1,6	0,03	357	7	b.d.	b.d.	b.d.
B17528a.2	96,2	34,1	6,8	1,5	384	59	48,5	11,2	2,7	0,32	131	3	0,7	0,09	0,3
B17528b.1	7,3	2,6	b.d.	b.d.	459	17	7,9	1,8	2,6	0,33	137	5	b.d.	b.d.	0,3
B17551	150,1	35,6	b.d.	b.d.	660	17	16,5	4,7	6,6	1,20	200	54	b.d.	b.d.	1,1

± 2SE	In	± 2SE	Sn	± 2SE	Te	± 2SE	Pt	± 2SE	Au	± 2SE	Pb	± 2SE	Bi	± 2SE
b.d.	2,7	3,1	1334	158	54,1	4,6	0,6	0,1	34,2	20,7	111	4	12,6	0,9
0,1	0,3	0,4	2902	294	45,7	3,6	0,2	0,0	28,9	19,3	2391	191	77,9	5,9
0,2	0,2	0,3	112424	12658	6,8	0,4	3,5	0,5	11,7	7,6	687	53	25,3	0,4
0,1	0,2	0,3	4625	596	31,8	1,6	9,1	1,3	10,3	8,2	743	101	24,0	1,6
0,1	0,2	0,2	118	15	10,1	0,8	0,2	0,0	7,1	4,7	3862	473	16,6	1,1
0,0	0,2	0,3	331	39	30,7	1,9	0,2	0,0	15,2	8,9	5060	241	25,5	1,7
b.d.	0,5	0,7	79	11	16,1	0,7	0,2	0,0	4,1	3,4	740	112	16,0	1,0
1,2	b.d.	b.d.	24	3	105,0	7,2	0,7	0,1	20,7	13,5	16437	1465	32,3	1,1
b.d.	0,3	0,3	2017	252	59,5	3,2	0,2	0,0	4,2	3,3	2052	269	22,5	1,5
0,1	0,4	0,5	812	111	32,1	1,4	0,3	0,0	15,4	12,8	433	63	10,0	0,7
0,1	0,2	0,2	3	0	6,6	0,2	0,5	0,1	39,7	22,9	1686	97	3,5	0,2
0,1	0,2	0,2	897	88	11,6	1,0	0,4	0,1	6,9	4,5	2918	197	9,8	0,8
b.d.	0,3	0,5	538	52	13,1	1,1	0,2	0,0	8,3	5,3	431	28	5,6	0,4
0,1	0,4	0,5	471	57	15,2	0,1	0,1	0,0	8,2	4,5	547	45	6,7	0,3
b.d.	0,7	1,0	11418	1033	16,7	1,6	7,2	1,1	22,8	14,1	913	47	15,3	1,3
b.d.	b.d.	b.d.	1852	227	10,6	0,2	0,2	0,0	7,9	4,3	1387	123	17,6	0,8
0,1	0,3	0,4	1622	199	98,1	3,3	0,1	0,0	7,2	3,9	528	53	11,9	0,5
b.d.	0,4	0,5	1390	174	52,9	3,5	0,2	0,0	6,6	3,4	410	50	9,1	0,2
b.d.	0,4	0,6	1455	184	32,6	2,6	0,1	0,0	6,4	3,3	498	65	10,5	0,2
0,1	3,0	4,1	6657	847	117,8	11,2	17,5	1,9	41,3	20,9	542	76	35,3	0,5
0,1	0,1	0,2	492	53	18,9	1,3	0,4	0,1	58,8	41,2	1660	159	13,3	1,0
0,3	0,3	0,4	1132	100	3,2	0,3	2,6	0,4	3,3	2,0	123	7	2,5	0,2
0,1	0,3	0,4	23993	3129	25,7	3,1	0,2	0,0	6,5	3,2	741	121	198,5	1,7
0,1	0,1	0,2	2273	239	44,1	2,4	0,3	0,0	20,9	13,5	290	19	17,6	0,2
0,1	0,2	0,2	2277	237	24,8	1,3	0,2	0,0	24,1	15,5	251	17	20,3	0,3
b.d.	0,2	0,3	2786	284	55,9	2,8	0,5	0,1	37,6	24,3	301	20	20,5	0,5
0,2	2,2	3,0	n.d.	n.d.	44,8	2,5	0,3	0,0	58,6	44,8	1048	131	157,5	10,6
0,1	1,9	2,7	4258	467	45,4	2,6	0,3	0,0	22,7	14,7	843	59	21,0	0,1
1,5	1,5	2,1	6795	751	16,7	1,1	4,8	0,7	23,8	17,0	2860	290	10,9	0,8
0,1	0,3	0,4	5819	667	32,5	2,1	2,9	0,4	36,9	27,0	965	104	31,4	2,2
0,1	0,7	1,1	2185	287	45,9	6,1	13,5	1,7	82,3	39,7	1302	227	21,4	0,3
0,1	0,3	0,4	7049	847	11,5	0,8	0,1	0,0	4,1	2,7	355	34	4,5	0,2
b.d.	0,3	0,4	11056	1465	13,8	2,0	0,2	0,0	6,2	3,0	1113	201	20,4	0,4
b.d.	0,3	0,5	4628	628	10,6	1,8	0,5	0,1	5,9	2,8	1428	292	14,0	0,6
b.d.	0,2	0,3	961	94	5,6	0,3	0,2	0,0	3,8	2,5	269	20	7,2	0,3
b.d.	0,2	0,3	1586	152	9,8	0,4	0,2	0,0	6,1	3,9	521	41	16,7	0,7
b.d.	0,3	0,5	3777	488	29,0	5,1	0,5	0,1	14,4	6,6	346	75	16,2	0,8
b.d.	2,3	3,1	98	12	21,0	1,6	4,2	0,7	44,2	29,0	8	1	8,8	0,5
b.d.	4,1	5,5	76	9	34,0	2,6	1,6	0,3	29,8	19,6	9	1	11,2	0,6
0,3	0,7	1,2	52	7	10,2	1,9	0,2	0,0	4,8	2,2	3181	723	12,6	0,8
214,7	5,2	6,5	n.d.	n.d.	39,0	1,5	376	91	24	21	737	138	286,9	20,9
b.d.	0,4	0,5	1353	127	126,8	5,4	0,8	0,1	8,1	5,2	244	20	72,2	3,5
0,1	0,6	0,9	733	66	59,2	2,3	0,4	0,0	19,6	12,5	293	29	10,0	0,6
0,1	0,3	0,4	389	34	33,5	1,3	0,1	0,0	7,4	4,7	322	35	9,4	0,7
0,3	b.d.	b.d.	159	18	60,6	4,0	10,5	1,6	148,3	96,8	103	9	30,7	0,9

Tab. B4: Results of LA -ICP-MS trace element analysis of the As-Ni-copper artefacts in ppm. For all samples n=10 point analyses were peformed. The errors are given as two standard errors (abbr.: b.d.=below detection limit).

Sample	Cr	±2SE	Mn	±2SE	Co	±2SE	Ni	±2SE	Zn	±2SE	Ge	±2SE	As	±2SE	Se
30-12-264	1.3	0.3	43.8	9.9	214	34	5665	159	38.6	9.5	1.3	0.1	14091	989	166
30-12-272.1	10.7	3.2	2.5	0.7	66	9	5854	172	18.0	4.4	0.1	0.0	9814	713	177
30-12-272.2	b.d.	b.d.	b.d.	b.d.	65	8	5669	181	11.6	2.8	0.3	0.0	8923	695	114
30-12-284	9.6	9.7	22.1	101.9	448	89	81567	4952	289.4	117.7	1.6	0.4	115455	8722	5249
30-12-321	0.2	0.1	11.3	1.7	52	11	1637	90	26.9	10.4	0.8	0.1	9422	701	143
30-12-382	3.4	1.3	2.7	3.8	83	25	2406	125	35.4	14.8	0.8	0.1	6542	479	132
30-12-416	1.6	0.5	1.0	0.8	506	92	11330	1559	53.5	16.4	0.1	0.0	15966	1130	562
30-12-696	1.4	0.4	0.9	0.3	15	3	1207	64	9.3	1.5	0.2	0.0	4219	378	53
31-17-186	0.7	0.2	23.5	12.8	32	6	7534	621	15.7	5.0	0.2	0.0	3551	254	422
31-17-205	151.8	42.8	9.5	3.5	353	58	7284	368	29.2	4.2	0.6	0.0	22258	2009	201
31-17-217.2	0.2	0.1	3.6	1.3	345	74	6301	189	32.2	7.8	0.8	0.1	28269	1988	200
31-17-217.3	0.4	0.2	3.8	1.2	366	83	6469	298	39.6	10.5	0.8	0.1	26286	1951	239
31-17-265	1.2	0.3	1.6	0.6	135	22	708	36	172.0	25.2	1.2	0.1	6255	562	46
B16937	b.d.	0.6	28.5	6.2	98	309	11649	265	27.9	9.1	0.9	0.2	9814	1330	381
B16954	2.4	0.4	16.0	1.9	1874	8	4941	706	56.0	2.4	1.3	0.1	14755	1198	673
B16996	1.5	b.d.	5.2	0.1	49	40	13867	204	16.7	10.8	1.2	0.1	13210	2033	1285
B17022	b.d.	b.d.	0.4	1.2	210	24	3600	2018	21.9	102.5	1.0	3.1	21091	535	254
B17327	b.d.	0.2	3.5	1.1	124	32	34206	129	172.0	6.8	3.9	0.3	5499	641	2013
B17330	0.9	1.0	3.0	0.4	193	1198	2496	70	40.2	1365.5	5.3	0.1	6978	136	38
B17410	1.6	0.5	1.0	0.2	767	5	1091	70	7398.3	15.1	0.9	0.1	1353	682	66
B17469	1.9	0.2	0.4	0.2	30	75	1247	389	91.4	15.6	0.8	3.3	7473	1340	123
B17478	1.0	95.9	0.4	3.3	545	123	11808	374	67.4	6.6	20.6	0.0	23300	2111	174
B17479	b.d.	b.d.	13.5	0.4	679	16	8287	581	26.0	8.0	0.1	0.2	14698	945	64
B17480	b.d.	0.8	1.1	0.3	100	15	9442	137	44.3	2.8	1.3	0.0	9790	864	1503
B17494	3.8	0.4	0.7	1.8	94	109	2306	959	15.8	14.4	0.2	0.1	9126	3748	225
B17495	1.4	0.4	5.2	0.2	596	53	17226	292	38.3	8.5	2.1	0.1	39218	1920	275
B17496	1.5	480.0	0.6	20.8	310	b.d.	5822	15	36.6	29.9	2.4	0.2	20514	5	596

sample nr.	Cr	±2SE	Mn	±2SE	Co	±2SE	Ni	±2SE	Zn	±2SE	Ge	±2SE	As	±2SE	Se	±2SE	Rh	±2SE
30-12-253-1	11.1	15064	142	69.2	57.2	216	3049	4174	17.6	596	0.4	5.6	19.3	19.8	8.4	12.1	0.4	1.7
30-12-253-3	3898	794	256	12.6	74.5	11.8	2518	384	30.8	1774	0.3	9.0	3.3	15.6	1.4	12.5	0.1	3.6
30-12-446	3.2	7.1	1.2	15.9	0.2	b.d.	35.0	2.4	3.9	2.6	0.2	b.d.	9.7	6.0	4.9	6.90	4.6	7.2
30-12-605	6.3	6.6	3.9	23.4	0.2	3.9	1.2	11.6	71.9	10.6	0.2	b.d.	2.5	10.2	1.5	20.4	1.5	402
30-12-754	0.2	0.1	b.d.	b.d.	b.d.	b.d.	13.8	0.5	2.3	0.01	b.d.	b.d.	120	1.7	5.4	0.06	3.4	0.004
30-12-773	0.3	0.02	0.9	0.03	0.4	b.d.	25.4	0.7	14.9	7.8	b.d.	b.d.	307	8.4	6.1	0.11	3.5	0.014
B16926a	1.1	0.1	0.1	0.004	b.d.	b.d.	2.0	0.3	7.2	0.3	b.d.	b.d.	3.0	0.2	4.0	0.02	1.8	0.008
B16931a	4.8	0.3	0.5	0.01	b.d.	b.d.	1.1	0.1	2.1	0.1	b.d.	b.d.	2.8	0.3	1.6	0.07	1.7	0.012
B16931b	3.4	0.2	1.8	0.1	0.3	0.04	1.0	0.04	2.6	0.03	b.d.	b.d.	3.7	0.2	1.6	0.05	1.9	0.016
B17078a	0.1	0.3	1.6	0.2	0.6	0.1	1.1	0.6	21.5	2.2	0.1	0.03	5.8	2.1	0.2	0.28	0.1	0.002
B17082a	15.1	1.8	14.3	0.3	1.9	0.2	19.6	0.9	82.3	0.7	0.3	0.02	6.2	0.4	0.3	0.03	0.2	0.002
B17084	0.3	0.0	b.d.	b.d.	0.5	0.2	4.5	0.1	1.4	0.02	b.d.	b.d.	5.7	0.9	5.8	0.09	2.7	0.008
B17553b	0.4	0.1	0.2	0.0	b.d.	b.d.	6.9	0.2	2.9	0.03	b.d.	b.d.	4.4	0.2	1.7	0.10	1.8	0.006

±2SE	Pd	±2SE	Cd	±2SE	In	±2SE	Te	±2SE	Pt	±2SE	Au	±2SE	Pb	±2SE	Bi
23	0.1	0.01	0.6	0.08	0.5	0.7	31.2	3.3	0.0	0.01	16.8	0.9	3782	375	59
22	0.2	0.03	0.2	0.03	0.6	0.8	29.3	2.2	0.1	0.02	7.4	0.4	697	84	260
15	0.2	0.03	0.4	0.05	0.4	0.5	20.7	1.3	0.3	0.06	6.4	0.4	536	84	123
730	2.6	0.45	4.7	4.46	19.2	23.5	1230	909	5.6	0.55	553	53	4887	1160	2099
32	b.d.	b.d.	0.3	0.04	0.5	0.6	33.1	3.3	b.d.	b.d.	7.3	0.7	1706	221	216
21	0.1	0.02	0.2	0.08	0.4	0.5	35.9	9.2	0.5	0.05	6.3	0.6	2214	459	107
69	0.2	0.03	0.5	0.08	4.8	6.1	128.2	13.9	0.2	0.02	23.7	2.1	2447	389	332
8	b.d.	b.d.	0.2	0.03	0.1	0.1	4.0	0.4	0.3	0.05	19.9	1.2	1621	284	49
53	0.1	0.01	0.3	0.04	0.3	0.4	53.5	5.1	0.1	0.01	19.7	1.7	326	42	10
31	0.2	0.03	0.3	0.04	0.3	0.4	47.6	5.4	0.2	0.04	30.9	1.9	10433	1449	90
29	0.1	0.01	0.1	0.01	0.1	0.2	32.4	3.2	0.0	0.00	65.9	5.3	8218	1341	625
38	0.1	0.01	0.1	0.01	0.1	0.1	39.0	4.2	0.1	0.01	61.4	4.9	8380	3600	487
7	0.3	0.04	0.2	0.04	0.6	0.7	23.1	2.5	0.2	0.03	13.2	0.8	2088	319	90
102	0.3	0.07	0.6	0.24	2.6	3.1	47.2	12.6	0.3	0.07	70.4	1.8	3620	493	268
195	0.5	0.03	1.4	0.07	2.5	0.7	122.5	7.3	0.5	0.15	30.3	1.6	2595	95	714
39	0.2	b.d.	0.5	0.02	0.6	0.4	63.3	5.7	0.9	0.06	26.4	0.7	736	226	25
309	b.d.	0.07	0.2	0.09	0.3	1.4	39.3	15.5	0.3	0.30	10.7	4.2	2340	399	87
6	0.4	0.01	0.7	0.03	1.0	0.5	103.3	1.0	1.4	0.05	63.3	0.1	4190	624	393
10	0.1	0.03	0.2	0.10	0.4	0.3	8.5	1.8	0.3	0.02	2.3	1.1	5387	501	330
19	0.2	0.03	0.5	0.04	0.2	0.3	17.3	2.8	0.2	0.03	17.9	0.3	1644	5477	28
33	0.2	0.02	b.d.	b.d.	0.2	0.7	27.9	9.6	0.3	0.02	5.2	1.2	26036	378	158
16	0.1	0.02	0.0	0.04	0.8	0.3	67.4	5.6	b.d.	b.d.	11.9	0.9	1720	1180	55
229	0.1	0.04	0.2	0.05	0.3	0.5	49.0	12.3	0.0	0.03	5.2	1.0	5668	813	52
34	0.3	0.01	0.3	0.04	0.4	0.9	120.3	5.1	0.3	0.01	16.8	2.2	2957	170	79
42	0.1	0.04	0.2	0.05	0.8	0.5	49.7	9.7	0.1	0.04	36.1	1.1	690	31	56
91	0.2	0.06	0.4	0.05	0.4	0.7	69.2	12.8	0.2	0.08	17.2	1.2	313	528	210
25	0.4	18.41	0.4	11.32	0.5	19.1	99.4	27.3	0.4	0.01	19.8	51.6	5137	16	24

Tab, B5: Results of LA-ICP-MS trace element analysis of the tin bronze artefacts in ppm. For all samples n=10 point analyses were peformed. The errors are given as two standard errors (abbr.: b.d.=below detection limit).

Pd	±2SE	Cd	±2SE	In	±2SE	Sn	±2SE	Sb	±2SE	Te	±2SE	Pt	±2SE	Au	±2SE	Pb	±2SE	Bi	±2SE
5.3	9.7	3.1	14.1	0.4	8.4	23.4	752	3.5	282	1.4	13.7	1.4	16.2	86.4	736	2526	1344	88.7	157.2
1.3	33.2	1.0	9.2	0.3	25.2	1.6	2026	0.4	982	0.6	17.5	1.4	62.4	0.7	570	59	4062	2.6	99.8
3.8	8.6	1.9	11.1	0.2	21.0	7.7	9.9	17.3	9.6	1.7	10.0	2.6	5.3	315	33.6	16036	1798	680	75.6
4.4	6.3	2.2	9.3	0.1	20.8	1.0	9.4	1.8	10.1	0.6	11.3	2.3	5.0	348	64.8	1377	254	364	57.6
4.5	0.006	2.3	0.002	0.2	0.008	3.2	0.008	28.9	0.1	1.3	0.01	1.2	0.03	596	0.2	8870	17.5	536	0.09
5.2	0.016	2.7	0.004	0.2	0.02	4.2	0.01	36.1	0.1	1.5	0.01	1.2	0.04	662	1.1	9276	13.1	674	0.24
4.5	0.006	2.3	0.002	0.2	0.018	0.2	0.1	1.0	0.01	0.9	0.00	2.2	0.2	323	0.2	2498	8.6	254	0.03
4.0	0.014	2.1	0.004	0.1	0.036	7.3	0.02	0.9	0.2	38.8	0.3	10.2	0.8	4615	5.2	2354	7.4	1199	0.32
4.9	0.032	2.6	0.008	0.2	0.04	7.4	0.02	1.0	0.03	34.4	0.4	17.1	1.0	5720	6.8	2265	8.8	1127	0.42
0.9	0.1	0.5	0.036	0.1	0.2	551	29.4	0.4	0.1	0.1	0.01	0.3	0.6	10.0	0.2	127	1.7	0.2	0.01
1.1	0.1	0.8	0.022	0.1	0.1	62.3	0.9	4.7	0.1	0.2	0.01	0.6	0.5	2.1	0.02	109	2.7	24.9	0.03
4.9	0.014	2.4	0.004	0.2	0.1	0.9	0.03	0.9	0.02	13.8	0.1	1.6	0.02	1407	1.1	4830	9.6	1056	0.22
7.6	0.018	3.9	0.004	0.3	0.024	23.5	0.1	8.6	0.02	1.4	0.02	4.6	0.1	1025	1.4	8249	20.6	1069	0.66

Tab. B6: Results of LA-ICP-MS trace element analysis of the silver artefacts in ppm. For all samples n=10 point analyses were peformed. The errors are given as two standard errors (abbr.: b.d.=below detection limit).

B.3 Copper isotope analysis

sample nr.	material	δ65Cu	±2SE
30-12-280a	Ag	0.054	0.212
30-12-429	Ag	0.260	0.047
30-12-605	Ag	0.206	0.031
30-12-754	Ag	0.016	0.017
30-12-773	Ag	1.393	0.100
B17084	Ag	0.098	0.017
31-17-266	As-Ni-Cu	-0.206	0.059
35-1-422.3	As-Ni-Cu	-0.231	0.193
B16409.2	As-Ni-Cu	-0.225	0.022
B16409.3	As-Ni-Cu	-0.358	0.003
B16409.4	As-Ni-Cu	-0.263	0.087
B17276.2	As-Ni-Cu	-0.061	0.068
B17356.3	As-Ni-Cu	-0.077	0.021
B17356.4	As-Ni-Cu	-0.189	0.075
B17426.1	As-Ni-Cu	-0.122	0.071
B17445	As-Ni-Cu	0.055	0.104
B17460.2	As-Ni-Cu	-0.268	0.061
B17528a.2	As-Ni-Cu	0.215	0.077
30-12-205	Bronze	-0.044	0.041
30-12-217.2	Bronze	0.323	0.114
30-12-217.3	Bronze	-0.057	0.026
30-12-272.1	Bronze	-0.219	0.054
30-12-272.2	Bronze	-0.202	0.064
30-12-321	Bronze	-0.141	0.011
30-12-382	Bronze	-0.029	0.025
30-12-696	Bronze	-0.504	0.016
31-17-186	Bronze	-0.198	0.059
31-17-265	Bronze	0.005	0.047
B16954	Bronze	-0.693	0.037
B16996	Bronze	-0.315	0.034
B17327	Bronze	-0.107	0.016
B17480	Bronze	-0.273	0.011

*Tab. B7: Results of **in situ** fsLA-ICP-MS Cu isotope analysis of the silver- and copper-based artefacts in‰. For all samples n=3-7 point analyses were peformed. The errors are given as two standard errors.*

sample nr.	material	δ65Cu	±2SE
30-12-446	Ag	0.181	0.055
30-12-605	Ag	0.418	0.060
B16926a	Ag	-0.169	0.060
B16931a	Ag	1.519	0.051
B16931b	Ag	0.326	0.055
B17553b	Ag	0.316	0.053
30-12-696	Bronze	-0.139	0.056
98-9-164	Copper	0.332	0.052
B17551	As-Ni-Cu	0.938	0.053

Tab. B8: Results of MC-ICP-MS Cu isotope analysis of drilled silver- and copper-based artefacts in ‰. The errors are given as two standard errors.

		$^{65}Cu/^{63}Cu$	2SD	2SE
NIST976_01	0.445979	0.000102	0.000026	
NIST976_02	0.445947	0.000181	0.000033	
NIST976_03	0.445998	0.000090	0.000018	
NIST976_04	0.446040	0.000049	0.000009	
NIST976_05	0.446036	0.000065	0.000012	
NIST976_06	0.446039	0.000123	0.000035	
Blank ^{63}Cu	0.0131	[V]		
Blank ^{65}Cu	0.0059	[V]		

Tab. B9: Results of fsLA-ICP-MS Cu isotope analysis of absolute $^{65}Cu/^{63}Cu$ ratios of the measured NIST976 for each measurement day. The errors are given as two standard errors.

B.4 Lead isotope analysis

sample nr.	206Pb/204Pb	± 2SE	207Pb/204Pb	± 2SE	208Pb/204Pb	± 2SE
30-12-264	17,900	0,003	15,664	0,002	38,032	0,006
30-12-272-1	18,305	0,010	15,678	0,009	38,485	0,026
30-12-272-2	18,305	0,007	15,679	0,005	38,512	0,017
30-12-284	18,532	0,005	15,731	0,004	38,582	0,009
30-12-285	18,679	0,007	15,623	0,006	38,631	0,016
30-12-321	17,697	0,013	15,673	0,013	37,768	0,028
30-12-373	18,561	0,006	15,668	0,005	38,715	0,016
30-12-375	18,632	0,004	15,685	0,004	38,849	0,013
30-12-380	18,590	0,005	15,664	0,003	38,741	0,009
30-12-382	17,835	0,002	15,654	0,002	37,942	0,006
30-12-416	17,654	0,003	15,651	0,002	37,848	0,007
30-12-696	18,918	0,006	15,692	0,005	39,106	0,022
31-17-186	18,884	0,019	15,707	0,007	39,103	0,031
31-17-193	18,542	0,006	15,635	0,005	38,679	0,028
31-17-201	18,752	0,004	15,706	0,003	38,889	0,012
31-17-205	17,989	0,013	15,651	0,012	38,037	0,034
31-17-217-3	18,519	0,011	15,658	0,013	38,722	0,045
31-17-265	18,685	0,008	15,649	0,005	38,815	0,023
31-17-266	18,531	0,004	15,650	0,002	38,776	0,015
31-17-267	18,674	0,005	15,657	0,003	38,829	0,012
31-17-352	18,782	0,021	15,687	0,006	38,946	0,029
33-35-79	18,915	0,006	15,696	0,004	39,058	0,022
35-1-422.1	18,680	0,005	15,664	0,003	38,838	0,011
35-1-422.2	18,678	0,004	15,674	0,002	38,817	0,010
35-1-422-3	18,665	0,004	15,666	0,003	38,802	0,010
35-1-479	18,516	0,003	15,680	0,003	38,723	0,009
B16409.1	18,540	0,005	15,701	0,002	38,766	0,015
B16409-2	18,609	0,004	15,687	0,003	38,843	0,009
B16409-3	18,598	0,003	15,680	0,003	38,824	0,009
B16409-4	18,610	0,003	15,686	0,002	38,834	0,007
B16937	17,783	0,008	15,659	0,006	37,754	0,020
B16954	17,774	0,005	15,645	0,006	37,926	0,020
B16996	18,922	0,008	15,703	0,006	39,158	0,017
B17022.1	17,633	0,003	15,642	0,005	37,680	0,017
B17276-2	18,436	0,011	15,686	0,005	38,576	0,027
B17317	18,701	0,004	15,668	0,003	38,879	0,011
B17327	17,586	0,006	15,643	0,003	37,610	0,010
B17330	17,635	0,005	15,635	0,003	37,654	0,009
B17351	18,560	0,005	15,668	0,003	38,727	0,016
B17356-2	18,844	0,004	15,682	0,003	39,041	0,010
B17356-3	18,838	0,004	15,681	0,003	39,048	0,010
B17356-4	18,839	0,004	15,680	0,003	39,037	0,011
B17389	18,642	0,003	15,662	0,003	38,829	0,008
B17422	18,664	0,003	15,672	0,002	38,872	0,009
B17426-1	18,368	0,004	15,659	0,003	38,537	0,011
B17426-2	18,368	0,004	15,656	0,003	38,525	0,012
B17445	18,765	0,003	15,692	0,003	38,910	0,010
B17460-2	18,661	0,003	15,673	0,002	38,851	0,010
B17469	17,798	0,005	15,616	0,004	37,807	0,015
B17474	18,447	0,007	15,612	0,005	38,560	0,016
B17478	18,068	0,003	15,661	0,003	38,161	0,009
B17479	17,383	0,005	15,627	0,004	37,371	0,013
B17480	17,711	0,004	15,639	0,003	37,737	0,012
B17494	18,164	0,007	15,683	0,008	38,118	0,026
B17495	18,949	0,011	15,717	0,009	39,335	0,023
B17496	18,639	0,008	15,645	0,007	38,768	0,021
B17508.2	19,709	1,006	17,189	0,893	41,098	1,992
B17516	18,662	0,006	15,652	0,004	38,807	0,016
B17528a-1	18,351	0,008	15,613	0,009	38,415	0,040
B17528a-2	18,590	0,024	15,642	0,014	38,712	0,060
B17528b-1	18,649	0,005	15,661	0,004	38,825	0,011
B17551	18,495	0,011	15,634	0,009	38,599	0,023

Tab. B10: Results of LA-MC-ICP-MS Pb isotope analysis of the copper-based artefacts. The errors are given as two standard errors.

sample nr.	$^{206}Pb/^{204}Pb$	± 2SE	$^{207}Pb/^{204}Pb$	± 2SE	$^{208}Pb/^{204}Pb$	± 2SE
30-12-253-1	18.673	0.011	15.681	0.010	38.864	0.030
30-12-253-3	18.661	0.025	15.667	0.022	38.853	0.053
30-12-446	18.636	0.003	15.677	0.003	38.823	0.009
30-12-605	18.609	0.006	15.675	0.005	38.797	0.014
30-12-773	18.648	0.006	15.654	0.006	38.784	0.017
B16926a	18.644	0.007	15.681	0.007	38.822	0.018
B16931a	18.916	0.009	15.693	0.007	39.050	0.020
B16931b	18.945	0.003	15.708	0.003	39.108	0.010
B17078a	18.651	0.003	15.684	0.003	38.852	0.009
B17082a	18.564	0.004	15.645	0.003	38.676	0.011
B17084	18.764	0.003	15.695	0.003	38.939	0.010
B17553a	18.619	0.004	15.650	0.004	38.735	0.011
B17553b	18.615	0.018	15.657	0.013	38.759	0.042

Tab. B11: Results of LA-MC-ICP-MS Pb isotope analysis of the silver artefacts. The errors are given as two standard errors.

sample nr.	$^{206}Pb/^{204}Pb$	± 2SE	$^{207}Pb/^{204}Pb$	± 2SE	$^{208}Pb/^{204}Pb$	± 2SE
AgA2	17.396	0.004	15.545	0.003	37.273	0.010
BAM376	17.869	0.116	15.785	0.124	37.897	0.283
bronzeA_01	17.177	0.371	15.490	0.038	36.924	0.403
bronzeA_02	16.835	0.325	15.249	0.237	36.252	0.618
bronzeA_03	17.106	0.231	15.478	0.020	36.847	0.248
bronzeA_04	17.159	0.371	15.476	0.032	36.896	0.394
bronzeA_06	17.108	0.318	15.483	0.030	36.857	0.346
NIST610_01	16.876	0.202	15.370	0.170	36.607	0.455
NIST610_02	16.831	0.263	15.322	0.236	36.550	0.556
NIST610_03	17.059	0.003	15.526	0.003	37.026	0.008
NIST610_04	17.057	0.005	15.523	0.006	37.019	0.020
NIST610_05	17.059	0.004	15.526	0.003	37.027	0.008
NIST610_06	17.061	0.005	15.526	0.003	37.029	0.008
NIST610_07	17.059	0.016	15.526	0.014	37.027	0.034
NIST610_08	17.059	0.003	15.525	0.002	37.026	0.008
RAgGP6	20.753	0.009	15.870	0.007	39.593	0.021

Tab. B12: Results of LA-MC-ICP-MS Pb isotope analysis of the standards. AgA2, BAM376, bronze A, and RAgGP6 are secondary standards. The NIST610 analyses are given as means of each measurement day. The errors are given as two standard errors.

	^{204}Pb	^{206}Pb	^{207}Pb	^{208}Pb
Blank [V]	0.000054	0.000205	0.000160	0.000267

Tab. B13: The mean blanks of the Pb isotopes measured by LA-MC-ICP-MS.

Day 1						
sample nr.	**$^{206}Pb/^{204}Pb$**	**± 2SD**	**$^{207}Pb/^{204}Pb$**	**± 2SD**	**$^{208}Pb/^{204}Pb$**	**± 2SD**
30-12-696	18.934	0.003	15.705	0.003	39.147	0.010
98-9-164	18.576	0.093	15.644	0.076	38.686	0.188
B17551	18.495	0.011	15.634	0.009	38.599	0.023
30-12-446	18.636	0.003	15.677	0.003	38.823	0.009
30-12-605	18.609	0.006	15.675	0.005	38.797	0.014
30-12-773	18.648	0.006	15.654	0.006	38.784	0.017
B16926a	18.644	0.007	15.681	0.007	38.822	0.018
B16931a	18.916	0.009	15.693	0.007	39.050	0.020
B16931b	18.944	0.003	15.708	0.003	39.108	0.010
B17078a	18.651	0.003	15.684	0.003	38.852	0.009
B17082a	18.564	0.004	15.645	0.003	38.676	0.011
B17084	18.764	0.003	15.695	0.003	38.939	0.010
B17553a	18.619	0.004	15.650	0.004	38.735	0.011
B17553b	18.613	0.003	15.644	0.003	21.800	0.470
NBS981	16.941	0.003	15.496	0.003	36.722	0.009
	^{204}Pb	**^{206}Pb**	**^{207}Pb**	**^{208}Pb**		
Blank [V]	0.00052	0.00942	0.00806	0.01997		

Day 2						
sample nr.	**$^{206}Pb/^{204}Pb$**	**± 2SD**	**$^{207}Pb/^{204}Pb$**	**± 2SD**	**$^{208}Pb/^{204}Pb$**	**± 2SD**
98-9-164	18.557	0.499	15.611	0.415	38.602	1.021
B17553b	18.600	0.006	15.629	0.006	38.650	0.019
NBS981	16.934	0.005	15.489	0.005	36.691	0.012
	^{204}Pb	**^{206}Pb**	**^{207}Pb**	**^{208}Pb**		
Blank [V]	0.00002	0.00027	0.00021	0.00055		

Tab. B14: Results of MC-ICP-MS Pb isotope analysis of the standards and samples. The errors are given as 2 SD. The samples 98-9-164 and B17553b were measured on two days. The standard NBS981 is given as mean. The mean blank intensities of each day are given in [V].

C Catalogue

Forword to the catalogue

This catalogue includes photos, microscopy pictures, and BSE (back-scattered electrons) images of the artefacts analysed and discussed in this study. In addition, archaeological data were included, as (when available) e.g. tomb, dating, and the different registration numbers of the Penn Museum. Photos of sample locations are included, when available.

As mentioned in chapter 1 Samuel K. Nash worked as a volunteer at the Penn Museum in Philadelphia. He is a trained metallurgical engineer and joined the Museum of Applied Science Center for Archaeology (MASCA) in 1995 and became later a Research Associate at the Penn Museum.

In the course of the Mesopotamian Metals Project Nash investigated the mounted samples of the copper based artefacts of Ur regarding their metallography. His handwritten notes were thankfully provided by the Penn Museum for research purposes and allowed to be published (September, 13th, 2018).

In order to complement the analytical data, the notes were included in the catalogue as a copy of the handwritten original for each artefact, where available. To facilitate the readability the handwritting was transcribed, digitised, and subjoined to the handwritten notes. Please note that crossed out parts were not digitised. The pages of the catalogue were arranged, so the notes are to the left side of a double page and the pictures to the right. The author assumes no responsibility for the correctness, completeness or quality of the transcription. Nash‘s notes are always marked by the header: „Samuel K. Nash‘s Notebook“.

30-12-264

Museums nr. 30-12-264.1

Field Nr.	U.11486
Old Registration Nr.	none
MMP NR.	Ur 127
Material	As-Ni-Sn-Cu
Object	Adze
Dating	Early Dynastic
Tomb	PG 1038
Type of Tomb	Private
EPMA	x
Laser (Trace)	x
Laser (CuI)	
Sol (CuI)	
Laser (LIA)	x
Sol (LIA)	30-12-22

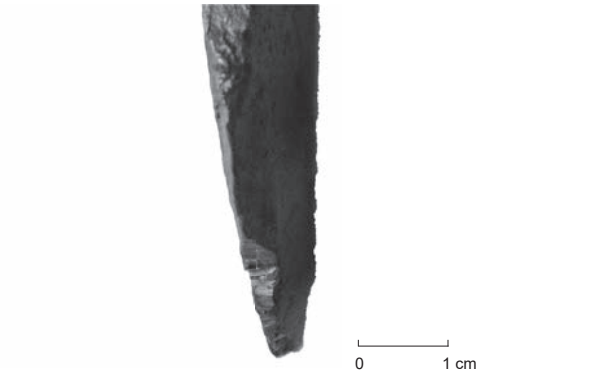

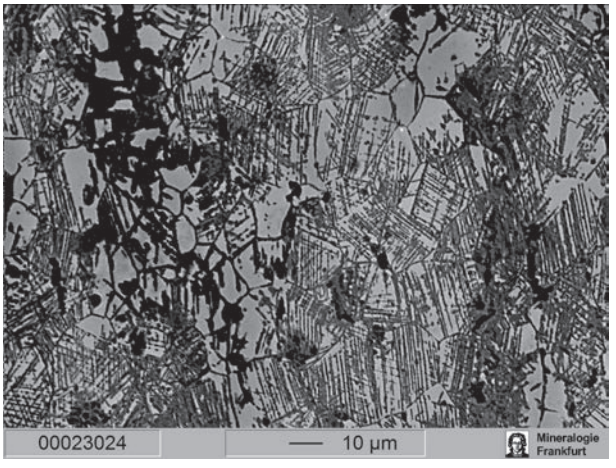

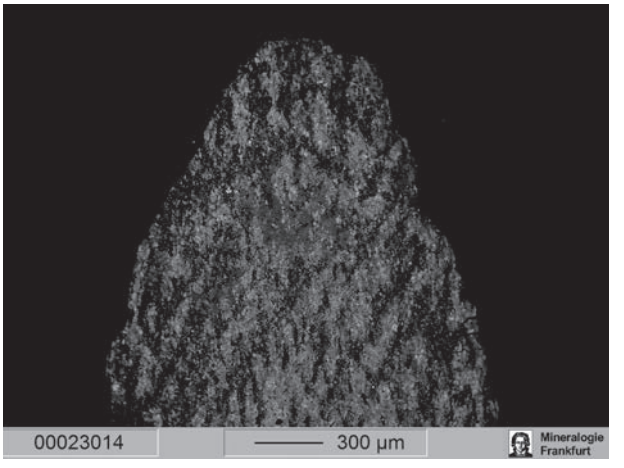

30-12-272

Museum nr. 30-12-272.1-2

Field Nr.	U.12740
MMP NR.	Ur 536
Material	Bz
Object	Mirror
Dating	Not Dated
Tomb	PG -5 m below surface, loose in soil
Type of Tomb	Private
Citation	Cleziou and Berthoud 1982, 15
Notes	Woolley's Object Catalogue identifies U.12740 as mirror
EPMA (ffm)	x
Laser (Trace)	x
Laser (CuI)	x
Sol (CuI)	
Laser (LIA)	x
Sol (LIA)	
PIXE-Analyses	Cu 88.1, Sn 9.3, As 0.69, Ni 0.5

Samuel K. Nash's Notebook

30-12-272 Ur 536
Intergranular corrosion has completely penetrated the periphery of this spatula which has an unusually high tin content, i.e., 11.6 %. The unaffected core beneath the corrosion zone consists of annealed, twinned, polygonal grains, arranged in bands that resist resolution, indicative of a significant degree of alloy segregation. The inclusions content is low and consists of small, spheroidal sulfides. The VHN averages between 85-92, ca., 88.5.
Some of the inclusions are elongated and fragmented indicating directional working prior to the final annealing treatment of the central section of this specimen.

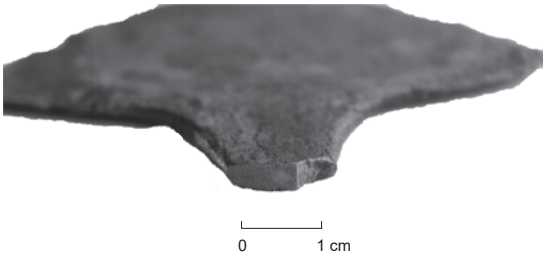

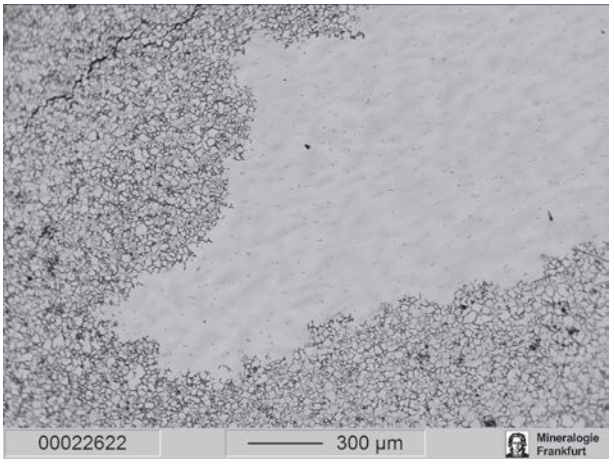

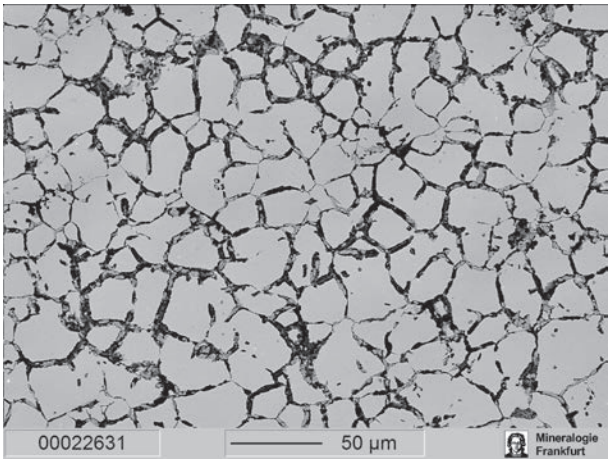

30-12-284

Museum nr. 30-12-284.1

Field Nr.	U.11866a
MMP NR.	Ur 122
Material	Bz
Object	Dagger
Dating	Early Dynastic
Find context	U.11868 (=BM 122560) Cylinder Seal, superimposed rows of animals. Note BM 122560 is included in British Museum: Western Asiatic Seals I (pl. 23c)
Tomb	PG 1162
Type of Tomb	Private
EPMA	x
Laser (Trace)	x
Laser (CuI)	
Sol (CuI)	
PIXE-Analyses	As, 0.30%; Sn, 12.0%; Ni, 0.20%

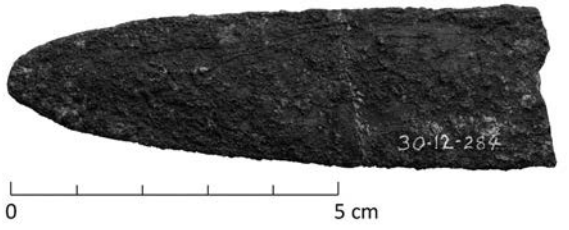

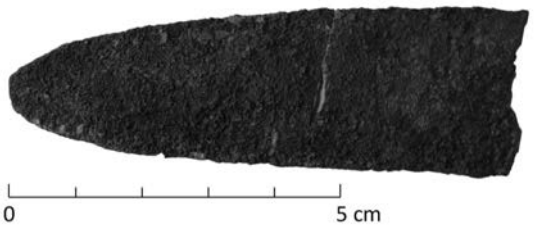

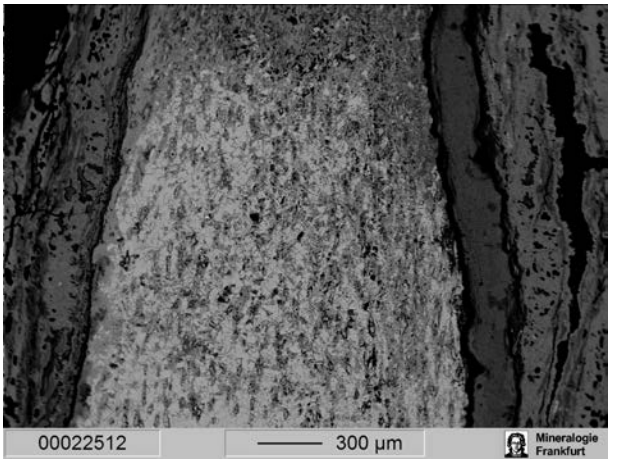

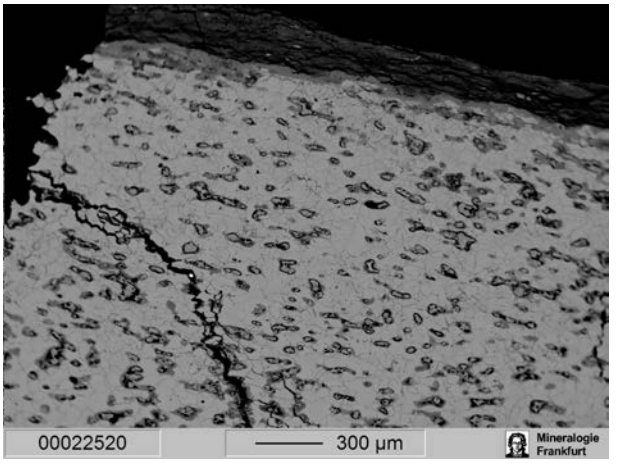

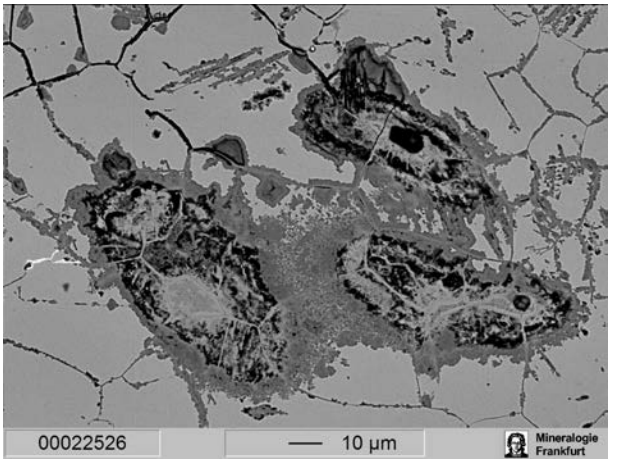

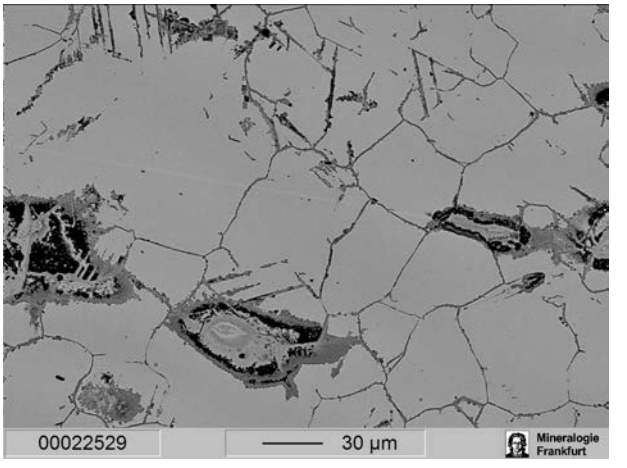

30-12-285

Museum nr. 30-12-285.1

Field Nr.	U.12005, probably wrong U. Number
MMP NR.	Ur 120
Material	As-Cu
Object	Chisel
Dating	Not Dated
Tomb	PG 1212
Type of Tomb	Private
Notes	The chisel does not appear to match with the description as a copper axe or the drawing on the PG 1212 card (blade)
EPMA	x
Laser (Trace)	x
Laser (CuI)	
Sol (CuI)	
Laser (LIA)	x
Sol (LIA)	
PIXE-Analyses	As, 0.66%; Sn, 0.053%; Ni, 0.34%

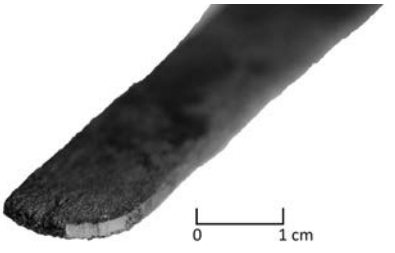

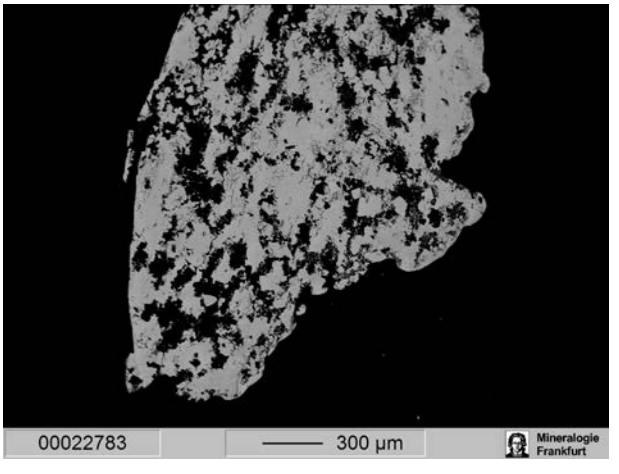

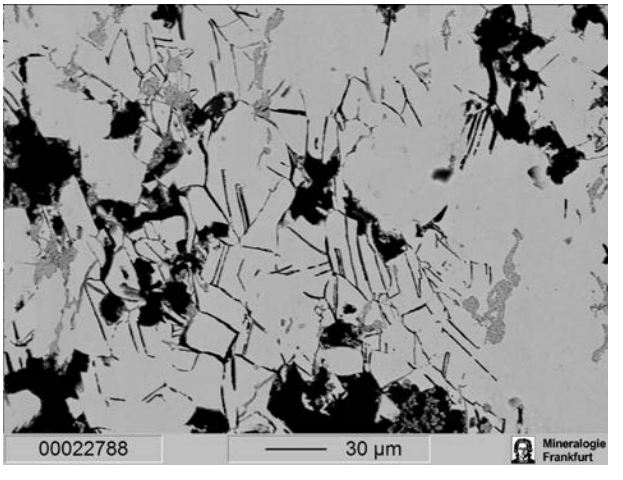

30-12-321

Museum nr. 30-12-321.1

Field Nr.	U.11494
MMP NR.	Ur 126
Material	Bz
Object	Spatula
Dating	Early Dynastic
Tomb	PG 1047
Type of Tomb	Private
EPMA	x
Laser (Trace)	x
Laser (CuI)	x
Sol (CuI)	
Laser (LIA)	x
Sol (LIA)	
PIXE-Analyses	As, 0.90%; Sn, 16.0%; Ni, 0.20%

Samuel K. Nash's Notebook

Ur 126 (30-12-321)
The fine equiaxed grains of this artifact (GS 7-8) are perfectly outlined by intergranular corrosion. However most of this initially hot worked specimen was subjected to subsequent heavy cold working. The latter process rendered the metal susceptible to stress corrosion cracking, and this feature is clearly evident in several areas. The absence of twinning is indicative of any post cold deformation annealing.

Ur 126 (30-12-321)
The entire oblong cross section of this spatula has suffered severe corrosion. That form of attach clearly outlines the equiaxed grain structure (GS 7-8), and accentuated the slip line traces introduced during post annealing cold work. A good deal of porosity and grain loss has occurred to corrosion as well. In places where corrosion is heaviest, large cracks formed evidence of stress corrosion cracking. Hardness impressions made in non-corroded metal yielded an average of VH=118

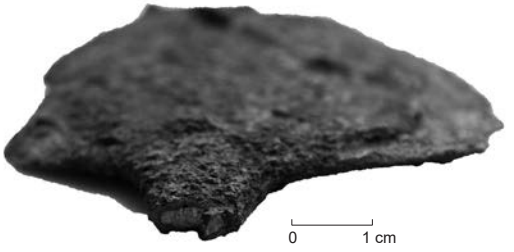

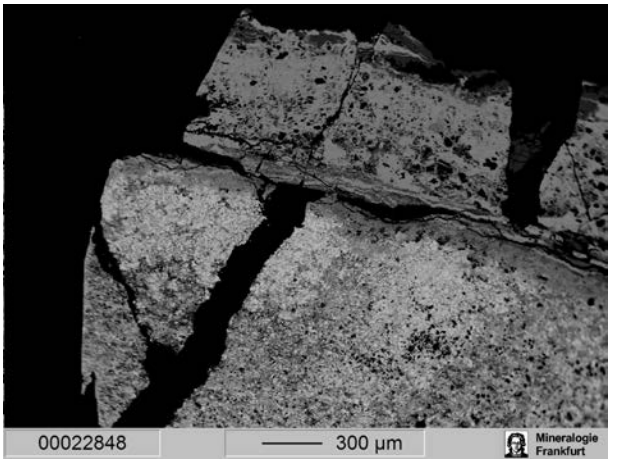

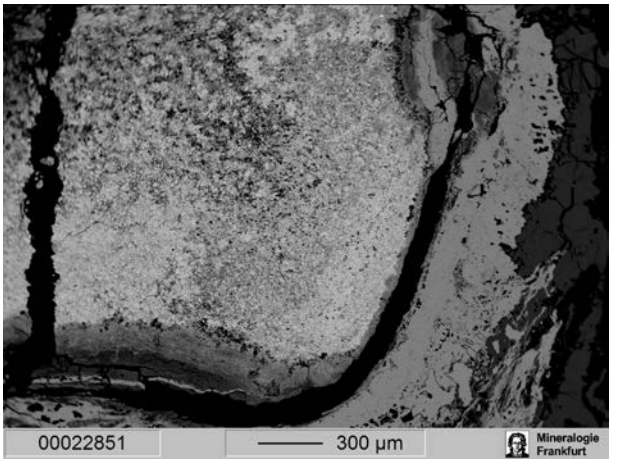

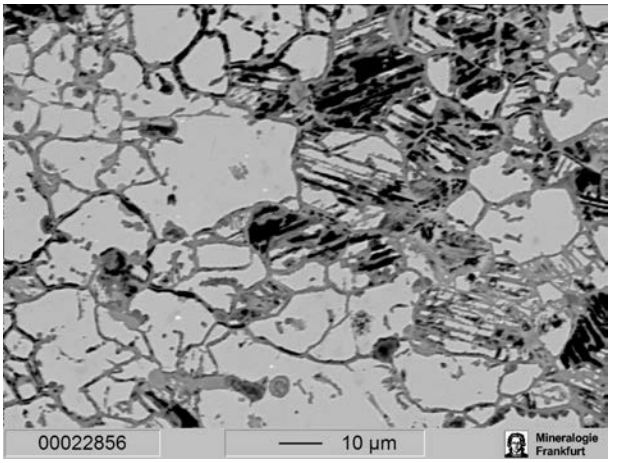

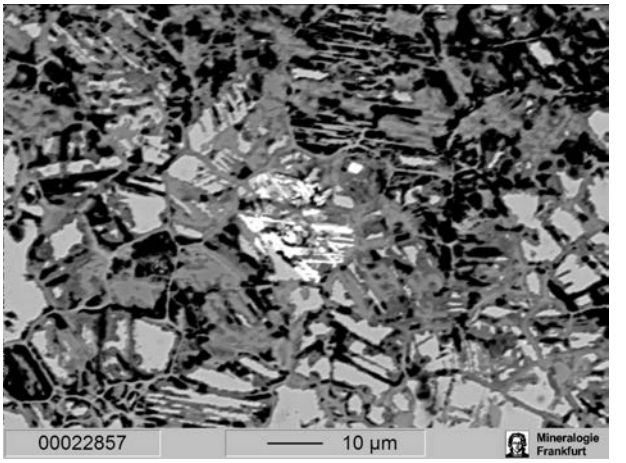

30-12-373

Museum nr. 30-12-373.1

Field Nr.	U.11212c
MMP NR.	Ur 116
Material	As-Cu
Object	Needle
Dating	Not Dated
Find context	U.12112 (IM 7453) Two Cylinder Seals
Tomb	PG 1249
Type of Tomb	Private
Notes	Field photograph (1284)
EPMA	x
Laser (Trace)	x
Laser (CuI)	
Sol (CuI)	
Laser (LIA)	x
Sol (LIA)	
PIXE-Analyses	As, 1.1%; Sn, 0.18%; Ni, 0.76%

Samuel K. Nash's Notebook

Ur 116 (30-12-373)
The circular cross section of this toggle pin has suffered severe corrosion both at its surface and over rather large areas within the interior. In both instances corrosion appears to have attached the metal a grain-at-a-time, rather than penetrating for some distance along grain boundaries. The remnant metal consists of polygonal shaped, annealed, twinned grains, GS 5-6. Non metallic inclusions of the sulfide type are globular in appearance, fairly numerous and uniformally spread throughout the cross section.

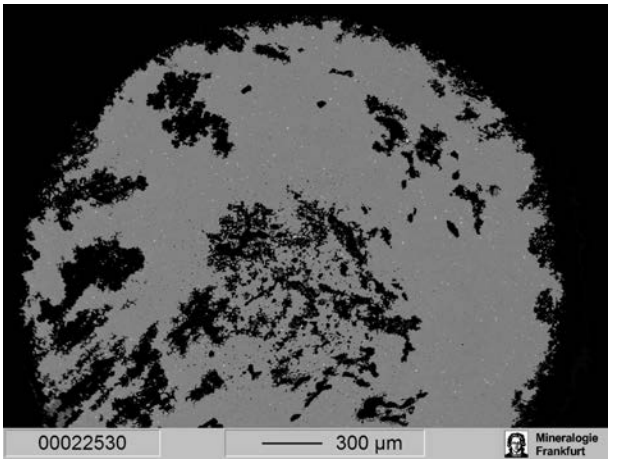

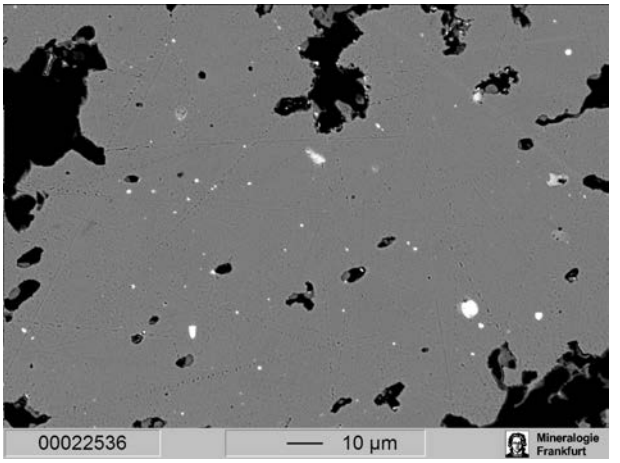

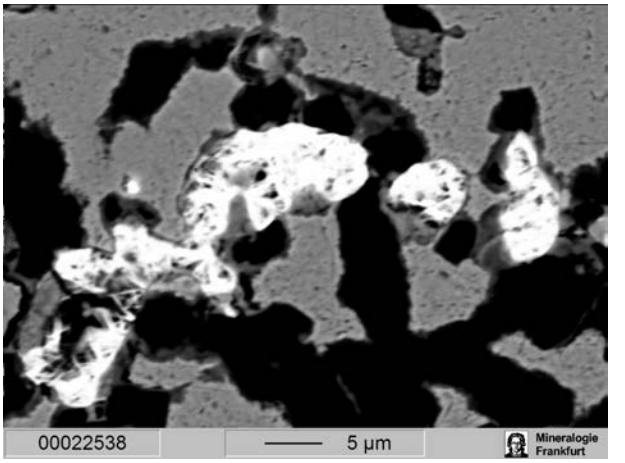

30-12-375

Museum nr. 30-12-375.1

Field Nr.	U.12606
MMP NR.	Ur 104
Material	As-Cu
Object	Needle
Dating	Akkadian
Tomb	PG 1339
Type of Tomb	Private
Notes	Dated with pottery
EPMA	x
Laser (Trace)	x
Laser (CuI)	
Sol (CuI)	
Laser (LIA)	x
Sol (LIA)	

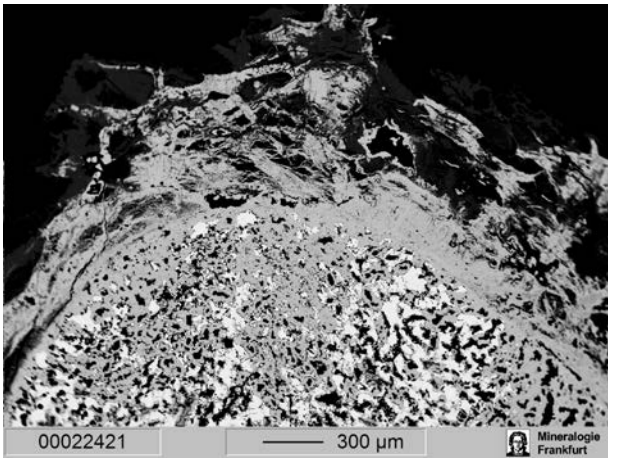

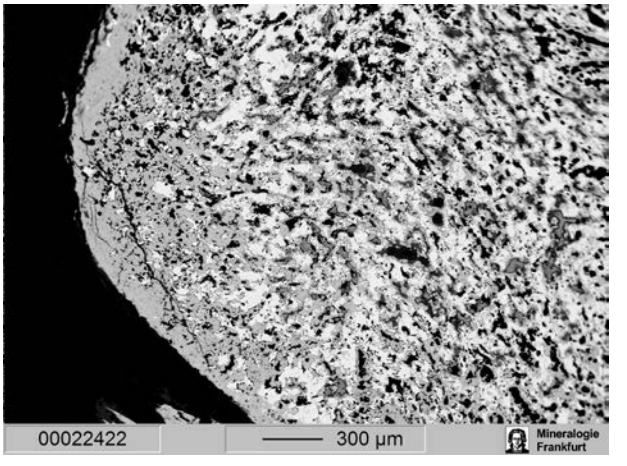

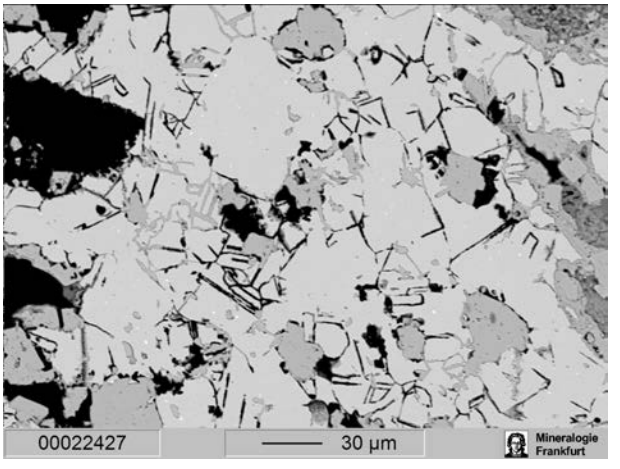

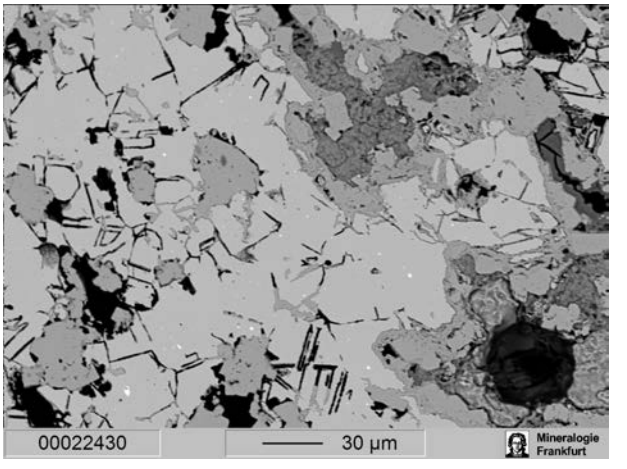

30-12-380

Museum nr. 30-12-380.1

Field Nr.	U.12054
MMP NR.	Ur 118
Material	As-Cu
Object	Pin
Dating	Akkadian
Tomb	PG 1230
Type of Tomb	Private
Notes	Dated with pottery
EPMA	x
Laser (Trace)	x
Laser (CuI)	
Sol (CuI)	
Laser (LIA)	x
Sol (LIA)	
PIXE-Analyses	As, 2.5%; Sn, 0.18%; Ni, 2.0%

Samuel K. Nash's Notebook

Ur 118 (30-12-380; U12654) ***9/19/10***

Corrosion of a predominantly pitting type has left the cold worked perimeter of this pin specimen in a highly serrated condition. The microstructure which initially consisted of annealed, twined, equiaxed grains is now penetrated by slits and cross-slit lines that extend from the perimeter to the center of the specimen. Grain size is ~5-6. A high density of duplex sulfide-type inclusions is also present.

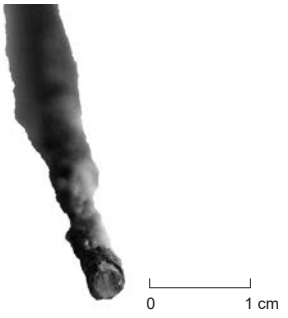

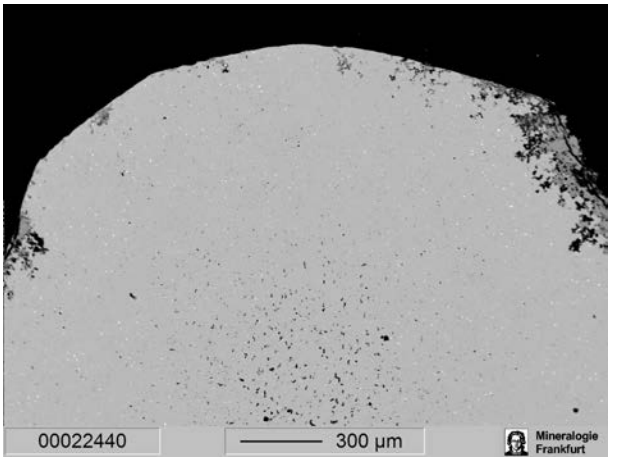

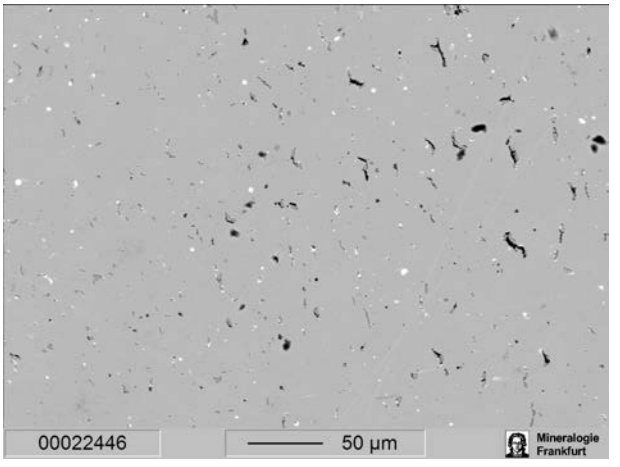

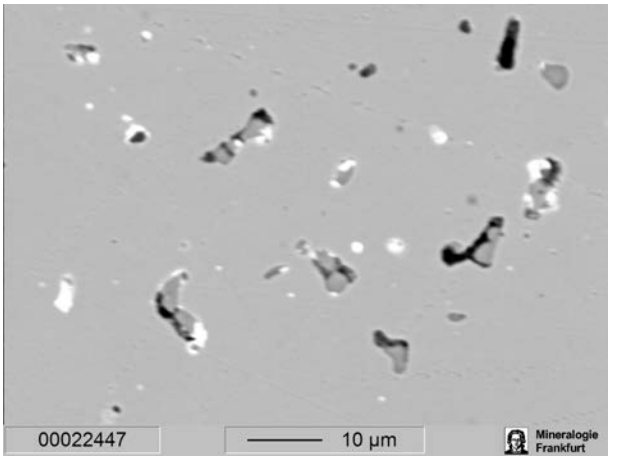

30-12-382

Museum nr. 30-12-382.1

Field Nr.	U.12680F
MMP NR.	Ur 95
Material	Bz
Object	Needle
Dating	Postakkadian-Ur III
Find context	U.12680 = BM 122499, 122566, 123711 - weird cylinder seal
Tomb	PG 1387
Type of Tomb	Private
Notes	BM says Elamite, Collon says Postakkadian - Ur III
EPMA	x
Laser (Trace)	x
Laser (CuI)	x
Sol (CuI)	
Laser (LIA)	x
Sol (LIA)	

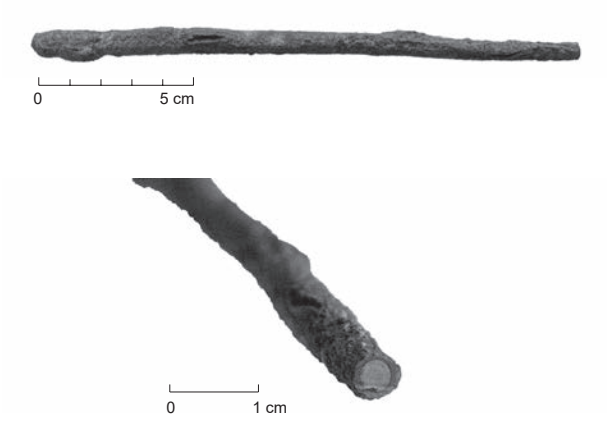

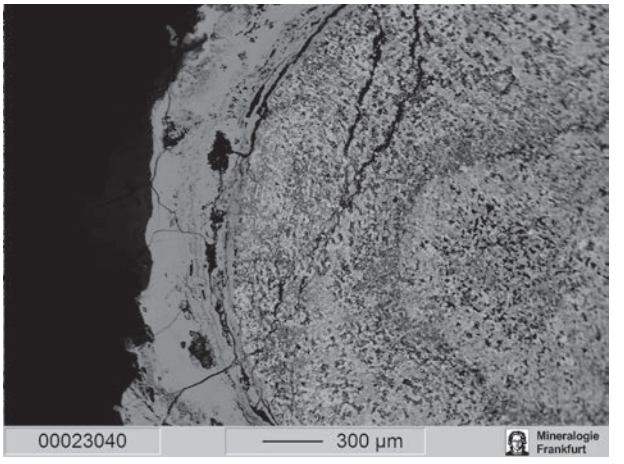

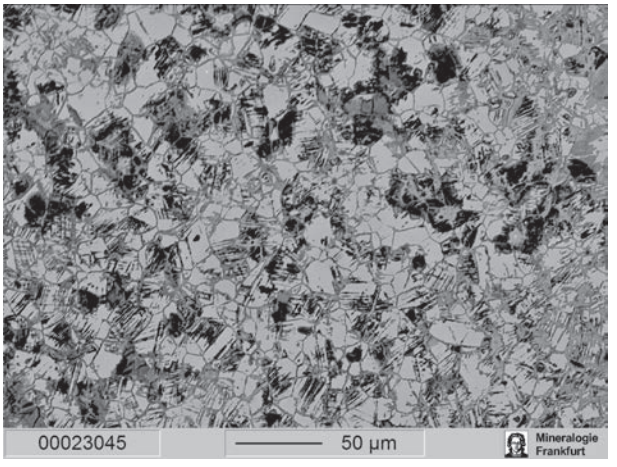

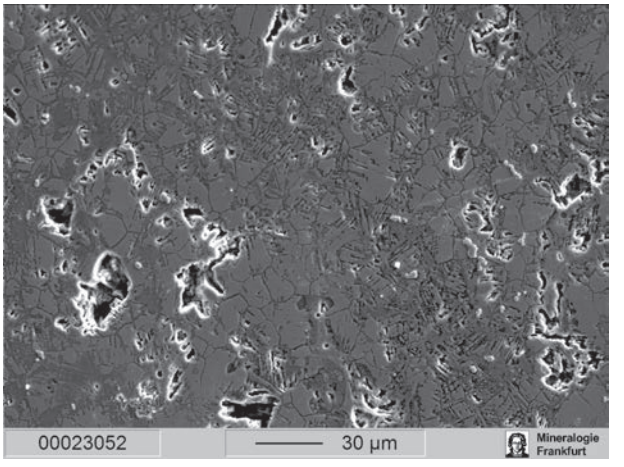

30-12-416

Museum nr. 30-12-416.1

Field Nr.	U.12350b
MMP NR.	Ur 105
Material	Bz
Object	Needle
Dating	Ur III
Find context	U.12350a (IM 14568) Cylinder Seal = UE 2, pl. 199, supposed a spread eagle = Post akkadian (?) Collon says Ur III
Tomb	PG 1336
Type of Tomb	Private
Notes	Collon says Ur III
EPMA	x
Laser (Trace)	x
Laser (CuI)	
Sol (CuI)	
Laser (LIA)	x
Sol (LIA)	

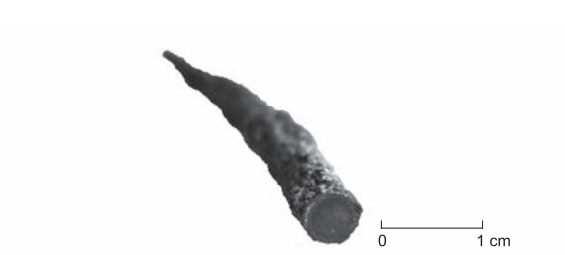

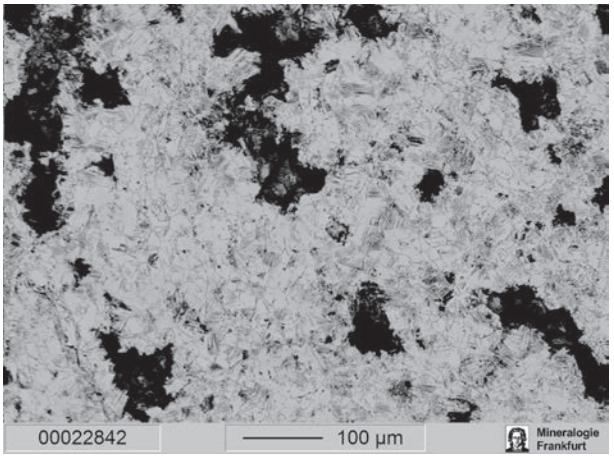

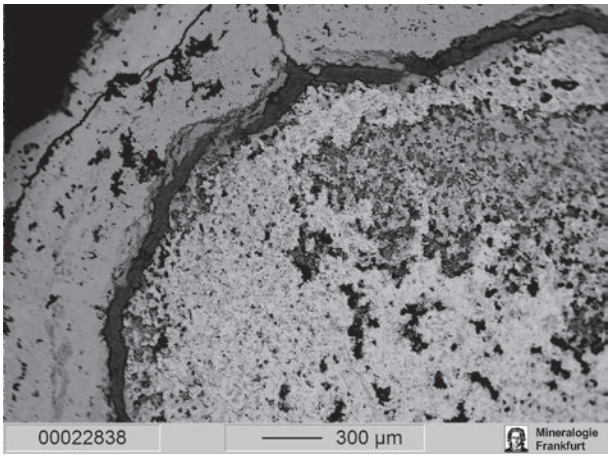

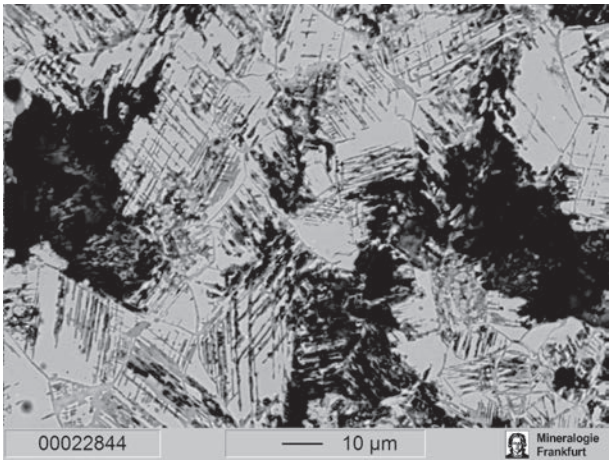

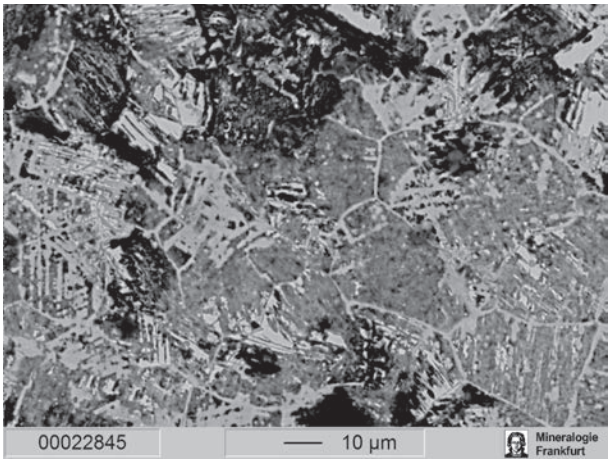

30-12-696

Museum nr. 30-12-696

Field Nr.	U.12435
Material	Bz
Object	Harp/Bull's Head
Dating	Early Dynastic
Tomb	PG 1332
Type of Tomb	Royal
EPMA	x
Laser (Trace)	x
Laser (CuI)	x
Sol (CuI)	x
Laser (LIA)	x
Sol (LIA)	x

Woolley, 1934, plate 116

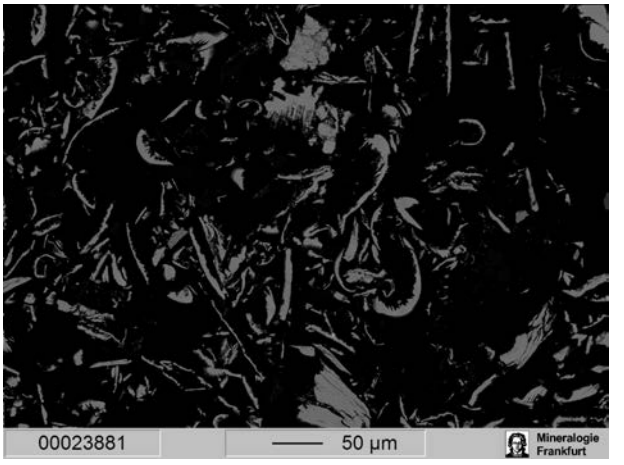

31-17-186

Museum nr. 31-17-186.1

Field Nr.	U.14238
MMP NR.	Ur 547
Material	Bz
Object	Axe
Dating	Early Dynastic
Tomb	PG 1687
Type of Tomb	Private
Notes	Woolley says ED
EPMA	x
Laser (Trace)	x
Laser (CuI)	x
Sol (CuI)	
Laser (LIA)	x
Sol (LIA)	
Misc	Casting structure
PIXE-Analyses	As, 0.33%; Sn, 18.9%; Ni, 1.2%

Samuel K. Nash's Notebook

U 033 Ur 547
✓ 31-17-186 [U14238]
Shafthole axe
Grave PG 1687
PIXE analysis: .....
PIXE data: As (0.33%) Sn (18.9%) Ni (1.2%)
Metallographic sample: .....
This highly corroded shafthole region of an axe is characterized by a cast microstructure consisting of coarse dendrites. Within the remnant portion there is a high density of what appear to be sulfide-type inclusions. Porosity is present throughout.

U 056 Ur 126

Samuel K. Nash's Notebook

Ur 547 Hardness scan taken at random (31-17-186)

47.1-46.8	*93.9*	
38.4-39.2	*77.6*	
43.4-41.7	*85.1*	
38.4-39.7	*78.1*	
40.9-40.2	*81.1*	*AV=88.3*
48.3-47.7	*96.0*	*VHN=95.1*
47.0-42.4	*94.4*	
46.0-46.5	*92.5*	
43.6-44.4	*88.0*	
46.5-47.0	*93.5*	
43.7-43.4	*87.1*	
45.6-47.1	*92.7*	
	1060.0	

Composition: As (0.33 %); Sn (18.9 %); Ni (1.29 %)

Microstructure: Cast, dendritic.

Note: Hardness impressions (100 grnload) taken only in clear metal areas able to accommodate the entire hardness impression. A second corroded phase, most likely high tin delta (δ) phase is present too, but it is completely corroded and was therefore not included in the hardness impressions. Question: is the data above the "true" hardness of this specimen?

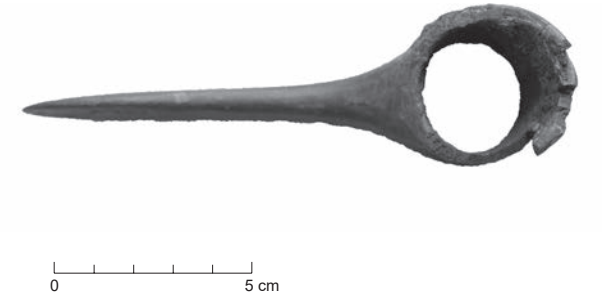

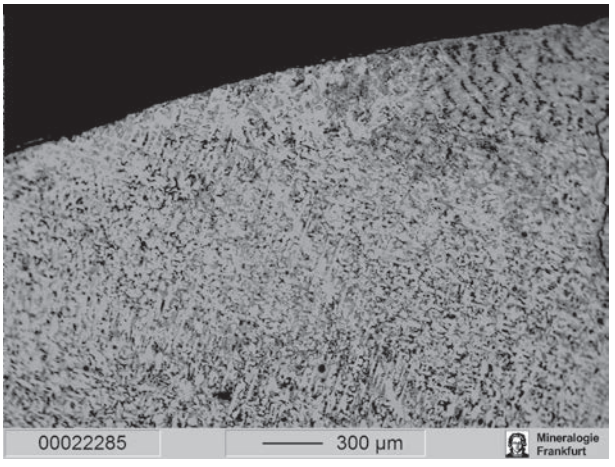

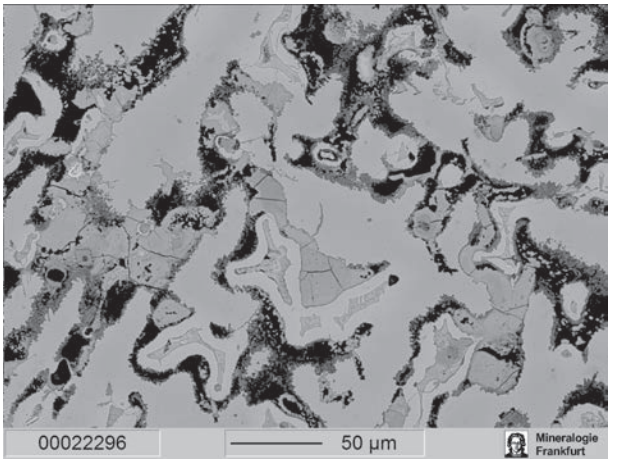

31-17-193

Museum nr.31-17-193.1

Field Nr.	U.14301
MMP NR.	Ur 74
Material	As-Cu
Object	Axe
Dating	Early Dynastic
Find context	U.14303: a bead supposed with a spread eagle on it
Tomb	PG 1738
Type of Tomb	Private
Notes	Woolley says ED
EPMA	x
Laser (Trace)	x
Laser (CuI)	
SoI (CuI)	
Laser (LIA)	x
SoI (LIA)	
PIXE-Analyses	As, 1.9%; Sn, 0.12%; Ni, 0.85%

Samuel K. Nash's Notebook

Ur 26 31-17-193
Heavy corrosion attack along the edge has also penetrated the matrix segmenting the remaining metal into several islands. The inclusions shapes still reflect their interdendritic origin, no evidence of working either hot or cold is visible. Main shape is prismatic with very straight boundaries; the grains themselves are fully recrystallized and twinned. This artifact was thoroughly annealed after casting to produce its evident microstructure.

[Following an etch with alcoholic FeCl3, some slight remnants of coring effects still visible].

[Note: Re etched with Klemm's III to tint. This is now in dessicator]

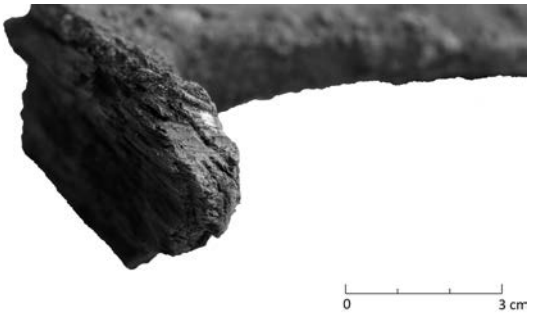

31-17-201

Museum nr. 31-17-201.1

Field Nr.	U.14304
MMP NR.	Ur 73
Material	As-Cu
Object	Adze
Dating	Early Dynastic
Tomb	PG 1739
Type of Tomb	Private
Notes	Woolley says ED
EPMA	x
Laser (Trace)	x
Laser (CuI)	
Sol (CuI)	
Laser (LIA)	
Sol (LIA)	
PIXE-Analyses	As, 2.9%; Sn, <0.024%; Ni, 3.0%

Samuel K. Nash's Notebook

✓ U 018 Ur 073
30-17-201 [U14304]
Shafthole adze
PIXE analysis: On the lower rim of the shafthole
PIXE data: As (2.9%) Sn (0.024%) Ni (3.0%)
Metallographic sample: From lower edge of socket
The inclusions in this specimen are small, well distributed and predominantly of the sulfide type, though some have a duel dark/light appearance. The shape of the inclusions bespeaks their dendritic origin. The microstructure consists of annealed, twinned, equiaxed grains (G.S., 5-6); however, an underlying dendritic pattern becomes visible when a ferric chloride etchant is used for increased contrast. Voids, a remnant of the dendritic shrinkage are a prominent feature.

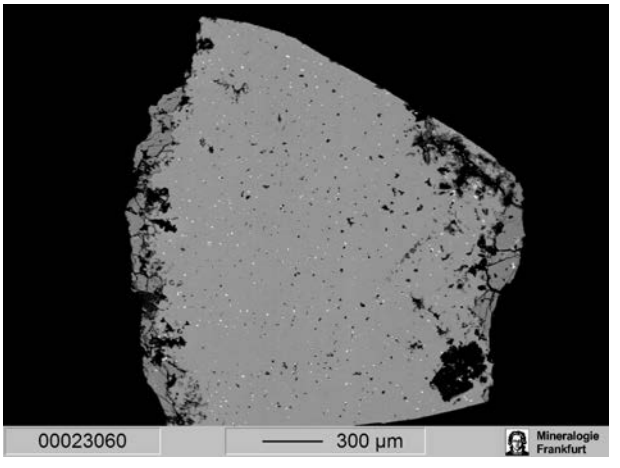

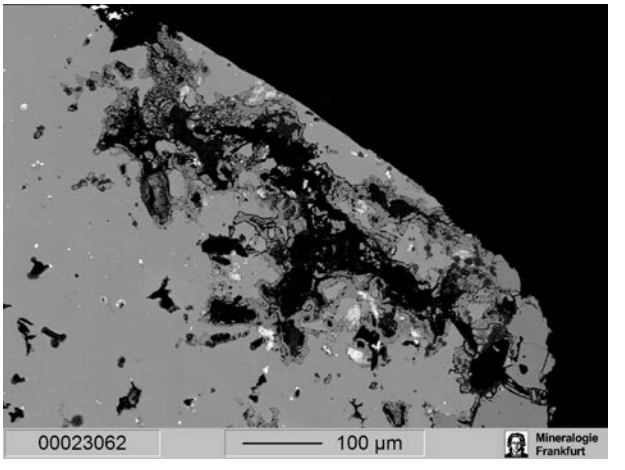

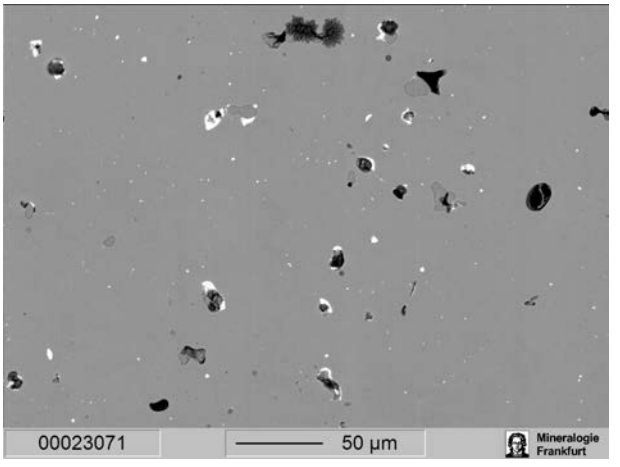

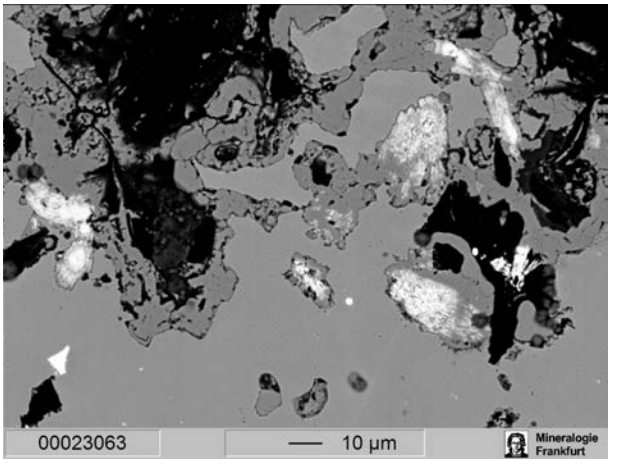

31-17-205

Museum nr. 31-17-205.1

Field Nr.	U.13528
MMP NR.	Ur 91
Material	Bz
Object	Adze
Dating	Early Dynastic
Tomb	PG 1520
Type of Tomb	Private
Notes	Woolley says ED
EPMA	x
Laser (Trace)	x
Laser (CuI)	x
Sol (CuI)	
Laser (LIA)	x
Sol (LIA)	
PIXE-Analyses	As, 1.4%; Sn, 4.5%, Ni, 0.75%

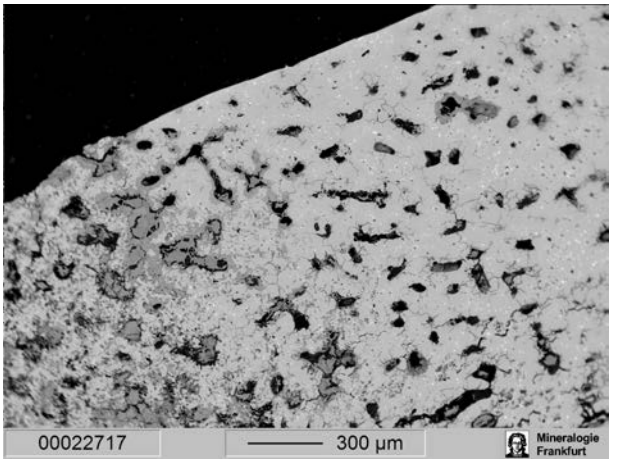

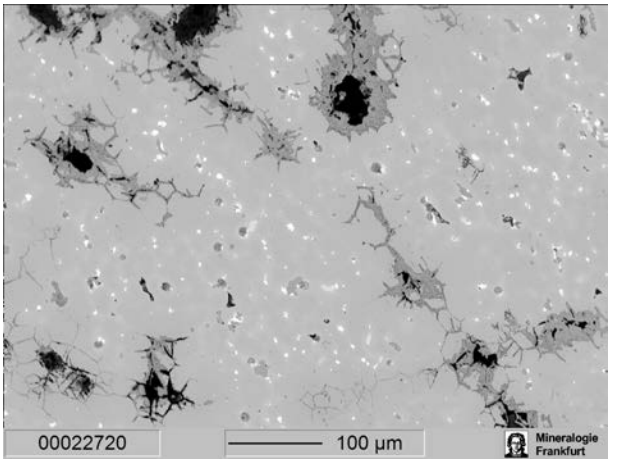

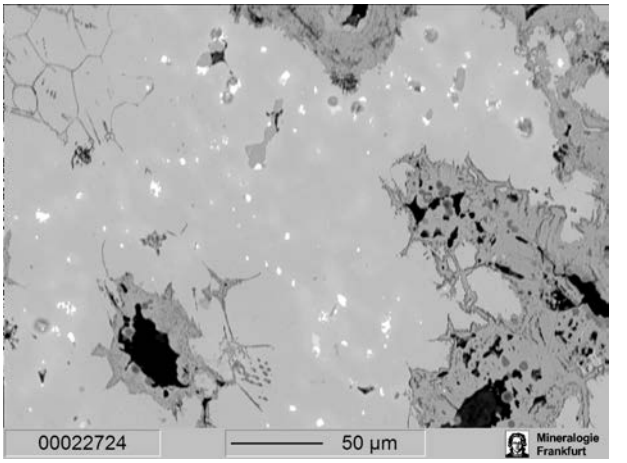

Samuel K. Nash's Notebook

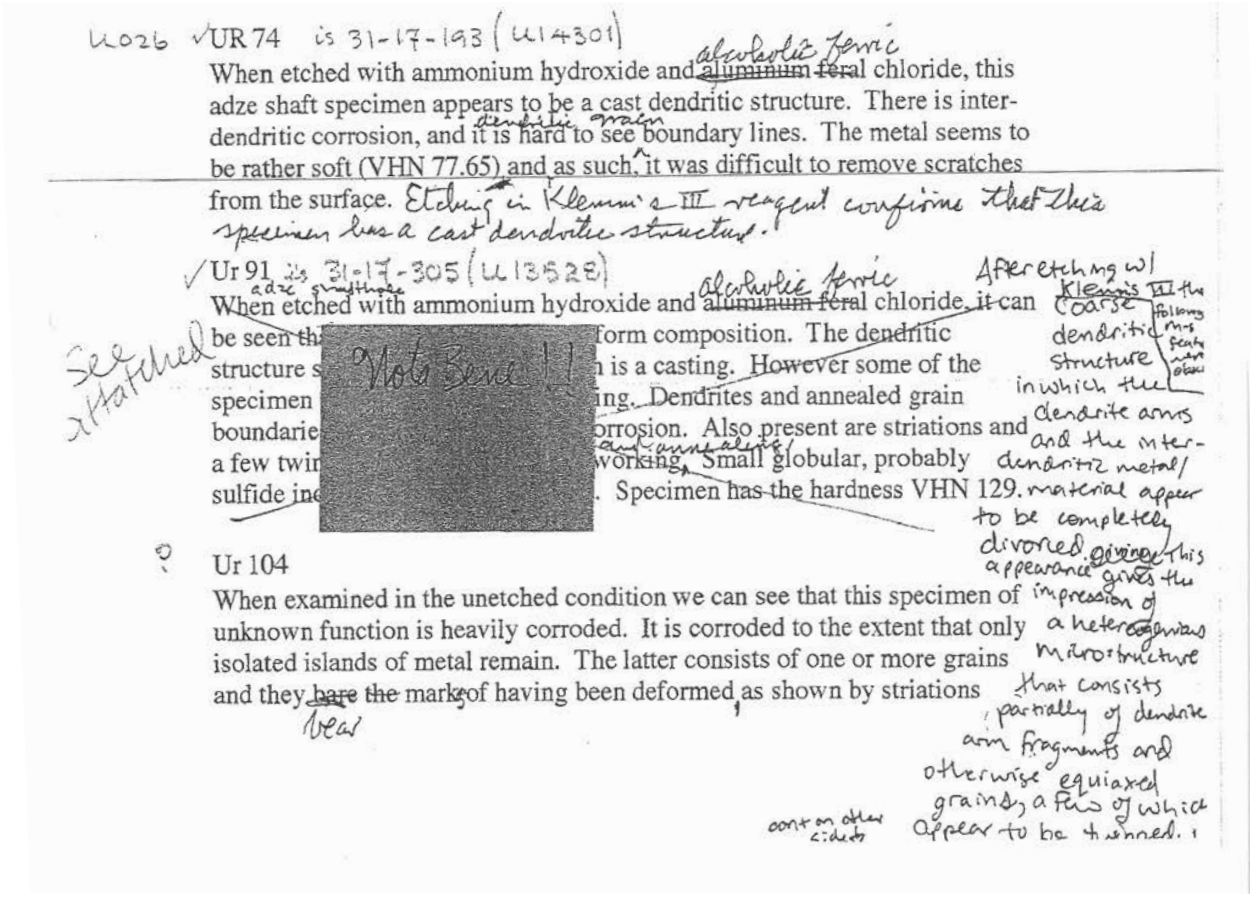

U026 ✓UR 74 is 31-17-193 (U14301)
When etched with ammonium hydroxide and ~~aluminum feral~~ alcoholic ferric chloride, this adze shaft specimen appears to be a cast dendritic structure. There is inter-dendritic corrosion, and it is hard to see dendritic grain boundary lines. The metal seems to be rather soft (VHN 77.65) and as such, it was difficult to remove scratches from the surface. Etching in Klemm's III reagent confirms that this specimen has a cast dendritic structure.

✓Ur 91 is 31-17-305 (U13528)
adze shafthole
When etched with ammonium hydroxide and ~~aluminum feral~~ alcoholic ferric chloride, it can be seen th[redacted]form composition. The dendritic structure s[redacted]n is a casting. However some of the specimen [redacted]ing. Dendrites and annealed grain boundarie[redacted]orrosion. Also present are striations and a few twin[redacted]working. Small globular, probably sulfide inc[redacted]. Specimen has the hardness VHN 129.

See attached

Not Sent !!

After etching w/ Klemm's III the following micro features were observed: Coarse dendritic structure in which the dendrite arms and the inter-dendritic metal/material appear to be completely divorced. This appearance gives the impression of a heterogeneous micro-structure that consists partially of dendrite arm fragments and otherwise equiaxed grains, a few of which appear to be twinned.

Ur 104
When examined in the unetched condition we can see that this specimen of unknown function is heavily corroded. It is corroded to the extent that only isolated islands of metal remain. The latter consists of one or more grains and they ~~bare the~~ bear marks of having been deformed as shown by striations

cont on other side

Saved in "Ur Micrographs"

U 13528 Ur 91
31-17-305
Shafthole Adze
PIXE analysis.....
PIXE data:

After etching with Klemm's III, the following micro structural features were observed. Coarse dendritic structure in which the dendrite arms and the inter-dendritic material appear to be completely divorced. This appearance gives the impression of a heterogeneous microstructure that consists partially of dendrite arm fragments and otherwise equiaxed grains, a few of which appear to be twinned. It seems reasonable to conclude that this specimen had been annealed, and other micro structural features such as striations are probably the result of deformation owing to cold working. Inclusions randomly dispersed appear to be of the sulfide type. A silvery appearing structure is present in some of the dendritic metal.

31-17-217.2-3

Museum nr. 31-17-217.2-3

Field Nr.	U.14252
MMP NR.	Ur 525
Material	Bz
Object	Adze
Dating	Early Dynastic
Tomb	PG 1698
Type of Tomb	Private
Notes	Woolley says ED, Haft of axe intact
EPMA	x
Laser (Trace)	x
Laser (CuI)	x
Sol (CuI)	
Laser (LIA)	
Sol (LIA)	
PIXE-Analyses	As, 2.2%; Sn, 5.2%; Ni, 0.78%

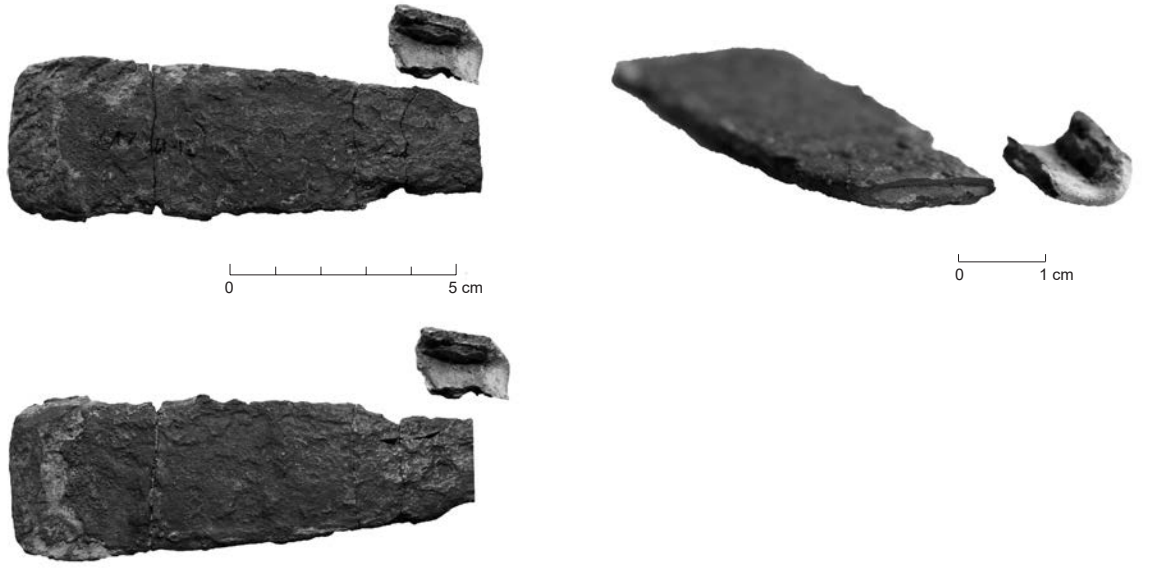

31-17-265

Museum nr. 31-17-265.1

Field Nr.	U.6642
MMP NR.	Ur 317
Material	Bz
Object	Bow
Dating	Late 2nd Mill BC or early 1st Mill BC
Find context	U.6638 (Silver bowl); Iron artefacts
Tomb	K.P., L-M, 10-1 Giparu
Type of Tomb	Private
Citation	Woolley UE VIII p. 37-38, Woolley UE IX, pp. 112-114
Notes	UE 8, (pp. 37-38) and 9
EPMA	x
Laser (Trace)	x
Laser (CuI)	x
Sol (CuI)	
Laser (LIA)	x
Sol (LIA)	

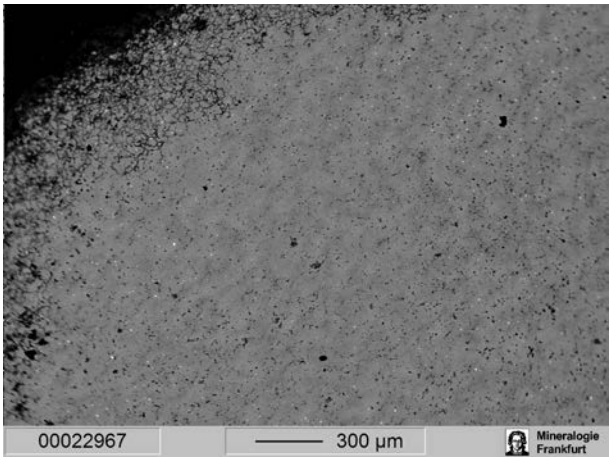

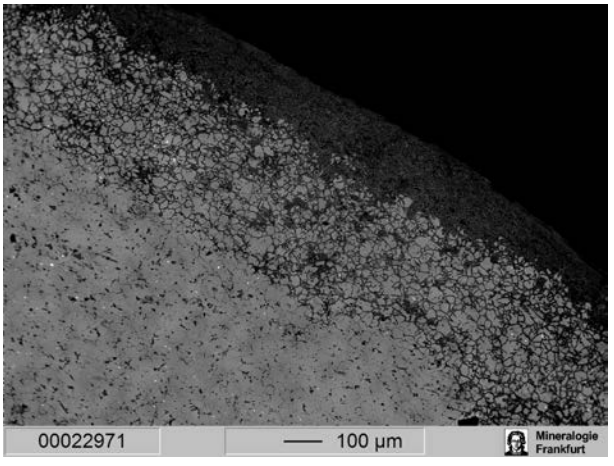

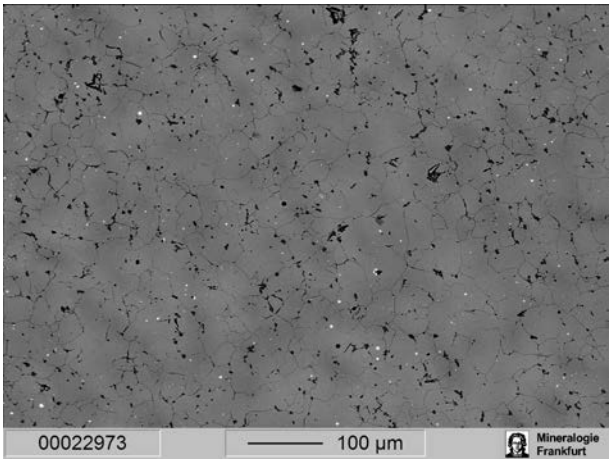

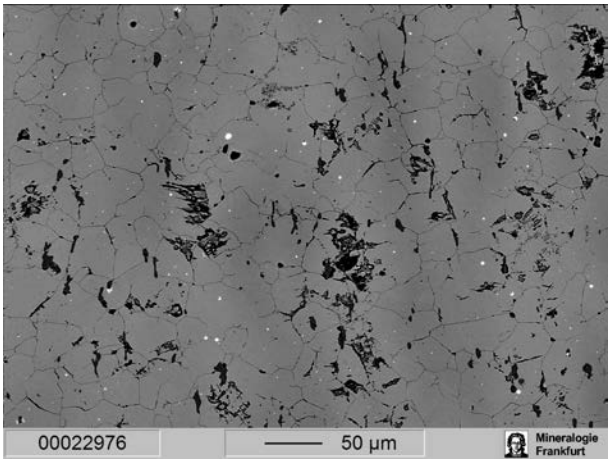

31-17-266

Museum nr. **31-17-266.1**

Field Nr.	U.14061
MMP NR.	Ur 542
Material	As-Cu
Object	Pin
Dating	Early Dynastic
Find context	U.14041 (31-17-7) Cylinder Seal = UE 2, pl. 195)
Tomb	PG 1625
Type of Tomb	Private
EPMA	x
Laser (Trace)	x
Laser (CuI)	x
Sol (CuI)	
Laser (LIA)	x
Sol (LIA)	
PIXE-Analyses	As, 2.4%; Sn, <0.018%; Ni, 2.1%

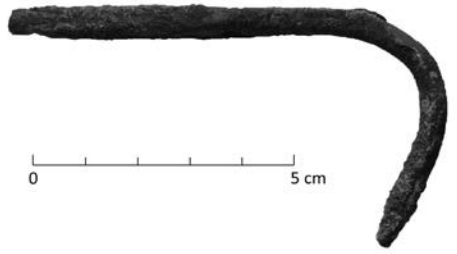

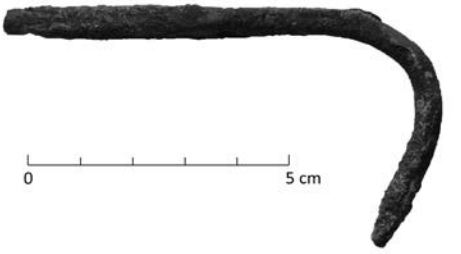

31-17-267

Museum nr. 31-17-267.1

Field Nr.	U.14924
MMP NR.	Ur 530
Material	As-Cu
Object	Hook
Dating	Late Uruk
Tomb	Pit F, T, square E7, level 8 - 8.5m
Type of Tomb	Private
Citation	Woolley UE IV pl. 30, p. 179
Notes	cf. UE 4, pp. 67 and 179 and pl. 30
EPMA	x
Laser (Trace)	x
Laser (CuI)	
Sol (CuI)	
Laser (LIA)	x
Sol (LIA)	
PIXE-Analyses	As, 1.1%; Sn, <0.010%; Ni, 0.28%

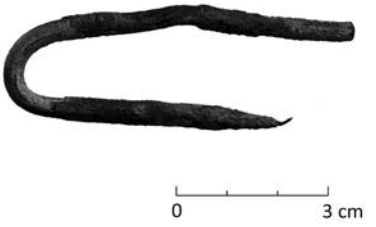

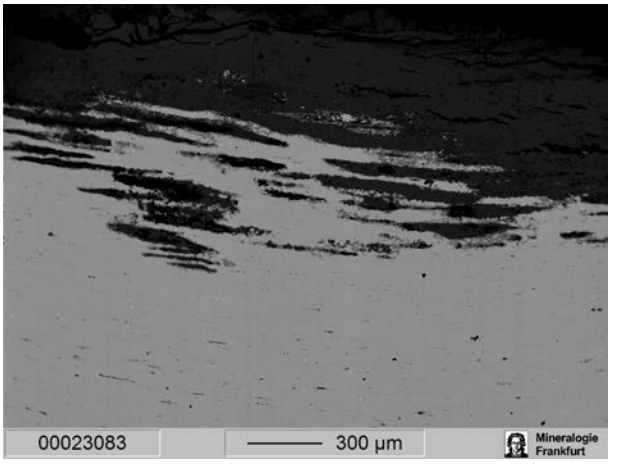

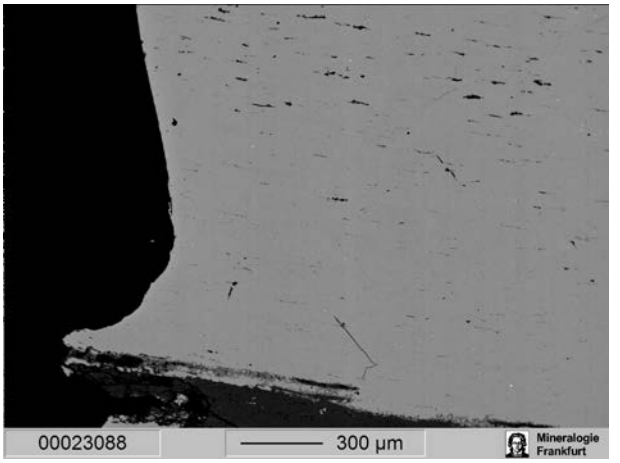

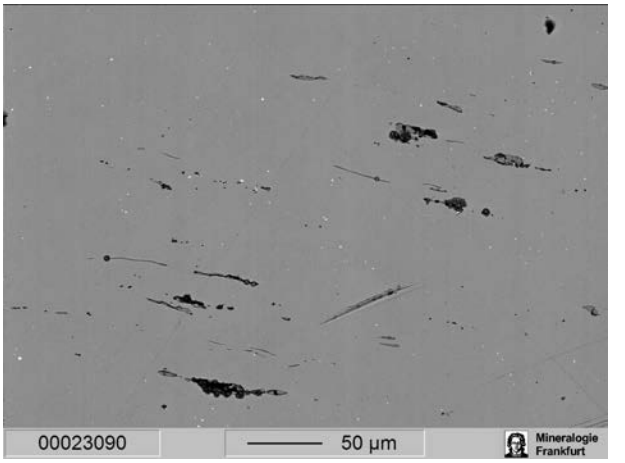

31-17-352T

Museum nr. 31-17-352T

Field Nr.	U.12778F
MMP NR.	Ur 539
Material	Cu
Object	Needle/pin shaft
Dating	Jemdet Nasr / ED I
Tomb	Pit G, levels 7.5-8m below plano-convex brick pavement (dates 3100 BCE)
Type of Tomb	Private
Notes	Pit G NW of PG 777
EPMA	x
Laser (Trace)	x
Laser (CuI)	
Sol (CuI)	
Laser (LIA)	x
Sol (LIA)	
PIXE-Analyses	As, 0.30%; Sn, <0.018%; Ni, 0.11%

https://www.penn.museum/collections/

Samuel K. Nash's Notebook

Ur 539, 31-17-352 ***4/11/06***

In oblong section of this specimen
Both the corrosion products and the remaining metal of this specimen appear in stratified layers. The two metal layers furthest from the center appear coherent, whereas the central portion has been heavily invaded by corrosion leaving it totally disrupted. The microstructure of the metal consists of blocky grains which appear both annealed and heavily twinned. Present also within the metal are sulfide type inclusions that appear as clusters in many areas.
VHN=99
Grain size approximately GS 6-7

Ur 001 31-17-352

Consists of two sections: transverse / circular; longitudinal section of rodshape. Heavily corroded with intergranular penetration throughout cracks in long section are situated both along the length and at right angles thereto. The crack paths suggest stress corrosion as the cause. High density of slate blue globular inclusions (could be matte) that in some areas are strung out and dispersed in a way that suggests eutectic formation. A higher degree of porosity is present in the central portion of both sections, perhaps a consequence of gas evolution during the original casting process. The grain structure shows the effects of hot working – a clear texture is evident in the long direction although the grains themselves are fairly equiaxed.

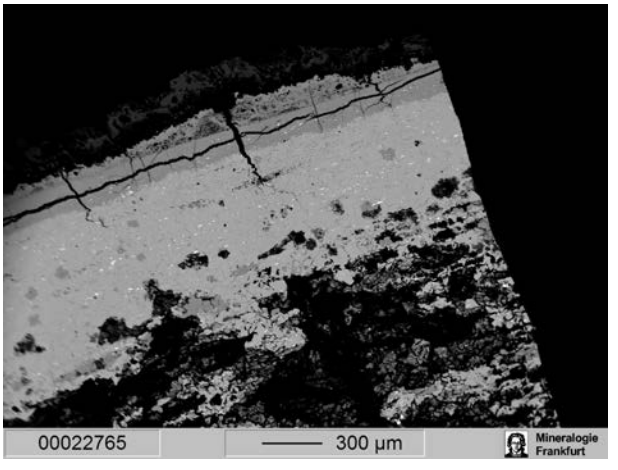

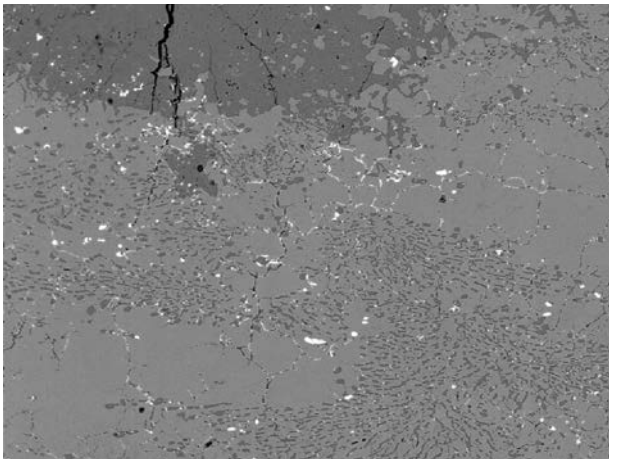

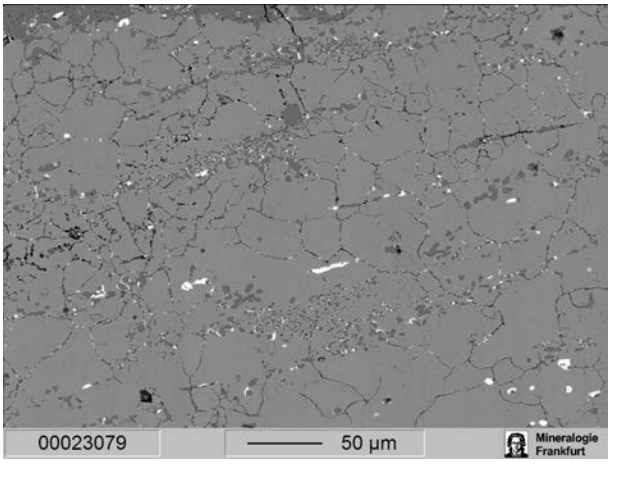

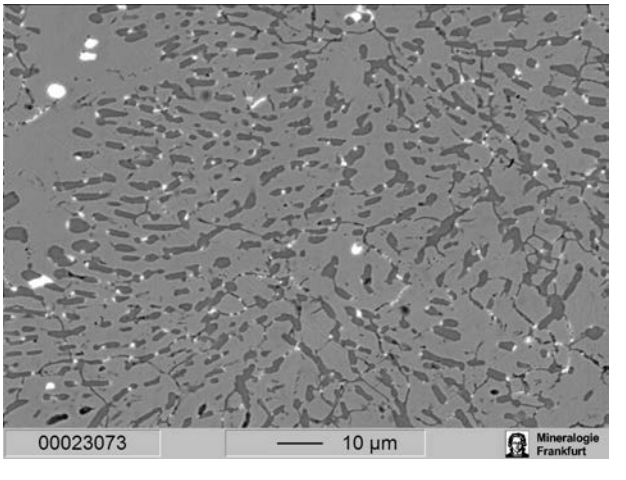

33-35-79

Museum nr. **33-35-79.1**

Field Nr.	U.18461
MMP NR.	Ur 137
Material	As-Cu
Object	Pin
Dating	Jemdet Nasr
Tomb	Pit W, JN 78b
Type of Tomb	Private
EPMA	x
Laser (Trace)	x
Laser (CuI)	
Sol (CuI)	
Laser (LIA)	
Sol (LIA)	
PIXE-Analyses	As, 2.1%; Sn, <0.012%; Ni, 2.8%

Samuel K. Nash's Notebook

U 002 Ur 137
33-35-079 [U18461]
Pike
Pin
Pit W, JN Grave 76b
PIXE analysis: On .....
PIXE data: As (2.1%) Sn (<0.012%) Ni (2.8%)
Metallographic sample: .....
The inclusions here are frequently of a duel composition and show a definite tendency towards alignment along the long axis of the specimen. The latter is an indication of working at elevated temperatures; however, the actual fragmented state of the inclusions is indicative of a cold-working preceding a final annealing treatment. The latter step produced essentially equiaxed, twined grains that vary widely in size —an indication of solute segregation.

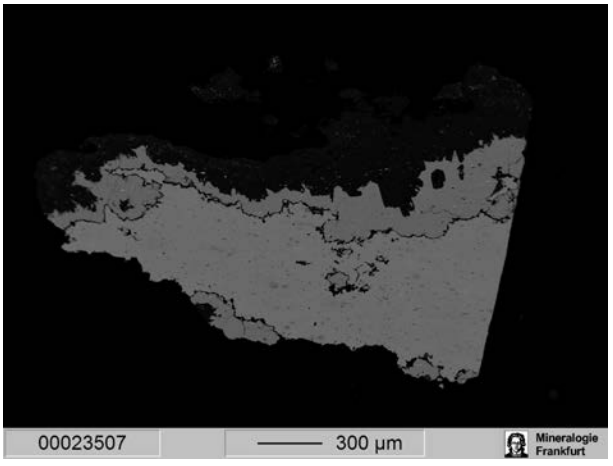

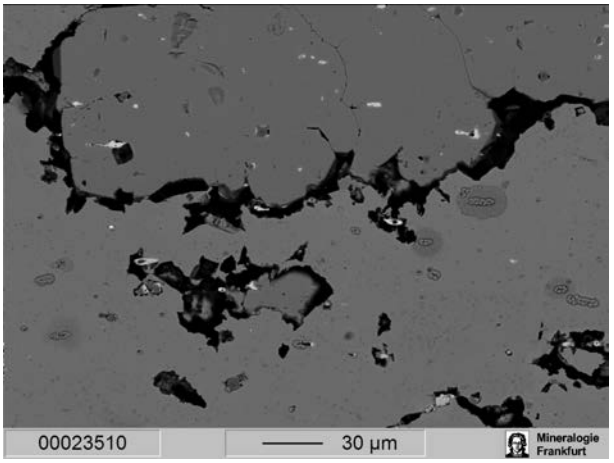

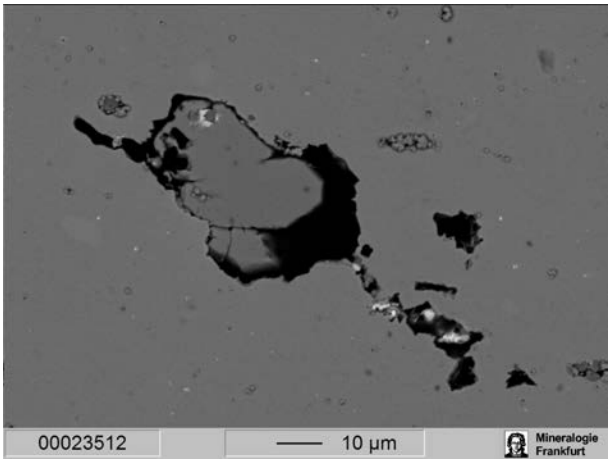

35-1-422.1-3

Museum nr. 35-1-422.1-3

Field Nr.	U.18935
MMP NR.	Ur 85, Ur 147
Material	Cu
Object	Dagger
Dating	Akkadian
Find context	cf. U.18926 Cylin der Seal UE 10, 131; UE IV
Tomb	Pit X PJ/G series 100
Type of Tomb	Private
Notes	Woolley says Sargonid
EPMA	x
Laser (Trace)	x
Laser (CuI)	
Sol (CuI)	
Laser (LIA)	
Sol (LIA)	
PIXE-Analyses	As, 3.6%; Sn, <0.032%; Ni, 2.3%

Samuel K. Nash's Notebook

Ur 85 35-01-422
This section has the thickness of a thin sheet. Inclusions are highly oriented indicating direction of initial hot working and subsequent cold working. Uniform fairly fine grained annealed, twinned recrystallized, broken edge contains numerous strain markings. The edge of the original shows uniform moderate corrosion layer.

Ur 147 [35-1-422]
Deep, intensive, pitting corrosion has effectively consumed the periphery of this blade specimen. The remaining metal probably adjacent to a cutting edge, has a heavily cold worked microstructure; the latter deformation has essentially erased outlining prior grain structure. An etching effect indicates non uniform composition in the forming light banding.
VHN: 195

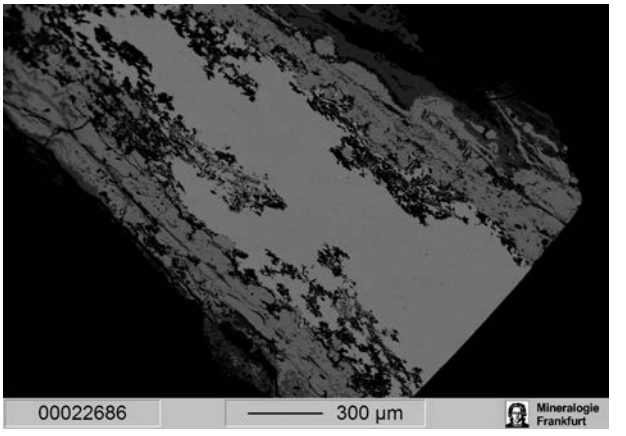

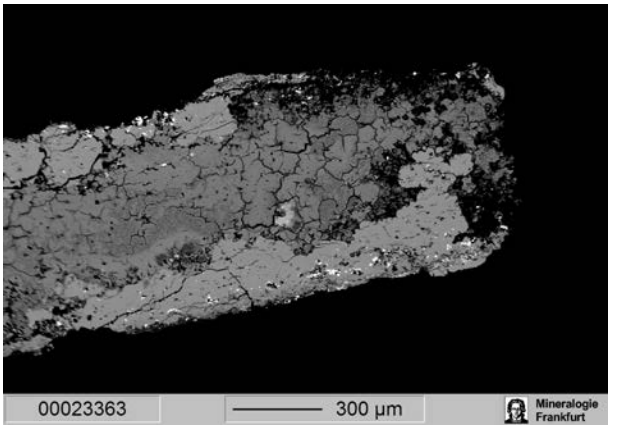

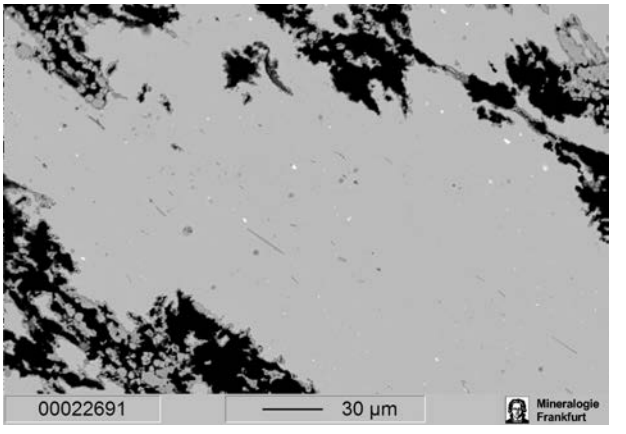

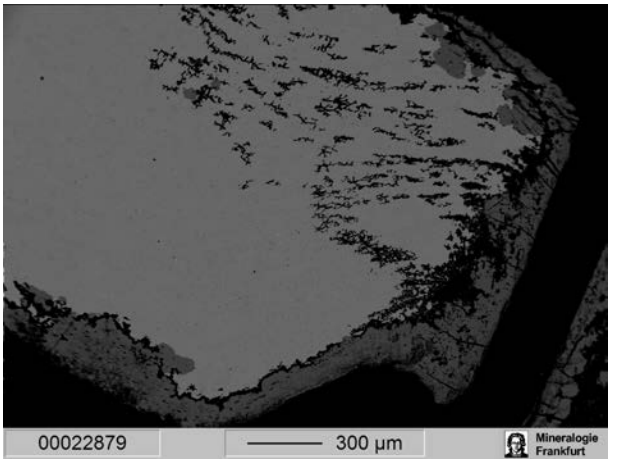

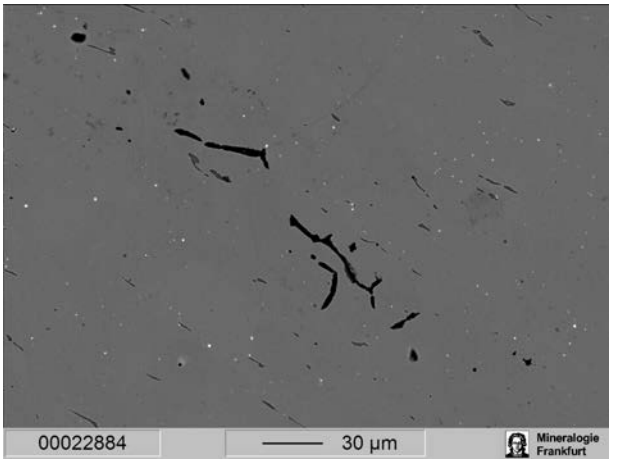

35-1-479

Museum nr. 35-1-479.1

Field Nr.	U.19102
MMP NR.	none
Material	s-Cu
Object	Pin
Dating	Early Dynastic
Tomb	Pit X PJ, found with U 19101 (copper pin) in ruins of a of the B series (plundered); UE IV: Pit X
Type of Tomb	Private
Notes	Woolley says ED
EPMA	x
Laser (Trace)	x
Laser (CuI)	
Sol (CuI)	
Laser (LIA)	x
Sol (LIA)	

98-9-164

Museum nr. 98-9-164

Field Nr.	none
MMP NR.	none
Material	Cu
Object	Copper ingot
Dating	Not Dated
Tomb	unknown
Type of Tomb	unknown
Notes	Probably not from Ur, but from Nippur, and of different dating
EPMA	x
Laser (Trace)	
Laser (CuI)	
Sol (CuI)	x
Laser (LIA)	
Sol (LIA)	x

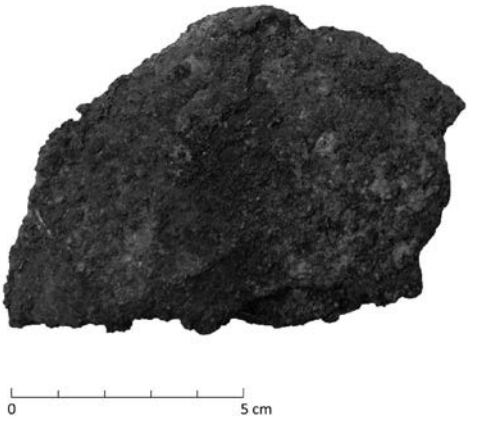

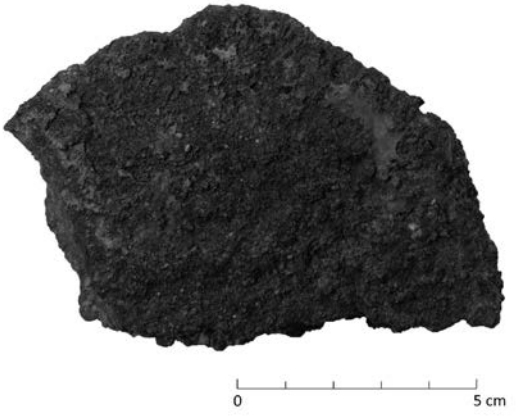

B16409.1-4

Museum nr. **B16409.1-4**

Field Nr.	U.6510
MMP NR.	Ur 96
Material	As-Cu
Object	Needle
Dating	Ur III - Isin Larsa
Tomb	EH (=series of houses) DT (probably DT=-Dim-tabba)
Type of Tomb	Private
Notes	Babylonian Section Catalogue says „Larsa Level“; B16409.1 is probably from another artefact, due to its different Pb isotopes and chemical composition
EPMA	x
Laser (Trace)	x
Laser (CuI)	
SoI (CuI)	
Laser (LIA)	x
SoI (LIA)	

Samuel K. Nash‘s Notebook

Ur 96 B16409
The border of this specimen has the appearance of having been broken from its source. In this narrow region some striations as well as intergranular corrosion attack are visible. A high density of at least two inclusions compositions are present; the black spots may be either lead or porosity. Some of the inclusions are somewhat elongated, but most have a spherical shape. Major corrosion has penetrated into the specimen center.
In the etched condition, the grain structure is equiaxed – resembling ferrite rather than typical prismatic Cu-Sn grains. The presence of a fine grain boundary precipitate may be the cause of this grain boundary movement. [See Martin and Doherty: Pg. 241-3]. Strain markings accentuated by etching are visible throughout the specimen interior. Some twinning is evident.

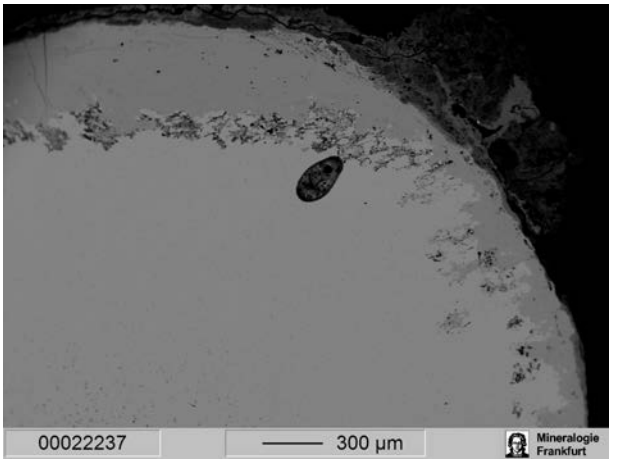

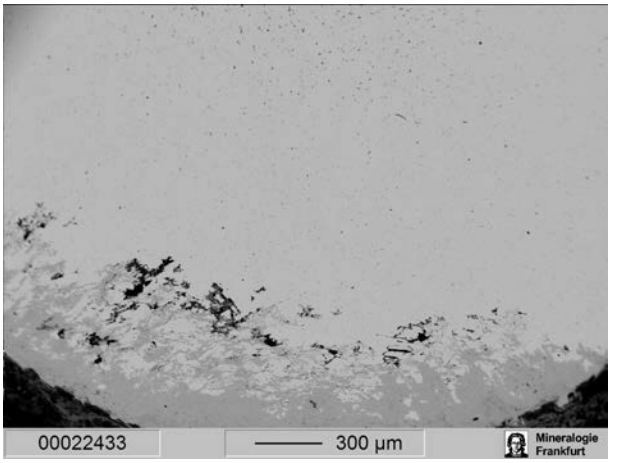

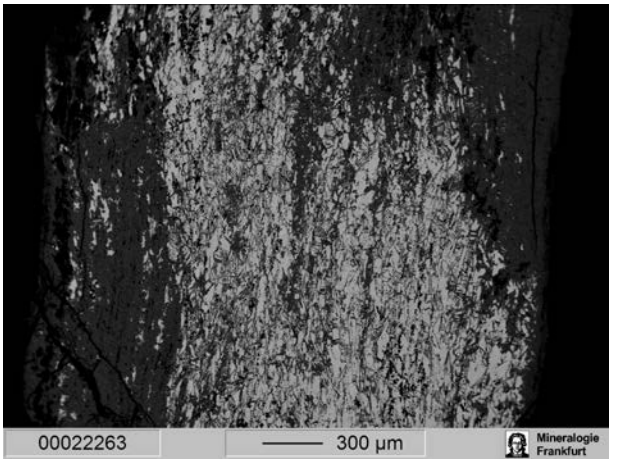

B16937

Museum nr. **B16937.1**

Field Nr.	U.10744
MMP NR.	Ur 132
Material	Bz
Object	Bracelet
Dating	Akkadian
Tomb	PG 0906
Type of Tomb	Private
Notes	Woolley says Akkadian
EPMA	x
Laser (Trace)	x
Laser (CuI)	
Sol (CuI)	
Laser (LIA)	x
Sol (LIA)	
PIXE-Analyses	As, 0.29%; Sn, 14.2%; Ni, 0.34%

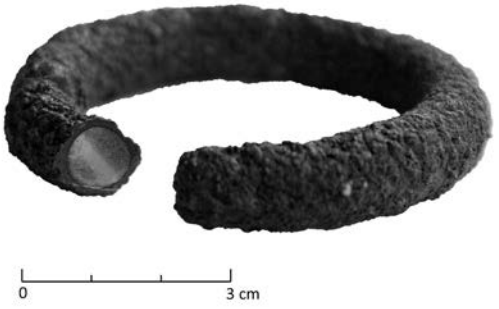

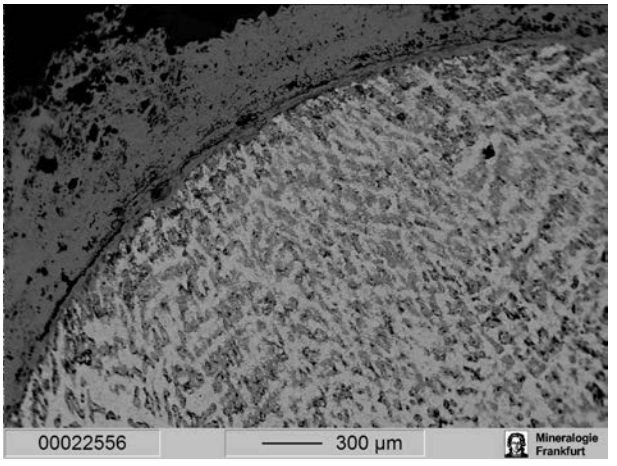

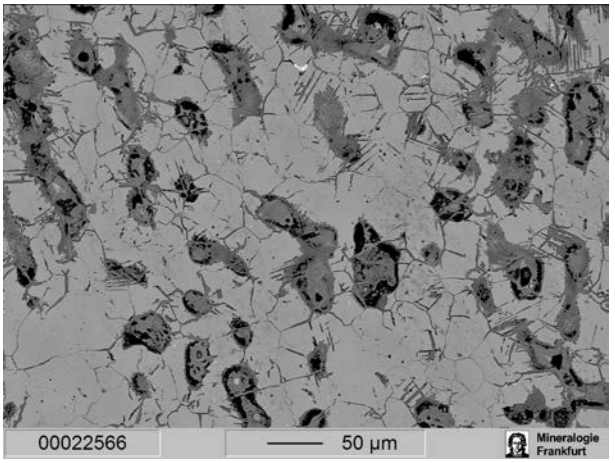

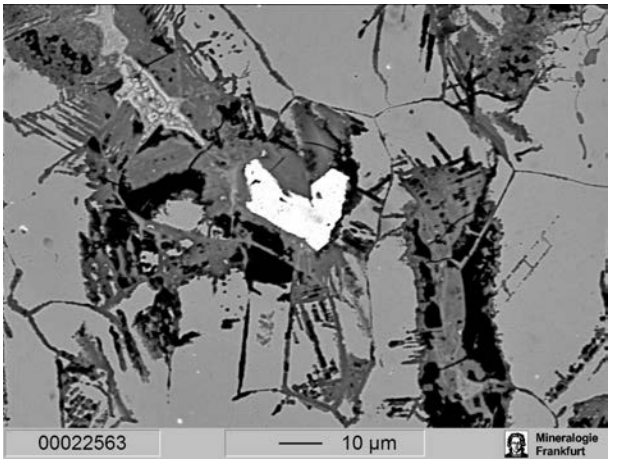

B16954

Museum nr. B16954.1

Field Nr.	U.9599
MMP NR.	Ur 160
Material	Bz
Object	Pin
Dating	Early Dynastic
Tomb	PG 0662
Type of Tomb	Private
Notes	Woolley says ED
EPMA	x
Laser (Trace)	x
Laser (CuI)	x
Sol (CuI)	
Laser (LIA)	
Sol (LIA)	
PIXE-Analyses	As, 0.24%; Sn, 12.6%; Ni, 0.10%

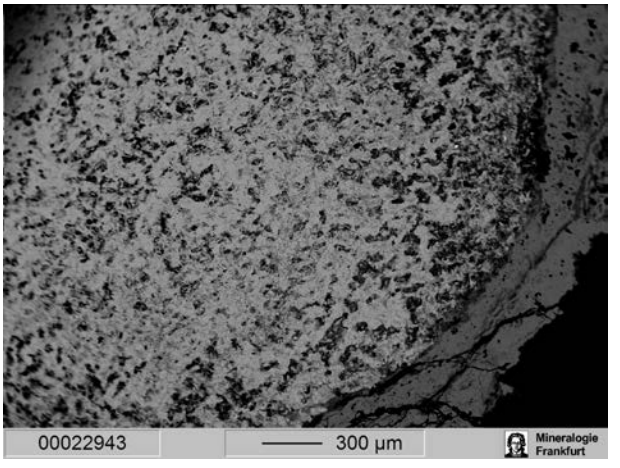

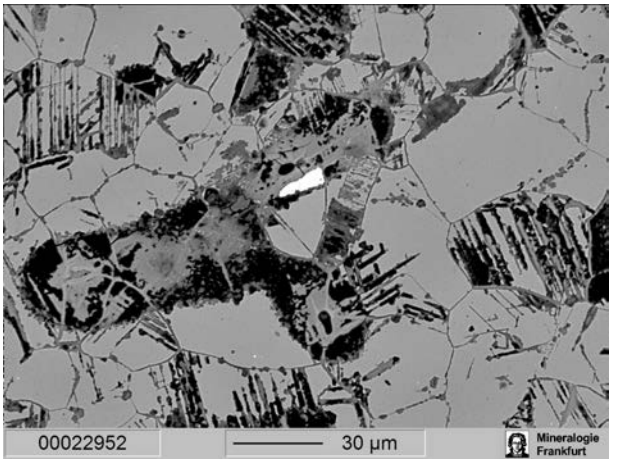

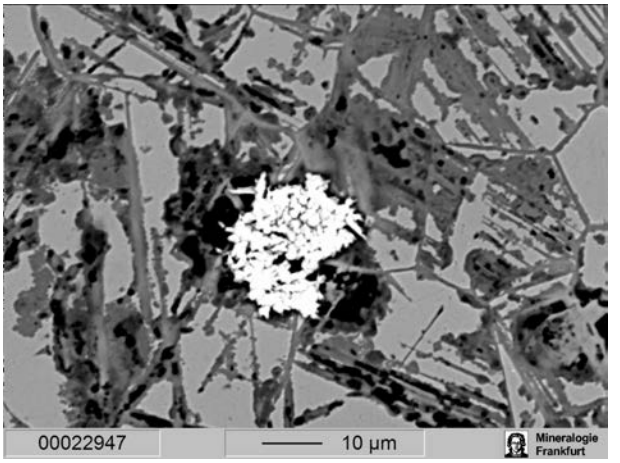

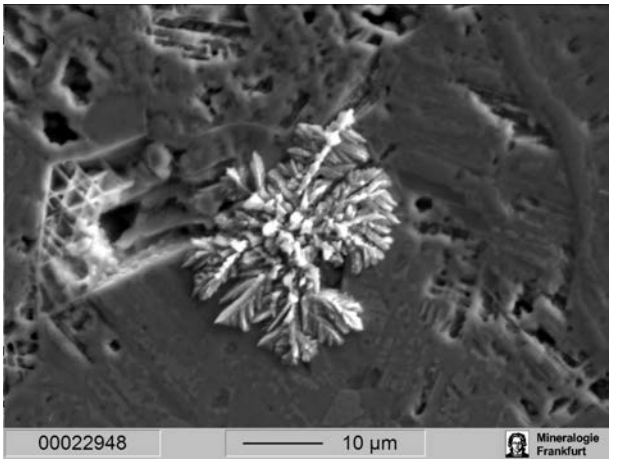

B16996

Museum nr. B16996.1

Field Nr.	U.9964
MMP NR.	Ur 177
Material	Bz
Object	Pin
Dating	Early Dynastic
Tomb	PG 0777
Type of Tomb	Royal
EPMA	x
Laser (Trace)	x
Laser (CuI)	x
Sol (CuI)	
Laser (LIA)	x
Sol (LIA)	

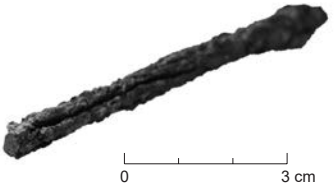

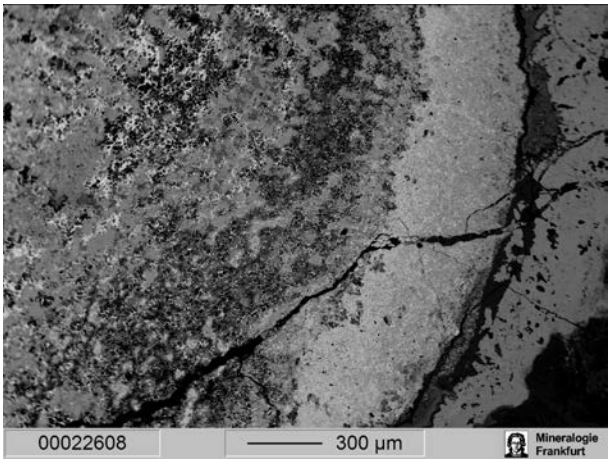

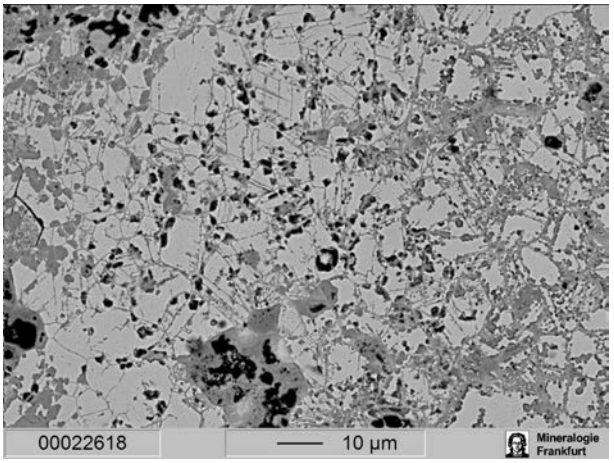

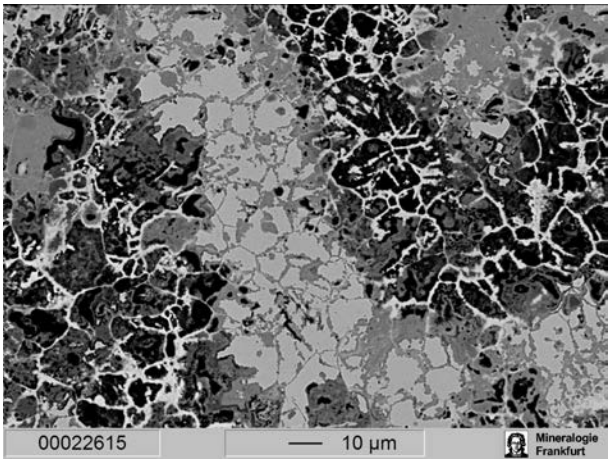

B17022

Museum nr. B17022.1

Field Nr.	U.9720
MMP NR.	Ur 164
Material	Bz
Object	Pin
Dating	Akkadian
Find context	cf. U.9721 (B17024) Cylinder Seal Tomb PG 0681
Type of Tomb	Private
EPMA	x
Laser (Trace)	x
Laser (CuI)	
Sol (CuI)	
Laser (LIA)	
Sol (LIA)	
PIXE-Analyses	As, 1.4%; Sn; 5.1%; Ni, 0.42%

Samuel K. Nash's Notebook

Ur 64 (B17022)
The unetched microstructure consists of an intergranularly corroded central core and a concentric ring of heavily intergranular corrosion separated from the core by a void. The main body also consists of equiaxed grains that are the consequence of original hot working. Grain size, in general is small GS 6-9, and is distributed in patches. A lack of homogeneity both in respect to composition and deformation is indicated. Numerous voids are present as well as a loss of individual grains from the matrix.

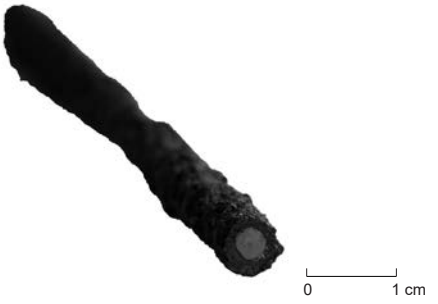

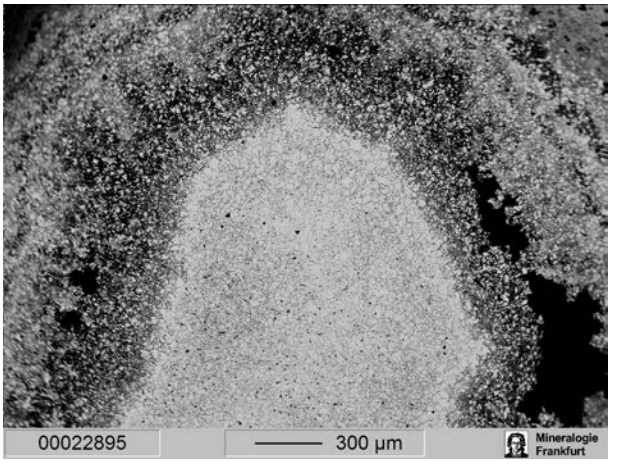

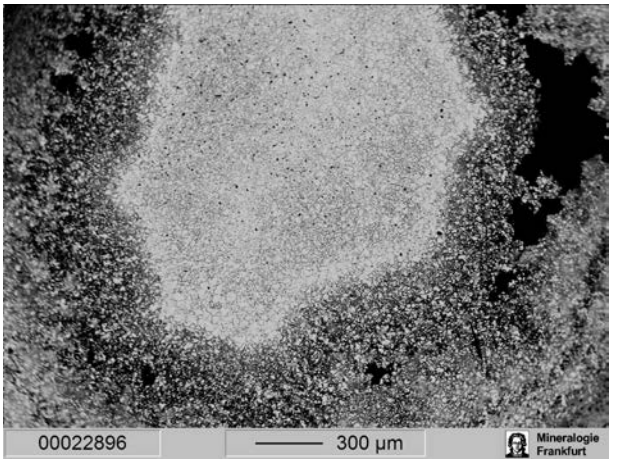

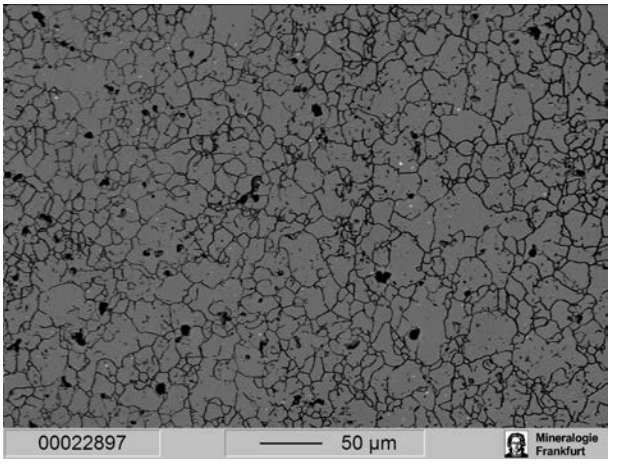

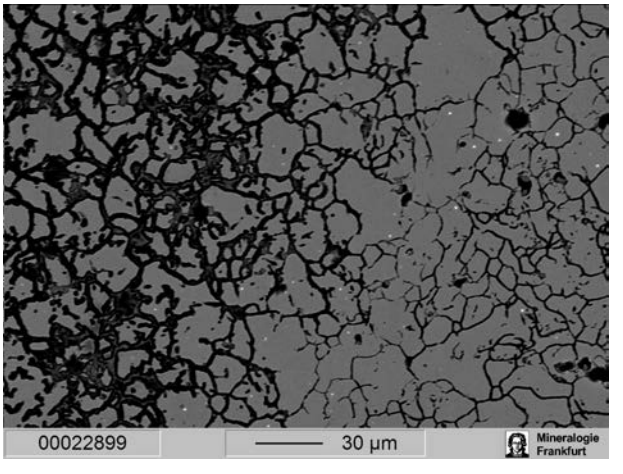

B17276.2

Museum nr. B17276.2

Field Nr.	U.10794
MMP NR.	Ur 533
Material	As-Cu
Object	Knife
Dating	Late Akkadian-Ur III
Find context	cf. U.10796 (B17569) Cylinder seal
Tomb	PG 0825
Type of Tomb	Private
Notes	Collon puts this kind of seal as Post-Akkadian to Ur III
EPMA	x
Laser (Trace)	x
Laser (CuI)	x
Sol (CuI)	
Laser (LIA)	x
Sol (LIA)	
PIXE-Analyses	As, 0.98%; Sn, <0.026%; Ni, 0.20%

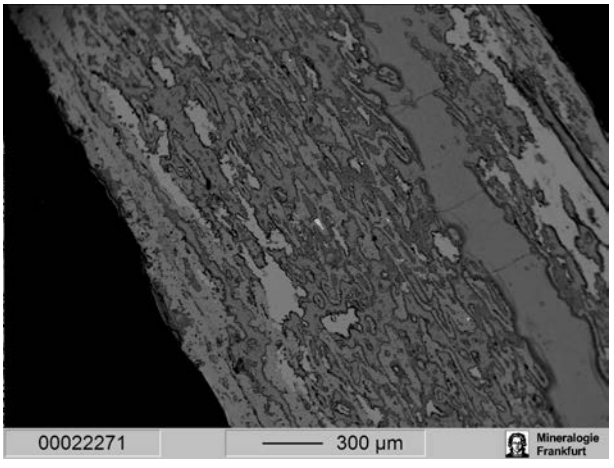

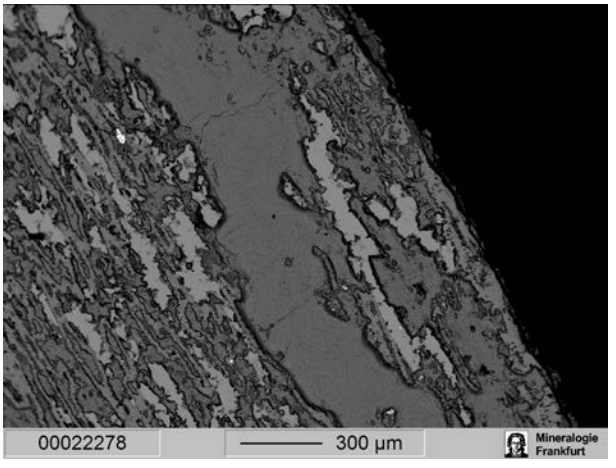

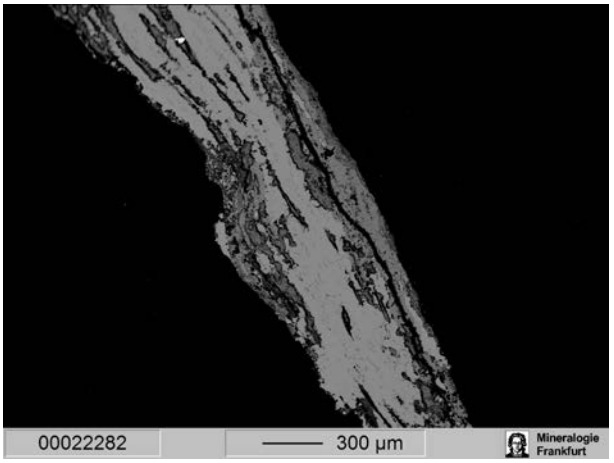

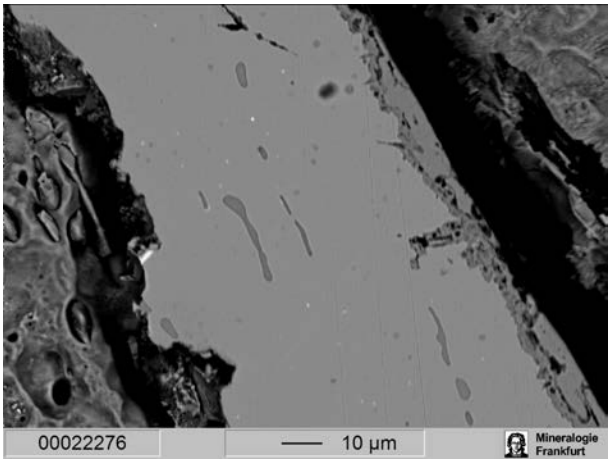

B17317

Museum nr. B17317.1

Field Nr.	U.9525
MMP NR.	Ur 153
Material	As-Cu
Object	Pin
Dating	Early Dynastic
Tomb	PG 0619
Type of Tomb	Private
Notes	Woolley says ED
EPMA	x
Laser (Trace)	x
Laser (CuI)	
Sol (CuI)	
Laser (LIA)	x
Sol (LIA)	
PIXE-Analyses	As, 1.8%; Sn, <0.027%; Ni, 1.0%

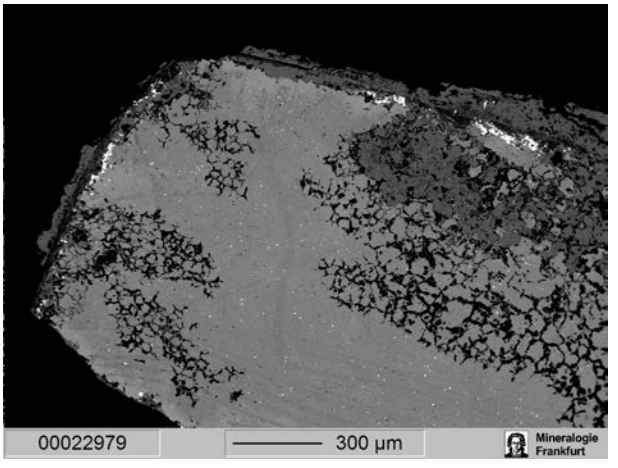

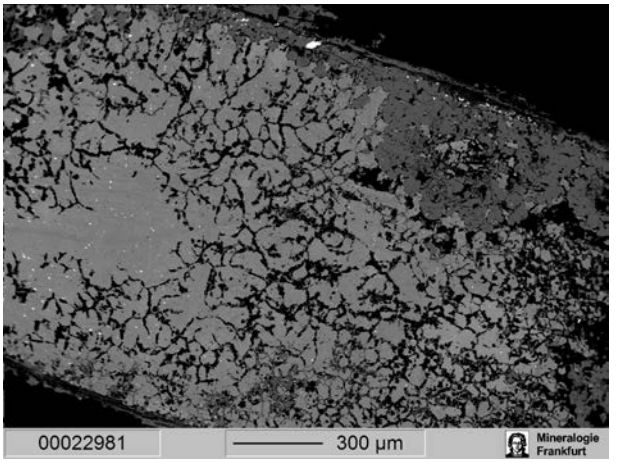

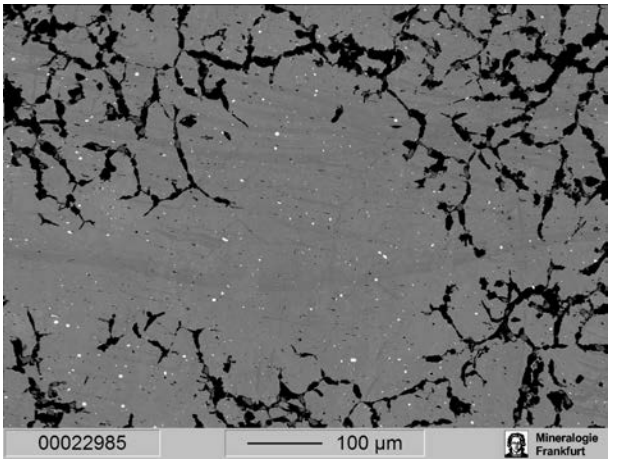

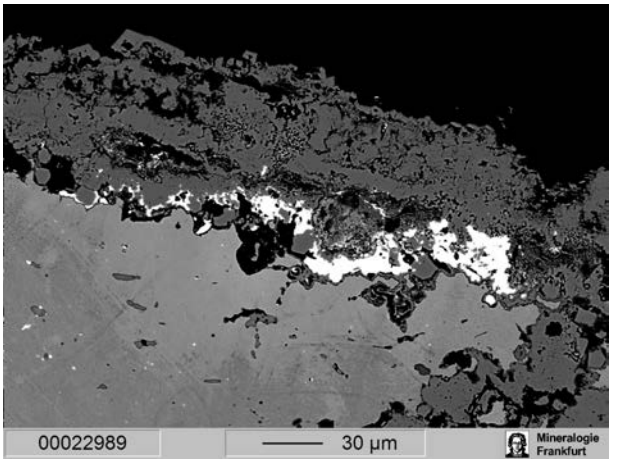

B17327

Museum nr. B17327.1

Field Nr.	U.8651
MMP NR.	Ur 62
Material	Bz
Object	Dagger
Dating	Early Dynastic
Tomb	PG 0049 TTE
Type of Tomb	Private
Notes	Woolley says ED
EPMA	x
Laser (Trace)	x
Laser (CuI)	x
Sol (CuI)	
Laser (LIA)	
Sol (LIA)	
PIXE-Analyses	As, 2.1%; Sn; 9.6%; Ni; 1.1%

Samuel K. Nash's Notebook

Ur 62 Dagger / knife B17327 (U.08501) ***2/20/06***

In the unetched condition, it is evident that intergranular corrosion has penetrated the entire specimen. At the specimen's periphery strain lines resulting from coldworking are present, and, in some instances, entire grains have been lost. The well delineated grains size is: GS 5; and consists of equiaxed grains.

In the etched condition it is clear that the original cutting edge of this dagger / knife has been lost in corrosion. The remnant microstructure consists of annealed twinned grains, the penultimate result of segmential deformations and heat treatment. The hardness of this specimen varies between VH 105-114.

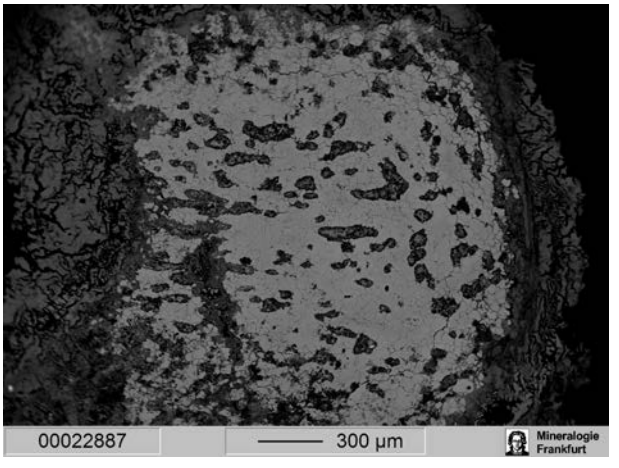

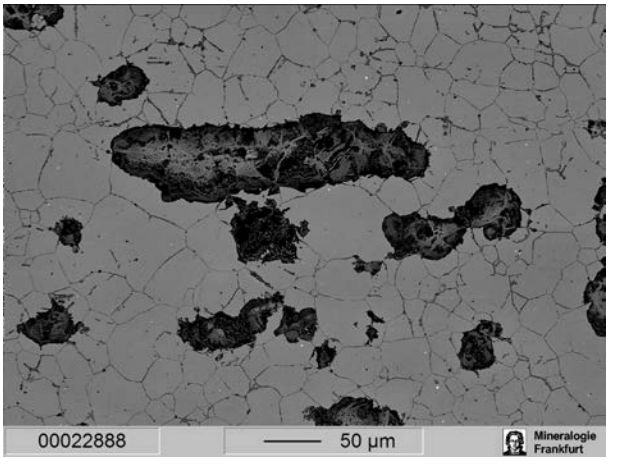

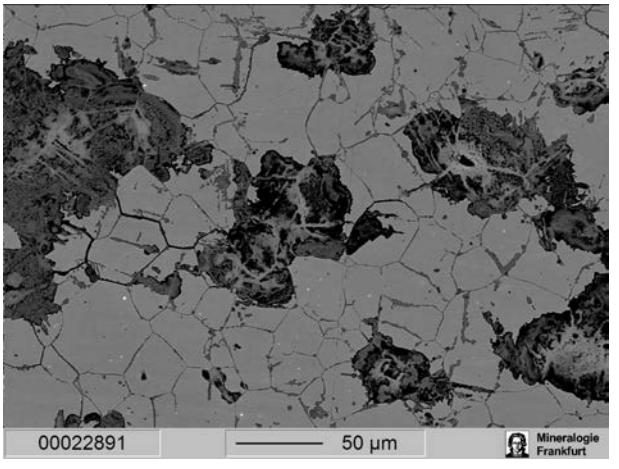

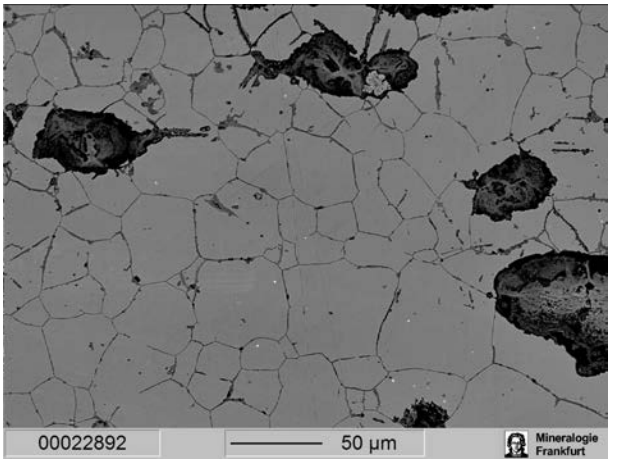

B17330

Museum nr. B17330.1

Field Nr.	U.9138-39
Material	Bz
Object	Blade
Dating	Early Dynastic
Tomb	PG 0537 (=PG 580)
Type of Tomb	Royal
EPMA	x
Laser (Trace)	x
Laser (CuI)	
Sol (CuI)	
Laser (LIA)	x
Sol (LIA)	
Misc	corroded

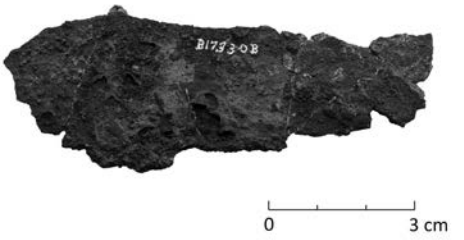

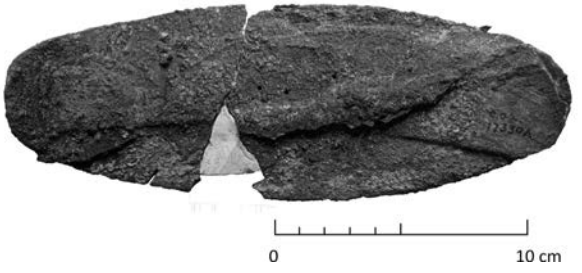

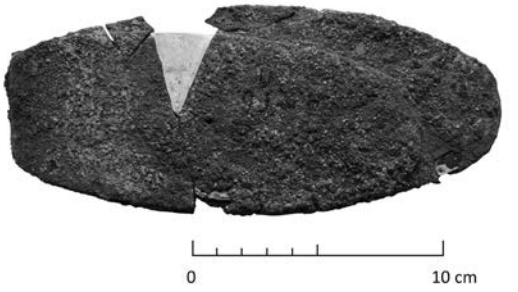

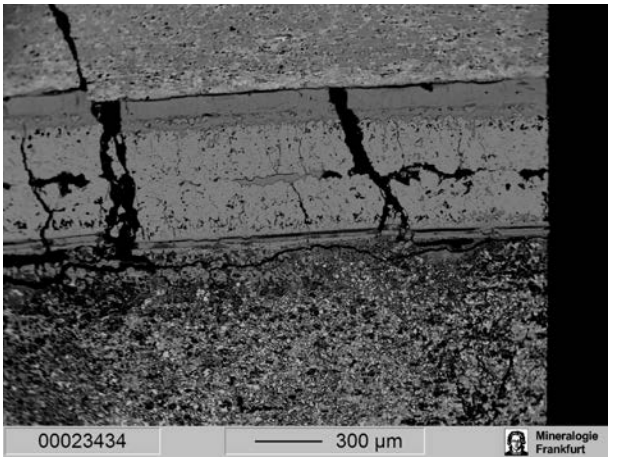

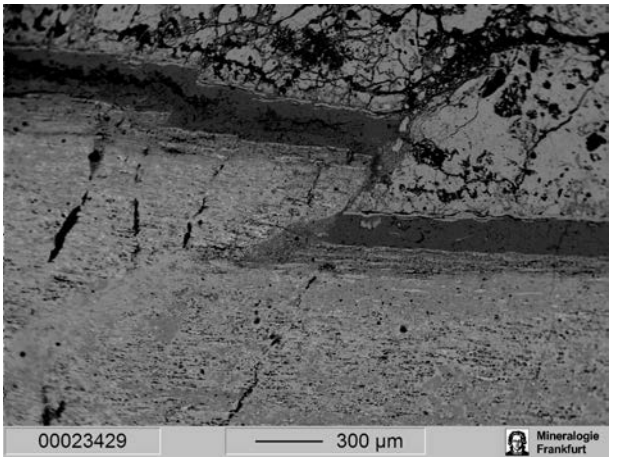

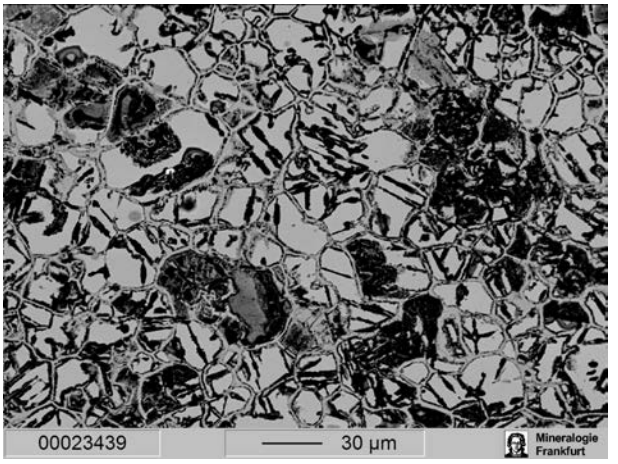

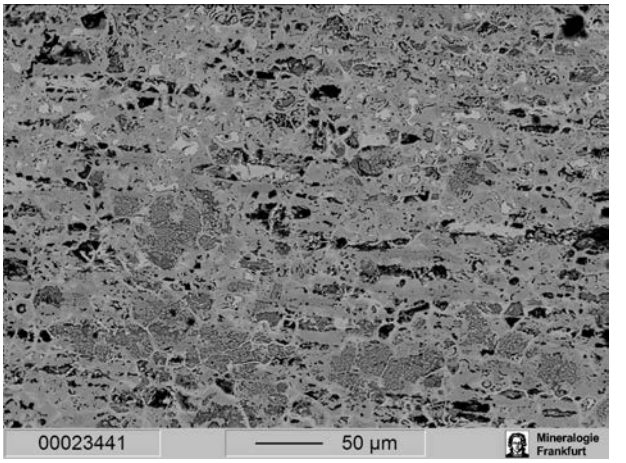

B17335

Museum nr. B17335.1

Field Nr.	U.9963C
Material	Cu
Object	Spearhead
Dating	Early Dynastic
Tomb	PG 0777
Type of Tomb	Royal
Citation	Woolley UE II, pl. 224; pp. 56, 81, 306, 439, 551
Notes	Parallel with B17333a-b
EPMA	x
Laser (Trace)	x
Laser (CuI)	
Sol (CuI)	
Laser (LIA)	
Sol (LIA)	
PIXE-Analyses	As, 0.55%, Sn, 6.5%; Ni, 0.31%

Samuel K. Nash's Notebook

Ur(?) B17335 ***3/13/06***

The matrix microstructure of this specimen of severely corroded pike is coarsely lamellar in appearance. A few undistorted grains clusters are present too. One possible explanation of the latter appearance is that the original dentritic microstructure was folded repeatedly while being hot worked. Neither hardness measurements nor photographs are considered worth doing, given this specimen's condition.

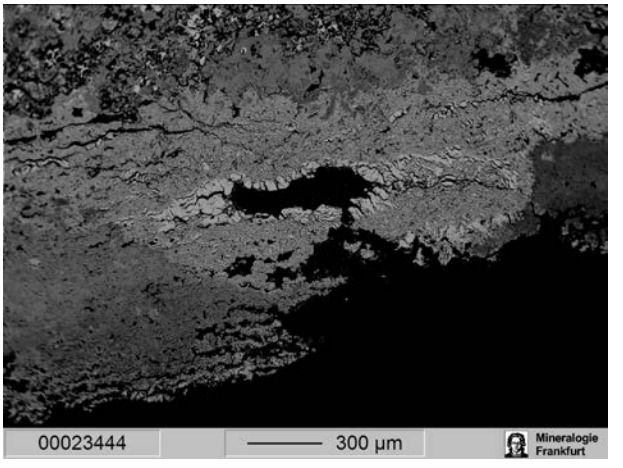

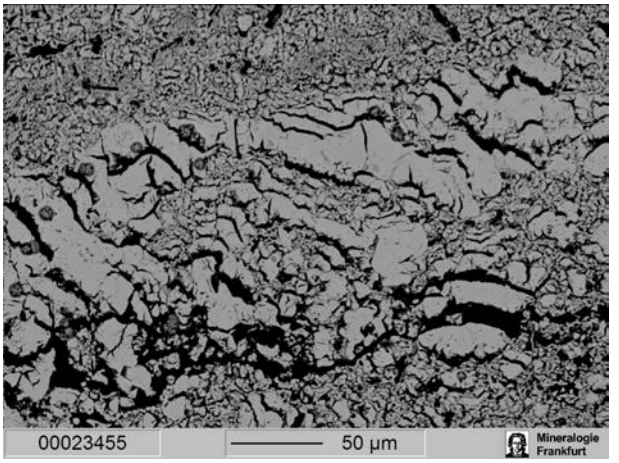

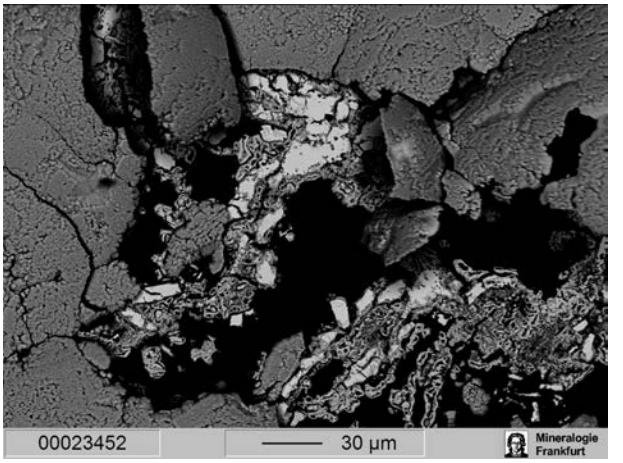

B17347

Museum nr. B17347.1

Field Nr.	U.9518
Material	Bz
Object	Spearhead
Dating	Early Dynastic
Tomb	PG 0617
Type of Tomb	Private
Notes	Woolley says ED
EPMA	x
Laser (Trace)	
Laser (CuI)	
Sol (CuI)	
Laser (LIA)	
Sol (LIA)	
Misc	heavily corroded

Samuel K. Nash's Notebook

Ur 537 (CBS-17347)

The progression of corrosion from the outer surfaces to the interior of this specimen of a knife-dagger, has resulted in a laminar-like appearance. Corrosion has clearly outlined the grain boundaries of the remaining metal, which appears to have very few non metallic inclusions. The grains themselves are equiaxed and were formed in a hot working operation; grain size is 5-6.
The average hardness of the same was found to be
VHN

			VHN
47.5-44.0	91.5	88.6	
45.0-44.1	89.1	93.4	Av=97.8
46.2-43.7	89.9	91.8	
41.9-41.5	83.4	107	
41.1-41.8	82.9	108	

Ur CBS 17347 ***SKN***

Corrosion: Heavily attacked throughout and at grain boundaries, sharply delineating the grain structure – hot rolled, equiaxed grains (GS~6). Layered structure as a result of prior hot deformations. Inclusions: Very low density; small spherically shaped are black in color.

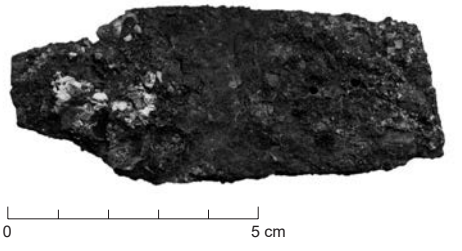

B17351

Museum nr. B17351.1

Field Nr.	U.10777
MMP NR.	Ur 134
Material	As-Cu
Object	Dagger
Dating	Early Dynastic
Tomb	PG 0849
Type of Tomb	Private
EPMA	x
Laser (Trace)	x
Laser (CuI)	
Sol (CuI)	
Laser (LIA)	
Sol (LIA)	
PIXE-Analyses	As, 2.1%; Sn; 1.4%; Ni, 1.9%

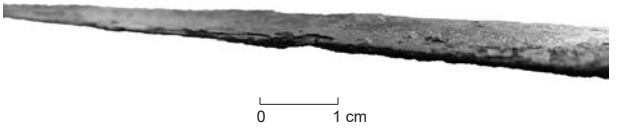

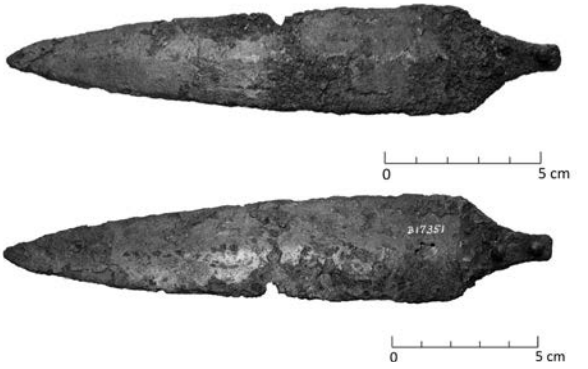

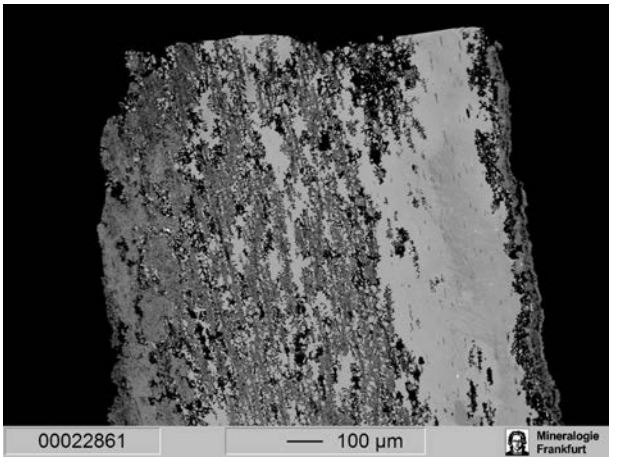

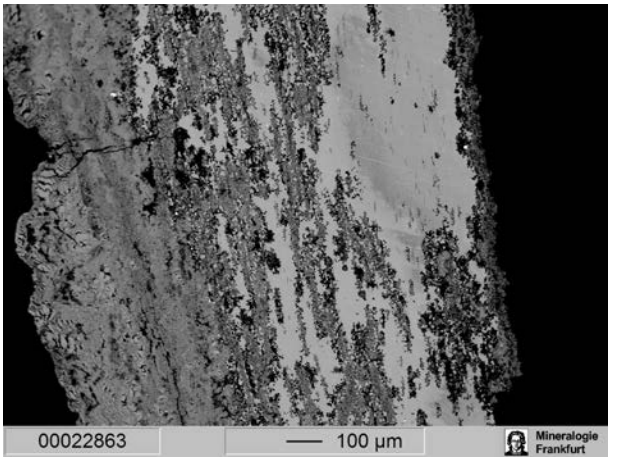

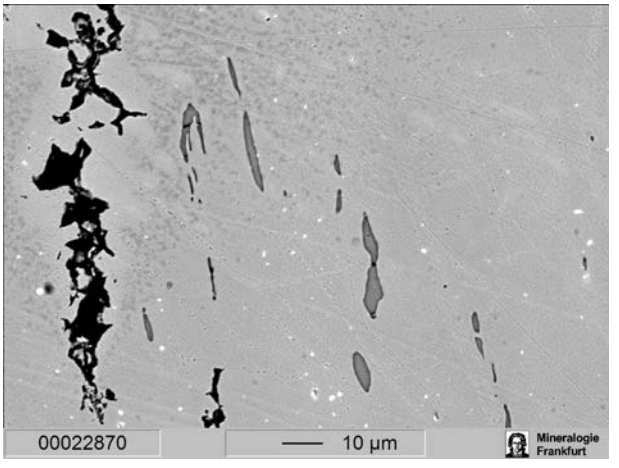

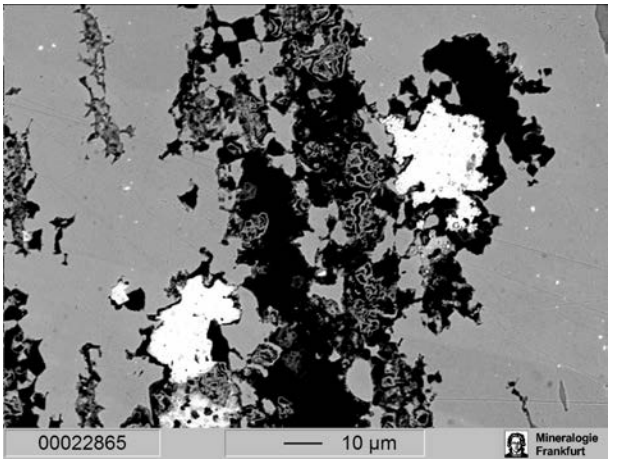

B17356.2-4

Museum nr. B17356.2-4

Field Nr.	U.9904
MMP NR.	Ur 528
Material	As-Cu
Object	Nail
Dating	Early Dynastic
Tomb	PG 0580
Type of Tomb	Royal
EPMA	x
Laser (Trace)	x
Laser (CuI)	
Sol (CuI)	
Laser (LIA)	x
Sol (LIA)	
PIXE-Analyses	As, 1.5%; Sn, 0.070%; Ni, 0.81%

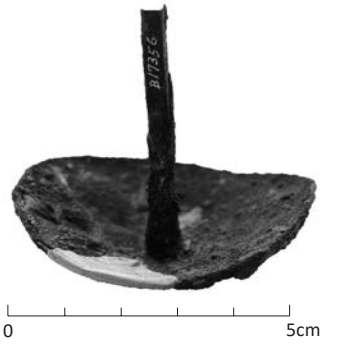

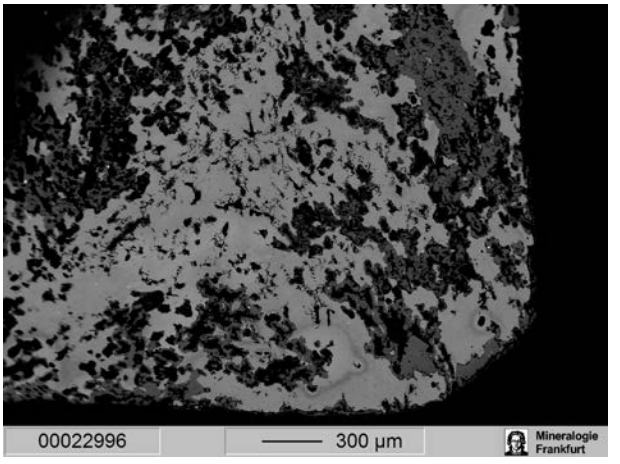

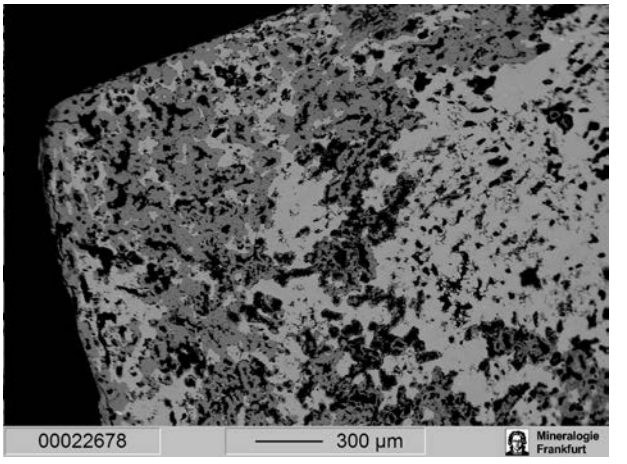

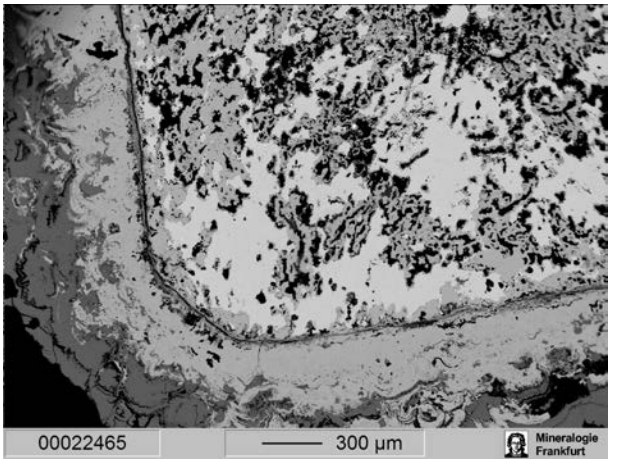

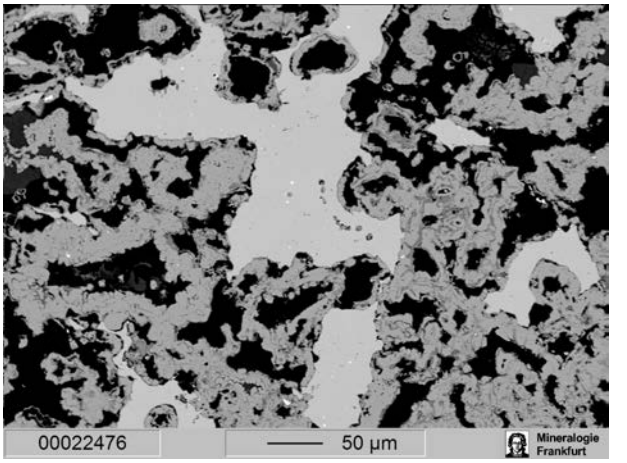

B17389

Museum nr. B17389.1

Field Nr.	U.8649
MMP NR.	Ur 143
Material	As-Cu
Object	Needle
Dating	Early Dynastic
Tomb	PG 0049 TTE
Type of Tomb	Private
EPMA	x
Laser (Trace)	x
Laser (CuI)	
Sol (CuI)	
Laser (LIA)	x
Sol (LIA)	
PIXE-Analyses	As, 1.6%; Sn, 0.13%; Ni, 0.55%

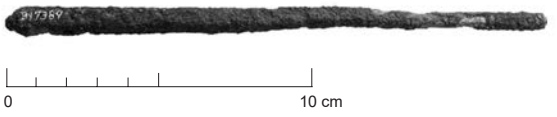

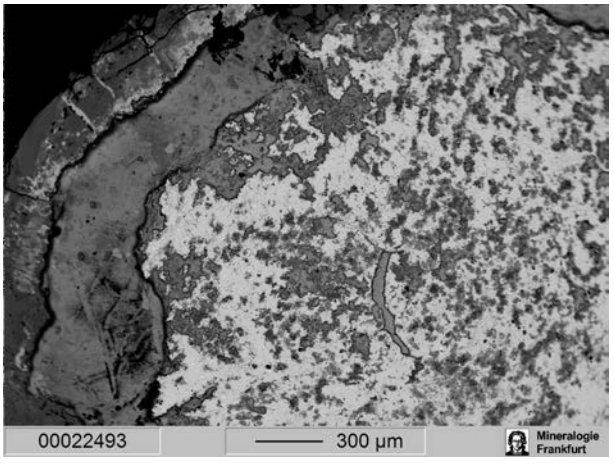

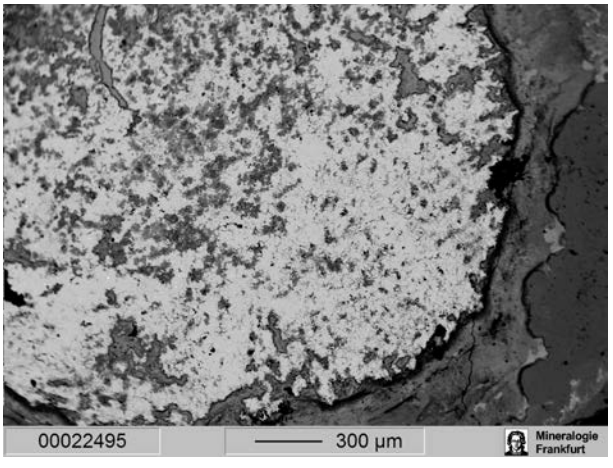

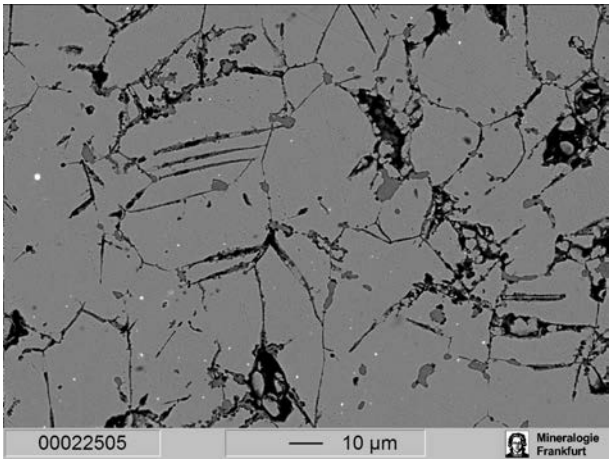

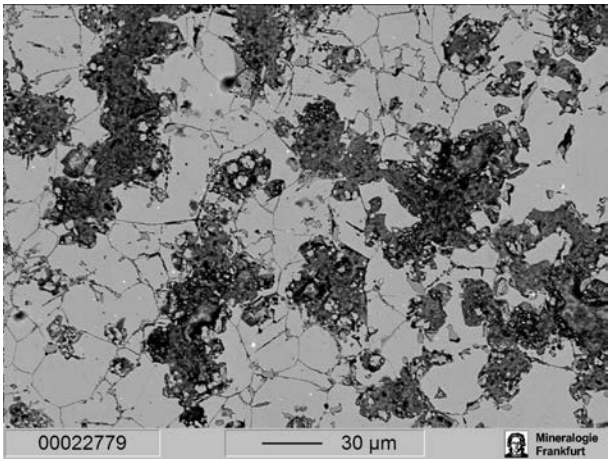

B17410

Museum nr. B17410.1

Field Nr.	U.9017
MMP NR.	Ur 23
Material	Cu
Object	Axe
Dating	Early Dynastic
Tomb	PG 0466 TTF
Type of Tomb	Private
EPMA	x
Laser (Trace)	x
Laser (CuI)	
Sol (CuI)	
Laser (LIA)	
Sol (LIA)	
PIXE-Analyses	As, 1.5%; Sn, 0.80%; Ni, 0.14%

B17411

Museum nr. B17411.1

Field Nr.	U.7931
MMP NR.	Ur 59
Material	Cu
Object	Axe
Dating	Early Dynastic
Tomb	PG 0068 TTE
Type of Tomb	Private
Notes	Find spot PG 68 TTE, 1.8 m below surface
EPMA	x
Laser (Trace)	x
Laser (CuI)	
Sol (CuI)	
Laser (LIA)	
Sol (LIA)	
Misc	heavily corroded

B17418

Museum nr. B17418.1

Field Nr.	U.7856
MMP NR.	Ur 139
Material	Cu
Object	Axe
Dating	Early Dynastic
Tomb	PG 0016 TTE
Type of Tomb	Private
Notes	Woolley says ED
EPMA	x
Laser (Trace)	x
Laser (CuI)	
Sol (CuI)	
Laser (LIA)	
Sol (LIA)	
Misc	corroded

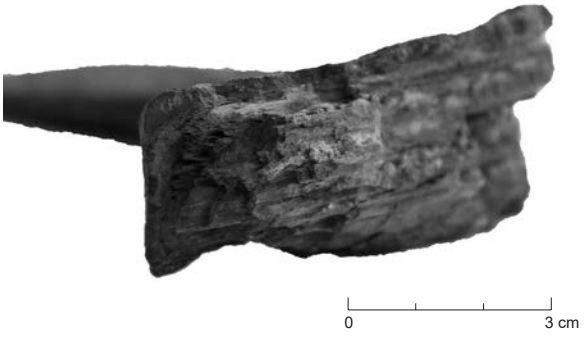

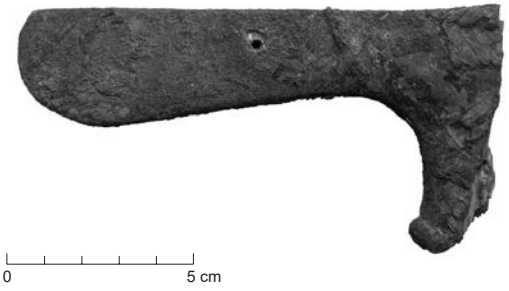

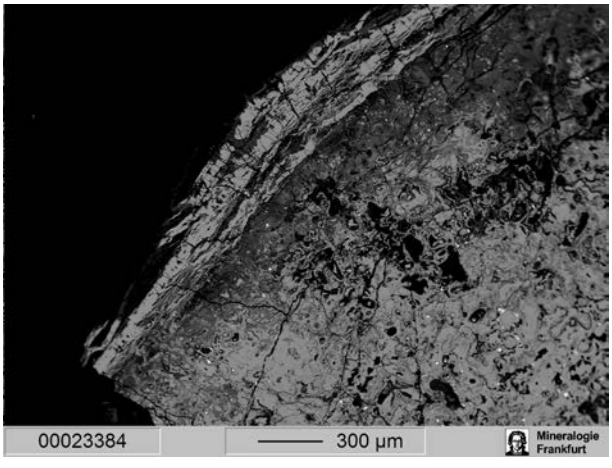

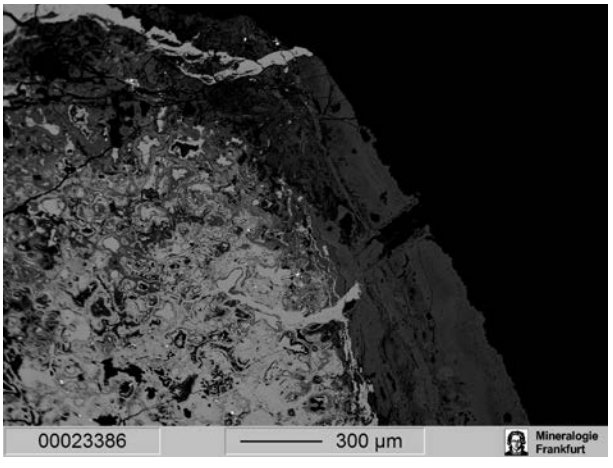

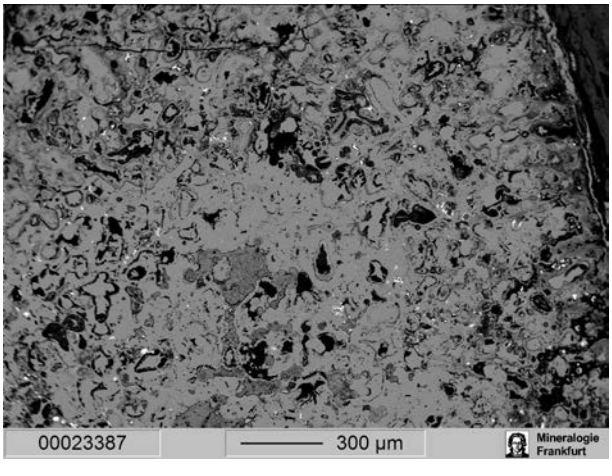

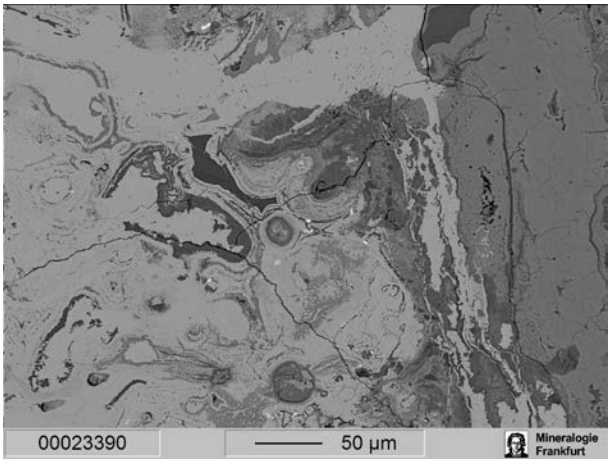

B17422

Museum nr. B17422.1

Field Nr.	U.8986A
MMP NR.	Ur 21
Material	As-Cu
Object	Anklet
Dating	Akkadian
Find context	U.8988 (BM 120572) Cylinder Seal with Inscription mentioning Enheduanna (Daughter of Sargon)
Tomb	PG 0503 TTF
Type of Tomb	Private
EPMA	x
Laser (Trace)	x
Laser (CuI)	
Sol (CuI)	
Laser (LIA)	x
Sol (LIA)	

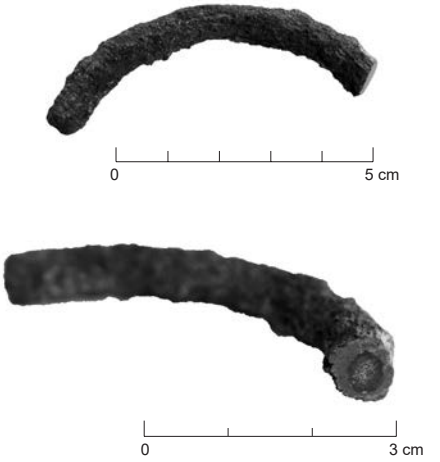

B17426.1-2

Museum nr. B17426.1-2

Field Nr.	U.8546
MMP NR.	Ur 535
Material	As-Cu
Object	Chisel (does not look like a dagger as Woolley describes it)
Dating	Early Dynastic (?)
Tomb	PG not known
Type of Tomb	Private
Notes	U.8546 is written on a blade, does not look like a dagger, as Woolley describes it in his cards, but more like a chisel
EPMA	x
Laser (Trace)	x
Laser (CuI)	x
Sol (CuI)	
Laser (LIA)	x
Sol (LIA)	
PIXE-Analyses	As, 1.6%; Sn, 9.7%; Ni, 0.41%

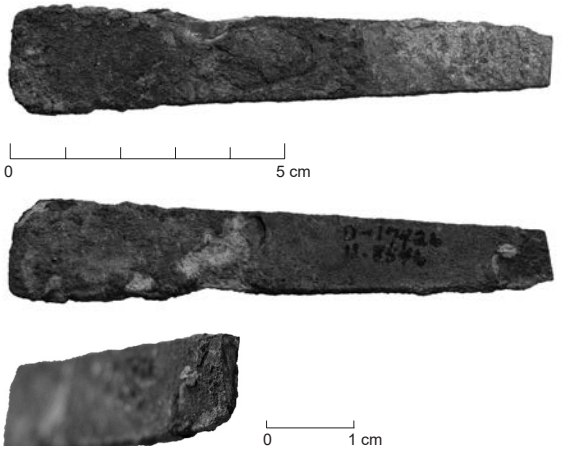

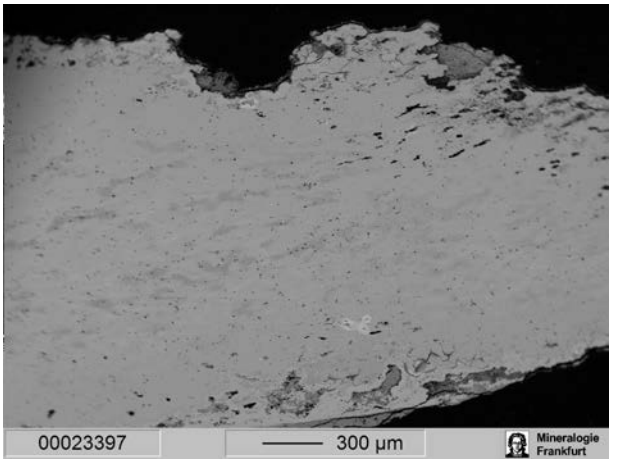

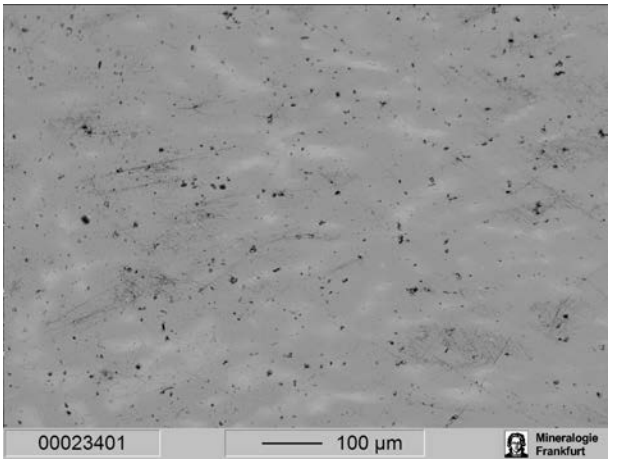

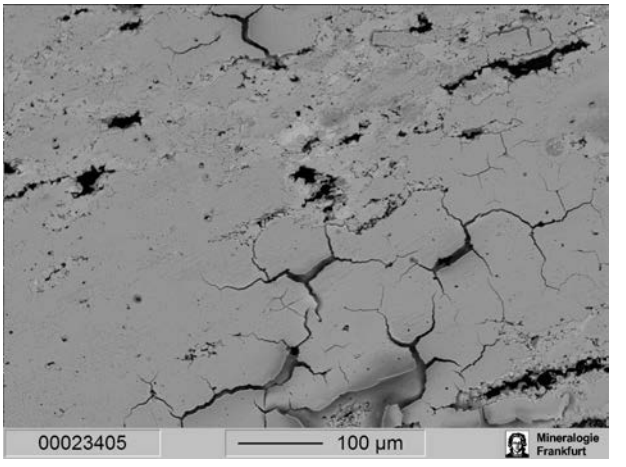

B17445

Museum nr. B17445.1

Field Nr.	U.8366
MMP NR.	Ur 61
Material	As-Cu
Object	Saw
Dating	Early Dynastic
Tomb	PG 0121 TTE
Type of Tomb	Private
Notes	Woolley says ED
EPMA	x
Laser (Trace)	x
Laser (CuI)	x
Sol (CuI)	
Laser (LIA)	x
Sol (LIA)	

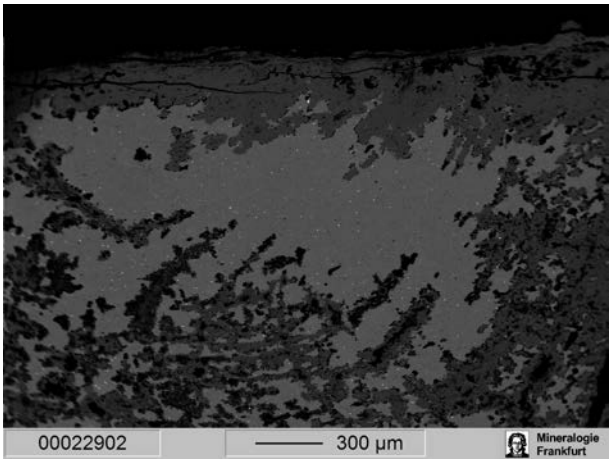

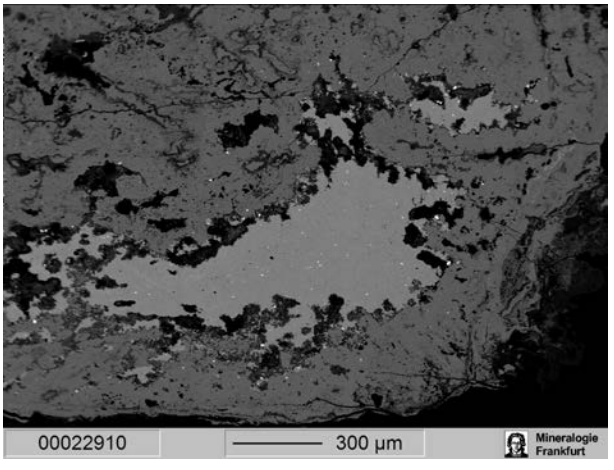

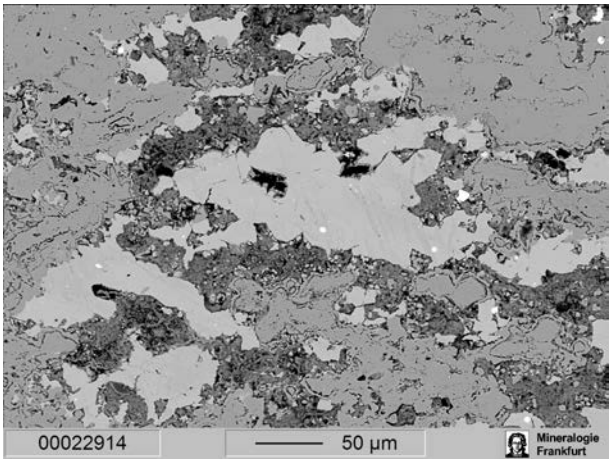

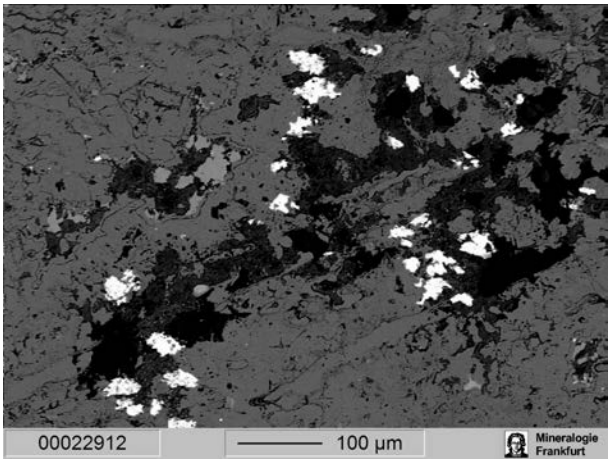

B17460.1-2

Museum nr. B17460.1-2

Field Nr.	U.8474
MMP NR.	Ur 526
Material	As-Cu
Object	Dagger
Dating	Ur III
Tomb	PG 0304 TTE
Type of Tomb	Private
EPMA	x
Laser (Trace)	x
Laser (CuI)	
Sol (CuI)	
Laser (LIA)	
Sol (LIA)	
PIXE-Analyses	As, 3.0%; Sn, 0.12%; Ni, 2.1%

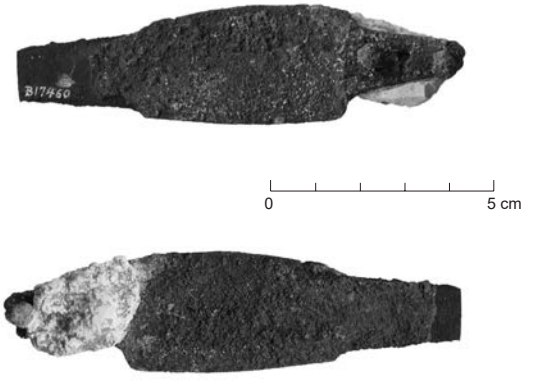

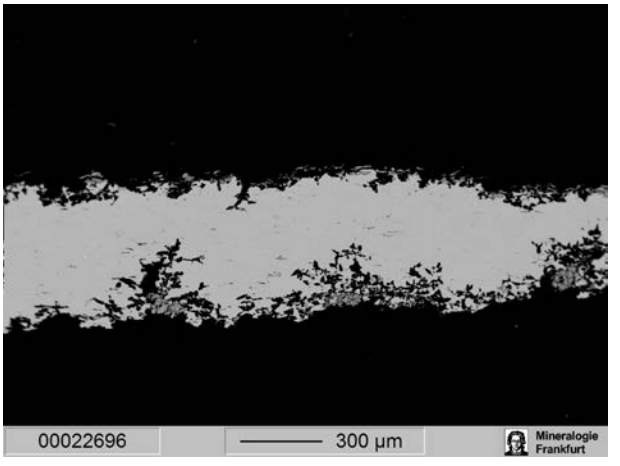

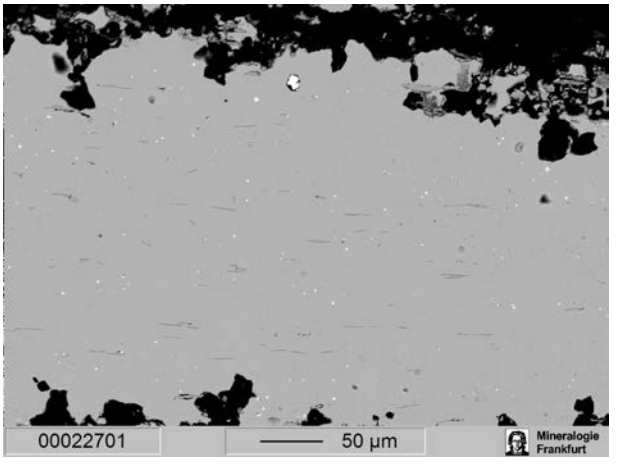

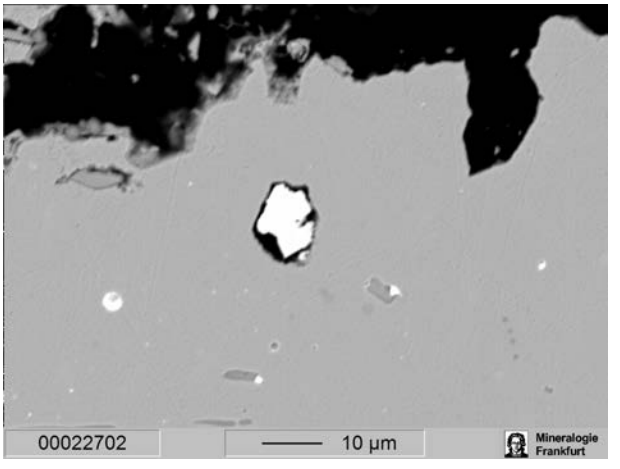

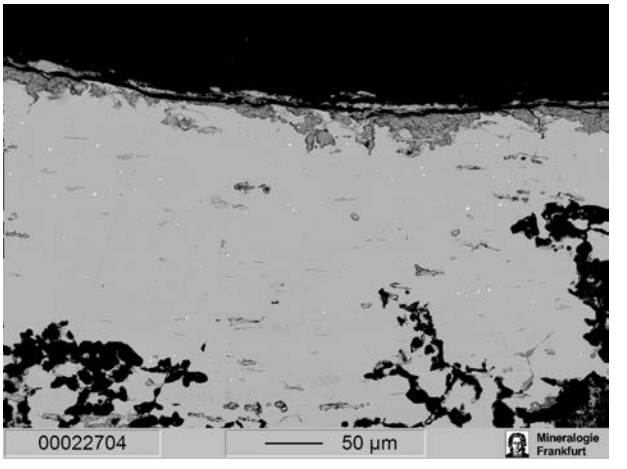

B17469

Museum nr. **B17469.1**

Field Nr.	U.9013
MMP NR.	Ur 18
Material	Bz
Object	Bracelet
Dating	Akkadian
Tomb	PG 0478 TTF
Type of Tomb	Private
Notes	Woolley says Akkadian
EPMA	x
Laser (Trace)	x
Laser (CuI)	
Sol (CuI)	
Laser (LIA)	x
Sol (LIA)	

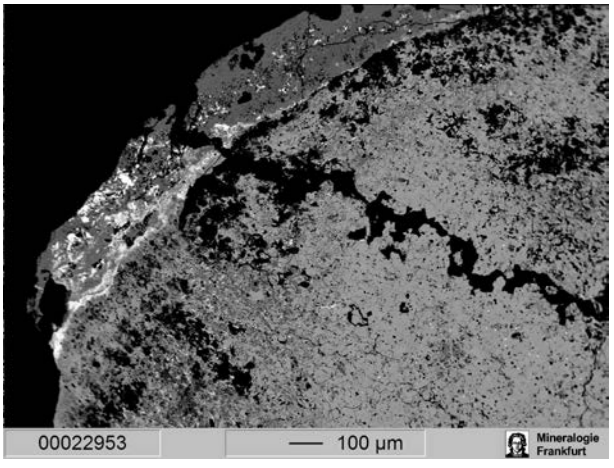

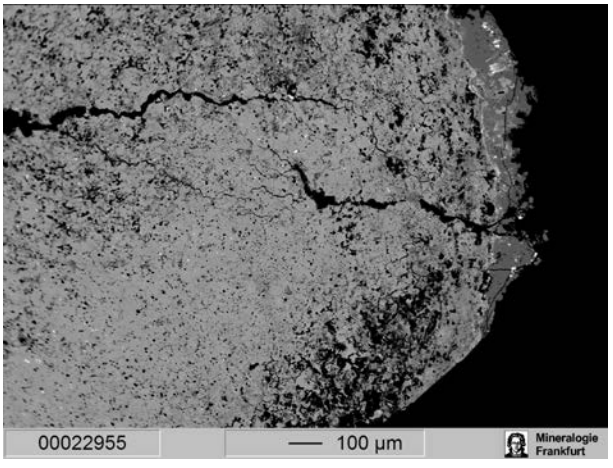

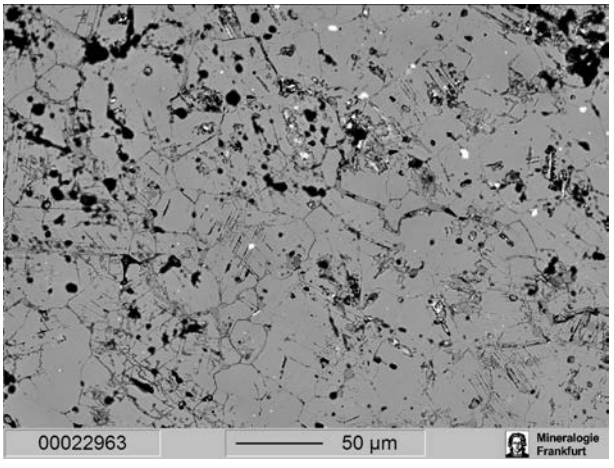

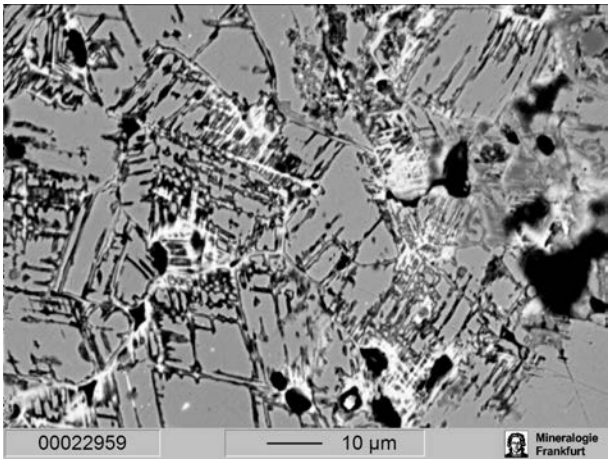

B17474

Museum nr. B17474.1

Field Nr.	U.8318
MMP NR.	Ur 6
Material	As-Cu
Object	Chisel
Dating	Early Dynastic
Tomb	PG 0163 TTE
Type of Tomb	Private
Notes	Woolley says ED
EPMA	x
Laser (Trace)	x
Laser (CuI)	
Sol (CuI)	
Laser (LIA)	
Sol (LIA)	
PIXE-Analyses	As, 1.7%; Sn, 0.15%; Ni, 0.88%

Samuel K. Nash's Notebook

U 009 Ur 006
B17474 [U08318]
Chisel
Grave PG 0163
PIXE analysis: On .....
PIXE data: As (1.7%) Sn (0.15%) Ni (0.88%)
Metallographic sample: .....
The inclusions, which are of the sulfide type, are small, but in many instances fragmented—indicative of the final cold-working. The grain structure, originally annealed, equiaxed and twinned, shows all the markings of extensive final cold-worked deformation. Moreover, grain size varies considerably from area to area. Thus effect is attributable to elemental segregation and the way it influenced grain growth in the metal's heat treatment history.

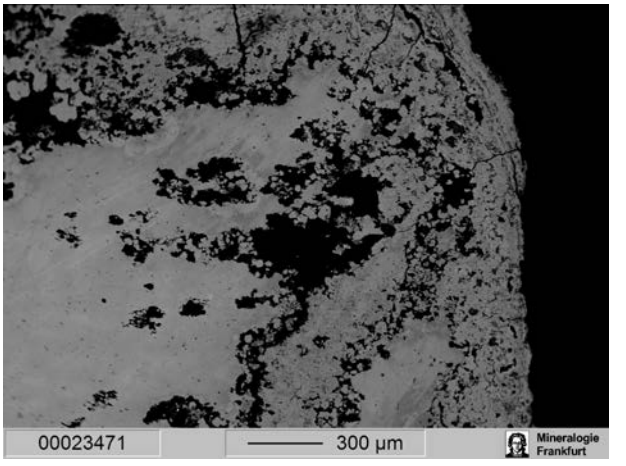

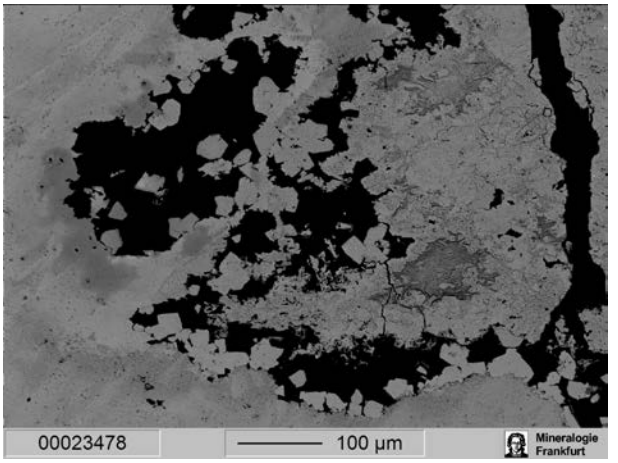

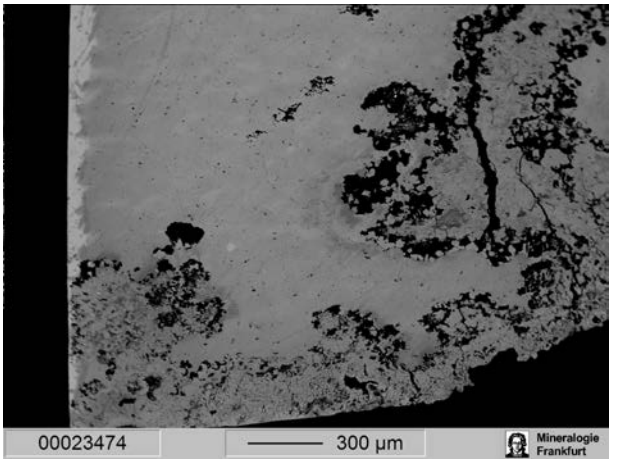

B17478

Museum nr. B17478.1

Field Nr.	U.8560
MMP NR.	Ur 10
Material	As-Cu
Object	Chisel
Dating	Early Dynastic
Tomb	PG 0317 TTE
Type of Tomb	Private
Notes	Woolley says ED
EPMA	x
Laser (Trace)	x
Laser (CuI)	
Sol (CuI)	
Laser (LIA)	
Sol (LIA)	
PIXE-Analyses	As, 2.4%; Sn, <0.009%; Ni, 0.67%

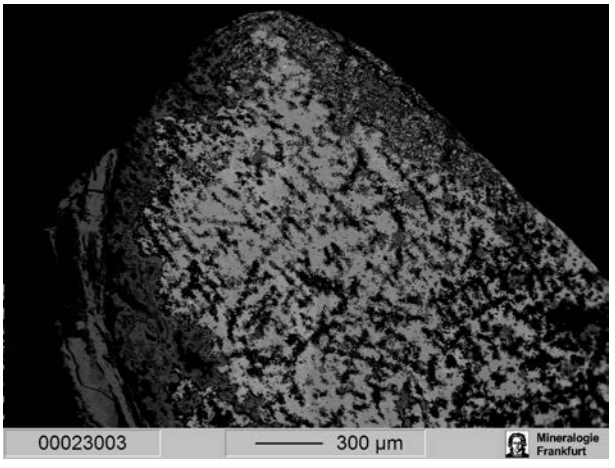

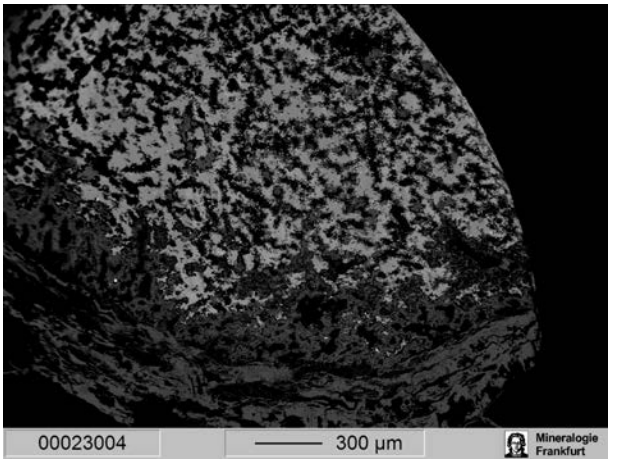

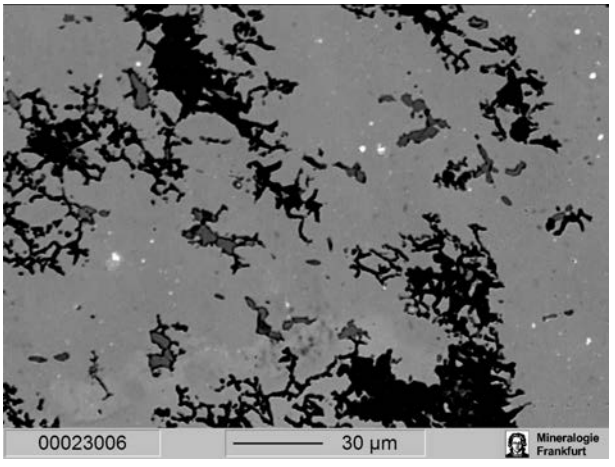

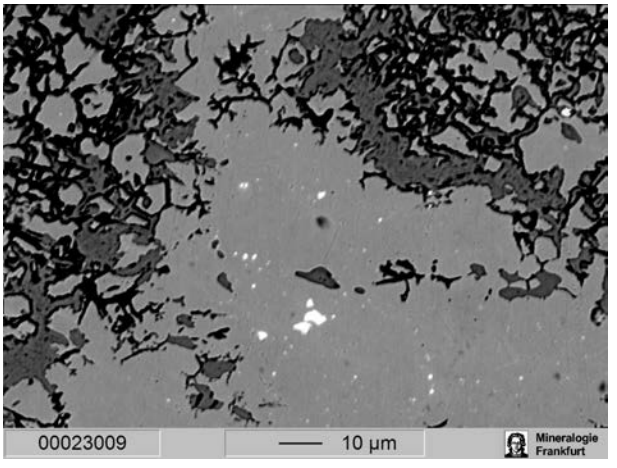

B17479

Museum nr. B17479.1

Field Nr.	U.9353
MMP NR.	Ur 150
Material	Bz
Object	Axe
Dating	Early Dynastic
Tomb	PG 0580
Type of Tomb	Royal
EPMA	x
Laser (Trace)	x
Laser (CuI)	
Sol (CuI)	
Laser (LIA)	x
Sol (LIA)	
PIXE-Analyses	As, 0.72%; Sn, 7.3%; Ni; 1.3%

Samuel K. Nash's Notebook

Ur 150 B17479

All that remains of this specimen of an adze, taken at the shaft hole, are a few isolated grains of clean metal. The latter contains significant amount of gas porosity; that is understandable given the place from which the specimen was taken.

Despite the poverty of metal, it is nevertheless clear, even in the unetched condition, that the microstructure is dendritic, i. e., that of a casting and that islands of the α-δ eutectoid are present. Etching, simply accumulates the latter microstructure features. The hardness, taken in the only area large enough to accommodate the VHN impressions, average of 87.3. (No photo taken)

Hardness		HV	VHN	
43.5-44.7		88.2	95.3	
46.5-47.5		94.0	84.0	
45.7-45.	7	91.4	88.8	avg=87.3
47.7-51.4		99.1	75.6	
44.7-44.6		89.3	93.0	

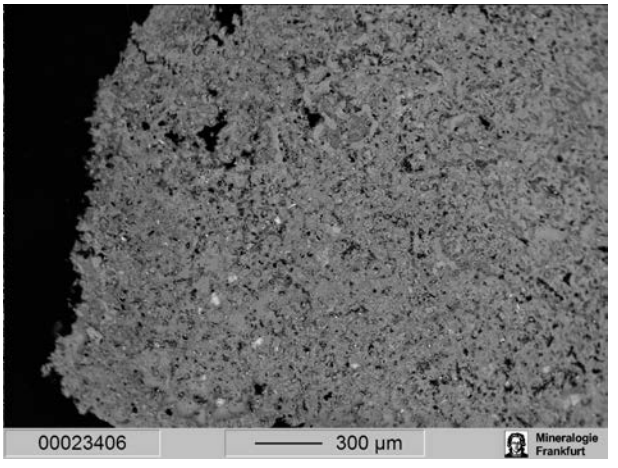

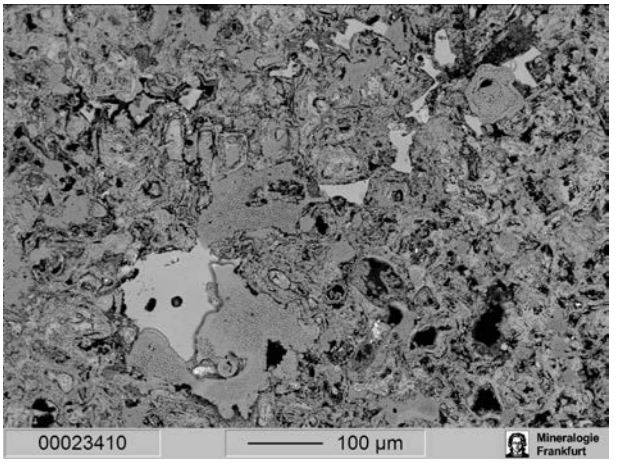

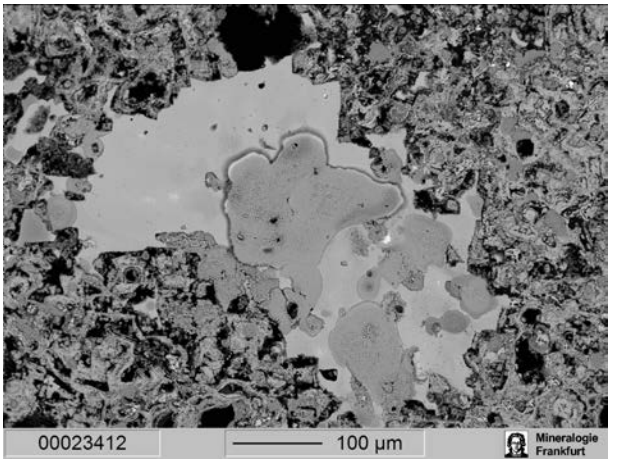

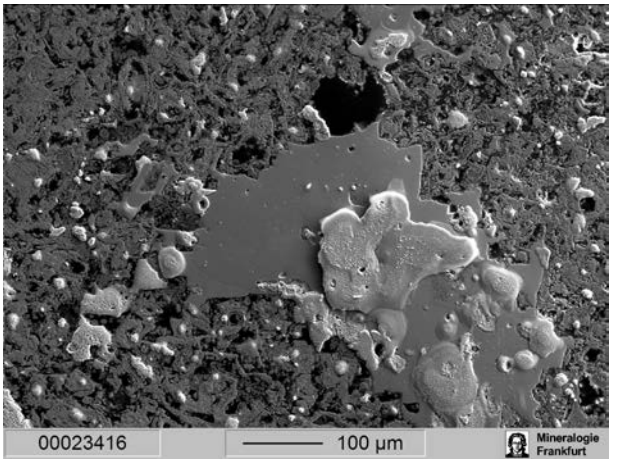

B17480

Museum nr. B17480.1

Field Nr.	U.9141C-F
MMP NR.	Ur 19
Material	Bz
Object	Spearheads soldered by oxidation
Dating	Early Dynastic
Tomb	PG 0537 (= PG 580)
Type of Tomb	Royal
EPMA	x
Laser (Trace)	x
Laser (CuI)	x
Sol (CuI)	
Laser (LIA)	x
Sol (LIA)	
PIXE-Analyses	As, 0.35%; Sn, 10.2%; Ni, 0.42%

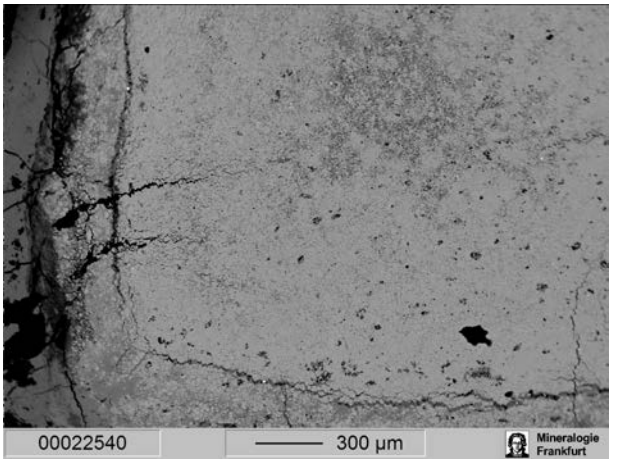

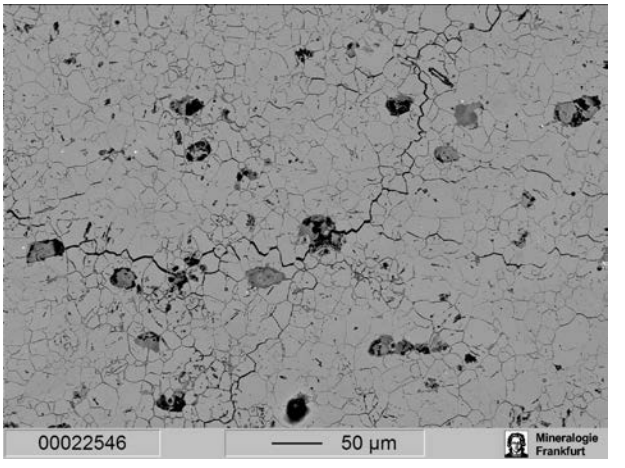

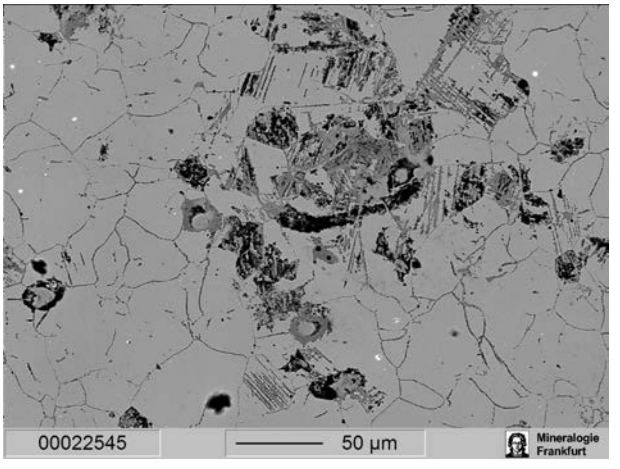

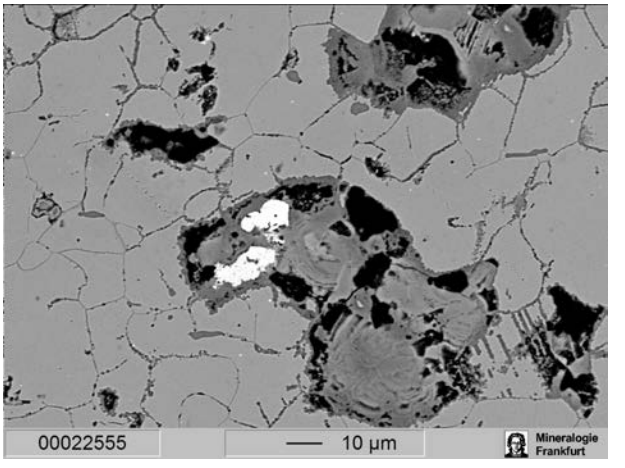

B17488

Museum nr. B17488.1

Field Nr.	U.10165
MMP NR.	Ur 53
Material	As-Cu
Object	Pin
Dating	Early Dynastic
Find context	U.10168 (BM 121561) Cylinder Seal
Tomb	PG 0780
Type of Tomb	Private
EPMA	x
Laser (Trace)	
Laser (CuI)	
Sol (CuI)	
Laser (LIA)	
Sol (LIA)	
PIXE-Analyses	As, 2.8%; Sn, <0.017%; Ni, 2.4%

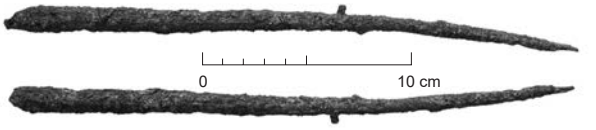

B17495

Museum nr. B17495.1

Field Nr.	U.10358
MMP NR.	Ur 135
Material	Bz
Object	Pin
Dating	Akkadian
Find context	U.10359 (BM 121549) Cylinder Seal
Tomb	PG 0832
Type of Tomb	Private
EPMA	x
Laser (Trace)	x
Laser (CuI)	
Sol (CuI)	
Laser (LIA)	x
Sol (LIA)	
PIXE-Analyses	As, 1.5%; Sn, 12.6%; Ni, 1.1%

Samuel K. Nash's Notebook

U065 / UR 135 & B17495 (U10358)

When examined in the unetched condition, it is readily apparent that this pin specimen has suffered uniform trans-granular corrosion. Corrosion is so extensive that the specimen has suffered grain loss, especially in the periphery. Grain size (GS7) is clearly delineated by corrosion. The effects of cold working manifest in striations and are fairly evident throughout this cross section. This specimen was too corroded to measure hardness.

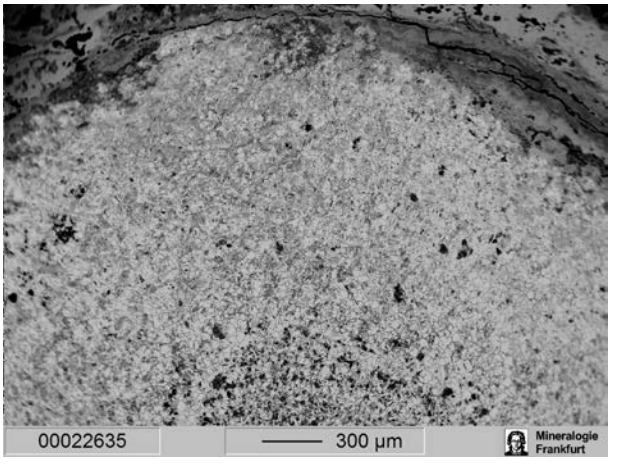

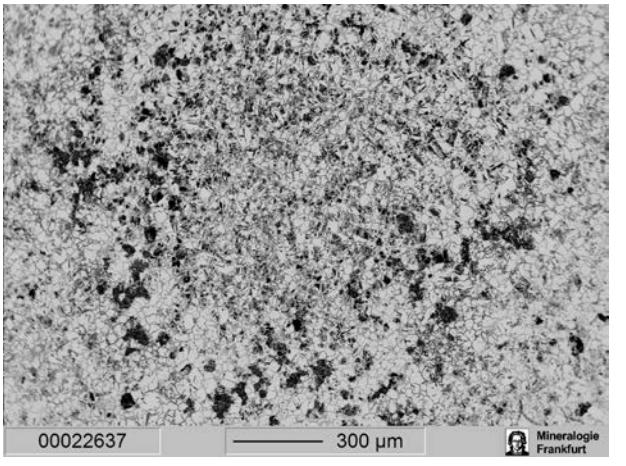

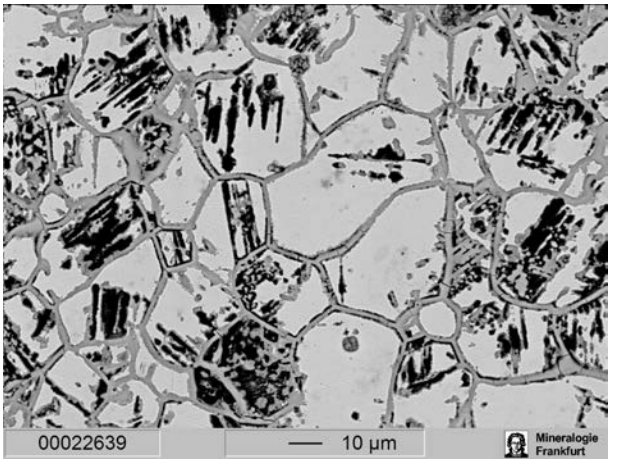

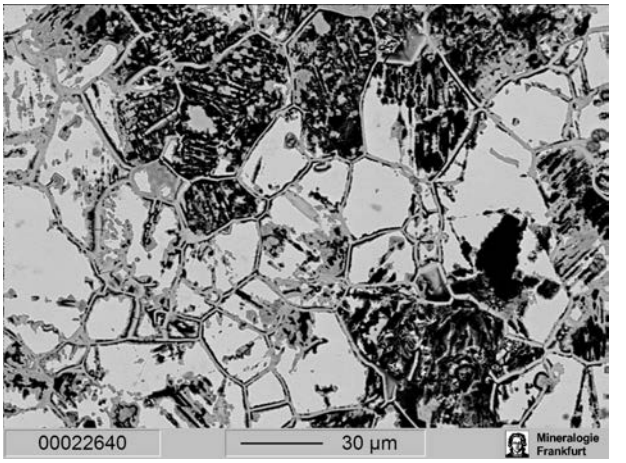

B17496

Museum nr. B17494.1 = B17496.1

Field Nr.	U.10196
MMP NR.	Ur 174
Material	Bz
Object	Pin
Dating	Akkadian
Find context	U.10192 (B17594) Cylinder Seal cf. UE 2, pl. 211.
Tomb	PG 0766
Type of Tomb	Private
Notes	Woolley classifies PG 766 as Akkadian
EPMA	x
Laser (Trace)	x
Laser (CuI)	
Sol (CuI)	
Laser (LIA)	x
Sol (LIA)	
Misc	Samuel K. Nash misnamed the specimen as B17494, the real name appears to be B17496

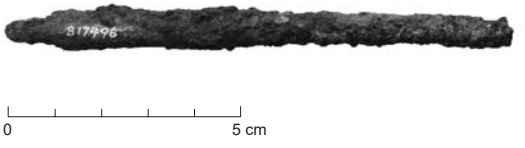

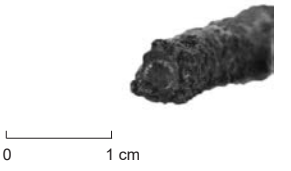

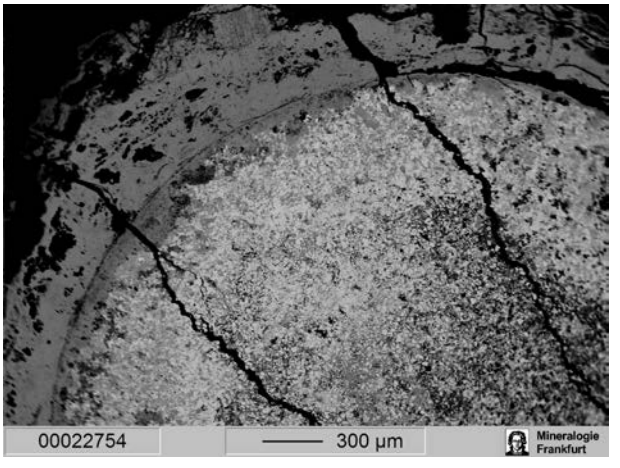

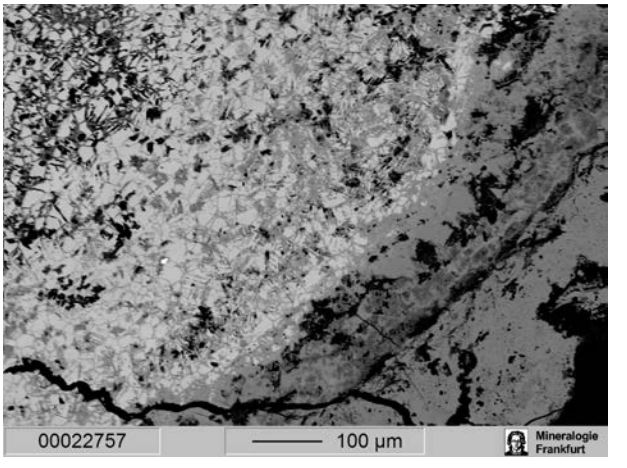

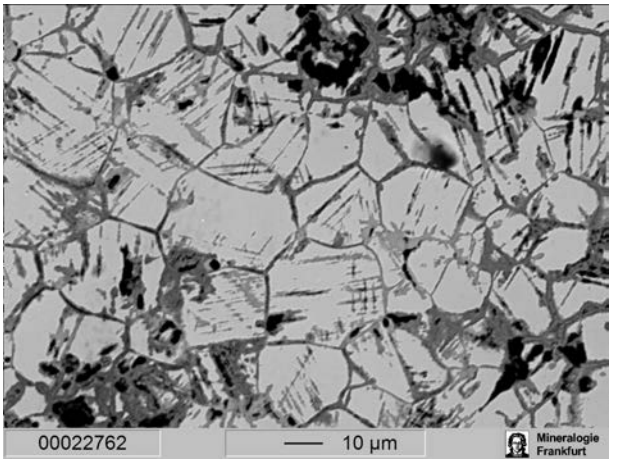

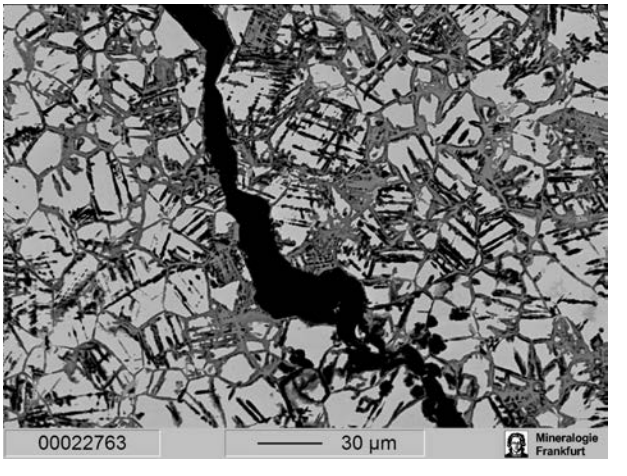

B17508

Museum nr. B17508.1-2

Field Nr.	U.9933
MMP NR.	Ur 169
Material	Ni-Cu
Object	Dagger
Dating	Early Dynastic
Tomb	PG 0737
Type of Tomb	Private
EPMA	x
Laser (Trace)	x
Laser (CuI)	
Sol (CuI)	
Laser (LIA)	
Sol (LIA)	
PIXE-Analyses	As, 0.40%; Sn, 0.012%; Ni, 10.7%

Samuel K. Nash's Notebook

UR 169 – B17508 (10% Ni) 3/01/06 Scanned 3/21/06
The tip of this dagger has been almost completely lost to corrosion. The little metal that remains shows strong evidence of directional work based upon the elongation of the sulfide-type inclusions. The microstructure is strongly banded. Grains visible at high magnification have been flattened and elongated; they were originally annealed twinned and polygonal in shape. The average VHN is 124.5. Yet actual hardness numbers

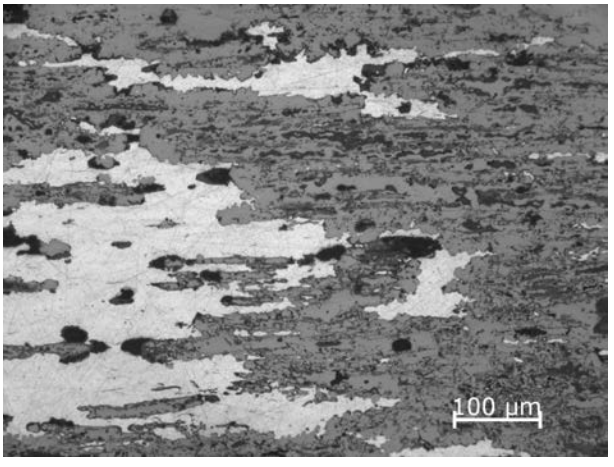

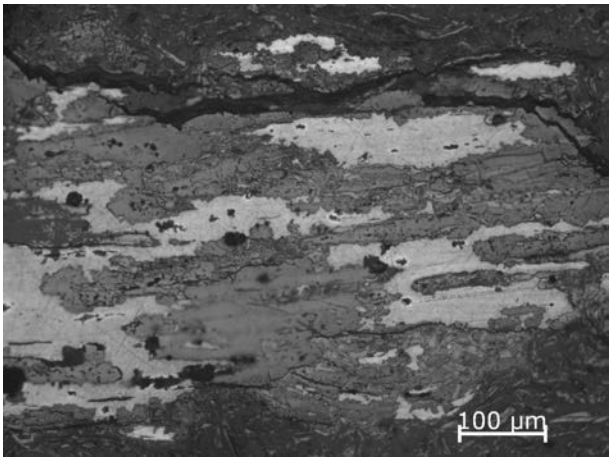

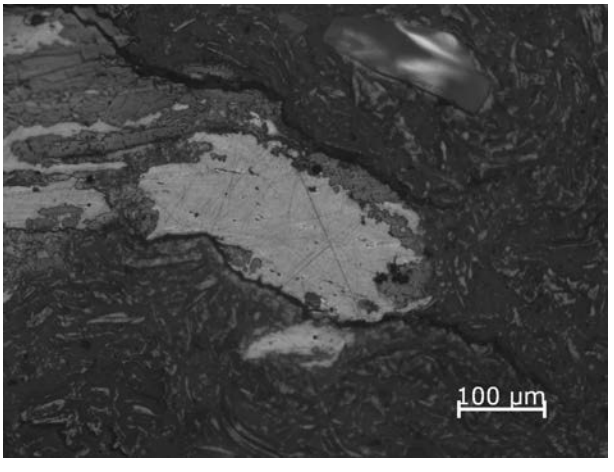

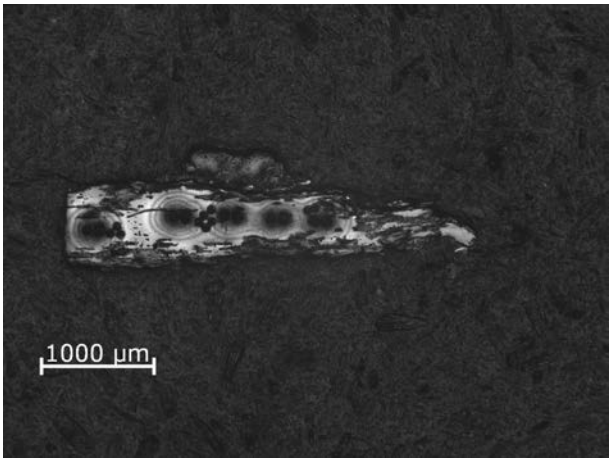

B17516

Museum nr. B17516.1

Field Nr.	U.9213
MMP NR.	Ur 26
Material	As-Cu
Object	Knife
Dating	Not Dated
Tomb	PG 0556
Type of Tomb	Private
EPMA	x
Laser (Trace)	x
Laser (CuI)	
Sol (CuI)	
Laser (LIA)	x
Sol (LIA)	
PIXE-Analyses	As, 1.7%; Sn, <0.013%; Ni, 0.95%

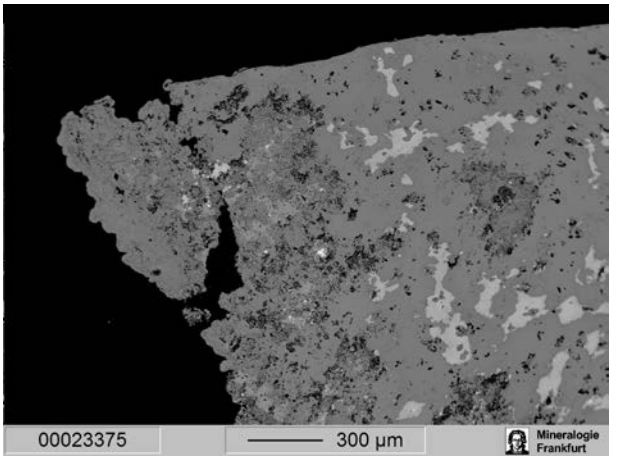

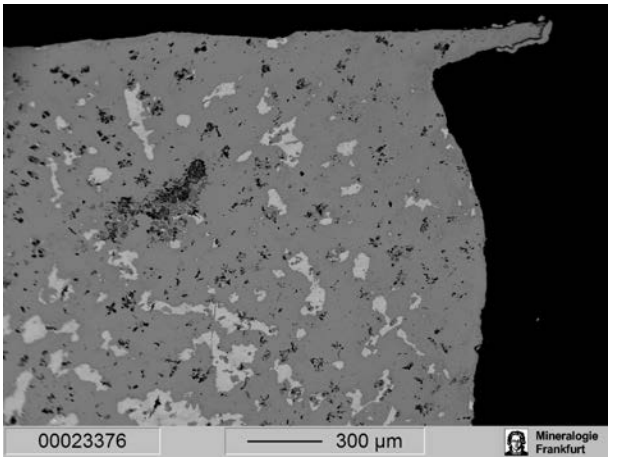

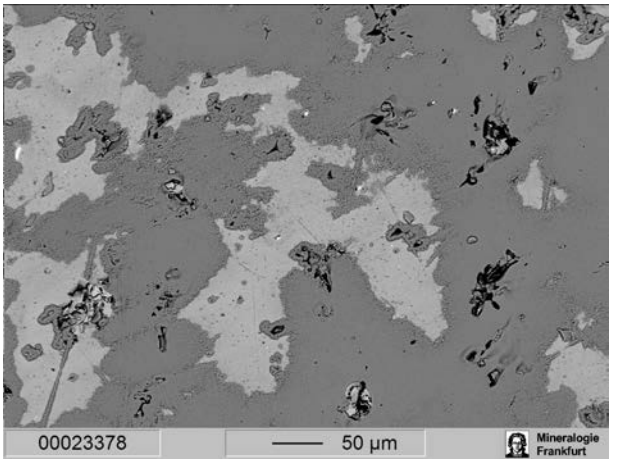

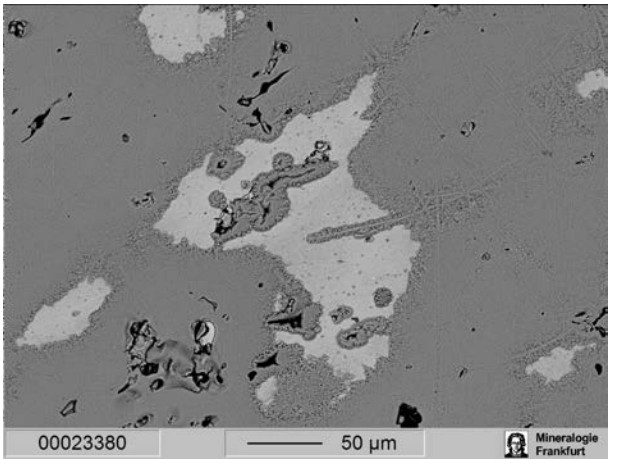

B17525

Museum nr. B17525.1

Field Nr.	U.9342
MMP NR.	Ur 56
Material	Cu
Object	Harpoon
Dating	Early Dynastic
Tomb	PG 0580 TTE
Type of Tomb	Royal
EPMA	x
Laser (Trace)	x
Laser (CuI)	
Sol (CuI)	
Laser (LIA)	
Sol (LIA)	

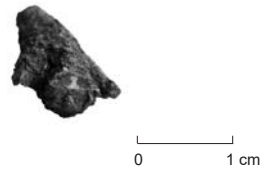

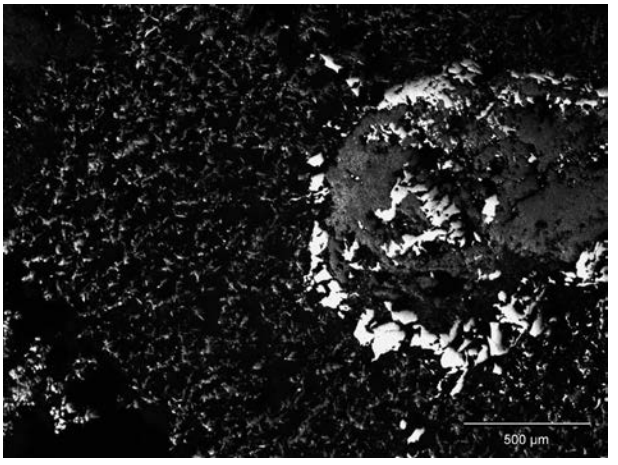

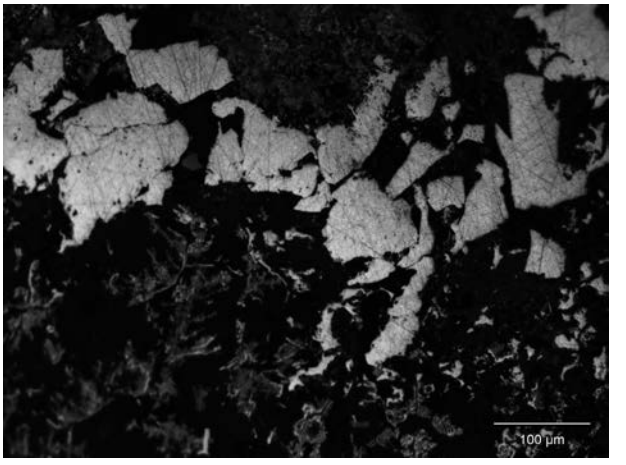

B17528A, -B

Museum nr. B17528a.1-2, -b

Field Nr.	U.9336
MMP NR.	Ur 52
Material	As-Cu
Object	2 Spearheads
Dating	Early Dynastic
Tomb	PG 0580
Type of Tomb	Royal
EPMA	x
Laser (Trace)	x
Laser (CuI)	x
Sol (CuI)	
Laser (LIA)	x
Sol (LIA)	
PIXE-Analyses	As, 1.3%; Sn, 0.045%; Ni, 0.99%

Samuel K. Nash‘s Notebook

Ur 17528 (U.09336) Ur 531
This specimen is identified as a barbed point; however it appears to be a wire form in the shape of a ring with overlapping ends. That it had been heavily deformed by coldworking or wire drawing is evident in the strongly aligned fractured condition of the nonmetallic inclusions. Deformations and therefore annealed grain size is non uniform – it is more intensive in the outer periphery than in the interior of the specimen. The latter condition is reflected in the grain size variation of the annealed grains. The effect of a final light coldworking is apparent in the deformed twinned grains. The hardness of the specimen showed a variation between VH 89-93.

CBS 17528A Ur52

This roughly circular cross section specimen has been effectively disintegrated by corrosion into individual small clusters and grains. The microstructure and the remnant metal shows coarse twined grains indicative of prior cold working and annealing at a fairly high temperature. Contains one dark etching and one very light etching phase: Can thus be a two phase structure? Doesn't seem likely, given the composition - Intensity and twinning visibly varies with the etchant.

Note: The twined leget etching phase is situated mainly around the specimen periphery; the dark etching phase is predominantly centrally situated. It looks almost like the light phase is penetrating the dark one. Has the light phase been preferentially corroded away at the center of the specimen?

Could this be a case 8 inverse segregation?

CBS 17528B Ur 52 ***I. 8.1 Dessicator***

This small circlet of finely (drawn?) wire consists of two overlapping legs. (See photo at 100x). The wire was hot formed as indicated by the elongated inclusions which are quite numerous. Etched with alcoholic FeCl3 the microstructure shows a fairly coarse grained field of twinned grains. The grain shapes suggest that they could have been the result of the hot working operation rather than a cold working and annealing treatment. The corrosion of this artifact is of the surface pitting type, with minor intergranular penetration.

(Question: Why is this sample designated the variation of CBS17528A when they don't look at all alike?)

Ur 52

This square cross sectional specimen of a handle has been so severely corroded that only a nodule of clear metal remains at its center. The microstructure consists of annealed, twinned, equiaxed grains – GS ~5 – that exhibit the effects of segregation in the form of mottling or bending. The remaining metal is relatively free from inclusions which are of sulfide-type.

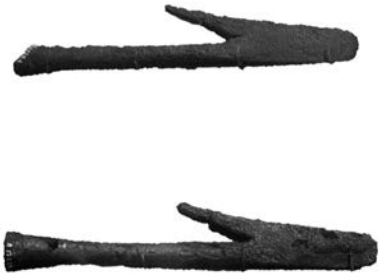

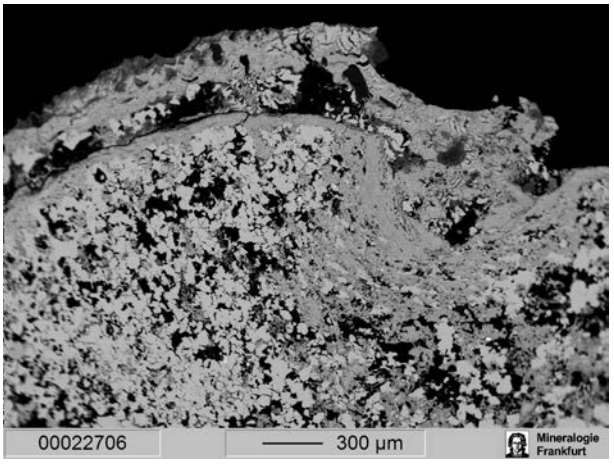

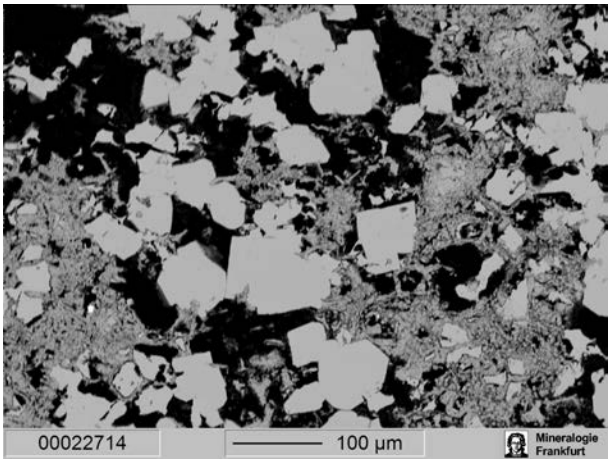

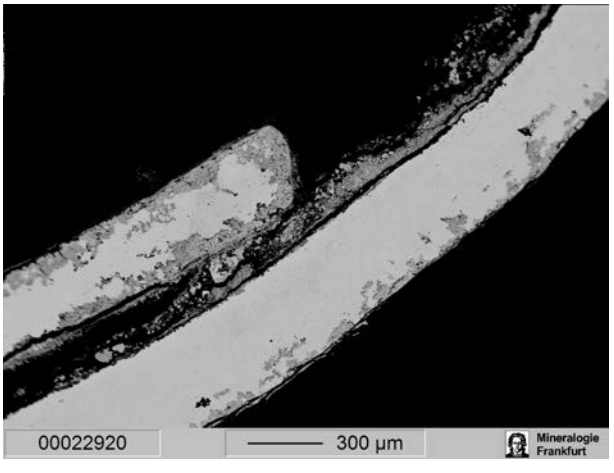

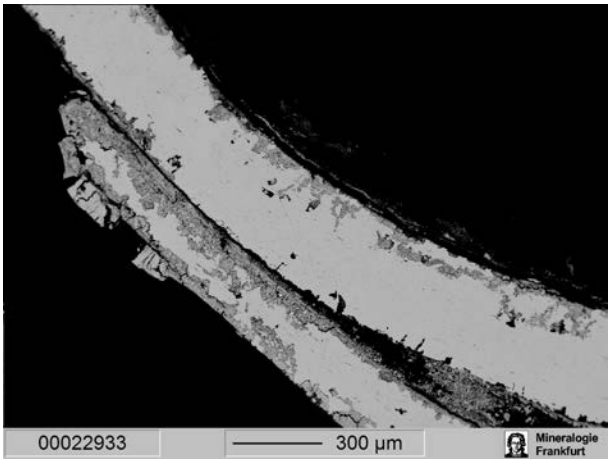

B17551

Museum nr. B17551

Field Nr.	U.9324
Material	As-Cu
Object	Rein Ring
Dating	Early Dynastic
Find context	cf. U.8557 stone relief
Tomb	PG 0580
Type of Tomb	Royal
Citation	Woolley, 1934, UE II, pp. 48, 433, 544
EPMA	x
Laser (Trace)	x
Laser (CuI)	
Sol (CuI)	x
Laser (LIA)	
Sol (LIA)	x

B17596

Museum nr. B17596.1

Field Nr.	U.10196
MMP NR.	Ur 173
Material	As-Cu
Object	Pin
Dating	Late Akkadian - Ur III
Tomb	PG 0762
Type of Tomb	Private
EPMA	x
Laser (Trace)	x
Laser (CuI)	
Sol (CuI)	
Laser (LIA)	x
Sol (LIA)	
PIXE-Analyses	As, 1.1%; Sn, 0.038%; Ni, 0.10%
Misc	Samuel K. Nash misnamed it as B17496, the true number is B17596

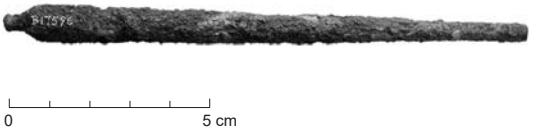

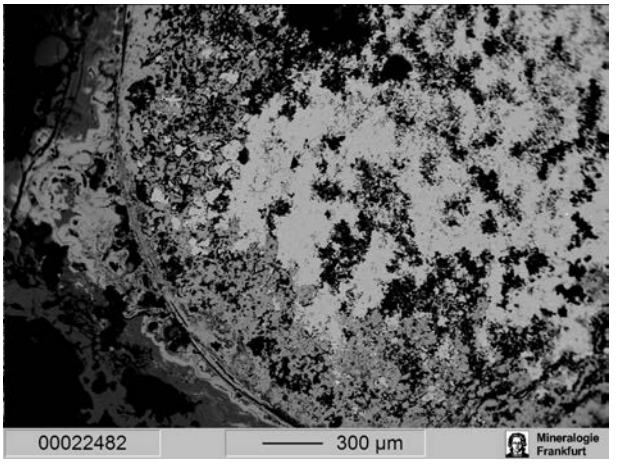

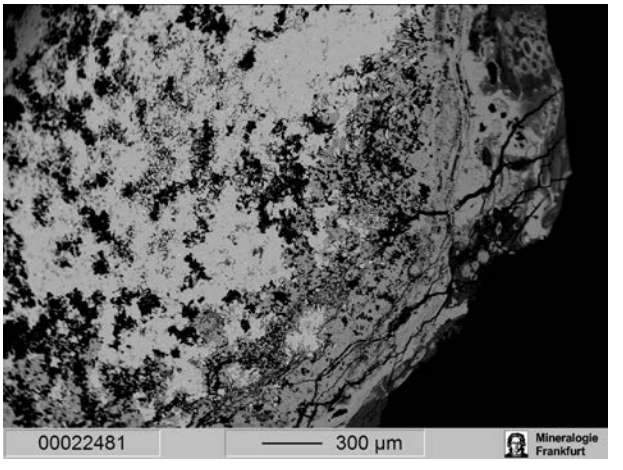

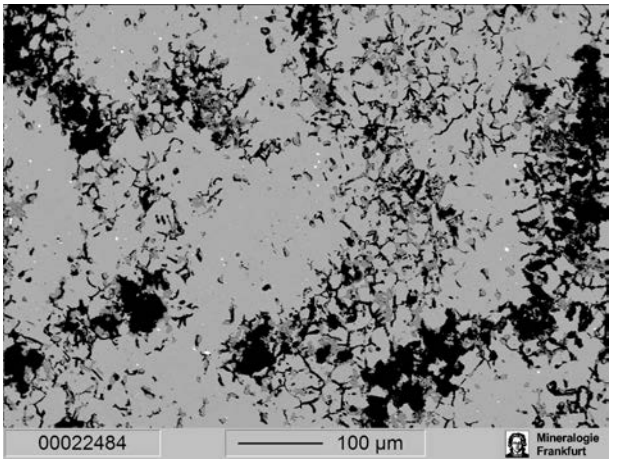

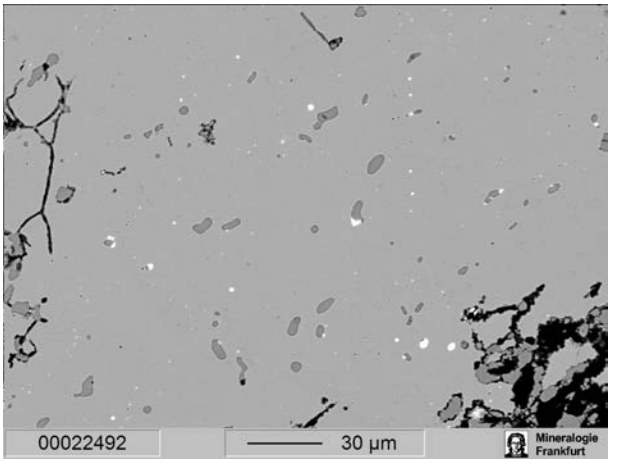

30-12-253.1-3

Museum nr. 30-12-253.1-3

Field Nr.	U.12355a
Material	Ag
Object	Lyre
Dating	Early Dynastic
Tomb	PG 1237
Type of Tomb	Great Death Pit
Note	The microstructure is recrystallised during electrochemical restoration and does not exhibit the original microstructure
EPMA	x
Laser (Trace)	x
Laser (CuI)	
Sol (CuI)	
Laser (LIA)	x
Sol (LIA)	

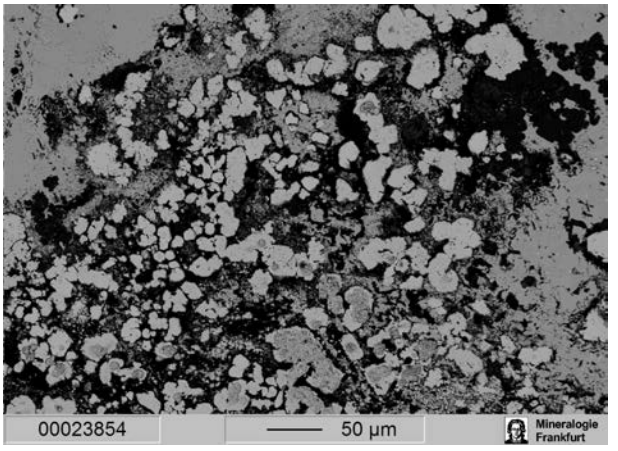


Woolley, 1934, plate 112

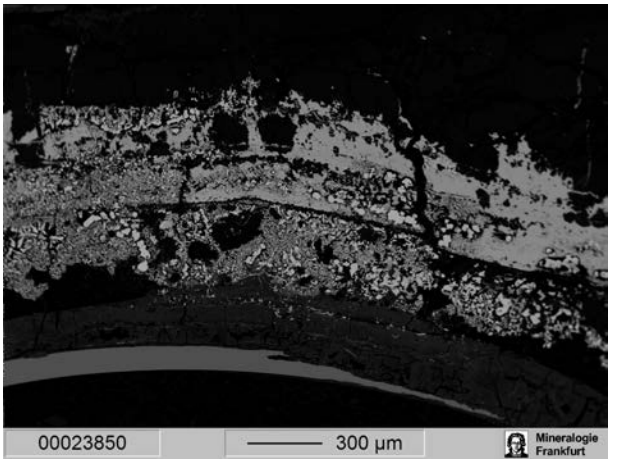

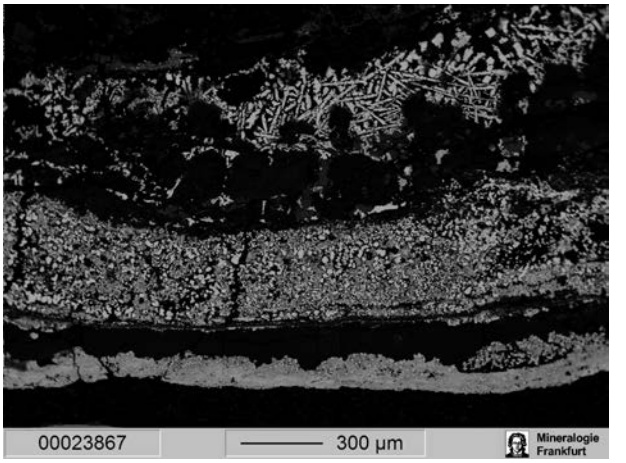

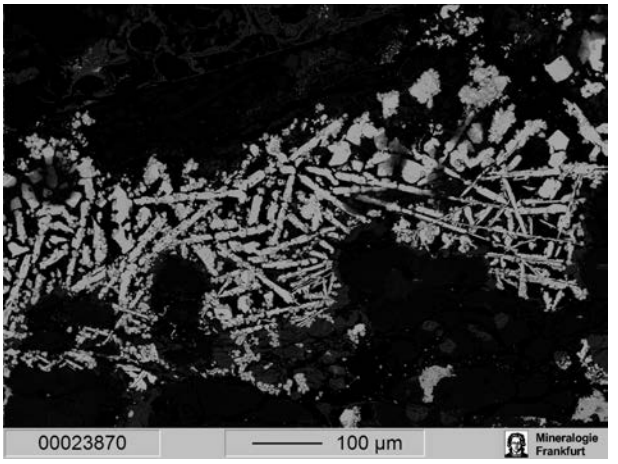

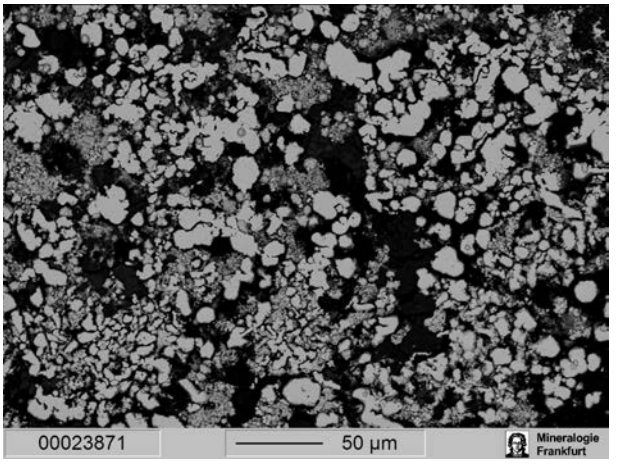

30-12-429

Museum nr. 30-12-429

Old Registration Nr.	B18184
Material	Ag
Object	Toe rings, finger rings, earrings and beads
Dating	unknown
Tomb	unknown
Type of Tomb	unknown
EPMA	
Laser (Trace)	
Laser (CuI)	x
Sol (CuI)	
Laser (LIA)	
Sol (LIA)	
Misc	corroded

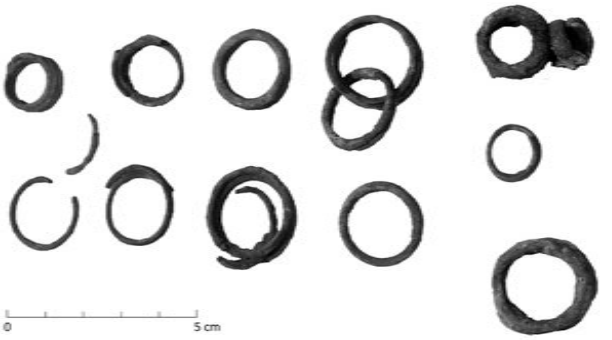

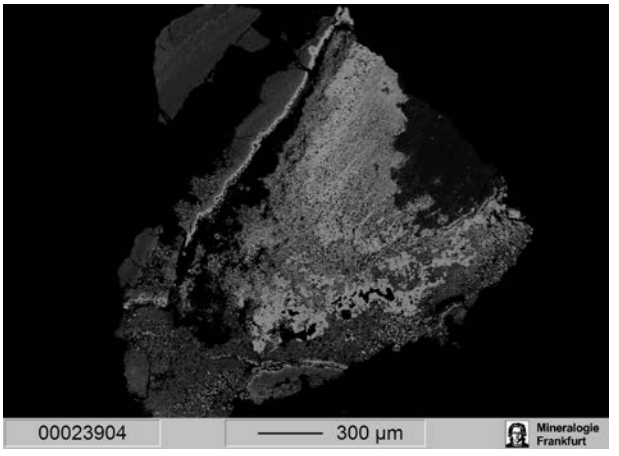

30-12-446

Museum nr. 30-12-446

Field Nr.	U.12388g
Material	Ag
Object	Pin
Dating	Early Dynastic
Tomb	PG 1237, body 30, renumbered body 49
Type of Tomb	Great Death Pit
EPMA	x
Laser (Trace)	x
Laser (CuI)	
Sol (CuI)	x
Laser (LIA)	x
Sol (LIA)	x

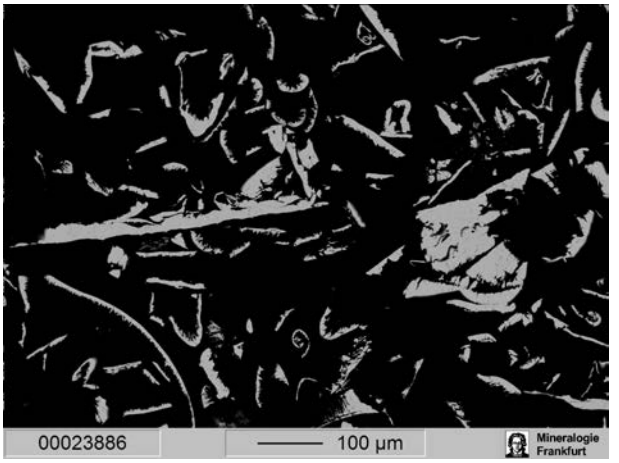

30-12-605

Museum nr. 30-12-605

Material	Ag
Object	Hair coil
Dating	unknown
Tomb	unknown
EPMA	x
Laser (Trace)	x
Laser (CuI)	x
Sol (CuI)	x
Laser (LIA)	x
Sol (LIA)	x

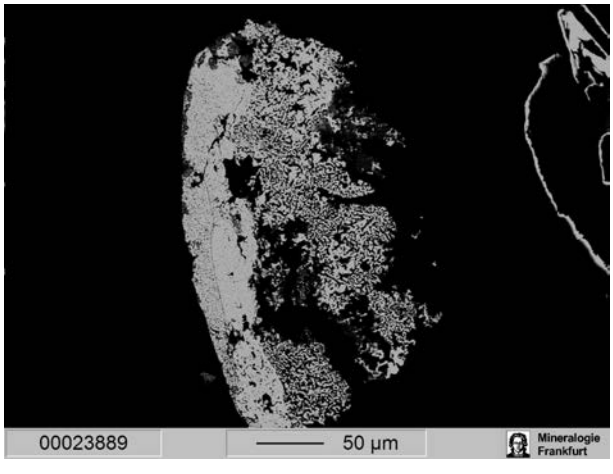

30-12-611

Museum nr. 30-12-611

Field Nr.	U.12425a
Material	Ag
Object	Rolled Ribbon
Dating	Early Dynastic
Tomb	PG 1237/69 9 (renumbered body 56)
Type of Tomb	Great Death Pit
EPMA	
Laser (Trace)	
Laser (CuI)	
Sol (CuI)	
Laser (LIA)	x
Sol (LIA)	

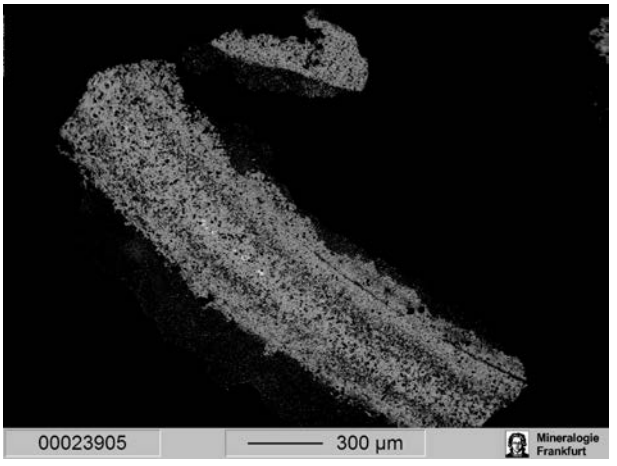

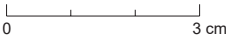

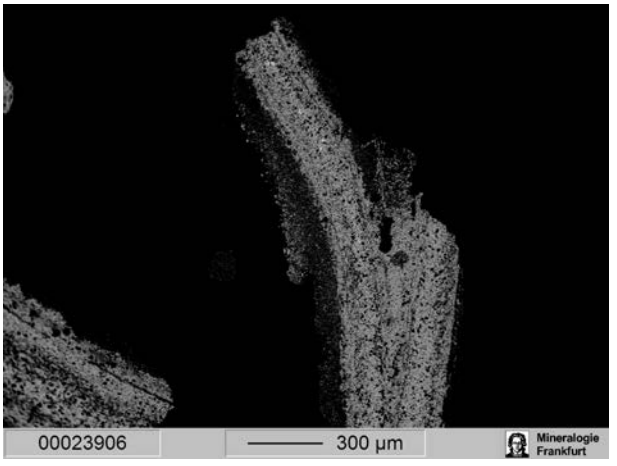

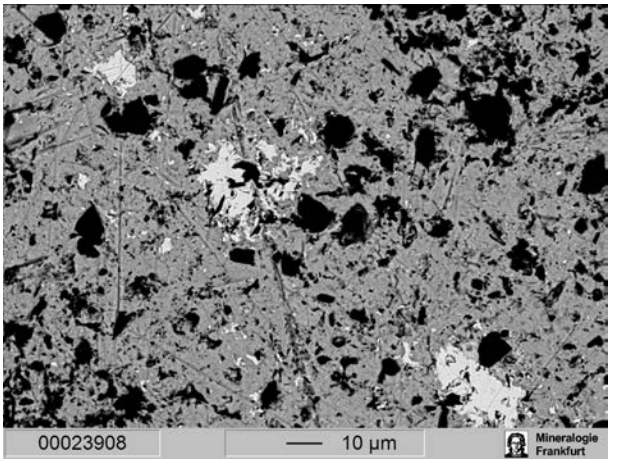

30-12-733

Museum nr. 30-12-733

Field Nr.	U.12423i
Material	Ag
Object	Pin
Dating	Early Dynastic
Tomb	PG 1237/67 (renumbered body 9)
Type of Tomb	Great Death Pit
EPMA	x
Laser (Trace)	x
Laser (CuI)	x
Sol (CuI)	
Laser (LIA)	x
Sol (LIA)	x

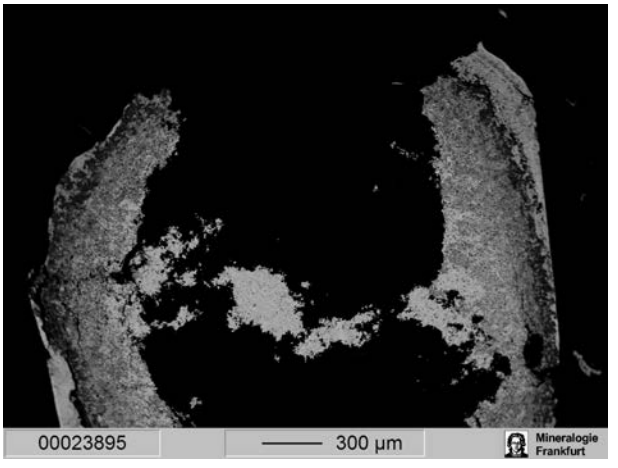

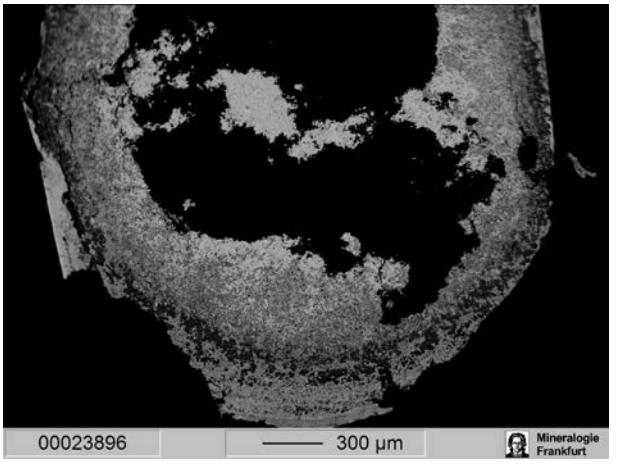

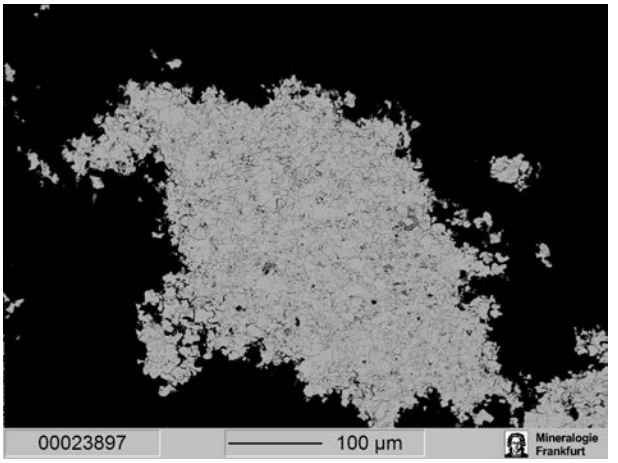

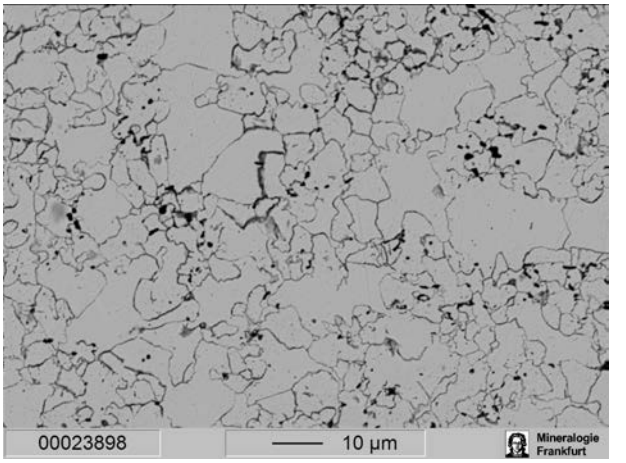

30-12-754

Museum nr. 30-12-754

Field Nr.	U.12369c
Material	Ag
Object	Pins
Dating	Early Dynastic
Tomb	PG 1237/11 (renumbered body 44)
Type of Tomb	Great Death Pit
EPMA	x
Laser (Trace)	x
Laser (CuI)	x
Sol (CuI)	
Laser (LIA)	x
Sol (LIA)	

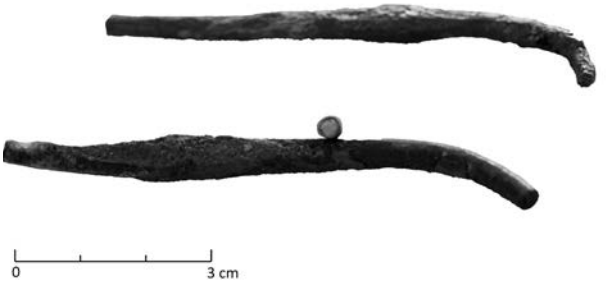

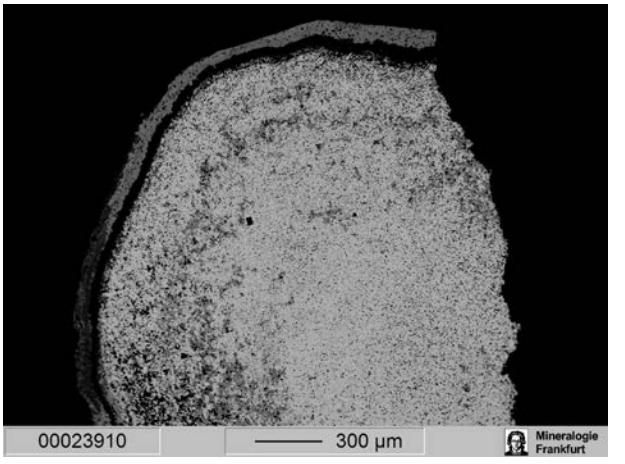

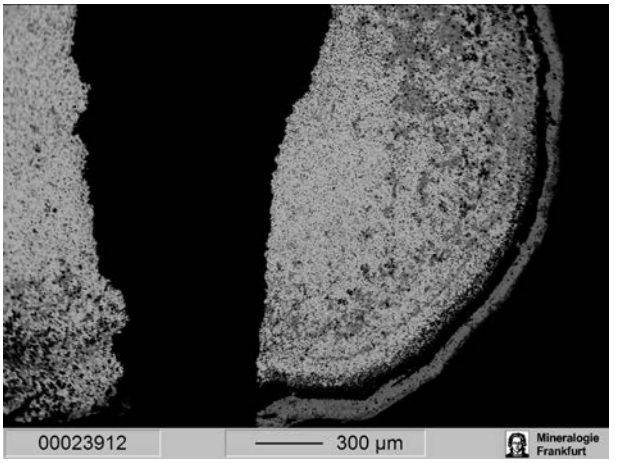

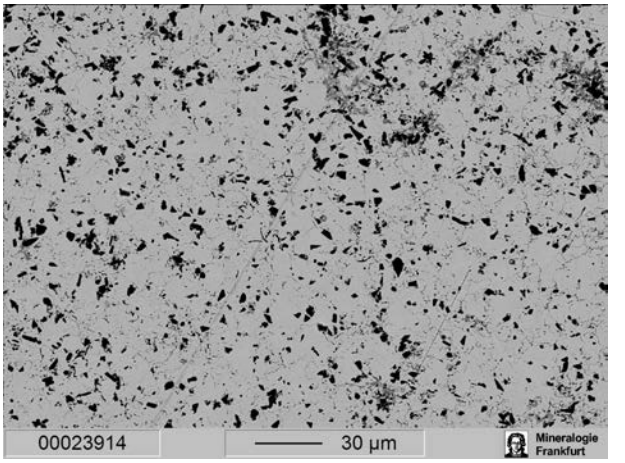

31-17-280a

Museum nr. 31-17-280a

Field Nr.	U.14324
Material	Ag
Object	Ring
Dating	unknown
Tomb	unknown
EPMA	x
Laser (Trace)	
Laser (CuI)	x
Sol (CuI)	
Laser (LIA)	x
Sol (LIA)	

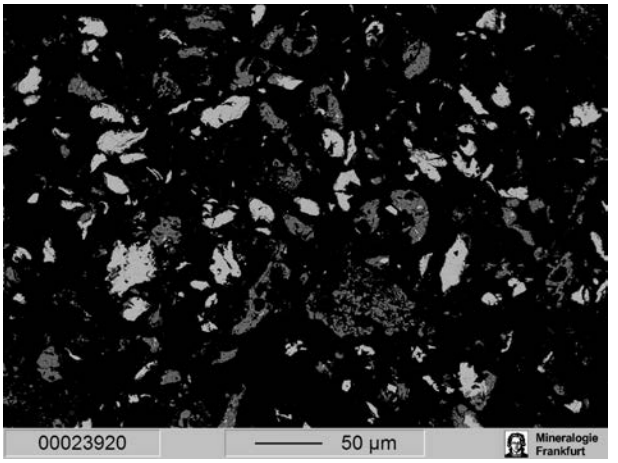

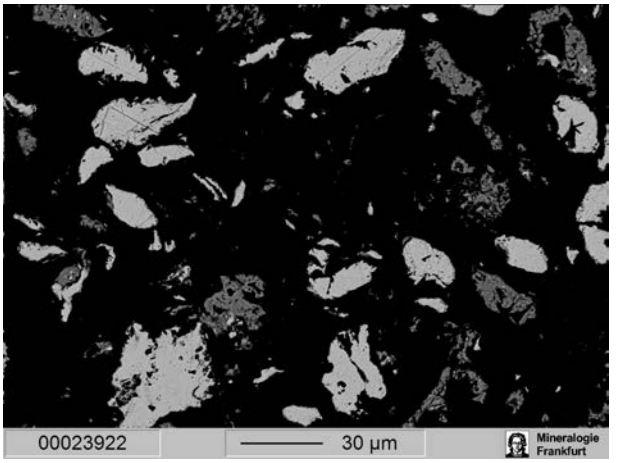

B16926a

Museum nr. B16926a

Material	Ag
Object	Pin
Dating	Akkadian / Late Akkadian
Tomb	PG 673
EPMA	x
Laser (Trace)	x
Laser (CuI)	
Sol (CuI)	x
Laser (LIA)	x
Sol (LIA)	x

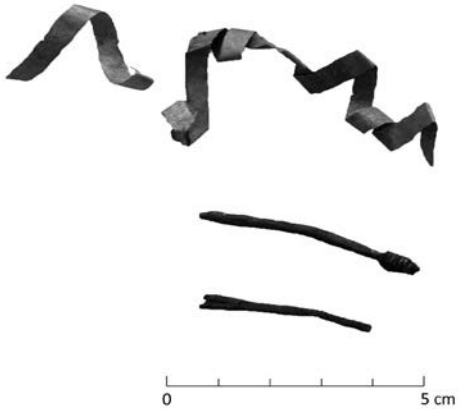

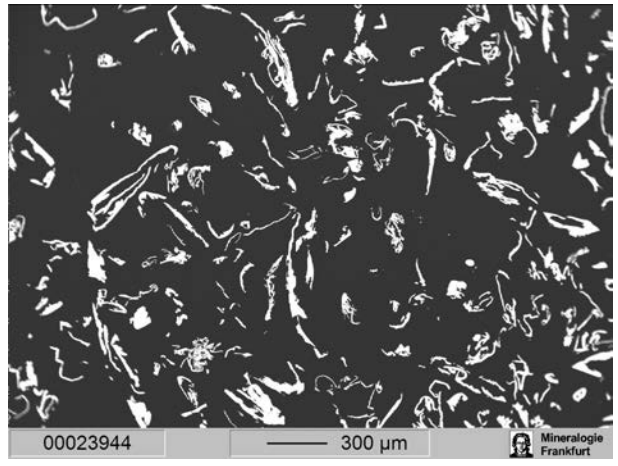

B16931a, -b

Museum nr. B16931.a, -b
Field Nr. U.9630a
Material Ag
Object 2 Bracelets
Dating Akkadian / Late Akkadian
Find context cf. U.9634,B16935 Cylinder Seal
Tomb PG 673
EPMA x
Laser (Trace) x
Laser (CuI)
Sol (CuI) x
Laser (LIA) x
Sol (LIA) x

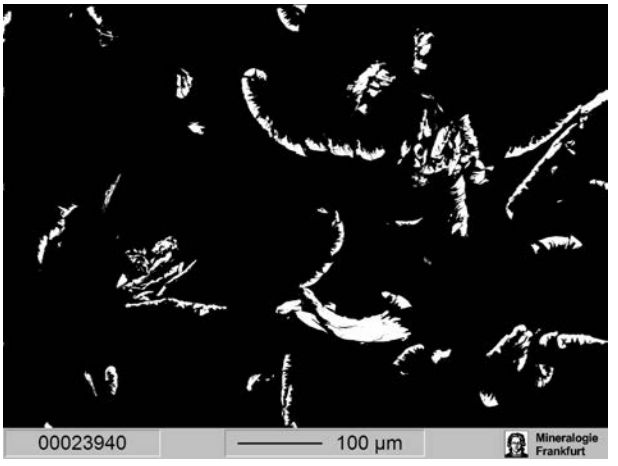

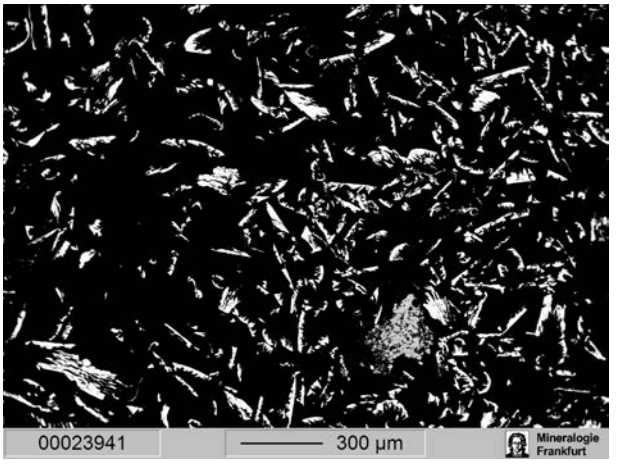

B17000/B17588

Museum nr. B17000/B17588

Field Nr. U.9786 / U.9787
Material Ag-Au-Lapis lazuli
Object Fragments of a diadem
Dating Early Dynastic
Tomb PG 777
Type of Tomb Royal
EPMA x
Laser (Trace)
Laser (CuI)
Sol (CuI)
Laser (LIA)
Sol (LIA)

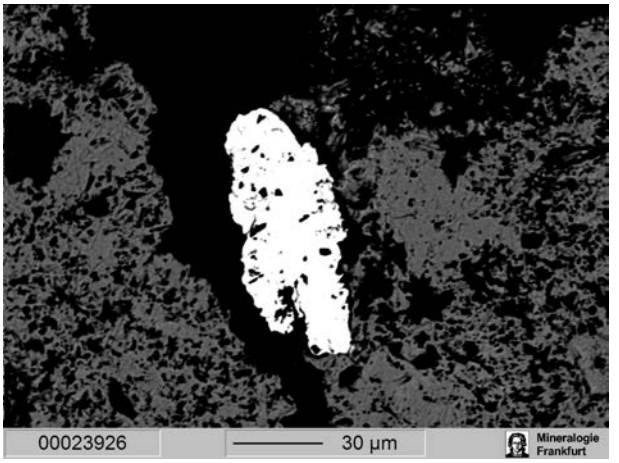

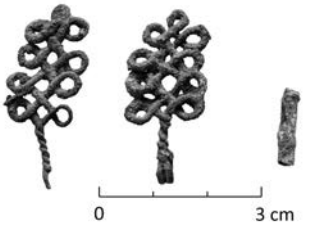

B17078a

Museum nr. B17078a

Field Nr.	U.10472
Material	Ag
Object	Spearhead
Dating	Early Dynastic
Tomb	PG 789
Type of Tomb	Royal
Note	The microstructure is recrystallised during electrochemical restoration and does not exhibit the original microstructure
EPMA	x
Laser (Trace)	
Laser (CuI)	
Sol (CuI)	
Laser (LIA)	
Sol (LIA)	x

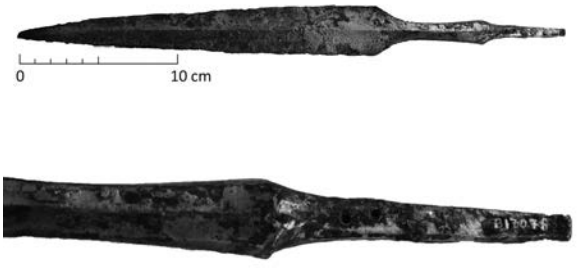

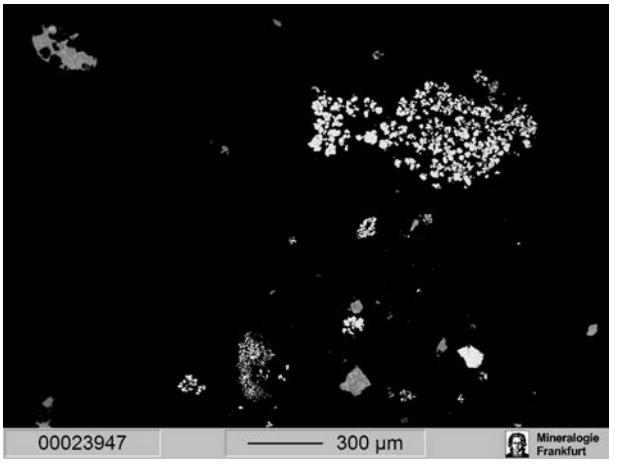

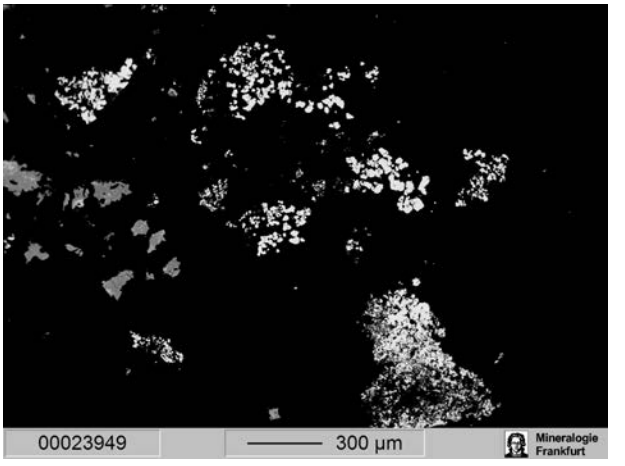

B17082a

Museum nr. B17082a

Field Nr.	U.10860
Material	Ag
Object	Tumbler
Dating	Early Dynastic
Tomb	PG 800
Type of Tomb	Puabis Tomb
Note	The microstructure is recrystallised during electrochemical restoration and does not exhibit the original microstructure
EPMA	
Laser (Trace)	
Laser (CuI)	
Sol (CuI)	
Laser (LIA)	
Sol (LIA)	x

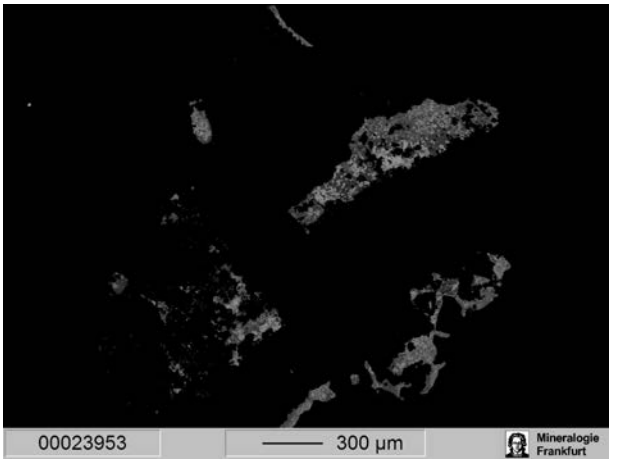

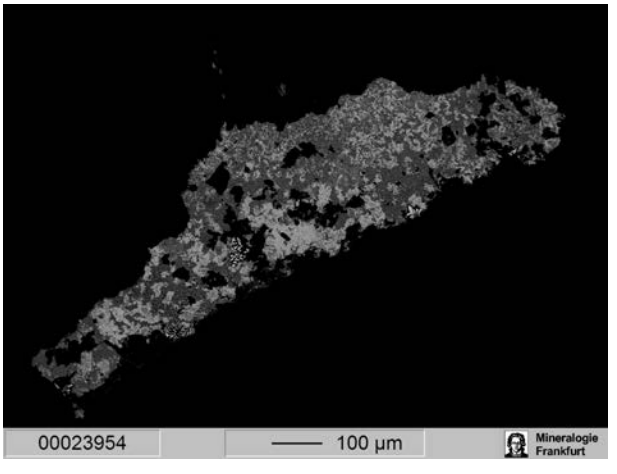

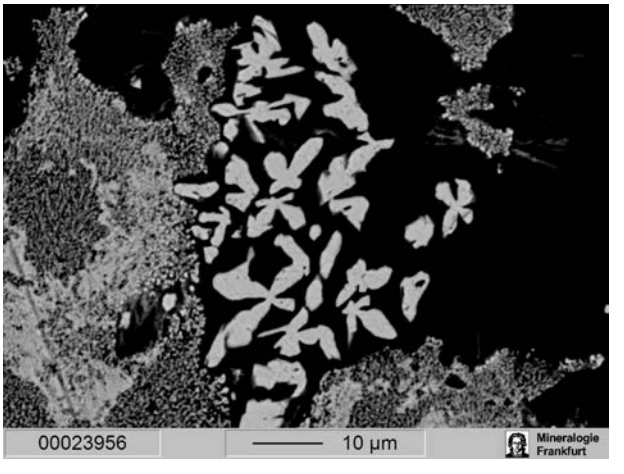

B17084

Museum nr. B17084

Field Nr.	U.8013A
Material	Ag
Object	Bracelet
Dating	Early Dynastic
Find context	cf. U.8006 (B16889) Cylinder Seal
Tomb	TTE PG 55
Type of Tomb	
EPMA	x
Laser (Trace)	x
Laser (CuI)	x
Sol (CuI)	
Laser (LIA)	
Sol (LIA)	x

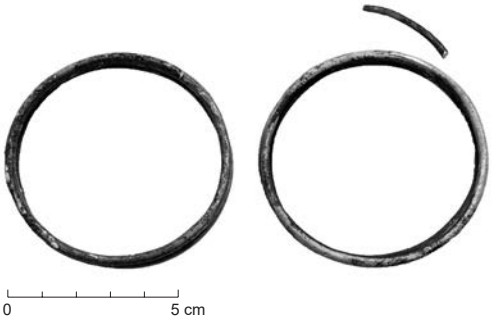

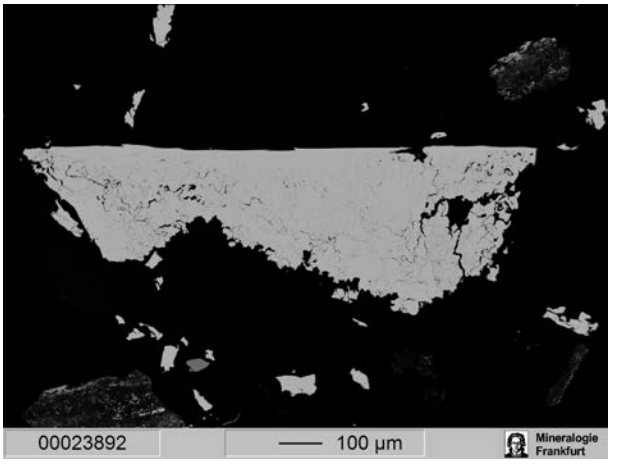

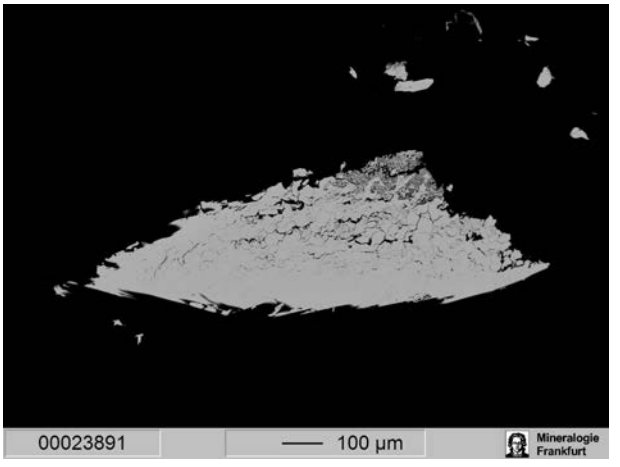

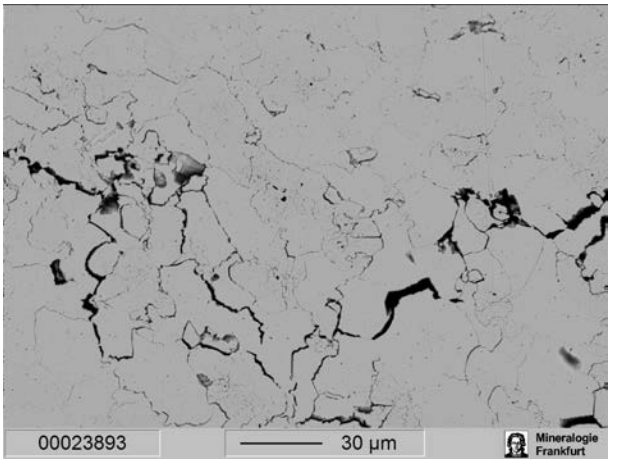

B17553

Museum nr. B17553

Field Nr.	U.8599
Material	Ag
Object	Bracelet
Dating	Early Dynastic
Tomb	TTE PG 333
Type of Tomb	
EPMA	x
Laser (Trace)	x
Laser (CuI)	
Sol (CuI)	x
Laser (LIA)	x
Sol (LIA)	x